Conference Proceedings

2000 International Conference on

MATHEMATICAL METHODS IN ELECTROMAGNETIC THEORY
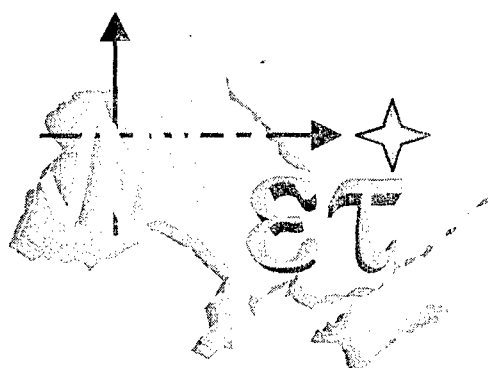
MM T 2000

Kharkov, Ukraine

September 12-15, 2000

TICRA

REPORT DOCUMENTATION PAGE

Form Approved OMB No. 0704-0188

Public reporting burden for this collection of information is estimated to average 1 hour per response, including the time for reviewing instructions, searching existing data sources, gathering and maintaining the data needed, and completing and reviewing the collection of information. Send comments regarding this burden estimate or any other aspect of this collection of information, including suggestions for reducing this burden to Washington Headquarters Services, Directorate for Information Operations and Reports, 1215 Jefferson Davis Highway, Suite 1204, Arlington, VA 22202-4302, and to the Office of Management and Budget, Paperwork Reduction Project (0704-0188), Washington, DC 20503.

1. AGENCY USE ONLY (Leave blank)	2. REPORT DATE September 12-14, 2000	3. REPORT TYPE AND DATES COVERED 2001 Final Report

4. TITLE AND SUBTITLE
International Conference on Mathematical Methods in Electromagnetic Theory (MMET 2000) Held in Kharkov, Ukraine on September 12-15, 2000. Conference Proceedings, Volume 2.

5. FUNDING NUMBERS
F61775-00-WF084
F68171-00-M-6175

6. AUTHOR(S)

7.
8. PERFORMING ORGANIZATION NAME(S) AND ADDRESS(ES)
Institute of Radiophysics and Electronics
National Academy of Sciences
Ulitza Akademika Proskury, 12
Kharkov 210085 Ukraine

8. PERFORMING ORGANIZATION REPORT NUMBER
ISBN 0-7803-6347-7

9. SPONSORING/MONITORING AGENCY NAME(S) AND ADDRESS(ES)
EOARD
PSC 802 Box 14
FPO AE 09499-0039

10. SPONSORING/MONITORING AGENCY REPORT NUMBER
CSP 00-5084

11. SUPPLEMENTARY NOTES
See also ADA383855, MMET 2000, Vol. 1. This work relates to Department of the Air Force grant issued by the European Aerospace Office of Research and Development. The United States has a royalty free license throughout the world in all copyrightable material contained herein.

12a. DISTRIBUTION/AVAILABILITY STATEMENT
Approved for Public Release. U.S. Government Rights License. All other rights reserved by the copyright holder. (Code 1, 20)

12b. DISTRIBUTION CODE
A

12. ABSTRACT (Maximum 200 words)

This is Volume 2 of the final Conference Proceedings of the International Conference on Mathematical Methods in Electromagnetic Theory (MMET 2000) held in Kharkov, Ukraine on September 12-15, 2000. Topics covered include theoretical and applied aspects of: antenna theory, asymptotic methods, particle beams, complex media, computational techniques, eigenvalue problems, electromagnetic theory, fiber optics, function-theoretic methods, gratings and frequently, inverse problems, lasers, linear accelerator models, nonlinear phenomena, open wavelengths, plasma and waves, radomes, remoting sensing models, waveguide circuits and CAD and more.

13. SUBJECT TERMS
EOARD, Foreign reports, Ukraine, Electromagnetics, Computational electromagnetics, Antennas

15. NUMBER OF PAGES

16. PRICE CODE

17. SECURITY CLASSIFICATION OF REPORT UNCLASSIFIED	18. SECURITY CLASSIFICATION OF THIS PAGE UNCLASSIFIED	19. SECURITY CLASSIFICATION OF ABSTRACT UNCLASSIFIED	20. LIMITATION OF ABSTRACT UL

NSN 7540-01-280-5500

Standard Form 298 (Rev. 2-89)
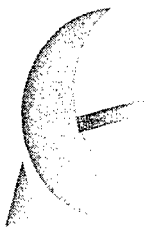Prescribed by ANSI Std. 239-18
298-102

20011206 135

Conference Proceedings

2000 International Conference on

MATHEMATICAL METHODS
IN ELECTROMAGNETIC THEORY

MM T 2000

Volume 2

Kharkov. Ukraine

September 12-15, 2000

AQ F02-02-0376

Organized and sponsored by

IEEE AP/MTT/AES/ED/GRS/LEO Societies East Ukraine Joint Chapter

in cooperation with

Ukrainian National URSI Committee
Scientific Council of NAS on Radio Physics and Microwave Electronics
Institute of Radio-Physics and Electronics of NAS
Institute of Radio Astronomy of NAS
Kharkov National University

technically co-sponsored by

IEEE AP, MTT and ED Societies
URSI

*We wish to thank the following for their contribution to the success
of this conference:*

IEEE ED, MTT, AP and NPS Societies
IEEE Region 8 Office
URSI
European Office of Aerospace R & D
European Research Office, USARDSG-UK
TICRA

2000 International Conference on Mathematical Methods in Electromagnetic Theory

MMET*2000 Chairman

Prof. E. I. Veliev, IRE NAS, Kharkov

MMET*2000 Organizing Committee

Prof. V. S. Bakirov, Rector, Kharkov National University

Mrs. N. Y. Bliznyuk, IRE NAS, Kharkov
Conference secretary and Website designer

Prof. V. I. Naidenko, National TU - Kiev Polytechnical Institute
Special representative in Kiev

Prof. A. B. Samokhin, Moscow TU of Radio, Electronics and Automation
Special representative in Moscow

Ms. I. A. Tishchenko, IRE NAS, Kharkov
Proceedings and program editor

Mr. A. D. Ustimenko, IRE NAS, Kharkov

Dr. I. Y. Vorgul, Kharkov National University
Arts and technical assistance

Prof. V. M. Yakovenko, Director, IRE NAS, Kharkov

MMET*2000 Chairman

Prof. E. I. Veliev, IRE NAS, Kharkov

MMET*2000 Technical Program Committee

Co-Chairmen:

Prof. A. I. Nosich, IRE NAS, Kharkov, Ukraine
Dr. W. Ross Stone, IEEE AP-S & URSI, La Jolla, USA

Members:

Prof. T. M. Benson, University of Nottingham, UK
Prof. L. Bertel, Universite de Rennes 1, France
Prof. V. S. Buldyrev, St. Petersburg University, Russia
Prof. N. Engheta, University of Pennsylvania, USA
Prof. F. Gardiol, Ecole Polytechnique, Lausanne, Switzerland
Prof. G. Hanson, University of Wisconsin-Milwaukee, USA
Prof. M. Hashimoto, Osaka Electro-Communication University, Japan
Prof. T. Hinata, Nihon University, Tokyo, Japan
Prof. M. Idemen, Isik University, Istanbul, Turkey
Prof. A. S. Ilinsky, Moscow State University, Russia
Prof. N. A. Khizhnyak, National Center – KIPT, Kharkov, Ukraine
Prof. A. A. Kirilenko, IRE NAS, Kharkov, Ukraine
Prof. K. Kobayashi, Chuo University, Tokyo, Japan
Prof. M. Marciniak, Institute of Telecommunications, Warsaw, Poland
Prof. Z. T. Nazarchuk, PMI NAS, Lviv, Ukraine
Prof. A. G. Nerukh, Kharkov TU of Radio Electronics, Ukraine
Prof. Y. Okuno, Kumamoto University, Japan
Prof. Y. S. Shifrin, Kharkov TU of Radio Electronics, Ukraine
Prof. I. A. Sukhoivanov, Kharkov TU of Radio Electronics, Ukraine
Prof. K. Tanaka, Gifu University, Japan
Prof. O. A. Tretyakov, Kharkov National University, Ukraine
Prof. E. N. Vasiliev, Moscow Power Engn. Institute – TU, Russia
Prof. D. M. Vavriv, IRA NAS, Kharkov, Ukraine
Dr. S. N. Vorobiov, IRA NAS, Kharkov, Ukraine
Prof. T. Yamasaki, Nihon University, Tokyo, Japan
Prof. G. I. Zaginailov, Kharkov National University, Ukraine

CHAIRMEN'S WELCOME

Dear colleagues:

We are very glad to see so many new and familiar faces at MMET*2000, especially of those speakers who have come to MMET for the third and forth time since 1990. This proves that mathematics, computational electromagnetics and physics of microwaves still attract time and efforts of researchers. This also proves that the conference is held at the right place and in the right time. One of the main features of the MMET series of conferences is English as working language. This may be liked or not but it is clear that this single factor has opened many new and exciting opportunities for the scientists of Ukraine and the Former Soviet Union to meet their Western colleagues and communicate in the recognized professional language. Results are seen in the visits, joint projects and publications of Ukrainian scientists and their colleagues from Europe, Japan and USA. Joint papers accepted to the program of MMET are getting common, with some speakers coming from their posts in foreign laboratories. Another feature is accessibility that is guaranteed by convenient location of Kharkov and good transportation network. This city has been for centuries on the crossroads between Ukraine, Russia, Black Sea and the Caucasus and acquired a unique cosmopolitan spirit and broad-mindedness. Still another feature is affordability for low-income participants: registration fee is split into several convenient parts to meet variety of incomes, cheaper accommodations are available. MMET started as a school-seminar for young scientists, and by tradition it keeps a number of absolutely one-of-a-kind opportunities for younger participants. These are reduced registration fee and a moderate travel support, plus a chance of winning an award of the conference that includes a fee waiver for the next meeting. All this would never be possible without very kind and efficient support of a number of international organizations and professional societies.

This year the Technical Program Committee adopted more strict selection criteria. The rate of acceptance of contributed papers was 78% (186 out of 240 submitted). It means that one of every five papers had no chance to be accepted. We hope that their authors will be luckier next time. Local Organizing Committee has shown its best in preparing the proceedings, running the facilities, managing the conference events, and arranging the social program. A new feature was frequently updated Web site of the conference. We are grateful to all the members of LOC and TPC for their contribution to the success of MMET*2000.

Thank you for coming to participate, enjoy the conference, make friends, discuss new joint projects, and plan to attend future MMETs.

Eldar I. Veliev and Alexander I. Nosich

TABLE OF MMET*2000 PAPERS GEOGRAPHY

ENTITY	PAPERS
KHARKOV	80
RUSSIA	48
UKRAINE (non-Kharkov)	20
JAPAN	7
TURKEY	6
POLAND	4
BELARUS	3
ITALY	3
UKRAINE+GERMANY	3
UKRAINE+JAPAN	3
GEORGIA	2
USA	2
UKRAINE+RUSSIA	2
UKRAINE+TURKEY	2
RUSSIA+UK	2
UK	1
The NETHERLANDS	1
TAIWAN	1
BULGARIA+ GERMANY	1
RUSSIA+POLAND	1
UKRAINE+USA	1
UKRAINE+FRANCE	1
UKRAINE+UK	1
UKRAINE+CANADA	1
UKRAINE+ISRAEL	1
UKRAINE+CHINA	1
GEORGIA+USA	1
TOTAL	199

TABLE OF CONTENTS

· ·

Volume I

COMPUTATIONAL TECHNIQUES

ANALYTICAL REGULARIZATIONS

SIGNAL PROCESSING

PROPAGATION AND REMOTE SENSING

ANTENNA THEORY

COMPLEX MEDIA, BEAMS AND PLASMAS

....

Volume II

OPTICAL NETWORKS

SCATTERING AND RADAR CROSS SECTION

GUIDED WAVES

EIGENVALUE PROBLEMS

GRATINGS AND FREQUENCY-SELECTIVE SURFACES

INVERSE AND SYNTHESIS PROBLEMS

IONOSPHERIC ELECTROMAGNETICS

FUNCTION-THEORETIC METHODS

OPTICAL

NETWORKS

NUMERICAL EVALUATION OF BINARY OPTICAL ELEMENTS WITH SUBWAVELENGTH STRUCTURES

Masayuki Fujimoto, Yoichi Okuno and Toyonori Matsuda[*]

Department of Electrical and Computer Engineering, Kumamoto University

2-39-1, Kurokami, Kumamoto 860-8555, Japan

E-mail: fujimo@st.eecs.kumamoto-u.ac.jp

[*]Kumamoto National College of Technology

2659-2, Nishigoshi, Kumamoto 861-1102, Japan

ABSTRACT

The diffraction characteristics of a diffractive device with binary subwavelength gratings are evaluated by the use of FDTD method. The field patterns are computed for sevral grating parameters. The transmitted fields are analyzed in terms of the effective refractive indices, which are determined by the duty ratio and grating period and depend on the polarization of the incident light. Numerical results show that the device works as an optical lens.

INTRODUCTION

The optical behavior of a subwavelength grating with a period p smaller than the wavelength is dependent on the polarization of the incident light. Subwavelength gratings exhibit form-birefringence and may be used as artificial anisotropic materials [1]. A binary relief grating which can devert the power of the incident light into a single diffracted order has been proposed [2]. The so-called blazed grating can be replaced with the subwavelength binary grating which is composed of unequal-width ridge. By varying the duty ratio of the grating, it may be treated as an artificial distributed-index medium. Making use of this properties of the grating, a binary diffractive lens has been considered [3,4].

As a binary diffractive profile treated in this paper modulates transmitted phase retardation of light wave in grating region by varying duty ratio, the device is so large in dimension and so complicated in its profile. We therefore employ the FDTD method [5] which is a useful computational technique for a wide variety of problems to investigate diffraction characteristics of the binary diffractive profiles with subwavelength elements. We design a binary optical lens and its performance.

SYSTEM CONFIGURATION

Fig.1. *Diffraction geometry and parameters.*
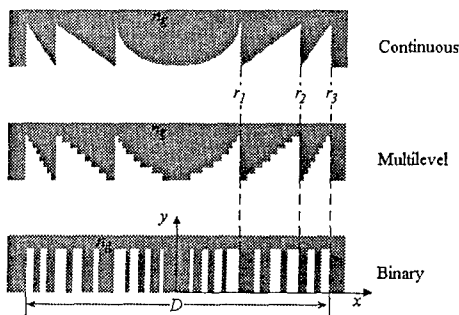
As shown in Fig. 1, the diffractive lenses analyzed in this paper are the surface relief structures of continuous, multilevel and binary profile. The incident region and the focal region are filled with isotropic and homogeneous media with refractive indices, n_g and n_0, respectively. The structures are assumed to be uniform in the z-directions. The etch depth of the Fresnel zone plate is given by

$$h(x) = \mathrm{mod}[\phi(x), 2\pi]/[(n_0 - n_g)k_0], \qquad (1)$$

where $\phi(x) = k_0 n_0 (f - \sqrt{x^2 + f^2})$, $k_0 = 2\pi/\lambda_0$, λ_0 is the free-space wavelength and f is the focal length. The plate has the discontinuities at positions,
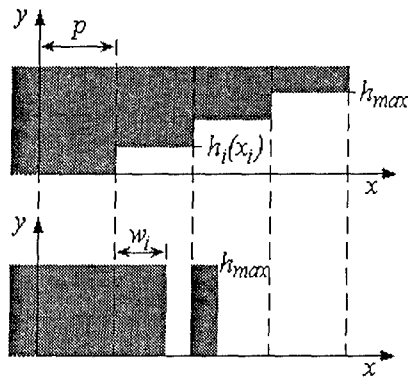
$$r_m = [2m\lambda_0 f + (m\lambda_0)^2]^{1/2}, \text{ where } m=1, 2, 3. \quad (3)$$

For multilevel profile, the profile is divided into q pixels with a common width p. The depth is sampled at the pixel midpoints, $x_i = (-q/2+i-0.5)p$, where $i=1, 2,..., q$, $q=D/p$ and D is the width of the lens. The quantized depths are given by

$$h_i(x_i) = \text{int}[h(x_i)/h_d + 0.5]h_d, \quad (4)$$

where $h_d=h_{max}/(N-1)$ is the step height, N is number of levels and $h_{max} = \lambda_0/(n_g - n_0)$.

Fig. 2. *Transition from multilevel profile to subwavelength grating.*

DETERMINATION OF SUBWAVELENGTH STRUCTURES

Here we describe the details of how to replace the multilevel profile with the subwavelength grating. The profile of multilevel lens is also divided into q ridge-groove pairs, with period p. Because the physical height of the grating (h_{max}) is fixed, the phase difference between the adjacent partitions is adjusted by varying duty ratio t_i. To determine the grating duty ratio t_i, it is assumed that the duty ratio corresponds to the difference of the depth of the partitioned pixel. According to Fig. 2, the duty ratio is given by, $t_i=1-h(x_i)/h_{max}$, where $i =1, 2,..., q$. Therefore the ridge width is given by $w_i = t_i p$. With the assumption, all parameters required for constructing ridge-width-modulated grating with subwavelength period can be caluculated. The lens parameters are set to be as follows: $n_g = 1.5, n_0 = 1, D = 12\lambda_0, q = 40, p = 0.3\lambda_0, h_{max} = 2.0\lambda_0$

NUMERICAL RESULTS

The total electric field for the TE (electric field parallel to z axis) polarized, normally incident plane wave is shown in Figs. 3 and 4, for the 16-level and the binary diffractive lens profile, respectively. In parts (a) of Figs. 3 and 4 the distribution of the absolute value of the complex amplitude E_z is shown, while in parts (b) of Figs. 3 and 4 the Poynting vector is shown. In both cases the focasing effect of the diffractive lens is demonstrated. The diffracted field is concentrated near the same focal point in both cases.

Similar diffracted pattern is analyzed in the case of the continuous diffractive lens. Figure 5 shows the diffracted field of the binary, continuous and 16-level diffractive profile in the y-direction ($x=0$). Though immediately bihind the lens the diffracted patern of the binary lens is different from that of other lenses, the peak of the diffracted power is located at the focal point. Figure 6 shows the diffracted field in the x-direction ($y=-4\lambda_0$).

CONCLUSION

The diffraction characteristics of the three different diffractive lenses have been eveluated by the FDTD method. We have shown that the binary subwavelength element with appropriate shapes and arrangements of the subwavelength structures works as an optical lens.

REFERENCES

[1] M. Born and E. Wolf, " Principles of Optics," Pergamon Press, Oxford, 1980.
[2] M. Schmitz et al., J. Soc. Am. A, vol.12, no. 11, pp.2458-2462, 1995.
[3] Z. Zhou et al., J. Soc. Am. A, vol.12, no. 5, pp.1104-1112, 1995.
[4] K. Hirayama et al., J. Soc. Am. A, vol.13, no. 11, pp.2219-2231, 1996.
[5] K. S. Yee, IEEE Trans. Antennas Propag., vol.4, no. 3, pp.302-307, 1966.
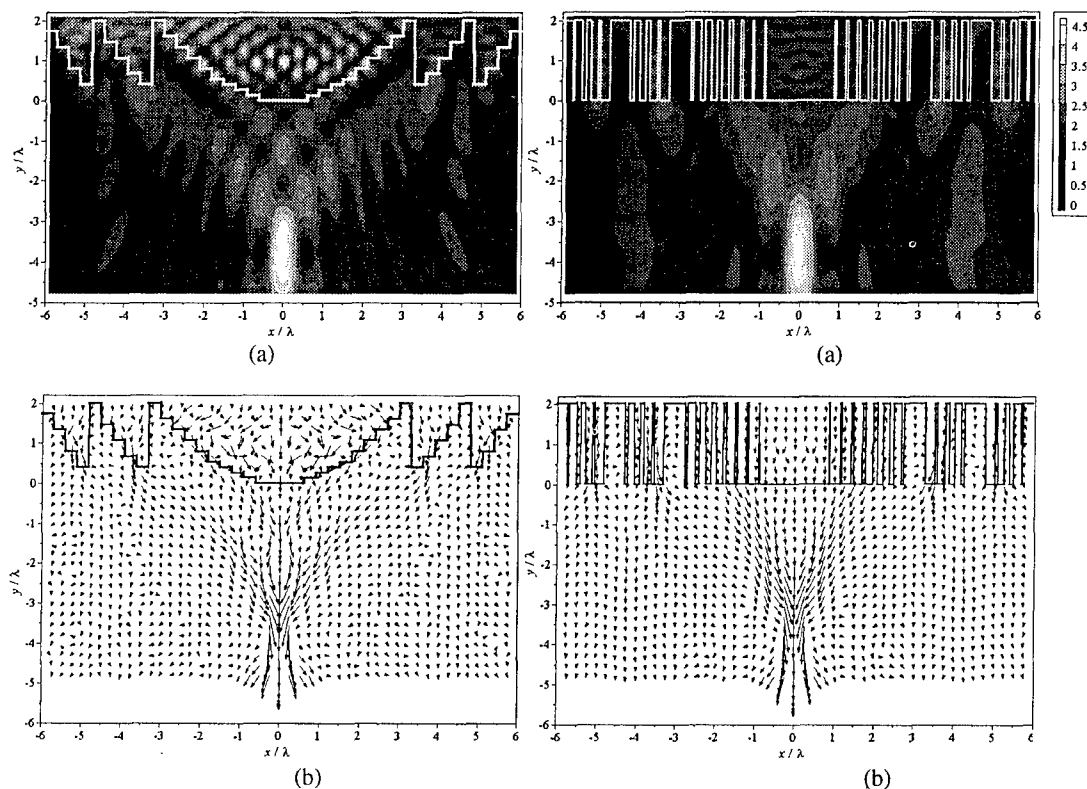
Fig. 3. *(a) Field distribution for 16-level lens. Absolute value of E_z is plotted. (b) The Poynting vector.*

Fig. 4. *(a) Same as Fig. 3, but binary lens. (b) The Poynting vector.*
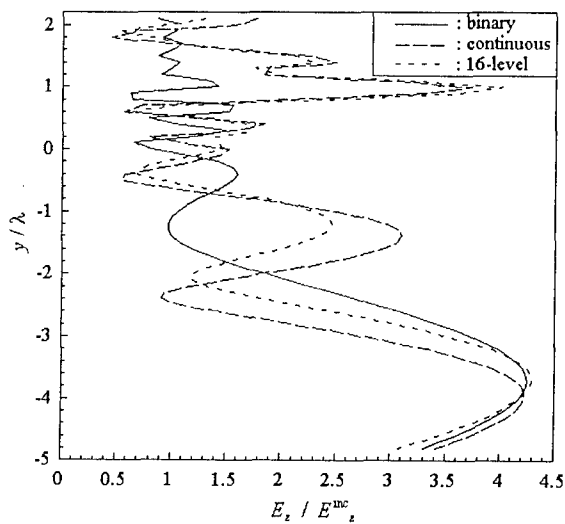
Fig. 5. *Field patterns in y-direction (x=0).*
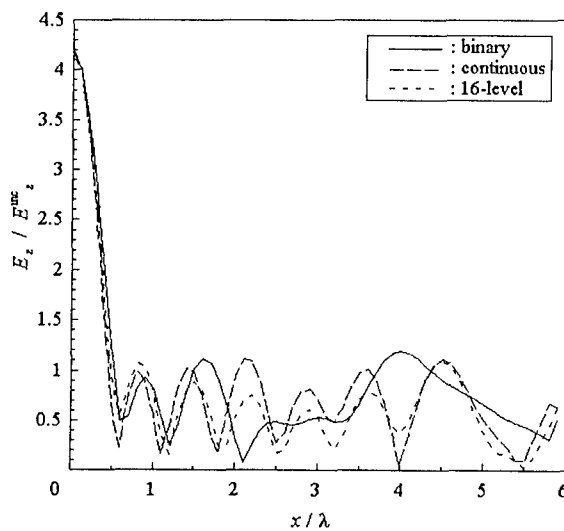
Fig. 6. *Field patterns in x-direction ($y=-4\lambda_0$).*

MATHEMATICAL ANALYSIS AND NUMERICAL SIMULATION OF THE GUIDED MODES OF THE WEAKLY GUIDING OPTICAL FIBERS

Evgenii Karchevskii and Rafail Dautov

Kazan State University, Kazan, Russia
Email: Evgenii.Karchevskii@ksu.ru

A mathematical formulation for the guided modes of the weakly guiding optical fibers is derived from the two-dimensional Helmholtz equation. The original problem is reduced to a spectral problem for the Helmholtz equation in a bounded domain with nonlocal boundary condition. This formulation leads to a nonlinear eigenvalue problem for a family of self-adjoint compact operators. The main spectral properties of these operators are established. Then the min-max principle provides an expression of the nonlinear dispersion relation, which connects the propagation constants of guided modes with the frequency. Various existence results are proved and complete description of dispersion curves (monotonicity, asymptotic behavior, existence of cutoff values) is carried out. A finite element scheme follows from the operator formulation of the problem. This scheme leads to a nonlinear eigenvalue problem for a family of self-adjoint matrix operators. The existence results for this problem are proved. For its solution we propose an efficient method. Practical opportunities of this algorithm are shown by the results of numerical experiments.

INTEGRAL EQUATIONS IN ELECTROMAGNETIC WAVE SCATTERING BY TWO-DIMENSIONAL DIELECTRIC LENSES AND SHELLS

Artem V. Boriskin*, and Svetlana V. Boriskina

Institute of Radiophysics and Electronics, National Academy of Sciences, Proskury str. 12, Kharkov 61085, Ukraine, *) e-mail: a_boriskin@yahoo.com

ABSTRACT

In this paper, integral equations for a two-dimensional (2D) wave diffraction by a two-layer arbitrary shaped dielectric scatterer are presented for both *E*- and *H*-polarization cases. The surface potential approach and the method of analytical regularization are used to obtain a Fredholm second-kind matrix equation. Efficient numerical algorithm based on this approach can be used for studying such physical effects as whispering-gallery (WG) mode resonances, focusing effect, beam directivity degradation due to a dielectric shell, etc., with applications to the design of cylindrical dielectric lenses and radomes.

INTRODUCTION

We study 2D problems of a field transmission through and scattering by a lossy two-layer arbitrarily shaped dielectric scatterer. Depending on the source location relatively to the scatterer, the problem can be considered as a 2D model of either a dielectric radome (❶) or a dielectric lens (❷) (Fig.1).

Curved dielectric radomes are widely applied in today microwave and millimeter-wave antenna technologies for protection of antennas from the impact of environment [1]. Dielectric lenses are used as focusing devices for a laser beam at the input to an optical-fiber network. In the microwave range, lenses are candidate antennas for many communication systems. They are attractive due to the wide band, multiple beams and mechanical scanning [2]. However, existing simulation tools are almost entirely based on high-frequency approximations having unclear and uncontrollable accuracy and not taking a full account of all the interactions between different parts of scatterer [3,4]. This prevents one from studying the physics of the wave phenomena in accurate and reliable manner, and thus calls for a development of novel approaches.
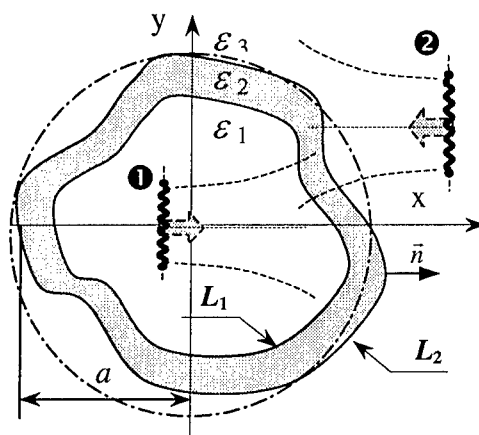
Fig.1 Geometry of the problem

INTEGRAL-EQUATION APPROACH

Consider a problem of the electromagnetic wave diffraction by an arbitrarily shaped dielectric shell with permittivity ε bounded with smooth curves L_1 and L_2. Total field must satisfy the Helmholtz equation with the wavenumber $k_s = k\sqrt{\varepsilon_s}$ in the s-th layer, the radiation condition at infinity, and the continuity conditions on the boundaries. The latter conditions can be written as follows:

$$U_s^{tot} = U_{s+1}^{tot}, \quad \alpha_s^2 \frac{\partial U_s^{tot}}{\partial r}\bigg|_{r=L_s} = \alpha_{s+1}^2 \frac{\partial U_{s+1}^{tot}}{\partial r}\bigg|_{r=L_{s+1}} \tag{1}$$

where s=1,2; $U_1^{tot} = U_0 + U_1^{sc}$; $U_2^{tot} = U_2^{sc} + U_2^{rad}$; $U_3^{tot} = U_3^{rad}$ and parameter α_s depends on the polarization: $\alpha_s = Z_s$ or $1/Z_s$ in the *E*- or *H*-case, respectively, $Z_s = (\varepsilon_s / \mu_s)^{1/2}$ is the normalized intrinsic impedance of the *s*-region, and $\varepsilon_1 = \varepsilon_3 = 1$, $\varepsilon_2 \equiv \varepsilon$.

Further formulas refer to the inner case ❶. Representing the fields in every region in terms of single-layer surface potentials over the contour of the scatterer cross section and applying the conditions (1), one obtains a set of the coupled first-kind integral equations (IEs) with respect to the unknown potential densities.

After the parametrization of the curves L_i : $x_i = x_i(t)$, $y_i = y_i(t)$ (*i=1,2*) and the usage of the properties of the single-layer potential limiting values, IEs take the following form:

$$\alpha_2^2 \int_0^{2\pi} \tilde{\varphi}_2^1 G_\varepsilon(t,t_1)dt_1 + \alpha_2^2 \int_0^{2\pi} \tilde{\psi}_2^2 G_\varepsilon(t,t_2)dt_2 - \int_0^{2\pi} \tilde{\varphi}_1^1 G(t,t_1)dt_1 = U_0(t) \tag{2}$$

$$\frac{1}{2}\left\{\frac{\tilde{\varphi}_2^1 + \tilde{\psi}_1^1}{L_1} + \frac{\tilde{\varphi}_2^2}{L_2}\right\} + \alpha_2^2 \int_0^{2\pi} \tilde{\varphi}_2^1 \frac{\partial G_\varepsilon(t,t_1)}{\partial n}dt_1 + \alpha_2^2 \int_0^{2\pi} \tilde{\psi}_2^2 \frac{\partial G_\varepsilon(t,t_2)}{\partial n}dt_2 - \int_0^{2\pi} \tilde{\varphi}_1^1 \frac{\partial G(t,t_1)dt_1}{\partial n}dt_1 = \frac{\partial}{\partial n}U_0(t) \tag{3}$$

$$\alpha_2^2 \int_0^{2\pi} \tilde{\psi}_2^1 G_\varepsilon(t,t_1)dt_1 + \alpha_2^2 \int_0^{2\pi} \tilde{\varphi}_2^2 G_\varepsilon(t,t_2)dt_2 - \int_0^{2\pi} \tilde{\psi}_3^2 G(t,t_2)dt_2 = 0 \tag{4}$$

$$\frac{1}{2}\left\{\frac{\tilde{\psi}_2^1}{L_1} + \frac{\tilde{\varphi}_2^2 + \tilde{\psi}_3^2}{L_2}\right\} + \alpha_2^2 \int_0^{2\pi} \tilde{\psi}_2^1 \frac{\partial G_\varepsilon(t,t_1)}{\partial n}dt_1 + \alpha_2^2 \int_0^{2\pi} \tilde{\varphi}_2^2 \frac{\partial G_\varepsilon(t,t_2)}{\partial n}dt_2 - \int_0^{2\pi} \tilde{\psi}_3^2 \frac{\partial G(t,t_2)}{\partial n}dt_2 = 0 \tag{5}$$

Here, the superscript and subscript of the unknown potentials correspond to the subscript of its argument and the layer, respectively; $\tilde{\varphi}(\tilde{\psi})_s^{1,2} = \varphi(\psi)_s^{1,2} \cdot L_{1,2}$ (note that $\psi_1^1 = \varphi_3^2 = 0$); $L_{1,2}$ are the coefficients which appear due to parametrization of the contours of integration:

$L_{1,2} = L(t_{1,2}) = \left[(dx_{1,2}/dt_{1,2})^2 + (dy_{1,2}/dt_{1,2})^2\right]^{1/2}$; $G(\vec{r},\vec{r}_1)$ is the free-space Green's function and $G_\varepsilon(\vec{r},\vec{r}_2)$ is the Green's function of the homogeneous medium with permittivity ε:

$$G(t,t_1) = (i/4) \cdot H_0^{(1)}(k|\vec{r} - \vec{r}_1|), \quad G_\varepsilon(t,t_1) = (\alpha i/4) \cdot H_0^{(1)}(k\sqrt{\varepsilon}|\vec{r} - \vec{r}_1|), \tag{6}$$

$\partial / \partial n$ is the normal derivative, n is the normal unit vector; $t_{1,2}$ are new parameters which uniquely characterize the contours: $x_{1,2} = x_{1,2}(t_{1,2})$, $y_{1,2} = y_{1,2}(t_{1,2})$, where $0 \le t_{1,2} \le 2\pi$. Further we invert analytically the singular or main parts, at $\vec{r} \to \vec{r}_{1,2}$ of IEs (2)-(5) exploiting the fact that the set of exponents: $\left\{e^{imt_{1,2}}\right\}_{m=-\infty}^{\infty}$ used as global basis in Galerkin's scheme is also a set of orthogonal eigenfunctions of canonical-shape IEs. This results in the following set of four coupled infinite-matrix equations:

$$\begin{cases} \alpha_2^2\left(\sum_{m=-\infty}^{\infty}\psi_{2m}^1 B1_{nm} + \sum_{m=-\infty}^{\infty}\varphi_{2m}^2 C1_{nm}\right) - \sum_{m=-\infty}^{\infty}\varphi_{1m}^1 A1_{nm} + \psi_{2m}^1 b1_n + \varphi_{2m}^2 c1_n - \varphi_{1m}^1 a1_n = u_n \\[2mm] \alpha_2^2\left(\sum_{m=-\infty}^{\infty}\psi_{2m}^1 \tilde{B}2_{nm} + \sum_{m=-\infty}^{\infty}\varphi_{2m}^2 \tilde{C}2_{nm}\right) - \sum_{m=-\infty}^{\infty}\varphi_{1m}^1 \tilde{A}2_{nm} + \psi_{2m}^1 b2_n + \varphi_{2m}^2 c2_n - \varphi_{1m}^1 a2_n = ka\tilde{u}_n \\[2mm] \alpha_2^2\left(\sum_{m=-\infty}^{\infty}\psi_{2m}^1 B1_{nm} + \sum_{m=-\infty}^{\infty}\varphi_{2m}^2 C1_{nm}\right) - \sum_{m=-\infty}^{\infty}\psi_{3m}^2 D1_{nm} + \psi_{2m}^1 b1_n + \varphi_{2m}^2 c1_n - \varphi_{3m}^2 d1_n = 0 \\[2mm] \alpha_2^2\left(\sum_{m=-\infty}^{\infty}\psi_{2m}^1 \tilde{B}2_{nm} + \sum_{m=-\infty}^{\infty}\varphi_{2m}^2 \tilde{C}2_{nm}\right) - \sum_{m=-\infty}^{\infty}\psi_{3m}^2 \tilde{D}2_{nm} + \psi_{2m}^1 b2_n + \varphi_{2m}^2 c2_n - \varphi_{3m}^2 d2_n = 0 \end{cases} \quad , n = 0, \pm 1, \ldots \tag{7}$$

$$A1\{\tilde{A}2,B1,\tilde{B}2,C1,\tilde{C}2,D1,\tilde{D}2\}_{nm} = \frac{1}{4\pi^2} \int_0^{2\pi} \int_0^{2\pi} A1\{\tilde{A}2,B1,\tilde{B}2,C1,\tilde{C}2,D1,\tilde{D}2\}(t,t_1)e^{int}e^{imt_1}dtdt_1 ,\tag{8}$$

$$u_n = \frac{1}{2\pi}\int_0^{2\pi} u_0 \cdot e^{-int}dt , \quad \tilde{u}_n = \frac{1}{2\pi}\int_0^{2\pi}\frac{d}{dn}u_0(t)\cdot e^{-int}dt , \quad \varphi_s^{1,2}\{\tilde{\psi}_s^{1,2}\} = \frac{2}{i\pi}\sum_{m=-\infty}^{\infty}\varphi_{sm}^{1,2}\{\psi_{sm}^{1,2}\}\cdot e^{imt_{1,2}} ,\tag{9}$$

$$\tilde{B}2\{\tilde{C}2\}_{nm}(t_{1,2}) = ka\sqrt{\varepsilon}\cdot\tilde{B}2\{\tilde{C}2\}_{nm} - iL_{1,2(n-m)}/\pi , \quad \tilde{A}2\{\tilde{D}2\}_{nm}(t_{1,2}) = ka\cdot\tilde{A}2\{\tilde{D}2\}_{nm} + iL_{1,2(n-m)}/\pi , \tag{10}$$

$$B1\{C1\} = G_\varepsilon(t,t_{1,2}) - \overset{0}{G}_\varepsilon(t,t_{1,2}), \qquad A1\{D1\} = G(t,t_{1,2}) - \overset{0}{G}(t,t_{1,2}),\tag{11}$$

$$B2\{C2\} = \frac{\partial}{\partial n}G_\varepsilon(t,t_{1,2}) - \frac{\partial}{\partial n}\overset{0}{G}_\varepsilon(t,t_{1,2}), \qquad A2\{D2\} = \frac{\partial}{\partial n}G(t,t_{1,2}) - \frac{\partial}{\partial n}\overset{0}{G}(t,t_{1,2})\tag{12}$$

$$a1_n = d1_n = J_n(ka)H_n(ka), \qquad b1_n = c1_n = J_n(ka\sqrt{\varepsilon})H_n(ka\sqrt{\varepsilon}),\tag{13}$$

$$a2_n = d2_n = i/\pi - ka\cdot J_n'(ka)H_n(ka) \qquad b2_n = c2_n = i/\pi + ka\sqrt{\varepsilon}\cdot J_n'(ka\sqrt{\varepsilon})H_n(ka\sqrt{\varepsilon}),\tag{14}$$

Thus, we performed a semi-inversion based on the extraction of the frequency-dependent singular part corresponding to the free space scattering from a 'canonical-shape' circular cylinder of radius a, as suggested in [5]:

$$\overset{0}{G}(t,t_{1,2}) = (i/4)\cdot H_0^{(1)}\left|2kaSin((t-t_{1,2})/2)\right|, \quad \overset{0}{G}_\varepsilon(t,t_{1,2}) = (i/4)\cdot H_0^{(1)}\left|2ka\sqrt{\varepsilon}Sin((t-t_{1,2})/2)\right|\tag{15}$$

The set (7) can be written as a single matrix equation $[T]_{4n,4n}[X]_{4n} = [S]_{4n}$, where matrix $[T] = [I+P]$, I being an identical operator and P a compact one in l_2^4. It has four blocks due to two boundaries of layer and two unknown density functions for each boundary. Vector $[S]$ is defined by the source location, and $[X]$ is the sought vector of unknown expansion coefficients. Truncation numbers of the blocks should be taken in coordinated manner and depend on the smoothness of the boundaries: the smoother the curve, the smaller value of truncation number enables one to obtain the required accuracy of calculations.

Some radome and lens shapes can require quite large matrices to be solved especially if high dielectric contrasts are involved. Then specialized time and memory saving algorithms [6] should be used. It is possible because the matrix $[T]$ is a so-called "sparse linear matrix" and has blocks of none-zero elements only along the main diagonal. The number of zero blocks increases for multi-layer scatterers. Besides, none-zero blocks have diagonal structure as well: values of block elements decrease with the distance from its main diagonal (the smoother the curve the faster the decrement). It enables one to estimate the size of each block for a required accuracy. Note that in any case the working matrix size is ten-fold reduced with respect to the rough moment-method recommendation 'ten points per lambda along the boundary'.

REFERENCES

[1] J.-H. Chang, K.-K. Chan, Analysis of two-dimensional radome of arbitrary curved surface, *IEEE Trans. Antenna Propagat.*, vol. AP-38 , no. 10 , pp. 1565-1568 , 1990.

[2] C. A. Fernandes, 'Shaped dielectric lenses for wireless millimeter-wave communications', *IEEE Antennas Propagat. Magazine*, vol. AP-41, no. 5, pp. 141-151, Oct. 1999.

[3] A. T. Greenwood, J.-M. Jin, 'A field picture of wave propagation in inhomogeneous dielectric lenses', *IEEE Antennas Propagat. Magazine*, vol. AP-41, no.5, pp. 9-18, Oct. 1999.

[4] H. Mieras, 'Radiation pattern computation of a spherical lens using Mie series', *IEEE Trans. on Antennas Propagat.*, vol. AP-30, no.6, pp. 1221-1224, Nov. 1982.

[5] S. V. Boriskina, A. I. Nosich, 'Method of analytical regularization in the problems of wave scattering by dielectric cylinders of arbitrary cross section', *Radio Physics and Radio Astronomy*, vol. 3, no. 3, pp. 310-318, 1998 (in Russian).

[6] W. Press, S. Teukolsky, W. Vetterling, B. Flannery, 'Numerical recipes in Fortran 77: the art of scientific computing', *Cambridge Univ. Press*, 2nd edition, vol. 1, Chap. 2 (www.nr.com).

ELECTROMAGNETIC WAVE DIFFRACTION
ON AN N-BRANCHING OF A PLANE WAVEGUIDE

Raskina O.A., and Tumakov D.N.

Kazan State University
P.O.Box 234 Kazan, 420503, Russia
E-mail: pnb@ksu.ru

We consider the branching of a planar waveguide with metallic walls into N metallo-dielectric waveguides. Let x-axis be oriented along the propogation direction of the wave and z-axis be directed along the waveguide interface. Metallic separation planes are $z = b_j$, $j = 1, ..., N$.

Let TE-polarized electromagnetic mode fall from the left unperturbed waveguide $(x < 0)$. The diffracted field is presented in the following form

$$U_j^+(x,z) = \sum_{n=1}^{\infty} B_n^j e^{-i\gamma_{nj}x} \sin \frac{\pi n}{b_j - b_{j-1}}(z - b_{j-1}),$$

$$x > 0, \quad b_{j-1} \le z \le b_j, \quad j = 1, ..., N,$$

$$U^-(x,z) = \sum_{n=1}^{\infty} A_n e^{i\gamma_n x} \sin \frac{\pi n}{a} z, \quad x < 0, \quad 0 \le z \le a,$$

where

$$\gamma_{nj} = \sqrt{k_j^2 - \left(\frac{\pi n}{b_j - b_{j-1}}\right)^2}, \quad \gamma_n = \sqrt{k_a^2 - \left(\frac{\pi n}{a}\right)^2}, \quad n = 1, 2, ...$$

Field conjugation conditions at $x = 0$ (continuity of tangential parts of vectors E and H) reduce the problem to the system of functional equations. Let us now introduce the integral operators determinated by kernels for $j = 1, ..., N$

$$K_j^+(t,z) = \frac{2}{b_j - b_{j-1}} \sum_{m=1}^{\infty} \frac{1}{\gamma_{mj}} \sin \frac{\pi n}{b_j - b_{j-1}}(t - b_{j-1}) \sin \frac{\pi n}{b_j - b_{j-1}}(z - b_{j-1}).$$

Since these integral operators have the eigen functions $\sin \dfrac{\pi i}{b_j - b_{j-1}} t$ and the eigen values $\dfrac{1}{\gamma_{ij}}$, the following identity is valid

$$\int_{b_{j-1}}^{b_j} \sum_{n=1}^{\infty} B_n^j \gamma_{nj} \sin \frac{\pi n}{b_j - b_{j-1}}(z - b_{j-1}) K_j^+(t,z) dt = \sum_{n=1}^{\infty} B_n^j \sin \frac{\pi n}{b_j - b_{j-1}}(z - b_{j-1}). \quad (1)$$

In the case of this identity, eliminating coefficients B_n^j, we obtain the system of functional equations with respect to coefficients A_n. Galerkin method with basis functions $\sin \dfrac{\pi k}{a} z$ leads to infinite system of linear algebraic equations (ISLAE).

$$A_k \frac{a}{2} + \sum_{n=1}^{\infty} A_n \alpha_{kn} = A^0 \beta_k, \quad k = 1, 2, \ldots, \tag{2}$$

$$\alpha_{kn} = \sum_{j=1}^{N_1} \frac{2a^4 (b_j - b_{j-1})}{\pi^2} \gamma_n \times$$

$$\times \left(\sum_{m=1}^{\infty} \left[(-1)^m \sin \frac{\pi n b_j}{a} - \sin \frac{\pi n b_{j-1}}{a} \right] \left[(-1)^m \sin \frac{\pi k b_j}{a} - \sin \frac{\pi k b_{j-1}}{a} \right] \times \right.$$

$$\left. \times \sum_{m=1}^{\infty} \frac{1}{\gamma_{mj}} \frac{m^2}{[m^2 a^2 - n^2 (b_j - b_{j-1})^2][m^2 a^2 - k^2 (b_j - b_{j-1})^2]} \right),$$

$$\beta_k = -\frac{a}{2} \delta_{k,n_0} + \sum_{j=1}^{N_1} \frac{2a^4 (b_j - b_{j-1})}{\pi^2} \gamma_{n_0} \times$$

$$\times \left(\sum_{m=1}^{\infty} \left[(-1)^m \sin \frac{\pi n_0 b_j}{a} - \sin \frac{\pi n_0 b_{j-1}}{a} \right] \left[(-1)^m \sin \frac{\pi k b_j}{a} - \sin \frac{\pi k b_{j-1}}{a} \right] \times \right.$$

$$\left. \times \sum_{m=1}^{\infty} \frac{1}{\gamma_{mj}} \frac{m^2}{[m^2 a^2 - n_0^2 (b_j - b_{j-1})^2][m^2 a^2 - k^2 (b_j - b_{j-1})^2]} \right).$$

Theorem 1. *The problem of diffraction on branching of planar waveguide with metallic walls is equivalent to ISLAE* (2) *for the expansion coefficients over eigen functions of the unperturbed waveguide* A_n.

An approximate solution of ISLAE (2) can be found by the reduction method. With this in mind, we truncate the external and infinite sums, in α_{kn} and β_k in (2). The transformed coefficients α_{kn} and β_k are designated as $\tilde{\alpha}_{kn}$, $\tilde{\beta}_k$. Consequently, the system (2) takes the form

$$A_k \frac{a}{2} + \sum_{n=1}^{N_1} A_n \tilde{\alpha}_{kn} = A^0 \tilde{\beta}_k, \quad k = 1, \ldots, N_1, \tag{3}$$

The following constants estimates for the values of m_1 и m_2 defined in [1], can be obtained on the basis inequalities [2]

$$m_1^2 \leq \left[\frac{2a^4(b_j - b_{j-1})}{\pi^2} N\right]^2 \sum_{k=1}^{N_1} \sum_{n=1}^{N_1} |\gamma_n|^2 (1+n^2)^{-\alpha} \times$$

$$\times \left|\sum_{m=N_2+1}^{\infty} \frac{1}{\gamma_{mj}} \frac{m^2}{[m^2 a^2 - n^2(b_j - b_{j-1})^2][m^2 a^2 - k^2(b_j - b_{j-1})^2]}\right|^2 \leq \text{const} \ln N_1 \cdot N_1^{-2\alpha},$$

$$m_2^2 \leq \left[\frac{2a^4(b_j - b_{j-1})}{\pi^2} DN\right]^2 \sum_{k=N_1+1}^{\infty} \sum_{n=1}^{N_1} |\gamma_n|^2 (1+n^2)^{-\alpha} \times$$

$$\times \left|\sum_{m=1}^{N_2} \frac{1}{\gamma_{mj}} \frac{m^2}{[m^2 a^2 - n^2(b_j - b_{j-1})^2][m^2 a^2 - k^2(b_j - b_{j-1})^2]}\right|^2 \leq \text{const} \ln N_1^3 \cdot N_1^{-2\alpha},$$

$$D = \max \frac{(b_j - b_{j-1}) \sum_{m=1}^{\infty} \frac{1}{|\gamma_{mj}|} \frac{m^2}{|m^2 a^2 - n^2(b_j - b_{j-1})^2| |m^2 a^2 - k^2(b_j - b_{j-1})^2|}}{(b_i - b_{i-1}) \sum_{m=1}^{\infty} \frac{1}{|\gamma_{mi}|} \frac{m^2}{|m^2 a^2 - n^2(b_i - b_{i-1})^2| |m^2 a^2 - k^2(b_i - b_{i-1})^2|}},$$

where the maximum takes on i, j, k.

The latter estimates allow us to formulate

Theorem 2. *SLAE* (3) *has the single solution in the space* $\overline{H}_\alpha$ $(0 < \alpha \leq 1)$, *when its right-hand side belongs to* $\overline{l}_2$.

Theorem 3. *ISLAE* (2), *which corresponds to the problem of diffraction on branching, has the single solution in the space* H_α $(0 < \alpha \leq 1)$, *when its right-hand side belongs to* l_2.

REFERENCES

[1] N.B.Pleshchinskii. On abstract theorie of approximated methods for solving of linear operator equations, Izv. vuzov, Matem., 2000, No. 3, 39-47.
[2] N.B.Pleshchinskii, D.N.Tumakov, Method of fractional fields for the scalar coordinate diffraction problems of the electromagnetic waves in the classes of distributions, Kazan Mathematical Society, Preprint 2000-1, Kazan, 2000 (in Russian).

COMPARATIVE ANALISYS OF SOME NUMERICAL TECHNIQUES FOR MODELLING OF SPATIAL TRANSIENT REGIMES IN IRREGULAR PLANAR STRUCTURES

E.V.Bekker*, E.A.Romanova*, L.A.Melnikov*, M.Marciniak**

** Saratov State University, Astrakhanskaja 83, 410026, Saratov, Russia,
Phone: 7-8452-515195, Fax: 7-8452-240446, e-mail:* ella@engels.san.ru

*** National Institute of Telecommunications , Szachowa 1, 04-894
Warsaw, Poland, Phone: (+48 22) 812 00 72, Fax: (+48 22) 812 83 47*

Irregular optical nonlinear waveguides can provide functions such as pulse compression, logic operations, and amplification [1]. There is an interest to correct characterization of the spatial transient regimes in the waveguides. We compared the collocation method [2], and the Beam Propagation Method combined with the Fast Fourier Transform [3] and Finite-Difference method [4] (FFT-BPM and FD-BPM) applied to the investigation of the transient regime in an irregular planar waveguide.

We solved the scalar wave equation for slowly varying field amplitude:

$$\left(2i\frac{\partial}{\partial z} + \frac{\partial^2}{\partial x^2} + a^2((2\pi/\lambda)^2 n (x,z)^2 - \beta^2)\right)E(x,z) = 0, \tag{1}$$

where β is the propagation constant, $n(x,z)$ is the refractive index profile of the waveguide, x, z are transversal and longitudinal coordinates normalised to a^2, and βa^2, respectively, λ is the wavelength, a is the index profile spatial characteristics (in the case of the waveguide with step-index profile, a is the core radius).

The collocation method is based on converting the scalar wave equation into a matrix total differential equation using the orthogonal collocation method which may be stated as follows. The partial differential equation is assumed to be satisfied exactly at some points along the transversal coordinate. These points are known as the collocation points. The total field is expressed as a linear combination of some orthogonal functions. So, by applying the collocation principle, the scalar wave equation can be converted into a set of total differential equations, which can be solved further numerically by using any standard procedure, such as the Runge-Kutta method.

All the methods mentioned are efficient in investigation of the total field propagation in fibers (in the case of FFT-BPM it is necessary to use the Fast Fourier-Bessel Transformation). Besides, all the methods are suitable for the study of the total field propagation in non-linear structures.

In a parabolic-index waveguide:

$$n(x) = n_1(1 - \Delta(\frac{x}{a})^2), \tag{2}$$

the collocation method is more efficient then FFT-BPM. It takes a smaller calculation time and enables one to achieve better accuracy by using less collocation points. In the case of the step-index waveguide we used the eigenfunctions of the parabolic index waveguide (Hermite-Gauss functions) as expansion functions in the collocation method. We calculated the condition numbers of the propagation matrices to find the effective parameters of the

expansion functions w (effective width of the expansion functions), and to determine the propagating step Δz. The condition numbers of the matrices were about 500. The dependence of the condition numbers of the propagation matrix corresponding to a step-index waveguide ($a=2.$ μm, refractive indices 1.4725, and 1.467) on the width of the Hermite-Gauss functions is shown in Fig.1 It is necessary to use the longitudinal step being about 0.01 of the diffraction length. Hence, the method becomes less efficient if using not eigenfunctions as a basis. However, the usage of the eigenfunctions of the waveguide with varying step-index profiles is problematic because it requires a complicated modification of computer code for each index profile.

In the FD-BPM method the loss due to numerical errors in the waveguides slightly depends on the propagation step size when in the FFT-BPM method it increases sufficiently [4]. Therefore, the FD-BPM technique is more efficient for the investigation of the field propagation in the waveguides with symmetrical and asymmetrical step-index profiles. However the FD-BPM method scheme is stable only in the case of paraxial approximation when the collocation method as well as the FFT-BPM method can be realised both in the cases of non-paraxial and paraxial beam propagation. The most interesting is to compare the description of the radiation field by the FD-BPM and FFT-BPM methods in order to investigate the radiation field propagation in paraxial and non-paraxial approximations.
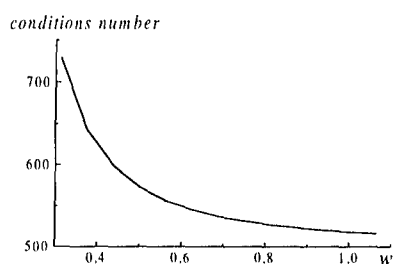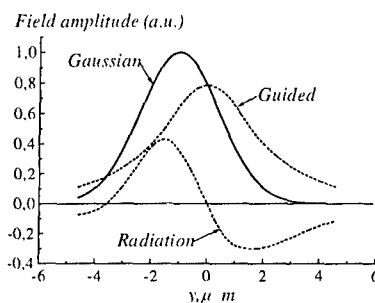
Fig.1   Fig.2

We have applied the FD-BPM and FFT-BPM methods to study the propagation of the radiation field excited by symmetrical and asymmetrical Gaussian beams in a single-mode planar waveguide [5]. The incident radiation field was taken as a part of the incident total field:

$$E_{radiation} = E_{total} - E_{guided},\qquad(3)$$

where the guided mode field E_{guided} is proportional to a normalized guided mode field Ψ_0 with some complex amplitude α:

$$E_{guided} = \alpha\Psi_0.\qquad(4)$$

We have considered an asymmetric excitation of a planar waveguide by the Gaussian beam of TE-polarized light at 1.53 μm wavelength. It has $1/e$ amplitude width of 4 μm. The guiding layer has a width of 2.3 μm and a refractive index of 1.491. The refractive index of the outer layers is 1.479. Fig.2 presents the Gaussian input beam and its modal and radiation parts field distributions. The propagation of the extracted radiation part of the field was calculated by the FFT-BPM and by FD-BPM methods. The FFT-BPM computational parameters were chosen in such a way that a part of the non-propagating (evanescent) spectrum and the whole propagating spectrum of the field were included in the k_y-space computational window in order to ensure exact modelling of the field propagation. In the most of experiments the computational grid of 256 transversal points, the longitudinal step $\Delta z=0.5$ μm, and the

transversal step $\Delta x=0.25$ μm were used. The FD-BPM method used the iterative procedure proposed in [4] for solution of (1), with computational grid of 256 transversal points, the longitudinal step of $\Delta z=2.5$ μm, and the transversal step of $\Delta x=0.25$ μm. The time needed to simulate the radiation field propagation in the waveguide in various computational grids is shown in Fig.3 (150 μm). The FD-BPM computation time was 12 times smaller than with FT-BPM.
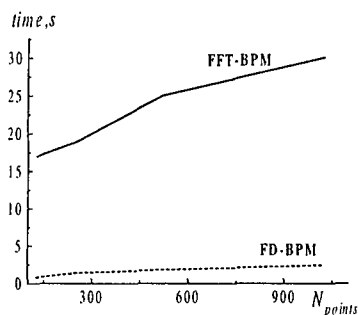
Fig.3
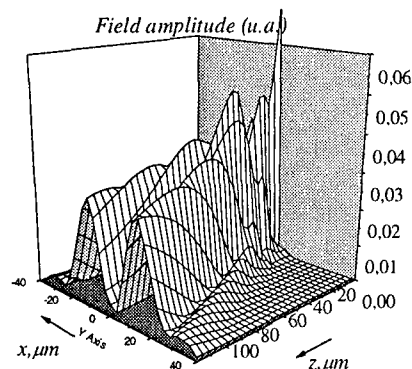
Fig.4

Propagating in the waveguide, the radiation field leaves the region of the inner layer (Fig.4). Fig.5 a,b demonstrates the input radiation field (solid line), and the radiation field at the distance 150 μm, calculated by FD-BPM (dotted line), and by FFT-BPM (dashed line) methods. Fig.5a corresponds to the case of symmetrical field excitation, and Fig.5 b corresponds to the 2. μm shift of the Gaussian beam. The radiation field distributions calculated by two methods look slightly different at some distances. The dependence of the field power difference in the vicinity of the inner layer ($x=-30\mu m$ to 30 μm, $\tau=P_{rad}/P_G$, $\Delta\tau= \tau_{FD} - \tau_{FFT}$) is shown in Fig.6.

a

b
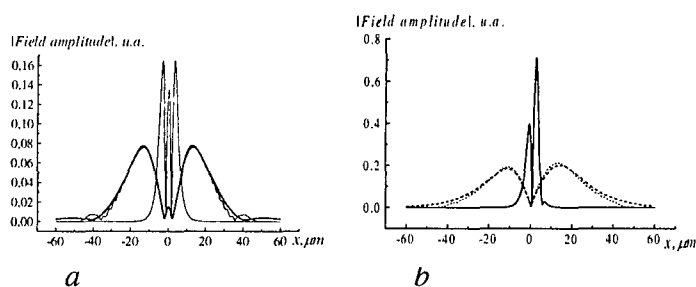
Fig.5
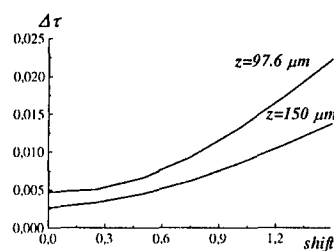
Fig.6

Thus FD-BPM was shown to be the most efficient in the analysis of the transient regimes in planar waveguides, however, in the paraxial approximation that is used in FD-BPM, the field propagates in the inner layer at the longer distances.

REFERENCES

1. Naomichi Okamoto and Shingo Ito // J. of Quantum Electron. 1988. V. 24. N.10. pp. 1966-1969.
2. A.S.Sharma, S.B.Banerjee // Opt.Lett.,V.14, N.1, pp.96-98, 1989.
3. J.Van Roy, J.van der Donk, P.E.Lagasse // J.Opt.Soc.Amer., V.71, p.803, 1983.
4. Y.Chung, N.Dagli // J.of Quantum Electron., V.26, N.8, pp.1335-1339, 1990.
5. M.Marciniak, B.Jaskorzynska // Opt.and Quant.Electron., V.27, pp. 977-985, 1995.

PHOTONIC BAND GAP STRUCTURE CREATED FROM ARTIFICIAL OPALS

V. V. Lysak, I. A. Sukhoivanov, and A. A. Chernoblavskiy

Kharkov State University of Radio Electronics
Lenin av. 14, Kharkov, 61166, Ukraine
Ph. +380 572 409 484, E- mail: Lysak@kture.kharkov.ua

Photonic bandgap (PBG) materials or photonic crystals represent a new paradigm in quantum and nonlinear optics. These materials were predicted theoretically as a means to realize two fundamentally new optical principles:

1)   the localization and trapping of light in a bulk material [1];
2)   the complete inhibition of spontaneous emission [2], [3] over broad frequency range.

The novel consequences of PBG material flow directly from the implementation of these two underlying principles.

Unlike optical cavities which confine light in one spatial dimension, the PBG materials facilitate coherent localization of light in all spatial directions.

By implanting dopes in a bulk material we can engineer an arbitrary number of individual localize states which weakly interact with each other inside a PBG material, but which maintain their immunity from vacuum modes outside the PBG material. These facilities the development of large scale integrated optical circuits within a PBG in which the nature of radiative dynamics is controlled by the local density of states of photons within the photonic crystal rather than the free space of density of states outside the photonic crystal.

Moreover the PBG structure may exhibit a much richer variety of nonlinear effects than conventional waveguides and optical fibers. The main of them are:

1.   anomalous superradiant emission rates [4];
2.   low threshold nonlinear optical response[5];
3.   highly nonclassical states of light within the PBG in the form of quantum gap solitons [6];
4.   collective switching of two-level atoms from ground to excited state with low intensity applied laser field [7].

Nowadays three types of structures are actively investigated:

a) 1D PBGs. The most common realization is the optical waveguide Bragg – grating with symmetrical [8] chirped and double-chirped [9] structure.

b) 2D PBGs are the photonic crystal fibers [10].

c) 3D PBGs [11].

By relatively simple and potentially useful method [12] that has allowed us to obtain a periodic structure consists of the cubic-close-packed colloidal particles (for example, silica colloids from Nissan Chemical Industries)

Figure 1. PBG structure from artificial opal.

with relatively large domain sizes $(\approx 1 cm^2)$. These 3-D lattices have a crystalline structure similar to that of an opal with packing density (~74%). It can also be increased to 95-100% by sintering the sample at elevated temperatures.

Owning to its 3-D periodicity, a crystalline assembly of colloidal particles strongly diffracts light along certain directions for a certain range of frequencies, forming the so-called stop-bands [13] the similar as we observed in the 1-D PBG structures which had been investigated using of the transfer matrix technique. The opals exhibit only narrow stop bands but missed the completely gap. But we know that when the stop bands are wide enough and can overlap for both polarization along all dirrections, this material is said to exhibit a complete PBG [14]. One of the way to increase the refractive-index contrast between the components of considrered periodic structure is considered below.

The transmittanse for a general N-period refractive-index potential is given by [15]:

$$T_N = 1 + \frac{sin^2(N\beta)}{sin^2(\beta)}\left(\frac{1}{T}-1\right)$$

where T_N is the transmittance for the N-periodic structures; β is the Bloch phase, associated with the infinite periodic structure; T is the transmittanse of the unit cell; N is the number of periods.

We have calculated (1) for the special case of the 1-D PBG structures – the quarter wave stack (we assume that the periodic structure is nonabsorbent and infinite). The result of this numerical calculation is shown in Fig.2.
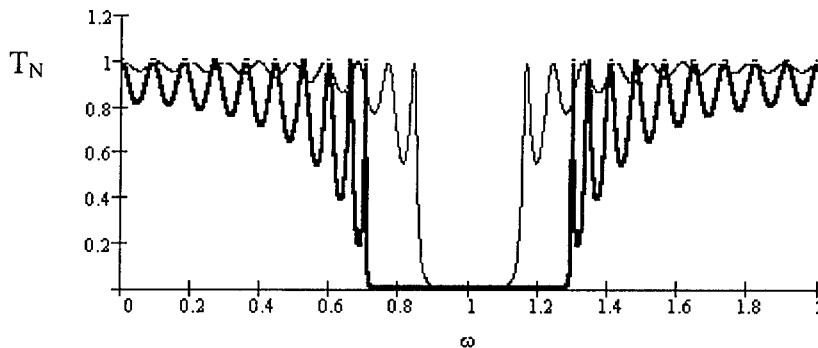
Figure 2. Dependence of the dimensionless transmittance for a ten – period (N=10) quarter wave stack with $n_1=1$, $n_2=1.5$ (thin curve); $n_1=1$, $n_2=2.5$ (thick curve) on the dimensionless frequency $\Delta\omega/\omega_0$. (We chose the changes of refractive-index contrast arbitrarily).

It is easy to note that the width $\Delta\omega/\omega_0$ of PBG increases from 33% to 48%. The result of this calculation of the 1-D PBG structure can be successfully carried over the 3-D homogeneous periodic structure (for example, artificial opal).

This assumption has been justified in practice by producing the "inverse opal". One of the methods for generating this inverted structure is to infiltrate artificial opal with a high dielectric material and to subsequently etch out of the SiO_2 spheres, leaving behind a connected network of high dielectric material with filling ratios around f = 0.26. As a result we obtain inverted structure like a Swiss cheese (Fig.1).

The infiltration and etching out enhances the dielectric contrast and it leads to exhibition of the complete PBG in this structure with relative size $\Delta\omega/\omega_0 = 4.25\%$ (Fig. 3).

And for the end of our discussion it is very interesting to compare our theoretical conclusions experimental data: dependence of the gap size as a function of index of refraction for a close-
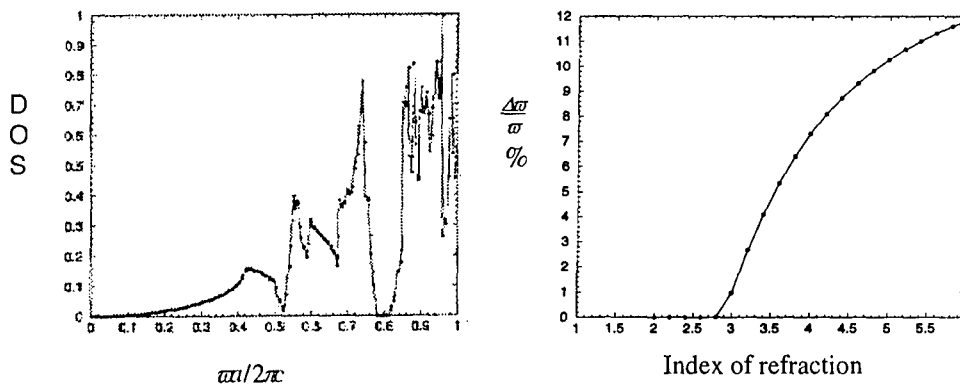
Figure3. Dependence of the density of states(DOS) for a close-packed fcc lattice of air spheres in silicon ("inverse opal") on dimensionless frequency ($\varpi a / 2\pi c$, where a-the constant lattice).
Figure4. Dependence of the gap size as a function of index of refraction for a close-packed fcc lattice of air spheres in a high dielectric matrix.

packed fcc lattice of air spheres in a high dielectric matrix (Fig. 4). And we can easily note that our theoretical assumption is in a very good agreement with the experiments.

REFERENCES

[1]. S. John, „Electromagnetic absorption in a disordered medium near a photon mobility edge," *Phys. Rev. Lett.,* vol.53, p. 2169,1984.

[2]. V. P. Bykov, „Spontaneous emission from a medium with a band spectrum," *Sov. J. Quant. Electr.,* vol. 4, p. 861, 1975.

[3]. E. Yablonovitch, „Inhibited spontaneous emission in solid –state physics and electronics," *Phys. Rev. Lett.,* vol. 58, pp. 2059 - 2062, 1987.

[4]. S. John and T. Quang, „Localization of superradiance near a photonic band gap," *Phys. Rev. Lett.,* vol. 74, p. 3419, 1995.

[5]. S. John and T. Quang, „Resonant nonlinear dielectric response in a photonic band gap material," *Phys. Rev. Lett.,* vol. 76, p. 2484, 1996.

[6]. S. John and V. I. Rupasov, „Multi-photon localization and propagating quantum gap solitons in a frequency gap medium," *Phys. Rev. Lett.,* vol. 79, p. 821, 1997.

[7]. S. John and T. Quang „Collective switching and inversion without fluctuation of two-level atoms in confined photonic systems," *Phys. Rev. Lett.,* vol. 78, p.1888, 1997.

[8]. I. Nefedov, Yu. Morozov, V. Gusyatnikov, A. Zheltikov, "Pulse transmission through controllable semiconductor photonic band gap structure," Proc. of 2nd international Workshop LFNM'2000, Kharkov, May 23, 2000, pp. 9 – 12.

[9]. F. X. Kaertner, N. Matuschek, et al. "Design and fabrication of double – chirped mirrors," Opt. Lett. Vol. 22, No. 11, p. 831 – 833, 1997.

[10]. P. J. Bennett, T. M. Monro, et al, "Towards practical holey fibre technology: fabrication, splicing and characterization", Proc. of 25th international conference ECOC'99, Nice, September 26-30, 1999, pp. I20 – I23.

[11]. J. G. Flemmming and S. Y. Lin, "Three-dimensional photonic crystal with a stop band from 1.35 to 1.95 mkm," Opt. Lett., pp. 49-51, 1999.

[12]. S.H.Park, D.Qin, and Y.Xia, "Cristalization of meso-scale particles over a large areas," Adv. Matter., vol.10, pp. 1028-1032, 1998.

[13]. P. L. Flaugh, S. E. O'Donnel, and S. A. Asher, "Development of a new optical wavelength rejection filter: Demonstration of its utility in Raman spectroscopy," Appl. Spectrosc., vol.38, pp. 847-850,1984

[14]. J. D. Joannopoulos, P. R. Villeneuve, and S. Fan, "Photonic crystals: Putting a new twist on light," Nature, vol.386, pp.143-149, 1997.

[15]. D. W. L. Sprung, H. Wu ,and J. Martorell, Am. J. Phys. 61,1118 (1993).

RESEARCH AND REALIZATION METHODS OF CONSTRUCTION OF STRICT OPTICAL ORTHOGONAL CODES FOR TRANSFER MULTIMEDIA OF INFORMATION AND DISTRIBUTIVE APPENDICES

A. Prigoda[1], J. Speidel[2], R. Frich[2], and I. Sukhoivanov[1]

[1] Kharkov State Technical University of Radio Electronics
Kharkov, 61166, Ukraine
E-mail: Sukhoivanov@kture.kharkov.com

[2] The University of Stuttgart, Institute of Telecommunications, Germany
E-mail Frich@uni-stuttgart.de

ABSTARCT
The algorithm for most compact construction packages of strict optical orthogonal codes (OOC) is offered. It allows to solve problems connected with designing of large flexible fiber-optic code-division multiple-access networks and complex hierarchical structures. The given algorithm can be used for producing and calculating of all optical coders/decoders of the given fiber code-division multiple-access network.

CONSTRUCTION OF OOC PACKAGES USING LINEAR ALGORITHMS
The result of this algorithm is the package of optical orthogonal code words with weight ω for L users. The model of the algorithm uses parts A and B of the theorem 1 [1]. We shall analyze this algorithm.

Structurally, the linear algorithm can be divided into three stages: creation of the first code word, construction others L -1 code words and computing of the code words length in the package. The attention must be paid to such splitting because it almost completely repeats the structure of the theorem 1 and is logically connected with it.

Once consecutive performance of all three stages of the linear algorithm has been done *a(n,w,1)* packages of an non-periodic strict OOC will be constructed.

This algorithm was realized using the programming language C. Dependence of the code word length from the users number *n(L)* (Figures 1) and the dependence of length of code words from the code word weight *n(w)* (Figure 2) were established. Length of code words in packages was determined using the algorithm that is much minimally than possible length of the code word in a package appreciated using the theorem 2 [1].

An essential conclusion must be noted that follows from the realization of the linear algorithm. We obtained a linear increase of the length of code words in a package from the first word to last word if we consider each code word separately while constructing the code words package using the minimizing principle of
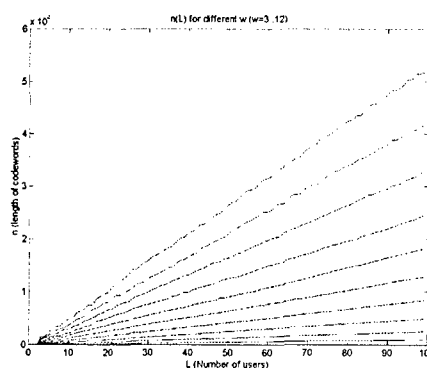
Figure 1 - Dependence of code words length in a OOC package on the number of active users for various values of the code word weight

meaning distances. Consequently, the length of the last code word determines the length of code words in the package and the difference between lengths between of the first and the last code words in a package will be large. Thus, the linear algorithm uses not rationally the space of meaning distances for all code words of a package.

ALGORITHMS WITH THE "TREELIKE" CONSTRUCTION OF OOC PACKAGES

An alternative algorithm was constructed taking into account the experience of the linear algorithm realization and the analysis of its application. It takes into account the lacks of linear algorithm. Namely, it satisfies to the minimal possible length of code words in the package appreciated the theorem 2; it most rationally uses space of meaning distances for all code words of the package.

Figure 2 - Dependence of code words length in a OOC package on a code words weight for various user numbers

The conclusion was made after the long logic analysis of directions of the algorithm construction. It was proposed to build an algorithm of the OOC packages construction including a minimizing principle, where the length of code words in a package decreases from first word to last; because the length of code words in a package increased from first to last code word in a package, and it led to negative consequences in the previous algorithm. By the imposed condition, while constructing the i-th code word we obtain the array of code words with the identical length. The structure of algorithm is as follows.

Zero stage. Finding of a minimal possible n for a code word with the weight w. The use of the found meaning as an entrance in the first stage.

The first stage. The finding of all families of code words for a range of lengths of code words from n_{max} up to n_{min}, where n_{max} is defined by the theorem 2 [1].

The second stage. Optical orthogonal word chooses from the received families of code words with the different length. For this purpose the part B of the theorem is used.

The third stage. Choosing of packages OOC with maximal number of code words in a package from all received packages.

The results of the alternative algorithm working remind a tree, where the number of all possible code words of identical length decreases from first to last, from the high to the root.

The fourth stage. We compare the received L with the given. If the received value is less than the required one, then n must be increased in the first step and calculations repeated. In other words, we increase the length of code words in a package until the maximal length L is equal to the required.

It is possible to compute a package OOC for the given number of the users for given weight of a code word. We also can calculate the optimum number of the users for a OOC package with given maximal length of code words and given weight of a code word using this algorithm. Unfortunately, it was not possible to develop a program for complete realization of the algorithm because of its "treelike" structure a great number of the data must be processed. The test examples shown almost completely coincidence with the estimated results of the minimal possible length of OOC packets for the given values of L and of w, obtained using theorem 2 (Table 2.1).
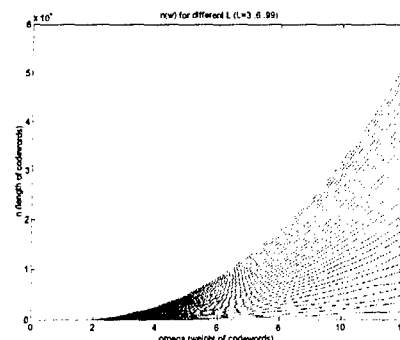
Table 1 - Packages of exact OOC obtained from the "treelike" algorithm

ω	n	$C_i=\{a_1^{(i)}, a_2^{(i)}, \ldots, a_\omega^{(i)}\}$ for $a(n, \omega, 1)$ exact OOC	
3	21	$C_1=\{1, 2, 3\},\ C_2=\{1, 3, 6\},\ C_3=\{1, 4, 11\}$	
4	29	$C_1=\{1, 2, 8, 12\},\ C_2=\{1, 3, 6, 15\}$	
4	57	$C_1=\{1, 2, 12, 25\},\ C_2=\{1, 5, 22, 27\},$ $4, 20, 29\},\ C_4=\{1, 8, 16, 28\}$	$C_3=\{1,$
4	57	$C_1=\{1, 2, 13, 28\},\ C_2=\{1, 5, 23, 25\},$ $4, 20, 29\},\ C_4=\{1, 9, 15, 22\}$	$C_3=\{1,$
4	57	$C_1=\{1, 2, 15, 25\},\ C_2=\{1, 5, 23, 26\},$ $3, 20, 29\},\ C_4=\{1, 9, 16, 21\}$	$C_3=\{1,$

The considered algorithm has the following advantages: 1. The resulting length of code words in a package is maximal approached to minimal possible for given L and w; 2. It can be used to compute a OOC package with the optimum length for the maximal users number using only one initial parameter, i.e. the weight of a code word; 3. It produces some packages of OOC after final settlements with identical L, n and w, characterized by the different set of code words. It can be used for designing of networks with a high level of branching.

CONCLUSIONS

Obtaining of several OOC packages at once is an essential advantage because a real OCDMA network is characterized by a high number of intermediate optical stars. Moreover, the real network has a block hierarchical structure. Each block of the first level represents an optical star and certain number of users and each block of the second level has an optical star and certain number of blocks of the first level and so on. Any optical star must have the OOC package in each level of any hierarchical level. Therefore, the computing of OOC packages of each star using linear algorithm requires a large time period because the presence of the operator for the parameter input of each optical star is necessary. The "treelike" algorithm allows to set up parameters so that the whole set of OOC packages for an OCDMA network with any complexity of hierarchy will be constructed at once. In other words, the necessity of the operator comes to a minimum.

The disadvantage is the necessity of processing of a large number of code words for finding an optimum optical orthogonal package. It requires significant expenses of the computing time and resources of the computer.

Having the mentioned disadvantage, this algorithm still remains very actual. The computing time of an OOC package using this algorithm will be paid back by increasing the speed of the information transfer in the OCDMA network, because a OOC package must be calculated promptly.

REFERENCES

[1] Zhang J.-G., " Flexible optical fiber CDMA networks using strict optical orthogonal codes for multimedia brodcasting and distribution applications, " IEEE Transactions on brodcasting, vol. 45, NO. 1, March 1999, pp. 106-115.

SPECTRAL INDEX METHOD APPLIED TO THE ANALYSIS OF WHISPERING GALLERY MODES IN SEMICONDUCTOR DISK RESONATORS

S. Greedy, P. Sewell, and T. M. Benson

School of Electrical and Electronic Engineering, University of Nottingham
Nottingham, NG7 2RD, UK
E-mail: eexscg@nottingham.ac.uk

ABSTRACT
A computationally efficient modelling method is presented that allows for the analysis of the whispering gallery (WG) modes supported by dielectric resonator structures. The approach is based on the Spectral Index (SI) method that has traditionally been applied to rib waveguides with rectangular cross section. The principle of effective widths is used in order to simplify the problem, producing a method that is simple in its application and so is ideally suited for use in an iterative design environment. The method provides both accurate resonant wavelengths and field profiles that give a practical insight into the behaviour of the structures that is invaluable to the design process. This approach is shown to provide results that are in excellent agreement with those obtained through other more numerically intense methods.

INTRODUCTION
The high Q-factors that are obtainable from dielectric resonators and their ability to support whispering gallery modes (WGMs) make them ideal components for inclusion in modern optoelectronic integrated circuits (OEICs). Strongly confined, air-clad resonator structures with radii of only a few microns may be realised with negligible loss. Such structures exhibit high Q-factors [1-2], which thus make them an attractive proposition for elements in wavelength-division multiplexing (WDM) circuits [3].

An analysis technique based on the well-proven Spectral Index (SI) method [4] is presented that allows for the efficient analysis of air-clad disk and ring resonators. The method provides a simple transcendental equation that is readily solved in a matter of seconds using a personal computer, providing results in the form of modal propagation constant and field profiles. This approach provides significant insight into the performance of the resonator, revealing important design characteristics such as the Q-factor (or finesse) and the free spectral range (FSR). The method maintains a high degree of computational efficiency and so is well suited to an iterative design process. Although more accurate methods exist, such as those employing finite difference (FD) schemes, the computational requirements of these methods are high and for the most part the accuracy provided by these methods is not required during an initial design process.

THEORY
The following will consider an air clad dielectric disk resonator as illustrated in figure 1(a), where n_g and n_s are the refractive indices of the guiding and substrate layers respectively, with $n_g > n_s > n_{air}$. The method proceeds by introducing the concept of effective widths, whereby the true boundaries of the structure are displaced by an amount determined from physically consistent arguments. On these new boundaries the field is set to zero, figure 1(b), yielding an equivalent problem, which is significantly easier to solve.

(a)

(b)
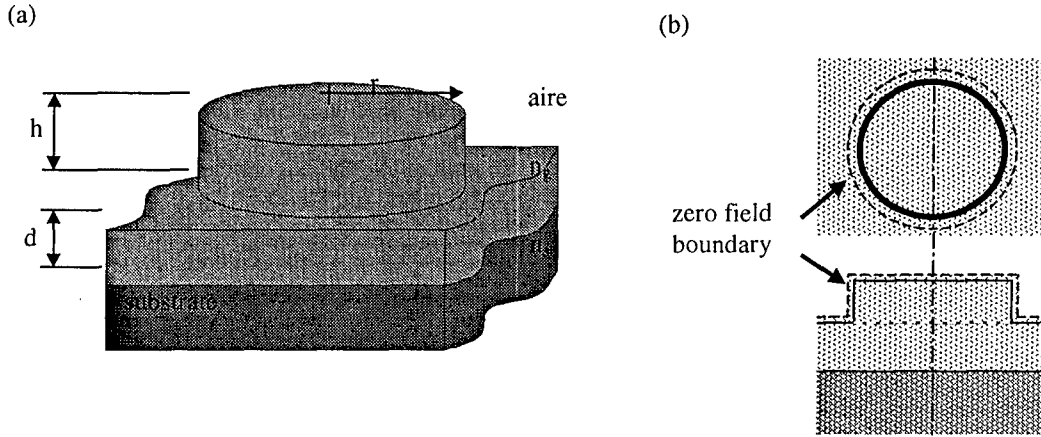
Figure 1. (a) Schematic illustration of disk resonator, (b) zero field boundaries.

The field in each region of the equivalent structure is expressed as a superposition of local solutions of the wave equation. The field in the disk can be expressed as:

$$\psi(r, y) = \sum_m A_m J_n(\alpha_m r) \frac{\sin(\gamma_m (y + h))}{\sin(\gamma_m h)} \quad (1)$$

Ψ represents rE_r and rH_r for the TE and TM like modes respectively, m is the number of terms used in the field expansion, A_m are coefficients, J_n is the Bessel function of order n whose argument, $(\alpha_m r)$, is such that the function is zero at the effective boundary. Below the disk a Hankel transform of the field is taken yielding:

$$\psi(r, y) = \int_c \partial s \, s\tilde{\psi}(s) J_n(sr) e^{-j\sqrt{k_L^2 - s^2} y} \quad (2)$$

where c is an appropriate contour. The expressions (1) and (2) are then matched with a variational expression, [4], to yield the final transcendental equation:

$$k_y \tan(k_y h) = \int_c \partial s \, s |\tilde{\psi}(s)|^2 \Gamma(s) \quad (3)$$

where $\Gamma(s)$ is a transfer function dependant upon the form of the layered media below the disk and c is an appropriate contour determined by the boundary conditions imposed at infinity. In (3) k_y and $\Gamma(s)$ are functions of angular frequency, ω, which is the only free variable. Values of ω are thus sought in the complex frequency plane for which (3) is satisfied. The Q-factor is then defined as $|\lambda_{real}/2\lambda_{imag}|$.

RESULTS

A disk resonator was considered, figure 1(a), with $n_g = 3.44$ (GaAs), $n_s = 3.40$ (GaAlAs), $r = 4.5\mu m$, $h = 4.5\mu m$ and $d = 5\mu m$. Solutions of (3) were sought in order to identify the WG modes supported by the structure. WG modes can be classified as either $WGE_{n,m,l}$ or $WGE_{n,m,l}$ where the subscripts n,m,l denote the number of azimuthal, radial and axial variations respectively. The following presents results for the $WGE_{n,1,1}$ WG modes. The results from the SI method were compared with those obtained from two semi-vectorial finite difference (SVFD) schemes of increasing accuracy, $SVFD_1$ providing the higher accuracy through use of a higher density mesh. Figure 2 compares resonant wavelengths (real component) and Q-factors obtained by each method. It is seen that the agreement in the resonant wavelength is excellent and that the Q-factors are in close agreement. It is noted this is a very challenging problem for the FD methods, requiring a large computational space and high quality absorbing boundary conditions.

(a)   (b)
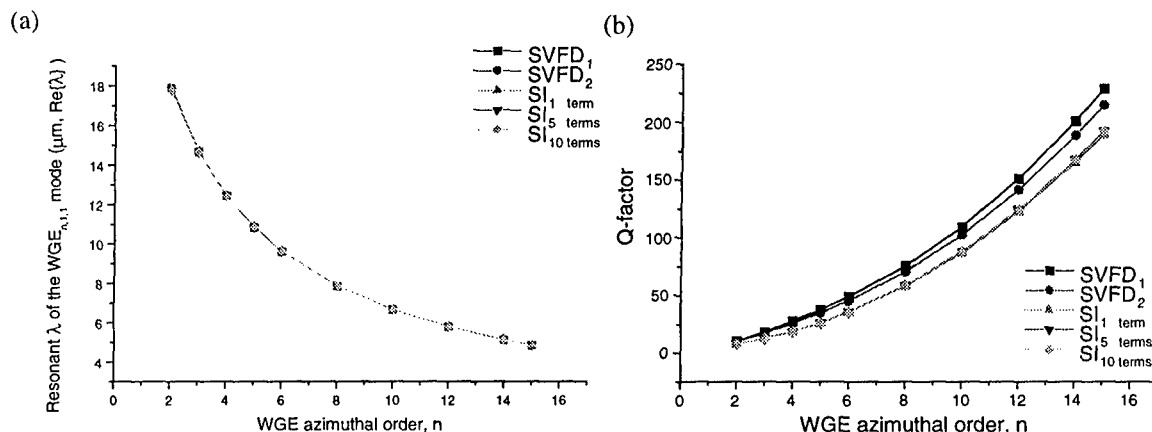
Figure 2. Numerical results, SI v SVFD; (a) resonant wavelength, (b) Q-factor.

CONCLUSION

We have presented a new method for the design and analysis of dielectric disk resonators. The method provides results that provide a significant insight into the behaviour of these devices with minimal computational effort. The method is shown to provide sufficient accuracy for practical implementation within an iterative design environment.

REFERENCES

[1] S. C. Hagness, D. Rafizadeh, S. T. Ho, A. Taflove, "FDTD Microcavity Simulations: Design and Experimental Realization of Waveguide-coupled Single-mode Ring and Whispering-gallery Mode Disk Resonators", *IEEE Journal of Lightwave Technology*, vol. 15, 1997.

[2] R. Orta, P. Savi, R. Tascone, and D. Trinchero, "Synthesis of Multiple Ring-Resonator Filters for Optical Systems", *IEEE Photon. Tech. Lett.*, vol. 7, pp.1447-1449, 1995.

[3] B. E. Little et al., "Microring resonator channel dropping filters", *IEEE J. Lightwave Tech.*, vol. 17, pp.704-715, 1999.

[4] P. C. Kendall, P. N. Robson, "*Rib Waveguide Theory by the Spectral Index Method*", Research Studies Press and Wiley, 1990.

SCATTERING

AND

RADAR CROSS SECTION

.λ

LOW-GRAZING-ANGLE SCATTERING BY A TRIANGLE MODEL OF AN OCEAN WAVE

Alexander G. Tyzhnenko

Department of Mathematics, Kharkov Economic University,

9-A Prosp. Lenina, Kharkov, Ukraine. E-mail: alex@alexgt.kharkov.ua

ABSTRACT. The boundary value problem (BVP) is reduced to the 1-D integral equation of the 1st kind and then to the ill-conditioned matrix equation. A new iterative method is proposed to such equations solving, which produces a robust and adequate solution. This solution is compared with the genetic algorithm solution and good agreement obtained. A strong backscattering for $1°$ grazing angle is revealed from a resonant-sized foaming-like ocean wave, that is comparable in order with radar "sea-spikes".

INTRODUCTION. The investigation of wave-scattering by the ocean surface has been an area of active research. The particular interest was gone up in the nowadays to the low-grazing-angle (LGA) scattering from the rough sea-surface. Numerous experimental works has indicated some unexpected phenomena in LGA backscatter [1], such as "sea-spikes". The experiments pointed to incipient or actively breaking water waves as a source of anomalous scattering. To explain the anomalous scattering phenomena the theoretical investigation is need to the electromagnetic scattering from gravity waves. Some recent studies have focused on deterministic targets with analytical extending the target as a flat surface to infinity [2]. The magnetic field integral equation (MFIE) was solved in these papers. It is known that MFIE and EFIE solutions suffer from the problem of spurious resonances at the eigenfrequencies. This phenomenon has been noted by several authors [3].

Figure 1

In this paper resonance-sized scatterers are investigated in the numerical electromagnetics using deterministic gravity wave models. The proposed method of a BVP solving is immune to spurious resonances and can be applied to LGA scattering from resonant-sized geometries for arbitrary small grazing angles, that is a hard point of numerical investigations.

THEORETICAL AND NUMERICAL FORMULATION. We consider the perfectly electrically conducting (PEC) realization of the ocean. A triangular model of a breaking wave is used (see Fig. 1 where $A(-a_1, 0)$, $B(0, b)$, and $C(0, a_2)$) with analytical extending the target as a flat surface to infinity. The incident TM-wave has only a z-directed electric field: $E_0(x, y) = \exp(-jk_{01}x + jk_{02}y + j\omega t)$. Here: $k_{01} = k_0 \sin i_0$, $k_{02} = k_0 \cos i_0$, $k_0 = \omega / c$, and i_0 is the incident angle. We find the scattered electric field as Witteker's integral [4]

$$E(x, y) = \int_{-\infty}^{\infty} \exp(-j\xi x - jhy)A(\xi)d\xi \qquad (1)$$

where $h \equiv h(\xi) = \sqrt{k_0^2 - \xi^2} = -j\sqrt{\xi^2 - k_0^2}$ and $\mathrm{Im}\, k_0 = -0$. The function (1) satisfies the wave equation and radiation condition in the upper half-plane for any integrable function
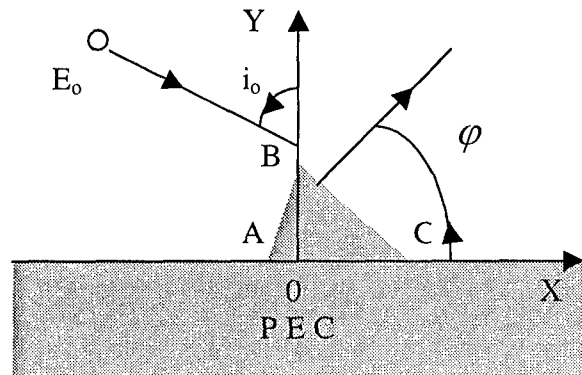
$A(\xi)$. The boundary condition satisfaction in the TM case leads to the integral equation (IE) for unknown function $A(\xi)$:

$$\int_{-\infty}^{\infty} \exp(-j\xi x - jhf(x))A(\xi)d\xi = -\exp(-jk_{01}x + jk_{02}f(x)) \qquad (2)$$

where the target's height-function $y = f(x)$ is defined as

$$f(x) = \begin{cases} \varphi(x), & x \in [-a_1, a_2] \\ 0, & otherwise \end{cases}, \varphi(x) = \begin{cases} (a_1 + x)b/a_1, & -a_1 \le x \le 0 \\ (a_2 - x)b/a_2, & 0 \le x \le a_2 \end{cases} \qquad (3)$$

The unknown spectral function $A(\xi)$ can be decomposed as

$$A(\xi) = A_1(\xi) + B(\xi) \qquad (4)$$

where $A_1(\xi) = -\delta(\xi - k_{01})$ determines the wave reflected from the plane $y = 0$. The substitution of (4) into (2) yields an IE of the 1st kind for the spectral function $B(\xi)$:

$$\int_{-\infty}^{\infty} \exp(-j\xi x - jhf(x))B(\xi)d\xi = F(x) \qquad (5)$$

with the right-hand side function

$$F(x) = \exp(-jk_{01}x)\left[\exp(-jk_{02}f(x)) - \exp(jk_{02}f(x))\right] \qquad (6)$$

that differs from zero only inside the interval $[-a_1, a_2]$. To solve the IE (5) over the whole interval R_1, we apply the Fourier transform to the both sides of equation with preliminary multiplication by $\exp(-\sigma|x|)$. Two methods are used in this paper for ill-conditioned system solving, which results from IE (5) while discretization. The first is an iterative method and the second is a genetic algorithm.

ITERATIVE METHOD. A new iterative scheme is proposed to solve an ill-conditioned ME

$$KX = F \qquad (7)$$

where K is a square matrix, X and F are vectors or matrices. The method is based on the *LU*-decomposition of specific form:

$$K = L + U$$

where

$$L = \begin{pmatrix} \alpha & 0 & 0 & \cdots \\ k_{21} & \alpha & 0 & \cdots \\ k_{31} & k_{32} & \alpha & \cdots \\ \cdots & \cdots & \cdots & \ddots \end{pmatrix}, \quad U = \begin{pmatrix} k_{11} - \alpha & k_{12} & k_{13} & \cdots \\ 0 & k_{22} - \alpha & k_{23} & \cdots \\ 0 & 0 & k_{33} - \alpha & \cdots \\ \cdots & \cdots & \cdots & \ddots \end{pmatrix}.$$

Then, the Eq. (7) can be rewritten in the iterative form:

$$X = \tilde{F} + \tilde{K}X , \quad \tilde{F} = L^{-1}F, \quad \tilde{K} = -L^{-1}U$$

This equation gives the iterative process

$$X^{(n)} = \tilde{F} + \tilde{K}X^{(n-1)} . \qquad (8)$$

The convergence depends on the right-hand side (F) and the decomposition parameter (α). Numerical investigation shows the following convergence condition fulfills for some F and α:

$$\|K^n \tilde{F}\| = \beta_n \|\tilde{F}\|, \quad \sum_{n=0}^{\infty} \beta_n = S < \infty \qquad (9)$$

In that case the solutions make up a compact set in a Banach space. Then, the tendency of discrepancy to zero for consequently $X^{(n)}$ ensures the tendency of approximate solution $X^{(n)}$ to an exact solution of Eq. (7), according to [5]. This method was compared with genetic algorithm and an excellent accordance was revealed.

NUMERICAL RESULTS. The scattering from a triangularly modeled breaking wave on a plane surface in PEC approximation is studied. The particular increasing of backscattering from a foaming-like breaking wave modeled with triangular target is detected for it's height $b=1.5\lambda_0$. For the most important case of strong LGA scattering from a foaming-like wave, the normalized scattering patterns for 1° grazing angle was calculated with the aid of two methods (Fig. 2).

The both algorithms are stopped at the same discrepancy of 0.04. We can see an excellent
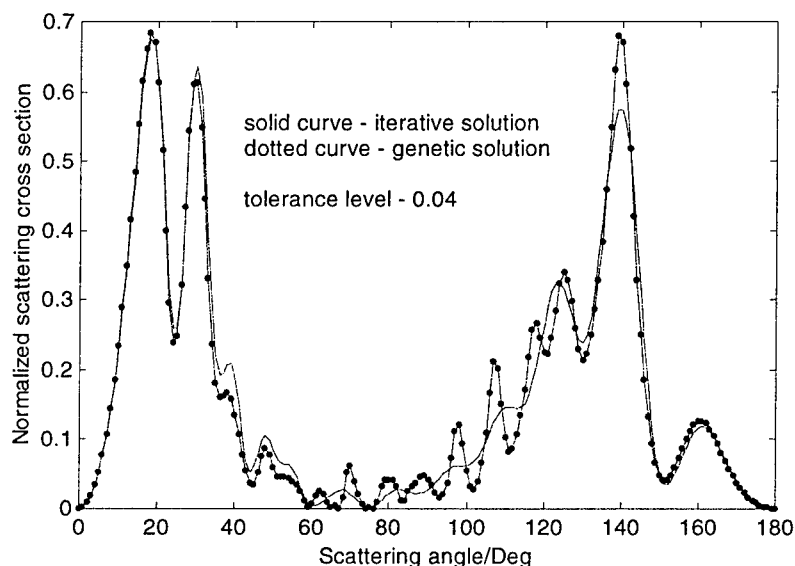
Figure 2

agreement of both methods. This result proves the robustness and adequacy of proposed method and genetic algorithm. Compared with minimal backscattering from foaming-like wave (for $b=\lambda_0$), the RCS may enlarged at 2.2922 dB for $i_0 = 88°$ and at 2.2104 for $i_0 = 89°$ if increasing the wave's height to $1.5\lambda_0$. The RCS from a breaking wave may enlarge in thousand times (~ 3dB) when the steepening wave transforms to the foaming one. This calculated effect is of the same order with a strong radar backscattering for H-polarization (so named "sea-spikes").

REFERENCES

[1] Y. Liu, S. Y. Frasier and R. E. McIntosh, "Measurement and classification of low-grazing-angle radar sea-spikes", *IEEE Trans. Antennas Propagat.*, vol. 46, pp. 27-40, Jan. 1998.

[2] D. H. Holliday, L. L. DeRaad, Jr., and G. J. St-Cyr, "Forward-backward: a new method for computing low-grazing angle scattering", *IEEE Trans. Antennas Propagat.*, vol. 44, pp. 722-729, May 1996.

[3] A. I. Nosich, "The method of analytical regularization in wave-scattering and eigenvalue problems: foundations and review of solutions", *IEEE Antennas and Propagation Magazine*, vol. 41, pp. 34-48, June 1999.

[4] E.T. Witteker and C.N. Watson, *A Course of Modern Analysis*, Cambridge Univ. Press, 1927.

[5] A. N. Tikhonov and V. J. Arsenin, *"Ill-posed problems solving methods"*, "Nauka", Moskow, p. 38, 1986 (in Russian).

REFLECTION OF A PLANE WAVE FROM A CYLINDER WITH FRACTAL PROPERTIES OF THE SURFACE (far-field region)

V. M. Onufriyenko, P. A. Samolchev, and T. I. Slyusarova

Zaporozhye State Technical University,
Zhukovsky Str. 64, Zaporozhye, 69063, Ukraine
e-mail: onufr@zstu.zaporizhzhe.ua

ABSTRACT

In this paper, the diffraction of a plane electromagnetic wave by a cylinder with fractal properties of the surface is researched. The results of designing of *integro-differential* model of the conductive cylinder are represented on the basis of representations of fractal geometry of a surface of actual explorers. The obtained α-characteristics of electromagnetic field generation has allowed making specification in the classical theory of a diffraction of electromagnetic waves on conductive bodies.

INTRODUCTION

For the description of the fractal properties of actual physical objects [1], the α-characteristics of components of electromagnetic field are introduced [2,3]. The fractal nature of objects (curves, surfaces, volumetric bodies, etc.) is taken into account through the Hausdorff measure, which is defined by means of the fractional *integro-differential* calculation [4,5], and the degree of fractality is taken into account by the α-values. Development of an *integro-differential* electromagnetic field model is considered that is further used for solving the problem of diffraction of a plane wave on a cylinder with fractal properties of the surface.

FORMULATION OF THE PROBLEM

Let us formulate the problem of determining the influence of the fractal properties of a cylindrical metal surface on the components of a monochromatic electromagnetic field. We assume that the field $\dot{E}^0, \dot{H}^0$ of the incident wave is known, the conductive body, and the enclosing medium has parameters ε_a and μ_a. Under the effect of the primary field on surface S of the body, the electrical fractal currents are produced which induces the secondary electromagnetic field $\dot{E}, \dot{H}$. As it was noted in [3], the usage of the formulas of fractional integration and differentiation enables one to characterize geometrical features of curves and surfaces. Further, instead of the vectors $\dot{E}, \dot{H}$, their α-characteristics $\dot{E}^\alpha = I^\alpha\left(D^\alpha \dot{E}\right)$, $\dot{H}^\alpha = I^\alpha\left(D^\alpha \dot{H}\right)$ will be considered. Suppose that a plane linearly polarized electromagnetic wave is incident on a perfectly conducting circular cylinder of radius a normally to its axis. Introduce a cylindrical coordinate system $x = r \cdot \cos\varphi$, $y = r \cdot \sin\varphi$, $z = z$ the z-axis coinciding with the axis of cylinder, and the angle φ is for the azimuth. Consider the case of the vector $\dot{E}^0$ parallel to the z-axis. The electric field of the incident wave has only z-component:

$$\dot{E}^0(r,\varphi) = E_0 \cdot e^{ikx} = E_0 \cdot e^{ikr \cdot \cos\varphi}, \quad k = \omega \cdot \sqrt{\varepsilon_a \cdot \mu_a}.$$

The considered problem is two-dimensional (no dependence on the coordinate z), therefore the Helmholtz equation for the secondary electric field becomes

$$\frac{1}{r} \cdot \frac{\partial}{\partial r}\left(r \cdot \frac{\partial\left(D^\alpha \dot{E}\right)}{\partial r}\right) + \frac{1}{r^2} \cdot \frac{\partial^2\left(D^\alpha \dot{E}\right)}{\partial \varphi^2} + k^2 \cdot D^\alpha \dot{E} = 0; \quad r \ge a; \quad 0 \le \varphi \le 2\pi. \quad (1)$$

The function $D^\alpha \dot{E}$ on a surface S should satisfy the terminal condition, which has a form as $D^\alpha \dot{E}(a,\varphi) = -E_0 \cdot e^{ika\cdot\cos\varphi}$. It satisfies the condition of radiation in the infinitely remote points: at $r \to \infty$, in the expression for the function $D^\alpha \dot{E}(r,\varphi)$ there should be only the components with the phase factor e^{-ikr} corresponding to a wave propagating from the origin to infinity.

Thus, the solution of the equation (1) satisfying the radiation condition is the function

$$D^\alpha \dot{E}(r,\varphi) = \sum_{m=0}^{\infty} D^\alpha \dot{E}_m(r,\varphi) = \sum_{m=0}^{\infty} D_m \cdot H_m^{(2)}(k \cdot r) \cdot \cos(m\varphi), \qquad (2)$$

where D_m is some constant determined from the terminal condition;

$$m = 0: \quad D_0 = -E_0 \cdot \frac{J_0(k \cdot a)}{H_0^{(2)}(k \cdot a)}; \quad m = 1,2,3,\dots: \quad D_m = -E_0 \cdot 2 \cdot i^m \cdot \frac{J_m(k \cdot a)}{H_m^{(2)}(k \cdot a)}. \qquad (3)$$

Substituting (3) into (2), we obtain a resulting expression for the secondary electric field, which appears due to the plane wave incident on the perfectly conducting circular cylinder of radius a with fractal properties of the surface

$$D^\alpha \dot{E} = -\bar{z}_0 \cdot E_0 \cdot \left\{ \frac{J_0(ka)}{H_0^{(2)}(ka)} \cdot H_0^{(2)}(kr) + 2\sum_{m=1}^{\infty} i^m \frac{J_m(ka)}{H_m^{(2)}(ka)} \cdot H_m^{(2)}(kr) \cdot \cos(m\varphi) \right\}. \qquad (4)$$

NUMERICAL RESULTS

After fractional integration, the α-characteristic of the secondary electric field (fractality is taken at the angle φ) is obtained as

$$\dot{E}_\varphi^\alpha = -\bar{z}_0 \cdot \frac{E_0}{\Gamma(\alpha)} \cdot \left\{ \frac{J_0(ka)}{H_0^{(2)}(ka)} \cdot H_0^{(2)}(kr) \cdot \int_0^\varphi \frac{1}{(\varphi-t)^{1-\alpha}} dt + 2\sum_{m=1}^{\infty} i^m \frac{J_m(ka)}{H_m^{(2)}(ka)} \cdot H_m^{(2)}(kr) \cdot \int_0^\varphi \frac{\cos(mt)}{(\varphi-t)^{1-\alpha}} dt \right\}$$

The polar graphics for the modulus of the secondary electric field in the far-field region are presented in Fig.1. Fig.1a) demonstrates a comparison of the classical and fractal approaches. In Fig.1b), the results of calculations for the fractal cylinders of different values of ka are presented.
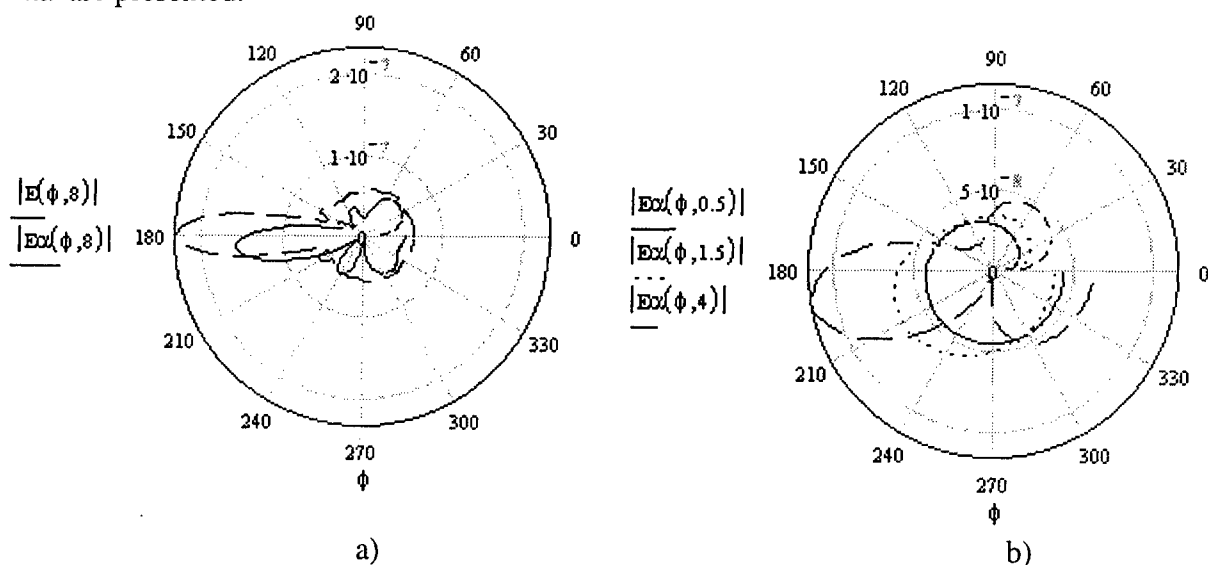
Fig.1

CONCLUSION

The obtained α-characteristics of the electromagnetic field have enabled us to generalize classical theory of diffraction of electromagnetic waves on conducting bodies. Diffraction of a plane electromagnetic wave on a cylinder with fractal properties of surface has been studied. The results of developing an *integro-differential* model of conducting cylinder are presented on the basis of representations about fractal geometry of the surface of actual scatterer. The obtained numerical data demonstrate a comparison between the classical and fractal approaches.

REFERENCES

[1] The fractals in physics // Proceedings 6th International Symposium on Fractals in Physics.
    (Triest, Italy, July 9-12,1985): Tr. from English // Edited by L. Pietronero, E. Tozotti.-
    M.:Mir,1988.-672 p. (in Russian).

[2] Onufriyenko V. On "α-features" a of electrical waves above impedance plane //
Conference
    Proceedings 12th International Conference on Microwaves and Radar. - Vol. 1. – Krakov
    (Poland). - 1998. - P. 212-215.

[3]   Onufriyenko V. M., Lysokon I. V., Samolchev P. A., Slyusorova T. I. The
electromagnetic
    waves on the fractal border of the division of two environments // Radioelectronika,
    informatyka, upravlinnya.- Zaporizhzhya: ZSTU. - 1999. - № 1. - P. 20-23. (in Ukrainian
)

[4]   Samko S. G., Kilbas And. A., Marichev O. I. The integrals and derivatives of the
fractional
    order and their some applications.- Minsk: Nauka i tehnika, 1987.-688 p. (in Russian)

[5] Engheta N. On the Role of Fractional Calculus in Electromagnetic Theory // IEEE
Antennas
    and Propagation Magazin. - Vol. 39. - N 4, August 1997.-P. 35-46.

[6]   V. Onufrienko. Physical-geometrical interpretation of α-characteristics of
electromagnetic
    field.//Radiofisika i elektronika. Institute of Radiophysics and Electronics of the
National
    Academy of Sciences of Ukraine, Vol.4, No.1, pp.7-10,1999 (in Ukrainien).

APERTURE COUPLING IN THE BODIES POSSESING A FINITE SYMMETRY GROUP

A.S. Ilinski[*], I.A. Zagorodnov[*], and R.P. Tarasov[**]

[*] Moscow State University, Moscow, Russia
[**] Research Institute of Pulse Techniques, Moscow, Russia
e-mail: celd@cs.msu.ru

ABSTRACT

A numerical method for predicting the field penetrating an arbitrary opening in a symmetric body is considered. The method is based on the usage of coordinate functions of irreducible representations of the group $\{\tau_N\}$ of symmetries of the cavity. It enables one to reduce calculation time by the factor $\sim N^2$ and to construct numerically an inverse operator for arbitrary excitation function. Required machine memory is also reduced by the factor N.

INTRODUCTION

A numerical method for predicting the field penetrating an arbitrary opening in a symmetric body is described here. The cubic cavity with an arbitrary aperture in its shell is an example of such item. This cavity has the group of symmetries O_h of the order 48. If a cavity has a finite group of symmetries $\{\tau_N\}$ of the order N, it is possible to develop a numerical method of the problem solution based on using of coordinate functions of irreducible representations of the group $\{\tau_N\}$ of symmetries of the considered cavity [1], [2].

The aperture coupling problem can be reduced to three problems. In the first problem the induced surface current density J is found for the apertureless body. In the second problem the aperture tangential E-field is found. In the third problem the surface current $\tilde{J}$ which yields the internal field is found. The first and the third problems can be reduced to an integral equation on the cavity shell S with the same operator. The second problem can be reduced to an equation on aperture S_0. In case of the group $\{\tau_N\}$ of the order N the integral equation on the surface S is reduced to the $\sim N$ disconnected equations on the $1/N$ part of the surface S.

Thus operator matrix of the integral equation becomes block diagonal one in the basis of coordinate functions of irreducible representations of the group $\{\tau_N\}$ of symmetries of the cavity. It allows reduce calculation time by a factor $\sim N^2$ and numerically to construct an inverse operator. Machine storage is also reduced by a factor N.

In the paper the numerical results for a cubic surface without one face and for a cylinder located in a sphere with a narrow slot irritated by an incident plane wave are given.

STATEMENT OF THE PROBLEM AND BASIC RELATIONS

The geometry under consideration is a cavity with an aperture S_0 in its perfectly conducting shell S. The screen $S_1 = S \setminus S_0$ is irradiated by a monochromatic field E_0, H_0, spreading in a homogeneous medium with an inductivity ε and a magnetic conductivity μ. Full field can be noted as $H = H_1 + H_0$, $E = E_1 + E_0$, where E_1, H_1 is a scattered field represented as

$$H_1 = \nabla \times A_1 J_1, \quad E_1 = -(i\omega\varepsilon)^{-1}\nabla \times \nabla \times A_1 J_1, \tag{1}$$

where ω is a circular frequency, and the vectorial potentials are determined by expression

$$A_1 J_1(x) = \int_{S_1} \left(\exp(ik|x-y|)/4\pi\right) J_1(y) d\mu(y), \quad k = \omega\sqrt{\varepsilon\mu}, \quad S_1 = S \setminus S_0.$$

The problem can be reduced to a following integral equation on a surface $S_1 = S \setminus S_0$:

$$N_1 J_1(x) = F_1(x), \quad x \in S_1, \quad N_1 J_1 = 2n \times \nabla \times \nabla \times A_1 J_1, \quad F_1 = 2i\omega\varepsilon n \times E_0. \tag{2}$$

In turn the problem for the closed surface S can be also reduced to an equation

$$N\hat{J}(x) = F(x), \quad x \in S, \quad F = 2i\omega\varepsilon n \times E_0, \tag{3}$$

which can be written in matrix representation

$$\begin{bmatrix} N_0 & N_{01} \\ N_{10} & N_1 \end{bmatrix} \begin{bmatrix} \hat{J}_0 \\ \hat{J}_1 \end{bmatrix} = \begin{bmatrix} F_0 \\ F_1 \end{bmatrix}.$$

The solution of equation (2) is equivalent to the solution of following matrix equation

$$\begin{bmatrix} 0 \\ J_1 \end{bmatrix} = \begin{bmatrix} \hat{J}_0 \\ \hat{J}_1 \end{bmatrix} + \begin{bmatrix} B_0 & B_{01} \\ B_{10} & B_1 \end{bmatrix} \begin{bmatrix} \tilde{F}_0 \\ 0 \end{bmatrix},$$

where functions $J_1(x)$, $x \in S_1$, and $\tilde{F}_0(x)$, $x \in S_0$, are unknown ones and matrix $B = N^{-1}$.

Hence, if the matrix B is known, the solution of the equation (2) can be found by formulas $\hat{J} = BF$,

$\tilde{F}_0 = -(B_0)^{-1}\hat{J}_0$, $\quad \tilde{J} = B\tilde{F}$, $\quad \tilde{F} = \begin{bmatrix} \tilde{F}_0 & 0 \end{bmatrix}^T$, $\quad J_1 = \hat{J}_1 + \tilde{J}_1$. The field inside cavity can be found

through expression (1) or by representation $H_1 = \nabla \times A\tilde{J}$, $E_1 = -(i\omega\varepsilon)^{-1}\nabla \times \nabla \times A\tilde{J}$.

Let's enter a vectorial bundle $T_1S \oplus T_2S$, where T_1S is a tangential bundle of polar vectors and T_2S is a bundle of axial vectors. The transformation τ_k from group $O(3)$ of orthogonal transformations of space induces an automorphism τ_k^+ of the bundle $T_1S \oplus T_2S$: $\tau_k^+(F_1(x), F_2(x)) \to \left(\left[\tau_k^* F_1\right](x), \ |\tau_k|\left[\tau_k^* F_2\right](x)\right)$, where τ_k^* is a transposition of a vector field.

If the boundary surface S has group of symmetries $\{\tau_N\}$ than the operator N of the integral equation (3) is invariant one concerning group $\{\tau_N\}$: $\tau_k^+ N = N\tau_k^+$, $\tau_k \in \{\tau_N\}$.

NUMERICAL METHOD

Manifold S, possessing a symmetry group $\{\tau_N\}$, can be represented as $S = \bigcup_{i=1}^{N} \tau_i F$, $Int(\tau_i F \cap \tau_j F) = 0, \forall i \neq j$. We can uniquely assign an operator function $\hat{N}(\tau_i) = \hat{N}(\tau_i, \tau_1) = P(\tau_i)NQ(\tau_1)$ defined on the group $\{\tau_N\}$ to the operator N which act in the space $L_p(S)$. Here $P(\tau_i)$: $L_p(S) \to L_p(F)$, is a contraction operator defined by relation $\left[P(\tau_j)\varphi\right](x) = \left[\tau_j^+\varphi\right](x) = \left[\hat{\varphi}(\tau_j)\right](x)$, $x \in S$, and $Q(\tau_i): L_p(F) \to L_p(S)$ is a prolongation operator defined by relation: $\left[Q(\tau_j)\hat{\varphi}(\tau_k)\right](x) = [(\tau_j^{-1})^+ \hat{\varphi}(\tau_k)](x)$ at $x \in \tau_j S_1$ and $\left[Q(\tau_j)\hat{\varphi}(\tau_k)\right](x) = 0$ at $x \notin \tau_j S_1$.

The operation of the operator N on a function φ can be noted as the right operator convolution on group $\{\tau_N\}$: $\hat{f}(\tau_i) = \sum_{j=1}^{N} \hat{N}(\tau_j^{-1}\tau_i)\hat{\varphi}(\tau_j)$, where the label $f = N\varphi$ is entered. The operator function for the inverse operator $B = N^{-1}$ can be found under the formula $\hat{B}(\tau_i) = \sum_{j=1}^{p} d_{\lambda_k} tr\left(\tilde{B}(\lambda_k)U_{\lambda_k}(\tau_j)\right)$, where

$\tilde{B}(\lambda_k) = \left[\tilde{N}(\lambda_k)\right]^{-1}$ and $\tilde{N}(\lambda_k) = \sum_{s=1}^{N} \hat{N}(\tau_s)U_{\lambda_k}(\tau_s^{-1})$.

The numerical approximation of the operator N was derived by a method of mechanical cubages. The formulas coincide with the ones gained in a collocation method at piecewise approximation of currents. The cavity shell S was approximated by an Euclidean complex.

NUMERICAL RESULTS

Let us consider a problem of a diffraction of a flat linearly polarised electromagnetic wave on a cavity D with group O_h, which is a non-commutative group of order 48. The body with the group O_h is determined by defining of a fundamental area in 1/48 part of space (just as the body of revolution is determined by

defining of a generator). For example, a cube and an octahedron have group O_h. In the paper the cubic cavity will be surveyed.

The matrix N^h of a discrete problem is a block matrix of order 48 with blocks of order $2n$, where n is a number of simplexes on fundamental area F. Thus we need only one block column of the matrix N^h as the other columns are gained from the first by permutations. It allows in 48 times to reduce the volume of machine storage. The group O_h has 10 irreducible representations: 4 one-dimensional, 2 two-dimensional and 4 three-dimensional. Hence instead of an inversion of the block matrix N^h of order 48 it is necessary to invert only four block matrixes of order 1, two matrixes of order 2 and four matrixes of order 3. This approach allows constructing an inverse matrix $B^h = (N^h)^{-1}$. For an inversion of the matrixes the Gauss method was used. Thus the number of operations was reduced in $\sim 10^3$ times.

In fig. 1 the quantity $|H_1 + H_0|/|H_0|$ in H - plane is shown. The scattering surface S_1 is a surface of a cube S without one face S_0. The plane wave is falling on the aperture S_0 with vector E along an edge a of the cube of wave size $ka = 12$. In fig. 2 the quantity $|H_1 + H_0|/|H_0|$ in H - plane is shown. The scattering surface can be represented as $S_1 = S_C \cup S_{Sp} \setminus S_0$, where S_C is a surface of a cylinder, located in a sphere S_{Sp} with a slot S_0, which is located along the equator of the sphere. The plane wave is falling on aperture S_0 with vector E along the equator. The surface $S = S_C \cup S_{Sp}$, which possesses group D_{nh} was approximated by an Euclidean complex with $\sim 2 \cdot 10^4$ simplexes. The structure has wave sizes: $R = 3r$, $l = 2r$, $a = 0.42r$, $b = 1.9r$, $kr = 2.06$, where R is a radius of the sphere S_{Sp}, r is a radius and l is a high of the cylinder S_C, a and b are length of sides of the slot S_0.
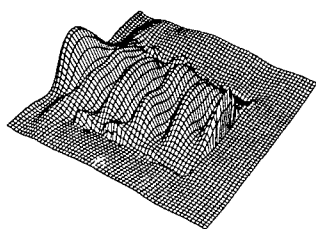
Fig. 1. H-field for the cubic cavity   Fig. 2. H-field for the cylinder inside a spherical cavity
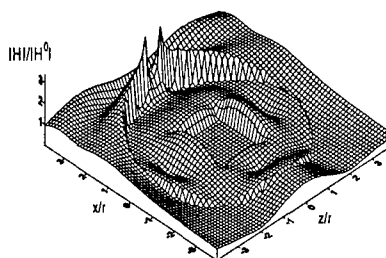
REFERENCES

[1] R.P.Tarasov "The computational stability of boundary equations of the first kind in problems of diffraction near resonances", Comp. Math. Math. Ph.,V.39, P.907-932.
[2] I.A. Zagorodnov, A.S. Ilinski, R.P. Tarasov, "Grid boundary equations on conducting surfaces with symmetries and their numerical analysis in diffraction problems on a sphere", Computational Mathematics and Mathematical Physics, (submitted).

PLANE ELECTROMAGNETIC WAVE SCATTERING AND DIFFRACTION IN A STRATIFIED MEDIUM

A. Maher, and N.B. Pleshchinskii

Kazan State University
P.O.Box 234 Kazan, 420503, Russia
E-mail: pnb@ksu.ru

The two-dimensional jump problem for the Helmholtz equation in a stratified medium is considered. Preliminary two auxiliary overdetermined Cauchy problems for a half-plane and for a strip in Sobolev classes of distributions of slow growth at infinity are solved and explicit representations of their solutions are given.

It is shown that the jump problem in the case of a multilayered medium can be reduced to a set of equations for the Fourier transforms of the boundary distributions for each layer. This set of equations can be transformed to two equations only. The jump problem for the Helmholtz equation is equivalent to a scattering problem for a plane electromagnetic wave in a multilayered space.

The diffraction problem for an electromagnetic plane wave at a finite set of metallic strips in a stratified space is considered. It is proved that this problem is equivalent to an integral equation with a logarithmic singularity in the kernel.

THE JUMP PROBLEM AND THE CAUCHY PROBLEMS

We assume that the lines $z = h_j$, $h_1 < h_2 < \ldots < h_n$ separate the half-planes $D_0 : z < h_1$, $D_n : z > h_n$ and the strips $D_j : h_j < z < h_{j+1}$, $j = 1..n - 1$ in the plane (x, z). We will search the solutions of the Helmholtz equation

$$\frac{\partial^2 u}{\partial x^2} + \frac{\partial^2 u}{\partial z^2} + k^2 u(x, z) = 0, \quad z > 0 \tag{1}$$

in the Sobolev space $H_s(R_2^+)$, $s > 3/2$ of distributions of slow growth at infinity satisfying the conjugation conditions

$$u(x, h_j + 0) - u(x, h_j - 0) = a_j(x), \quad \frac{\partial u}{\partial z}(x, h_j + 0) - \frac{\partial u}{\partial z}(x, h_j - 0) = b_j(x), \quad j-1..n. \tag{2}$$

If the representations of the solutions in the domains D_0 and D_n contain the outgoing into the half-planes waves [1], then we call the solution $u(x, z)$ of the jump problem as outgoing into infinity. We denote $\Delta h_j = h_{j+1} - h_j$ and

$$\gamma_j^0(\xi) = \{|\xi| > k_j : +i\sqrt{\xi^2 - k_j^2}; \quad |\xi| < k_j : -\sqrt{k_j^2 - \xi^2}\}.$$

The following statements are valid.

Lemma 1 . *The solution $u_n(x, z)$ of the equation (1) in the domain D_n belongs to the class of solutions outgoing into a half-plane $z > h_n$ and satisfies the boundary conditions*

$$u_n(x, h_n + 0) = u_n^+(x), \quad \frac{\partial u_n}{\partial z}(x, h_n + 0) = v_n^+(x)$$

if and only if when Fourier transforms of the boundary functions satisfy the equality

$$V_n^+(\xi) - i\gamma_n^0(\xi) U_n^+(\xi) = 0. \tag{2}$$

Thus the Fourier transform of $u_n(x,z)$ is the solution of the equation

$$(k_n^2 - \xi^2 - \zeta^2)U_n(\xi,\zeta) = \frac{1}{\sqrt{2\pi}} e^{ih_n\zeta}[V_n^+(\xi) - i\zeta U_n^+(\xi)] \quad . \tag{3}$$

Lemma 2 . *The solution $u_0(x,z)$ of the equation (1) in the domain D_0 belongs to the class of solutions outgoing into a half-plane $z < h_0$ and satisfies the boundary conditions*

$$u_0(x,h_1 - 0) = u_1^-(x), \quad \frac{\partial u_0}{\partial z}(x,h_1 - 0) = v_1^-(x)$$

if and only if the Fourier transforms of the boundary functions satisfy the equality

$$V_1^-(\xi) + i\gamma_0^0(\xi)U_1^-(\xi) = 0. \tag{4}$$

Thus, the Fourier transform of $u_0(x,z)$ is the solution of the equation

$$(k_0^2 - \xi^2 - \zeta^2)U_0(\xi,\zeta) = -\frac{1}{\sqrt{2\pi}} e^{ih_1\zeta}[V_1^-(\xi) - i\zeta U_1^-(\xi)] \quad . \tag{5}$$

Lemma 3 . *The solution $u_j(x,z)$ of the equation (1) in the domain D_j, $j = 1..n-1$ satisfies the boundary conditions*

$$u_j(x,h_j + 0) = u_j^+(x), \quad \frac{\partial u_j}{\partial z}(x,h_j + 0) = v_j^+(x),$$

$$u_j(x,h_{j+1} - 0) = u_{j+1}^-(x), \quad \frac{\partial u_j}{\partial z}(x,h_{j+1} - 0) = v_{j+1}^-(x)$$

if and only if the Fourier transforms of the boundary functions satisfy the equalities

$$[V_j^+(\xi) - i\gamma_j^0(\xi)U_j^+(\xi)] - e^{+i\Delta h_j\gamma_j^0(\xi)}[V_{j+1}^-(\xi) - i\gamma_j^0(\xi)U_{j+1}^-(\xi)] = 0, \tag{6}$$

$$e^{+i\Delta h_j\gamma_j^0(\xi)}[V_j^+(\xi) + i\gamma_j^0(\xi)U_j^+(\xi)] - [V_{j+1}^-(\xi) + i\gamma_j^0(\xi)U_{j+1}^-(\xi)] = 0. \tag{7}$$

Thus, the Fourier transform of $u_j(x,z)$ is the solution of the equation

$$(k_j^2 - \xi^2 - \zeta^2)U_j(\xi,\zeta) = \frac{1}{\sqrt{2\pi}} e^{+ih_j\zeta}[V_j^+(\xi) - i\zeta U_j^+(\xi)] - \frac{1}{\sqrt{2\pi}} e^{+ih_{j+1}\zeta}[V_{j+1}^-(\xi) - i\zeta U_{j+1}^-(\xi)]. \tag{8}$$

Lemma 1 is proved in [1], the complete proof of Lemma 3 is given in [2].

Theorem 1. *The Fourier transform of the solution of the jump problem (1), (2) in the stratified medium can be obtained from the equations (3), (5) and (8), where $V_j^\pm(\xi), U_j^\pm(\xi)$ satisfy the equations (2), (4), (6), (7) and*

$$U_j^+(\xi) - U_j^-(\xi) = A_j(\xi), \quad V_j^+(\xi) - V_j^-(\xi) = B_j(\xi), \quad j = 1..n. \tag{9}$$

We denote that sometimes the homogeneous jump problem has nontrivial solutions in the class of distributions outgoing from the media interfaces into half-spaces. It is shown in [2] that the set of equations (2), (4), (6), (7) and (9) can be transformed to only two equations.

DIFFRACTION PROBLEM ON THE SET OF METALLIC STRIPS

Suppose a set of ideally conducting infinitely thin metallic strips are placed at the media interfaces, and at the line $z = h_j$, $j = 1..n$ the intervals $[\alpha_{jk}, \beta_{jk}]$, $k = 1..m_j$ correspond to the strips. We introduce a set of functions $\phi_j(x)$, $j = 1..m_j$ determined on the intervals $[\alpha_{jk}, \beta_{jk}]$, $k = 1..m_j$, respectively. We assume that the source wave has the potential $\tilde{u}(x, z)$.

Theorem 2. *The diffraction problem on the set of metallic strips in the stratified medium is equivalent to the integral equation*

$$\frac{1}{2\pi} \int_{-\infty}^{+\infty} \int_{-\infty}^{+\infty} U_j(\xi, \zeta) e^{-i\xi x} e^{-i\zeta h_j} d\xi d\zeta =$$

$$= \{ j = n : -\tilde{u}(x, h_n + 0), \ x \in (\alpha_{nk}, \beta_{nk}); \quad j \neq n : 0, \ x \in (\alpha_{jk}, \beta_{jk}) \} \qquad (10)$$

by functions $\phi_j(x)$, $j = 1..m_j$, *where* $U_j(\xi, \zeta)$ *are the Fourier transforms of the solutions* $u_j(x, z)$ *of the jump problem and*

$$a_j(x) = 0, \quad j = 1..n - 1; \quad a_n(x) = -\tilde{u}(x, h_n + 0);$$

$$b_j(x) = \{ \phi_j(x), \ x \in (\alpha_{jk}, \beta_{jk}); \quad 0, \ x \notin (\alpha_{jk}, \beta_{jk}) \}, \quad j = 1..n - 1;$$

$$b_n(x) = \{ \phi_n(x), \ x \in (\alpha_{nk}, \beta_{nk}); \quad -\frac{\partial \tilde{u}}{\partial z}(x, h_n + 0), \ x \notin (\alpha_{nk}, \beta_{nk}) \}.$$

The solution of integral equation (10) with logarithmic singularity in the kernel can be found by Galerkin method.

REFERENCES

[1] Pleshchinskaya I.E., Pleshchinskii N.B., The Cauchy problem and potentials for elliptic partial differential equations and some of their applications, Advances in Equations and Inequalities (A.E.I.) (ed. J.M. Rassias), Athens, Greece, 1999.

[2] A.Maher, N.B.Pleshchinskii, The jump problem for the Helmholtz equation in stratified medium and its applications (in preparation) (in Russian).

NUMERICAL METHOD OF SOLVING THE SINGULAR INTEGRAL EQUATIONS OF WAVE SCATTERING BY A PENETRABLE POLYGONAL CYLINDER

L. N. Ilyashenko and A. I. Nosich

Institute of Radio-Physics and Electronics NASU
ul. Proskury 12, Kharkov 61085, Ukraine

The problem of an H-polarized wave scattering by a dielectric polygonal cylinder is considered. To obtain a set of the first-kind Fredholm singular integral equations (IEs), single-layer potentials are used. A Galerkin method of moments with special basis is applied for reducing IEs to an infinite-matrix equation having favorable features.

INTRODUCTION

Solving the problems of wave scattering often comes to singular IEs [1]. For example, this can be done by applying potential theory together with boundary conditions on the scatterer surface. There are various ways of a further numerical treatment, all of them being based on reduction of IEs to a matrix equation. Some results obtained in the diffraction by smooth cylinders were presented in [2,3]. However, the existence of edges makes computations with smooth expansion functions inaccurate [3]. One of the ways to overcome this difficulty is to take into account a solution singularity in the neighborhood of geometric singularity by using appropriate basis [4-6]. As known, the methods that do not exploit analytical inversion of a singular part of the full problem operator, fail to minimize the error of computations. Therefore, we propose a method that is a modification of [4-6] for dielectric polygonal cylinders.

FORMULATION OF THE PROBLEM AND THE METHOD OF SOLUTION

The geometry of the considered scattering problem is shown in Fig. 1. The incident field
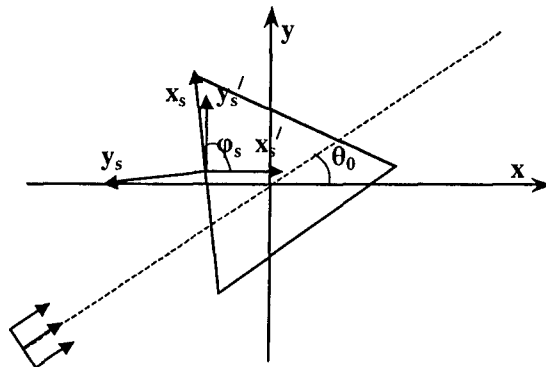
Fig.1. Geometry of the problem

is an H-polarized plane wave: $H^i = e^{ik\cos\theta_0 + ik\sin\theta_0}$. The scatterer is a uniform dielectric cylinder whose cross-section is a regular triangle of the side size *2d* and relative permittivity is ε.
Denote the internal domain of the scatterer as Ω and its contour as *L*. Present he total field inside Ω as H^ε and decompose it outside Ω as $H^i + H^{sc}$. The incident and the scattered fields have to satisfy the Helmholtz equation in free space, for $r \notin \Omega (r \in ext\,\Omega)$, the field H^{sc} has to satisfy similar equation with wavenumber $k\varepsilon^{1/2}$, for $r \in \Omega$. On the scatterer contour *L*, the continuity conditions should be satisfied:

$$\left(H^{i}+H^{sc}\right)_{L}=H^{\varepsilon}\Big|_{L},\frac{\partial}{\partial n}\left(H^{i}+H^{sc}\right)_{L}=\frac{1}{\varepsilon}\frac{\partial}{\partial n}H^{\varepsilon}\Big|_{L}\tag{1}$$

The scattered field must also satisfy the Sommerfeld radiation condition at infinity. Eventually, the condition that the energy in any bounded domain of space is finite should be satisfied as well.

A fundamental solution of the wave equation is the Green's function depending on the distance between two points on the plane, $r, r' \in \Re^{2}$:

$$G(r,r')=\frac{i}{4}H_{0}^{(1)}(k|r-r'|) \quad \text{and} \quad G_{\varepsilon}(r,r')=\frac{i\varepsilon}{4}H_{0}^{(1)}(k\sqrt{\varepsilon}|r-r'|)\tag{2}$$

We shall seek the solution of the boundary value problem as a pair of single-layer potentials uniformly satisfying the Helmholtz equation and radiation condition [1], with unknown densities $p \in C(\partial\Omega)$, $q \in C(\partial\Omega)$:

$$H^{\varepsilon}(r)=\int_{L}G_{\varepsilon}(r,r')p(r')ds \quad H^{sc}(r)=\int_{L}G(r,r')q(r')ds\tag{3}$$

By using the conditions on L and the properties of the normal derivative limiting values for a single-layer potential [1], the following set of singular IEs is obtained:

$$\begin{cases}\displaystyle\int_{L}p(r')G_{\varepsilon}(r,r')ds'-\int_{L}q(r')G(r,r')ds'=H^{i}(r) \\[2mm] \displaystyle\frac{p(r)}{2\varepsilon}+\frac{1}{\varepsilon}\int_{L}p(r')\frac{\partial}{\partial n}G_{\varepsilon}(r,r')ds'+\frac{q(r)}{2}-\int_{L}q(r')\frac{\partial}{\partial n}G(r,r')ds'=\frac{\partial}{\partial n}H^{i}(r)\end{cases}\tag{4}$$

The method of numerical solution of (4) is based on the decomposition of polygonal cylinder to three flat-facet key elements. Correspondingly, the scattered and internal field functions are expressed as a superposition of the fields generated by each facet. Therefore, in the plane of cross-section, introduce a common coordinate system (XY) and three local coordinate systems $(X_{s}O_{s}Y_{s})$, with the origin O_{s} placed in the center of the s-th facet of the cylinder, and $O_{s}Y_{s}'$ axis being normal to the s-th facet (see Fig. 1). Then the set (4) is takes a form of six coupled IEs in terms of the local unknown functions p_{i} and q_{i} (i=1,2,3)

$$\begin{cases}\displaystyle\frac{di}{4}\sum_{i=1}^{6}\int_{-1}^{1}p_{i}(t)K_{ij}(t,t_{0})dt=f_{j}(t_{0}) \\[3mm] \displaystyle\frac{p_{j}(t_{0})+p_{j+3}(t_{0})}{2}+\frac{di}{4}\sum_{i=1}^{6}\int_{-1}^{1}p_{i}(t)M_{ij}(t,t_{0})dt=\tilde{f}_{j}(t_{0})\end{cases}\quad (j=1,2,3)\tag{5}$$

where the following notations have been used:

$$q_{i}=p_{i+3}\ \ (i=1,2,3)\quad K_{ji}(t,t_{0})=\varepsilon H_{0}^{(1)}\left(\sqrt{\varepsilon}R_{ij}(t,t_{0})\right)\qquad \text{if i = 1,2,3}\tag{6}$$

$$K_{ji}(t,t_{0})=-H_{0}^{(1)}\left(R_{i-3,j}(t,t_{0})\right)\qquad \text{if i = 4,5,6}\tag{7}$$

$$M_{ji}(t,t_{0})=\frac{k^{2}d\sqrt{\varepsilon}}{R_{ji}}\left[\left(t_{0}-\frac{a_{j}}{d}\right)-\left(t-\frac{a_{i}}{d}\right)\cos(\varphi_{i}-\varphi_{j})+\frac{b_{i}}{d}\sin(\varphi_{i}-\varphi_{j})\right]H_{1}^{(1)}\left(\sqrt{\varepsilon}R_{ji}(t,t_{0})\right)$$

$$\text{if i = 1,2,3}\tag{8}$$

$$M_{ji}(t,t_{0})=\frac{k^{2}d\sqrt{\varepsilon}}{R_{j,i-3}}\left[\left(t_{0}-\frac{a_{j}}{d}\right)-\left(t-\frac{a_{i-3}}{d}\right)\cos(\varphi_{i-3}-\varphi_{j})+\frac{b_{i-3}}{d}\sin(\varphi_{i-3}-\varphi_{j})\right]H_{1}^{(1)}\left(R_{j,i-3}(t,t_{0})\right)$$

$$\text{if i = 4,5,6}\tag{9}$$

Here, R_{ij} is the distance between the points t and t_{0}, φ_{i} is the angle between the x_{i}-axis of a local coordinate system and the x-axis of the common coordinate system, (a_{i}, b_{i}) are the

coordinates of the origin of a local coordinate system. Besides, in the right-hand parts, we have

$$f_j(t_0) = \exp\left(ikd\left[\left(t_0 + \frac{a_j}{d}\right)\cos(\theta_0 - \varphi_j) + \frac{b_i}{d}\sin(\theta_0 - \varphi_j)\right]\right)$$

$$\tilde{f}_j(t_0) = ikd\cos(\theta_0 - \varphi_i)\exp\left(ikd\left[\left(t_0 + \frac{a_j}{d}\right)\cos(\theta_0 - \varphi_j) + \frac{b_i}{d}\sin(\varphi_i - \varphi_j)\right]\right)$$

(10)

In the scattering by a perfectly electric conducting (PEC) polygonal cylinder, a technique of reducing the IEs similar to (5) to the infinite-matrix equation of the Fredholm second kind was presented in [6]. It was done in the Fourier-transform domain. We propose to solve (5) in the space domain, by projecting them onto local bases of the weighted Chebyshev polynomials of the first kind. As known, for numerical efficiency, is desirable to decompose the kernels in a sum of regular and singular parts and invert the latter. The mentioned basis functions diagonalize the singular IE operator corresponding to a PEC strip scattering [4,5]. Therefore, it is expected that our algorithm is better suited for the polygonal scatterers than the previous ones from [2,3].

CONCLUSION

A method of numerical solution of the wave-scattering by dielectric polygonal cylinders is proposed. It is based on decomposition of the total scattered field into the partial contributions of separate interacting facets, and on further usage of semi-inversion concept. Numerical results obtained by this method agree well with the published earlier. This can be applied to a scatterer with arbitrary number of edges. Besides, it can be developed into a universal solver of the scattering from electrically large objects, through the segmentation technique.

REFERENCES

[1] D. Colton, P. Kress. *Integral Equation Methods in Scattering Theory*, Wiley, NY, 1983.

[2] R. M. James, "On the use of Fourier series/FFT's in the solution of boundary integral equations for EM scattering", *IEEE Trans. Antennas and Propagation*, vol. 42, no 9, pp. 1309-1316, 1994.

[3] S. V. Boriskina, A. I. Nosich. "Method of an analytical regularization in the problems of wave diffraction by dielectric cylinders of arbitrary cross-sections", *Radio Physics and Radio Astronomy*, vol. 3, no3, 1998, pp. 310-318.

[4] S. N. Vorobiov, S. L. Prosvirnin, "Method of Moments in the scattering of electromagnetic waves by a metallic strip", *Doklady Akademii Nauk Ukrainy*, Kiev, 1984, pp.138-145 (in Russian).

[5] A.Matsushima, T. Itakura. "Singular integral equation approach to electromagnetic scattering from a finite periodic array of conducting strips", *J. of Electromagnetic Waves and Applications*, vol. 5, No. 6, 1991 , pp.545-562.

[6] E. I. Veliev, V. V. Veremey, "Numerical-analytical approach for the solution to the wave scattering by polygonal cylinders and flat strip structures", in M. Hashimoto, M. Idemen and O.A., Tretyakov (Eds.), *Analytical and Numerical Methods in Electromagnetic Wave Theory*, Chapter 10, pp. 471-514, Science House, Tokyo, 1993.

GENERALIZED WIENER-HOPF TECHNIQUE FOR WEDGE SHAPED REGIONS OF ARBITRARY ANGLES

V. Daniele

Dipartimento Elettronica, Politecnico di Torino,
C.so Duca degli Abruzzi 2410129 Torino (Italy)
E-mail:daniele@polito.it

ABSTRACT

A new technique for solving diffraction problems in angular shaped regions is here presented. This technique applies both for impenetrable wedge and penetrable wedges. The functional equations obtained through this technique present different difficulties of solution according to the geometry of the problem. For example for half-planes and impenetrable or isorefractive rigth wedges we deal with classic matrix W-H equations. On the contrary dealing with arbitrary media or with not right wedges, we have to introduce new functional equations that we call generalized Wiener-Hopf equations. This paper describes some properties of the generalized Wiener-Hopf equations.

INTRODUCTION

The Wiener-Hopf technique is a powerful and general method for solving discontinuity diffraction problems. However usually it is assumed that for wedge shaped regions these geometries (except for particular wedge angles) do not allow Wiener-Hopf equations. The aim of this work is the introduction of the Wiener-Hopf technique also for arbitrary angular wedges and for penetrable regions filled with different media. The obtained results are new functional equations that generalize the classic Wiener-Hopf equations. Our method is based on a generalization of the method used to deduce W-H equations for right angle regions. In particular, through the introduction of oblique coordinates, new equations have been obtained, relating the unilateral Fourier transforms of electromagnetic field in two different directions [1].

By using these equations and by imposing the boundary conditions on the interfaces separating the different homogeneous regions, we can obtain the functional equations relevant to every wedge problem involving not penetrable or penetrable media [1]. In order to give an example in the following a wedge with two face impedances excited by an E-polarized plane wave has been considered (Maliuzhinets problem). Let the axis z of a cartesian coordinates system be parallel to the electric field E ($E=E_z$) and the axis x coincident with the symmetry axis of the wedge and directed outside. By introducing as unknowns the following unilater Fourier transforms defined on the positive real semi axis ($x \geq 0$, $y=0$ or $\varphi=0$):

$$V_+(\eta) = \int_0^\infty E_z(x,0)e^{j\eta x}dx, \quad I_+(\eta) = -\int_0^\infty H_x(x,0)e^{j\eta x}dx,$$

where ω, k and μ are the angular frequency, the propagation constant and the permeability in the medium outside the wedge respectively.
The functional equation are [1]:

$$M(\eta(\alpha)) \begin{vmatrix} V_+(\eta(\alpha)) \\ I_+(\eta(\alpha)) \end{vmatrix} = M(\eta(-\alpha)) \begin{vmatrix} V_+(\eta(-\alpha)) \\ I_+(\eta(-\alpha)) \end{vmatrix} \qquad (1)$$

where

$$M(\eta) = \begin{vmatrix} \dfrac{\xi}{-(\xi\cos\Phi + \eta\sin\Phi)z_+ + \omega\mu} & -\dfrac{\omega\mu}{-(\xi\cos\Phi + \eta\sin\Phi)z_+ + \omega\mu} \\[2mm] -\dfrac{\xi}{-(\xi\cos\Phi + \eta\sin\Phi)z_- + \omega\mu} & -\dfrac{\omega\mu}{-(\xi\cos\Phi + \eta\sin\Phi)z_- + \omega\mu} \end{vmatrix} =$$

$$= M(\eta(\alpha)) = \tilde{M}(\alpha) = \begin{vmatrix} \dfrac{\alpha\cos\Phi + \tau\sin\Phi}{-\alpha\ z_+ + \omega\mu} & -\dfrac{\omega\mu}{-\alpha\ z_+ + \omega\mu} \\[2mm] -\dfrac{\alpha\cos\Phi + \tau\sin\Phi}{-\alpha\ z_- + \omega\mu} & -\dfrac{\omega\mu}{-\alpha\ z_- + \omega\mu} \end{vmatrix}, \qquad M(\eta(-\alpha))) = \tilde{M}(-\alpha)$$

and $z_\pm$ are the the normal impedances on the boundaries $\phi = \pm\Phi$ of the wedges, $\xi = \sqrt{k^2 - \eta^2}$, $\tau = \sqrt{k^2 - \alpha^2}$, $\alpha = \alpha(\eta) = \eta\ \sin\Phi + \xi\cos\Phi$, $\eta(\alpha) = \alpha\ \sin\Phi - \tau\cos\Phi$,

$\eta(-\alpha(\eta)) = \eta_2(\eta) = \eta\cos 2\Phi - \sqrt{k^2 - \eta^2}\sin 2\Phi$.

Eq.1 is a particular case of the functional equations in the Fourier domain, that in general may be written in the following form:

$$G(\eta)F_+(\eta) = F_-(a(\eta)) + F_-(b(\eta)) + F_i(\eta) \qquad (2)$$

where $G(\eta)$ (matrix kernel) and $F_i(\eta)$ (source vector) are known functions depending on the complex variable η and F_+ and F_- are the unknown vectors. The substantial difference with respect to the classic Wiener–Hopf equations is the presence in this functional equation of the known mappings $a(\eta)$ and $b(\eta)$. In fact, while the unknown $F_+(\eta)$ is a classic plus function, i.e. regular in the half-plane $Im[\eta] \geq 0$, in the second member $F_-(a(\eta)) = F_-(a)$ is a minus function in the a-plane, i.e.regular in the half-plane $Im[a] \leq 0$, and $F_-(b(\eta)) = F_-(b)$ is a minus function in the b-plane, i.e.regular in the half-plane $Im[b] \leq 0$. We can call the previous equation Generalized Wiener Hopf equation. In some particular cases (half planes or right wedge unpenetrable or isorefractive) we have $a(\eta) = b(\eta) = \eta$ leading to classic W-H equation that can be solved with the factorization technique.

The major advantages of the introduction of these equations is that they characterize all wedge problems involving both unpenetrable regions and penetrable ones even with anisotropic or bianisotropic media filling them[1].

ON THE SOLUTIONS OF GENERALIZED WIENER-HOPF EQUATIONS

Wiener-Hopf technique for solving the classic equations is based on the decomposion and the factorization of generic functions in plus and minus functions (i.e. regular respectively in the half plane $Im[\eta] \geq 0$ and $Im[\eta] \leq 0$). Also dealing with Generalized Wiener-Hopf equations, decomposition and factorization constitute the key for obtaining the solutions. However, whereas the classic decomposition is very easy to obtain, the generalized decomposition is more difficult and in general lead to Fredholm integral equations.

Decomposition
Let consider a function F(η) which is a Fourier transform of a function f(y), and m(η) an analitical function of η regular on a strip containing the real axis of the plane η. The generalized decomposition of a function (with respect the mapping m(η)) consists in getting the two decomposing functions so that:

F(η)= F₊(η)+F₋(m(η))

where the functions F₊(η) and F₋(m(η)) are respectively a plus function in the η plane (i.e. regular in half plane Im[η]≥0) and a minus function in the m plane (i.e. regular in half plane Im[m]≤0). If there are not singularities of F(η) between the real axis Im[η]=0 and the image of Im[m]=0 on the η plane (this condition is not rescrittive), we obtain the following Fredholm integral equation of the second kind for the decomposing F₊(η):

$$F_+(\eta)+\frac{1}{2\pi j}\int_{-\infty}^{\infty}\left(\frac{1}{m(\eta')-m(\eta)}\frac{dm}{d\eta'}-\frac{1}{\eta'-\eta}\right)F_+(\eta')d\eta'=\frac{1}{2\pi j}\int_{\gamma}\frac{F(\eta')}{m(\eta')-m(\eta)}\frac{dm}{d\eta'}d\eta'$$

where γ runs on the real axis η' leaving above the singular point η. Note that the particular case m(η)=η leads to the classic Cauchy decomposition formula.

Factorization
Following the same ideas introduced in the classic factorization we can get to the generalized factorization of scalar kernel G(η)=G₋(m(η))G₊(η), through the logaritmic generalized decomposition: log[G(η)]= ψ₋(m(η)) + ψ₊(η). It yields:

$$G_-(m(\eta)) = e^{\psi_-(m(\eta))}, \qquad G_+(\eta) = e^{\psi_+(\eta)}$$

This factorization technique can be extended also to matrix factorization in many cases.
In particular it is possible to reduce the generalized factorization of rational matrices to scalar decompositions. This allows to factorize arbitrary matrices with Pade' approximations.

Solution of the generalized equations
The process of decomposition and factorization allow us to extend the Wiener-Hopf technique to obtain the solution of the generalized equations:

G(η)F₊(η)= F₋(m(η))+ Fᵢ(η)

In this particular case, the generalized factorization of the kernel G(η) and the generalized decomposition: (G₋(m(η)))⁻¹F₀(η)= X₊(η)+ X₋(m(η)), lead to the solutions:

F₊(η) = (G₊(η))⁻¹ X₊(η),   F₋(m(η))=- G₋(m(η))X₋(m(η))

To conclude it must be observed that always we can reduce the arbitrary generalized equation (2) to Fredholm equations. However this procedure sometime requires a process of matrix factorization.

REFERENCES
[1] V. Daniele: "Generalized Wiener-Hopf technique for wedge shaped regions of arbitrary angles", Rep.1-2000, Dipartimento Elettronica, Politecnico Torino, Jan.2000.

PLANE WAVE DIFFRACTION BY THE RIGHT-ANGLED WEDGE COATED WITH THE THIN BI-ISOTROPIC LAYERS

Sergei G.Vashtalov and Olga A.Dotsenko*

Department of Radiophysics, Tomsk State University
36 Prospekt Lenina, Tomsk, 634050, Russia
E-mail: vash@re.tsu.ru

*Department of Radiophysics, Tomsk State University
36 Prospekt Lenina, Tomsk, 634050, Russia
E-mail: dol@elefot.tsu.ru

ABSTRACT

In this paper, the diffraction problem is considered for the plane electromagnetic wave incident on a right-angled perfectly conducting wedge, whose metallic faces are coated with thin layers of the bi-isotropic materials. Generalized second-order impedance boundary conditions for thin covering is used. We applied the Sommerfeld-Maliuzhinets integral to spectral representation of the total electromagnetic field. The total field must satisfy the Helmholtz equation, the edge condition and the proper conditions at infinity.

INTRODUCTION

The recent years have witnessed of enormous growth in the research activity focusing on the wave interaction with complex materials, namely, with chiral, bi-isotropic and bi-anisotropic media [1]. The scientists elaborate new methods of the calculation for such materials.

In this paper, the diffraction problem is considered for the plane electromagnetic wave incident on a right-angled perfectly conducting wedge, the metallic faces of which are coated with thin layers of the bi-isotropic materials. It is a special case of problem, which was considered in paper [2]. The covering is very thin; therefore it is possible to use generalized impedance boundary conditions for its simulation [3-6], which contains field derivatives above the first order. However, the standard boundary conditions on the edge are not sufficient for the extraction of a unique solution studying the scattering on the objects with edges. Therefore it is necessary to introduce the so-called contact conditions that prescribe certain relations between the field and its derivatives on the edge.

The problem is considered with the help of the modified Maliuzhinets technique [2,4,6]. The Maliuzhinets functional equations are obtained for the transform of the Sommerfeld-Maliuzhinets integral. The general solution of these equations contains three unknown constants, which are chosen from the radiation condition and the contact condition on the edge of the wedge.

FORMULATION OF THE PROBLEM

Let us consider the diffraction of the H-polarized time-harmonic ($e^{-i\omega t}$ time dependence is understood) electromagnetic plane wave $H_z^i(r,\varphi) = exp[-ikr\cos(\varphi - \varphi_0)]$ in an angular region $|\varphi| < 3\pi/4$, where $k = \omega\sqrt{\varepsilon_0\mu_0}$, μ_0 и ε_0 are the free space permeability and

permittivity, respectively. The faces of the wedge $\varphi = \pm 3\pi/4$ are coated with thin layers of bi-isotropic materials, the thickness of which are $d_\pm$. Hereinafter the symbol sequence of kind $\pm$ means that the upper (lower) sign corresponds to the face $\varphi = +3\pi/4$ $\left(\varphi = -3\pi/4\right)$ of wedge. A plane wave is incident in the direction φ_0. In the polar coordinate system (r, φ) the generalized impedance boundary conditions [5] on the faces of the wedge can be expressed as:

$$\left[\mp \frac{1}{ikr} \frac{\partial}{\partial \varphi} - p_\pm \left(1 + \frac{1}{k^2 N_\pm^2} \frac{\partial^2}{\partial r^2} \right) \right] H_z(r, \pm 3\pi/4) = 0 \tag{1}$$

where $p_\pm = ikd_\pm \mu_\pm$, $N_\pm^2 = n_\pm^2 \cos^2 \Theta_\pm - \kappa_\pm^2$, $n_\pm^2 = \varepsilon_\pm \mu_\pm$, $\sin \Theta_\pm = \chi_\pm / n_\pm$, $\varepsilon_\pm$ and $\mu_\pm$ are the complex permittivity and permeability of the layers, $\kappa_\pm \geq 0$ are the chirality parameters, $\chi_\pm \geq 0$ are the non-reciprocity parameters. The total field $H_z(r, \varphi)$ must satisfy the Helmholtz equation, the edge condition and the proper conditions at infinity. Nevertheless, these conditions are not sufficient to solve completely the present boundary problem. It is necessary to add a contact condition. The contact condition is required for the boundary conditions (1), which is possible to write in the following form [7]:

$$\lim_{r \to 0} \left[\frac{1}{t_+} \frac{\partial}{\partial r} H_z(r, +3\pi/4) - \frac{1}{t_-} \frac{\partial}{\partial r} H_z(r, -3\pi/4) \right] = 0 \tag{2}$$

where $t_\pm = N_\pm^2 / p_\pm$.

METHOD OF SOLUTION

We applied the Sommerfeld-Maliuzhinets integral [8] to spectral representation of the z-component of the total magnetic field in the form

$$H_z(r, \varphi) = \frac{1}{2\pi i} \int_\gamma e^{-ikr \cos \alpha} S(\alpha + \varphi) d\alpha, \tag{3}$$

where γ is the double loop Sommerfeld contour. From boundary conditions (1) the system of functional equations is obtained:

$$a_\pm(\alpha) S(\alpha + 3\pi/4) - a_\pm(-\alpha) S(-\alpha + 3\pi/4) = 2C_\pm \sin \alpha \tag{4}$$

where $C_\pm$ are arbitrary constants. Variable coefficients $a_\pm(\alpha)$ in this system are polynomials of $\sin \alpha$ and contained the complex Brewster angles, which are given in paper [2]. The general solution of the system of equations (4) can be written in the following form:

$$S(\alpha) = \left[\sigma(\alpha, \varphi_0) + C_+ S_+(\alpha) + C_- S_-(\alpha) + C \Psi(\alpha) \right] \Psi(\varphi_0) \tag{5}$$

where C is an arbitrary constant. The function $\sigma(\alpha, \varphi_0)$ is the meromorphic solution of the corresponding homogeneous system (4) with $a_\pm(\alpha) = 1$. The functions

$$S_\pm(\alpha) = \mp \frac{\mu}{2\pi i} \int_{-i\infty}^{i\infty} \frac{\sin \mu \tau}{\cos \mu \tau \mp \sin \mu \alpha} \frac{\sin \pi d \tau}{a_\pm(\tau) \Psi(\tau \pm \Phi)} \tag{6}$$

are the partial solutions of the non-homogeneous system (4), regular in the strip $|Re\alpha| < 3\pi/4$.

The function $\Psi(\tau)$ is combination of special meromorphic Maliuzhinets functions [8], which

depend on the complex Brewster angles. Maliuzhinets function, for angle $\varPhi = 3\pi/4$, has of importance $\varPsi_{3\pi/4}(\alpha) = \left(4\cos^2\frac{\alpha}{6} - 1\right)\!/3\cos\frac{\alpha}{6}$.

CONCLUSIONS

The problem, which we have considered is an example of a bi-isotropic conducting wedge, included angle for which, the exact solution can be found for a plane wave at normal incidence. From the boundary conditions, using Maliuzhinets theorem, we obtained a system of functional equations for the angular spectral function. The total solution of this system is a combination of three arbitrary constants and a special meromorphic Maliuzhinets functions, which contained the Brewster angles. The arbitrary constants are chosen from a system of linear algebraic equations. In conclusion we have computed the constants, which are the solution of the system of algebraic equations.

REFERENCES

[1] Tretyakov, S.A. (1994) Electrodynamics of complex media: chiral, bi-isotropic and some bi-anisotropic materials, *Radiotekhnika i elektronika*, **Vol.39 no. 10**, pp. 1457-1470 (in Russian)

[2] Vashtalov, S.G. and Fisanov, V.V. (1997) Plane wave diffraction by the wedge coated with the thin bi-isotropic layers. In: *Advances in Complex Electromagnetic Materials, ed. by A. Priou et al.* Dordrecht: Kluver. Pp. 201-206.

[3] Senior, T.B.A. and Volakis, J.L. (1989) Derivation and application of class of generalized boundary conditions, IEEE *Trans.*, **Vol. AP-37 no. 12**, pp. 1566-1572

[4] Osipov, A.V. (1994) General solution for a class of diffraction problems, *J.Phys.A: Math.Gen.,* **Vol.27**, pp. L27-L32

[5] Tretyakov, S.A. (1994) Approximate boundary conditions for a thin bi-isotropic slab. *Radiotekhnika i Electronika,* **Vol.39 no 2**, pp.184-192 (in Russian)

[6] Abbaspur-Tamijani A. and Safavi-Naeini. S. (1998) Electromagnetic wave diffraction by a multi-layer coated wedge: normal incidence. IEEE Antennas and Propagation Society Int. Symp. Atlanta, Georgia, **Vol.3**, pp. 2148-2151

[7] Rojas R.G., Ly H.C., Pathak P.H. (1991) Electromagnetic plane wave diffraction by a planar junction of two thin dielectric/ferrite half planes. Radio Sci., **Vol. 26 no 3**, pp. 641-660.

[8] Maliuzhinets, G.D. (1958) Excitation, reflection and radiation of surface waves from a wedge with given face impedances. DAN USSR, **Vol.121 no 3**, pp.436-439 (in Russian)

DIFFRACTION PROBLEMS FOR AN ELECTROMAGNETIC WAVE ON A STRIP AND FOR ELASTIC WAVE ON A DEFECT IN COMPARISON

Gousenkova A.A.

Kazan State University

P.O.Box 234 Kazan, 420503, Russia, E-mail: pnb@ksu.ru

ABSTRACT

Diffraction problems for an electromagnetic wave on an ideally conducting infinitely thin metallic strip, placed on the media interface of two homogeneous isotropic dielectric media, and diffraction problems for an elastic wave on a defect in the form of a split or a thin inclusion, disposed on the media interface of two homogeneous isotropic elastic media, in the case of the two-dimensional field are considered. The formulations and the methods of solving these problems are given in comparison. It is shown that the most similar are the diffraction problems, in which the number of the wave modes propagated in the medium coincides.

FORMULATION OF THE PROBLEM

We will consider diffraction problems for an electromagnetic TE-wave on an ideally conducting infinitely thin metallic strip $\{ z = 0, \alpha < x < \beta \}$, placed on the media interface of two homogeneous isotropic dielectric media, and diffraction problems for an elastic wave on the defect in the form of a split or a thin inclusion $\{ z = 0, \alpha < x < \beta \}$, disposed on the media interface of two homogeneous isotropic elastic media. Assume that the body forces are absent. Let us consider the plane problem when the field is two-dimensional ($\partial / \partial y = 0$), omitting the time factor e^{-ikt}. The incident field for $z > 0$ and for $z < 0$ is given. We will search the field, arising in the diffraction for a TE-wave and an elastic wave on a strip and on a defect, respectively.

It is possible to consider diffraction problems in the case of an electromagnetic and elastic medium from common mathematical point of view, in spite of differences of physical nature. To solve diffraction problems we will use the method of the Fourier transform in the class S'.

Diffraction problems in the case of one type of waves. It is well known (see e.g. [1]), that there is one type of waves in a homogeneous isotropic dielectric medium and at the antiplane deformation in a homogeneous isotropic elastic medium. Therefore we will at first consider the plane diffraction problem for the TE-wave on the strip and the antiplane diffraction problem for the elastic wave on the defect.

In the case of the antiplane deformation on the assumptions for the unique non-zero component $w(\cdot, \cdot)$ of the displacement vector we have the Helmholtz equation

$$\frac{\partial^2 w}{\partial x^2} + \frac{\partial^2 w}{\partial z^2} + k^2(z)w = 0, \quad k(z) = \{k_+, \ z > 0; \ k_-, \ z < 0\}. \tag{1}$$

To solve the diffraction problem it is necessary to find a solution of (1) for $z > 0$ and for $z < 0$ in the class $\tilde{S}'$ of outgoing from the straight line $z = 0$ into the half-planes $z > 0$ and $z < 0$ solutions [2], satisfying the conditions of the media interface

$$\frac{\partial w}{\partial z}(x,0 \pm 0) + \frac{\partial w_0}{\partial z}(x,0 \pm 0) = 0, \quad x \in (\alpha, \beta),$$

$$[w(x,z)]\big|_{z=0} = 0, \qquad \left[\frac{\partial w}{\partial z}(x,z)\right]\Bigg|_{z=0} = 0, \quad x \notin (\alpha, \beta), \qquad (2)$$

where $w_0(\cdot,\cdot)$ is the incident wave,

$$[w(x,z)]\big|_{z=0} = w(x,0+0) - w(x,0-0), \qquad \left[\frac{\partial w}{\partial z}(x,z)\right]\Bigg|_{z=0} = \frac{\partial w}{\partial z}(x,0+0) - \frac{\partial w}{\partial z}(x,0-0).$$

In order to find the field, arising by the diffraction of the elastic wave on the defect, it is necessary to consider two auxiliary problems [2], [3]: the Cauchy problem for the equation (1) in the half-plane $z > 0$ with the boundary conditions

$$w(x,0) = w_0(x), \qquad \frac{\partial w}{\partial z}(x,0) = w_1(x), \quad x \in R$$

and the jump problem for the Helmholtz equation at the plane z with the conditions

$$[w(x,z)]\big|_{z=0} = a(x), \qquad \left[\frac{\partial w}{\partial z}(x,z)\right]\Bigg|_{z=0} = b(x), \quad x \in R.$$

One can obtain an integral equation equivalent to the diffraction problem for the elastic time harmonic wave on the defect in the case of the antiplane deformation

$$\frac{i}{2\pi}\int_\alpha^\beta a(t)\int_{-\infty}^{+\infty} \frac{\gamma_+(\xi)\gamma_-(\xi)}{\gamma_+(\xi)+\gamma_-(\xi)}\exp(i\xi(t-x))d\xi dt = -\frac{\partial w_0}{\partial z}(x,0), \quad x \in (\alpha, \beta), \qquad (3)$$

on the assumption that $\dfrac{\partial w_0}{\partial z}(x,0\pm 0) = \dfrac{\partial w_0}{\partial z}(x,0), \quad x \in (\alpha, \beta)$. Then the field, arising by the diffraction of the elastic wave on the defect, is determined by the equality

$$w_\pm(x,z) = \frac{1}{2\pi}\int_\alpha^\beta a(t)\int_{-\infty}^{+\infty} \frac{\pm\gamma_\mp(\xi)}{\gamma_+(\xi)+\gamma_-(\xi)}\exp(\pm i\gamma_\pm(\xi)z + i\xi(t-x))d\xi dt.$$

In the case of the electromagnetic medium on the above assumptions we will search a solution of (1) for $z > 0$ and for $z < 0$ in the class $\tilde{S}'$, satisfying the conditions (2) and

$$w(x,0\pm 0) + w_0(x,0\pm 0) = 0, \quad x \in (\alpha, \beta).$$

The diffraction problem for the TE-wave on the metallic strip is solved analogously to the considered diffraction problem for the elastic wave on the defect. The integral equation equivalent to the problem, similar to (3), is obtained in [2].

Diffraction problems in the case of two types of waves. It is well known that there are two types of waves in a homogeneous isotropic elastic medium in the general case. Oscillatory processes in an elastic medium are more complicated than in an electromagnetic medium and they are accompanied by mutual transformations of longitudinally and lateral waves, if a body has the boundary.

It is possible to show that the diffraction problem for the elastic time harmonic wave on the defect, coupling in the homogeneous isotropic elastic medium, when there are two types of waves, but the boundary conditions for the longitudinally and lateral potentials are separated, is reduced to the two considered diffraction problems [3]. The integral equations are equivalent to the diffraction problem, are similar to the equations of the diffraction problem for an electromagnetic wave on the unclosed plane cylindrical screens, located in one plane, obtained in [4].

Consider the diffraction problem for an elastic wave on the defect in the case of different media. The boundary conditions for the longitudinally and lateral potentials are not separated, therefore it is conveniently to use the formulation of the problem in the displacements. To

solve the problem it is necessary to find a solution of the Lame equations

$$(\lambda(z) + 2\mu(z))\frac{\partial^2 u}{\partial x^2} + (\lambda(z) + \mu(z))\frac{\partial^2 v}{\partial x \partial z} + \mu(z)\frac{\partial^2 u}{\partial z^2} + \rho(z)k^2(z)u = 0,$$

$$\mu(z)\frac{\partial^2 v}{\partial x^2} + (\lambda(z) + \mu(z))\frac{\partial^2 u}{\partial x \partial z} + (\lambda(z) + 2\mu(z))\frac{\partial^2 v}{\partial z^2} + \rho(z)k^2(z)v = 0,$$

for $z > 0$ and for $z < 0$ in the class $\tilde{S}'$, satisfying the conjugation conditions

$$u(x, 0 \pm 0) + u_0(x, 0 \pm 0) = 0, \quad v(x, 0 \pm 0) + v_0(x, 0 \pm 0) = 0, \quad x \in (\alpha, \beta),$$

$$[u(x, z)]\big|_{z=0} = 0, \quad \left[\frac{\partial u}{\partial z}(x, z)\right]\bigg|_{z=0} = 0, \quad [v(x, z)]\big|_{z=0} = 0, \quad \left[\frac{\partial v}{\partial z}(x, z)\right]\bigg|_{z=0} = 0, \quad x \notin (\alpha, \beta).$$

Here $u(\cdot, \cdot)$, $v(\cdot, \cdot)$ are the displacement components, the Lame constants $\lambda(\cdot)$, $\mu(\cdot)$ and the density $\rho(\cdot)$ are determined analogously to $k(\cdot)$; $u_0(\cdot, \cdot)$, $v_0(\cdot, \cdot)$ determine the incident field. Two integral equations equivalent to the plane diffraction problem for the elastic time harmonic wave on the defect are obtained in [3] by the method used by us for solving the diffraction problem in the case of the antiplane deformation.

In [5], integral equations with logarithmic singularities in the kernels of the static problems of the plane elasticity theory for bodies with defects are solved numerically by the Bubnov-Galerkin method. It is possible to use this method also to solve the diffraction problems, the integral equations of which have a logarithmic singularity in the kernels.

Note that if there are points in an electromagnetic medium with identical physical characteristics, then in the case of an elastic medium, by the presence of two wave modes, this method is true only under a certain condition [1].

It is well known that there are not longitudinal waves in the Maxwell theory. However, lateral waves have a polarization: the TE- and TM-polarized waves are considered. For lateral waves in an isotropic medium one distinguishes horizontal and vertical polarizations: the SH- and SV-waves are considered, respectively. In the case of a homogeneous anisotropic electromagnetic or elastic medium the problem becomes more complicated. This is associated with an increase of the number of wave modes.

Thus, the most similar are the diffraction problems in the case of electromagnetic and elastic media, in which the numbers of wave modes coincide. Note that the general approach to the diffraction problems in the case of elastic and electromagnetic media is possible because of the consideration of general diffraction problems, scattered waves are not introduced from physical considerations.

REFERENCES

[1] Grinchenko V.T., Meleshko V.V., Time Harmonic Oscillations and Waves in Elastic Bodies, Kiev: Naukova dumka, 1981 (in Russian).
[2] Pleshchinskaya I.E., Pleshchinskii N.B., The Cauchy problem and potentials for elliptic partial differential equations and some of their applications, Advances in Equations and Inequalities (A.E.I.) (ed. J.M. Rassias), Athens, Greece, 1999.
[3] Gousenkova A.A., Plane diffraction problem for elastic wave on a defect (in preparation) (in Russian).
[4] Il'inskii A.S., Smirnov Yu.G. Diffraction for Electromagnetic Waves on Conducting Thin Screens (Pseudodifferential Operators in Diffraction Problems), Moscow, IPRJR, 1996.
[5] Gousenkova A.A., Pleshchinskii N.B. Integral equations with logarithmic singularities in the kernels of the boundary value problems of the plane elasticity theory for domains with a defect, Appl. Math. and Mech, 2000, V. 64, No. 1, 137-144 (in Russian).

ON THE SOMMERFELD REPRESENTATION

V.Daniele [1], M.G. Floreani [2], R.E. Zich[2]

[1] Politecnico di Torino, Dip. Elettronica, c.so Duca degli Abruzzi 24, 10129 Torino

[2] Politecnico di Milano, Dip. Elettrotecnica, Piazza Leonardo da Vinci 32
20133 Milano, Italy. E-mail: daniele@polito.it

ABSTRACT
The Sommerfeld integral is a very important field representation particularly in the electromagnetic problems involving angular shaped regions. For example, we recall that even the powerful Maliuzhinets method is based on the use of Sommerfeld integral. However, although it has been widely studied and used, many questions are still open and in particular it is not perfectly clear when it is possible to apply it and when it is not. Here, we deduce the Sommerfeld integral starting from the inverse Laplace transform of the field satisfying the wave equation. It is shown that, for this purpose, it is necessary to know in detail the properties of the singularities in the spectral domain.

INTRODUCTION
Suppose that an electromagnetic field, $E_z(\rho,\varphi)$, is defined in an homogeneous arbitrary angular region with propagation constant k. We can introduce the unilateral Fourier transform $V_+(\eta)$ (or Laplace Transform) of this field:

$$V_+(\eta,\varphi) = F_+\left[E_z(\rho,\varphi)\right] = \int_0^\infty E_z(\rho,\varphi)e^{j\eta\rho}d\rho \qquad (1)$$

and the integral Fourier representation:

$$E_z(\rho,\varphi) = \frac{1}{2\pi}\int_\gamma V_+(\eta,\varphi)e^{-j\eta\rho}d\eta \qquad (\rho \geq 0) \qquad (2)$$

The function $V_+(\eta,\varphi)$ is a plus function as it implies the regularity on the halfplane above the Bromwich contour γ (Fig.1a). We have 'a priori' no knowledge of the singularities on the halfplane under that contour. These may be branch points and discrete singularities (in Fig.1a we show a cut corresponding to the branch point $\eta= k$). The plane-wave poles are particularly important and they are all on the segment joining the branch points $-k$ and k. In all the cases of practical interest, $V_+(\eta,\varphi)$ is a solution of a functional equation whose coefficients depend on the ξ variable defined by:

$$\xi = \sqrt{k^2 - \eta^2} \qquad (3)$$

Ambiguities can be avoided making a unique definition of this double-value function by choosing one of the two branches. We choose the branch so that $\xi=k$ for $\eta=0$ and the branch lines so that $Im[\xi]\leq 0$ in all the η plane, this means to assume arcs of equilateral hyperbola (Fig.1a) as the conventional branch lines in the η-plane. We say that this branch of the double-value function ξ is the proper one (the other one is the improper branch). It is useful to imagine the η-plane as a two-sheeted complex plane with branch cuts providing the means of passing from one sheet to the other. The sheet where ξ assumes the proper value will be called in the following "proper sheet".
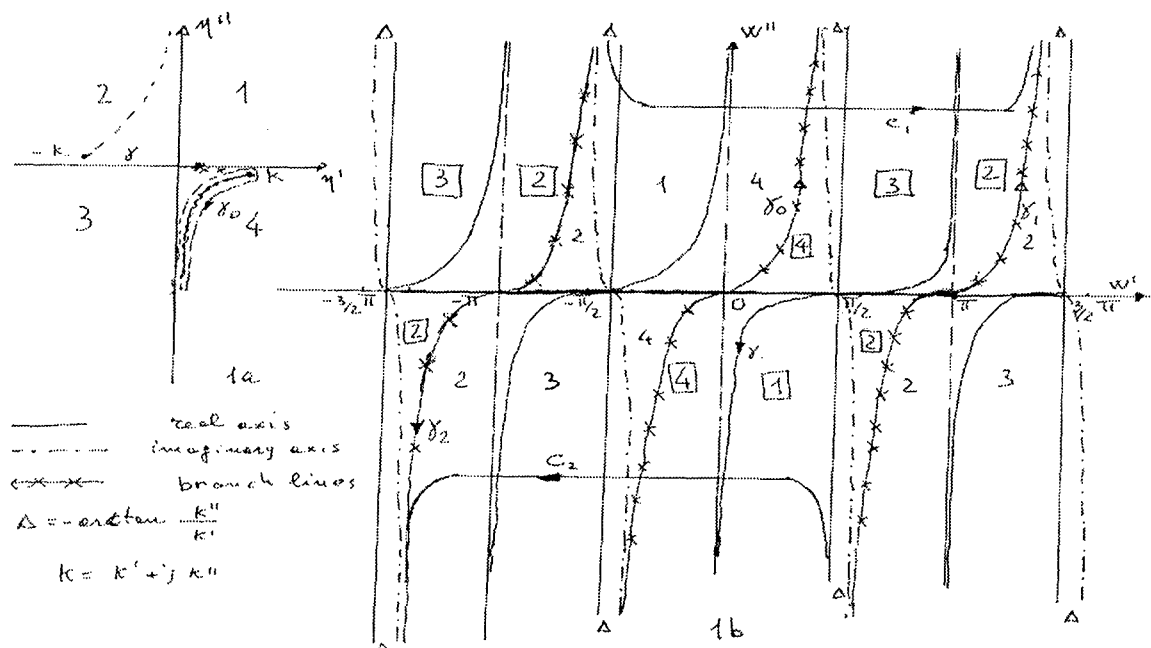
Fig 1

a : η-plane.
b : w-plane.

DEDUCTION OF THE SOMMERFELD INTEGRAL

In order to relate the Fourier representation (2) with the Sommerfeld integral, it is necessary to make some assumptions about the singularities of $V_+(\eta,\varphi)$: a) $+k$ is the only branch point, b) the number of the poles is finite and they are $(-k, k)$ on the proper quadrant 4 of the η-plane (Fig.1a). These assumptions form a sufficient condition for the Sommerfeld representation to hold. We can deform the Bromwich contour γ on the closed line γ_0 surrounding the conventional branch line relevant to k (Fig.1a). It follows:

$$E_z(\rho,\varphi) = \frac{1}{2\pi}\int_{\gamma_0} V_+(\eta,\varphi)e^{-j\eta\rho}d\eta - j\sum_i \operatorname{Re} s(V_+(\eta_i,\varphi)e^{-j\eta_i\rho}) \qquad (4)$$

where the minus sign in front of the residues follows from the clock direction of the half circumference closing the real axis in the lower halfplane. Note that $\xi = \sqrt{k^2 - \eta^2}$ is real on γ_0. In particular, it is negative on the right border of the branch line and positive in the left border. Let us introduce now the w plane (Fig.1b):

$$\eta = k\,\mathrm{Cos}[w], \quad \xi = k\,\mathrm{Sin}[w] \qquad (5)$$

where $k = k' + j\,k''$, $k'' < 0$. With this mapping both the proper and improper sheets of the η-plane lie down the w-plane. In particular in the range $-\pi \le \mathrm{Re}[w] \le \pi$, the improper sheet $(\mathrm{Im}[\xi] \ge 0)$ maps to the regions denoted with 1,2,3 and 4 whereas the proper sheet to the regions with the same number in $\langle$ (Fig.1b). Note that the segment of the real axis defined by $0 \le w \le \pi$ belongs to the proper sheet whereas the segment of the real axis defined by $-\pi \le w \le 0$ belongs to the improper sheet. Taking into account the relation

$$(6) \quad w = \mathrm{ArcCos}[\eta/k] = w' + j\,w'' = -j\,Log[\frac{\eta + j\sqrt{k^2 - \eta^2}}{k}]$$

the transformation (5) maps any point of the η-plane to infinite points. In the range $-\pi \leq$ Re[w]$\leq \pi$, they are only two and differ by sign. Hence, one of them lies is in the image of the proper sheet and the other in the image of the improper sheet. The position of the poles of $V_+(\eta,\varphi)$ means that for $-3\pi/2 \leq$ Re[w]$\leq 3\pi/2$ we can have poles in the region 4 in $\langle$ and on the real segment $0\leq$Re[w]$\leq \pi$. Under the mapping $\eta \rightarrow w$, (4) becomes:

$$E_z(\rho,\varphi) = \frac{1}{2\pi}\left[\int_{\gamma_0} f[w,\varphi]e^{-jkCos[w]\rho}dw + 2\pi j \sum_i \text{Re}\, s(f[w,\varphi])_i \, e^{-jkCos[w_i]\rho})\right] \qquad (7)$$

$$f(w,\varphi) = k\, V_+(k\cos[w,\varphi])\, Sin[w], \qquad (8)$$

We now consider two cases. In the first case we suppose that no branch points are present. Then (7) reduces only to residues, the function f(w,φ) is a function of w that is odd and 2π–periodic, and we define the Sommerfeld function s(w,φ) as :

$$s(w,\varphi) = -f(w+\pi, \varphi) \qquad (9)$$

Notice that the poles of s[w,φ] are those of f[w] translated of $-\pi$. Taking into account their positions, if the curves c_1 and c_2 are suitable chosen, the translation of $-\pi$ keeps these poles in the region bounded by γ_1, c_1, γ_2 and c_2 (Fig.1b). Moreover it results that Res[s(w,φ)]$_{w=wi-\pi}= -$Res[f(w,φ)]$_{w=wi}$ and by the residue theorem it is possible to obtain:

$$\int_{\gamma_1+\gamma_2} s[w,\varphi]e^{+jkCos[w]\rho}dw - \int_{c_1+c_2} s[w,\varphi]e^{+jkCos[w]\rho}dw = 2\pi j\sum_i \text{Re}\, s(s[w,\varphi])_{w=w_i-\pi}\, e^{jkCos[w_i-\pi]\rho} = -E_z(\rho,\varphi)$$

However, the periodicity of s(w,φ) means that the first integral vanishes, so that

$$E_z(\rho,\varphi) = \int_{c_1+c_2} s[w,\varphi]e^{+jkCos[w]\rho}dw \qquad (10)$$

If the branch points are present, (8) defines f(w,φ) only if w belongs to the images of the proper sheet (regions with the number in $\langle$ in Fig.1a). One can define f(w,φ) everywhere by using a process of analytic continuation, but this makes f(w,φ) neither odd nor period function of w. In this case we define implicitly s[w,φ] (that is not periodic!) by:

$$f(w,\varphi) = s[w+\pi,\varphi]- s[w-\pi,\varphi] \qquad (11)$$

Non-periodicity of s[w,φ] implies that its poles are those of $f(w,\varphi)$ translated of π and $-\pi$. Again in the region enclosed by $\gamma_1, c1, \gamma_2$ and c_2 we can have only the poles of $f(w,\varphi)$ that are translated of $-\pi$, and the residue theorem leads to (10). The previous result stands for every plus function. In order to relate it to the Sommerfeld integral it is necessary to consider that the field satisfies the wave equation. Then we obtain:

$$f(w,\varphi) = f_1(w+\varphi) + f_2(w-\varphi) \qquad (12)$$

Now we can relate f_1 and f_2 to two functions s_1 and s_2 defined by (9) or (11) and obtain the sought Sommerfeld representation:

$$E_z(\rho,\varphi) = \frac{1}{2\pi}\left[\int_{c_1+c_2} s[w+\varphi]e^{+jkCos[w]\rho}dw\right], \qquad s(w)= s_1(w)-s_2(-w)$$

RADIATION EFFICIENCY OF COUPLED HORIZONTAL ELECTRICAL DIPOLES OVER A LOSSY HALF-SPACE

Peter L. Tokarsky

Kharkiv State Technical University of Radio Electronics
14, Lenin Av., Kharkiv, 61166, Ukraine, Phone: +380 572 409 430, Fax: +380 572 409 113
E-mail: shifrin@kture.kharkov.ua

ABSTRACT

The problem of radiating coupled horizontal electrical Hertzian dipoles, placed close to the plane interface of two dielectric media, is considered. The relations for calculating the mutual impedance, radiation resistance and loss resistance between the dipoles and also the radiation efficiency of antenna array composed of such elements are found. The computation results are discussed.

INTRODUCTION

The study of properties of an antenna placed over a lossy half-space occupies an important place in the antenna theory. However, despite a great number of publications on this subject, the influence of the ground parameters on the antenna element interaction, and on the antenna arrays efficiency has not been adequately investigated. In the papers [1-2], a rigorous impedance approach to the analysis of the radiation efficiency of the coupled vertical dipole antennas close to the air-ground interface is developed. In this work the approach is applied to investigate the similar performances of the horizontal electric dipoles (HED) over lossy half-space.

THEORY

Let us consider an antenna array of N electrical Hertzian dipoles located in a close proximity to the plane interface between two media. The dipoles are centred 33 at the points $Q_n(x_n, y_n, z_n)$ $(n = 1, 2, \ldots, N;\ z_n > 0)$ of the Cartesian coordinate system ($\vec{x}^0, \vec{y}^0, \vec{z}^0$), and their electric dipole moments are $\vec{p}_n = \vec{y}^0 I_n l_n$, where I_n is the n-th dipole current amplitude and l_n is its length. The medium 1 (air), where the dipoles are placed, has the permittivity ε_1, permeability μ_1 and conductivity $\sigma_1 = 0$ and occupies the upper half-space $z > 0$. The medium 2 (earth) with electrical parameters ($\varepsilon_2, \mu_2, \sigma_2$) occupies the lower half-space $z < 0$. The dipole array input power P_{in} can be represented as a sum $P_{in} = P_\Sigma + P_d$, where P_Σ is the power radiated into the upper half-space, i.e. the useful power, and P_d is the power transmitted through the interface and dissipated in the ground, i.e. the lost power [3]. In this case the antenna array efficiency is $\eta = P_\Sigma / P_{in}$. All these powers can be found as:

$$P_{in} = \sum_{m=1}^{N}\sum_{n=1}^{N} P_{mn} = \sum_{m=1}^{N}\sum_{n=1}^{N} I_m R_{mn} I_n^*, \quad P_{\Sigma,d} = \sum_{m=1}^{N}\sum_{n=1}^{N} P_{\Sigma,d\,mn} = \sum_{m=1}^{N}\sum_{n=1}^{N} I_m \Re_{\Sigma,d\,mn} I_n^*, \quad (1)$$

where Z_{mn}, $\Re_{\Sigma mn}$, $\Re_{dmn}$ are, respectively, mutual impedance, mutual radiation and mutual loss resistance [4] between m-th and n-th dipoles, $\Re_{\Sigma mn} + \Re_{dmn} = \mathrm{Re}\{Z_{mn}\} = R_{mn}$.

To obtain the mentioned quantities, we use the plane-wave representation [5] of the electromagnetic fields of the n-th HED as follows: $\vec{E}_n = \vec{E}_{n\infty} + \Delta \vec{E}_n$, $\vec{H}_n = \vec{H}_{n\infty} + \Delta \vec{H}_n$,

where $\vec{E}_{n\infty}$, $\vec{H}_{n\infty}$ are the HED fields above the perfect ground, $\Delta\vec{E}_n$, $\Delta\vec{H}_n$ are correction terms:

$$\Delta E_{n\,x,y,z} = \int_{-\infty}^{\infty}\int_{-\infty}^{\infty}\Delta e_{n\,x,y,z}\, e^{-j\Psi}\, dv_x dv_y ; \qquad \Delta H_{n\,x,y,z} = \int_{-\infty}^{\infty}\int_{-\infty}^{\infty}\Delta h_{n\,x,y,z}\, e^{-j\Psi}\, dv_x dv_y ; \quad (2)$$

$$\Delta e_x = jZ_{01}C\frac{v_x v_y(\gamma_1^2 T_\varepsilon + k_1^2 \tilde{T}_\mu)}{k_1\gamma_1(v_x^2 + v_y^2)}e^{j\Psi_n} ; \qquad \Delta h_x = C\frac{v_y^2 T_\varepsilon + v_x^2\tilde{T}_\mu}{k_1\gamma_1(v_x^2 + v_y^2)}e^{j\Psi_n} ;$$

$$\Delta e_y = jZ_{01}C\frac{v_y^2\gamma_1^2 T_\varepsilon - v_x^2 k_1^2\tilde{T}_\mu}{k_1\gamma_1(v_x^2 + v_y^2)}e^{j\Psi_n} ; \qquad \Delta h_y = -C\frac{v_x v_y(T_\varepsilon - \tilde{T}_\mu)}{v_x^2 + v_y^2}e^{j\Psi_n} ;$$

$$\Delta e_z = Z_{01}v_y T_\varepsilon\, e^{j\Psi_n} ; \qquad \Delta h_z = -jC\frac{v_x}{\gamma_1}\tilde{T}_\mu\, e^{j\Psi_n} ;$$

$$C = \frac{k_1^2 I_n l_n}{8\pi^2} ; \quad T_\varepsilon = \frac{2\gamma_2\varepsilon_1}{\gamma_1\varepsilon_2 + \gamma_2\varepsilon_1} ; \quad T_\mu = \frac{2\gamma_2\mu_1}{\gamma_1\mu_2 + \gamma_2\mu_1} ; \quad \tilde{T}_\mu = \frac{\gamma_1\mu_2}{\gamma_2\mu_1}T_\mu = \frac{2\gamma_1\mu_2}{\gamma_1\mu_2 + \gamma_2\mu_1} ;$$

$$j\Psi = jk_1(v_x x + jv_y y) + \gamma_1 z ; \qquad j\Psi_n = jk_1(v_x x_n + jv_y y_n) - \gamma_1 z_n ;$$

$$k_{1,2} = \omega\sqrt{\tilde{\varepsilon}_{1,2}\,\mu_{1,2}} ; \quad \tilde{\varepsilon}_{1,2} = \varepsilon_{1,2}\left(1 - j\sigma_{1,2}/\omega\varepsilon_{1,2}\right); \quad \gamma_{1,2} = \sqrt{k_1^2 v^2 - k_{1,2}^2} , \quad v = \sqrt{v_x^2 + v_y^2} .$$

Using math expressions (2) by the induced EMF method [6], the mutual impedance between m-th and n-th HED are obtained: $Z_{mn} = Z_{mn\infty} + \Delta Z_{mn}$, where $Z_{mn\infty}$ corresponds to the perfect ground, ΔZ_{mn} is the addition due to real ground properties:

$$\frac{\Delta Z_{mn}}{R_{00}} = -j\frac{3}{2}\int_0^\infty\left(\frac{j\gamma_1}{k_1}T_\varepsilon A + \frac{k_1}{j\gamma_1}\tilde{T}_\mu B\right)e^{-\gamma_1(z_m + z_n)}v\,dv , \qquad (3)$$

where

$$\left.\begin{array}{c}A\\B\end{array}\right\} = J_0(k_1 v\rho_{mn})\left\{\begin{array}{c}\sin^2\varphi_{mn}\\\cos^2\varphi_{mn}\end{array}\right\} + \frac{J_1(k_1 v\rho_{mn})}{k_1 v\rho_{mn}}\cos 2\varphi_{mn} ;$$

$$\rho_{mn} = \sqrt{(x_m - x_n)^2 + (y_m - y_n)^2} ; \quad \varphi_{mn} = \arctan\frac{y_m - y_n}{x_m - y_n} .$$

For determining the mutual loss resistance $\Re_{dmn}$ and mutual radiation resistance $\Re_{\Sigma mn}$ the Poynting vector method is used [1,2]. The obtained results can be expressed in form:

$$\frac{\Re_{dmn}}{R_{00}} = j\frac{3}{2}\int_0^\infty\left(\left[\frac{\gamma_1 - \gamma_1^*}{4k_1}|T_\varepsilon|^2 - \mathrm{Im}\left\{\frac{\gamma_1}{k_1}T_\varepsilon\right\}\right]A + \left[\frac{\gamma_1 - \gamma_1^*}{4k_1}|T|^2 + \mathrm{Im}\{T\}\right]B\right)e^{-\gamma_1 z_n - \gamma_1^* z_m}v\,dv ; \quad (4)$$

$$\frac{\Delta\Re_{\Sigma mn}^{\theta\theta}}{R_{00}} = -j\frac{3}{2}\int_0^1\left(\mathrm{Re}\left\{T_\varepsilon\,e^{-\gamma_1(z_m + z_n)}\right\} + \frac{1}{2}\left(|T_\varepsilon|^2 - T_\varepsilon - T_\varepsilon^*\right)e^{\gamma_1(z_m - z_n)}\right)\frac{\gamma_1}{k_1}A v\,dv ; \qquad (5)$$

$$\frac{\Delta\Re_{\Sigma mn}^{\varphi\varphi}}{R_{00}} = j\frac{3}{2}\int_0^1\left(\mathrm{Im}\left\{T\,e^{-\gamma_1(z_m + z_n)}\right\} + \left[\frac{\gamma_1}{2k_1}|T|^2 - \mathrm{Im}\{T\}\right]e^{\gamma_1(z_n - z_m)}\right)B v\,dv ; \qquad (6)$$

$$\Re_{\Sigma mn} = \Re_{\Sigma mn}^{\theta\theta} + \Re_{\Sigma mn}^{\varphi\varphi} ; \quad R_{00} = 20k_1^2 l_m l_n ; \quad T = \frac{k_1}{\gamma_1}\tilde{T}_\mu .$$

NUMERICAL RESULTS

As an example, the radiation efficiency of the equidistant linear phased antenna array composed of the N HED has been investigated. The array elements are spaced on the z-axis with step $d = \lambda/2$, and the bottom dipole is placed at a distant $h = \lambda/2$ from the interface. It is assumed that currents in the antenna array have the uniform amplitude distribution ($I_n = I_0 = \text{Const}$) and progressive phase distribution. The parameters of the ground are $\varepsilon_2/\varepsilon_1 = 10$, $\sigma_2 = 0.01 (\Omega \cdot m)^{-1}$, $\mu_2/\mu_1 = 1$, frequency is 6 MHz. Fig.1 shows the efficiency of the arrays versus the beam-pointing angle in xOz-plane. As seen, when the beam is scanned within the elevation plane, the antenna array efficiency is varied and its behaviour depends on the number of the elements N. The maximal efficiency values are observed at the evaluation angles $\alpha = 90° - \theta_0 \approx 15° ...45°$,
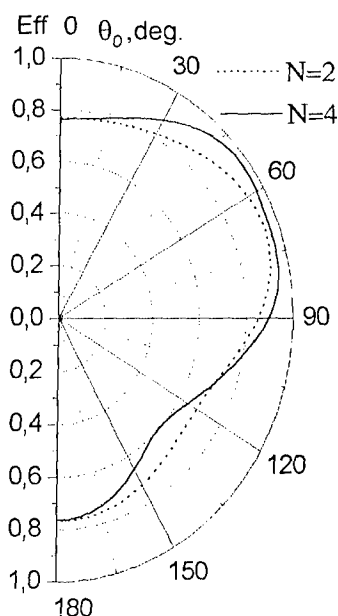
and minimal is at α close to $-30° ...-45°$. The efficiency of the in-phase excited array, whose beam is pointing along the interface, is about $0.85...0.9$. Unfortunately, we have not found in the literature any data on the efficiency for the dipole array above the ground, but only for the single dipole above the earth [3]. Therefore, in order to verify the offered here method, we have computed the efficiency of the single HED and compared it with the similar results in [3]. The agreement between both results was very good.

Fig.1

CONCLUSIONS

The developed approach can be useful for estimation of the power budget for various horizontal antenna structures over the earth, especially for HF antenna arrays.

REFERENCES

[1] P. L. Tokarsky, «Mutual Resistances and Efficiency of Electrical Dipoles Located Near an Interface of Two Media», *Radio Physics and Radio Astronomy*, vol. 3, no. 4, September,1998, pp.434-440. (In Russian).

[2] P. L. Tokarsky, «Radiation Efficiency of Coupled Vertical Dipole Antennas Located Above a Lossy Half-Space», *Proc. of the IIIrd Intern. Conference on Antenna Theory and Techniques* (ICATT-99). Ukraine, Sevastopil, SSTU, 1999, p. 158-159.

[3] P. M. Hansen, «The Radiation Efficiency of a Dipole Antenna Located Above an Imperfectly Conducting Ground», *IEEE Trans. on Antennas and Propagation*, vol. AP-20, no.11, pp.766-770, 1972.

[4] P. L. Tokarsky, «Mutual Coupling in a System of Radiators with Joule Losses», *Radiotekhnika i Elektronika*, vol. 31, no. 9, pp.1717-1723, 1986. (In Russian). English translation: *Soviet Journal of Communications Technology and Electronics*, no. 3, pp. 9-14, 1987.

[5] G. T. Markov, A. F. Chaplin, «Excitation of Electromagnetic Waves», Moscow: Energiya, 1967. (In Russian).

[6] D. M. Sazonov, «Microwave Circuits and Antennas», Mir Publishers Moscow, 1990.

ELECTROMAGNETIC SCATTERING FROM CAVITIES WITH COMPLEX OBJECTS INSIDE

Vladimir N. Kisel', and Anatoly I. Fedorenko

Institute for Theoretical and Applied Electrodynamics,
Joint Institute for High Temperatures, Russian Academy of Sciences
ITAE, Izhorskaya, 13/19, Moscow, 127412, Russia
E-mail: kis@eldyn.msk.ru, fed@eldyn.msk.ru

ABSTRACT

The communication deals with the 3-D electromagnetic model elaboration and numerical investigation of scattering properties of jet engine inlets accounting for real shape of the air duct and presence of the engine first stage to be the main scatterer. The basis of the model is the utilization of equivalence theorem and integral expressions for electromagnetic fields in conjunction with the iterative techniques to improve the accuracy of the surface currents evaluation on the duct walls and termination (e.g. blade structure). Results of numerical investigations are presented together with the indexes of computer program performance for various types of engine intakes including curved ones (S-type) and ducts with complex blade structure inside.

PROBLEM SOLUTION

It is well known that jet engine inlets often do determine the scattering properties of the whole airplane. Different authors devoted their attention to the modeling of scattering from the inlets but numerical algorithm enhancements and elaboration of more adequate electromagnetic models do not miss their actuality. The main difficulties arise because of the model is to provide the correct data on scattered fields for very large size of cavity (from tenths to hundreds wavelengths) with the realistic accounting for the complex termination – the first stage of the engine (e.g., blade structure). Cross section variations and winding of the most modern engine air ducts prevent from using the analytical methods of the theory of guided waves to calculate the electromagnetic wave penetration through the cavity. The required accuracy is difficult to be realized and verified if the algorithm is based upon high frequency asymptotic techniques (like rays). So the basis of developed 3D model is the utilization of equivalence theorem and the integral expressions for electromagnetic fields together with the Kirchhoff approximation (edge diffraction is being neglected).

Surface currents on the cavity walls are calculated via iterations organized similar to [1]

$$\vec{J}_0 = 2\vec{n} \times \vec{H}^i, \quad \vec{J}_m(p) = 2\vec{n} \times \vec{H}^i + 2\vec{n} \times \int_{S_3} \vec{J}_{m-1}(q) \times \nabla G(p,q) dS, m \geq 1, \quad p \in S_3,$$

where $\vec{H}^i$ is the incident field, G is the free space Green's function, $\vec{n}$ is the unit vector of the inner normal to the cavity walls, $\vec{J}_m$ is the vector of the surface current density on the inner surface S_3 defined on the m-th iteration, p and q are observation and integration points, incident field is produced by equivalent electrical and magnetic currents distributed over the inlet aperture S_1. In [1] after the convergence of the process has been achieved the calculated distribution of $\vec{J}$ is used to determine tangent components of scattered field on the inlet aperture S_1. Then the far scattered field is calculated using these components via Kirchhoff's approximation. Despite of many advantages and numerical efficiency of this technique

comparing to direct solution of integral equation the calculation time remains still unsatisfactory. So, if calculations are performed involving ordinary workstation with single Intel Pentium III-733 processor the maximum overall dimensions of the cavity are restricted to several wavelengths provided the time of problem solution is not to exceed several hours. It should be mentioned that the time expenses are proportional to the squared surface of the cavity (i.e. the surface where the electrical and magnetic currents are to be determined) in the best case when the number of iterations does not grow with cavity dimensions enlarging.

In the present work, the necessary numerical efficiency is achieved in the following way. The inner volume of intake is divided to form the waveguide part and the termination, as shown on Fig.1. Then the waveguide part (or the duct) may be considered as the connection of some sections, each of them consisting of inlet, outlet apertures and lateral surface. The quantity of sections depends upon the duct length. Numerical efficiency is increased due to considering the propagation of waves (incident and reflected from the termination) separately for each section. It is appropriate on the high frequencies when Kirchhoff's approximation provides a satisfactory accuracy and the effects of edge diffraction and additional interaction between different sections are relatively

Fig.1.

small. As a result, now the calculation time depends upon the duct length (i.e. sections quantity) linearly. Further improvement to the algorithm efficiency is provided due to special way of integrand calculation. The technique is based upon a linear interpolation of surface currents and rigorous calculation of ∇G in additional nodal points of quadrature formula. This offered to sparse the grid of observation points by $1,5 \div 2$ times (in linear units) thus enlarging maximum overall dimensions of cavity (section) without a loss of accuracy.
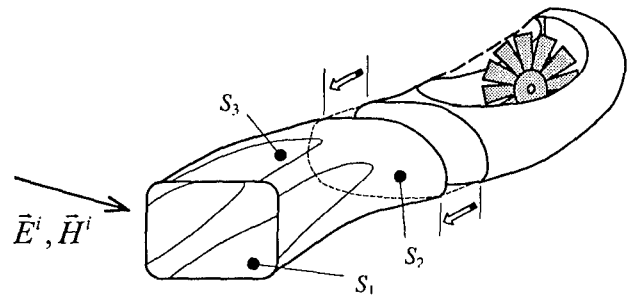
After the waveguide part has been divided by sections each of them consisting of inlet, outlet apertures and lateral surface, we organize a step-by-step calculation of the surface electric and magnetic current densities over the outlet aperture due to predetermined currents on the inlet one for every section. This process is repeated until the termination (with the loading or blade structure) is being reached. The calculation of currents on the inner conducting surface is realized via iterations like in [1]. But the secondary (scattered) field is determined rather on the outlet surface of given section than on inlet one. It is evaluated by integrating the fields of currents distributed over inlet aperture and lateral interior surface. The mentioned algorithm of integrand approximation is also used and iterations themselves are organized in slightly different way (as in more efficient Ziedel's process). The determined tangent components of scattered field on outlet aperture are treated as radiating sources that induce field in the volume of the next section. The excitation of the section with blade structure is calculated in the same iteration process. After the currents on blades and interior lateral surface have been determined, the secondary field is evaluated. Observation points are placed on the input aperture of termination now. Tangent components of the secondary field are the equivalent source to generate the wave propagating along the duct from the termination to the inlet aperture. This process is evaluated in the same way as for the incident wave with the interchanging of inlet and outlet surfaces.

The initial excitement currents on inlet aperture S_i are defined as tangent components of incident plane wave. The scattered field (in the far zone of outer region) is calculated via the integration of tangent components of the secondary wave propagating from the termination. This integration is performed over the same aperture S_i.

NUMERICAL RESULTS

The backscattering diagrams of radar cross section (RCS) per squared wavelength calculated for two different cavities are presented below. RCS of rectangular cavity with straight walls and constant cross section (being the square $6\lambda \times 6\lambda$) and with the length $\approx 25,5\lambda$ is shown in Fig.2. Here the curves 1 and 2 depict the case of conducting flat termination (2 are the test

Fig.2.   Angle of incidence, deg.

Fig.3.   Angle of incidence, deg.
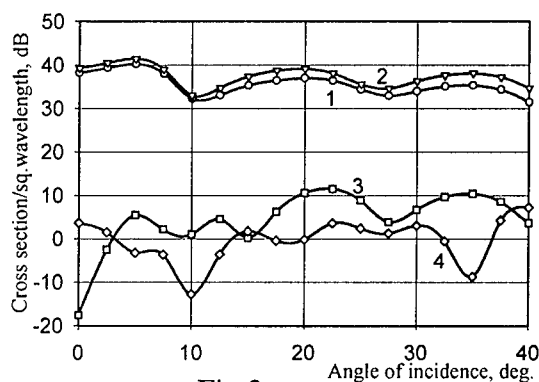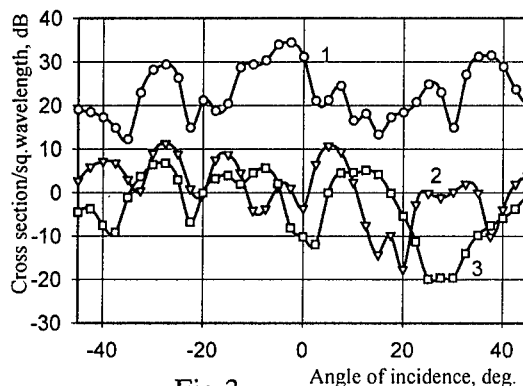
results obtained via usual modal techniques, they are plotted to demonstrate reasonable accuracy of calculations), 3 and 4 are the results for RCS (for co- and cross-polarization correspondingly) if the blade structure is placed instead of termination plate. Blade structure consists of 20 blades ($\approx 0,8\lambda \times 1,6\lambda$), each of them being turned by 45° with respect to axis. The results for S-type duct with varying cross section are shown in Fig.3. The cross section perimeter, the axis length and blade structure geometry are the same as in previous case, but the axis has two bends by 25,5° with the curvature radii 16λ (see legend to fig.3). Here curve 1 plotted for the case of flat metal plate termination, curves 2 and 3 are again the results for RCS of cavity with blade structure placed inside instead of plate (co- and cross polarization data). It is evident that RCS decreases sufficiently in the case of blade structure presence but it is still significant. Another feature to point out is that cross-polarization component in scattered field is close to that for co-polarization.

The calculation time for each of shown diagram (Pentium III-500 based workstation was used) lies between 45-90 minutes. We would like to note in conclusion that similar techniques are realized to treat the cavities with interior walls coated with radar absorbing material.

REFERENCES

[1] Obeleiro-Basteiro F., Rodrigues J.L., Burkholder R.J. An iterative physical optics approach for analyzing the electromagnetic scattering by large open-ended cavities// IEEE Trans. Antennas and Propagation, V.AP-43, no.4, pp.356-361, 1995.
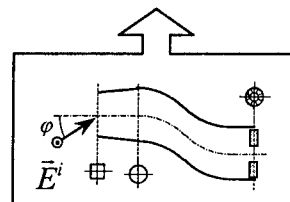
MATHEMATICAL MODELING OF ELECTROMAGNETIC WAVE SCATTERING BY THE COMPLICATED TERRAIN RELIEF

A.Y. Shramkov

Kharkov Military University, Kharkov, Ukraine

ABSTRACT

A calculation method for the plane electromagnetic wave scattering by the complex terrain relief is proposed. The relief model is constructed on the basis of digital maps of terrain using the finite element method. An approximated surface is divided by triangular elements. Scattering problem is solved for every relief element (physical optics approach). Resulted scattered field is calculated by adding the fields scattered by separate relief elements. The example of calculation results for field scattered by the portion of natural ground surface is presented.

A correct solution of many radar and electrodynamics problems is impossible without the information about values of electromagnetic field scattered by the terrain relief at given points of free space.

To solve the problem of electromagnetic waves scattering by the underlying surface with a sufficient accuracy, we offer to use a spatial model of a relief which takes into account its three-dimensional character. The relief model is built on the basis of digital maps of terrain using the finite element method [1]. It represents a collection of relief heights in knots of a regular rectangular grid covering given area.

The approximated surface is divided by triangular elements, vertexes of which are the knots of a grid. The size of triangles should satisfy the following requirements. At first, it should exceed by far the radar wavelength. Secondly, the observation point should be in the far zone of the element. Besides, the triangles' size should ensure maximum adequacy of relief approximation.

It is well known that the main contribution to the scattered field is from the relief plots situated in a main ray of the radar pattern. Therefore, to simplify the calculations without loosing the accuracy it is enough to solve the scattering problem only for relief elements, which are situated inside this area.

Besides, relief plots, which are invisible either from the radar disposition point or from the observation point, are eliminated from analysis. For determination of relief elements visibility, the method of tracing is used [2].

The sizes of the area to be analyzed are so large, that the difference between the wave paths from different relief elements to the observation point can be rather big. Consequently, for every observation point the relief elements are sorted due to boundaries of differenced volume.

Then we obtain solution of the scattering problem for every relief element, taking into account the above mentioned reasons and supposing that the considered area of relief is in the far zone of radar antenna. The incident field represents a nonuniform plane wave modulated by a radar pattern and factors, caused by wave amplitude attenuation when it propagates from the radar to separate relief elements.

On the surface of every element, the equivalent densities of electrical and magnetic currents (in the approximation of physical optics) are found. The relief element surface has electrodynamic parameters of the specific type of terrain ground.

The information about electrodynamic parameters of terrain in the analyzed area can be obtained from the digital maps of terrain.

The obtained current densities on the element surface allow to calculate values of scattered field by using an integral representation of the field derived from the Lorenz lemma [3].

The well known formulas of Kirchhoff allow us to write the expression for the scattered electromagnetic field as

$$
j\omega\vec{p}\vec{E}^{pac}(x_0) = \int_S \left[\vec{H}^\perp(x)\vec{E}_0(x|x_0,\vec{p}) - \vec{H}_0^\perp(x|x_0,\vec{p})\vec{E}(x) \right] ds =
$$

$$
= \int_S \left(\vec{H}^\perp \vec{E}_0 + \vec{E}^\perp \vec{H}_0 \right) ds_x \approx \sum_{i=1}^M \int_{S_i} \left(\vec{H}_i^\perp \vec{E} + \vec{E}_i^\perp \vec{H} \right) ds , \tag{1}
$$

where $\vec{H}_i^\perp$, $\vec{E}_i^\perp$ are the equivalent densities of the electrical and magnetic currents on a surface of separate element in an approximation of physical optics; $\vec{E}_0(x|x_0,p), \vec{H}_0(x|x_0,\vec{p})$ are the field components at the point x, generated by the electric dipole with a vector-moment $\vec{p}$, located at the point x_0.

We shall obtain the asymptotic expressions for the field $\vec{E}_0(x|x_0,p), \vec{H}_0(x|x_0,\vec{p})$ by placing a point x_0 at the infinity in the direction of the vector $\vec{r}^0$

$$
\vec{E}_0(x|x_0,p) \sim \left[\vec{r}_i^0 \times (\vec{p} \times \vec{r}_i) \right] \Omega(r_i) e^{-jk_0(\vec{r}_i^0 \vec{x}_0)} , \tag{2}
$$

$$
\vec{H}_0(x|x_0,\vec{p}) \sim \frac{1}{j\omega\mu_0} \vec{\nabla} \times \vec{E}_0 \sim \Omega(r_i)(\vec{p} \times \vec{r}_i^0)\sqrt{\frac{\varepsilon_0}{\mu_0}} e^{-jk_0(\vec{r}_i^0 \vec{x})} , \tag{3}
$$

where $\Omega(r_i) = \frac{1}{\varepsilon_0} k_0^2 \frac{e^{jk_0 r_i}}{4\pi r_i}$; r_i is a distance from the center of separate triangle to the observation point.

Thus field scattered by single relief element is

$$
\vec{p}\vec{E}^{pac}(\vec{r}^0) = \frac{1}{j\omega} \sqrt{\frac{\varepsilon_0}{\mu_0}} \sum_i \Omega(r_i) \int_{S_i} [(\vec{H}^\perp(x)(\vec{p} - \vec{r}_i^0(\vec{p}\vec{r}_i^0)))\sqrt{\frac{\mu_0}{\varepsilon_0}} +
$$

$$
+ \vec{E}^\perp(x)(\vec{p} \times \vec{r}_i^0)] e^{-jk_0(\vec{r}_i^0 x)} ds_i . \tag{4}
$$

Densities in the $\vec{E}^\perp$, $\vec{H}^\perp$ in the boundaries of the same triangular element are supposed to be constant and equal to the values at one of triangle vertexes. The integration on triangular area will be carried out in the barycentric coordinates.

The field scattered by relief is calculated by adding fields scattered by separate elements. The summation is carried out over the relief elements which are pre-selected. The influence of radar pattern and various distances from radar disposition point to different elements is taken into account.

The example of calculation results for field scattered by the portion of natural ground surface is presented in Fig.1.

The general view of the model of the relief portion which was used for calculations is presented in Fig.2.

Thus, the described method allows to calculate the electromagnetic field scattered by the complex terrain relief at any point of free space.
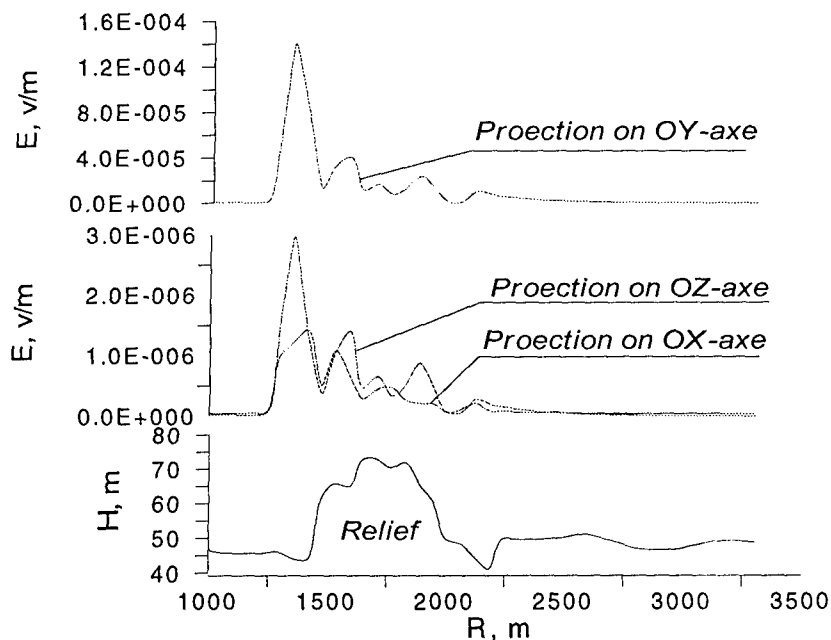
Fig. 1
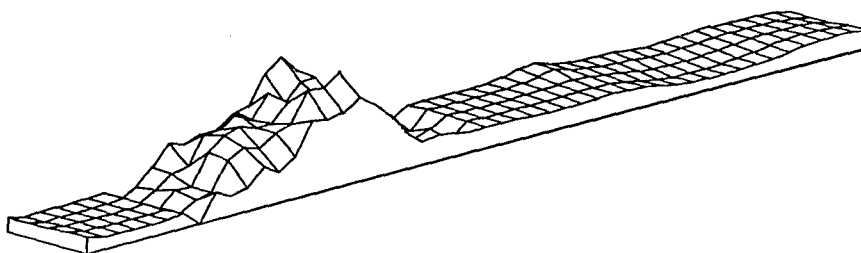
Fig. 2

REFERENCES
[1] Sukharevsky O.I., Batyev V.D., Entys M.Y., Shramkov A.Y. Restitution of relief spatial model. // Scientific works collection. Information Systems. - Kharkov: NAS of Ukraine, Petrov's Academy of Science and Art, Kharkov military university. 1998. - Vol.2 (10). - p. 141-146.
[2] D. F. Rogers Procedural Elements for Computer Graphics. M.: Mir, 1989. (In Russian)
[3] Sukharevsky O.I.   The generalized lemma of Lorenz and integral representation of some electrodynamics problems solution // Radiotechnics and electronics. - 1987. - Vol.11. - p. 2255-2262. (In Russian)

THE SCATTERING BY A PERFECTLY CONDUCTING PARABOLOID OF ROTATION WITH AN ABSORBING COATING OF THE EDGES

S.V. Nechitaylo, S.V.Orekhov, and K.I.Tkachuk

Kharkov Military University, Kharkov, Ukraine

ABSTRACT

In this paper, the plane electromagnetic wave scattering by perfectly conducting paraboloid of rotation with toroidal absorbing coating of edge is considered. The calculation method is based on combination of the solution (in the near-field zone) of the model problem of the plane electromagnetic wave scattering by perfectly conducting wedge with absorbing cylinder on the edge [1] and asymptotic high-frequency methods. Calculation results are presented.

THE TECHNIQUE OF SOLUTION

Calculations were carried out using the technique developed in [2]. The Stratton-Chu-type integral representation was used as a main calculation formula. The asymptotic expressions of this representation in the far-field zone can be written as:

$$\vec{H}^S(\vec{r}^0) = jk_0 \frac{\exp(jk_0 |\vec{x}^0|)}{4\pi |\vec{x}^0|} \vec{I}(\vec{r}^0) \times \vec{r}^0; \tag{1}$$

$$\vec{E}^S(\vec{r}^0) = \sqrt{\mu_0/\varepsilon_0}\, \vec{H}^S(\vec{r}^0) \times \vec{r}^0, \tag{2}$$

where $\vec{r}^0$ is the unit vector of the direction to the observation point, $\vec{x}^0$ is radius-vector of the observation point, μ^0, ε^0 are permeability and permittivity of free space, $k_0 = \omega\sqrt{\varepsilon_0\mu_0}$,

$$\vec{I}(\vec{r}^0) = \int_S \left[\vec{H}^\perp - \sqrt{\varepsilon_0/\mu_0}(\vec{E}^\perp \times \vec{r}^0) \right] \exp\left[-jk_0(\vec{r}^0\vec{x}^0) \right] dS, \tag{3}$$

$\vec{E}^\perp = \vec{n} \times \vec{E}$, $\vec{H}^\perp = \vec{n} \times \vec{H}$, S is an arbitrary closed surface which encloses the scatterer, $\vec{n}$ is the normal to the surface S.

Let us select the surface of integration as a surface coinciding with the paraboloid surface S_1 everywhere except the neighbourhood of edge. In the cross-section orthogonal to the edge the integration surface S_0 is the part of circle with radius ρ_0. $S = S_0 + S_1$ and, respectively, in (3):

$$\vec{I}(\vec{r}^0) = \vec{I}_{S_0}(\vec{r}^0) + \vec{I}_{S_1}(\vec{r}^0) \tag{4}$$

The integral $\vec{I}_{S_0}(\vec{r}^0)$ can be calculated by technique [2], which uses the solution of the model problem of the plane EM wave scattering by perfectly conducting wedge with absorbing cylinder on the edge [1].

Since all geometrical sizes of the surface S_1 are sufficiently large in comparison to λ the contribution of the surface S_1 can be calculated in physical optics approximation. The integrand in $\vec{I}_{S_1}(\vec{r}^0)$ is rapidly oscillating function. Therefore, $\vec{I}_{S_1}(\vec{r}^0)$ can be calculated by the cubature formula for integral of the following form: $I = \int_S \exp[jk\Omega(\vec{r})]f(\vec{r})dS$. For this, the triangulation of the paraboloid surface and its piecewise-plane approximation with transformation to the barycentric coordinates was performed.

Using the above described technique, the calculation of RCS for perfectly conducting paraboloid both with toroidal absorbing coating and without it was carried out. To obtaine stable characteristic (since the RCS of paraboloid strongly depends on sounding wave-length) it is necessary to average the RCS at a certain wave range.

RESULTS OF NUMERICAL CALCULATIONS
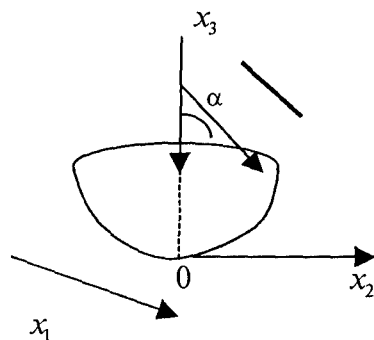
Fig.1.

was 0,5 m, focus was 1m. The wavelength was 0,05m and the average was carried out in the wavelength range 0,03..0,07m. The dependence of $\sigma = \sqrt{RCS}$ on angle *fi* is presented in Figs.2..9. The edge contribution to the total RCS is shown by a dotted line, smooth surfers contribution - by dot-dash line and the total RCS - by solid line. The vector of incident wave was located in the plane $X_2 O X_3$ (Fig.1). *Fi* is the angle

The calculation was performed for paraboloid of the following sizes: height between negative direction of axis OX_3 and the incident wave vector. So, the value of angle *fi*=180 corresponds to the axial sounding of paraboloid. The calculations have shown that at sounding direction deviation of 1-2 degrees from the paraboloid axis the integral $\bar{I}_{S_0}(\bar{r}^0)$ in (4) can be evaluated with a sufficiently good accuracy by the

stationary phase method. In the monostatic and for axial sounding, $\bar{I}_{S_0}(\bar{r}^0)$ was computed by numerical integration over the whole edge. In Figs.2..5 values of σ as function of *fi* are presented for perfectly conducting paraboloid. In Figs.6..9 the result of calculation of σ are presented for paraboloid, whose edge is covered with absorbing material with $\varepsilon = 20 + j0,1$ and $\mu = 1,35 + j0,85$. The calculations were carried out for two types of sounding signal polarization: parallel (Figs.2,3,6,7), perpendicular (Figs.4,5,8,9) to the tangent to the edge at bright point. The analysis of results has shown that at $fi = 90^0..140^0;220^0..270^0$ there are no bright points at paraboloid and the edge dominates the contribution to RCS (Figs.3,5,7,9).
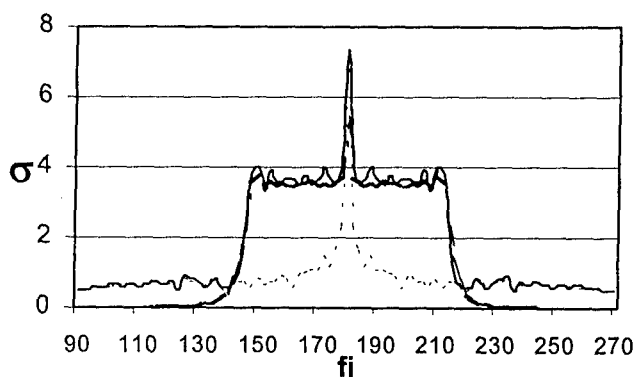
Fig.2
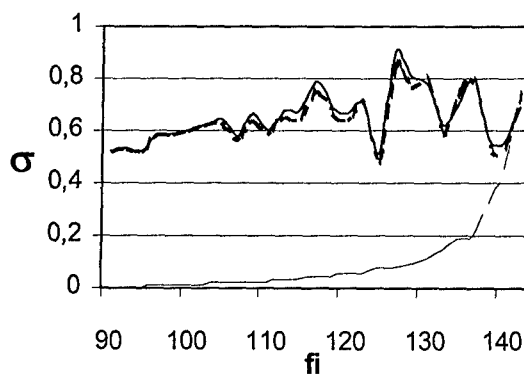
Fig.3
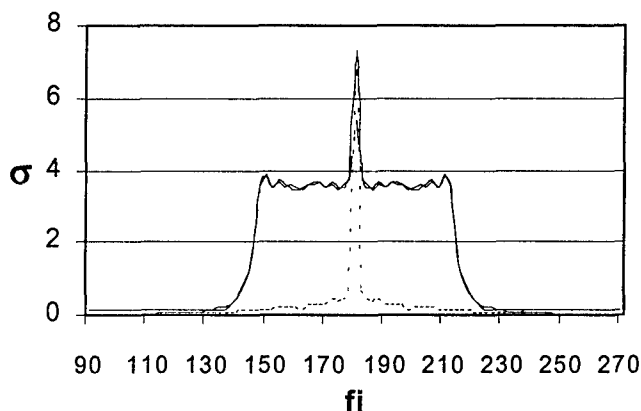
Fig.4
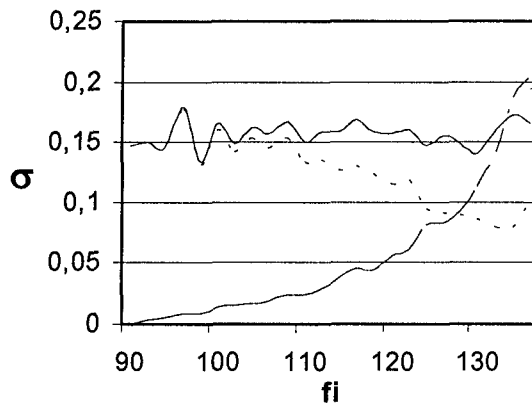
Fig.5
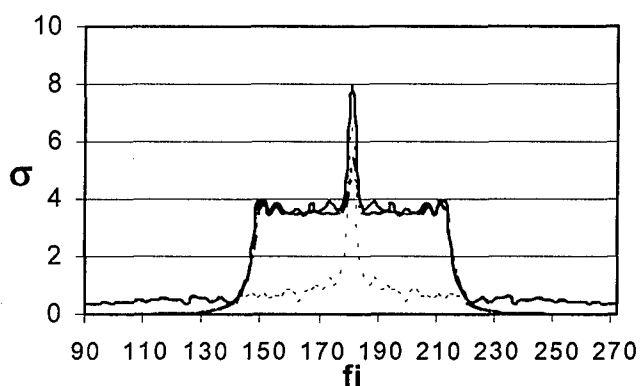
Fig.6
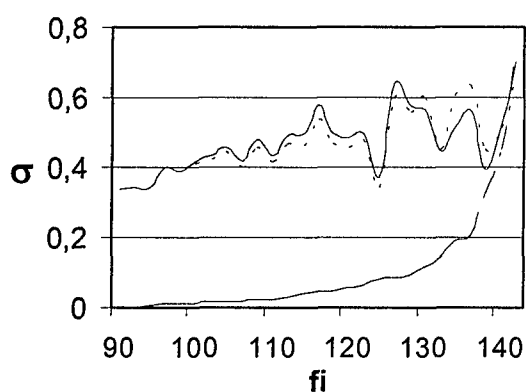
Fig.7
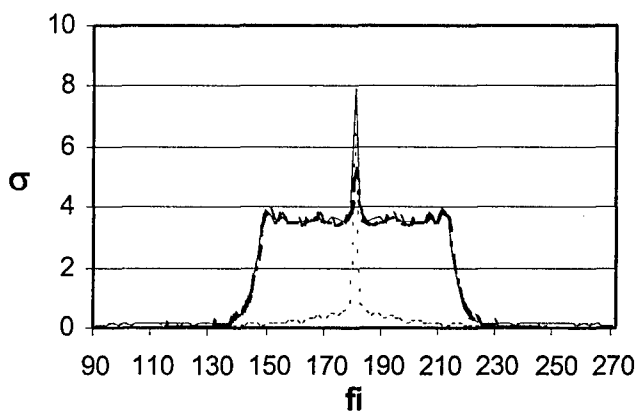
Fig.8
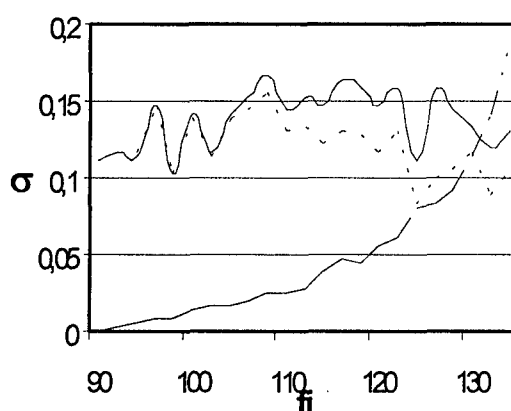
Fig.9

REFERENCES

[1] Sukharevsky O.I., Dobrodnyak A.F.// Izv. Vuzov. Radiofizika.1988.vol.31. №9.p.1074. (In Russian).
[2] Vasilets V.A, Gorelyshev S.A., Sazonov A.Z., Sukharevsky O.I. "Electromagnetic scattering by complex shape objects partly coated with absorbing materials". Report in this conference.

APPROXIMATE METHODS FOR SOLVING PROBLEMS OF THE ELECTROMAGNETIC SCATTERING FROM LOCAL INHOMOGENEITIES AND PARTIAL RADIATION CONDITIONS

A. S. Ilinski

Moscow State University, Moscow, Russia

E-mail: celd@cs.msu.ru

At the present time, problems of the electromagnetic wave theory play an important role in science and technology. Progress in radio astronomy, radio navigation, creation of satellite communication systems, antenna design, etc., is impossible without fundamental investigations of the wave radiation, reflection, and scattering in the presence of an inhomogeneous medium. Development of methods of medium remote probing is also important.

A theoretical study of electromagnetic processes is reduced to an investigation of solutions to the Maxwell equations for an inhomogeneous medium, which satisfy certain boundary conditions imposed on bodies of arbitrary shapes. Usually, an investigation of wave processes is a multiparameter problem, which can be successfully solved using simulation methods. An important class of mathematical models of wave stationary processes which occur in unbounded regions of the three-dimensional space includes models of the electromagnetic wave propagation in waveguides and stationary electromagnetic scattering from a body embedded in a locally inhomogeneous medium. Usually, a problem of the electromagnetic scattering is formulated as follows [1].

In an unbounded space region, medium characteristics are described by permittivity and permeability tensors $\hat{\varepsilon}(M)$ and $\hat{\mu}(M)$ whose components are variable functions of coordinates. The medium can contain a well conducting body D with certain boundary conditions imposed on its surface. The medium characteristics are constant and the medium is homogeneous ($\hat{\varepsilon}(M) \equiv \varepsilon_0$, $\hat{\mu}(M) \equiv \mu_0$) at a finite distance from the surface of body D. The incident field can be produced by external electric and magnetic currents localized at a finite distance from the body or on its surface. In this formulation, the mathematical problem is reduced to solving the Maxwell equations in an unbounded region D_e outside D

$$rot\,\vec{H} = -i\omega\hat{\varepsilon}\vec{E} + \vec{j}$$
$$rot\,\vec{E} = i\omega\hat{\mu}\vec{H}$$

(1)

where $\vec{j}$ is a finite compact function satisfying the boundary condition

$$\left[\vec{n}\vec{E}\right]\Big|_{\partial D} = Z\left[\vec{n}\left[\vec{n}\vec{H}\right]\right]\Big|_{\partial D}$$

(2)

Here, $\vec{n}$ is the inward normal to surface ∂D of the body and Z is the surface impedance specified at each point of ∂D.

At infinity, the fields must satisfy the radiation condition, which provides the single-valuedness of the problem under consideration and the absence of waves arriving from infinity. When boundary ∂D is finite, the radiation condition is formulated in the form of the Sommerfeld—Rellich condition

$$\lim_{R \to \infty} \int_{S_R} \left| \left([\vec{i}_R \vec{E}] + \sqrt{\mu_0/\varepsilon_0} [\vec{i}_R [\vec{i}_R \vec{E}]] \right) \vec{i}_R \right|^2 ds = 0 \qquad (3)$$

where $\vec{i}_R$ is the outward normal to sphere S_R with the center at a fixed point $O \in D$.

In addition to the limit amplitude principle, the limit absorption principle proposed by A. G. Sveshnikov [2], proves to be rather efficient. According to this principle, a unique solution to the stationary problem for a lossless medium is found as a limit solution to the stationary problem for a lossy medium when the absorption factor approaches zero. The limit absorption principle enables one to formulate the analytical radiation conditions in waveguides and in the problems of scattering from infinite periodic surfaces. Applications of the limit principles are analyzed in [3, 5, 6].

For a body of an arbitrary shape and an arbitrary inhomogeneous medium, diffraction problem (1)—(3) cannot be solved analytically and one has to apply numerical methods. In this case, the solution is approximated in an unbounded region. In order to develop efficient numerical methods, it seems natural to solve the problem in a bounded region whose diameter is as small as possible. To this end, the radiation conditions must be imposed on a finite boundary Σ_{R_0} rather than at infinity. It is assumed that, outside this boundary, the medium is homogeneous and the field can be reconstructed analytically. The Sommerfeld—Rellich limit conditions and limit principles cannot be directly used when applying numerical methods in a bounded region. Using these limit conditions and principles, one should formulate the analytical boundary conditions on Σ_{R_0}.

In this situation, the partial radiation conditions are the most suitable. These conditions were introduced [3] and formulated by A. G. Sveshnikov for the exterior diffraction problem [7].

The partial radiation conditions consist in the following. As known, the system of the homogeneous Maxwell equations with constant ε_0 and μ_0 has a countable system of solutions $\{\vec{E}_n, \vec{H}_n\}$ which satisfy the radiation conditions at infinity. This system of solutions can be found using the method of separation of variables in the spherical coordinates. One can enumerate these solutions so that the values $n > 0$ and $n < 0$ correspond to the electric and magnetic waves, respectively. Applying the Vekua theorem, one can prove that system $\{\vec{E}_n, \vec{H}_n\}$ is complete on an arbitrary closed surface and a solution to problem (1)—(3) satisfying the radiation conditions can be represented outside Σ_{R_0} in the form of the expansion

$$\begin{matrix} \vec{E} \\ \vec{H} \end{matrix} = \sum_n a_n \begin{matrix} \vec{E}_n \\ \vec{H}_n \end{matrix} \qquad (4)$$

where coefficients a_n are the same for the electric and magnetic fields. Representation (4) is valid on Σ_{R_0}. Thus, we obtain the condition, which couples the tangential components of the electric and magnetic fields on Σ_{R_0}. The operator coupling the tangential components on Σ_{R_0} is linear but not local. It couples the value of $\vec{E}$ at a point on the surface with the values of $\vec{H}$ at all the points on the surface. When Σ_{R_0} is a sphere, due to the orthogonality

of the spherical wave fields on a sphere, the partial radiation conditions can be written in the form

$$\beta_n^* \int_{\Sigma_{R_0}} \left[\vec{E} \vec{H}_n^* \right]_r ds = \beta_n \int_{\Sigma_{R_0}} \left[\vec{E}_n^* \vec{H} \right]_r ds \, ,$$

where $\beta_n = \int_{\Sigma_{R_0}} \left[\vec{E}_n \vec{H}_n^* \right]_r ds \, .$

On an arbitrary surface, the conditions are of a complicated form (see [1, 2]).

The method of deriving the partial radiation conditions is of principal importance. It consists in the following. In order to solve the boundary-value problem in the region outside surface Σ_{R_0}, the solution is represented analytically. This representation is used for formulating a nonlocal condition on finite surface Σ_{R_0}. This circumstance enables one to formulate the partial radiation conditions for certain regions with the boundaries at infinity. These classes of regions include waveguides, horns, and periodic surfaces.

In [I], A. G. Sveshnikov first formulated and justified the partial conditions for a regular waveguide. Later, the partial radiation conditions were often applied for numerical solutions of diffraction problems using the projection methods [7]. It is important that, in these works, both the exact solution and the approximate solution, which was found using the projection method exactly, satisfied the partial radiation conditions. However, one can use the general principle of formulating the partial radiation conditions in order to obtain discrete approximate partial conditions for mesh functions. To this end, the problem is discretized outside Σ_{R_0}, its solution satisfying the radiation conditions is represented analytically, and a coupling between the discrete representations of $\vec{E}$ and $\vec{H}$ is established on Σ_{R_0}.

REFERENCES
[1] A.G. Sveshnikov, *Direct and Inverse Problems of Electromagnetics, in* Problems of Mathematical Physics and Computational Mathematics, Moscow, Nauka, 1977, p.287 (in Russian).
[2] A.G.Sveshnikov, *On the Radiation Principle*, DAN SSSR, 1950, V.75, No. 5 (in Russian).
[3] A.G. Sveshnikov, *The Limit Absorption Principle for a WaveGuide*, DAN SSSR, 1951, V.80, No.3, P.345 (in Russian).
[4] A.N.Tikhonov and A.A.Samarskii, *On the Radiation Principle*, ZhETPh, 1948, V.18, No.2 (in Russian).
[5] A.G.Sveshnikov and A.S. Ilinski, *A Direct Method for Solving Problems of Scattering from a Local Inhomogeneous Body*, Zhurnal Vychislitel'noi Matematiki I Matematicheskoi Fiziki, 1971, V. 11, No. 4, P.960 (in Russian).
[6] A.S. Ilinski, *A Method for Investigating Problems of Scattering from a Periodic Structure*, Zhurnal Vychislitel'noi Matematiki I Matematicheskoi Fiziki, 1974, V. 14, No. 4, P.1063 (in Russian).
[7] A.G. Sveshnikov, *Scattering from a bounded body*, DAN SSSR, 1969, V.184, No.1 (in Russian).

COMBINED UTILIZATION OF EIGENFUNCTIONS AND INTEGRAL EQUATIONS TO CALCULATE THE FIELDS INSIDE INHOMOGENEOUS DIELECTRIC BODIES

Vladimir N. Kisel', Anna V. Alpatova[*], and Nataly N. Kisel'[*]

Institute for Theoretical and Applied Electrodynamics,
Joint Institute for High Temperatures, Russian Academy of Sciences
127412, ITAE, Izhorskaya, 13/19, Moscow, RussiaE-mail: kis@eldyn.msk.ru
[*]Taganrog State University of Radio Engineering
347928, TSURE, Nekrasovsky, 44, GSP-17A, Taganrog, RussiaE-mail: airpu@tsure.ru

ABSTRACT

The communication deals with the solution of 2-D model problem of excitation of a uniform dielectric circular cylinder with nonuniform dielectric object called 'inclusion' contained within. The aim is reached by a combination of two rigorous techniques, namely eigenfunction expansions (EE) and volume integral equations (IE). The solution leads to a system of linear algebraic equations, whose unknowns represent the field values over the inclusion cross-section. The developed model can be efficiently utilized to solve the electromagnetic compatibility problems, to construct composite materials with predetermined electromagnetic properties and, especially, when investigating the electromagnetic fields influence on biological structures. In the last case, the cylinder is a good model of a bath with matching liquid, where the investigated object is immersed, or a model of some biological structures such as arm, leg, etc.

PROBLEM DEFINITION

Let the circular cylinder with radius R and permittivity ε_2 be placed in the free space which permittivity is assumed to be 1, Fig.1. Axis Oz of cartesian and cylindrical coordinate systems (x, y, z) and (r, φ, z) coincides with the axis of cylinder. The inner region of cylinder contains a nonuniform dielectric inclusion V_j with the permittivity $\varepsilon(x,y)$. The cylinder is illuminated by the plane wave $\vec{E}^i = \vec{i}_z E^i$, the propagation direction of the incident wave is perpendicular to the cylinder axis. The fields outside, inside the cylinder and in the volume of inclusion are to be determined.
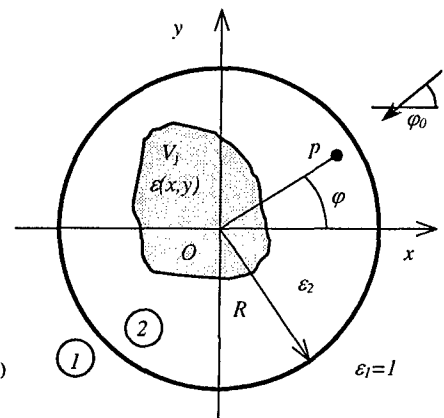
SOLUTION

Let write the incident field as follows

$$E^i = E_0 e^{ik_1(x\cos\varphi_0 + y\sin\varphi_0)} = E_0 e^{ik_1 r \cos(\varphi - \varphi_0)} = E_0 \sum_{n=-\infty}^{\infty} i^n J_n(k_1 r) e^{-in(\varphi - \varphi_0)}$$

Here k_1 is the free space wavenumber, $J_n(.)$ is the Bessel function. The electric field has single z-component. In the region 2 (at $r \leq R$) it can be represented as a sum

$$E = E_0 \sum_{n=-\infty}^{\infty} i^n b_n J_n(k_2 r) e^{-in(\varphi - \varphi_0)} + E^{pol},$$

where k_2 and G_2 are the wavenumber and the Green's function of the unbounded space filled with the substance of region 2, $E^{pol} = k_2^2 \int_{V_j} (\varepsilon - 1) E G_2 dV$ is the field radiated by polarization

currents $j^{pol} = i\omega\varepsilon_0\varepsilon_2(\varepsilon-1)E$. Making use of the superposition principle, the following IE for the field $E(p \in V_j)$ can be derived

$$E - k_2^2 \int_{V_j} (\varepsilon-1)EG_2 dV = E_0 \sum_{n=-\infty}^{\infty} i^n b_n J_n(k_2 r)e^{-in(\varphi-\varphi_0)} . \tag{1}$$

Then we write the fields E and H in region 1 (at $r \geq R$) and use the boundary conditions:

$$E_0 \sum_{n=-\infty}^{\infty} i^n J_n(k_1 R)e^{-in(\varphi-\varphi_0)} + E_0 \sum_{n=-\infty}^{\infty} i^n c_n H_n^{(2)}(k_1 R)e^{-in(\varphi-\varphi_0)} = E_0 \sum_{n=-\infty}^{\infty} i^n b_n J_n(k_2 R)e^{-in(\varphi-\varphi_0)} + E^{pol}\Big|_{r=R}$$

$$E_0 k_1 \sum_{n=-\infty}^{\infty} i^n J_n'(k_1 R)e^{-in(\varphi-\varphi_0)} + E_0 k_1 \sum_{n=-\infty}^{\infty} i^n c_n H_n^{(2)'}(k_1 R)e^{-in(\varphi-\varphi_0)} = $$

$$= E_0 k_2 \sum_{n=-\infty}^{\infty} i^n b_n J_n'(k_2 R)e^{-in(\varphi-\varphi_0)} + k_2^2 \int_{V_j} (\varepsilon-1)E(-\mathrm{rot}_\varphi(\vec{i}_z G_2)\big|_{r=R})dV \tag{2}$$

Making use of G_2 expression in cylindrical coordinate system, the electrical and magnetic fields produced by polarization currents can be written in similar fashion, e.g.

$$E^{pol}\Big|_{r=R} = -\frac{ik_2^2}{4} \sum_{n=-\infty}^{\infty} \left[\int_{S'} (\varepsilon-1)E e^{-in(\varphi_0-\varphi')} J_n(k_2 r')dS' \right] e^{-in(\varphi-\varphi_0')} H_n^{(2)}(k_2 r)\Big|_{r=R} ,$$

where S' is the inclusion cross section. Then S' is divided by M small elements $\{S_j\}_{j=1}^M$ and integral S' is calculated using, say, rectangular quadrature rule. As a result, the convenient expressions to be used in (2) are obtained

$$E^{pol}\Big|_{r=R} = E_0 \sum_{n=-\infty}^{\infty} i^n e_n H_n^{(2)}(k_2 r)\Big|_{r=R} e^{-in(\varphi-\varphi_0)} , \quad i\omega\mu_0 H_\varphi^{pol}\Big|_{r=R} = k_2 \sum_{n=-\infty}^{\infty} i^n e_n H_n^{(2)'}(k_2 r)\Big|_{r=R} e^{-in(\varphi-\varphi_0)}$$

$$e_n = \sum_{m=1}^M E_m d_{nm} , \qquad d_{nm} = -\frac{ik_2^2}{4} i^{-n} \int_{S_m} (\varepsilon_m-1)e^{-in(\varphi_0-\varphi')} J_n(k_2 r')dS' ,$$

where E_m is a field at the center of m-th element (r_m, φ_m) related to E_0, ε_m is the m-th element permittivity related to the permittivity of region 2 matter.
Satisfying (2) term-by-term the following expressions are obtained:

$$J_n(k_1 R) + c_n H_n^{(2)}(k_1 R) = b_n J_n(k_2 R) + e_n H_n^{(2)}(k_2 R) , \tag{3}$$

$$k_1 J_n'(k_1 R) + k_1 c_n H_n^{(2)'}(k_1 R) = k_2 b_n J_n'(k_2 R) + k_2 e_n H_n^{(2)'}(k_2 R) .$$

Solving of (3) to define b_n leads to the expressions

$$b_n = b_n^{(1)} + b_n^{(2)} e_n , \quad \text{where} \quad b_n^{(1)} = A_n / C_n , \quad b_n^{(2)} = B_n / C_n , \quad A_n = \begin{vmatrix} H_n^{(2)}(k_1 R) & H_n^{(2)'}(k_1 R) \\ J_n(k_1 R) & J_n'(k_1 R) \end{vmatrix} ,$$

$$\tag{4}$$

$$B_n = \begin{vmatrix} H_n^{(2)}(k_2 R) & \sqrt{\varepsilon_2} H_n^{(2)'}(k_2 R) \\ H_n^{(2)}(k_1 R) & H_n^{(2)'}(k_1 R) \end{vmatrix} , \quad C_n = \begin{vmatrix} H_n^{(2)}(k_1 R) & H_n^{(2)'}(k_1 R) \\ J_n(k_2 R) & \sqrt{\varepsilon_2} J_n'(k_2 R) \end{vmatrix}$$

These formulae for b_n are substituted into the right side of IE (1). The integral in the left side of (1) is written as a sum that appears after dividing S' и V_j by the same elements S_m and V_m

$$k_2^{\ 2}\int_{V_j}(\varepsilon-1)EG_2dV=\sum_{m=1}^{M}E_m g_{lm}, \quad g_{lm}=k_2^{\ 2}\int_{V_m}(\varepsilon_m-1)G_2(p\in V_l,q\in V_m)dV_q, \quad l=1,2,...,M.$$

The coefficients g_{lm} are calculated analytically in cylindrical coordinate system while the squares S_m are replaced with equivalent circles of radius $a_m=\sqrt{S_m/\pi}$.

Then we write the IE (1) for every observation point p_l, $l=1,2,...,M$ and thus obtain the linear algebraic equations system with respect to the field values at these points and over S_l :

$$E_l-\sum_{m=1}^{M}a_{lm}E_m=f_l, \quad a_{lm}=g_{lm}+\sum_{n=-\infty}^{\infty}i^n d_{nm}b_n^{(2)}J_n(k_2r_l)e^{-in(\varphi_l-\phi_0)}, \quad f_l=\sum_{n=-\infty}^{\infty}i^n b_n^{(1)}J_n(k_2r_l)e^{-in(\varphi_l-\phi_0)}.$$

More convenient expressions are derived through substituting d_{nm}, rearranging the series and relating a_{lm} and B_n to $J_n^{\ 2}(k_2R)$. After the system has been solved (i.e. the fields in the volume of inclusion have been determined) it is possible to calculate b_n from (4), then use (3) to define c_n and evaluate the fields both inside and outside of cylinder.

NUMERICAL RESULTS

The results of test calculations are presented in Fig.2. The reference solution was found via usual eigenfunctions techniques. It is easily seen that the agreement is quite good (curves of the field constant values placed upper are calculated via reported technique, lower ones are obtained using EE). This field distribution is also depicted as a 3D surface. The geometrical parameters and electromagnetic properties are shown in the scheme supplied.
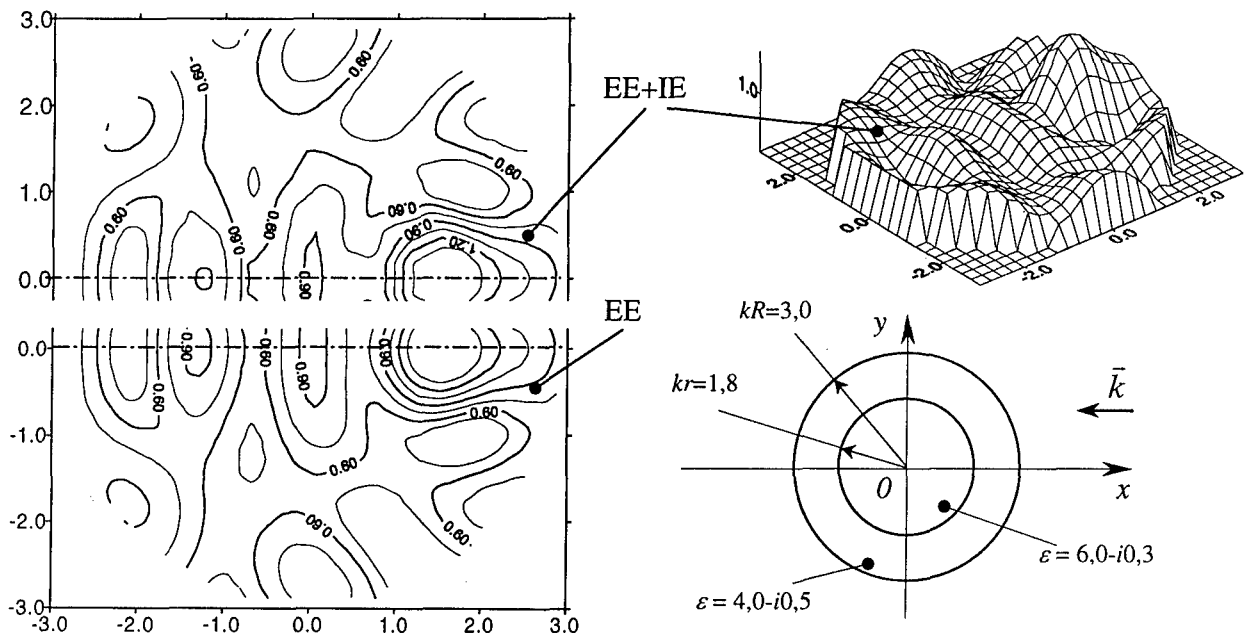
Fig.2.

ELECTROMAGNETIC WAVE SCATTERING FROM AN IMPEDANCE PLANE COVERED WITH A DIELECTRIC LAYER

Yuriy V. Yukhanov

Taganrog State University of Radio Engineering
Antennas & Radio Transmitting Devices, 44, Nekrasovsky, GSP-17A
347928 Taganrog, RUSSIA e-mail: airpu@tsure.ru

ABSTRACT
The problem of a plane wave scattering from inhomogeneous periodic impedance plane, which is covered with a homogeneous layer of lossy dielectric, is solved in rigorous formulation. The solution is obtained in closed analytical form. The wave is scattered from a plane with non-specular reflecting reactance [1] produced by the periodic groove structure. The grooves are filled with a low-loss dielectric and covered with a uniform dielectric layer.

In [1], the problems of synthesis and analysis of a reactance plane, which reflects the incident plane electromagnetic wave in a certain direction, were considered. Real structures realizing impedance covering (as, for example, ribbed structures filled with dielectric), are not perfect, and so they are not reactant due to the presence of losses. The impedance always has nonzero real part. In the antenna applications this is not desirable. In electromagnetic structures purposed for the control of the object scattering characteristics, the real part of impedance (Re $Z \geq 0$) can be an additional parameter, whose optimization enables one to extend functional abilities of such structures. The present work is devoted to the analysis of a plane with passive inhomogeneous periodic impedance Z (ReZ≥0) covered with a layer of homogeneous dielectric, which reflects the incident plane H-polarized wave in a certain direction. Consider an impedance plane S_3 located at ($y=0$) in the Cartesian coordinates. At the height Δ, a parallel homogeneous lossy-dielectric layer ($\varepsilon=\varepsilon'-i\varepsilon''$; $\mu=\mu'-i\mu''$) is located, with thickness d. The impedance structure, which reflects an H-polarized plane wave with the incidence angle $\varphi = \varphi_i^0$ (Fig.1) into the wave with certain reflection angle $\varphi = \varphi_0$, is cut on the surface S_3..According to [1], requested scattering properties are provided by the following reactance:

$$Z(x) = iZ_0 tg\, \eta x, \qquad (1)$$

where $\eta = k(\cos\varphi_i^0 + \cos\varphi_0)$.

Introduction of small losses into the impedance structure (1) (by the substitution $\dot{\eta} = \Gamma(1 - i\alpha)$) leads to the following periodic distribution of impedance:

$$Z(x) = Z_0 \frac{S_1 e^{i\Gamma x} - S_2 e^{-i\Gamma x}}{S_1 e^{i\Gamma x} + S_2 e^{-i\Gamma x} + S_0}, \qquad (2)$$

where $\Gamma = 2\pi/L = k(\cos\varphi_i^0 + \cos\varphi_0)$;

$S_0 = -i\alpha; S_{1,2} = 0.5 e^{\pm\alpha\pi}$; and L is the impedance
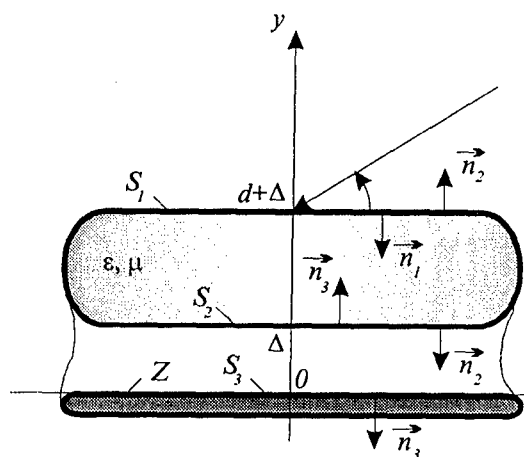
Fig.1

structure period. If $\alpha = 0$, the expression (2) coincides with the formula (1).

Consider the solution of the problem about plane wave

$$H_z^i = e^{ik(x\cos\varphi_i + y\sin\varphi_{11})}$$

scattering on the considered structure.

Represent the magnetic field $H_z(x)$, which is to be found, on the impedance plane $(y=0)$, as follows:

$$H_z(x) = (S_1 e^{i\Gamma x} + S_2 e^{-i\Gamma x} + S_0)H(x)H_z^i(x).$$

Taking into account that the function $H(x)$ is periodic in the interval $[0,L]$, use its expansion in terms of complex Fourier series

$$H(x) = \sum_{m=-\infty}^{\infty} X_m e^{im\Gamma x}.$$

Then, one can obtain, from the system of integral equations for each structure region (Fig.1), with the unknowns as the spectral densities of the components of the electromagnetic field vectors, the following three-diagonal system of linear algebraic equations of band-type, where the unknowns are the expansion coefficients X_m :

$$
\begin{cases}
\dots\dots\dots\dots\dots\dots\dots\dots\dots\dots\dots\dots\dots\dots\dots\dots\dots\dots \\
\dots D_{-1}X_{-2} + S_0 X_{-1} + C_{-1}X_0 \dots\dots\dots\dots\dots = 0; \\
\dots\dots\dots\dots\dots D_0 X_{-1} + S_0 X_0 + C_0 X_1 \dots\dots\dots = I_i; \\
\dots\dots\dots\dots\dots\dots D_1 X_0 + S_0 X_1 + C_1 X_2 \dots = 0, \\
\dots\dots\dots\dots\dots\dots\dots\dots\dots\dots\dots\dots\dots\dots\dots\dots\dots\dots
\end{cases} \tag{3}
$$

where $\quad I_i = 2\dfrac{G_2(-\eta_i)}{G(-\eta_i)} e^{ikd\sin\varphi_i}$; $\qquad D_m = S_1(1 + \dfrac{Z_0}{G_m}\dfrac{P_{2m}}{P_{1m}})$; $\qquad C_m = S_2(1 - \dfrac{Z_0}{G_m}\dfrac{P_{2m}}{P_{1m}})$;

$G_m = \sqrt{\kappa_m^2 - k^2}\,/\,ik$;

$$\begin{Bmatrix} A_m \\ B_m \end{Bmatrix} = G_m \begin{Bmatrix} ch \\ sh \end{Bmatrix}(\gamma_{2m}h) + G_{2m}\begin{Bmatrix} sh \\ ch \end{Bmatrix}(\gamma_{2m}h); \quad P_{1\,2',m} = \dfrac{A_m G_{2m}}{G_m}\begin{Bmatrix} ch \\ sh \end{Bmatrix}(\gamma_m\Delta) + B_m\begin{Bmatrix} sh \\ ch \end{Bmatrix}(\gamma_m\Delta);$$

$G_{2m} = \sqrt{\kappa_m^2 - k_2^2}\,/\,ik\varepsilon_2$; $\kappa_m = -\eta_i - m\Gamma$, $m=0,\pm1,\pm2,\dots$; and $\eta_i = k\cos\varphi_i$; $d=h+\Delta$.

In (3), higher-order harmonics X_m can be expressed through X_{-1}, X_0 и X_1 as follows:

$$X_{m+1} = -\dfrac{S_0 X_m + D_m X_{m-1}}{C_m}, \quad m=1,2,\dots$$

$$X_{m-1} = -\dfrac{S_0 X_m + C_m X_{m+1}}{D_m}, \quad m=-1,-2,\dots, \tag{4}$$

The coefficients of expansion X_{-1}, X_0 и X_1 , in their turn, can be determined by solving the set (3) directly, in the form

$$X_1 = AX_{-1}; \quad A = \dfrac{D_1}{C_{-1}}\dfrac{p}{q}; \quad X_{-1} = \dfrac{2}{D_0 + AC_0 - p\dfrac{S_0^2}{C_{-1}}}; \quad X_0 = -\dfrac{2qS_0 A}{D_1[D_0 + AC_0 - p\dfrac{S_0^2}{C_{-1}}]}, \tag{5}$$

where the factors p and q are expressed after the chain ratios:

$$p = 1 - \cfrac{D_{-1}C_{-2}}{D_{-2}C_{-3}}\cfrac{1}{\cfrac{S_0^2}{D_{-2}C_{-3}} - \cfrac{1}{1 - \cfrac{D_{-3}C_{-4}}{D_{-4}C_{-5}}\cfrac{1}{\cfrac{S_0^2}{D_{-4}C_{-5}} - \cfrac{1}{1 - \cfrac{D_{-5}C_{-6}}{D_{-6}C_{-7}}\cfrac{1}{\cfrac{S_0^2}{D_{-6}C_{-7}} - \cfrac{1}{1 - \dots\dots}}}}}} ;$$

$$\text{and } q = 1 - \cfrac{D_2 C_1}{D_3 C_2}\cfrac{1}{\cfrac{S_0^2}{D_3 C_2} - \cfrac{1}{1 - \cfrac{D_4 C_3}{D_5 C_4}\cfrac{1}{\cfrac{S_0^2}{D_5 C_4} - \cfrac{1}{1 - \cfrac{D_6 C_5}{D_7 C_6}\cfrac{1}{\cfrac{S_0^2}{D_7 C_6} - \cfrac{1}{1 - \dots\dots}}}}}} .$$

Thus, we have managed to obtain an analytical solution for the total field of the periodic impedance plane S_3 in the closed form, as follows:

$$H_z(x) = \sum_{m=-\infty}^{\infty} X_m \left\{ S_0 e^{ix(\eta_i + m\Gamma)} + S_1 e^{ix[\eta_i + (m+1)\Gamma]} + S_2 e^{ix[\eta_i + (m-1)\Gamma]} \right\}. \tag{6}$$

This is a discrete spectrum of slow and fast plane waves propagating along the impedance structure with the phase velocities equal to $v_{\phi m} = ck/(m\Gamma \pm \eta_i)$.

The scattering pattern $F(\varphi)$ of the impedance plane, as well as that of any periodic structure, can be presented in a form of a product of the unit element (single period) pattern, $F_0(\varphi)$ and the pattern of the whole system, $F_p(\varphi)$

$$F(\varphi) = F_0(\varphi) F_p(\varphi). \tag{7}$$

Due to the impedance structure periodicity, it is possible to obtain the expressions for $F_0(\varphi)$ and $F_p(\varphi)$ in elementary functions.

The system factor $F_p(\varphi)$ behavior is conditioned by the period L of the impedance structure, being indepent on the impedance distribution curvature (Z_0) (2). The scattering pattern of the unit element $F_0(\varphi)$, in opposite, depends not only on the values of L and Z_0, as it was found in [1], but also on the impedance structure parameter α and the dielectric layer parameters ε and μ. Note that the value of the structure period L determines spatial orientations of the patterns $F_0(\varphi)$ and $F_p(\varphi)$. The parameters Z_0, α and ε, μ determine the comparative ratio of the spatial harmonic amplitudes for the scattered field. Consequently, they can be used to control the main and side lobes intensities. The obtained analytically closed rigorous solution of the problem involving an impedance plane under a layer of homogeneous dielectric enables one to optimize the impedance distribution and thus provide required scattering characteristics for the objects of various applications.

REFERENCES

1. Y. V. Yukhanov, Analysis and Synthesis of Impedance Plane, *Proc. Int. Conf. Mathematical Methods in Electromagnetic Theory (MMET*98),.* Kharkov, Ukraine, 1998. vol. 1, pp. 118-120.

PERFORMANCE OF 2D REFLECTOR ANTENNA SYSTEM İN A CİRCULAR DİELECTRİC RADOME REİNFORCED WİTH AN INNER RESİSTİVE GRATİNG

Taner Oğuzer
Dokuz Eylül University
Electrical and Electronics Eng. Dept.
Tınaztepe Campus, Buca, Izmir/TURKEY
Phone:90(232)4531008/1171, E-mail:taner.oguzer@eee.deu.edu.tr

ABSTRACT

A reflector antenna system with a concentric dielectric radome and inner resistive grating problem is solved by regularization. This is performed only for E-polarization case. Numerical results are verified by some truncation error functions. Besides various radiation patterns are obtained.

INTRODUCTİON

Although the general shape of the reflectors are 3D parabolic, two dimensional cylindrical reflector antennas are sometimes used in application. The general solution techniques are asymptotic ones like PO,GTD,PTD or complex ray tracing and Gaussian beam composition of the feed pattern. The other alternative is purely numerical methods like a popular one MoM. In mathematical point of view both asymptotic and numerical methods don't guarantee the accuracy and convergency. However, they can be used in the solution of a large class of problems. On the other hand another way of solution of the scattering problems is analytical-numerical methods. In these methods the problem is decomposed into singular and regular parts. The singular part is converted by some analytical way and problem is regularized. The remaining part is then inverted by an efficient numerical method. A popular regularization method is Riemann-Hilbert technique (RHT) which is outlined in [1]. Then in [2], RHT is used in the 2D reflector antenna problems by combining it with complex source point method. Sometimes reflector antenna systems are located inside a dielectric radome which protects the system from the enviromental conditions. The analysis of the reflector antenna systems with the concentric dielectric radome is presented in [3]. Besides in [4], the radiation of a complex line source in a cylindrical radome of metal-dielectric grating is studied by using the general surface impedance boundary condition model.

In the present study we located the reflector antenna system in a concentric dielectric radome which is reinforced with an inner resistive grating. This is extension of [3] and only difference is the inner grating. In [4], the radome is very thin compare to free space wavelength (|khl<<1). But in this geometry the thickness of the radome may be arbitrary so the presented geometry is more realistic. There are two boundary conditions on the grating and on the reflector respectively.These two conditions state two integral equations. Since the grating is resistive the first problem is Fredholm 2nd kind and no need to regularization. We regularized the second integral equation by RHT.

FORMULATİON

The geometry of the problem is a two dimensional perfectly conducting and infinitely thin symmetrical front-fed circular screen which is illuminated by a directive feed antenna(Figure 1). This reflector antenna system is covered by a concentric dielectric radome reinforced with an inner resistive grating. The permittivity of the lossy dielectric radome is denoted as ε_r. The inner grating is assumed to be very thin compared to free space wavelength and electric and magnetic resistivities R and S are expressed by using plane wave transmission through planar slab. The grating is made up of good conductor so R is small and S may be very large i.e. resistive case. The thickness of grating is greater then the skin depth of conductor(impenetrable case). Therefore there is a very small but finite thickness and this makes R and S values of the air part of the grating very large. Then we can assume the tangential electric field on the air part of the grating is continuous as well on the conductor part.

The requirements for the rigorous solution of the present boundary value problem can be stated as the satisfaction of the Helmholtz equation, Sommerfeld radiation condition and the boundary conditions on the pec reflector screen and on the resistive grating. The basic electric field integral equations (EFIE) are obtained for E-polarization case by applying the boundary conditions. The integral equation on the grating can be written as

$$\int_{M_i} G_{zz}^{E}(\vec{r},\vec{r}')J_z^{E1}(\vec{r}')d\vec{r}' + \int_M G_{zz}^{E}(\vec{r},\vec{r}')J_z^{E2}(\vec{r}')d\vec{r}' + E_z^{in}(\vec{r}) = RJ_z^{E1}(\vec{r}) \qquad \vec{r} \in M_i \, (r=c) \qquad (1)$$

$$J_z^{E1}(\vec{r}) = 0 \qquad \vec{r} \in S_i \ (r=c) \qquad (2)$$

The integral equation on the circular pec screen;

$$\int_{M_i} G_{zz}^{E}(\vec{r},\vec{r}')J_z^{E1}(\vec{r}')d\vec{r}' + \int_M G_{zz}^{E}(\vec{r},\vec{r}')J_z^{E2}(\vec{r}')d\vec{r}' + E_z^{in}(\vec{r}) = 0 \quad \vec{r} \in M \,(r=a) \qquad (3)$$

$$J_z^{E2}(\vec{r}) = 0 \qquad \vec{r} \in S\,(r=a) \qquad (4)$$

M_i and S_i are metal and slot parts of the grating where $i=1,2,3,...$Furthermore M and S are metal and slot parts of the reflector screen. J_z^{E1} and J_z^{E2} are current densities on the metalic parts.E_z^{in} is the incident field radiation which is located at a complex position. $G_{zz}^{E}(r,r')$ defined in [3] is the 2D Green's function in the presence of a dielectric radome layer. Therefore the effect of the radome is included into the Green's function.

All the parameters are expressed in terms of Fourier Series and substituted into the equations. Then Dual Series are obtained. First integral equation on grating is already Fredholm 2nd kind and no need to regularization so Fourier Inversion Procedure is used to solve. The other integral equation is Fredholm 1st kind and singular. We regularized it by RHT. Therefore the whole problem is reduced to a algebraic equation system which is Fredholm 2nd kind and regular.

NUMERİCAL RESULTS

Firstly the convergent nature of accuracy is shown in Figure 2. The variation of the directivity and the truncation errors versus truncation number Ntr is presented in Figure 2(a) and 2(b) respectively. Two types of truncation error is plotted. The first one for directivity $\Delta_d = |D^{Ntr+1} - D^{Ntr}|/D^{Ntr}$ and the second one for current $\Delta_c = \max|x_n^{Ntr+1} - x_n^{Ntr}|/\max|x_n^{Ntr}|$ .The results shows that the accuracy increases with the increasing Ntr. On the other hand Figure 3(a) presents the total electric field (Ez) and the error in boundary condition($B_z = E_z - RJ_z$) and both are defined on the grating. It is clear that the boundary conditions are satisfied on the metal part of the grating. The variation of the current distribution on the grating surface is expressed in Figure 3(b) and it is really drops zero at the slot region. Finally Figure 4 is a representation of the radiation plots for two different θ_{ap}' values.When θ_{ap}' becomes larger the edge effects increases so the difference between $\varepsilon_r=1$ and $\varepsilon_r=2+0.2*i$ cases increases. One result of the greater edge effects is the higher levels of the sidelobes.

CONCLUSİON

Reflector antenna system inside a dielectric radome-inner resistive grating problem is solved by regularization only for E-polarization case. Real metal cases R goes to very small values so this solution becomes non-regular. Then problem may be solved for pec metal grating instead of the resistive grating case.

REFERENCES
[1] A.I.Nosich,"Green's function-Dual series approach in wave scattering from combined resonant scatteres" in Analytical and Numerical Methods in Electromagnetic Wave Theory, Science House, 1993
[2] T.Oğuzer,A.Altıntaş and A.I.Nosich,"Accurate simulation of reflector antennas by complex source-dual series approach" IEEE Transactions on AP vol.43 no:8 pp 793-802 August 1995
[3] T.Oğuzer,"Analysis of circular reflector antenna covered by concentric dielectric radome" IEEE Transactions on AP *accepted for possible publication.*

[4] A.Altıntaş,S.Quardani and V.B.Yurchenko,"Complex source radiation in a cylindrical radome of metal-dielectric grating" IEEE Transactions on AP vol.47 no:8 pp 1293-1301 August 1999
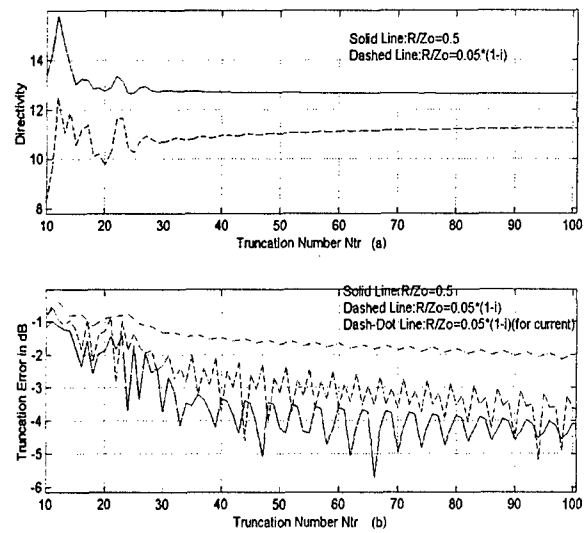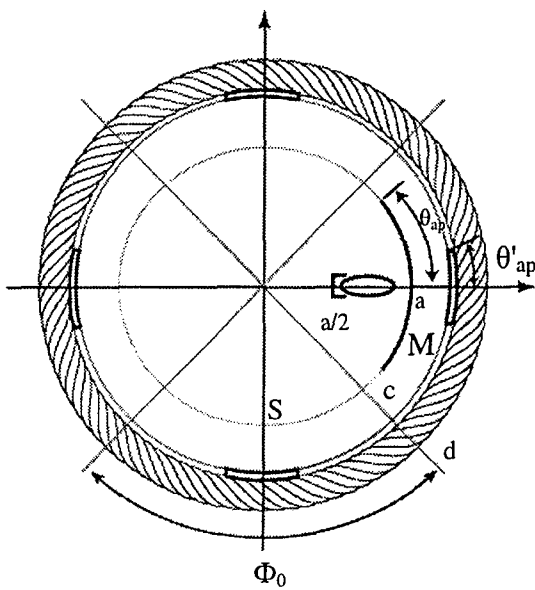
Figure 1: Geometry of the problem
Figure 2:Relative accuracy of the solution.
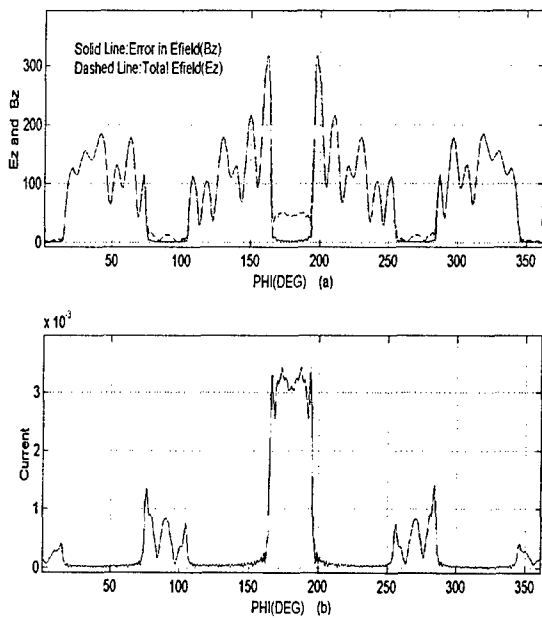
Figure 3 :Current,electric field and error in boundary
in conditions on the grating for ka=15,kc=25,kb=3,Ntr=100
eps_r=2+0.2i and aperture angle 15 degree
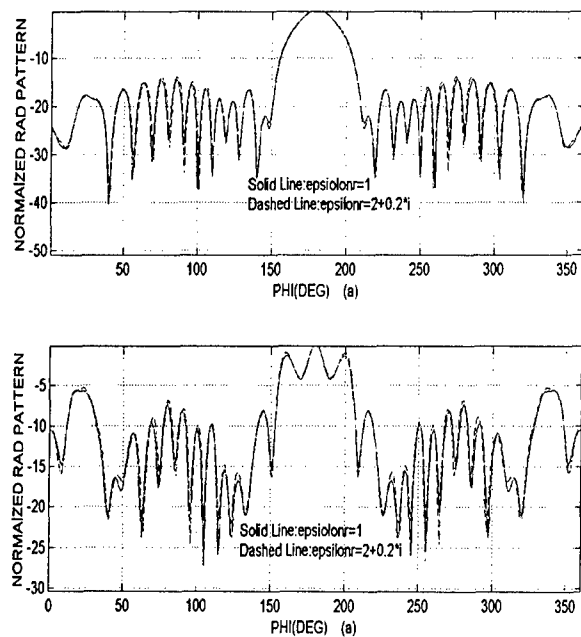
Figure 4:Radiation patterns for same parameters
(a) teta_ap=1 degree and in(b) teta_ap=10 degree.

ANALYSIS OF INDUCTION RESPONSES FROM METAL OBJECTS USING THE METHOD OF AUXILIARY SOURCES

F. Shubitidze, K. O' Neill, S. Haider, K. Sun and K. Paulsen

Thayer School of Engineering, Dartmouth College, Hanover, NH, 03755
Email: Fridon.Shubitidze@dartmouth.edu
Fax: +603 6463856

ABSTRACT

The method of auxiliary sources (MAS) is developed for analyzing low frequency response of conducting and permeable objects. The method uses elementary auxiliary magnetic dipoles/charges to produce the unknown fields. Sources are located on virtual surfaces that usually conform to, but do not coincide with the real surface of the object, where application of the boundary conditions determines unknown source coefficients. The source fields automatically satisfy Maxwell's equations and, using point collocation on the real surface, one avoids all singularities and all integrations. Accuracy in satisfying the boundary conditions can be evaluated explicitly using non-collocation points. Typical, highly efficient results here show low frequency response of spheroids and cylinders depending on object size and shape.

INTRODUCTION

The detection and identification of unexploded ordinance (UXO) is currently a subject of intensive investigation. While UXO consists of sizable, highly conducting and permeable bodies, it is extremely difficult to distinguish them reliably from typically clutter. Consequent false alarms increase cleanup costs enormously. Resent research and field experience show superior UXO detection performance by sensors operating at sub-radar frequency; this has spawned new analyses of scattering by low frequency electromagnetic induction (EMI) [1-3]. For the frequencies considered (~ 10 Hz to ~ 100s of kHz), displacement currents are negligible compared to conduction currents. Conduction currents in the soil, J_s, are also negligible, relative to those in metallic targets. Thus, the dielectric properties of the environment are relatively unimportant. In this work we demonstrate the ease of MAS for EMI scattering simulation, showing accuracy in comparison to the analytical solution for sphere [4].

FORMULATION

Consider a permeable, conducting 3-D object placed a primary magnetic field with time dependence $e^{i\omega t}$ (Fig.1). The primary field induces eddy currents within the object, which produce secondary (scattered) fields outside. With $\partial \vec{D} / \partial t \sim 0 \sim Js$, the external magnetic is
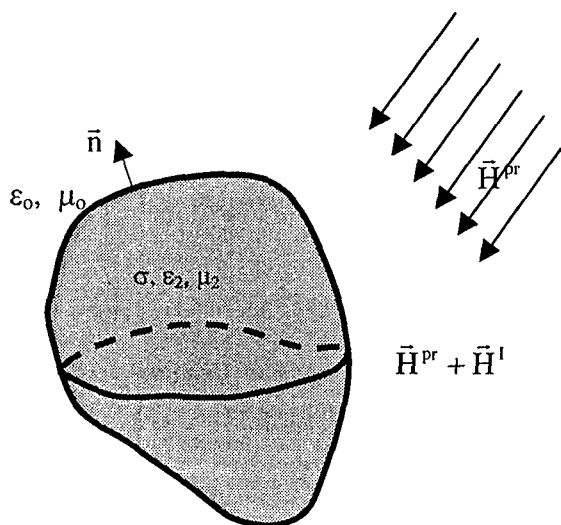
Fig.1 Geometry general EMI problem

irrotational and can be represented as gradient of the scalar potential, $\vec{H}_1^{sc} = -\nabla\varphi$, where φ satisfies the Laplace equation. The approximate secondary field outside of the object (region 1) is expressed as

$$\vec{H}_1^{sc}(\vec{r}) = \sum_{n=1}^{N} \rho_n \nabla G(\vec{r}_n, \vec{r}), \quad \text{where } G(\vec{r}_n, \vec{r}) = \frac{1}{4\pi\mu_0 |\vec{r} - \vec{r}_n|} \tag{1}$$

G is the fundamental solution of the Laplace equation for φ, $\vec{r}$ is the observation point position vector; $\vec{r}_n$ and ρ_n are position vector and unknown scaler coefficient of the nth source, respectively. These sources are located at points distributed over a secondary surface, approximately following but inside the real surface. We compute the external secondary field by assuming that these sources radiate into an infinite homogeneous medium with the properties of the exterior space.

Inside of the target (region 2) we cannot apply the same simplification of the Maxwell's equations as outside of it. The magnetic field inside the target is expressed as

$$\vec{H}_2(\vec{r}) = \sum_{n=1}^{N} k_2^2 \vec{\Pi}^m(\vec{r}_n, \vec{r}) + \nabla\nabla \cdot \vec{\Pi}^m(\vec{r}_n, \vec{r}) \quad \text{where } \vec{\Pi}^m(\vec{r}^n, \vec{r}) = \frac{1}{4\pi\mu_2} \frac{\vec{P}_n e^{-jk_2|\vec{r} - \vec{r}_n|}}{|\vec{r} - \vec{r}_n|} \tag{2}$$

$\vec{\Pi}^m$ is the fundamental solution of the Helmholtz equation, $k_2 = \sqrt{-j\omega\sigma\mu_2}$, $\vec{P}_n$ is the nth unknown magnetic dipole source coefficient. These sources reside on an auxiliary surface slightly outside and approximately following the real surface. Each vector $\vec{P}_n$ consists of 2 components approximately parallel to the real surface (equivalently, two crossed magnetic current elements), or 1 component for a cylindrically symmetrical problem. We compute the internal total field by assuming that these sources radiate into an infinite homogeneous medium with the properties of the metallic target material.

The relation between the external and internal fields is dictated by the continuity conditions at the real surface. Specifically, the tangential components of the magnetic field and the normal component of the magnetic flux density must be continuous across real surface,

$$[\vec{n} \times (\vec{H}_1^{sc} + \vec{H}^{inc})] = [\vec{n} \times \vec{H}_2], \quad \vec{n} \cdot (\vec{B}_1^{sc} + \vec{B}^{inc}) = \vec{n} \cdot \vec{B}_2 \tag{3}$$

where $\vec{n}$ is a unit normal vector on the real surface. Enforcing (3) at selected collocation points on the real surface provides the matrix equation that is solved for the unknown coefficients $\{\rho_n\}$, $\{\vec{P}_n\}$. Once the unknown coefficients are determined, we may compute the field readily at all points.

RESULTS

To demonstrate the accuracy of the method we consider a primary magnetic field, $\vec{H}^{pr} = \hat{z}H_0$, acting on a sphere with material properties σ, μ_2 and radius a. Because of rotational symmetry, the number of auxiliary sources and boundary condition points is equal. Fig. 2 show normalized secondary magnetic from the sphere as a function of the characteristic parameter $|k_2|a$ (the induction number), for the case with $\mu_r = \mu_2/\mu_0 = 10$, compared with the exact solution [4]. We see excellent agreement.
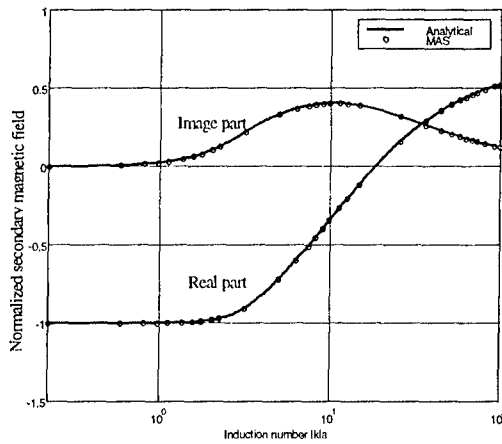
Fig.2 Normalized secondary magnetic field versus induction number, sphere radius a=5cm, μ_r=10; σ=10^7
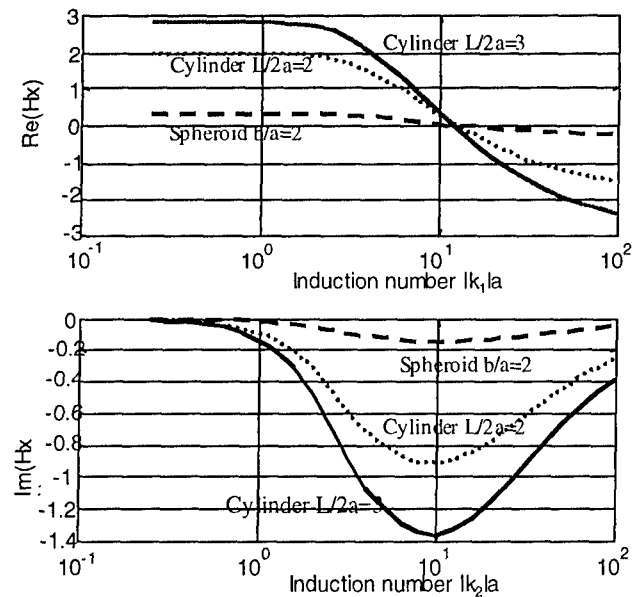
Fig. 3. Transverse case; μ_r=10

Fig.3 shows real and imaginary normalized EMI response with $\vec{H}^{pr} = \hat{x}H_o$, transverse to the targets' major axes. Scattered far fields were obtained above target centroids, in the direction of the primary field. For the cylinder L/2a=2 or 3, where L is cylinder length an a its radius; and for the spheroid b/a=2. All targets have the same transverse radius a. Thus the smaller cylinder has the essentially the same aspect ratio as the spheroid; the larger cylinder is twice as long as the first. The spheroid produces a more diverging secondary field than the L/2a cylinder, hence a weaker response, illustrating shape factor. The longer cylinder produces a stronger response than the shorter one, illustrating size factor. The real parts are positive at low frequencies due to induced volume magnetization in line with the primary field. As frequency increases the secondary field opposes the primary field and response becomes negative. The imaginary part shows a characteristic peak, when volume currents have their maximum effect. This is absent in the near static limit (Ik$_2$Ia ~ 0) and in the high frequency limit, when essentially all eddy currents are on the surface. All these results make physical sense, and serve as a reality check on the results.

REFERENCE

[1]   N. Geng, K. E. Baum, L. Carin. "On the Low Frequency Natural Responses of Conducting and permeable Target." IEEE Trans. Geosci. Remote Sens., Vol. 37, pp 347-359, 1999.
[2]   D.K Keiswetter, I.J.Won, B.Barrow, T. Bell, "Object identification using multifrequency EMI data", UXO forum   1999, Alexandria, Virginia May 24, 1999.
[3]   L. Collins, P.Gao, J. Moulton, L. Makowsky, R. Weaver, D Keiswetter, I.J. Won. "Detection of Low metal mines using frequency domain EMI." UXO forum 1999, Alexandria, Virginia May 24, 1999.
[4]   J.R. Wait, "A conducting sphere in a time varying magnetic field". Geophysics, vol. 16, pp. 666-672, 1951
[5]   Karkashadze D., Zaridze R. "The Method of Auxiliary Sources in Applied Electrodynamics", LATSIS Symposium, Zurich, 1995.

PLANE WAVE SCATTERING ON A REFLECTOR ANTENNA LOCATED OVER AN IMPEDANCE PLANE

Yuriy V. Yukhanov, Alexandr Yu. Yukhanov

Taganrog State University of Radio Engineering, Tagatrog, Russia
E-mail: airpu@tsure.ru

ABSTRACT

The influence of an impedance plane on the efficient surface of diffusing (radar cross-section (RCS)) of parabolic antenna is considered in this paper. The features of diffusing are analyzed on the basis of combination of the method of physical optometrists (of physical optics) and integral equations. It was shown that due to the mutual reflections from the mirror antenna and impedance plane, the RCS can double increasing its angular sector. The results of numerical experiments are also presented.

The influence of the impedance plane on the radar cross-section (RCS) of parabolic mirror antennas (MA) is considered. The scattering characteristics are analyzed using the method of physical optics combined with the method of integral equations.Suppose the parabolic antenna S is located at an h distance from the S_0 homogeneous impedance plane (Fig.1), the antenna axis and S_0 making the θ_0 angle. The Cartesian co-ordinates zero point coincides with the parable focus, the x-axis being parallel to the S0 plane. The problem parameters are constant along the z-axis. Mirror and emitter fixing constructions are not considered. A plane electromagnetic wave $\vec{E}^i$, $\vec{H}^i$ ($\vec{H}^i = \vec{i}_z H^i_z$) is incident from the direction φ on the antenna. The Lorenz lemma in its integral form is used to solve the problem. The auxiliary source is the infinite in-phase line of the magnetic current with a singular amplitude. The auxiliary source field $\vec{E}^M, \vec{H}^M (\vec{H}^M = \vec{i}_z H^M_z)$ meets the same boundary conditions as the field under investigation
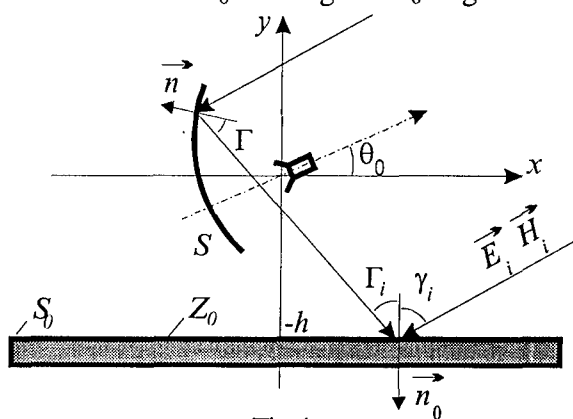
Fig.1

$$[\vec{n}\vec{E}^M (p,q)] = 0, \quad q \in S . \tag{1}$$

The field is the one of the magnetic current line scattered near the antenna. The boundary conditions introduced in (1) allow to avoid defining the field upon the S MA surface. Thus, the problem is reduced to the task of defining the tensor vector of magnetic field H_z on the homogeneous impedance plane S0 from the Fredholm second-kind integral equation:

$$H_z(x) = 2 \int\limits_{-\infty}^{\infty} Z_0 H_z^{M0}(x, x') H_z(x') dx' + 2 \int\limits_{-\infty}^{\infty} \{Z_0 H_z^{MA}(x, x') - E_x^{MA}(x, x')\} H_z(x') dx' +$$

$$+ 2H_z^i(x, \varphi^i) + 2H_z^{MA}(x, \varphi^i), \tag{2}$$

where $\vec{E}^M = \vec{E}^{M0} + \vec{E}^{MA}$; $\vec{H}^M = \vec{H}^{M0} + \vec{H}^{MA}$; $\vec{E}^{M0}, \vec{H}^{M0}$ is the free-space auxiliary current field; $\vec{E}^{MA}, \vec{H}^{MA}$ is the scattered auxiliary current field; Z_0 is the homogeneous impedance of plane S_0; $H_z^{MA}(x, \varphi^i)$ is the incident wave field in the $p \in S_0$ point, scattered by the antenna.

In the paper, $\vec{E}^{MA}, \vec{H}^{MA}$ are determined within the physical optics approximation. It became possible due to thorough electrical measurements of the antenna reflector.

The complicity of (2) is that the function is to be determined upon the infinite integral. We can avoid the difficulties by representing the field as a sum of the following fields:

$$H_z(x) = H_0(x) + H_1(x) + H_2(x), \tag{3}$$

where $H_0(x)$ is the magnetic field component induced waves upon the homogeneous plane S_0 in the absence of the MA S. It is the solution of the Fredholm second-kind integral equation

$$H_0(x) = 2 \int\limits_{-\infty}^{\infty} Z_0 H_z^{M0}(x, x') H_0(x') dx' + 2H_z^i(x)$$

as

$$H_0(x) = \frac{2 \cos \gamma_i}{\cos \gamma_i + Z_0} H_z^i(x); \tag{4}$$

$H_1(x)$ is magnetic field component induced by the scattered with MA S incident wave upon the homogeneous impedance plane S_0. It is the solution of the Fredholm second-kind equation

$$H_1(x) = 2 \int\limits_{-\infty}^{\infty} Z_0 H_z^{M0}(x, x') H_1(x') dx' + 2H_z^{MA}(x).$$

The equation was solved analytically. In case of Ma without the antenna component for $H_1(x)$ we obtain (Fig.1)

$$H_1(x) = -k \int\limits_S \cos \Gamma \frac{\cos \Gamma_i}{\cos \Gamma_i + Z_0} H_0^{(2)}(kR_{p,q}) e^{ik\rho \cos(\varphi - \varphi_i)} dS.$$

The magnetic field tensor component $H_2(x)$ is determined by the mutual reflection between S_0 and S planes. It is a cylinder wave reflected from MA and thus it decreases with the distance as $1/\sqrt{r}$. So, $H_2(x)$ is therefore commensurable to incident wave (H_z^i) on the finite plane interval S_0. The further task is to find the function of the rest of the magnetic field tensor for the impedance plane S_0. From the Fredholm second-kind integral equation for $H_2(x)$ for finite interval $[x_1, x_2]$,

$$H_1(x) - 2 \int\limits_{x_1}^{x_2} \{Z_0 H_z^M(x, x') - E_x^{MA}(x, x')\} H_1(x') dx' =$$

$$= 2 \int\limits_{x_1}^{x_2} \{Z_0 H_z^{MA}(x, x') - E_x^{MA}(x, x')\} [H_0(x') + H_T(x')] dx',$$

where $[x_1, x_2]$ interval value depends upon the disposition of plane and antenna, and upon the MA reflector measurements as well. The solution, in principle, is not a difficult one.
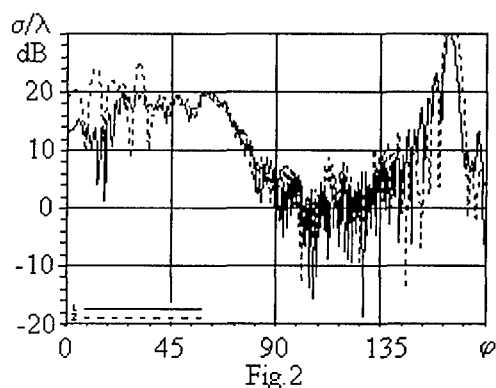
Fig. 2
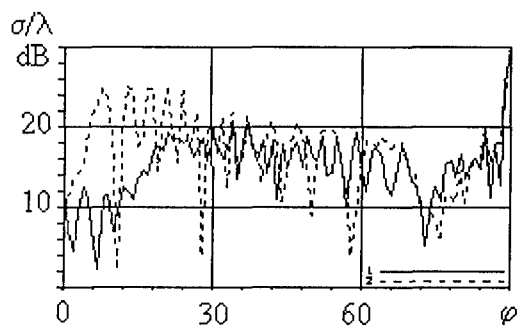
Fig. 3

The bi-static diagram of MA scattering for the non-symmetrical parabolic reflector (f=10λ, Ψ=60^0, θ_0=0^0) is shown (Fig.2). The MA is located over the ideal conducting surface with the length of 42λ x∈[-12λ,30λ], at *h=10λ* height (line 1) and *h=1λ* (line 2) with the incident wave angel of φ^i=30^0. Line 3 represents the case of MA reflector RCS in the free-space in the antenna axis direction. Calculations show that while increasing of the incident angel, the bi-static diagrams of MA scattering tends to widen the angel sector with the simultaneous increasing of RCS level in some directions.

Fig. 3 shows mono-static diagrams of the same antenna. The line numbers are the same as those for the previous cases.

The analysis of numerical results indicates that the MA S – surface S$_0$ system acts as corner reflector. It is especially evident for the low antenna position. For the axis by directions with angel (0^0÷15^0) the main contribution is due to the waves cross-reflections in the following sequence: S$_0$ $\Rightarrow$ S $\Rightarrow$ S$_0$. For the other directions the field created by cross-reflection sequence of S $\Rightarrow$ S$_0$ $\Rightarrow$ S prevails.

Due to these cross-reflections the mono-static diagram widens as much as twice and occupies the same angle sector as the bi-static diagram. It is, in fact, the whole of the upper hemisphere.

SCATTERING OF A PLANE ELECTROMAGNETIC WAVE BY A METAL-DIELECTRIC COMPOSITE CYLINDER

A. Y. Shepilko[1], and Y. V. Shepilko[2]

[1] Institute of Radio Astronomy, National Academy of Sciences of Ukraine
4 Chervonopraporna Ul., Kharkov, 61002,Ukraine

[2] Kharkov State Municipal Academy,
12 Revolyutsii Ul., 61002,Ukraine e-mail: shepsis@ksame.kharkov.com

INTRODUCTION

The scattering of a plane electromagnetic wave by an infinite circular metal-dielectric cylinder (CMDC) is considered. The metal part of cylinder is a sector of an arbitrary angle of opening. One may use such structures in order to model the properties of a wedge-shaped load, which is frequently used in electromagnetic control applications [1]. Since in some cases the analysis of the experimental data may be not reliable due to small magnitude of the measured reflection coefficient and relative errors of measurement equipment, there is a need for a closed-form analysis of the model structures [2]. In the presented study the method of re-expansion in the basis functions at a given interval is used [3,4]. The resulting field is presented in terms of the Bessel and Hankel functions. Applying the boundary condition to the Fourier series representation of the scattered field, the problem is reduced to the solution of a matrix equation with unknown expansion coefficients, which can be calculated with controlled accuracy. The scattered field is evaluated asymptotically and the backscattering radar cross section (BRCS) expression is derived. Accurate numerical results are presented in case of the *E*-polarized waves.

FORMULATION AND ANALYSIS

A 2-D cross section of the problem in cylindrical coordinates $(\rho,\ \varphi,\ z)$ is shown in Fig.1. Assume that CMDC is uniform in the z-direction. Cylinder is of radius a has a metallic sector opening of the angle δ, and $\varepsilon2$, $\varepsilon1$ are permittivities of CMDC and environment, respectively. Time-harmonic dependence is implied as $\exp(-i\omega t)$. A plane wave is incident on CMDC at the angle β with respect to the φ-axis. The field in the structure is presented as a superposition of the incident and scattered fields. The *E*-polarization implies that the incident electric field is parallel to the z-axis. To apply the boundary conditions at the cylinder, we expand the incident plane wave in terms of the Bessel functions [5]:
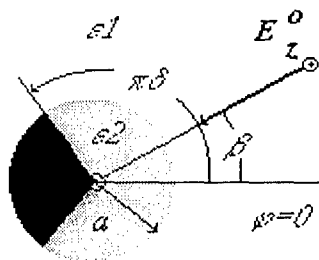
Fig.1 Geometry of the problem.

$$E_z^0 = \sum_{m=-\infty}^{\infty}(-i)^m J_m(k\rho)e^{im(\varphi-\beta)}\ , \qquad E_\varphi^0 = E_\rho^0 = H_z^0 = 0 \qquad (1)$$

The scattered field should satisfy a homogeneous Helmholtz equation at any point of space, except for a metal, and the boundary conditions at the metal. In view of the condition of radiation as well as condition of energy limitation in any finite region, we write analogous representations in terms of the Bessel functions and the Hankel functions of the first kind, for the electrical z-components of the scattered electromagnetic fields:

$$
E_z^1 = \begin{cases} \sum\limits_{m=-\infty}^{\infty} \beta_m H_m^{(1)}(k_1\rho)e^{im\varphi}, & \rho \geq a, \\ \sum\limits_{q=1}^{\infty} \alpha_q J_{qv}(k_2\rho)Sin(\varphi+\pi v)qv, & 0 \leq \rho \leq a, \end{cases} \tag{2}
$$

where $k=\omega/c$, $k_j = \sqrt{\varepsilon_j\mu}\,k$, ($\mu=1$, $j=1$ or 2), c is the velocity of light in vacuum, α_q, β_m are the expansion coefficients to be determined. Other field components can be found from the Maxwell equations.

Satisfying the boundary conditions for the total field on the metal and condition of continuity of the field outside the metal surface, and using the method of re-expanding in the basis functions at the intervals $[0, 2\pi]$ and $[-\pi./2, \pi/2]$ of the φ variation, we obtain the following matrix equation of the second kind.

$$
X_n \frac{H_n^{(1)}(k_1a)}{H_n^{(1)'}(k_1a)} = p_e \sum_{m=-\infty}^{\infty} X_m \sum_{q=1}^{\infty} \frac{J_{qv}(k_2a)}{J_{qv}'(k_2a)} V_{qv}^n Q_{qv}^m - p_e \sum_{m=-\infty}^{\infty} (-i)^m J_m'(k_1a)e^{-im\beta}
$$

$$
\sum_{q=1}^{\infty} \frac{J_{qv}(k_2a)}{J_{qv}'(k_2a)} V_{qv}^n Q_{qv}^m + (-i)^n J_n(k_1a)e^{-in\beta}, \quad n=0,\pm 1,\pm 2,..., \tag{3}
$$

where $p_e = \sqrt{\dfrac{\varepsilon_1}{\varepsilon_2}}$, $X_n = \beta_n H_n^{(1)'}(k_1a)$ and the prime denotes a derivative with respect to ρ.

Matrix coefficients V_{qv}^n and Q_{qv}^m are expressed through trigonometric functions [4]. The obtained equation, after certain transformations, can be analyzed numerically after a truncation to the finite order. Using asymptotic expansion of the Hankel functions, one may obtain the following expressions for BRCS and the amplitude function of the scattered field (AFSF), respectively:

$$
k_1\sigma_B = 4\left| \sum_{m=-\infty}^{\infty} \frac{X_m}{H_m^{(1)'}(k_1a)} e^{im(\beta-\pi/2)} \right|^2, \qquad A(\varphi) = \left| \sum_{m=-\infty}^{\infty} \frac{X_m}{H_m^{(1)'}(k_1a)} e^{im(\varphi-\pi/2)} \right| \tag{4}
$$

NUMERICAL RESULTS AND DISCUSSION

Figures 2-4 illustrate BRCS versus electrical diameter *ka* and AFSF, respectively. Relative computation error of BRCS and ASFS was less than *5.0%*. Analyzing the obtained results one can conclude that by varying the values of *ka*, *ε2* and *ε1*, the field reflected from CMDC with a wedge can be minimized.

REFERENCES

[1] B.M. Kats, V.P. Meschanov, N.F. Popova, V.D. Tupikin, *Elektronnaya Tekhnika, seriya SVCh,* no.4 (448), p.9, 1992 (in Russian)

[2] M.V. Davidovich, V.P. Meschanov, N.F. Popova, Electrodynamic model of a coaxial, *Radiotekhnika i Elektronika,* v.43, no 12, pp.1447-1453, 1998 (in Russian)

[3] V.I. Smirnov, *Course of Higher Mathematics,* Moscow, GITTL Publ., 1957, vol.2 (in Russian)

[4] Ye.V. Shepilko, Excitation and diffraction of electromagnetic field by infinite bodies

with cylindrical symmetry, *Ph.D. Thesis*, Kharkov State University, Kharkov, 1979 (in Russian).

[5] Ye.I. Ivanov, *Diffraction of Electromagnetic Waves by Two Bodies*, Minsk, Nauka i Tekhnika, 1968 (in Russian).
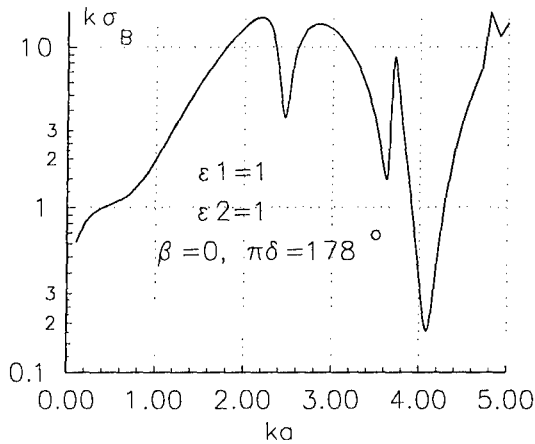
Fig.2. BRCS versus *ka*
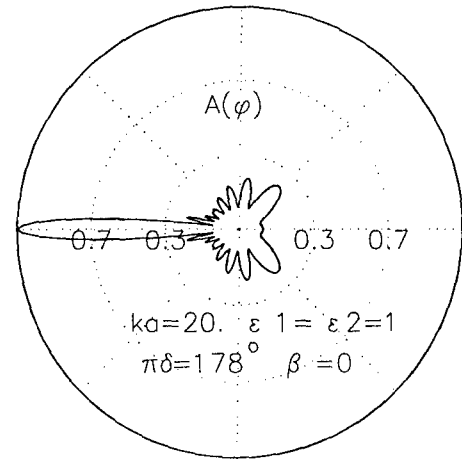
Fig.3. Normalized far-field versus φ
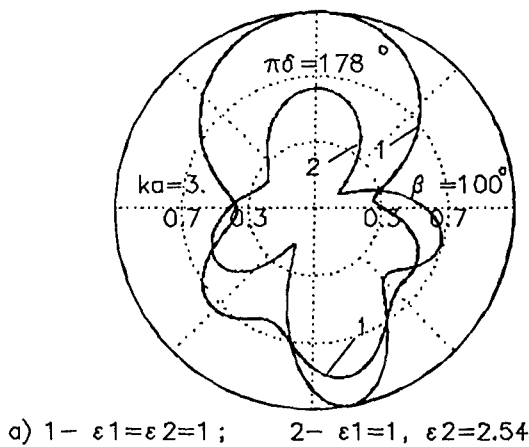
a) 1− $\varepsilon 1 = \varepsilon 2 = 1$;   2− $\varepsilon 1 = 1$, $\varepsilon 2 = 2.54$
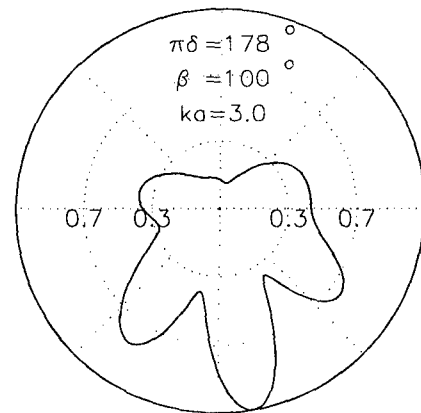
b) $\varepsilon 2 = 1$, $\varepsilon 1 = 2.54$,

Fig.4. Normalized far-field versus φ for various permittivities

GUIDED WAVES

SPECTRAL APPROACH TO THE SYNTHESIS OF THE WAVEGUIDE BANDSTOP FILTERS BASED ON DIELECTRIC RECTANGULAR POSTS

L. Minakova, and L. Rud

Institute of Radio Physics and Electronics, National Academy of Sciences of Ukraine
12 Acad. Proskura St., Kharkov, 61085, Ukraine
E-mail: rud@ire.kharkov.ua

ABSTRACT

A nontraditional approach to the synthesis of waveguide rejection cells of a dielectric rectangular post type is developed on the basis of an exact solution of corresponding spectral problem taking into account the dielectric loss. The results of synthesis of the rejection cells and optimization of bandstop filters are presented.

Waveguide bandstop filters are usually worked out on the basis of resonant cells that have smooth characteristics beyond the rejection frequency and have no spurious resonances within the whole waveguide operating band. As an example of such an element, *E*-plane stub in a rectangular waveguide may be mentioned [1]. The similar properties inhere in dielectric circular cylinders made from a high-permittivity material [2] and having the height equals to the one of a rectangular waveguide. The present communication is devoted to the evolution of approach, proposed in [1], on the synthesis of separate rejection cells and the multi-section bandstop filters based on dielectric posts of a rectangular cross-section shown in Fig.1. Such rejection cells are preferred since they are simple in fabrication and can be calculated with the aid of exact mathematical model that is more efficient than the one developed in [2] for dielectric cylinders. The last factor is important because the search of a cell configuration according to the given specification on its characteristics is a time-consuming procedure.
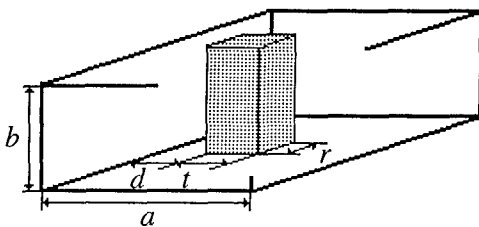
Fig. 1.

The utilized approach consists in searching two geometrical parameters describing the post dimensions according to the given complex dimensionless eigen-frequency $\kappa = a/\lambda$ of the first higher H_{201} oscillation that causes the resonant rejection of the incident H_{10} mode (so-called resonance on a "locked" mode). The eigen-frequency $\kappa_{201} = \kappa'_{201} + i\kappa''_{201}$, $\kappa''_{201} < 0$ and quality factor $Q_{201} = -\kappa'_{201}/2\kappa''_{201}$ of the H_{201} operating oscillation describe uniquely the resonant characteristics of the desired cell providing the specified rejection frequency $\kappa_0 \approx \kappa'_{201}\left(1 - (2Q_{201})^{-2}\right)^{1/2}$ and quality factor $Q \approx Q_{201}$. The developed numerical algorithm is based on solving the homogeneous system of non-linear equations

$$\begin{cases} \operatorname{Re} D(\kappa_0, Q, x_1, x_2) = 0 \\ \operatorname{Im} D(\kappa_0, Q, x_1, x_2) = 0 \end{cases} \tag{1}$$

Here $D(...) = \det F(...)$ where F is the matrix operator of the corresponding spectral problem on field natural oscillations of considered waveguide-dielectric resonators. Such a problem was strongly investigated in [3]. The solution of system (1) enables one to obtain the values of

x_1, x_2, corresponding to two post parameters (for example, $t/a, r/a$ or $d/a, r/a$), as functions of the given f_0 and Q. The desired solution of (1) was obtained by the Newton method.

The concrete results on the synthesis of separate resonator cells are presented in Fig. 2 for the case of rectangular dielectric cylinders located near a narrow waveguide wall (d=0) and made from the mentioned in [2] ceramic with $\varepsilon = 38.5(1 + i2 \cdot 10^{-4})$. With using the presented data, one can determine the post thickness t/a from Fig. 2(a) and the post length r/a from Fig. 2(b) according to the given values of κ_0 and Q. From the analysis of Fig. 2, it follows that the chosen value of Q is greater, the frequency range in which such a value can be reached is narrower. To extend this range, the structures with $d \neq 0$ should to be used.
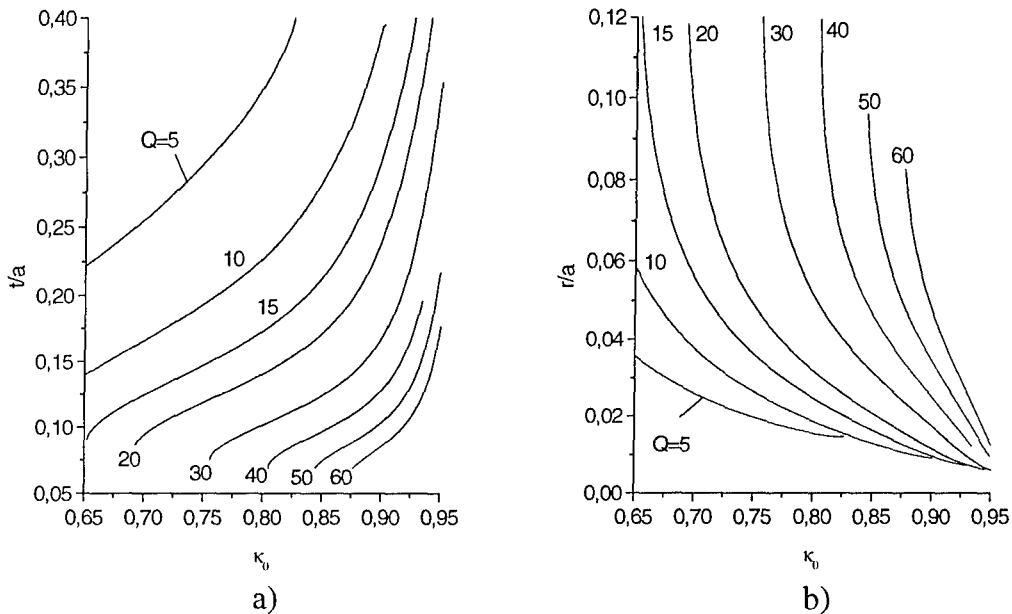
Fig.2.

The process of bandstop filter design includes two stages. The first one consists in obtaining the initial geometry of separate filter resonators. For that, the required values of Q for each filter resonator are obtained according to the given specification with the known procedure of designing bandstop filter-prototypes with quarter-wave couplings [4]. Further, the desired geometrical parameters of each resonator are defined with the aid of dependencies presented in Fig. 2. The second stage is the tuning of filter parameters by the optimization procedure. This procedure is based on the solution of the minimax many-variable problems by the method of steepest descent. The following goal function is used in the optimization procedure

$$F(\vec{x}) = \sum_{\substack{i=1 \\ f_l \leq f_i \leq f_a}}^{N_l} \left(\frac{L_i}{L_p}\right)^2 + \sum_{\substack{i=1 \\ f_b \leq f_i \leq f_c}}^{N_b} \left(\frac{L_s}{L_i}\right)^2 + \sum_{\substack{i=1 \\ f_d \leq f_i \leq f_r}}^{N_r} \left(\frac{L_i}{L_p}\right)^2 \qquad (2)$$

In (2), $\vec{x}$ is a vector of variable parameters, f_l, f_a are the beginning and end of the low-frequency pass band, f_b, f_c are the same of the filter stop band, and f_d, f_r are the same of high-frequency pass band. Values of L_p, L_s are the required insertion loss level within the pass band and stop band, respectively.

The characteristics of two optimized bandstop filters with the central relative frequency $\kappa_0 = 0.8$ and distances between separate resonators $s/a \approx \lambda_g/4$ and $s/a \approx 3\lambda_g/4$ are shown in Fig. 3(a) and Fig. 3(b), respectively (λ_q is the wavelength of H_{10} mode in a hollow rectangular waveguide at $\kappa = \kappa_0$). The straight, dash, and dot curves are related to the insertion, return, and dielectric loss, respectively. Initially synthesized resonators have the

a)   b)
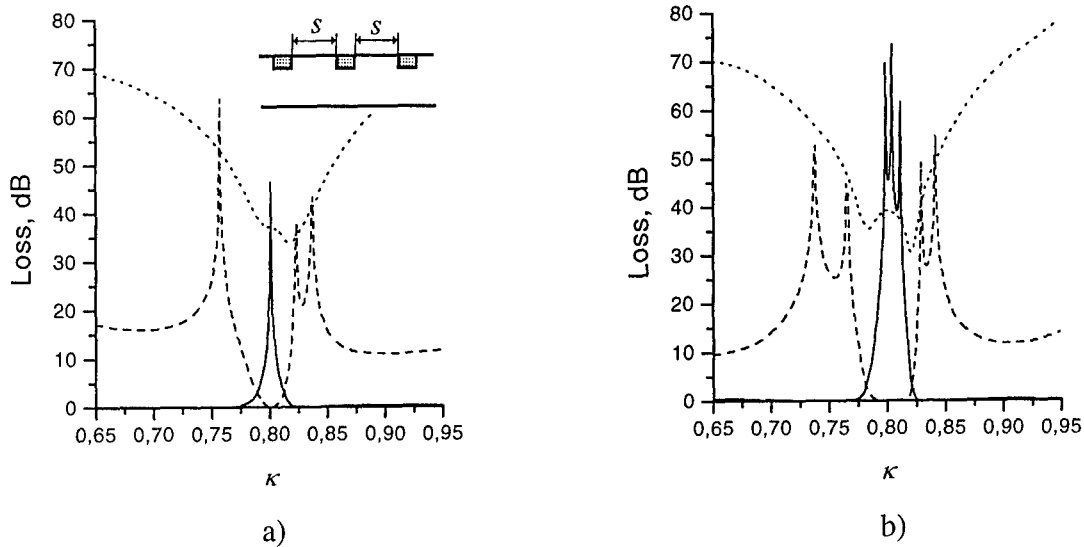
Fig. 3.

following qualities: $Q_1 = Q_3 \approx 31.5$, $Q_2 \approx 18$ for the cases of $s/a \approx \lambda_g/4$ and $Q_2 \approx 12$ for the case of $s/a \approx 3\lambda_g/4$. The values of Q_i, $i = 1,2$ were obtained for the filters having the 2% stop band at the level of $L_s = 20$ dB taking into account the corrections on qualities of coupling waveguides. From the comparable analysis of Fig. 3, one can conclude that the above-mentioned initial data are more suitable for the filters with $3\lambda_g/4$ coupling waveguides. The strong higher-mode interaction does not allow obtaining acceptable characteristics for the case of $s/a \approx \lambda_g/4$ when resonators are close to each other.

REFERENCES

[1] A.A. Kirilenko, L.A. Rud', and S.L. Senkevich, "Spectral approach to the synthesis of bandstop filters," *IEEE Trans. Microwave Theory Techn.*, vol. MTT-42, pp. 1387-1392, July 1994.
[2] R. Gesche, N. Lochel, "Scattering by a lossy dielectric cylinder in a rectangular waveguide," *IEEE Trans. Microwave Theory Techn.*, vol. MTT-36, pp. 137-144, Jan. 1988.
[3] L. Minakova, L. Rud, "Natural oscillations of waveguide-dielectric resonators based on sections of partially filled rectangular waveguides," *Radiophysics and Electronics*, Col. vol. IRE NASU, vol. 4, No. 3, pp. 71-77, 1999.
[4] D.L. Matthai, L. Young, and E.T.M. Jones, *Microwave Filters, Impedance-Matching Networks and Coupling Structures*, New York, McGraw-Hill, 1964.

MODELING OF ELEMENTS WITH CIRCULAR SYMMETRY PLACED IN A RECTANGULAR WAVEGUIDE MULTIPORT

Dmitry Kulik, and Anatoly Kirilenko

[1] Institute of Radiophysics and Electronics of NASU, Ukraine, Kharkov,
fax: 038 0572 441105, e-mail: kirilenko@ire.kharkov.ua

ABSTRACT

A set of algorithms based on matching the fields of radial waveguide (WG) and several rectangular ones is described. The proposed approach can be applied to calculate both the multiports with tuning posts and the turnstile junctions with coaxial WG.
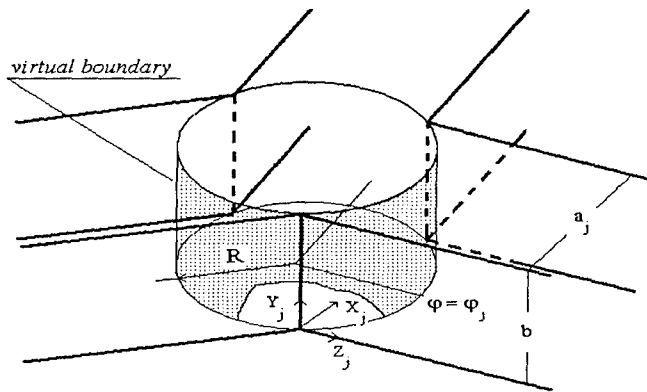
Fig.1

Available library of the key-building elements determines the versatility of the software of WG electromagnetic modeling based on the decomposition principle. In this view, attractive are such geometries as a set radial discontinuities placed into the junction of several rectangular WGs. A lot of widespread WG units may be treated in this manner, starting from the simplest angled bends [1], corners, tees and posts [2] and up to turnstile junction of circular coaxial and star-wise set of rectangular WGs, spaced in a plane. General considerations put into foundation of the series of corresponding numerical models are described in this paper.

First, consider the mode-matching operators arising at calculation a generalized star-wise junction of several rectangular WGs with some radial WG domain $(\rho > \hat{\rho})$. The electromagnetic fields of the radial and rectangular WGs can be presented respectively, as an expansion in the $TE(M)_y$-modes with $E(H)_y = 0$ and as conventional expansions in

$TE(M)_z$-modes. The decisive factor at the choice of discretization in application of the mode-matching procedure is that the fields of radial WG modes are orthogonal at a cylindrical surface and the ones of rectangular WG are orthogonal at plane rectangular cross-section section. It does not allow obtaining the second-kind matrix equation matching the fields at virtual cylindrical boundary (Fig.1) or at rectangles $z_j = 0$ only. On the other hand matching at $\rho = const$ allows simplifying the calculation of arising coupling integrals. Projecting the field matching equations at $\rho = R$ on the fields $e(h)_{qp}$ of the radial WG eigen-modes:

$$\int\left[\left(E(H)_\tau^{rect.WG} - E(H)_\tau^{rad.WG}\right) \times h(e)_{qp}^{h(e)^*}\right]\Big|_{x,y,z \in \rho = R} ds = 0 \text{, we have the following pair of matrix}$$

equations coupling the amplitudes of the incident (I) and outgoing (R) rectangular WGs modes and the amplitudes of fields in the radial WG region adjacent to the virtual boundary of field matching:

$$E^+ R + E^- I = P^E A + Q^E B \text{ and } H^+ R + H^- I = P^H A + Q^H B \qquad (1).$$

Here, $\mathbf{A}$ and $\mathbf{B}$ are the amplitudes of "standing" waves in radial WG, $\mathbf{E}^{\pm}, \mathbf{H}^{\pm}$ are the matrix of radial-rectangular WG coupling integrals arising at matching E-, H-fields and have line-block character according to number of ports, the diagonal matrices $\mathbf{P}^{E(H)}, \mathbf{Q}^{E(H)}$ are some kind of radial WG "standing" waves norms.

JUNCTIONS WITHOUT INSERTS

Though our main goal is the consideration of "the junctions with inserts", we have to discuss initially the simplest geometry. In the cases of star-wise junctions of rectangular WGs by common cylindrical domain without any inserts, $\mathbf{B} \equiv 0$ and we obtain, from (1), a required matrix relation between the incident and excited modes

$$\left(\mathbf{P}^{H^{-1}}\mathbf{H}^{+} - \mathbf{P}^{E^{-1}}\mathbf{E}^{+}\right)\mathbf{R} = -\left(\mathbf{P}^{H^{-1}}\mathbf{H}^{-} - \mathbf{P}^{E^{-1}}\mathbf{E}^{-}\right)\mathbf{I} \qquad (2).$$
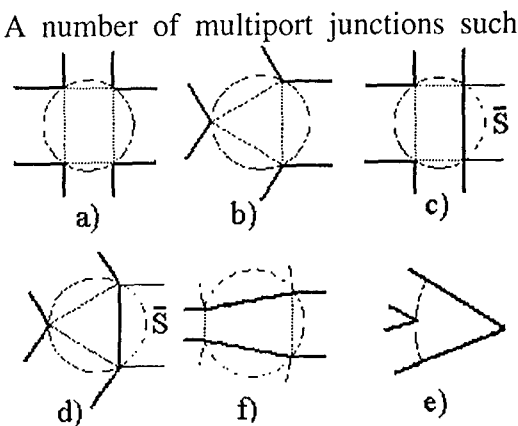
A number of multiport junctions such

Fig.2

as crosses (Fig.2a), Y-junctions (Fig.2b) and tees (Fig.2c) etc. can be calculated using this expression. This approach is close to one used in [1] for calculation of angled bends (fig.2e). The main numerical efforts fall on coupling integrals' calculation, the efficient way to do that using Jacoby-Angerra formulae being firstly proposed in [1].

There is a possibility to enlarge the list of possible applications. Based on some multiport problem and taking into account that placement of the short in "j"-th arm leads to relation $R^{(j)} = -I^{(j)}$, we can obtain the solution for a new geometry. The alteration of (2) consists in elimination of the "j"-th block in the matrix of right part and in replacing the "j"-th block of the left part by

$$\left(\mathbf{P}^{(j)H^{-1}}\mathbf{H}^{(j)+} - \mathbf{P}^{(j)E^{-1}}\mathbf{E}^{(j)+}\right) - \left(\mathbf{P}^{(j)H^{-1}}\mathbf{H}^{(j)-} - \mathbf{P}^{(j)E^{-1}}\mathbf{E}^{(j)-}\right)$$. These new geometries will be,

for example, a WG tee (Fig.2c) and a WG corner (Fig.2d) as the modifications of WG units shown correspondingly in Fig.2a and 2b. A smooth transition (Fig.2f) also belongs to the field of application of such algorithms. It should be noted that here we deal with an unusual situation of matching the fields of partial regions beyond the boundaries of considering geometry. The cylindrical fragments of this "matching surface" are marked as $\overline{S}$ in Fig.2. As this approach to modified structures will be used further we present here the Table that consists the amplitudes (*Amp*) and phases (*Phase*) of TE_{10} -mode reflection coefficient for the side port of H-tee (Fig.2c) calculated at different number of azimuth space harmonics in radial WG Q taken into account in (2). The right column of Table contain the data obtained by algorithm [3]. Waveguide dimensions are $23 \times 10\,\text{mm}^2$, frequency is 30 GHz.

Table

Q	8	16	24	algorithm [2]
Amp	0.49940	0.48610	0.48770	0.49000
Phase	-174.31	-171.81	-171.54	-171.27

JUNCTIONS WITH CIRCULAR INSERTS

Some junctions whose S-matrices can be found by the below described algorithms are shown in Fig.3 and Fig.4. Different kinds of tuning posts in cross, tees or in the straight WG (Fig.3) can be considered immediately and the others as different turnstile junctions of coaxial WG and several rectangular ones or conventional coaxial-to-rectangular WG launcher require additional calculations to obtain S-matrix (single-mode in coaxial) by a procedure described, for example, in [4]. The latter will be reduced to a thrice-repeated calculation of the geometry with a shortened coaxial arm.
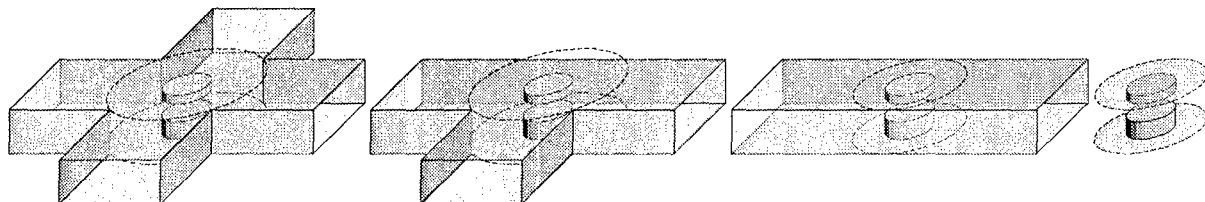
Fig.3
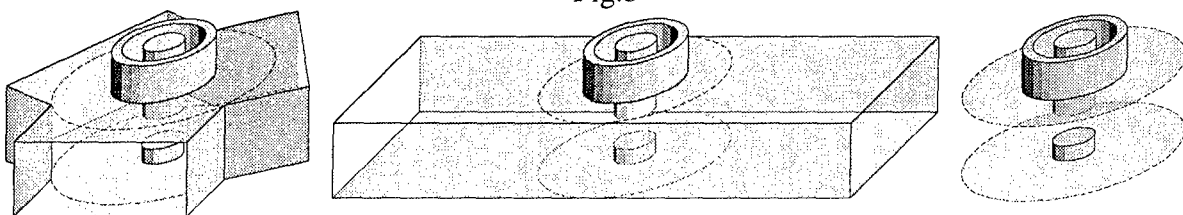
Fig.4

The idea consists in consideration of corresponding auxiliary problems shown in right parts of Fig.3 and 4 to obtain the relation that couples the amplitudes of radial WG field expansions on the "output" boundaries of various units in radial WG. All of such radial WG objects include point $\rho = 0$, and can be treated as some "reflective" ones and produce the relation of

type $V \begin{bmatrix} A \\ B \end{bmatrix} = 0$. Here, A and B are the vectors of coefficients of radial WG field expansion in

the region between "virtual boundary" (Fig.1) and external boundary of cylindrical insert. On the other hand taking into account (1) one can easy obtain

$$W^+R + W^-I = \begin{bmatrix} A \\ B \end{bmatrix}, \quad W^\pm = \begin{bmatrix} \left(Q^H P^E - Q^E P^H\right)^{-1}\left(Q^H E^\pm - Q^E H^\pm\right) \\ \left(P^H Q^E - P^E Q^H\right)^{-1}\left(P^H E^\pm - P^E H^\pm\right) \end{bmatrix}. \text{ Excluding } \begin{bmatrix} A \\ B \end{bmatrix} \text{ we find a}$$

required S-matrix of a multiport with insert from $S = -\left(V \ W^+\right)^{-1} V \ W^-$. Matrices V for cylindrical inserts may be found by conventional mode-matching procedure.

References

[1] F.Reisdorf und H.Knetsch, Wellenausbreitung im abgeknickten Rechteckhohlleiter, *NTZ*, H.7, 1972, 312-317.

[2] H.Yao, K.Zaki, A.Atia, R.Hershig, Full wave modeling of conducting posts in rectangular waveguides, *IEEE Trans. on MTT*, v.43, No.12, 1995, 2824-2829.

[3] L.Rud, Diffraction of waves on H-plane tee junction, *Radiotekhnika i Electronika*, v. 29, No.9, 1984, 1711-1719 (in Russian).

[4] Ma Z., Yamashita E., Port reflection coefficient method for solving multiport microwave network problems, *IEEE Trans. on MTT*, v.43, No.2, 331-337.

SUCCESSIVE APPROXIMATION METHOD FOR THE LINEAR SYSTEM OF DOUBLE LONGITUDINAL SLOTS IN A RECTANGULAR WAVEGUIDE

N. Blinova, A. Zhironkina, and L. Yatsuk

Kharkov National University, Svobody Sq. 4 , Kharkov, 61077, Ukraine

Email: Ludmila.P.Yatsuk@univer.kharkov.ua

ABSTRACT

An efficient approximation method is used to calculate energetic parameters and amplitude-phase distribution along a linear waveguide-slot antenna with double longitudinal slots in a broad wall of a rectangular waveguide having an arbitrary end loading. The approach is used when E-field in slots is approximated with only one sinusoidal function. The mutual coupling of the slots over a waveguide and free space is taken into account, as well as the thickness of a waveguide wall and dielectric filling of the slots.

INTRODUCTION

Linear waveguide-slot systems are widely used in antenna technique, especially in the class of frequency scanning antennas. One of the mostly used antennas of such kind is a system of longitudinal slots in a broad wall of a rectangular waveguide. The amplitude-phase distribution (APD) along an antenna changes with frequency. There are two causes of this change: firstly, slot radiation coefficients depend on the frequency and, secondary, the reflection and radiation coefficients of antenna depend on electric distances between the slots. The controllability of the frequency characteristics of slot energetic parameters is very desirable. One of the ways to reach it is the usage of double slots (two nearly located slots) and filling them with dielectric. The mutual coupling of slots in a double one usually widens the frequency characteristics of their energetic parameters, the dielectric filling makes them narrower. Thus, the combined application of these modifications gives enables one to obtain the required characteristics. Obvious, the usage of the double slots complicates the process of APD and energetic parameters computation for a multielement slot antenna especially when it has an arbitrary loading at the end. If, for this purpose, the well known method of induced magnetomotive forces [1] is used, the order of the corresponding system of linear algebraic equations (SLAE) doubles and the matrix elements become very complicated. The successive approximation method used in our previous works (for example [2]), is free from these shortcomings. The purpose of this paper is to illustrate the possibilities of this method in the case of the double-slot multielement systems and to study some of their electrodynamics properties.

CONSIDERATION

Statement of the problem. The waveguide of a cross section $axb= 23x10$ mm with longitudinal slots in its broad wall is considered. The thickness of the waveguide wall t is taken into account ($t= 1$ mm). The double slot is composed of slots with lengths L_1, L_2 and widths d_1, d_2. Coordinates of their centres and the centre of the whole group, which are calculated from the narrow wall, are x_{01}, x_{02} and x_0, respectively. The distribution of electric field in slots is supposed to be sinusoidal (one half-wave of sinusoid) along the slot and constant across it. If N-fold slots are considered, all these data must have the index n which indicates the order number of the slot considered. The reflection coefficient from the end loading of the

waveguide is $\dot{R}$ which can vary within the limits $0 \le |\dot{R}| \le 1$. The waveguide with slots is excited from a generator with the dominant wave H_{10} of unit amplitude. The amplitude distribution of slot voltages along the antenna and its radiation coefficient are to be determined.

The main idea of the successive approximation method. The first approximation reduces to the first expanding of an incident wave from the first slot to the last one. The first double slot is excited by the wave of unit amplitude $A_0 = 1$. The voltages on the inner surfaces S_1 and S_3 of the first slot $V_{11}^{(1)}, V_{13}^{(1)}$ and on the outer ones (S_2 and S_4) $V_{12}^{(1)}, V_{14}^{(1)}$ satisfy the 4-order SLAE (SLAE-4) of induced magnetomotive forces method [1]. The first figure in subscripts signifies the order number of double slot, the second – the number of the slot surface. The superscript in the brackets signifies the order number of a successive approximation. The amplitude $A_1^{(1)}$ of the wave exciting the second double slot is composed of three amplitudes: A_0 - of the wave incident on the previous slot and the amplitudes $A_{11}^{(1)}, A_{13}^{(1)}$, excited in direction $z > 0$ along the waveguide axis by the electric field on the surfaces S_1 and S_3.

$$A_1^{(1)} = A_0 + A_{11}^{(1)} + A_{13}^{(1)} \tag{1}$$

The voltages $V_{21}^{(1)}, V_{23}^{(1)}$ and $V_{22}^{(1)}, V_{24}^{(1)}$ on the second double slot are found from the SLAE-4 which is similar to the previous one, only magnetomotion forces in the right side of this system are stipulated by the amplitude $A_1^{(1)}$ (not by the A_0 already). This process spreads in the same way to the end of antenna. The wave passing the last double slot has the amplitude $A_N^{(1)}$:

$$A_N^{(1)} = A_{N-1} + A_{N1}^{(1)} + A_{N3}^{(1)} \tag{2}$$

This wave is reflected from the waveguide end loading. We mark the amplitude of reflected wave as

$$B_{N+1}^{(2)} = \dot{R} A_N^{(1)} \tag{3}$$

Here, the second approximation begins, in which we successively find the voltages on the slots with numbers *N, N-1, N-2* and so on. The voltages $V_{N1}^{(2)}, V_{N3}^{(2)}$ and $V_{N2}^{(2)}, V_{N4}^{(2)}$ again are to be found from the SLAE-4 with the amplitude $B_{N+1}^{(2)}$ stipulating the right side of it. The amplitude $B_N^{(2)}$ of the wave which goes to the $(N-1)$-th slot from the slot number N is composed of $B_{N+1}^{(2)}$ and amplitudes $B_{N1}^{(2)}, B_{N3}^{(2)}$, excited by voltages $V_{N1}^{(2)} + V_{N1}^{(2)}$, $V_{N3}^{(1)} + V_{N3}^{(2)}$:

$$B_N^{(2)} = B_{N+1} + B_{N1}^{(2)} + B_{N3}^{(2)} \tag{4}$$

This process continues in $z < 0$ direction down to the first slot and then the third approximation begins. Approximations with odd order-numbers correspond to the spreading of the wave process in $z > 0$ direction and the ones with the even order-numbers – in $z < 0$ direction. These processes include the slots interaction over a free space as well but for the briefness it was not mentioned above. The resulting voltages on the slots $V_{ni}^{(\mu)}$ are sums of voltages of all approximations:

$$V_{ni}^M = \sum_{\mu=1}^{M} V_{ni}^{(\mu)}, \tag{5}$$

where M is the number of approximations, *i* is the number of slot surface.

Calculations results. Fig.1 presents the radiation coefficient dependence on frequency for the single and double empty slots (curves 1,2) and ones filled with dielectric (permittivity $\varepsilon=5$, curves 3,4). Geometric parameters for the single slot are $L=16$mm and $x_0=2.5$mm, for the doubled slot - $L_1=L_2=16.6$mm, $x_{01}=1$mm, $x_{02}=4$.mm. The center of the system is $x_0=2.5$mm. The values for the slots filled with dielectric are: the single slot - $L=10.16$.mm, $x_0=2.5$mm, doubled slot - $L_1=L_2=10.6$mm. $x_{01}=1$mm, $x_{02}=4$mm. The widths of all slots are $d=1.5$ mm. It is clearly seen that in both cases the double slots have a wider band width than the single ones. The behavior of radiation coefficient for the linear antennas with 10 single and double slot radiators is plotted in Fig.2. Curves 1 and 2 correspond to the above mentioned single and double empty slots as elements of the array spaced by the distance of half- wavelength in the waveguide at the frequency $f=9.375$ GHz.. The low level of radiation coefficient at this frequency is a result of an unsatisfactory matching of the slot system with the half space [1]. The same situation occurs in the case of the system of double slots. However, in this case the curve goes a bit higher than one for the single slots and has no reduction of the radiation coefficient at low frequencies (9.0 GHz). If the condition of matching is fulfilled, the system of 10 single slots radiates nearly one half of power arriving from a generator (curve 3). Still the radiation coefficient of this function is reduced at high frequencies. Thus, the system of double slots is the best one.
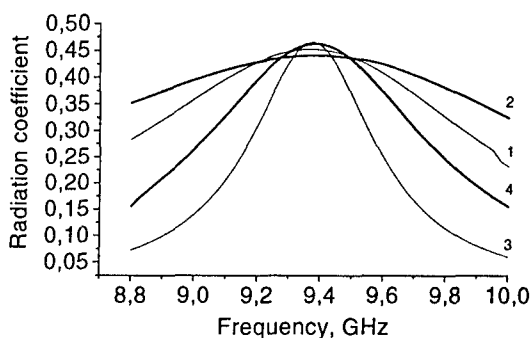
Figure 1
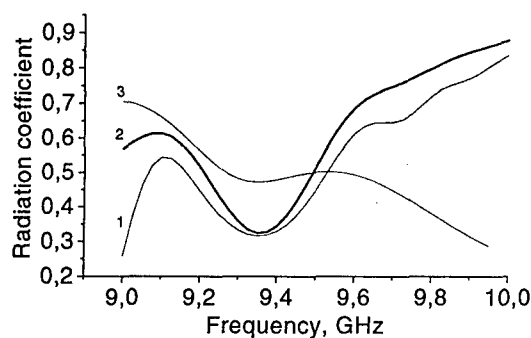
Figure 2

CONCLUSION

The obtained results show that that the applied successive approximation method gives correct description of physical regularities taking place in linear waveguide systems of doubled. slots. The developed computation program can be used for solving optimization problems for antennas with such slots.

REFERENCES

[1] Feld Ya., Benenson L. Antenna-feeder devices. part 2, M.: 1959, 551p. (In Russian)

[2] Yatsuk L.., Blinova N, Zhironkina. A. Linear system of X-slots in a waveguide with an arbitrary reflecting loading. Transactions of the 7-th International Crimea conference "Superhigh frequency technique and telecommunication technologies", Sevastopol, 1997, v.2, p.502-503, (In Russian).

NUMERICAL ANALYSIS OF AC LOSSES IN TRANSMISSION LINES COMPOSED OF ROUND WIRES

Akira MATSUSHIMA and Hiroyoshi SAKAMOTO

Department of Electrical and Computer Engineering, Kumamoto University
Kurokami 2-39-1, Kumamoto 860-8555 Japan   E-mail: matsua@eecs.kumamoto-u.ac.jp

Abstract   An accurate numerical analysis is presented for the AC effective resistance and the inductance of imperfectly conducting wire transmission lines. The number and the allocation of the wires are arbitrary. The analysis is based on integral equations combined with the moment method. The numerical results are shown for the resistance and inductance of two-wire and three-wire lines. The present technique is also applied to the microstrip lines and obtained good agreement with the results by other methods.

1. INTRODUCTION

The properties of wire transmission lines have been considered analytically through many years [1] because of the simplicity of the cross section shapes. From the viewpoint of application, approximate formulas for the characteristic impedance and the attenuation constant concerning various structures have been proposed [2]. The most of the above treatment, however, regards the lines as cylindrical bodies having infinite conductivity or surface impedance, and moreover, imposes the limitation with respect to the thickness of conductors or the distance among them. Because the available frequency range has been widened recently, it is important, in designing transmission lies, to grasp the variation of the AC loss and the characteristic impedance due to the skin and proximity effects. Therefore we desire the development of numerical methods and the construction of design formulas effective for all wire conductivity and frequency not only for the simple two-conductor lines but also for the multi-conductor coupled lines.

Based on the above motivations, this paper develops an accurate numerical technique for the AC resistance and the impedance of the transmission line composed of a set of imperfectly conducting round wires. The problem is formulated into the set of Fredholm type integral equations for the unknown current density that has been used in Refs. [3–5]. The computations are done for several transmission lines, and the characteristics are discussed physically. As an attempt to extend the applicability of the method, the microstrip line is analyzed by using the current filament model.

2. INTEGRAL EQUATIONS

As shown in Fig. 1, infinitely long wires, having the conductivity σ, the permittivity ε, the permeability μ ($\approx \mu_0$), and the radius a, are placed along the z axis. All wires are divided into three ($p = 1, 2, 3$) groups. The p-th group includes M_p ($m = 1, 2, \ldots, M_p$) wires and carries the current $I_p\hat{z}$, where $\hat{\ }$ denotes a unit vector. Here we impose the condition of the closed current, i.e., $I_1 + I_2 + I_3 = 0$. The time factor is assumed $\exp(j\omega t)$ and the field is treated as TEM under the quasi-stationary condition that $\sigma \gg \omega\varepsilon$.

The set of Fredholm type integral equations is given by [3–5]
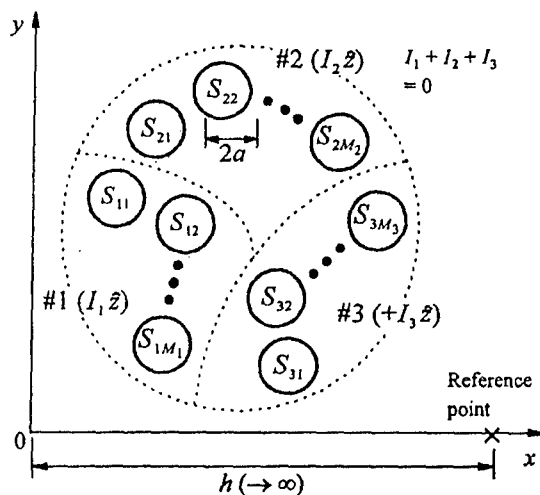
Figure 1: Geometry of the problem.

$$\tilde{J}_z(r) - \frac{j\omega\mu_0\sigma}{2\pi} \sum_{q=1}^{3} \sum_{n=1}^{M_q} \int_{S_{qn}} \tilde{J}_z(r') \log \frac{|r - r'|}{a} dS'$$

$$= \frac{C_p}{a^2} \quad \left(\begin{array}{l} r \in S_{pm}; \ p = 1,2,3; \\ m = 1, 2, \ldots, M_p \end{array} \right) \qquad (1)$$

where $r = x\hat{x} + y\hat{y}$ is the observation point, $r' = x'\hat{x} + y'\hat{y}$ is the point of the z-directed unknown current density $\tilde{J}_z$, and S_{qn} is the n-th cross section in the q-th group. The constant $C_p = -\sigma a^2(\partial\phi/\partial z)_{\#p}$ is also unknown, where ϕ is the scalar potential. The total current in each group is given by

$$I_q = \sum_{n=1}^{M_q} \int_{S_{qn}} \tilde{J}_z(r') dS' \quad (q = 1, 2, 3) \qquad (2)$$
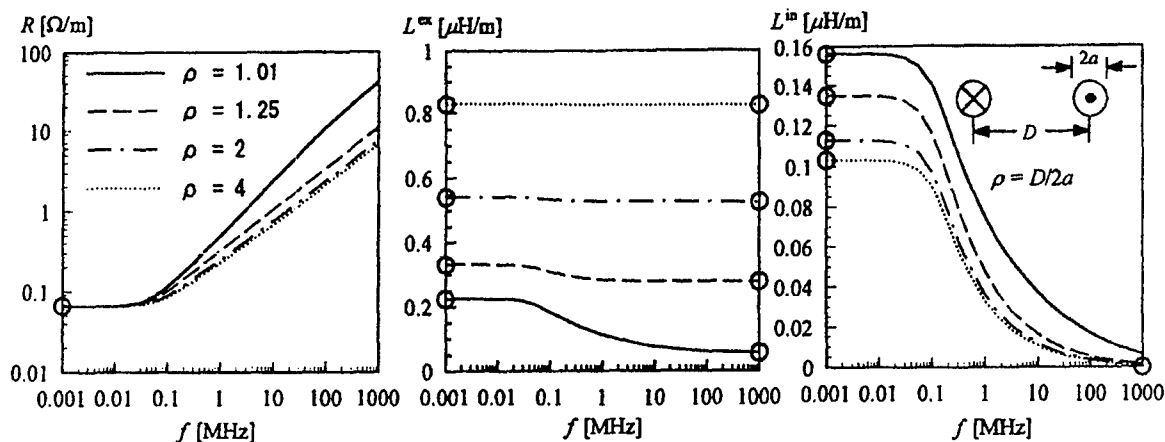
Figure 2: Frequency dependence of the effective resistance and the inductance for the parallel two-wire line. The circles are the exact values at $f \to 0$, ∞. $2a = 32.0$ mil $= 0.8128$ mm, $\sigma = 58$ MS/m.
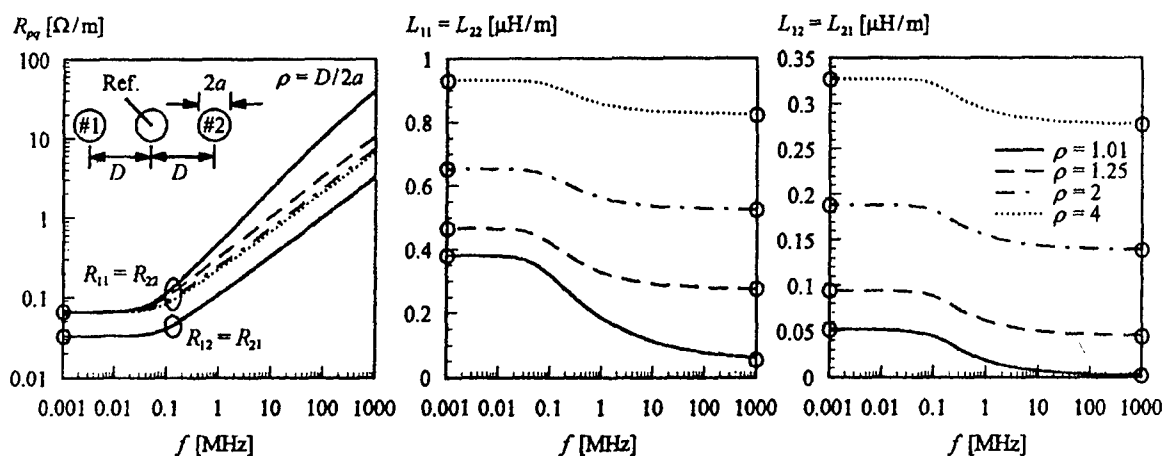
Figure 3: Frequency dependence of the effective resistance and the inductance for the parallel three-wire line. The circles are the exact values at $f \to 0$, ∞. $2a = 32.0$ mil $= 0.8128$ mm, $\sigma = 58$ MS/m.
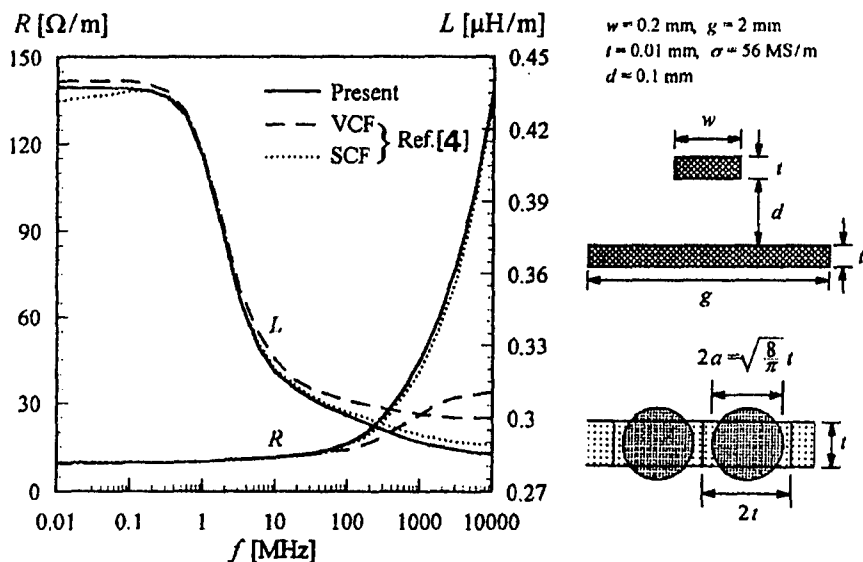
Figure 4: Frequency dependence of the effective resistance and the inductance for the microstrip line ($M_1 = 10$, $M_2 = 100$). The solid, broken, and dotted lines correspond to the present method, the volume-current formulation, and the surface-current formulation, respectively.

3. MOMENT METHOD

Let us solve Eq. (1) by the moment method. We set the local cylindrical coordinate system (r_{pm}, φ_{pm}). in which $r_{pm} = 0$ and $\varphi_{pm} = 0$ correspond to the center of S_{pm} and $+x$ direction, respectively. The unknown function is approximated by the finite sum as

$$\tilde{J}_z(r) \approx \frac{1}{a^2} \sum_{k=-K}^{K} f_{pmk} \frac{J_k(\beta r_{pm})}{J_k(\beta a)} e^{jk\varphi_{pm}} \tag{3}$$

where $J_k(\cdot)$ is the k-th order Bessel function, $\beta = \sqrt{-j\omega\mu_0\sigma} = e^{j3\pi/4}\sqrt{2}/\delta$ is the wave number, and $\delta = \sqrt{2/(\omega\mu_0\sigma)}$ is the skin depth.

Next we substitute Eq. (3) into Eq. (1) and derive a set of linear equations by the point matching method. We impose Eq. (1) at the $2K + 1$ points distributed at regular intervals. This leads us to

$$\sum_{q=1}^{3}\sum_{n=1}^{M_q}\sum_{k=-K}^{K} f_{qnk} \left[\delta_{pq}\delta_{mn} + \beta a G_k(r_{pml,qn})\right] e^{jk\varphi_{pml,qn}} = C_p \quad \left(\begin{array}{l} p = 1,2,3; \ m = 1,2,\ldots,M_p; \\ l = -K, -K+1, \ldots, K \end{array} \right) \tag{4}$$

where the local coordinate $(r_{pml,qn}, \varphi_{pml,qn})$ denotes the position of the l-th matching point on the circumference of S_{pm} with its origin being settled at the center of S_{qn}. The function G_k is defined by

$$G_k(r_{qn}) = \frac{\beta}{2\pi a} \int_{S_{qn}} \frac{J_k(\beta r'_{qn})}{J_k(\beta a)} e^{jk(\varphi'_{qn} - \varphi_{qn})} \log \frac{|r - r'|}{a} dS \tag{5}$$

and are evaluated analytically. We notice the lack of three conditions in Eq. (4), which is supplemented with Eq. (2). Substitution of Eq. (3) into Eq. (2) yields its linear expression of it.

4. NUMERICAL RESULTS

Figure 2 shows the property of the two-wire line composed of copper. The degree of separation is denoted by ρ: the situation of contact corresponds to $\rho = 1$. The circles are based on the exact formulas based on the models of uniform current ($f \to 0$) and surface current ($f \to \infty$), which agree well with the both edges of the curves. The raise of the effective resistance R mainly stems from the skin effect as $\rho = 4$. whereas the proximity effect is added if ρ is smaller. The external inductance becomes small and depends on the frequency when the wires are close. The internal inductance decreases monotonically as the frequency increases due to the skin effect.

Figure 3 concerns the three-wire line. The outer wires carry the signals and the center wire is the reference. From the symmetry $Z_{pq} = Z_{qp}$. The self values R_{pp} and L_{pp} are nearly equal to R and $L^{ex} + L^{in}$ in Fig. 2 for all f. That is, when the current flows only in two wires (#1–Ref. or #2–Ref.), we have little effect from the remaining one. On the other hand, the mutual resistance R_{pq} ($p \neq q$) is about half of $R_{pp}|_{\rho=4}$ and the mutual inductance L_{pq} ($p \neq q$) is 1/3–1/5 times as L_{pp}. This means that the amount of the crosstalk is not small. The circles denoting the limit values agree well with the edges of the curves.

Next we treat the microstrip line by using the filament model. As shown in the right side in Fig. 4. we regard the strips as the set of $t \times 2t$ rectangular elements (t: thickness) and replace them by round wires having the same area. The microstrip line is considered as 110 filaments. The behavior of R and L is similar to the previous figures. The results by the volume-current formulation (VCF) and the surface-current formulation (SCF) are added for reference. The present result is close to VCF and SCF at low and high frequencies, respectively. Considering that VCT (SCF) is precise when the current distribution is uniform (surface oriented), we can conclude that the present treatment is sufficiently effective.

5. CONCLUSIONS

We have computed the AC impedance of the wire transmission lines using the integral equations. The microstrip line was treated by the filament model and good results were obtained. This technique is therefore expected to be effective for the lines with more complicated cross section shapes.

References
    [1] R. W. P. King, "Transmission-line Theory," McGraw-Hill, New York, 1955.
    [2] B. C. Wadell, "Transmission Line Design Handbook," Artech House, Boston, 1991.
    [3] B. D. Popović et al., Proc. IEE, vol.119, no.5, pp.569–574, 1972.
    [4] T. K. Sarkar et al., Progress In Electromagnetics Research, vol.16, pp.153–173, 1997.
    [5] A. Matsushima et al., Trans. IEICE, vol.J81-C-I, no.11, pp. 626–633, 1998.

SELF AND MUTUAL ADMITTANCE OF WAVEGUIDE SYSTEM WITH AN IMPEDANCE FLANGE

S.A. Komarov and V.V. Scherbinin

Altai State University, 66 Dimitrov Str., Barnaul, 656099, Russia

Phone: (3852) 367047, E-mail: komarov@phys.dcn-asu.ru, scherbinin@phys.dcn-asu.ru

ABSTRACT

In this paper, the problem of radiation from finite array of identical waveguides with an impedance flange radiating in arbitrary stratified media has been solved. The problem can be reduced to a set of integral equations with respect to finite functions representing linear combinations of electrical and magnetic fields tangential components on apertures of waveguides. The stationary functional is performed for these equations on the basis of variational principle. The expressions for the matching characteristics of the system (reflection and transmission coefficients of waveguides, self and mutual admittance) are obtained in the closed form by using the functional. The flange impedance influence on the matching characteristics of two rectangular apertures on the single mode assumption is numerically investigated.

INTRODUCTION

Flanged waveguides can be applied as radiating systems and radiowave probes for diagnostics of native media and artificial materials. Our interest lies in developing theoretical methods of solving similar boundary problems. In the case of a perfectly conducting flange, the problem can be formulated as a set of integral equations for unknown functions that are the tangential to the flange components of electric field on the aperture of the waveguide. The method of moments or variational approach can be used for analysis. In the previous papers, the problems were solved for radiation in a plasma or dielectric half-space [1]. The extension of similar class of problems for the case of single radiator with an impedance flange was performed earlier [2-3].

THEORY

Consider an antenna array consisting of the N aperture radiators based on open-ended identical semi-infinite waveguides. The apertures of waveguides are located in a flat infinite flange, which coincides with the coordinate plane $\bar{\rho} = \{x, y\}$ and is characterized by an impedance ZZ_0 (Fig.1). The coordinates of aperture center number n is defined by the $\bar{\rho}_n$ vector $(n=1, \dots, N)$.
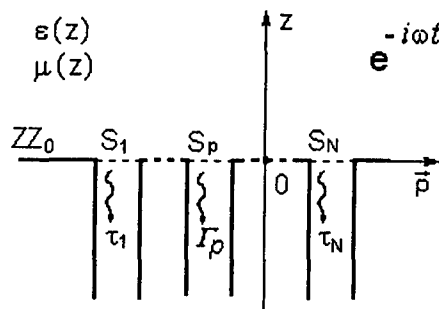
Fig. 1.

The mutual location and orientation of apertures is given by an arbitrary parallel displacement relatively to each other in this plane. The region $z > 0$ is characterized by the medium parameters $\varepsilon(z), \mu(z)$.

It is assumed that a waveguide with the number $n = p$ is excited by the dominant mode and that the fields vary in time as $e^{-i\omega t}$. The radiation occurs in the region $z > 0$. The matching characteristics and mutual coupling of waveguides must be determined. The problem is assumed to be linear, therefore, more general case of several excited waveguides can be analized using the superposition principle.

Using the impedance boundary conditions of the flange and the requirement of continuity of the tangential fields of apertures, a set of integral equations can be obtained by representing auxiliary finite functions $\vec{F}_n(\vec{\rho})$ as linear combinations of tangential fields of the apertures:

$$\vec{F}_n(\vec{\rho}) = \vec{E}_{tn}(\vec{\rho}, -0) - ZZ_0 \vec{u} \times \vec{H}_{tn}(\vec{\rho}, -0); \quad \vec{\rho} \in S_n. \tag{1}$$

For the set of integral equations, a stationary functional related to the matching and mutual coupling characteristics is introduced. An approximate solution of the problem can be found by using the variational principle and a model set of finite functions (1) on apertures. The single-mode approach is most simple, here suppose

$$\vec{F}_n(\vec{\rho}) = A_n \vec{\phi}_{0n}(\vec{\rho}), \tag{2}$$

where $\vec{\phi}_{0n}(\vec{\rho})$ is the orthonormal modal functions of the waveguide dominant mode of the given configuration, and A_n is the unknown complex amplitudes. The application of the variational principle in the single-mode approach to the set of integral equations allows to derive expressions for the dominant mode reflection coefficient Γ_p in the waveguide with number p and the transmission coefficients $\tau_n, (n \neq p)$. Each of the latter characterize the amplitude of the wave transmitted into the waveguide with number n:

$$\Gamma_p = \tfrac{1}{\alpha}\left(A_p - \beta\right), \quad n = p; \quad \tau_n = \tfrac{1}{\alpha} A_n, \quad n \neq p. \tag{3}$$

Here, $\alpha = 1 - ZZ_0 Y_0, \beta = 1 + ZZ_0 Y_0$; Y_0 is the admittance of infinite waveguide. The coefficients A_n can be found from the following algebraic set:

$$\sum_{m=1}^{N}\left(p_{nm} + \delta_{nm}\frac{Y_0}{\alpha}\right) A_m = \frac{2\delta_{np} Y_0}{\alpha}; \quad n = 1, \dots, N. \tag{4}$$

Here, δ_{nm} is Kronecker delta, coefficients p_{nm} are defined as

$$p_{nm} = \int\int\limits_{S_n S_m} \vec{\phi}_{0n}(\vec{\rho})\, \widetilde{G}(\vec{\rho} - \vec{\rho}')\, \phi_{0m}(\vec{\rho}')\, d\vec{\rho}'\, d\vec{\rho}, \tag{5}$$

$\widetilde{G}(\vec{\rho} - \vec{\rho}')$ is the dyadic Green's function containing the information about environment properties in the region $z > 0$.

Self and mutual admittances are connected with the reflection and transmission coefficients as [1,2]:

$$Y_p^s = Y_0 \frac{1 - \Gamma_p}{1 + \Gamma_p}, \quad Y_n^m = Y_0 \frac{\tau_n}{1 + \Gamma_p}. \tag{6}$$

NUMERICAL EXAMPLES

This approach was applied to the analysis of the matching and mutual coupling characteristics of two rectangular waveguides with an impedance flange. The reflection coefficients in the first waveguide Γ_1, transmission coefficient τ_2 in the second waveguide, admittances Y_1^s and Y_2^m under the formulas (3-6) were calculated.

Fig. 2 shows the dependence of $|\Gamma_1|$ and $|\tau_2|$ on the parameter k_0a (k_0 is free space wavenumber). Calculations were performed for the following parameters: $a = 2.3b$ (a and b are the dimensions of waveguide broad and sidewall, respectively), $L = 1.5b$ (L is the distance between centres of apertures), the mutual orientation of waveguides is shown in Fig. 2.
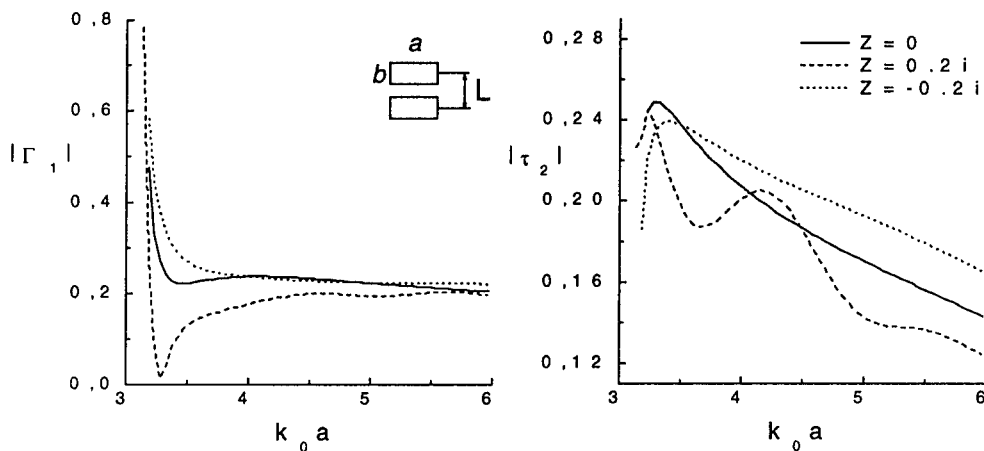
Fig. 2

Fig. 2 demonstrates the most noticeably influence of the impedance on the reflection coefficient in the vicinity of k_0a critical value. The capacitive impedance $Im(Z) > 0$ decreases $|\Gamma_1|$ and $|\tau_2|$; the inductive impedance $Im(Z) < 0$ increases these characteristics in comparison with the case of a perfectly conducting flange.

REFERENCES

1. *Gorgio V. Borgiotti* A Novel Expression for the Mutual Admittance of Planar Radiating Elements. IEEE Trans. on Antennas and Propagation, Vol. AP-16, No.3, pp.329-333.
2. *S.A. Komarov* Variational principle in the problem of reflection from semi-infinite waveguide with impedance flange. Izvesiya Vuzov, Radioelectronics, 1985, vol.28, No.3, pp.30-35. (in Russian)
3. *S.A. Komarov, V.V. Scherbinin* Reflection from circular semi-infinity waveguide with impedance flange. News of Altai State University, 1994, No.1, pp. 68-70 (http://tbs.dcn-asu.ru/news/1999/1/phys/TheNewsOfASU-1999-1-phys-04.pdf.zip) (in Russian)

PHYSICAL AND MATHEMETICAL ASPECTS OF SOME MODE MATCHING METHOD MODIFICATIONS

Alexander G. Yushchenko

Institute of Radiophysics and Electronics, National Academy of Sciences of Ukraine
12 Ul. Akademika Proskury, Kharkov, 61085, Ukraine; e-mail: AGYu@kpi.kharkov.ua

ABSTRACT

The effective mathematical approach making possible the understanding of different physical phenomena, which have been observed in complicated waveguide structures, from the standpoint of some properties of a semi-open resonator, based on cut -off waveguide splitters, has been discussed.

THE IDEAS WORLD AND THE WORLD OF PHYSICAL PHENOMENA

Albert Einstein and Leopold Infeld in their book "THE EVOLUTION OF PHYSICS: *The Growth of Ideas from Early Concepts to Reality and Quanta"* remarked "we were striving in broad touches to describe the attempts of human mind to find the relationship between the world of ideas and the world of phenomena". According to Einstein's opinion, "the most inconceivable characteristic of universe is that it is conceivable". Modern standpoint on the knowledge evolution allows to draw a conclusion about its homology with the biological evolution [1], but to refer ideas themselves to the categories of certain forms of lives in consciousness, as well as reproductionable programs (genetic algorithms and computer viruses) can refer to live forms in virtual reality [2,3]. In the author's opinion, the possibility of human cognition, as well as homology of evolution processes observed on different structural organization levels, is due to fundamental unities of creative processes of nature and consciousness [3]. It is essential that a fuller agreement of the observed phenomena with our theories is reached by means of inventing some new ideas and new notions, while new facts often compel us to abandon old theories.

This work is devoted to the consideration of the question of shaping the new electrodynamics concepts on a waveguide splitter as a certain semi-open resonator, the description of an efficient mathematical method of electrodynamics analysis of such kind of structures and the demonstration of a variety of different practical actions of the newly received knowledge for the microwave technology.

SOME WAYS OF OVERCOMING MATHEMATICAL MODELING PROBLEMS

In a physical-mathematical study, it is very often fruitful to compare physical and mathematical information on the subject of models world and physical world singularities correspondence. So, for example, mathematical singularities which are not backed up by the analyzed structure physics, point to the need of auditing of the mathematical method, while a priori knowledge about singularity, for instance, on the metallic wedge, will allow a priori use of field representation taking this particularity into account [4]. In paper [5] it is noted that in problems of the applied mathematical physic, failures connected with attempts to build efficient solutions in the form of series on certain function system, possessing completeness inside a considered area, but unfit for account of its boundary conditions, sometimes brought about some wrong conclusions about insolubility of the problem. Therefore, it was proposed to divide the problem into several auxiliary subproblems, for which it is possible to find series satisfying both the assumed equation and boundary conditions. In such a manner, the general solution of Dirichlet's problem and Neiman's problem for rectangular region was obtained in the work [6] as a sum of two uniform problems. The usage a similar approach to solving

scattering problems on waveguide discontinuities has allowed to get some series which converge rapidly and already in one-wave approximation allowed to receive the relative error not more than 1-2%, regardless of the type of the problem geometry and its complexity [7,8,9]. It is important to note that the adequacy of electrodynamic modelling performed on the basis of the Treftz method to real wave processes is due to the accuracy of satisfying the boundary conditions. In this case, the boundary conditions are satisfied termwise for the expansion of the field electrical components. To illustrate it, let us consider the geometry of the elementary problem about the waveguide expansion where the mode matching intervals have been shown (dashed lines):
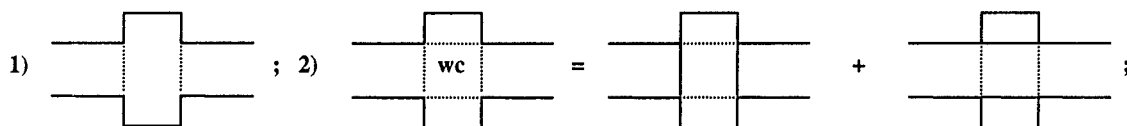
where 1) corresponds to traditional mode matching method and 2) -to the method discussed here.

Thus, for the case 2) the used Treftz method, in which an internal region (WGC) of "orthogonal waveguide coupling" containing no singular points inside the mode bases matching intervals, has been separated at the stage of selecting the problem geometry [8,9]. Experience shows that such an approach to solving not only scattering waveguide problems [7-9], but also eigenmode (scalar [10-14] and vector [15,16]) problems yields infinity rapidly converged equations. It should be pointed out that for the first case the one-wave approximations has no practical sense.

NOTION OF NEW TYPE OF RESONATOR BASED ON CUT-OFF SPLITTERS

The method described above enables one to analyze an electromagnetic field structure of different types of waveguide splitters and waveguides with complex cross sections. The most interesting results have been obtained under eigenmode problem statement concerning different types of waveguide splitters with and without dielectric filling [10-14]. It turned out that in the case, when splitter is formed by cut -off hollow waveguides, a limited number of eigenmodes exists in it that was confirmed experimentally. Hence, it follows that sections of cut-off waveguides operate as "spread" reflection boundaries for the field concentrated within the splitter area. In this case the term "spread" boundaries characterizes the fact that here it is impossible to indicate exactly the coordinates of reflecting surface, because the field attenuates from the borders of a WGC area in longitudinal directions of cut-off waveguides forming splitters. That is why when a splitter is excited by a propagating wave, for example H_{10}, the coupling quasi-eigen modes arise there, which condition the variety of their scattering properties, in the case when its arms are not cut-off [8,9]. According to their physical nature, they are analogues to the modes on "locked" waves in waveguide expansion or dielectric inserts. The main phenomenological difficulty in understanding this phenomenon was that the known resonators structures have certain metal or dielectric reflection boundaries and accommodate propagation of high order waves. The big contribution into the evolution of knowledge about the physics of phenomena in these structures was given by the "free oscillation model" with complex frequencies [17], that has brought about the refusal from previous standpoints which connect a sharp inflections of their amplitude -frequencies characteristics with appearance of high modes.

NEW CONCEPTION PRACTICAL ADAPTATION IN MICROWAVE TECHNOLOGY

The most practically important property of the discovered resonators was their semi-openness that ensures a possibility of access in a resonator area. Having filled one of the orthogonal waveguides by extended magnitodielectric bar (rectangular waveguides splitter

[9,12]) or plate (splitter of rounds waveguides and flat one [13,18,19]) and having chosen its sizes under condition of the waveguide being cut-off, one could locally test this object consecutively moving it through the area of splitter, connected with the main microwave tract. As quasi-eigen H modes frequencies correspond to critical frequencies of E waves of transmission lines, the necessity of studying the new lines, whose cross-sections have the form of splitters, became obvious [14-16]. Waveguide splitter eigenmodes have been also applied for the microwave filters designing based on the resonators of different classes [20]. In all cases, the new devices have proved to be better on many basic parameters than the known ones.

CONCLUSION

The developed conception about the new type of resonator based on cut-off waveguide splitter has changed the insight into phenomena physics of scattering waves on waveguides irregularities and has lead to the designing of unique new class of microwave devices.

REFERENCES

1. K. Popper," The Growth of Scientific Knowledge", *London*, 1969.
2. R. Dawkins, "The Selffish Gene". *Moscow:* Mir, 1993.
3. A. Yushchenko " The Evolution Megasynthesis Logic and The Causal Attributed of a Global Catastrophe",   Proc. Int. Conf. of BSEC: Disasters. *Kharkov,* May 23-25, 2000, p.270-276.
4. G. Zargano, A. Lerer, V. Laypin at al," Transmission Lines With Complex Cross Sections", *Rostov-na –Donu*, 1983. *(in Russian)*
5. A.Vlasov, " Method of Redefied Series", *Len.*, LGU: The Dynamic Theory of Seismic Waves, v.3, 1959. *(in Russian)*
6. L. Kantorovich and V. Krilov. "The Approximate methods of the Higher Analysis". *(in Russian)* Editions: *Moscow/Leningrad;* Russia: Fizmatgiz. 1962.
7. E. Kuhn. "A Mode Matching Method for Solving Field Problems in Waveguide and Resonators Circuits". *AEU.* No. 27, pp. 511-518. 1973.
8. V. Korobkin , S. Shibalkin, and A. Yushchenko , "The Coupling Quasi-eigen Modes in Waveguide Splitters". *Radiotech. Electron.*, v.39. No. 7, pp. 1107-1112. 1994.
9. A. Yushchenko, M. Ilchenko, S. Shibalkin et al, "The Non-destructive Microwave Test of an Extended Dielectric and Metallized Dielectric Structures Parameters by the Method of Electromagnetic Resonance of Waveguide Junctions", *Int. Conf. ISRAMT, Kiev, Ukraine*, v.2, pp.707-710, 1995.
10. V. Korobkin, V. Osintsev. "The Eigen Modes of Electromagnetic Field of a Dielectric Resonator in Waveguide Splitter". *Radiotech. Electron.*,v.30. No.3, pp. 417-421. 1985. *(in Russian)*
11. V. Korobkin, N. Pyatak, "The Eigen Modes of a Semi-open Waveguide Structure", *Radiotech. Electron.*, v.32, No.3, pp. 517-525, 1987.
12. V. Korobkin, V. Osintsev, "The Eigen Modes of the Cross-shape Splitter of Rectangular Waveguides with Magnetodielectric Filling", *ZhTF,* v.55, №10, 1985.
13. V. Korobkin, Yu. Makeev, A. Strizhachenko, "The Eigen Electromagnetic Modes of Half-Open Cylindrical Waveguide Junction With Dielectric Filling", *ZhTPh*, v. 56, No. 12, pp.2313-2319, 1986.
14. V. Korobkin, V. Osintsev," The Eigen Modes of the Rectangular Waveguide Placed Into Semi-Open Cross-Shaped Screen", *Conference on Waves and Diffraction*, Moscow, v.3, pp.20-22. 1990.
15. A. Yushchenko and S. Shibalkin. "The Electrodynamic Modelling of Waveguide Properties of Semi-open Transmission Lines based on Flat Waveguide Splitters", *IRMMW*, v. 15. N11, pp. 1523-1552. 1994. *(in Russian)*
16. A. Yushchenko, S. Shibalkin, M. Ilchenko, "The Eigenmodes Classification of the Cross-Shaped Waveguide Splitters", *22 th Conf. on IRMMW*, v. 2.8, pp. 126-127, USA, 1997.
17. L. Rud', Yu. Sirenko, V. Schestopalov, N. Yaschina, " The Numerical Investigations of the Free Oscillations Characteristic of an Open Waveguide Resonators", *IRE NANU*, Prep. № 316 -318, 1986.
18. A. Yushchenko, V. Chizhov, "Precision Microwave Testing of the Dielectric Substrates", *IEEE Instrumentation & Measurement*, v. 46, no. 2, pp. 507-510, April 1997.
19. M. Ilchenko, A. Yushchenko, Yu. Poplavko at al. " The Method of the Waveguide Junction Resonance for an Integrated Ferroelectric Films Investigation", *Proc. of 27 th UMC*, v. 2 , pp. 842-847, 1997.
20. M.E. Ilchenko, A.G. Yushchenko, V.V. Popov , " The Band Pass Filters Based on Resonators of Different Classes", *Int. Conf. ISRAMT, Kiev, Ukraine*, v.2, pp. 631-633 , 1995.

EIGEN REGIMES OF THE MULTILINK WAVEGUIDE FILTER WITH REACTIVE DIAPHRAGMS

V.B. Kazanskiy and V.V. Khardikov

Chair of Theoretical Radiophysics, Kharkov State University
4 Svobody sq., Kharkov, 61077, Ukraine
Tel: +38 0572 457257, e-mail: Vyacheslav.V.Khardikov@univer.kharkov.ua

ABSTRACT

The eigen regimes of a multilink waveguide filter with reactive diaphragms are investigated. The transcendental equation for complex frequencies and Q-factor of the eigen oscillations of the multilink waveguide filter with reactive diaphragms is presented. The dependences of the eigen frequencies and Q-factor of the eigen oscillations on the structure parameters are shown.

OBJECT OF RESEARCH

A cylindrical waveguide with the N infinitely thin and perfectly conducting radial or circular diaphragms placed on the equal distances (L) (fig.1) was considered. The waveguide has a radius a. The pieces-homogeneous layers between diaphragms are characterized by the permittivity (ε_j), permeability (μ_j) and longitudinal dimensions b_j ($j = 1,2$).
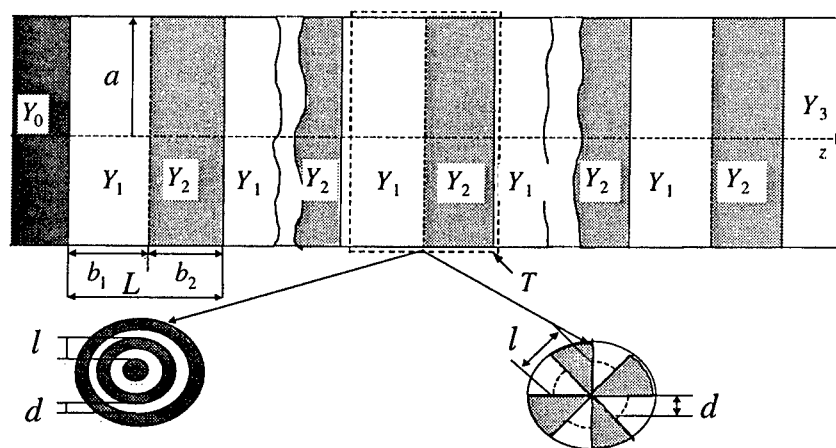
Fig.1. Multilink waveguide filter with reactive diaphragms.

The eigen oscillations of the symmetrical TE_{0n}- and TM_{0n}-waves were researched. The characteristic dimension of the diaphragms is supposed to be significantly smaller than the wave length ($\kappa = l/\lambda$), therefore there are no phenomena of the transformation of the wave types. In this approach, the amplitudes of the fields on the entrances of the neighboring periods are connected by the transfer matrix T of the equivalent four-pole. Taking into consideration the transfer matrixes of the input (T_0) and output (T_3) boundaries of the filter, the amplitudes of the fields of the radiation are defined by the operator correlation:

$$\begin{pmatrix} 0 \\ B_0 \end{pmatrix} = T_0 T^N T_3 \begin{pmatrix} A_{N+1} \\ 0 \end{pmatrix}. \tag{1}$$

The elements of the degree of the transfer matrix $T(t_{jk})$ were presented in [1] by the analytical formulas through the Mauguin polynomials $P_N(X)$, where $X = (t_{11} + t_{22})/2$.

The transcendental equation for the complex eigen frequencies was obtained from the condition of the existing of a nontrivial solution of (1):

$$P_{N-1}(X)/P_N(X) = t_{11} \pm t_{12}((Y_j - Y_3)/(Y_1 + Y_3)). \qquad (2)$$

There Y_j is the wave admittance of the regular part of the structure, and $Y_0 = Y_1$. The complex eigen frequencies $\kappa_c^\nu = \mathrm{Re}\kappa_c^\nu + i \cdot \mathrm{Im}\kappa_c^\nu$ (ν is the number of the resonance in the zones of the quasitransparent) are included in t_{jk} as the argument ($t_{jk}(\kappa_c^\nu)$). The upper sign in (2) corresponds to the TE_{0n}-waves and the lower sign corresponds to the TM_{0n}-waves.

ANALYSIS OF THE EIGEN REGIMES

The characteristic dependencies of the eigen frequencies κ_c^ν and Q-factor ($Q_\nu = -\mathrm{Re}\kappa_c^\nu/(2\mathrm{Im}\kappa_c^\nu)$) [2] of the oscillations on such structure parameters as filling parameter u of the diaphragms ($u = \cos(\pi d/l)$), L/a and b_1/L for filter were presented in Fig. 2-4 ($N = 3$) and Fig. 5 ($N = 2$).
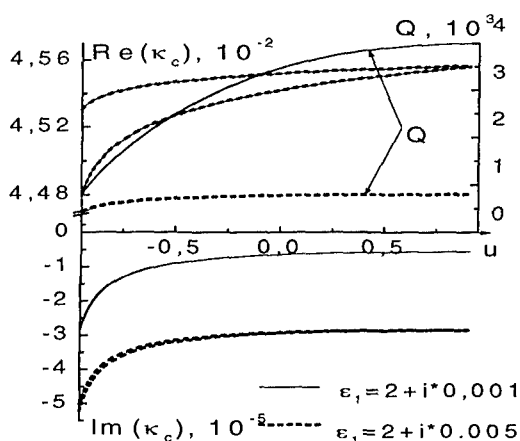
Fig.2. Dependences of κ_c^ν and Q_ν TE_{01}-
wave on u ($L/a = 2, a/l = 15, \varepsilon_i = \mu_i = 1$,
($i = 0,2,3$), $\mu_1 = 1$).
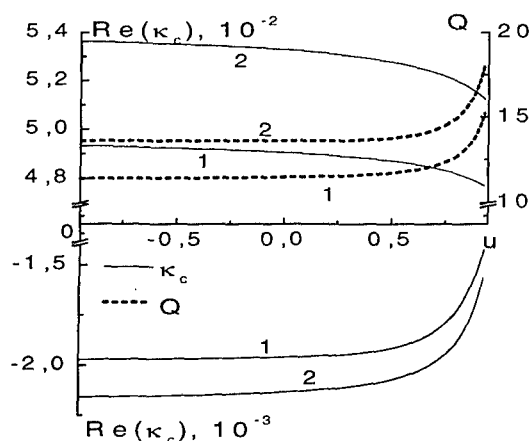
Fig.3. Dependences of κ_c^ν and Q_ν TM_{01}-
wave on u ($L/a = 2, a/l = 15, \varepsilon_i = \mu_i = 1$).

The influence of the connection between basis elements upon the spectrum of the eigen oscillations can be seen from the dependences of the $\kappa_c^\nu(u)$ and $Q_\nu(u)$ on the filling parameter u of the circular diaphragms (Fig. 2-3). These dependences are distinguished by a very small value of $\mathrm{Im}\kappa_c^\nu$ for the TE_{01}-wave (Fig. 2). In this case, the spectrum lines $\mathrm{Re}\kappa_c^\nu(u)$ in each quasitransparent zone are separated by small distances if the filling parameter is small ($u \le -0.5$), and they are very close if the filling parameter is large ($u > 0$). For the TM_{01}-wave the spectrum is wider (Fig. 3). This fact is conditioned by the polarization sensitivity of the diaphragms.

The absolute values of $\mathrm{Re}\kappa_c^\nu$, $\left|\mathrm{Im}\kappa_c^\nu\right|$ are decreasing and the Q-factor (Q_ν) is increasing, if the frequencies ($\sim L/\lambda$) are increasing (Fig. 4). Such behavior of κ_c^ν and Q_ν is typical for quasiopen structures.

The presence of the piece-homogenous regions ($\varepsilon_1 \neq \varepsilon_2$) changes the conditions of the radiation in the external waveguide canals. The extreme values appeared in dependences of the radiation losses ($\mathrm{Im}\kappa_c^\nu$) and the Q-factor (Q_ν) on the dimension of the inhomogeneous regions (Fig. 5).
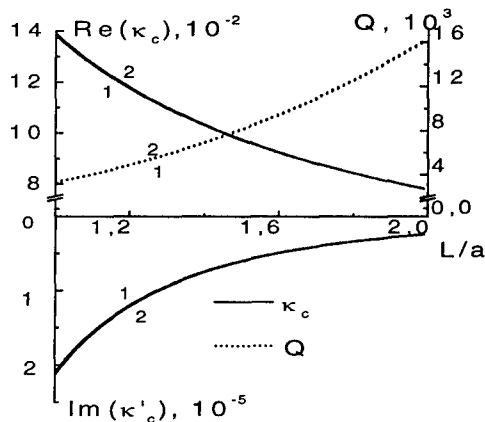
Fig.4. Dependences of κ_c^ν and Q_ν TE_{01}-wave on L/a. ($u=0$, $a/l=15$, $\varepsilon_i = \mu_i = 1$).
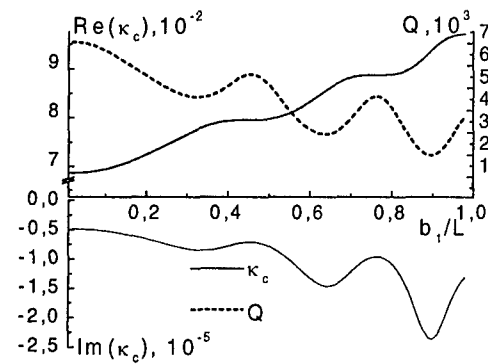
Fig.5. Dependences of κ_c^ν and Q_ν TE_{01}-wave on b_1/L. ($L/a=2$, $a/l=12$, $u=0$, $\varepsilon_2 = 2$, $\varepsilon_0 = \varepsilon_1 = \varepsilon_3 = 1$, $\mu_i = 1$).

The $\left|\mathrm{Im}\kappa_c^\nu\right|$ is increasing and the Q-factor (Q_ν)decreasing, when the dissipative losses ($\mathrm{Im}\varepsilon_1$) are increasing (fig. 2). In this case $\mathrm{Re}\kappa_c^\nu$ was almost constant.

CONCLUSIONS
The transcendental equation for complex frequencies and Q-factor of the eigen oscillations of the symmetrical cylindrical waves of the waveguide with an arbitrary number of the identically elements is presented. The dependences of the eigen frequencies for multilink waveguide filter with the reactive diaphragms on wave type, filling parameter of the diaphragm, dimension of the dielectric layers and dissipative losses are shown. Their computational algorithm does not depend on the wave type, waveguide canals and number of the identically elements. The presented results allow to select the optimum operation regime of the control devices depending on their functional purpose.

REFERENCES
[1] V.B. Kazanskiy, V.V. Podlozny, V.V. Khardikov " Investigation of Scattering Characteristics of a Sequence of Identical Elements Using Cayley-Hamiltone Theorem", Electromagnetic waves and electronic system, Russia, V.4, № 3,1999, pp. 19-27. (In Russian and English).
[2] Diffraction of the waves on gratings./ V.P. Shestopalov, L.N. Litvinenko, S.A. Masalov, V.G. Sologub.– Kharkov, 1973.–278 p. . (In Russian).

GENERALIZED ANALYSIS OF A COAXIAL WAVEGUIDE TO RADIAL WAVEGUIDE JUNCTION

Oleksey S. Kim

National Technical University of Ukraine

2110D, Radio Engineering Faculty, Polytekhnichna st., 12, Kyiv, 03056, Ukraine

E-mail: alex_kim@ucl.kiev.ua

ABSTRACT

A new mathematical model of a coaxial waveguide to radial waveguide junction is presented. The solution has been obtained in terms of generalized scattering matrices. At first, closed form expressions for elements of a generalized admittance matrix of the junction have been derived. Then, the generalized admittance matrix has been converted to a generalized scattering matrix.

INTRODUCTION

A coaxial waveguide to radial waveguide junction is widely employed as a part of coaxial-to-rectangular waveguide junctions, rotary joints and other variety of microwave devices. However, the diffraction problem of a coaxial waveguide to radial waveguide junction has not been solved in a generalized form so far. The known mathematical models are limited to the TEM mode in a coaxial line and formulated in terms of input admittance normalized to the coaxial aperture [1]. In this paper, the solution of the problem is obtained in terms of generalized scattering matrix, which describes all possible operation conditions of the junction.

Furthermore, along with the solution for a general junction between two radial waveguides [2], the presented approach allows analyzing biconical antennas with non-linear elements of cones taking into account the feed geometry.
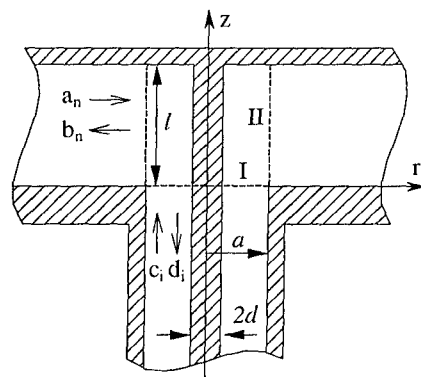
Fig. 1

MULTIMODE ANALYSIS OF THE JUNCTION

Geometry of the junction is presented in Fig. 1. Transversal (to the r-direction) components of the electric and magnetic fields in a radial waveguide are given by (azimuthal index m is omitted for brevity)

$$\vec{E}_\tau = \sum_{n=0}^{\infty} \left(a_n^E H_m^{(1)}(k_n r) + b_n^E H_m^{(2)}(k_n r) \right) \vec{\Phi}_n^E + \sum_{n=1}^{\infty} \left(a_n^H H_m'^{(1)}(k_n r) + b_n^H H_m'^{(2)}(k_n r) \right) \left(\vec{\Phi}_n^H \vec{e}_\varphi \right) \vec{e}_\varphi =$$

$$= \sum_{n=0}^{\infty} A_n^E \vec{\Phi}_n^E + \sum_{n=1}^{\infty} A_n^H \left(\vec{\Phi}_n^H \vec{e}_\varphi \right) \vec{e}_\varphi , \tag{1}$$

$$\vec{e}_r \times \vec{H}_\tau = \sum_{n=0}^{\infty} y_n^E \left(a_n^E H_m'^{(1)}(k_n r) + b_n^E H_m'^{(2)}(k_n r) \right) \left(\vec{\Phi}_n^E \vec{e}_z \right) \vec{e}_z -$$

$$- \sum_{n=1}^{\infty} y_n^H \left(a_n^H H_m^{(1)}(k_n r) + b_n^H H_m^{(2)}(k_n r) \right) \vec{\Phi}_n^H = \sum_{n=0}^{\infty} B_n^E \left(\vec{\Phi}_n^E \vec{e}_z \right) \vec{e}_z - \sum_{n=1}^{\infty} B_n^H \vec{\Phi}_n^H , \tag{2}$$

where indices E and H stand for TM and TE waves, respectively; $H_m^{(1)}$ and $H_m^{(2)}$ are Hankel functions of the first and second kind; $k_n = \sqrt{k_0^2 - \gamma_n^2}$; k_0 is the wave propagation constant in free space; $\gamma_n = n\pi/l$; $\vec{\Phi}_n^E$ and $\vec{\Phi}_n^H$ are the radial waveguide eigenfunctions

$$\vec{\Phi}_n^E = \cos(\gamma_n z)\cos(m\varphi)\vec{e}_z + \frac{m\gamma_n}{k_n^2 r}\sin(\gamma_n z)\sin(m\varphi)\vec{e}_\varphi; \tag{3}$$

$$\vec{\Phi}_n^H = -\frac{m\gamma_n}{k_n^2 r}\cos(\gamma_n z)\cos(m\varphi)\vec{e}_z + \sin(\gamma_n z)\sin(m\varphi)\vec{e}_\varphi; \tag{4}$$

$y_n^E = -j\dfrac{\omega\varepsilon\varepsilon_0}{k_n}$ and $y_n^H = -j\dfrac{k_n}{\omega\mu\mu_0}$ are the wave admittances.

At first, we define a boundary condition on the surface II as $E_\tau^{II} = 0$ and an exciting electric field on the surface I by

$$\vec{E}_\tau^I = \sum_i \left(C_i^{H,E} + D_i^{H,E}\right)Z_i^{H,E}\vec{h}_i^{H,E} \times \vec{e}_z = \sum_i G_i^{H,E}Z_i^{H,E}\vec{h}_i^{H,E} \times \vec{e}_z, \tag{5}$$

where $\vec{h}_i$ is the transverse magnetic field of the coaxial mode i; Z_i is the wave impedance of mode i: $Z_i^H = \dfrac{k_0 Z_0}{\gamma_i^H}\mu$, $Z_i^E = \dfrac{\gamma_i^E Z_0}{k_0\varepsilon}$; $\gamma_i^{H,E} = \sqrt{k_0^2\varepsilon\mu - \left(k_i^{H,E}\right)^2}$ is the propagation constant of mode i; $k_i^{H,E} = \lambda_i^{H,E}/a$ is the wave number of mode i; λ_i^E is the i-th root of the function $L_m(x) = J_m(x) - Y_m(x)J_m(xd/a)/Y_m(xd/a)$;

λ_i^H is the i-th root of the function $X_m'(x) = J_m'(x) - Y_m'(x)J_m'(xd/a)/Y_m'(xd/a)$;

J_m and Y_m are Bessel functions of the first and second kind, order m.

Then, the tangential magnetic fields on the surfaces II and I are found by using the Green's function for a coaxial resonator. These magnetic fields can also be represented through equation (2) and $\vec{H}_\tau^I = \sum_p F_p^{H,E}\vec{h}_p^{H,E}$. Making use of continuity of tangential magnetic fields on the surfaces I and II and following the Galerkin procedure for the resulting equations we obtain the elements of the generalized admittance matrix $Y^{(11)}$ and $Y^{(21)}$:

TM$_i \to$ TM$_i$ and TE$_i \to$ TE$_i$ mode coupling: $Y_{ii}^{(11)} = j\cos\left(\gamma_i^{H,E}l\right)/\sin\left(\gamma_i^{H,E}l\right)$;

TEM$\to$TEM mode coupling : $\qquad Y_{ii}^{(11)} = j\cos\left(k_0\sqrt{\varepsilon\mu}l\right)/\sin\left(k_0\sqrt{\varepsilon\mu}l\right)$;

TM$_i\to$TM$_n$ mode coupling: $\qquad Y_{ni}^{(21)} = \dfrac{4}{\varepsilon_n l}\dfrac{k_0\varepsilon}{k_i^E}\dfrac{\gamma_i^E}{\left(\gamma_i^E\right)^2 - \gamma_n^2}L_m'\left(k_i^E a\right)$;

TE$_i\to$TM$_n$ mode coupling: $\qquad Y_{ni}^{(21)} = \dfrac{4}{\varepsilon_n l}\left\{\dfrac{m\gamma_n}{(k_n)^2 a}\gamma_n + \dfrac{m\gamma_i^H}{\left(k_i^H\right)^2 a}\gamma_i^H\right\}\dfrac{X_m\left(k_i^H a\right)}{\gamma_n^2 - \left(\gamma_i^H\right)^2}$;

TM$_i\to$TE$_n$ mode coupling: $\qquad Y_{ni}^{(21)} = 0$;

TE$_i\to$TE$_n$ mode coupling: $\qquad Y_{ni}^{(21)} = -\dfrac{4}{\varepsilon_n l}\dfrac{\gamma_n}{\gamma_n^2 - \left(\gamma_i^H\right)^2}X_m\left(k_i^H a\right)$;

TEM$\to$TM$_n$ mode coupling: $\qquad Y_n^{(21)} = j\dfrac{4d}{\varepsilon_n al}\dfrac{k_0\sqrt{\varepsilon\mu}}{k_0^2\varepsilon\mu - \gamma_n^2}$; $\qquad \varepsilon_n = \begin{cases} 2, n = 0 \\ 1, n \neq 0 \end{cases}$.

Similarly, we obtain the other elements of the generalized admittance matrix $Y^{(12)}$ and $Y^{(22)}$. Transition from the admittance matrix to a scattering matrix yields the generalized scattering matrix of the junction between coaxial and radial waveguides.

RESULTS

Consider a cylindrical cavity formed by a short circuit in the radial waveguide (Fig. 2). Experimental results have been presented by Keam and Williamson [1] for the phase of the reflection coefficient for the partially filled with dielectric and hollow coaxial-line/cylindrical cavity junctions. The dimensions are $a = 1.525$ mm, $d = 3.5$ mm, $R = 41$ mm, $l = 150$ mm, $c = 24.12$ mm and $\varepsilon = 2.1$. Both cases for TEM coaxial mode excitation have been analyzed using the developed mathematical model. For the first case, four generalized scattering matrices have been progressively cascaded: of the junction between the hollow and filled coaxial waveguides, of the coaxial waveguide to radial waveguide junction, of the junction between the filled and hollow radial waveguides, and of the short circuit in the radial waveguide. The computed results are plotted in Fig. 3 along with Keam and Williamson's experimental values. One can see that theoretical and experimental results agree very well.
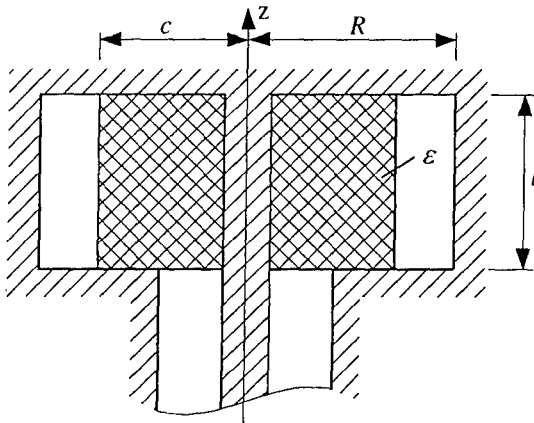
Fig. 2
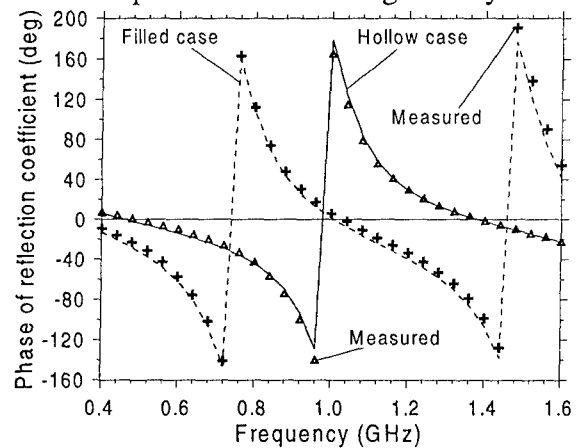
Fig. 3

CONCLUSION

A new approach to analysis of a coaxial waveguide to radial waveguide junction is presented. A key feature of the approach is the closed form expressions for elements of a generalized admittance matrix of the junction. Resulted generalized scattering matrix describes all possible operation conditions of the junction. Correctness of the developed mathematical model has been proved by a comparison with known results for cylindrical cavity excited by coaxial waveguide.

Presented solution can be incorporated into multimode analysis of coaxial-to-rectangular waveguide junctions, rotary joints and other variety of microwave and antenna devices.

REFERENCES

[1] R.B. Keam and A.G. Williamson, "Analysis of a general coaxial-line/radial-line region junction," *IEEE Trans. Microwave Theory Tech.*, vol. 41, pp. 516–520, Mar. 1993.

[2] F.F. Dubrovka and O.S. Kim, "A new mathematical model of omnidirectional dual-reflector antennas," *Radioelektronika (Izvestiya VUZ)*, vol. 42, no. 6, pp. 3–16, 1999 (in Russian; translation into English: *Radioelectronics & Communications Systems*, Vol. 42, No. 6, pp. 1–10, 1999)

MODELING AND OPTIMIZATION OF A NEW-TYPE BANDSTOP FILTER BASED ON MULTIAPERTURE IRISES

Lyudmila Mospan and Anatoly Kirilenko

Institute of Radiophysics and Electronics, National Academy of Science of Ukraine
12, Ul. Proskury, Kharkov, 61085, Ukraine
phone: 380 572 448518, fax: 380 572 441105, e-mail: kirilenko@ire.kharkov.ua

ABSTRACT

General properties of the single- and double-band rejection sections based on the multi-aperture irises have been investigated. A bandstop iris with two rejection resonances has been numerically investigated and measured. New type of three-section bandstop filter with three-slot irises has been designed, optimized and tested. The calculated results for an X-band bandstop filter have been confirmed with good accuracy in experiment.

INTRODUCTION

A bandstop iris for a rectangular waveguide was first reported in [1]. Recently, it was shown that a resonance of total rejection exists even for the simplest two-slot iris and that it is always located between two points of full matching [2]. The nature of the rejection resonance was also studied there, and it was shown that this resonance is the structure response to the excitation at the real frequency close to two natural oscillation complex frequencies. In this communication, the study of such elements as the components of bandstop filters is discussed.

NUMERICAL RESULTS

A numerical model under consideration was based on the generalized S-matrix technique The role of key element was played by the plane-step junction of the main rectangular waveguide and two (or three) waveguides of smaller cross-sections. Required full-wave S-matrix of this junction was calculated by the conventional mode-matching technique (see, for example, [3]). Numerical investigations show that the rejection resonance Q-factor is mainly determined by the difference between the widths of the iris slots. Varying both the height and the width of the iris slots can change the location of the resonance frequency. Fig. 1 shows the frequency responses of two-aperture irises, slots of which were cut right next to the wide walls of the rectangular waveguide WR90 (iris thickness is 0.48 *mm*, $a1 = 14.5$ mm, $a2 = 12.5$ mm, $b1 = b2 = 4.75$ mm (solid curve with square markers), $b1 = b2 = 3.75$ mm (solid curve), $b1 = b2 = 1.75$ mm (dashed curve)).The widths of the slots are fixed and their heights are changed decreasing from one curve to the other leading to the resonance sift to lower frequency together with making its Q-factor decreased. As it is seen, decreasing the heights of the slots does not necessarily leads to the increase in the Q-factor of the rejection resonance (as in single aperture irises). Note that even two "high" slots, taking approximately 90% of the waveguide height, provide a rejection effect (see the curve with square marks in Fig. 1). The latter is important with respect to the electrical breakdown properties. Similar to Fig.1 rejection responses are also formed by the three-slot irises, the topology of which is symmetrical with relation to the horizontal axis of the waveguide cross-section. This symmetry provides a rarefied spectrum of the higher-order modes and decreases mutual interaction of fringing fields for the irises being the sections of a filter with $\lambda_g /4$ distances between them. The latter makes the response more close to the one predicted by the circuit theory. A cumulative view of the dependence of the three-slot iris properties on the widths of the slots is given by Fig. 2, where equal-value curves for the rejection frequencies and the Q-factors (defined at the 3 *dB* level of insertion loss) are presented in the coordinates $(a1, a2)$. Fig. 2 enables one to estimate the dimensions of the iris slots that provide a required Q-factor and rejection resonance frequency

(iris thickness is 0.38 _mm_, heights of the slots are $b1 = 1.52$ _mm_, $b2 = 2.52$ _mm_). It is clear that close frequency responses can be obtained both for $a1 > a2$ and for $a1 < a2$. In the case of equal "electromagnetic" properties for the external pair of slots and the central one (roughly speaking in the vicinity of their equal dimensions), the Q-factor tends to infinity and the rejection resonance disappears. Note also that the rejection sections based on the irises with three slots of different dimensions possess an interesting feature of forming frequency responses with two rejection resonances. The frequency responses having two rejection spikes for the three-slot iris in _WR90_ (iris thickness is 0.48 _mm_, $a1 \times b1 = 13.1 \times 1$ mm^2, $a2 \times b2 = 14.2 \times 3$ mm^2, $a3 \times b3 = = 15.2 \times 3$ mm^2) are presented in Fig. 3. Calculated (solid line) and measured (triangle marks) curves are in good agreement although the maxima of insertion loss reach only 12 _dB_ and 19 _dB_ because of the finite conductivity. The existence of the pair of rejection resonances can be interpreted as a response of the open structure to the excitation of three natural oscillations with three different complex frequencies [2]. One of them has a low Q-factor of the coupling with input and output waveguides, whereas the other two have high Q-factors. As an example of application of multi-slot irises for the bandstop filter design, let us consider the structure shown in the insert in Fig. 4. The filter-prototype design was carried out according to the following specification: frequencies of the stopband are $f_1 = 10.2$ _GHz_, $f_2 = 10.3$ _GHz_ at the suppression level $L_s \geq 80$ _dB_, edge frequencies of passband $f_{p1} = 10.1$ _GHz_, $f_{p2} = 10.4$ _GHz_ with permissible insertion loss $L_p \leq 0.5$ _dB_. According to [4], we obtain the filter consisting of three sections, separated by the distances $l_1 = l_2 = \lambda_g / 4$. Obviously, the interaction of irises due to the fringing fields substantially influences both the skirt selectivity and the level of the passband insertion loss. The geometry optimization for the bandstop filter based on resonance irises was carried out with the aid of the goal function of conventional type:

$$g(\vec{x}) = \sum_k \left\{ \frac{L_s}{L_1(f_k^s)} \right\}^2 + \sum_i \left\{ \frac{L(f_i^p)}{L_p} \right\}^2 ,$$

where L_s and L_p are the required level of insertion loss in the stop band and the pass band respectively. The frequencies $\{ f_k^s \}$ and $\{ f_i^p \}$ correspond to the sets of sampling points within the stop and passbands, respectively. The vector of varying parameters $\vec{x}$ included all the filter dimensions except of the thickness of the irises and the location of the slot centers. The dimensions of two irises after optimization are presented in _Table_ 1.

Table. 1 Bandstop filter geometry

1st and 3rd irises		2nd iris			
$a1 \times b1$, mm^2	$a2 \times b2$, mm^2	$a1 \times b1$, mm^2	$a2 \times b2$, mm^2	$l1$, _mm_	$l2$, _mm_
14.31x1.87	12.53ō 2.09	14.25ō2.1	12.57ō1.98	9.92	9.95

The curve of the insertion losses for the optimized filter geometry, pictured in Fig. 5 by solid line, corresponds to the goal function with an increased weight of the lower part of the pass band. The resulting response is characterized by quite a steep left front near the lower edge of the stopband (0.22 _dB/MHz_). The lower part of the passband of approximately 500 _MHz_ has insertion loss exceeding no more than 0.15 _dB_. An experimental example of the filter has shown the losses of about 0.5 _dB_ within the band of 450 _MHz_ to the left of the stopband and even a steeper left front of the characteristic at the lower edge of the stopband (2.5 _dB/MHz_) with the maximum of insertion loss being equal to 42 _dB_. Corresponding data are marked by triangles in Fig. 4.

CONCLUSION

Thus, it has been shown that the multi-slot resonance irises, cross-sections of which contain several slots of different dimensions, form a frequency response containing a number of total rejection resonances equal to the number of slots having different "electromagnetic" properties minus one. Numerical analysis of the possibility to control the locations and the Q-factors of the total rejection resonances has shown that it is possible to develop easy-to-manufacture low-cost bandstop filters (one- and two-band) using the multi-slot irises. Three-section bandstop filter has been experimentally realized showing a high front steepness of the stopband frequency response.
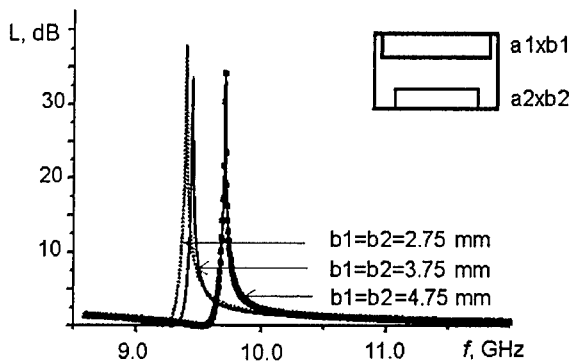
Fig. 1 Insertion loss for two-slot irises with different slot heights

Fig. 2 Plots $Q = Const$ and $f = Const$ for a three-slot symmetric iris with a single stopband

Fig. 3 Calculated (—) and measured (Δ) frequency responses for a two-stopband three-slot iris
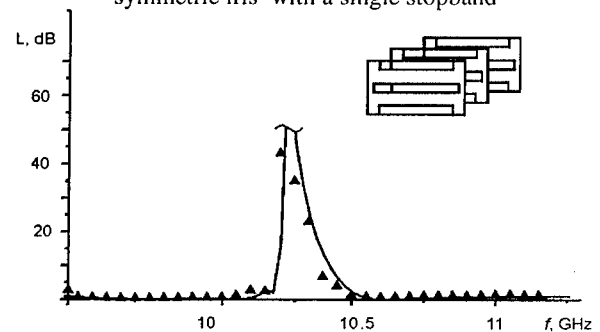
Fig. 4 Calculated (—) and measured (Δ) insertion loss for a bandstop filter based on three-slot irises

REFERENCES

[1] N.G.Paterson, I.Anderson, Bandstop iris for rectangular waveguide, *Electronics Lett.*, 1976.-v.12, N22.-pp.592-594.

[2] A.A.Kirilenko, L.P.Mospan, Reflection resonances of two-aperture irises in rectangular waveguide, *Proc of 29th Eur. Microwave Conf.*, Munich, Germany, 1999.- v.1.-pp.28-31

[3] H.Parzelt, F.Arndt "Double-plane steps in rectangular waveguides and their application for transformers, irises, and filters," *IEEE Trans. MTT*, vol.30, no5, pp.7711-777, 1982.

[4] G.L.Matthaei, L.Young, E.M.Jones, Microwave Filters, Impedance-Matching Networks and Coupling Structures, McGraw-Hill, 1972.

ELECTROMAGNETIC OSCILLATIONS
IN PERIODIC MEDIA OUTSIDE THE PASSBANDS

M.I. Ayzatsky

National Scientific Center "Kkarkov Institute of Physics and Technology"

1 Akademicheskaya Str., Kharkov, 61108, Ukraine

aizatsky@nik.kharkov.ua

ABSTRACT

In this paper we present the results of investigation of electromagnetic waves in a layered dielectric that is backed from one side by a metal plate. These waves attenuate in the direction of periodicity and propagate along the normal direction, so they can be treated as surface waves.

INTRODUCTION

It is well known [1] that in 1-D periodic media, there are two different basic electromagnetic eigen-oscillations supported without external currents and charges. In the certain frequency intervals (passbands) the electromagnetic oscillations represent wave process, which carry a constant power (in the case of absence of absorption) in the forward or backward direction. Between the passbands electromagnetic oscillations have a structure that is different from the previous case. In these frequency intervals electromagnetic oscillations transfer no energy in the direction of periodicity and have decreasing (increasing) dependence on the coordinate. These frequency intervals are called forbidden bands (stopbands). Today the 1-D periodic media are sometimes called 1-D photonic band gap (PBG) structures. Results of our investigations of the properties of electromagnetic oscillations in the stopbands of a layered structure are presented. Particularly, we have shown that, under some conditions, the eigen-functions, which yield the field distributions, can have zero values at certain planes normal to the direction of periodicity. By placing metal sheets at these planes, we can essentially change the properties of the waves reflected from finite number of dielectric layers lying on a metal plate and create dielectric-metal resonance systems having oscillations with increasing or decreasing field distributions along the coordinate z. These phenomena can be treated in terms of so-called "defect modes" [2] as the "surface defect levels" that arise as a result of existence of the interface between the medium with a band structure and the medium that can be considered as an infinite potential well. In this paper we present the results of investigations of the evanescent in one direction and propagating in the normal one electromagnetic waves in the case of a layered structure limited from one side by a metal (or in the case of periodicity reflected symmetrically relatively some plane).

MULTI-LAYER DIELECTRIC

Let us consider properties of eigen electromagnetic oscillations in a layered dielectric, which represents a periodical along the axis z set of layers with the thickness d_1 and d_2 and permittivities ε_1 end ε_2. In transversal directions (x, y), the layers are not limited. Dependence on time and transversal coordinate x shall be supposed as $\exp\{i\{k_x x - \omega t)\}$.

Dependence of the transversal components of electromagnetic field on the longitudinal coordinate z can be found from the Maxwell equations. For arbitrarily selected two adjoining layers $(i=1,2)$ (from which we shall count the periods $(s=0)$) tangential electric field components can be written as:

$$E_{\tau,i}^{(0)} = E_i^{(+)}e^{ih_i z} + E_i^{(-)}e^{-ih_i z}, \tag{1.1}$$

where $h_i = \omega/c\sqrt{\varepsilon_i - k_x^2 c^2/\omega^2}$ and $E_i^{(\pm)}$ are constants.

As the considered system is periodic along the axis z with period $D=d_1+d_2$, the field components within the period with number s can be determined by the expression:

$$E_{\tau,i}^{(s)} = \rho^s \left[E_i^{(+)} e^{ih_i(z-sD)} + E_i^{(-)} e^{-ih_i(z-sD)} \right] \tag{1.2}$$

where ρ is some complex number. It is easy to show that at the fixed frequency the boundary conditions for the field components are fulfilled only for two values of parameter ρ [3]: ρ_1 and $\rho_2 = 1/\rho_1$.

Inside the stopbans, $|\rho_1| < 1$. If $\kappa_x = k_x D / 2\pi = D / \lambda_x > 0$, there is a gap for the frequencies $0 < \Omega < \Omega_1$ ($\Omega = \omega D/(2\pi c) = D/\lambda$). This gap we shall call the zero stop band. Let us
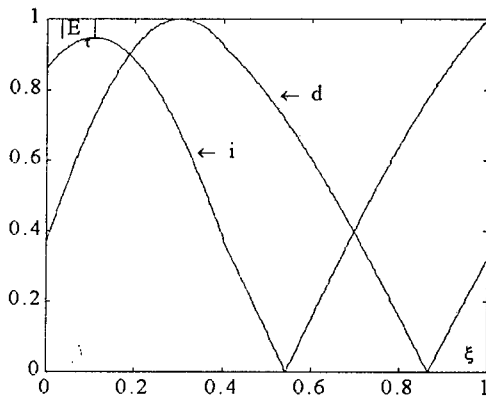
Fig. 1

consider a structure of an electrical field in some stop band. An example can be seen in Fig.1 where we show the dependences of the absolute value of E_τ on the normalized longitudinal coordinate $\xi = z/D$ within one period for the first stopband and $\kappa_x = 0.31$, $\Omega = 0.35$ ($n_1 = sqrt(\varepsilon_1') = 2$, $n_2 = sqrt(\varepsilon_2') = 1.38$, $\varepsilon_1'' = \varepsilon_2'' = 0$, $d_1 = n_2/(n_1+n_2)D$, $d_2 = n_1/(n_1+n_2)D$).

From Fig.1, it follows that both eigen non-propagating oscillations (d-decreasing: $|\rho_1| < 1$, i-increasing: $|\rho_2| > 1$) of layered dielectric have an interesting feature. In certain planes normal to the axis z, the tangential component of the electric field equals to zero [4]. Note that for two fundamental solutions these planes do not coincide. By putting in these planes metal planes, we can efficiently control the field distribution.

Indeed, a general solution of electromagnetic problem with a finite layered structure is represented as a sum of two fundamental (partial) solutions $E_\tau(z) = C_1 E_{\tau,1}(z) + C_2 E_{\tau,2}(z)$. If the metal plate is located at $z = z_*$, the following condition must be satisfied:

$$C_1 E_{\tau,1}(z_*) + C_2 E_{\tau,2}(z_*) = 0, \tag{1.3}$$

from which it follows that if $E_{\tau,1}(z_*) = 0$ ($E_{\tau,2}(z_*) = 0$), then $C_2=0$ ($C_1=0$). Thus, choosing some z_*, we can create the field distribution that corresponds only to one fundamental solution, i.e. either pure increasing or decreasing one.

Transversal planes with zero values of the tangential component of electric field exist in all gaps under some conditions, but for the zero gap they are located near the edge of the gap and if $\kappa_x \to 0$, the frequency width of this interval tends to zero.

Using the described circumstances, we can, firstly, essentially change the performances of waves reflected from a finite number of dielectric layers lying on a metal plate. Secondly, one can create metal-dielectric resonance systems based on non-propagating waves and having oscillations with increasing (decreasing) field distributions along the coordinate z. Results of these investigations will be given elsewhere. Here we shall present the results of exploring of the surface waves that can exist in the forbidden zones in the semi-limited layered dielectrics backed by a metal plate.

SURFACE WAVES IN A HALF-LIMITED LAYERED DIELECTRIC

Assume that the front surface of the metal plate has the coordinate $z=z_m$. The layered dielectric is spaced in such a way that a layer with the higher refractive index starts at the coordinate $z=0$. Changing the position of the front surface of the metal plate $(0<z_m<D)$, we can study different "surface levels" of electromagnetic oscillations. We shall consider the case when optical length of each layer equals a quarter of some reference wavelength λ_*, i.e., $d_i = \lambda_* /(4n_i)$. For perfect metal we have the boundary condition at $z=z_m$:

$$E_\tau(z = z_m) = C_1 E_{\tau,1}(z = z_m) + C_2 E_{\tau,2}\left(z = z_m\right).$$

If $E_{\tau,1}(z)$ corresponds to the decreasing solution then we have to suppose that $C_2=0$ and try to find such a frequency Ω and transversal wavenumber κ_x inside a forbidden band that $E_{\tau,1}(\Omega, \kappa_x, z = z_m) = 0$.

Fig. 2

In Fig.2 (s-polarization) and Fig.3 (p-polarization), we present the results of solving this dispersion equation (symbols $\{ \bullet \}$ -z_m=0,
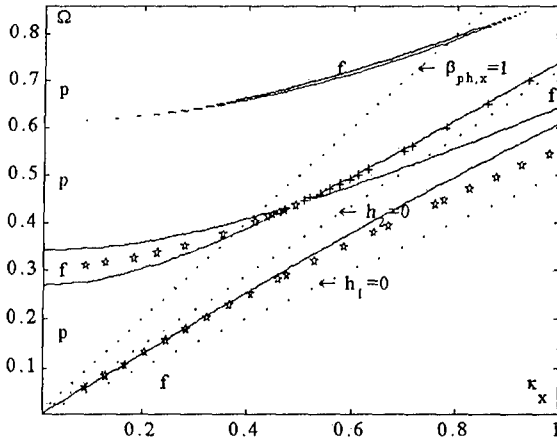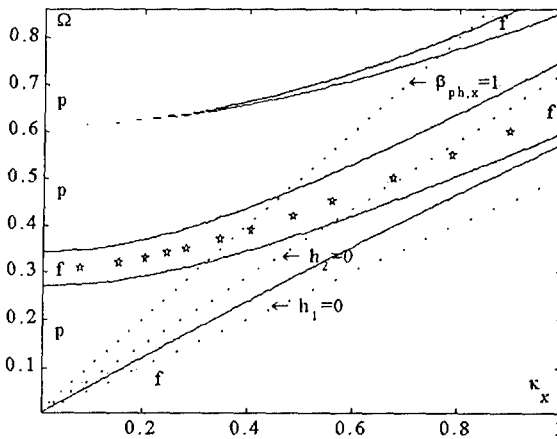
the layered medium starts with the more dense layer of n_1=2; and symbols $\{+\}$ - $z_m=d_1$, layered medium starts with the less dense layer of n_2=1.38) . Letters p mark passbands and letters f mark forbidden bands.

We can see that for s-polarization there are surface waves both for z_m=0 and $z_m=d_1$, but surface waves with p-polarization exist only when z_m=0. The surface wave in the zero forbidden band exists only for s-polarization when $0<z_m<d_1/2$ and $(d_1+d_2/2)<z_m<D$. In the first forbidden band for the s-polarization waves can travel along the x-axis with phase velocities less or greater than that of light

Fig. 3

$(0<z_m<d_1/2$ and $(d_1+d_2/2)<z_m<D)$ and they are slow waves if $d_1/2<z_m<(d_1+d_2/2)$.

For the p-polarization surface waves in the zero forbidden band cannot exist. In the first forbidden band waves travel along the x-axis with phase velocities less or greater than that of light only if $(0<z_m<d_1/2$ and $(d_1+d_2/2)<z_m<D)$. So, surface waves with the p-polarization do not exist if $d_1/2<z_m<(d_1+d_2/2)$.

Our preliminary simulations have shown that the studied surface waves can exist in the layered structures with finite number of layers backed from one side by the metal.

REFERENCES

[1] Brillouin L., Parodi M. *Propagation des Ondes dans les Milieux Periodiques*, 1956.

[2] Yablonovish E., Gmitter T.H., Meade R.D. et al. *Phys. Rev. Lett.* 1991, **67**, 3380.

[3] Khizhnyak N.A. Theory of waveguides with dielectric disks. *Radiotekhnika i Elektronika*, 1960, v.5, N.3, pp..413-421 (in Rusian).

[4] Ayzatsky M.I. Electromagnetic oscillations in periodic mediums and waveguides outside the passband. *Problems of Atomic Science and Technology*, 1999, N.3, p.6-9.

STUDY OF SURFACE FLUTE MODES PROPAGATION IN A CYLINDRICAL METAL WAVEGUIDES WITH NONCIRCULAR CROSS-SECTION AND PLASMA FILLING

V. Girka, I. Pavlenko, and S. Puzirkov

Kharkov National University, 4 Svobody sq., Kharkov, 61077, Ukraine,
e-mail: girka@pem.kharkov.ua

INTRODUCTION

Due to needs of modern radio-physics and plasma electronics, dispersion properties of the plasma filled waveguides of different geometries have been actively studied recently. Such waveguides are used as the main component of oscillators and amplifiers of high frequency electromagnetic waves and guiders of intense charged particle beams [1]. Theoretical study of surface flute modes (SFM) which can propagate along azimuthal angular direction in a cylindrical metal waveguide with non-circular cross-section can be useful for elaboration of various radio engineering and plasma electron devices.

That is why this paper is devoted to description of the SFM electromagnetic properties. They are studied analytically and numerically by using Maxwell equations for description of the SFM fields and cold plasma model with the aid of successive approximation method.

PROBLEM GEOMETRY AND ANALYTICAL STUDY

Consider a cylindrical metal waveguide which is completely filled with magneto-active plasma. An external uniform magnetic field $\vec{H}_0$ is oriented along the z axis. The radius of metal waveguide is characterized by the following expression: $R_2 = R_1(1 + h\cos N\varphi)$. Dependence of the SFM fields on coordinates and time is chosen in the following form: $f_m(r)\exp(im\varphi - i\omega t)$. Here h is a small parameter, ω is the wave frequency, m is the azimuthal wave number. We suppose here that $\dfrac{\partial}{\partial z} = 0$. If there is a narrow axial slot in the metal waveguide (it means that its angular size $\varphi_0 \ll 1$) then by using Maxwell's equations and two boundary conditions: the SFM fields are of finite value at the axis of the waveguide, and the tangential component of the SFM electric field is zero at the metal surface, one can find the following dispersion equation:

$$\frac{m\varepsilon_2}{kR_2\varepsilon_1\Psi_0^2} + \frac{I_m'(kR_2\Psi_0)}{\Psi_0 I_m(kR_2\Psi_0)} = \frac{-\varphi_0(J_m'(kR_2) + iN_m'(kR_2))}{2\pi(J_m(kR_2) + iN_m(kR_2))} , \tag{1}$$

where $\Psi_0^2 = \dfrac{\varepsilon_2^2 - \varepsilon_1^2}{\varepsilon_1}$, $I_m(x)$ is modified Bessel function, $J_m(x)$ and $N_{m(}(x)$ are the Bessel and Neiman functions, respectively, the prime means the derivative with respect to argument, $k = \omega/c$, ε_i is the plasma permeability tensor in the approximation of cold plasma. Solution of (1) has been found in the form: $\omega = \omega_0 + \Delta\omega - i\gamma$, where $|\Delta\omega| \ll \omega_0$, $\gamma \ll \omega_0$, ω_0 is the solution of (1) in the zero approximation ($\varphi_0 = 0$), $\Delta\omega_0$ and γ are real and imagine parts of

the first order approximation for the ω_0, respectively. In the limiting case one can find the following analytical expressions:

$$\Delta\omega \approx \frac{\varphi_0}{\pi}\Omega_e \; ; \; \gamma \approx -\varphi_0\left(\frac{kR_2}{2}\right)^{|2m|} \frac{m!^2}{\pi^2|m|} 2\Omega_e \, , \text{if } kR_2 \ll 1;$$

(2)

$$\Delta\omega \approx \frac{\varphi_0}{4\pi ka}\Omega_e \; ; \; \gamma \approx -\frac{\varphi_0}{2\pi}\Omega_e \, , \text{if } kR_2 \gg m,$$

here Ω_e is the Langmuir frequency.

In the case of the waveguide with non-circular cross-section one can find the following analytical expressions as a correction to ω_0. If the inequality $kR_2\Psi_0 \gg N,m$ is valid, then correction term is as follows:

$$\Delta\omega \approx -\frac{h^2}{2}\omega_0\left(1 + \frac{|\omega_e|}{\omega_0}2N\right).$$

(3)

However, in the opposite limiting case $kR_2\Psi_0 \ll N,m$ one can find another solution:

$$\Delta\omega \approx \frac{-h^2\omega_0}{2}\begin{cases} \dfrac{4N\omega_e^2}{kR_1\Omega_e} & \text{when } \omega_0 \to 0 \\[3mm] \dfrac{2N\omega_0}{|\omega_e|} & \text{when } \omega_0 \sim |\omega_e| \end{cases}.$$

(4)

RESULTS OF NUMERICAL STUDY

Numerical analysis of (1) enables one to obtain the results presented in Figure 1, where $\beta = \dfrac{\Omega_e^2}{\omega_e^2} = 50$. Lines marked by squares, triangles and diamonds have been obtained in the cases of m=2, 3 and 4, respectively.
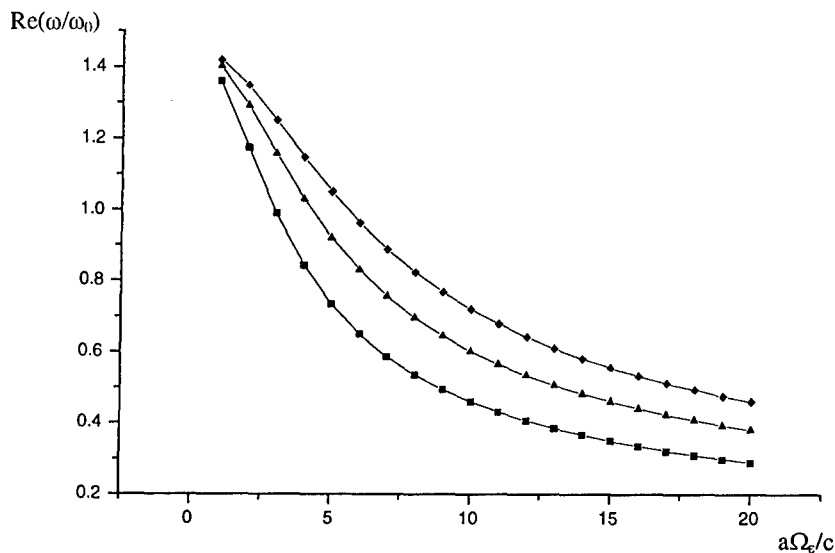
Fig. 1.

One can see that the SFM with small values of azimuthal wavenumbers damp more stronger than those with relatively great wavenumbers.

Figure 2 illustrates a results of spatial structure of the SFM magnetic field for the case $R_1 = 7\dfrac{c}{\Omega_e}$ and m=3.
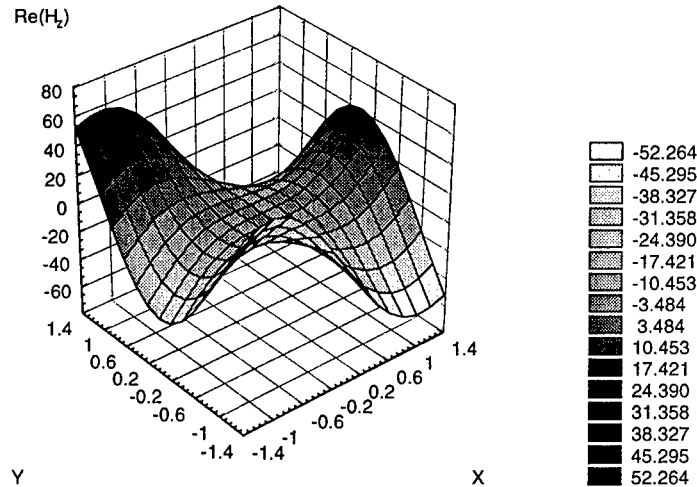
Fig. 2.

CONCLUSION

Dispersion properties of the SFM have been studied in the case of magnetoactive plasma-filled metal waveguide with the cross-section which is characterized by the equation $R_2(\varphi) = R_1(1 + h \sin N\varphi)$. Eigenfrequencies and spatial distributions of the SFM fields have been found and analyzed both analytically and numerically. The SFM damping caused by emission of their power through an axially directed narrow slot has been studied as well. It is found that these X-polarized modes are the fast waves: their magnetic component is much greater than both electric components; their wave power flow is directed mainly along a small azimuth angle. The SFM propagation can be considered as alternative method for wall conditioning in fusion devices during a microwave gas discharge.

The work was supported in part by the Science and Technology Center in Ukraine, project #1112.

REFERENCES

[1] Miller R.B. *An Introduction to the Physics of Intense Charged Particle Beams*. New York, Plenum, 1982.

DOMAIN-PRODUCT-TECHNIQUE ANALYSIS
OF A DIELECTRIC-LOADED H-PLANE RADIATOR

Ahmet S. Turk, and Vitaliy P. Chumachneko[1]
Electronics Engineering Department, Gebze Institute of Technology
41400 Gebze, Kocaeli, Turkey

ABSTRACT

A study of an H-plane structure composed of the feeding waveguide, horn and dielectric loading with polyhedral boundaries is described. The method of analysis is domain product technique (DPT). Results demonstrating improvements in radiation characteristics are presented for several configurations.

INTRODUCTION

Effects of dielectrics on radiation of electromagnetic horns have been examined by a number of authors. It was established that dielectric loading could provide significant improvements in some of their characteristics [1]. Because of complex geometry, many configurations of this type can be studied only experimentally or using direct numerical methods requiring long computing time and large storage capacity of computer.

This paper deals with a symmetric H-plane radiating structure composed of the feed, horn and dielectric embedding of a multiangular cross-section. One possible geometry is shown in Fig. 1. An efficient rigorous analysis of the structure is based on the DPT method [2,3]. Sample results showing reduction in the beamwidth and lowering the side lobe level are presented for several loaded radiators.

FORMULATION

Two regions form the structure considered. Region 1 is occupied by dielectric with relative permittivity ε. Region 2 contains a filament source extending along the z-axis. It is assumed that the waveguide supports a single TE_{10} mode and the source is far enough from the aperture so that the horn is excited either by dominant mode. Both regions may consist of more than one separate part. The profiles of region 1 and 2 are broken lines composed of $N^{(1)}$ and $N^{(2)}$ segments respectively. The length of the jth segment is $2f_j^{(p)}$. The time dependence is $\exp(i\omega t)$. λ is the free-space wavelength, $\qquad k^{(2)} = k_0 = 2\pi/\lambda \qquad$ and

Fig. 1 Geometry of the problem

$k^{(1)} = \sqrt{\varepsilon}k_0$. In addition to the basic system (x, y, z), a local Cartesian co-ordinate system $(x_j^{(p)}, y_j^{(p)})$ and an elliptic one $(\xi_j^{(p)}, \eta_j^{(p)})$ are introduced for the jth segment of the pth region $(j = \overline{1, N^{(p)}}, p = 1,2)$:
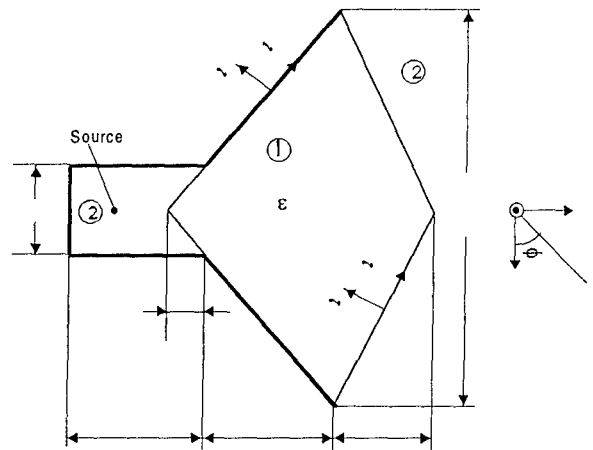
$$x_j^{(p)} = f_j^{(p)} \cosh \xi_j^{(p)} \cos \eta_j^{(p)}, \quad y_j^{(p)} = f_j^{(p)} \sinh \xi_j^{(p)} \sin \eta_j^{(p)} \tag{1}$$

Boundary value problem is formulated with respect to the single component of electromagnetic field E_z satisfying Helmholtz's equation with appropriate boundary, edge and radiation conditions. Denote electric field sought in regions 1 and 2 as $u^{(1)}$ and $u^{(2)}$. In every cross-sectional region, the field is constructed in the form of a sum as

$$u^{(1)} = \sum_{j=1}^{N^{(1)}} u_j^{(1)}, \qquad u^{(2)} = u_s + \sum_{j=1}^{N^{(2)}} u_j^{(2)} \tag{2}$$

Here, u_s is the known contribution of the source and terms $u_j^{(p)}$ ($j = \overline{1, N^{(p)}}, p = 1,2$) are given by expansions

$$u_j^{(p)} = \sum_{n=0}^{\infty} {}^p D_n^j \frac{Me_n^{(2)}(\xi_j^{(p)}, q_j^{(p)})}{Me_n^{(2)}(0, q_j^{(p)})} ce_n(\eta_j^{(p)}, q_j^{(p)}) \tag{3}$$

where $ce_n(\eta_j^{(p)}, q_j^{(p)})$ is the even angular Mathieu function of index n, $Me_n^{(2)}(\xi_j^{(p)}, q_j^{(p)})$ is the relevant radial Mathieu function and $q_j^{(p)} = (k^{(p)} f_j / 2)^2$. $\{{}^1 D_n^j\}$ and $\{{}^2 D_n^j\}$ are sequences of the unknown expansion coefficients. Substituting (2) and (3) into boundary conditions leads in the manner usual for DPT to an infinite matrix that can be solved after truncation. Validation of the theory and the pertinent computer code was performed in the case of an H-sectoral horn loaded by a quasi dielectric ($\varepsilon = 1$) insert. The results obtained are in complete agreement with the known solution [2] for the same configuration without loading.

NUMERICAL RESULTS

The radiation properties of the structure have been examined according to the procedure described in the previous section for a selected set of parameters. Some of the results are presented and discussed below.
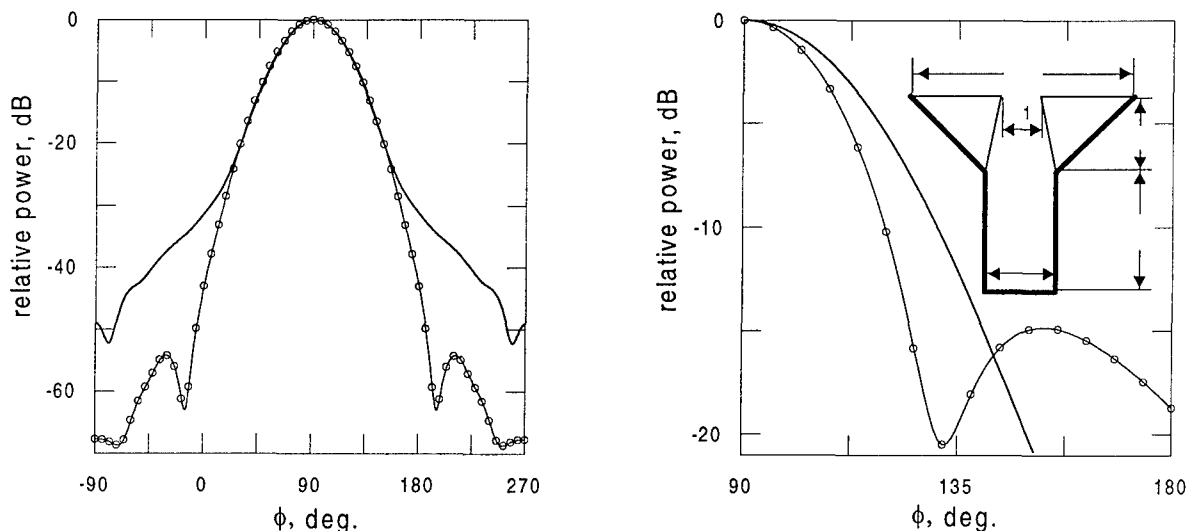
Fig. 2 Radiation pattern of unloaded and loaded horn shown in Fig. 1 for $a/\lambda = 0.75, q/a = 2$, $b/a = 1.5, c/a = 1.5, d/a = 0.16$ and $l/a = 0.5$. Solid line: unloaded; circles: loaded ($\varepsilon = 4$).

Fig. 3 Radiation pattern of unloaded and loaded horn for $a/\lambda = 0.75, q/a = 2, q_1/a = 0.23$, $c/a = 1.5$ and $b/a = 1$. Solid line: unloaded; circles: loaded ($\varepsilon = 2$).

Improvements in radiation characteristics of dielectric-loaded horns are usually archived at the expense of the new appreciable side lobes [1]. Results given in Fig. 2 demonstrate the opposite. The loading lowers significantly the level of the minor radiation. Fig. 3 shows far-field patterns calculated for the horn depicted in the background. The narrowing of the main beam, caused by dielectric slabs, is clearly seen. Fig. 4 shows the radiation pattern of the open-ended waveguide loaded with multiangular dielectric lens. It is seen that the lens increases directivity of the waveguide appreciably.
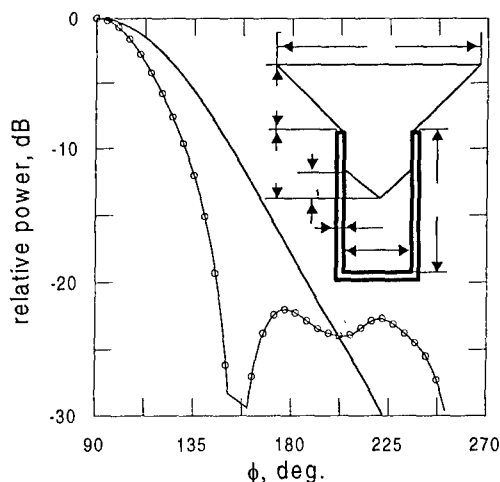
Fig. 4 Radiation pattern of unloaded and loaded open-ended waveguide for $a/\lambda = 0.75$, $q/a = 1.35, b/a = 1.5, l/a = 0.5, l_1/a = 0.1$ and $d/a = 0.2$. Solid line: unloaded; circles: loaded ($\varepsilon = 4$).
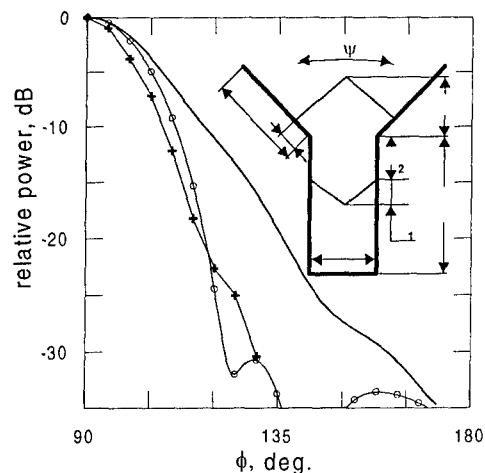
Fig. 5 Radiation pattern of unloaded and loaded horn for $\psi = 60^o, a/\lambda = 0.75, l/a = 2.95$, $r/a = 1.45, c/a = 2.1, c_1/a = 0.87, c_2/a = 0.3$ and $b/a = 2.97$. Solid line: unloaded; circles: loaded (data calculated for $\varepsilon = 2.586$); crosses: loaded (experimental data for $\varepsilon = 2.586$).

Parameters of the insert shown in Fig. 5 have been chosen with the aid of computational experiment to narrow the main beam and to lower simultaneously the side lobe level. In the same figure, the calculated radiation pattern is compared with the results of measurement performed for the H-sectoral horn with the waveguide dimensions 10 cm × 4 cm. As it is seen, agreement between the theory and experiment is quite satisfactory.

All numerical examples given were obtained by changing the input data only. On the whole, computation time depends on the dimensions of the antenna but is fairly short. For a structure with subdomain boundaries in the total electric length extending to 20 wavelengths, computation of the radiation pattern takes about 5 s with an IBM-PC-compatible computer based on Pentium-II CPU at 266 MHz.

REFERENCES
[1] M. Hamid, and A. Al-Sulaiman, "New types of dielectric-loaded horn antennas," *Int. J. Electronics*, vol. 55, no. 5, pp. 729-750, 1983.
[2] V. P. P'yankov, and V. P. Chumachenko, "Solution of H-plane radiation problem for two-dimensional horn with complex piecewise linear contour," *Izvestiya VUZ Radiofizika*, vol. 33, no. 5, pp. 604-610 (in Russian).
[3] V. P. Chumachenko, E. Karacuha and M. Dumanli, "An analysis of TE-scattering from a multiangular groove in a ground plane," *J. Elect. Waves Appl.*, vol. 13, pp. 381-396, 1999.

HIGH-Q WAVEGUIDE FILTER

Vladimir V. Podlozny, and Vyacheslav V. Khardikov

Chair of Theoretical Radiophysics, Kharkov National University
4 Svobody sq., Kharkov, 61077,Ukraine
E-mail: V.Podlozny@univer.kharkov.ua

ABSTRACT

A waveguide section filled periodically with magneto-dielectric layers and metal gratings is investigated. The amplitude-frequency characteristics, conditions of the resonant transparency and high-Q natural oscillations are obtained.

INTRODUCTION

The resonance properties of a periodic set of gratings of metal bars in free space have been investigated in [1]. The revealed high frequency selectivity of such a structure stimulates the investigation of a similar system in a waveguide as a filter. This paper deals with a periodic sequence of gratings and magneto-dielectric layers in a rectangular waveguide.

GEOMETRY

A section of a rectangular waveguide (a x b) is considered. There are N identical unit cells placed periodically with the period L along the z-axis (the direction of the wave propagation). A unit cell contains a grating of rectangular metal bars (h is the grating thickness, l is the grating period along the y-axis, g is the gap between the bars) between two dielectric layers. The latter are characterized by the thicknesses d_1 and d_2, permittivities ε_1 and ε_2, and permeabilities μ_1 and μ_2, respectively. The input and output waveguides are filled with magneto-dielectrics of permittivities ε_0, ε_3 and permeabilities μ_0, μ_3, respectively. The structure is homogeneous along the x-axis. We consider the single-mode regime of TE$_{m0}$-modes and use the long-wave approximation ($\ae = l/\lambda \ll 1$).
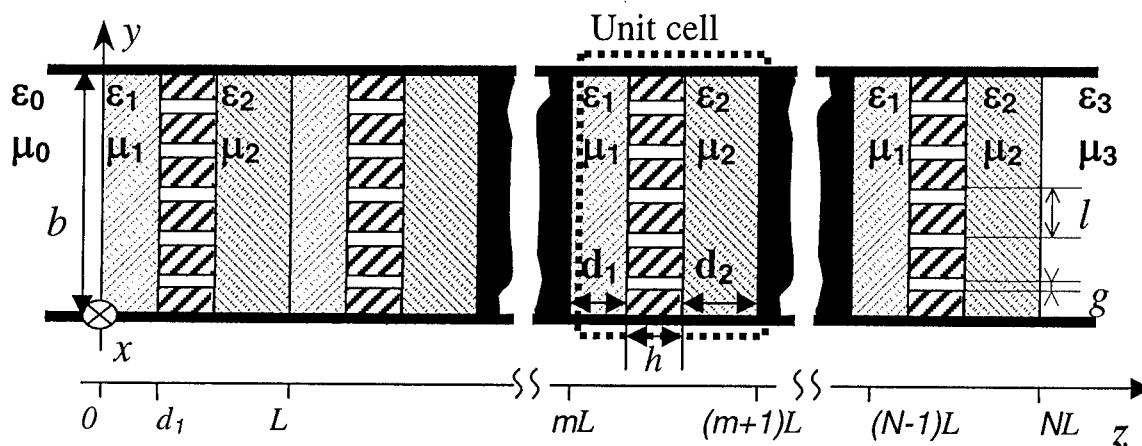
Fig.1 Geometry of multilayer periodic waveguide filter

METHOD OF SOLUTION

The diffraction problem of TE_{m0}-modes is solved by using the matrix approach and the theory of the matrix polynomial [2,3]. The transfer matrix $\mathbf{T}$ of the unit cell of the structure has been obtained from the solution presented in [4]. The transfer matrices of the input $\mathbf{T}_0$ and output $\mathbf{T}_3$ of the waveguide are determined using the standard boundary condition for the interface of homogeneous layers. The amplitude of the incident wave is related to the scattered field amplitudes by the product of $\mathbf{T}_0\mathbf{T}^N\mathbf{T}_3$. Direct analytical formulas of the reflection R and transmission τ coefficients are taken from [2] in terms of the Mauguin polynomials [5].

RESULTS

1. Reflection characteristics

There are wide stopbands and narrow passbands near high-Q resonances on the reflection characteristics of the structure (Fig.2), similarly to the structure with simpler unit cells [2]. Position and width of the bands result from the equation for the propagation constant of the relevant infinite waveguide [1,2]. The resonances in the passbands are determined by the zeros of the Mauguin polynomials $\cos(\pi v/N)=(t_{11}+t_{22})/2$, where $v=1,2,..N-1$ is the number of resonance, t_{11} and t_{22} are the elements of the transfer matrix $\mathbf{T}$. High Q-factors of the resonances result from the high selectivity of a single grating and weak electromagnetic coupling between the gratings in a set. The Q-factor can be evaluated using the ratio of the total number of the resonances (N-1) to the width of the corresponding passband $Q \sim (N-1)/(æ_{N-1}-æ_1)$. If $h/\lambda \ll 1$ and $\varepsilon_j=\mu_j=1$, then the passband width is $æ_{N-1}-æ_1=\cos(\pi/N)/\pi n(2|\ln\sin(\pi g/2l)|+\pi h/g)$, where n is the number of the passband.
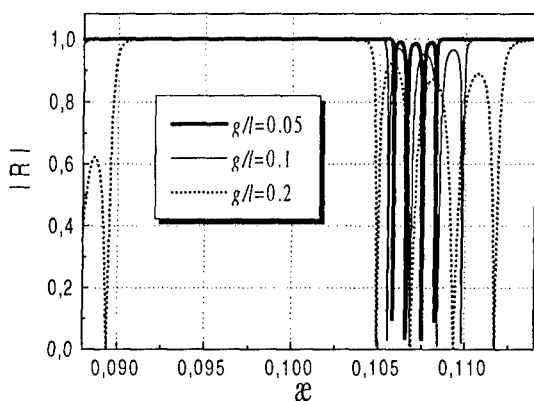
Fig.2 Frequency dependences of the reflection coefficient module, TE_{10}-mode, N=5, a/l=40, a/b=2, L/l=20, h/l=6, $\varepsilon_{0,2,3}$=1, ε_1=9+i0.001, μ_j=1, d_1/(L-h)=0.2.
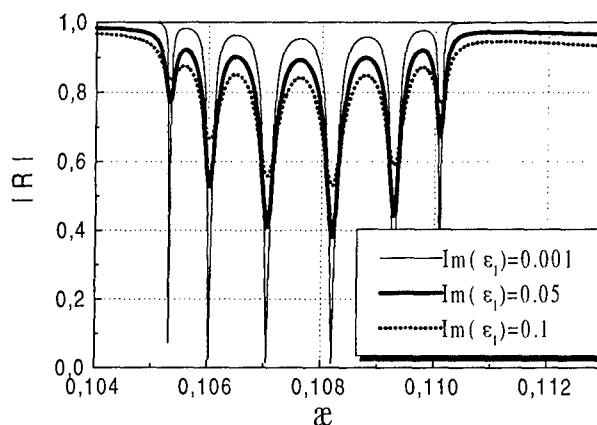
Fig.3 Frequency dependence of the reflection coefficient module, TE_{10}-mode, N=7, a/l=40, a/b=2, L/l=20, g/l=0.2, h/l=6, $\varepsilon_{0,2,3}$=1, Re(ε_1)=9, μ_j=1, d_1/(L-h)=0.2.

Insertion of magneto-dielectric layers between the gratings enables one 1) to improve the matching of the section with the input and output, 2) to decrease the total length of the structure, 3) to increase the number of the varying parameters, 4) to simplify the fabrication method. It is important to take into account the influence of the dissipative losses in the layers on Q-factor (Fig.3).

2. Natural Oscillations

Obtained analytical formulas for the scattering coefficients enable one to investigate the natural oscillations of the structure depending on the geometric, field and material parameters. Figs.4 and5 illustrate a typical behavior of the complex frequencies $æ_j^v = \text{Re}\,æ_j^v + i\,\text{Im}\,æ_j^v$ and Q-factors $Q_v = \text{Re}\,æ_j^v / \text{Im}\,æ_j^v$. It is important to notice that the Q-factors of the resonances grow with the increase of frequency (Fig.4). If the dissipative losses get greater, the absolute value $|\text{Im}\,æ_c|$ increases and Q-factor decreases (Fig.5).
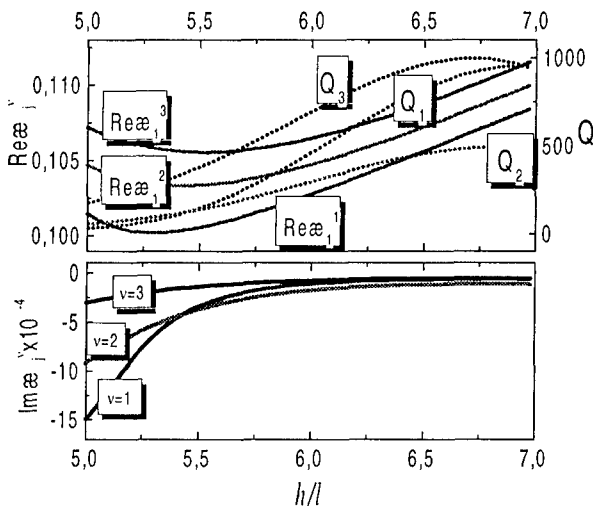
Fig.4 Dependence of the natural frequencies and Q-factor of the filter on the thickness of the grating, TE_{10}-mode, N=4, a/l=40, a/b=2, L/l=20, g/l=6, $\varepsilon_{0,2,3}$=1, ε_1=2, μ_j=1, $d_1/(L-h)$=0.1.
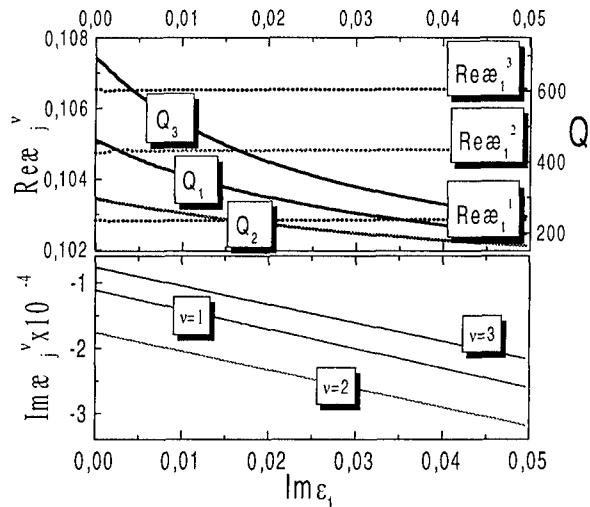
Fig.5 Dependence of the natural frequencies and Q-factor of the filter on the dielectric losses, TE_{10}-mode, N=4, a/l=40, a/b=2,L/l=20, h/l=6, $\varepsilon_{0,2,3}$=1, Re(ε_1)=2, μ_j=1, $d_1/(L-h)$=0.1.

CONCLUSION

Obtained results enable us to recommend the investigated structure as a basis of a high-Q waveguide filter of the TE_{mo}-modes. The presence of additional resonant magneto-dielectric layers before and behind of the grating in the unit cells enables one to modify the characteristics of the filter in a wide range. Analytical expressions for the resonance frequencies and Q-factors of the oscillations have been obtained. Their behavior has been illustrated by the dependences of the reflection coefficient and natural complex frequencies on the parameters of the system.

REFERENCES

[1] *Microwave and Optical Technology Letters*: 4/1999.
[2] *Electromagnetic Waves & Electronic Systems*: vol.4 3/1999.
[3] M. Born and E. Wolf, *Principles of Optics*, Oxford, 1980.
[4] V.P. Shestopalov, L.N. Litvinenko, C.A. Masalov, V.G. Sologub, *Diffraction of Waves by Gratings*, Kharkov: Kharkov State University Press, 1973 (in Russian).
[5] H. Levine, *Unidirectional Wave Motions*, Amsterdam, 1978.

ANALYSIS OF A LOADED E-PLANE
CROSS-SHAPED JUNCTION OF RECTANGULAR WAVEGUIDES

V.A. Karlov

Dept. of Radiophysics, Dniepropetrovsk University
13 Naukova St., Dniepropetrovsk, 49625, Ukraine, Tel: 28 0562 467995 (582338)

ABSTRACT
Using the method of overlapping regions, an electromagnetic model of an E-plane cross-shaped divider is developed. The coupling region of the cross-shaped divider includes rectangular resonance cavities. Numerical values of the scattering matrix coefficients have been obtained.

INTRODUCTION
Parameter determination of the measuring standards of reflection and transmission coefficients by numerical methods is a perspective tendency in the microwave metrology. E-plane cross-shaped junction of rectangular waveguides has a smooth scattering matrix coefficient behavior against frequency. The junction is used as a reference discontinuity in various measuring devices. Thus the comprehensive investigation of the junction properties is practically valuable.

ELECTROMAGNETIC MODEL OF THE WAVEGUIDE JUNCTION
In the present paper, electromagnetic calculation of the scattering matrix of the loaded E-plane cross-shaped junction of rectangular waveguides is made by means of the method of overlapping regions [1]. The configuration of the divider under consideration is shown in Fig. 1a.

a)   b)
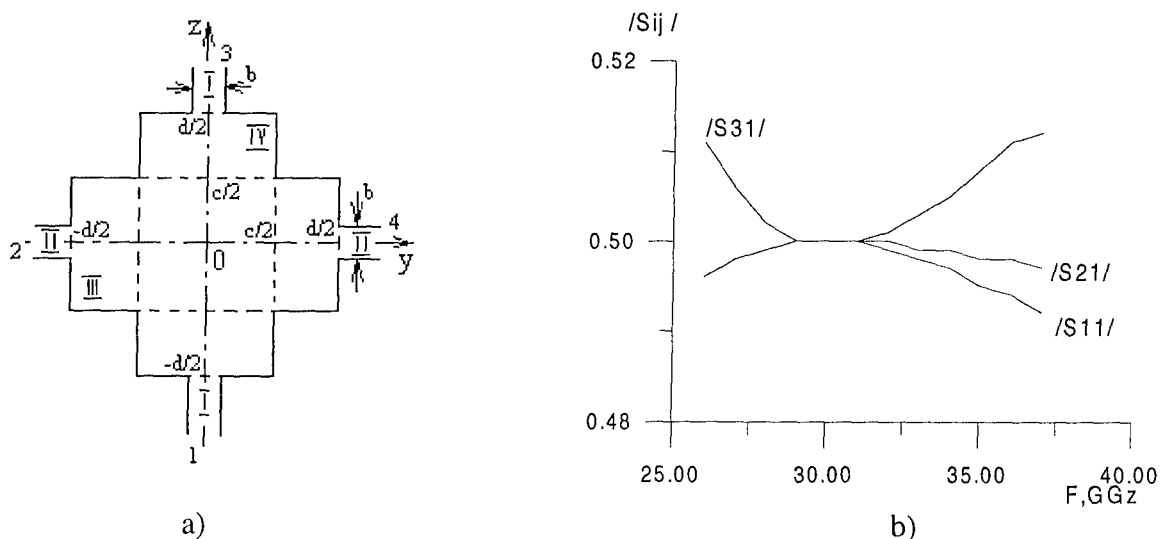
Fig. 1. (a) A loaded E-plane cross-shaped junction of rectangular waveguides. (b) The scattering matrix coefficients of loaded divider: $c=1.2b$, $d=1.97b$, $a \times b=7.2 \times 1.7$ mm.

The protruding arm, regions I and II, is a rectangular waveguide (of dimensions a and b, a being the broader dimension) which supports the dominant H_{10} mode only. In the junction, the modal fields must be of the H-type only (i.e., having no electric field component E_x), and their dependence on x takes the form of $\sin \pi/a(x+a/2)$. Regions I, II, III and IV are the overlapping regions with boundaries:

region I: $\quad -\dfrac{a}{2} \le x \le \dfrac{a}{2}$, $\qquad -\dfrac{b}{2} \le y \le \dfrac{b}{2}$, $\qquad -\infty < z < \infty$;

region II: $\quad -\dfrac{a}{2} \le x \le \dfrac{a}{2}$, $\qquad -\infty < y < \infty$, $\qquad -\dfrac{b}{2} < z < \dfrac{b}{2}$;

region III: $\quad -\dfrac{a}{2} \le x \le \dfrac{a}{2}$, $\qquad -\dfrac{d}{2} \le y \le \dfrac{d}{2}$, $\qquad -\dfrac{c}{2} < z < \dfrac{c}{2}$;

region IV: $\quad -\dfrac{a}{2} \le x \le \dfrac{a}{2}$, $\qquad -\dfrac{c}{2} < y < \dfrac{c}{2}$, $\qquad -\dfrac{d}{2} < z < \dfrac{d}{2}$.

For the selected simple regions, a system of integral equations has been derived. The solution has been obtained by the method of eigenfunctions. In the regions I and II, the H_x-components have been expanded in terms of the waveguides modes, and in the regions III and IV they have been expanded in terms of the resonator modes [2]. The electromagnetic problem constructed in this way enables us to determine the divider scattering matrix coefficients $S_{ij} = S_{ij}(a,b,c,d,F,N)$ as a function of geometrical sizes a, b ,c, d in the whole frequency band F of the single mode excitation. The number of the taken into account higher-order modes was N=15.

NUMERICAL RESULTS AND DISCUSSIONS
The device can be considered as a cross-shaped divider, which is loaded with waveguide irregularities in the form of step discontinuity of impedance. The properties of divider are investigated beforehand by the method of the loaded multi-port. Initial numerical values of the scattering matrix coefficients were calculated by using the rigorous solution of an electromagnetic problem. The values of reflection coefficients of the loads in the output ports were determined from the solution of the concrete problem.
Application of the divider as a 6-port transducer of complex signals demands the input power to be split into four equal parts. This can be achieved by using the principal mode H_{10} or by using higher non-propagating modes H_{1n}.

The situation of equal splitting under conditions of operating with higher modes H_{1n} is illustrated in Fig. 1b. The corresponding sizes of resonator cavities were *c=1.2b, d=1.97b*. With these sizes, the absolute value of S_{ij} lies between 0.49 and 0.51.

Fig. 2a displays the situation with operating mode H_{10}. The divider sizes were $d \approx 3/2\lambda_e$, $c=3b$. The parameters mentioned above correspond to the analysis of the divider loaded by steps in the rectangular waveguides with impedance ratio 1/3 by means of the theory of transmission lines.
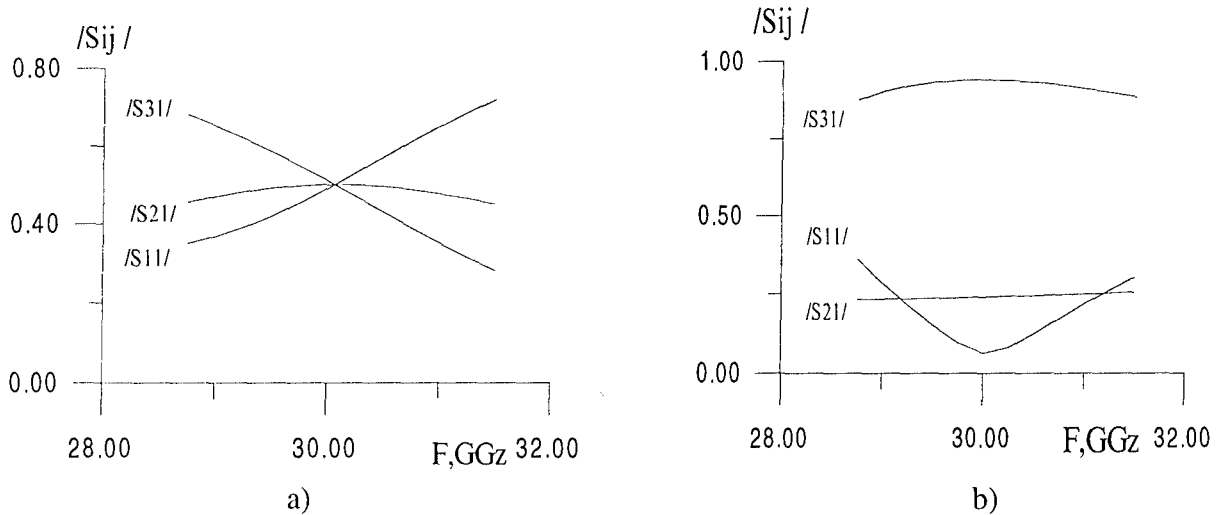
Fig. 2. The divider scattering matrix coefficients as a function of the cavity sizes d and c :
   a) $d=6.55b$, $c=3b$;   b) $d=4.7b$, $c=3b$.

If the lengths d of the resonator cavities are equal to $\lambda_e / 2$ and the width c is equal to $3b$, the effect of narrow-band matching in the input port has been observed. This situation is illustrated in Fig. 2b.
Therefore, the divider can be applied in practice using as the operating wave both the principal propagating mode and higher non-propagating modes H_{1n}. The obtained results

enable us to investigate the properties of the divider with different sizes of resonator cavities. They also show that the divider can be applied as a reference multiple-port discontinuity for the design of the analyzers of microwave circuits.

REFERENCES

[1]   Petrusenko I.V., Yakovlev A.B., Gnilenko A.B., 1994, "Method of partial overlapping regions for the analysis of diffraction problems", *IEE Proc.- Microw. Antennas Propag.*, vol. 141, pp. 196-198.

[2]   I.G. Prokhoda, V.A. Karlov. Matching of a cross-shaped junction of rectangular waveguides in the E-plan, *Izvestiya Vuzov MB i SSO USSR. Radioelektronika,* 1986, vol. 29, No. 2, pp. 90-92, (in Russian).

LONGITUDINAL SLOTS IN A RECTANGULAR WAVEGUIDE LOADED WITH A LAYERED DIELECTRIC

L. Yatsuk, A. Lyakhovsky, and A. Lyakhovsky

Kharkov National University, 4 Svobody Sq., Kharkov, 61077, Ukraine

E-mail: Ludmila.P.Yatsuk@univer.kharkov.ua

ABSTRACT

Longitudinal slot in a broad wall of a rectangular waveguide filled with a centrally positioned dielectric slab is considered. Radiation coefficients of the slot are studied using the modified eigen-wave method in the excitation problem. Dependence of radiation coefficient and resonance properties of the slot on geometry of the system, dielectric permittivity, width of the slot and its position in the waveguide wall have been studied in the X-band.

INTRODUCTION

Longitudinal slots in partially filled with dielectric waveguides are more difficult for theoretical studying than transversal ones. The scattering elements of a slot can be considered as functionals of the magnetic field H excited by the electric field in the slot in the source region. Magnetic current equivalent to the electric field in the slot, that is a surface one, is used as a source of this field. The density distribution function of this current contains the Dirac delta-function which causes difficulties of obtaining a convergent solution for the magnetic field. Using the eigen-wave method [1] or the method of the Green's function for the field [2] (the main methods of solving an excitation problem) one encounters the following difficulties. In both cases the expression for the H-field excited by a longitudinal magnetic current contains its density (and the Dirac delta-function as well) in the explicit form. This prevents one from obtaining the convergent expression for the inner admittance of the slot, without which it is impossible to obtain its power parameters (radiation coefficient and others). The authors of [2] did not write in their paper how they have overcome this difficulty. Modification of the eigen-wave method proposed in [3] permits to obtain a convergent solution for the H-field. The purpose of this paper is to illustrate the possibilities of this method for calculating the radiation coefficients of longitudinal slots in a waveguide with a dielectric slab and studying these slots' resonance properties.

DISCUSSION

Geometry of the system considered. A rectangular waveguide of a x b=23 x 10 mm cross section is partially filled with a centrally positioned dielectric slab of the width a_2 and permittivity ε. The waveguide wall thickness is supposed to be finite. The slab is parallel to the narrow walls of the waveguide. The coordinate system x,y,z is used inside the waveguide, z is longitudinal coordinate. The sot of length L and width d is cut in the broad wall of the waveguide, x_0 is displacement of the slot center from the narrow wall; u and v are local coordinates along and across the slot with the origin in its center.

The main steps of obtaining a slot power parameters are as follows. The electric field in the slot is presented as $\vec{e}_{s1} = V_1\vec{e}$ on the inner surface of the slot and $\vec{e}_{s2} = V_2\vec{e}$ on the outer one. Here, $\vec{e} = \vec{v}^0 e_v$, $e_v = \sin\left[\pi\left(u + L/2\right)/L\right]/d$, V_1 and V_2 are voltages between the slot edges in the bulges of the E-field, $\vec{v}^0$ is a unit vector along the v-axis. For simplicity, the our study was done by characterizing the E-field along the slot with the only one half-wave of a sinusoidal function and admitting E to be constant in the transverse direction. Magnetic field

H_z excited by the slot is to be found under the slot in order to obtain the inner slot admittance. Magnetic current which excites this field has the density $\vec{J}^{m} = \left[\vec{e}_{sl}, \vec{n}^{i} \right]$, where $\vec{n}^{i}$ is the unit vector normal to the inner slot surface. Taking into account the expression for the field $\vec{e}_{sl}$ we can represent $\vec{J}^{m}$ in the form

$$\vec{J}^{m} = \vec{z}^{0} e_{v}(u, v) \delta(y), \tag{1}$$

where $\vec{z}^{0}$ is a unit vector along z-axis, $\delta(y)$ is the Dirac delta-function, y is the coordinate along the axis normal to the inner slot surface where $y = 0$.

The above mentioned methods [1,2] yield the expression for the H_z-field that consists of the infinite sums of *LE-* and *LM*-waves and the divergent extra sum term:

$$\hat{H}_{z} = -\left(\vec{z}^{0}, \vec{J}^{m} \right) / \left(i \omega \mu_{a} \right), \tag{2}$$

where ω is the frequency, μ_{a} is the absolute magnetic permeability, i is imaginary unit.

The idea of the eigen-wave method modification is as follows. The set of potential eigen-functions $\vec{L}_{j} = \nabla \varphi_{j}^{m}$ was built for the waveguide with a dielectric slab. These functions are orthogonal in the cross section of the waveguide. This property was used in the series expansion of (2). The combination of three sums (over *LE-* and *LM*-waves and the last one) resulted in the convergent series. The *H*-field obtained was used for determining the longitudinal slots inner admittance and, after that, for calculation of their power parameters.

Calculation results.. Calculations were performed for the slabs having permittivities $\varepsilon = 10$ ($a_{2} = 1$ mm), $\varepsilon = 16$ ($a_{2} = 0.5$ mm and $a_{2} = 1$ mm). In all three cases the cut-off wavelengths of the H_{20}-mode were $\lambda_{c} \cong 24mm$, for the H_{10}-modes $\lambda_{c} = 62$, 60 mm and 72 mm, respectively, and in the band $24 \leq \lambda \leq 45$ mm the wavelengths in the waveguide were smaller than those in the free space. It is very useful in the scanning antenna design. For creating a required amplitude-phase distribution along antenna it is necessary to have possibility of variation of separate slot radiation coefficients $\left. |S_{\Sigma}|^{2} \right|_{res}$ in the limits:

$$0.05 \leq \left. |S_{\Sigma}|^{2} \right|_{res} \leq 0.5, \tag{3}$$

where subscript "res" means "resonance".

As a result of calculations it was shown that as unlike the empty waveguide, in the case of a waveguide with centrally positioned dielectric longitudinal slab the radiation coefficient increases with x_{0} approaching to the wall axis where the dielectric slab is placed. If permittivity ε is not high enough, $\left. |S_{\Sigma}|^{2} \right|_{res}$ may vary in much smaller limits. For example, if $\lambda = 31mm, \varepsilon = 10$, $a_{2} = 0.5$ mm, the radiation coefficient remains practically constant for all x_{0} .in the region where $\varepsilon = 1$. It was found that the most suitable geometry for fitting (3) is the following one: $\varepsilon = 16$, $a_{2} = 1$ mm, $d = 1.5$ mm (see Figure 1). The curve-numbers 1-9 in this Figure correspond to the displacements $x_{0} = 1$, 2.5, 4, 5, 6, 7, 8, 9, 10.25 mm. It is well seen that the electric length of resonance slot diminishes with the slot approaching to the dielectric. This effect was discussed in detail in [4]. The relative width of curves of $|S_{\Sigma}|^{2}(\lambda)$ is of great interest as well. In Figure 2, the relative width $\Delta\lambda/\lambda_{res}$ of radiation coefficient dependences on λ (curves plotted in Figure 1) are represented as a function of x_{0}. The shifts $\Delta\lambda$ were fixed at the level $0.5 \left. |S_{\Sigma}|^{2} \right|_{res}$. The curve order numbers correspond to the following cases: 1.-

$\varepsilon = 10, a_2 = 1mm, d = 1.5mm$, 2.-$\varepsilon = 16$, $a_2 = 0.5$ mm, $d = 1.5$ mm. 3.-$\varepsilon = 10$, $a_2 = 1$ mm, $d = 3$mm, 4.-$\varepsilon = 16$, $a_2 = 0.5$ mm, $d = 3$ mm, 5.-$\varepsilon = 16$, $a_2 = 1$ mm, $d = 1.5$ mm., 6-$\varepsilon = 16$, $a_2 = 1$ mm, $d = 3$ mm.. It is seen that these functions are rather irregular. The average level of $\Delta\lambda/\lambda_{res}$ does not vary significantly from that of the slots in an empty waveguide (about 15%). The tendency of widening of the functions $|S_\Sigma|^2(\lambda)$ is observed in most cases when x_0 is directly near the dielectric slab. In the middle parts of the curves, the oscillations of $\Delta\lambda/\lambda_{res}$ in the range of (3-4)% take place. Apparently it can be caused by the complicated structure of field in the waveguide considered and besides by not very accurate calculations of these functions. In order to reveal the real reason of these oscillations it is necessary to continue the investigations.
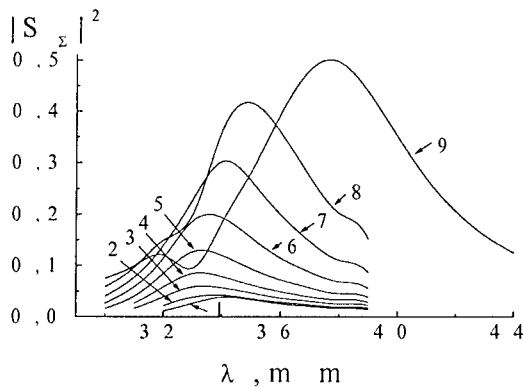
Figure 1
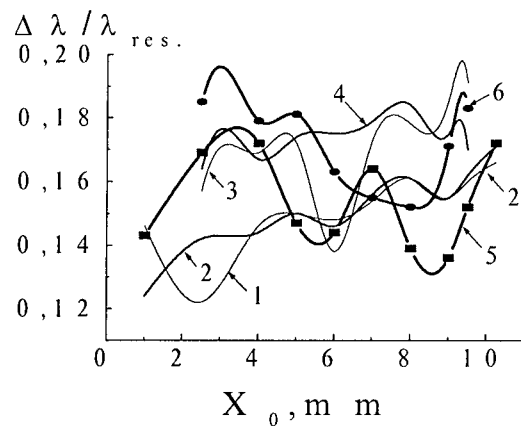
Figure 2

CONCLUSION

The results obtained make more clear the physical regularities taking place in the electromagnetic field radiation by a slot cut in a rectangular waveguide with a dielectric slab inside. These results may be used in the design of the scanning waveguide-slot antennas.

REFERENCES

[1] Wainstein L.A. *Electromagnetic Waves,* Moscow, Radio and Svyaz, 1988 (in Russian).

[2] Jubert J. And McNamara D.A. Longitudinal slots in broad wall of rectangular waveguide inhomogeneously loaded with dielectric slab, *Electronic Letters,* 1991, vol. 27, No 16, pp.1480-1482.

[3] Yatsuk L.P. Waveguide waves scattering from slot and wire-slot inhomogeneities, *Doctor of Sciences Thesis,* Kharkov State University , Kharkov, 1997, (in Russian)

[4] Yatsuk L.P., Lyakhovsky A.F., Lyakhovsky A.A. Electrodinamic Parameters of Narrow Slots in a rectangular Waveguide Filled with Three-Layered Dielectric. Theory and Experiment, *Proc. Int. Conf. Antenna Theory and Techniques,* Sevastopol, Ukraine, 1999, pp.360-362.

THE VORTEX LATTICE METOD IN THE SPECRAL PROBLEM OF A RECTANGULAR WAVEGUIDE WITH A LAMELLAR GRATING

V.V. Kamyshan, and O.P. Kamyshan

Kharkov National University, 4 Svobody sq., Kharkov, Ukraine

ABSTRACT

Interest to research and use of slowing-down electromagnetic systems (ES) in waveguides with rectangular grooves recently has been revived (see [1]). In the present work, in a rigorous manner the spectral problem of infinite rectangular waveguide for the longitudinal electrical (LE) waves [2] for ES with periodic slowing-down systems with any number of arbitrary size resonators in the period is considered. This work is a generalization of results of paper [3], where we considered a lamellar grating with one resonator in the period by using the discrete singularities (currents) method, also known as vortex lattice method.

The spectral problem for a rectangular waveguide with a grating on the wide wall can be reduced, by using the technique of [3], to a spectral problem for a two-dimensional (2D) ES (Fig. 1), whose cross-section by the plane XoZ is homogeneous along the axis oY and coincides with the similar cross-section of the initial structure. Starting from the Maxwell equations for 2D problem we obtain the set of singular integral equations (SSIE) with additional conditions (1), based on the method published in [5,6]:

$$
\left.
\begin{aligned}
&\sum_{q=1}^{Q} \int_{a_q}^{b_q} \left[G(z,\varsigma) + \delta_{pq} M_p(z,\varsigma) \right] F(\varsigma)\, d\varsigma = 0; \qquad z \in \left[a_p, b_p \right], \\
&\sum_{q=1}^{Q} \int_{a_q}^{b_q} K(z,\varsigma) F(\varsigma)\, d\varsigma = 0;
\end{aligned}
\right\} \; p = \overline{1,Q}, \quad (1)
$$

In the case of Q resonators in the period of slowing-down system, the kernels of the singular equations for the LE_m- waves are

$$
G(z,\varsigma) = \frac{1}{L} e^{ik_{z0}(z-\varsigma)} \left\{ -\operatorname{ctg}\frac{\pi}{L}(z-\varsigma) + i\frac{k_{z0}}{\gamma_0} \operatorname{cth}(\gamma_0 b) + \right.
$$

$$
\left. + i\sum{}' \left[\frac{k_{zn}}{\gamma_n} \operatorname{cth}(\gamma_n b) - \frac{|n|}{n} \right] e^{i\frac{2\pi}{L}(z-\varsigma)n} \right\};
$$

$$
M_p(z,\varsigma) = -\frac{1}{2L_p} \left\{ \operatorname{ctg}\frac{\pi}{2L_p}(z-\varsigma) + \operatorname{ctg}\frac{\pi}{2L_p}(z+\varsigma-2a_p) + \right.
$$

$$
\left. + 4\sum_{n=1}^{\infty} \left[\frac{k_n^{(p)}}{\gamma_n^{(p)}} \operatorname{cth}(\gamma_n b) - 1 \right] \sin k_n^{(p)}\left(z-a_p\right) \cos k_n^{(p)}\left(\varsigma-a_p\right) \right\}
$$

and the additional conditions are

$$
K_{pq}(\varsigma) = -\delta_{pq} \frac{1}{k} \operatorname{ctg}\left(kh_p\right) - \frac{i}{L}\sum \frac{1}{k_{zn}\gamma_n} \operatorname{cth}\left(\gamma_n b\right)\left[e^{ik_{zn}(b_p-\varsigma)} - e^{ik_{zn}(a_p-\varsigma)} \right].
$$

In these expressions the following notations are used

$$\gamma_n^2 = k_n^2 - k^2; \quad \left(\gamma_n^{(q)}\right)^2 = \left(k_n^{(q)}\right)^2 - k^2; \quad k_n^{(q)} = \frac{\pi}{L_q}n; \quad k_n = k_{zo} + \frac{2\pi}{L}n; \quad L_q = b_q - a_q,$$

The symbol $\sum'$ denotes the sum over $n = -\infty \ldots \infty$ excluding $n = 0$, k is the wavenumber in free space. Other notations are shown in Fig. 1. The required function $F(z)$ is connected to a longitudinal component of electric field on the border between the resonator and the space of interaction by expressions:

$$F(z) = E_z(x,z)\big|_{x=0}; \quad F_q(z) = E_{zq}(x,z)\big|_{x=0};$$

$$F(z) = F_q(z), z \in [a_q, b_q]; \quad q = \overline{1,Q};$$

Fig. 1
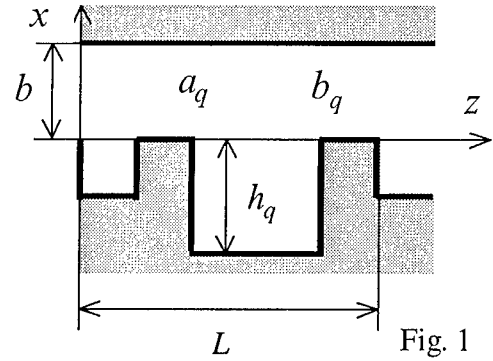
The z-component of the electric field in the space of interaction E_z^+, $(x > 0)$ and in resonators E_{zq}^-, $(x < 0)$ is presented as

$$E_z(x,z) = -\frac{i}{k}\sum_{n=-\infty}^{\infty} c_n \gamma_n \frac{\text{sh}(\gamma_n(b-x))}{\text{sh}(\gamma_n b)} e^{ik_{zn}z}; \qquad\qquad 0 \le x \le b, \quad (2)$$

$$E_{zq}(x,z) = \frac{i}{k}\sum_{n=0}^{\infty} c_n^{(q)} \gamma_n^{(q)} \frac{\text{sh}(\gamma_n^{(q)}(x+h_q))}{\text{sh}(\gamma_n^{(q)}b)} \cos k_n^{(q)}(z-a_q); \quad -h_q \le x \le 0, \quad (3)$$

and satisfy, together with the other components of electromagnetic field, the boundary conditions on the perfectly conducting metal surfaces of ES. Other components of electromagnetic field are expressed through the component E_z by using the Maxwell equations. The factor of decomposition (2) - (3) is determined through the SSIE solution $F(z)$ from expressions

$$c_n = \frac{ik}{L\gamma_n}\sum_{q=1}^{Q}\int_{a_q}^{b_q} F(\varsigma)e^{-ik_{zn}\varsigma} d\varsigma; \quad c_n^{(q)} = -\frac{ik}{L_q\gamma_n^{(q)}} \begin{cases} \displaystyle\int_{a_q}^{b_q} F(\varsigma)d\varsigma, & n=0 \\ \displaystyle 2\int_{a_q}^{b_q} F(\varsigma)\cos k_n^{(q)}(\varsigma-a_q), & n>0 \end{cases}$$

Longitudinal component of the field $E_z^{(w)}$ and dispersion curves $k^{(w)}(k_z)$ of the rectangular waveguide are expressed through the solution of 2D problem as follows: $E_z^{(w)}(x,y,z) = E_z^{\pm}(x,z)\cos k_y y$, $k^{(w)}(k_z) = \sqrt{k^2(k_z) + k_y^2}$, where $k_y = l\pi/a$; a is the width of the wall of rectangular waveguide along the axis 0Y, l is the index of the LE_{lm} - wave.

Fig. 2a - ES_a : $(b = 1.5; \ a_1 = 0; \ b_1 = 0.5; \ h_1 = 2;)$;

Fig. 2b - ES_b : $(b = 0.75; \ a_1 = 0; \ b_1 = 0.25; \ h_1 = 1; \ a_2 = 0.5; \ b_2 = 0.75; \ h_2 = 1;)$;

Fig. 2c - ES_c : $(b = 0.75; \ a_1 = 0; \ b_1 = 0.25; \ h_1 = 1; \ a_2 = 0.5; \ b_2 = 0.75; \ h_2 = 0.9)$.

The numbers in figures specify indices of the LE_m waves.

The normalized parameters ES_a and ES_b were chosen so that the geometrical sizes of these ES were identical and dispersion curves differed only because of the presence of computational mistakes in the matrix elements (of the order of 10^{-7}) and in calculations. For ES ES_c the height of resonators differs on 10%. Comparison of figures shows that small manufacturing errors in slowing-down systems can essentially change the shape of dispersion
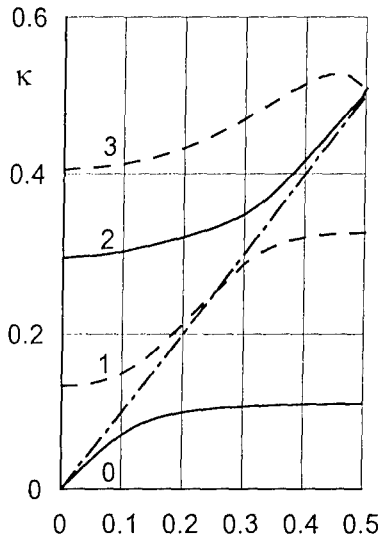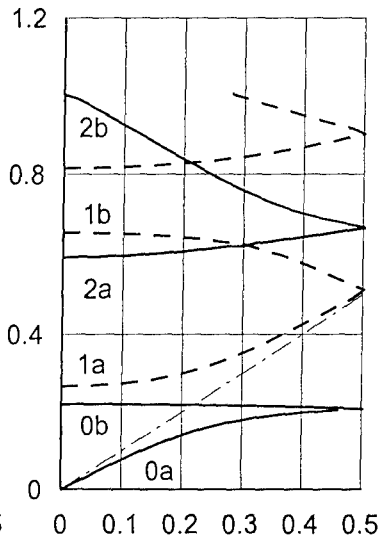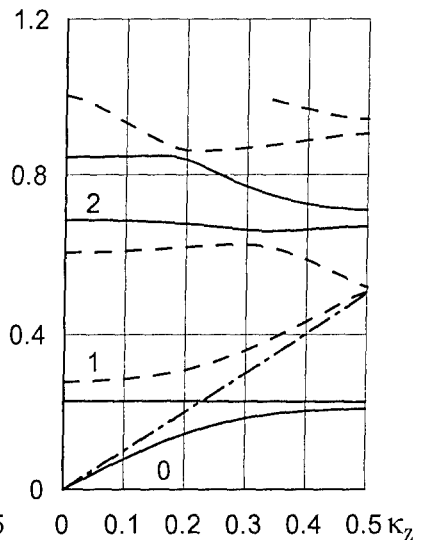
Fig. 2a   **Fig. 2b**   **Fig. 2c**

REFERENCES

[1] L.J.Louis, J.E.Scharer, J.H.Booske, *Physics of Plasmas*, v.5, p.2797-2895, 1998.
[2] R.A. Silin, V.P. Sazonov, *Slowing-Down Systems,* Moscow: Sov. Radio, 1966 (in Russian).
[3] V.V. Kamyshan, O.P. Kamyshan, *Proc. Int. Conf. Methods of Discrete Singularities in Physical Problems,* Orel, Russia, 2000, p. 246-249 (in Russian).
[4] L. Levin, *Theory of Waveguides,* Moscow: Radio i Svyaz, 1982 (Russian translation).
[5] Yu.V. Gandel, *Problems of Cybernetics,* Moscow: AN SSSR Publ., 1986. p. 166-183.
[6] Yu.V. Gandel, S.V. Eremenko, T.S. Polyanskaya, *Mathematical Problems of the Method of Discrete Currents,* Kharkov: Kharkov State University Press, 1992 (in Russian)..

NEW EXPLICIT SOLUTIONS IN TIME DOMAIN FOR WAVEGUIDE SIGNALS

Oleg A. Tretyakov and Zheng Yu

Kharkov National University, Kharkov, 61077, Ukraine

ABSTRACT

Study of electromagnetic phenomena in Time Domain (TD) within the scope of the classical approach has faced the problems of a principal nature [1]. Evolutionary Approach to Electromagnetics (EAE) has been proposed as an alternative tool capable to overcome the difficulties in the development of Electromagnetics for TD [2]. In this presentation, idea of EAE is explained and two examples of its application are demonstrated.

SCHEME OF *EAE*

A system of Maxwell's equations can be shortly written as an abstract operator equation *MX (R, t) = F(R,t)*, where *M* is Maxwell's operator, *X(R,t)* is the sought electromagnetic field, *F(R,t)* is the given function of impressed forces. *EAE* has been developed [2] starting from separation of Maxwell's operator as *M = W + B*, where *W* is a *linear self-adjoint* operator acting on waveguide transverse coordinates *r* of the position vector *R = r + az, (|z| = 1)* at the argument of *X(R,t)*. Operator *B* can be linear or nonlinear as the constitutive relations involved in *M* dictate it.

Operator *W* is self-adjoint due to the boundary conditions over the perfectly conducting waveguide surface involved in this definition. It has the eignevectors specified as the eigenfunctions of the operator eigenvalue equation $WY_i(r) = k_i Y_i(r)$, where $r \in S$, *S* is a waveguide cross-section. Spectrum k_i is real and discrete. Eigenvector set $\{Y_i (r)\}$ is complete. It originates a basis in the Hilbert space chosen as the space of solution. Projection of the solution sought onto the basis elements looks as $X(R,t) = \sum_{(i)} c_i(z,t) Y_i(r)$, where the scalar coefficients $c_i(z,t)$ are unknowns. A problems for them can be obtained via projecting of Maxwell's equations themselves onto the same basis elements $Y_i(R)$'s. This procedure results in a system of evolutionary (i.e. with time derivative) partial differential equations for $c_i(z,t)$. Operator *B* determines the type of these equations.

WAVEGUIDE MODES IN TD

Electromagnetic fields of TM and TE waveguide modes can be presented as

$$\vec{E}_n = \sqrt[-2]{\varepsilon_0} \left\{ V_n^e(z,t) \nabla \Phi_n(r) + z e_n(z,t) k_n^2 \Phi_n(r) \right\}, \tag{1}$$

$$\vec{H}_n = \sqrt[-2]{\mu_0} I_n^e(z,t) \left[z x \nabla \Phi_n(r) \right] ;$$

$$\vec{E}_m = \sqrt[-2]{\varepsilon_0} V_m^h(z,t) \left[\nabla \Psi_m(r) x z \right] , \tag{2}$$

$$\vec{H}_m = -\sqrt[2]{\mu_0}\left\{I_m^h(z,t)\nabla\Psi_m(r) + z h_m(z,t)v_m^2\Psi_m(r)\right\},$$

where ε_0, μ_0 are free constants. Potentials Φ_n and Ψ_m are normalized eigenfunctions of well studied eigenvalue problems for Laplacian, namely

$$(\Delta + \kappa_n^2)\Phi_n(r) = 0, \quad \Phi_n(r)|_L = 0, \quad \frac{\kappa_n^2}{S}\int_S |\Phi_n|^2 ds = 1; \qquad (3)$$

$$(\Delta + v_m^2)\Psi_m(r) = 0, \quad \frac{\partial}{\partial N}\Psi_m(r)|_L = 0, \quad \frac{v_m^2}{S}\int_S |\Psi_m|^2 ds = 1.$$

The above mentioned series $X(R,t) = \Sigma_{(i)}c_i(z,t)Y_i(r)$ is equivalent to presentation of electromagnetic field sought as a superposition of the waveguide modes.

EVOLUTIONARY EQUATIONS

When a waveguide is hollow, the amplitudes of longitudinal field components, i.e. and from (1) and (2) are solutions of unidimensional Klein-Gordon Equation (KGE), i.e.

$$\left(\partial_\tau^2 - \partial_\zeta^2\right)f(\tau,\zeta) = 0, \qquad (4)$$

where $\tau = v_m ct$, $\zeta = v_m z$ while $f \equiv h_m$, and $\tau = \kappa_n ct$, $\zeta = \kappa_n z$ while $f \equiv e_n$; $c = 1/\sqrt{\varepsilon_0\mu_0}$ - is the sped of light in the free space. Evolutionary equations for the amplitudes of transverse modal fields in the hollow waveguide turn into a set of simple direct formulas

$$I_m^h = \partial_z h_m, \quad V_m^h = -\partial_{ct}h_m, \quad V_n^e = \partial_z e_n, \quad I_n^e = -\partial_{ct}e_n \qquad (5)$$

system of equations (4), (5) should be supplemented by appropriate initial or/and boundary (with respect to z variable) conditions.

EXAMPLE OF EXPLICIT SOLUTION

Separation of variables in *KGE* (4) is evident: it results in monochromatic waveguide waves [3]. Furthermore, it turned out that it is possible to obtain a variety of new explicit solutions in the form of product, $f(\tau,\zeta) \equiv F[u(\tau,\zeta)] = U(u)V(v)$, where u, v are new real variables. The problem of finding the functions $u(\tau,\zeta)$, $v(\tau,\zeta)$ has been solved by Miller in his study of *KGE* by means of the group theory methods [4].
Two examples of such solutions are given below.

Case 1: $\tau - \zeta = \frac{1}{2}(u - \upsilon)^2$, $\tau + \zeta = \frac{1}{2}(u + \upsilon)^2$; $-\infty < u < \infty, 0 \spadesuit \upsilon < \infty$

These substitutions convert KGE (4) to a pair of equations for parabolic cylinder functions as

$$\frac{d^2U}{du^2} + \left(u^2 - \alpha\right)U = 0, \qquad \frac{d^2V}{dv^2} + \left(v^2 - \alpha\right)V = 0, \tag{6}$$

where variables *u, v* can be expressed in terms τ, ζ as follows

$$u = \left(\sqrt{|\tau| + |\zeta|} + \sqrt{|\tau| - |\zeta|}\right)\!/\sqrt{2}, \quad v = \left(\sqrt{|\tau| + |\zeta|} - \sqrt{|\tau| - |\zeta|}\right)\!/\sqrt{2},$$

provided that $|\tau| \geq |\zeta|$. When free parameter α is equal to $\pm i(2k+1)$ where $k = 0, 1, 2, \ldots$, then

$$F_\alpha \equiv F_k(u,v) = e^{\pm i\tau} H_{2k}\!\left(e^{\mp i\pi/4}u\right) H_{2k}\!\left(e^{\mp i\pi/4}v\right) \tag{7}$$

where H_{2k} are the Hermite orthogonal polynomials. This solution is valid in two quadrants of plane (τ, ζ) where inequality $|\tau| \geq |\zeta|$ holds. In the supplement, where inverse inequality $|\zeta| \geq |\tau|$ holds, the folowing substitutions are valid.

Case 2: $\zeta - \tau = \dfrac{1}{2}(u-v)^2, \quad \zeta + \tau = \dfrac{1}{2}(u-v)^2; \quad -\infty < u < \infty, \ 0 \spadesuit v < \infty$.

In this case, we have the other forms of equations for parabolic cylinder functions as

$$\frac{d^2U}{du^2} - \left(u^2 + \alpha\right)U = 0, \qquad \frac{d^2V}{dv^2} - \left(v^2 + \alpha\right)V = 0, \tag{8}$$

where

$$u = \left(\sqrt{|\zeta| + |\tau|} + \sqrt{|\zeta| - |\tau|}\right)\!/\sqrt{2}, \quad v = \left(\sqrt{|\zeta| + |\tau|} - \sqrt{|\zeta| - |\tau|}\right)\!/\sqrt{2}.$$

CONCLUSION

The Scheme of Evolutionary Approach to Electromagnetics is presented for the development of waveguide theory in Time Domain.

The Approach opens a prospect for evolutionary (i.e. with time derivative) partial differential equations obtained as a powerful tool for developing Electromagnetics in Time Domain.

Two examples of explicit solutions are presented for electromagnetic waves in a hollow waveguide different from the monochromatic waveguide modes.

REFERENCES

[1] P. Hillion, Some comments on electromagnetic signals; in Essays on the Formal Aspects of Electromagnetic theory, ed. A. Lakhtakia, World Scientific Publ. Co., Singapore, 1993.
[2] O.A. Tretyakov, Essentials of nonstationary and nonlinear electromagnetic field theory; in *Analytical and Numerical Methods in Electromagnetic Wave Theory*, ed. by M. Hashimoto, M. Idemen and O.A. Tretyakov, Science House Co., Tokyo, 1993.
[3] Van Bladel, J., 1985, Electromagnetic Fields, Hemisphere, Washington.
[4] W. Miller, J., 1977, Symmetry and Separation of Variables, Addison-Westley Publ. Co., Massachusetts.

.

.

EIGENVALUE

PROBLEMS

SPECTRAL PROPERTIES OF A PERIODIC PLASMA WAVEGUIDE

G.I. Zaginaylov, P.V. Turbin[1], K. Schuenemann[2], and J.-Y. Raguin[2]
Kharkov National University, Kharkov, 61077, Ukraine
[1]Scientific Center of Physical Technologies, Kharkov, 61145, Ukraine
[2]Tech. Univ. Hamburg-Harburg, 21071, Hamburg, Germany

ABSTRACT

Periodic waveguides have numerous applications in modern microwave technology mostly due to their two fundamental properties: support of slow waves; and existence of stop bands. These properties are common for a great number of waves in periodic mediums regardless from their nature. However, the reliable approach allowing an adequate analysis of dispersion properties of the plasma waves in periodic plasma-filled waveguides is addressed here for the first time.

Recently, periodical waveguide structures loaded with a magnetized plasma become a subject of intense experimental and theoretical investigations, since they are promising tools for using as interaction chambers in high-power microwave (HPM) electronic devices. They provide exclusively favorable conditions for enhancement power-handling capabilities, increase of a tunability and improvement of some other characteristics of HPM sources. As it is well-known, plasma-filled periodic waveguide supports two families of modes. One of them is high-frequency electromagnetic (EM) modes. The general dispersion properties of EM modes in plasma-filled periodic waveguides are very similar to those in vacuum periodic waveguides. They can be successfully analyzed using a conventional approach. Another is the family of purely plasma modes which are prototypes of the well-known Trivelpiece-Gould (TG) modes in smooth plasma waveguides. They were multiply observed in experiments, however, a detailed exploring of their spectral properties is extremely difficult both theoretically and experimentally. Detailed investigations showed that the dispersion diagrams for TG modes can not be analyzed on the basis of the conventional approach since the density of dispersion curves infinitely increases in the finite range of frequencies $0 < \omega < \omega_p$, where ω_p is the plasma frequency, producing a fundamentally new kind of spectral behavior, a so-called "dense" spectrum [1]. The properties of the "dense" spectrum have not been studied yet even qualitatively.

Quite recently, the novel approach to be more suitable for the treatment of the "dense" spectrum was suggested in [2]. It provides the formulation of the eigenvalue/eigefunction problem in terms of full fields avoiding the infinite determinantal dispersion relation. The obtained dispersion curves of the first approximation had no stop bands; yet it was unclear whether this was the consequence of the idealizations or such a feature is really inherent to the TG modes in periodic waveguides. The aim of this work is to develop a more accurate and detailed analysis of dispersion properties of TG modes in periodic plasma-filled waveguide based on the novel approach proposed in [2].

For the sake of simplicity consider as in [2] a planar waveguide with periodically varying thickness loaded with a uniform, cold, collisionless plasma embedded in a strong axial static magnetic field. All wave perturbations are assumed to be of TM polarization $\left(E_x, H_y, E_z \right) \sim e^{-i\omega t}$, $\left(\omega < \omega_p \right)$, electrostatic and symmetric with respect to the z-axis $\left(E_x(x, z) = E_x(-x, z) \right)$. Dispersion properties of TG modes in such a structure can be described by the functional equation [2]:

$$e^{ik_z \varphi(z)} \Psi(z + \varphi(z))(1 + \varphi'(z)) + e^{-ik_z \varphi(z)} \Psi(z - \varphi(z))(1 - \varphi'(z)) = 0, \qquad (1)$$

where $\Psi(z) = e^{-ik_z z} E_z(0, z)$, $\varphi(z) = |\varepsilon(\omega)|^{1/2} X_0(z)$, $x = X_0(z)$ is the equation of the periodic waveguide boundary: $X_0(z + d) = X_0(z)$, d is the period of the structure, k_z is the wavenumber of perturbations, $E_z(0, z) = E_z(x, z)|_{x=0}$ is the axial electric field on the waveguide axis, which is assumed to be quasiperiodic $E_z(0, z + d) = e^{ik_z d} E_z(0, z)$, the prime denotes differentiation about an argument.

Eq. (1) is correct in a rigorous mathematical sense provided that $\varphi'(z) \leq 1$ and valid in a qualitative sense if this condition is slightly broken [3].

A direct numerical analysis of (1) is hardly possible, since it describes the "dense" spectrum, i.e. each point in the $\omega - k_z$ plane inside the range $0 < \omega < \omega_p$ is the solution of (1). Indeed, let $k_{zm}(\omega)$ be the eigenvalues of (1) with the eigenfunctions $\Psi_m(z)$ where m is a transverse index. It is not difficult to see that $k_{zmn}(\omega) = k_{zm}(\omega) + nk_0$, where $k_0 = 2\pi/d$ are also the eigenvalues of (1). They have other eigenfunctions $\Psi_{mn}(z) = \Psi_m(z)e^{-ink_0 z}$. The set of curves $k_{zmn}(\omega) = k_{zm}(\omega) + nk_0$, where $m = 1, ..., \infty$, $n = 0, \pm 1, \pm 2, ..., \pm \infty$, entirely fill the range $0 < \omega < \omega_p$ in the $\omega - k_z$ plane [1]. Meanwhile it can be easily established that eigenvalues $k_{zmn}(\omega)$ and eigefunctions $\Psi_{mn}(z)$ taken at fixed m and different n define the same full field $E_{zm}(0, z)$, which is characterized only by transverse index m. So, one can use any of them to calculate the full field, others are spurious. Thus, before numerical calculations it would be reasonable to transform (1) in such a way as to get rid of spurious solutions.

For this, introduce a new function $F(z) = \int^z E_z(0, z') dz'$. For $F(z)$ we have the following problem:

$$\begin{cases} F(z + \varphi(z)) + F(z - \varphi(z)) = 0 \\ F(z + d) = e^{ik_z d} F(z) \end{cases} \qquad (3)$$

It is expedient to present $F(z)$ in the form $F(z) = \rho(z)e^{ik_z z + i\theta(z)}$. For two new unknown real functions $\rho(z)$ and $\theta(z)$ from (3) we can derive two separate problems:

$$\begin{cases} \rho(z + \varphi(z)) + \rho(z - \varphi(z)) = 0 \\ \rho(z + d) = \rho(z) \end{cases} \qquad (4)$$

$$\begin{cases} \dfrac{1}{2}[\theta(z + \varphi(z)) - \theta(z - \varphi(z))] = (m + 1/2)\pi - k_z \varphi(z) \\ \theta(z + d) = 2\pi nk_0 z + \theta(z) \end{cases} \qquad (5)$$

It can be easily seen that all spectral properties of our structure are defined by the problem (5), while the problem (4) has a simple and evident solution $\rho(z) = const$. According to the theorem about uniqueness of solution of a value-boundary problem for Maxwell equations, it is unique.

Now, the index n labeling the axially shifted branches can be omitted what enables us to get rid of spurious solutions and consider the problem describing the ordinary spectrum of waveguide modes:

$$\begin{cases} \dfrac{1}{2}\left[\theta\big(z + \varphi(z)\big) - \theta\big(z - \varphi(z)\big)\right] = (m + 1/2)\pi - k_z\varphi(z) \\ \theta(z + d) = \theta(z) \end{cases} \quad . \tag{6}$$

After that it is convenient to analyze (6) numerically. Numerical calculations have been performed for sinusoidal ripples: $X_0(z) = x_0\big(1 + \alpha\cos k_0 z\big)$.

Fig.1 displays the dispersion curve for the fundamental plasma mode. The locations of stop bands are defined by the relation: $\omega_{-q} < \omega < \omega_{+q}$, where $\omega_{\pm q} = \omega_p \Big/\Big(1 + \big(\pi q/x_0 k_0(1 \pm \alpha)\big)^2\Big)^{-1/2}$, $q = 1, 2, ..., \infty$.
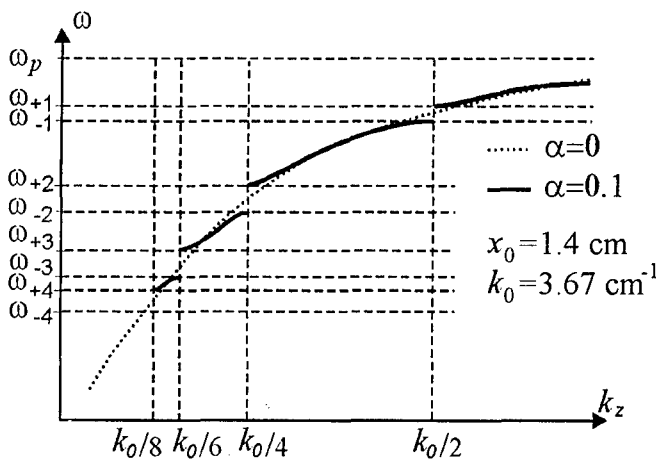
Fig. 1. The fundamental plasma mode $(m=0)$

As in the case of electromagnetic waves, group velocities of plasma waves at the boundaries of stop bands $\big(\omega = \omega_{\pm q}\big)$ tend to zero. Meanwhile the wavenumbers of plasma waves tend to $k_0/2q$, when the frequency approaches to the q – th stop band. At increasing q stop bands locate more densely and below the frequency defined from the condition $\alpha x_0 k_0|\varepsilon|^{1/2} \geq \pi/2$ they begin to overlap. Note, that our consideration is restricted by the condition $\alpha x_0 k_0|\varepsilon|^{1/2} \leq 1$ [3]. No stop bands for the fundamental plasma mode exist at $k_z > k_0/2$.

CONCLUSION

Revealed distinguishing features of periodic plasma waveguides can provide specific regimes of beam - plasma wave interaction as well as specific regimes of acceleration of charged particles which can not be realized in conventional vacuum periodic waveguides. The approach considered can be a gateway to their quantitative analysis.

REFERENCES

[1]. W.R.Lou, Y.Carmel, T.M.Antonsen, Jr., W.W.Destler, and V.I.Granatstein, Phys. Rev. Lett., 67, 2481 (1991).
[2]. G.I. Zaginaylov, A.A.Rozkov, J.-Y.Raguin, Phys. Rev. E, 60, 7391 (1999).
[3]. I.L.Verbitskii, G.I.Zaginaylov, IEEE Trans. Plasma Sci., 27, 1101 (1999).

COMPUTING COMPLEX PROPAGATION CONSTANTS OF DIELECTRIC WAVEGUIDES

E. Trifonov, and Y. Karchevskii

Kazan State University, 18 Kremlevskaya street, 420008, Kazan, Russia

E-mail: Evgenii.Karchevskii@ksu.ru

ABSTRACT

An approach for computing propagation constants of dielectric waveguides with arbitrary circuit of cross section is presented. The method is demonstrated by a numerical example of waveguides with circular and square cross sections. The convergence of this method is analyzed.

We shall now consider the propagation of electromagnetic waves in a cylindrical dielectric waveguide with constant permittivity ε_l embedded into a medium with constant permittivity $\varepsilon_2 < \varepsilon_l$. The cross section of the waveguide S_l is an area bounded with twice continuously differentiable circuit C. The permeability μ_0 is equal to 1 everywhere. Electromagnetic waves in such a structure satisfy the source-free Maxwell equations

$$rotH = \varepsilon\frac{\partial E}{\partial t}, \; rotE = -\mu_0\frac{\partial H}{\partial t}\,.$$

We represent unknown functions in the form of $E(x,y,z,t) = \mathrm{Re}\!\left(\overline{E}(x,y)e^{i(\omega t - \beta z)}\right)$, $H(x,y,z,t) = \mathrm{Re}\!\left(\overline{H}(x,y)e^{i(\omega t - \beta z)}\right)$. Expressing vector fields in terms of longitudinal magnetic and electric components $u = \overline{E}_z$, $v = \overline{H}_z$, we reduce the initial problem to the spectral problem (see [1]) of finding such values of parameter β which allow to obtain nontrivial solutions of system of the Helmholz equations

$\Delta u + \chi_j^2 u = 0$, $\Delta v + \chi_j^2 v = 0$, $M = (x,y) \in S_j, j = 1,2$ that satisfy the condition

$$u^+ - u^- = 0, \qquad v^+ - v^- = 0, \qquad M \in C,$$

$$\frac{1}{\chi_1^2}\left(\beta\frac{\partial u^-}{\partial \tau} - \omega\mu_0\frac{\partial v^-}{\partial v}\right) - \frac{1}{\chi_2^2}\left(\beta\frac{\partial u^+}{\partial \tau} - \omega\mu_0\frac{\partial v^+}{\partial v}\right) = 0, \quad M \in C,$$

$$\frac{1}{\chi_1^2}\left(\beta\frac{\partial v^-}{\partial \tau} + \omega\varepsilon_1\frac{\partial u^-}{\partial v}\right) - \frac{1}{\chi_2^2}\left(\beta\frac{\partial v^+}{\partial \tau} + \omega\varepsilon_2\frac{\partial u^+}{\partial v}\right) = 0, \quad M \in C,$$

and Reichard condition at infinity $\begin{pmatrix} u \\ v \end{pmatrix} = \sum_{n=-\infty}^{\infty}\begin{pmatrix} A_n \\ B_n \end{pmatrix} H_n^{(1)}(\chi_2 r)e^{inr}, r \geq R$.   Here,

$\chi_j = \sqrt{k_0^2 n_j^2 - \beta^2}$, $k_0 = \omega^2\varepsilon_0\mu_0$, $\varepsilon_j = \varepsilon_0 n_j$, $j = 1,2$, $\partial/\partial\tau(\partial/\partial v)$ is tangential (normal) derivative. We search for β in the Riemann surface Λ of the function $ln\chi_2(\beta)$. If β lies in the main "physical" sheet Λ_0^1 of this surface, which satisfy the conditions $Im\chi_2 \geq 0$ and $-\frac{\pi}{2} \leq \arg\chi_2 \leq \frac{3\pi}{2}$, then functions $\overline{E}_z, \overline{H}_z$ decrease exponentially in infinity. If β lies in the sheet Λ_0^2, which satisfy the conditions $Im\chi_2 \geq 0$ and $-\frac{\pi}{2} \leq \arg\chi_2 \leq \frac{3\pi}{2}$, then functions $\overline{E}_z, \overline{H}_z$ increase exponentially in infinity.

The numerical method of computing the propagation constants β is presented in [1]. We use the expressing unknown functions in terms of potential theory basic problem reduced to an equivalent system of singular integral equations with nonlinear introducing of spectral parameter β in kernels. The Galerkin method with trigonometric basis was suggested for numerical solution of this system. This method was used only for finding real dispersion characteristics.

The aim of present work was to test this method for finding complex propagation constants. First, we analyze singularities of kernels of integral operators. It was proved that these singularities can be extracted analytically. Integral operators with singularities were represented as a sum of operator

without singularities and operator with known eigenfunctions and eigenvalues. We use the Galerkin method based on eigenfunctions of singular operators. A program complex for numerical solution of this system was developed.

The method has two parameters, i.e. M-number of the integration point and N-number of basis functions in the Galerkin method. Our experiments show that the method has an interior convergence by M and N.

First, the circular cross section with radius R example was considered. In this case it is possible to formulate characteristic equation rigorously for the propagation constant β (see [2]). The calculations was done with $\varepsilon_1=2$, $\varepsilon_2=1$, $k_0R=4$. The differences Δ between the exact solution and approximating solution and the number of points of integration M for four roots are presented in Fig1. Here $h = \beta/k_0$. Increasing N does not make effect in this case because Galerkin's method resulting system is equivalent to characteristic equation. Besides, we can see that it is not necessary to take large M to obtain a good accuracy.
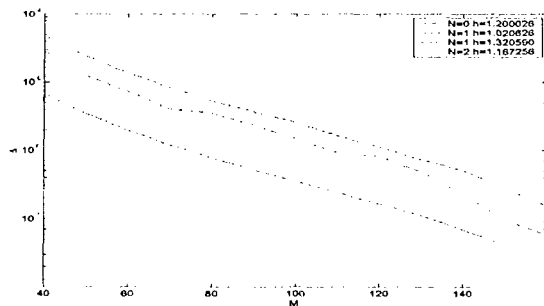
To analyze such complex modes we applied the method of [2], see Fig.2. The solid curves are for characteristic equation, the squares denote values computed by our method. Here $V = k_0 R(\varepsilon_1 - \varepsilon_2)^{1/2}$, $\varepsilon_1=61$, $\varepsilon_2=1$.
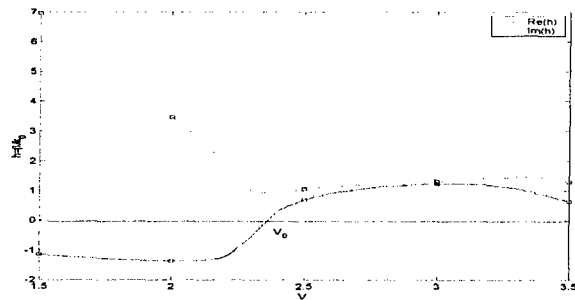
As seen (Fig 2), Re(β) changes its sign for $V=V_0$. It means that β moves from Λ_0^1 to Λ_0^2. Numerical experiments for waveguide with square cross section were carried out. Their result coincidences with [1] are presented in Fig3. We specify the square as

$$r(\varphi) = \left(\left(\frac{\cos\varphi}{d}\right)^{2m} + \left(\frac{\sin\varphi}{d}\right)^{2m}\right)^{-\frac{1}{2m}}.$$ Here $p = \frac{d}{\pi\omega}$, d is the length of square side. The dependence of calculation accuracy on the number of basis functions N for p=0.7 is shown in Fig4. As one can see, the method is convergent by N.
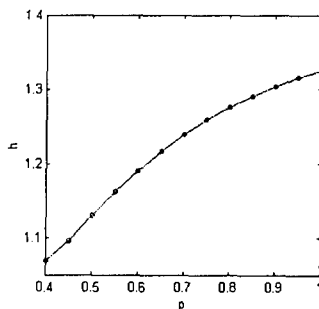
Fig 3
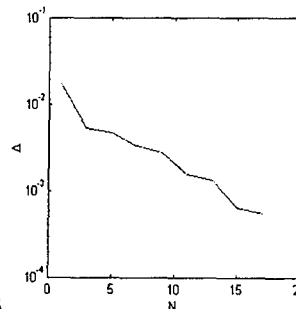
Fig 4

REFERENCES

[1] Karchevskii E.M. Determination of the Propagation Constants of Dielectric-Waveguide Eigenmodes by Methods of Potential Theory // Computational Mathematics and Mathematical Physics, Vol. 38, N 1, 1998, p. 132-136.

[2] Tomas F. Jablonski, "Complex modes in open lossless dielectric waveguides", J. Opt. Soc. Am. A/Vol. 11, 4/April 1994

CHIRAL LOW FREQUENCY RESONANCE ON AN ANISOTROPICALLY CONDUCTIVE CYLINDER WITH A THIN LONGITUDINAL SLOT

P. A. Malyshkin and A. D. Shatrov

Institute of Radio Engineering and Electronics, Russian Academy of Sciences
1 Vvedenskogo Sq., Fryazino, Moscow Region,141120, Russia
Tel. (7-095)526 92 66; Fax (7-095) 203 84 14; E-mail palmal@mail.ru

ABSTRACT

In this paper, we consider the problem diffraction of a circularly polarized wave by an anisotropically conductive cylinder of small radius with a thin longitudinal slot. It is shown that, for a certain relation between the pitch angle of the helical conductive lines and the angular dimension of the slot, one can observe a resonance phenomenon that is characterized by a sharp increase in the scattering cross-section; for a right-handed helix, this resonance phenomenon occurs only when the incident wave is left circularly polarized. At the resonance frequency, the scattered field is left-circularly polarized and has a uniform directional pattern.

It is known that certain cylindrical objects of small cross dimensions have resonance properties. These are, for instance, a metal cylinder with a longitudinal slot [1] and anisotropically conductive strip where the direction of conductivity makes a small angle with the edges of the strip [2]. The fields scattered by these objects are linearly polarized. In [3], a low frequency chiral resonance was observed in a hollow cylinder with the pitch angle of the helical conductive lines close to $\pi/2$. For right-handed helices, the resonance appears for right circularly polarized wave. The scattered field at the resonance is right circularly polarized and its angular directivity can be described by $\cos\varphi$.
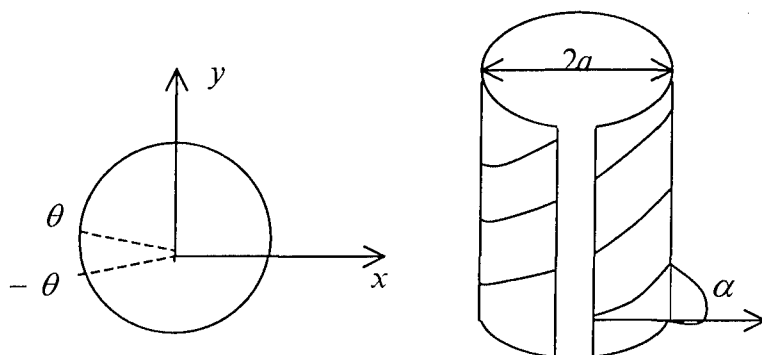
Fig. 1. Anisotropically conductive cylinder with a longitudinal slot.

In this work, we investigate a new electromagnetic object, which is a non-closed cylindrical surface with helical conductivity. We considered the diffraction of a circularly polarized plane wave propagating perpendicularly to the z axis by the surface $r = a$, $|\varphi| < \theta$ with the following anisotropic-conductivity boundary conditions:

$$E_z^+ = E_z^-, \quad E_\varphi^+ = E_\varphi^-, \quad E_z \sin\alpha + E_\varphi \cos\alpha = 0,$$

$$\left(H_z^+ - H_z^-\right)\sin\alpha + \left(H_\varphi^+ - H_\varphi^-\right)\cos\alpha = 0, \tag{1}$$

where α is the pitch angle of the helix. The z-components of the incident electromagnetic field are given by the formulas

$$H_z^0 = \exp\left[-ikr\cos(\varphi - \varphi_0)\right], \quad E_z^0 = \pm i\exp\left[-ikr\cos(\varphi - \varphi_0)\right]. \tag{2}$$

Hereinafter, the upper and lower indices correspond to the right and left hand circular polarized waves.

The problem is reduced to a integral-differential equation for the surface current $f(\varphi)$, which is related to the jump in the tangential component of the magnetic field by the formulas

$$H_z^+ - H_z^- = -f(\varphi)\cos\alpha, \quad H_\varphi^+ - H_\varphi^- = f(\varphi)\sin\alpha \tag{3}$$

The equation for $f(\varphi)$ is

$$\frac{d^2}{d\varphi^2}\int_{-\theta}^{\theta} A(\varphi-\varphi')f(\varphi')d\varphi' + \frac{d}{d\varphi}\int_{-\theta}^{\theta} B(\varphi-\varphi')f(\varphi')d\varphi' + \int_{-\theta}^{\theta} C(\varphi-\varphi')f(\varphi')d\varphi' = F(\varphi) \tag{4}$$

The kernels A, B, and C are determined by the Green's function for free space,

$$G(r,\varphi,r',\varphi') = \frac{i}{4}H_0^{(2)}\left\{k\left[r^2 + r'^2 - 2rr'\cos(\varphi-\varphi')\right]^{1/2}\right\}, \tag{5}$$

as follows:

$$A = \frac{\cos^2\alpha}{ka}G(a,\varphi,a,\varphi')\cos(\varphi-\varphi'),$$

$$B = \frac{\cos^2\alpha}{ka}\left[G(a,\varphi,a,\varphi') + a\frac{\partial}{\partial r}G(a,\varphi,a,\varphi')\right]\sin(\varphi-\varphi'), \tag{6}$$

$$C = ka\sin^2\alpha G(a,\varphi,a,\varphi') + ka\cos^2\alpha G(a,\varphi,a,\varphi')\cos(\varphi-\varphi').$$

The left-hand side of equation (4) is determined by the expression

$$F(\varphi) = \left[i\cos\alpha\cos(\varphi-\varphi_0) \mp \sin\alpha\right]\exp\left[-ika\cos(\varphi-\varphi_0)\right]. \tag{7}$$

The current $f(\varphi)$ obeys the conditions

$$f(\theta) = f(-\theta) = 0. \tag{8}$$

For the asymptotic case

$$ka \ll 1, \quad \mu = tg\alpha \ll 1, \quad \pi - \theta \ll 1, \tag{9}$$

an analytical solution is derived in the following form:

$$f(\varphi) = Df_0(\varphi), \tag{10}$$

where

$$f_0(\varphi) = \ln\left[\cos\frac{\varphi}{2} + \left(\cos^2\frac{\varphi}{2} - \cos^2\frac{\theta}{2}\right)^{1/2}\right] - \ln\cos\frac{\theta}{2}, \tag{11}$$

$$D = \frac{2ka(ka \mp 2\mu)}{1 + (ka)^2\left\{2 - i\frac{\pi}{2}\left[(ka)^2 + 4\mu^2\right]\right\}\ln\cos\frac{\theta}{2}}. \tag{12}$$

The total scattering cross-section σ calculated from the current (10) is determined by the formula

$$k\sigma = \frac{\pi^2}{8}(ka)^2\left[(ka)^2 + 4\mu^2\right]|D|^2\ln^2\cos\frac{\theta}{2}. \tag{13}$$

As it follows from (12), similarly to the case of a metal cylinder with a longitudinal slot, the resonant frequency is determined by the formula

$$ka = \left|2\ln\cos\frac{\theta}{2}\right|^{-1/2}. \tag{14}$$

Note that, at the frequency

$$ka = 2\mu, \tag{15}$$

a right circularly polarized wave does not interact with the cylinder. Therefore, a cylinder with the geometrical parameters μ and θ related by the formula

$$\mu^2 = 1\Big/ 8\left|\ln\cos\frac{\theta}{2}\right| \tag{16}$$

demonstrates ideal chiral properties at the resonant frequency (14). It does not interact with a right circularly polarized wave and strongly scatters a left circularly polarized wave. Fig.2 shows the scattering cross-sections versus the frequency for the left and right circularly polarized waves for $\theta = 175°$ and $\alpha = 12°$.
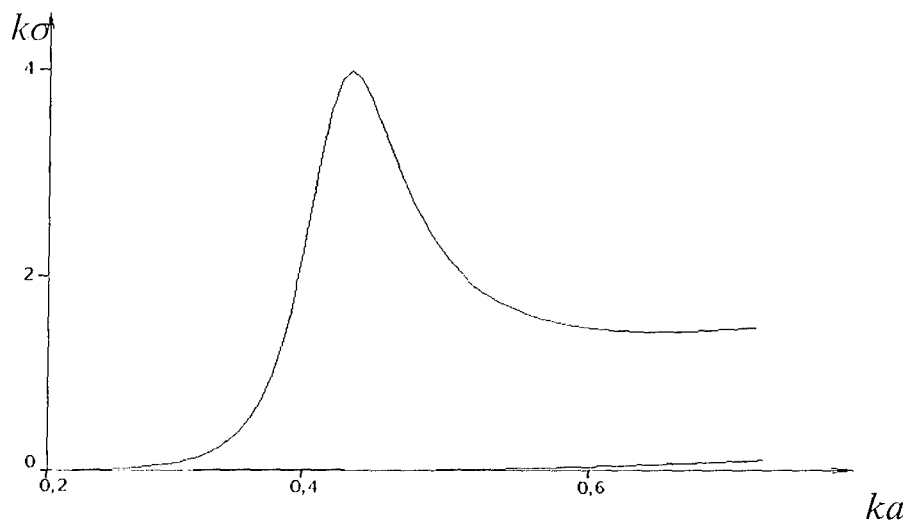
Fig. 2. Scattering cross-sections for left (resonance curve) and right circularly polarized waves for $\theta = 175°$, $\alpha = 12°$.

Thus, an anisotropically conductive cylinder with a longitudinal slot has a strong polarization selectivity with respect to left and right circularly polarized waves. This fact makes it possible to use such cylinders for the design of artificial chiral media and structures [4].

REFERENCES
1.   Nosich, A.I. and Shestopalov, V.P., An Electromagnetic Analogue of the Helmholtz Resonator, *Dokl. Akad. Nauk SSSR,* 1977, vol. 234, no. 1, pp. 53–56.
2.   Malyshkin, P.A. and Shatrov, A.D., Resonance Scattering of Electromagnetic Waves by a Narrow Anisotropically Conductive Strip, *Radiotekh. Elektron.,* 1999, vol. 44, no. 7, pp. 800–805.
3.   Sivov, A.N., Chuprin, A.D.. and Shatrov, A.D., Low-Frequency Resonance in a Hollow Circular Cylinder with Perfect Conductivity along Helical Lines, *Radiotekh. Elektron.,* 1994, vol. 39, no. 10, pp. 1534–1538.
4.   Katsenelenbaum, B.Z.. Korshunova, E.N., Sivov, A.N., and Shatrov, A.D.. Chiral Electromagnetic Objects, *Usp. Fiz. Nauk,* 1997, vol. 167, no. 11, pp. 1201–1212.

RESONANT SPECTRA OF THE WGM DIELECTRIC RESONATORS DEFORMED FROM THE CIRCULAR GEOMETRY

Svetlana V. Boriskina, Trevor M. Benson, Phillip Sewell and Alexander I. Nosich*

School of Electrical and Electronic Engineering, University of Nottingham, University Park, Nottingham NG7 2RD, UK
E-mail: eezsb@hermes.nottingham.ac.uk

*Institute of Radio Physics and Electronics
of National Academy of Sciences of Ukraine, Kharkov, Ukraine
E-mail: alex@emt.kharkov.ua

ABSTRACT

WGM cylindrical dielectric resonators deformed from the circular symmetry are of special interest for the design of new optoelectronic devices. They provide advantages for integration into microwave and optical circuits and obtaining directional emission from the WG-type lasers. The effect of increasing the deformation magnitude on the complex resonance frequencies of the WG-modes is studied using an efficient algorithm based on the method of analytical regularization.

INTRODUCTION

WGM dielectric resonators (DRs) are important elements of microwave, millimetre-wave and optical integrated circuits [1-4]. Their high quality factor, simplicity of fabrication, mechanical stability, good temperature compensation and suppression of spurious modes make them attractive for applications in a wide range of wavelengths and materials. Furthermore, they are also easily coupled to various waveguides and transmission lines. The fields of the WG modes are localised in the vicinity of the resonator contour, resulting in the high Q-factors of these modes. However, this also causes a strong dependence of the Q-factors on the shape and curvature of the contour. The intrinsic widths of the WG resonances of undeformed circular cylinders appear due to evanescent leakage and absorption losses in the dielectric material, while WGM oscillations in azimuthally-inhomogeneous DRs may have considerable radiation losses. However, along with inhomogeneities caused by fabrication inaccuracies, i.e., surface roughness or imperfect circular shape, deliberately formed inhomogeneities of DR are of special interest for the design of new devices. Such inhomogeneities are introduced in order to rarefy the DR spectrum and prevent a mode coupling (narrow sectorial cuts or inserts [2]), or obtain a directional emission of the WG-type lasers (gratings and small indentations on the circumference or substantial deformations from a circular symmetry [3]), and enlarge the coupling interaction length and air gap between a resonator and a waveguide (elliptic and racetrack ring resonators [3,4]). It has been demonstrated [3] that high-Q WG resonances can be excited in DRs deformed by up to 50% from the circular cylindrical symmetry.

The main goal of this paper is to study the effect of perturbations in the DR cross-section shape on the resonant frequencies and Q-factors of the WG modes. As conventional numerical methods can fail to give a correct description of the high-Q WG-mode resonances [5], we use the combination of two accurate mathematical techniques: the Green's function method to derive the set of the boundary integral equations (IE) and the Method of Analytical Regularization (MAR) [6] to convert them to a matrix equation with favourable features. Finally, it should be also noted that standard perturbation techniques cannot be used as the deformation of the DR cross-section causes a drastic shift of the resonant frequencies.

PROBLEM FORMULATION AND METHOD OF SOLUTION

Consider a deformed dielectric cylinder of cross-section S bounded by a smooth closed doubly continuously differentiable curve L ($x = a/\mu \cdot r(t)\cos t$, $y = ar(t)\sin t$) (Fig. 1). After presenting

the fields inside and outside DR as single-layer surface potentials over the DR contour and imposing the boundary conditions, a set of homogeneous singular IEs of the Fredholm first-kind can be obtained:

$$\int_L \varphi(\vec{r}_s) G_\varepsilon(\vec{r}, \vec{r}_s) dl_s - \int_L \psi(\vec{r}_s) G(\vec{r}, \vec{r}_s) dl_s = 0 \tag{1}$$

$$\frac{\varphi(\vec{r})}{2\alpha} + \frac{\psi(\vec{r})}{2} + \frac{1}{\alpha} \int_L \varphi(\vec{r}_s) \frac{\partial}{\partial n} G_\varepsilon(\vec{r}, \vec{r}_s) dl_s - \int_L \psi(\vec{r}_s) \frac{\partial}{\partial n} G(\vec{r}, \vec{r}_s) dl_s = 0 .$$

Here $\partial/\partial n$ is the outer normal derivative to the contour, $\alpha = 1$ or ε_b in the case of E or H polarization, $\varphi(\vec{r}_s)$ and $\psi(\vec{r}_s)$ are the unknown potential densities. Kernel functions G_ε, G are the Green's functions and are known to have the logarithmic singularities at $\vec{r} \to \vec{r}_s$. To handle the singular parts of the kernels of the IEs, we use the integral operator regularization (semi-inversion) based on the diagonalization of the singular part corresponding to a "standard" circular cylinder of some radius a_s:

$$G_0(t, t_s) = \frac{i}{4} H_0^{(1)} \left(2ka_s \left| (\sin(t - t_s))/2 \right| \right) . \tag{2}$$

This is advantageous for numerical modelling provided that the contour of the deformed DR is smooth and also provides readily the characteristics of the undeformed DR, useful for the purposes of comparison. By applying the Galerkin scheme, the problem being considered is reduced to a homogeneous Fredholm second-kind infinite-matrix equation:

$$AX = (I + B)X = 0,$$

where $$X = \{x_n\}_{n=-\infty}^\infty, \quad A = \{A_{mn}\}_{m,n=-\infty}^\infty, \quad I = \{\delta_{mn}\}_{m,n=-\infty}^\infty . \tag{3}$$

The resonant frequencies of the WG-modes of the resonator are determined as the points on the complex frequency plane for which nontrivial solutions of (3) exist. Specifically, we seek the values of dimensionless frequency parameter ka that are the singular points of the operator $A(ka)$, i.e., points at which the determinant of the matrix equation vanishes:

$$\det(A(ka)) = 0 . \tag{4}$$

The roots of (4) are found by searching in the complex plane with the Powell's hybrid method. Although in practice the matrix, which is used in (4), is truncated, the analytical regularization procedure reduces the impact of this and the method shows guaranteed and fast convergence with increasing the truncation number. Once the complex resonant frequency is determined, the resonance Q-factor can be obtained as:

$$Q = -\operatorname{Re}(ka)/2\operatorname{Im}(ka) . \tag{5}$$

NUMERICAL RESULTS AND DICUSSION

We consider elliptical (Fig.1a), quadrupolar (Fig.2a) and sinusoidally-corrugated (Fig.3a) resonators as examples of deformed circular-cylindrical geometries. Elliptical and quadrupolar deformations of DRs are frequently used to achieve a desired level of coupling with a waveguide via a wider air gap, which may relax the required fabrication tolerances and substantially improve filter characteristics. Circular DRs with periodically corrugated contours find applications when directional emissions are required. WG modes in DR are classified as $WGE_{mn}^\pm$ or $WGH_{mn}^\pm$ depending on polarization and symmetry. The first subscript m denotes the number of the azimuthal field variations, the second n denotes the number of the radial variations, index $\pm$ relates to the even/odd dependence on y. One can see that increasing the aspect ratio of the ellipse and quadrupole shifts all the resonances and spoils their Q-factors. Figs. 1-3b show that although deformed WGM DRs possess the merits of the circular WGM DRs, high Q-factor WG modes can only survive in the resonators, which are slightly deformed from the circle. If the deformation is

increased further, the Q-factors of the WG-modes decrease dramatically. It should also be noted that this effect is much stronger for small resonators, and if the DR size is enlarged, high-Q WG modes can still survive even in DRs with severe deformations of the contour.

CONCLUSIONS

Natural resonance frequencies of the WG-mode DRs deformed from circular geometry are studied by an efficient and numerically accurate method based on the analytical regularization of the
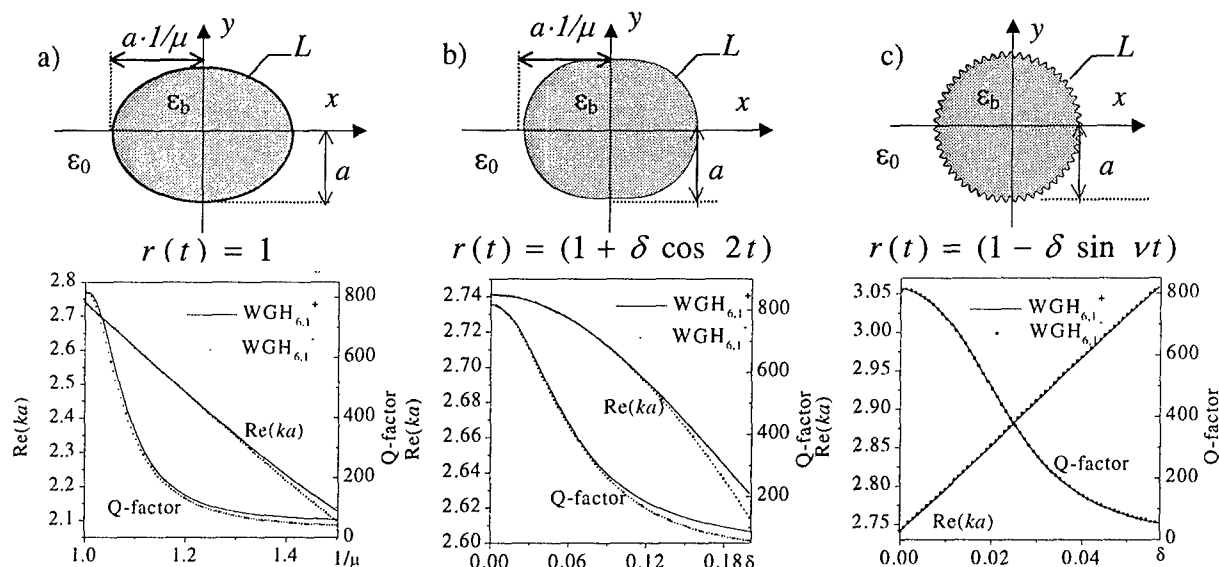
Fig. 1. Deformed resonator geometries, resonant frequencies and Q-factors of the same $WGH_{6,1}^{\pm}$ oscillations.

a) $\varepsilon_h = 10 + 0.01i$, b) $\varepsilon_h = 10 + 0.01i$, $1/\mu = 1$, c) $\varepsilon_h = 10 + 0.01i$, $v = 50$

contour integral equations. It is demonstrated how the resonance characteristics of the deformed DRs depart from those of the circular-cylindrical DRs. The method is applicable to various types of host media. Its accuracy is the same near and off sharp resonances that makes it an ideal tool for investigating practical design issues.

REFERENCES

[1] D. Cros and P. Guillon, "Whispering gallery dielectric resonator modes for W-band devices", *IEEE Trans. MTT*, v. 38, pp. 1667-1673, 1990.

[2] Y. Filipov, S. Kharkovsky, A. Kirichenko, "WG modes of nonuniform dielectric resonators", *Microwave Opt. Tech. Lett.*, v. 10, pp. 124-129, 1995.

[3] J.U.Nockel, A.D.Stone and R.K.Chang, "Q spoiling and directionality in deformed ring cavities", *Optics Letters*, v. 19, pp. 1693, 1994.

[4] Y. Kogami, Y. Tomabechi and K. Matsumura, "Resonance characteristics of whispering gallery modes in an elliptic disc resonator", *IEEE Trans. MTT*, v. 44, pp. 473-475, 1996.

[5] G.L. Hower, et al, "Inaccuracies in numerical calculations of scattering near natural frequencies of penetrable objects", *IEEE Trans. AP*, v. 41, pp. 982-986, 1993.

[6] A.I. Nosich, "The method of analytical regularization in wave scattering and eigenvalue problems", *IEEE AP Magazine*, v. 42, pp. 34-49, 1999.

NUMERICAL INVESTIGATION OF EIGEN OSCILLATIONS NEAR THE SYSTEM OF TWO STRIPS FORMING A CROSS IN THE CHANNEL

A. I. Makarov

Novosibirsk State University, Faculty of Mathematics and Mechanics,
Department of Hydrodynamics, 630090 Pirogova St. 2, Russia
e-mail: A.Makarov@hydro.nsc.ru

ABSTRACT

In this paper, the existence of eigenoscillations near the mentioned in the title system is proven. The number of oscillation modes is determined. Classification by groups of possible symmetry is carry out. Infinite matrix equation for the coefficients of corresponding expansion is obtained. This equation is investigated numerically. Obtained are the plots of eigenvalues versus the length of the cross. Approximate formula for the eigenvalues is found and investigated. The theory of the self-adjoint operators, the "Dirichlet-Neumenn bracket" and variational methods are used.

STATEMENT OF THE PROBLEM

We deal with a system of two identical strips forming a cross in the infinite channel of square cross-section. The point of strips' intersection is in the center of cross. All notations are shown in Figure 1. We investigate eigenoscillations with a harmonic time dependence.
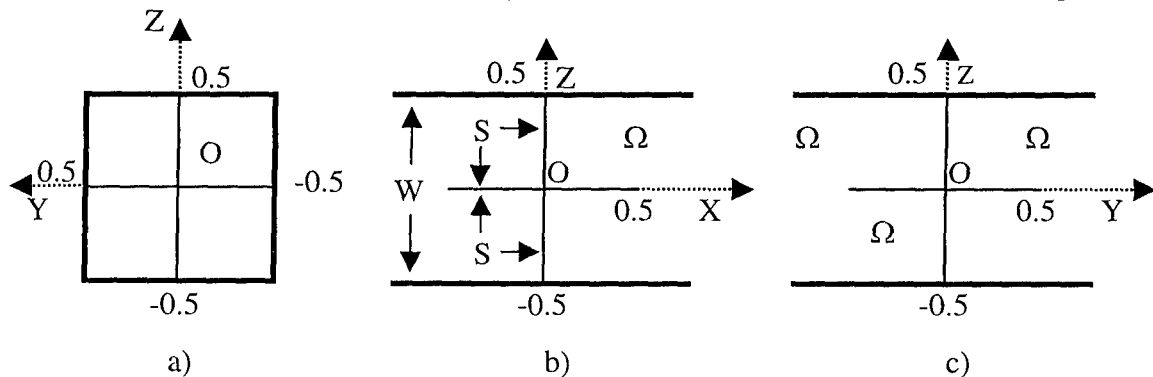
Fig. 1. Geometrical parameters of system of two strips forming a cross: a) front view; b) right lateral view c) top view.

Mathematical statement of problem for potential function $u(x,y,z)$ is:

$$\begin{cases} \Delta u + \lambda^2 u = 0 & in\ \Omega\,/\,S\,/\,W & -wave\ equation \\ \dfrac{\partial u}{\partial n} = 0 & on\ S \cup W & -Neumann\ condition\ , \\ \int_{\Omega_0}\left(u^2 + (\nabla u)^2\right)d\Omega_s < \infty & \Omega_0 \subset \Omega & -local\ energy\ condition \end{cases} \qquad (1)$$

Definition. Non trivial solution u(x,y,z) of SP is called eigenfunction of (1), the corresponding λ is called eigen (value) frequency.

It is assumed that the oscillations are odd with respect to the axes OY and OZ (the case of the even oscillations with respect to one of the axes leads to a problem with one strip in the

channel, that was studied in [1]). The system has a mirror symmetry with respect to the plane *OYZ*, so its solution can be presented as a direct sum of even and odd in variable *x* solutions.

THE THEOREM OF EXISTENCE

The self-adjoint extension *(-Δ)* has a positive continuous spectrum. The main difficulty is that discrete spectrum of problem (1) is imbedded in continuos spectrum of operator *(-Δ)*. Moreover, the Green's function of (1) is not unique [2] and it is necessary to add some condition, which provides the uniqueness of solution. On physical grounds we need to add the following condition (see more in [1]) (here, *S* is any cross-section of the channel):

$$\int_\Omega e^{i\lambda x} u(x,y,z)\,d\Omega = 0 \quad \Leftrightarrow \quad \int_S u(x,y,z)\,dS = 0 \; \forall x \tag{2}$$

According to (2), continuos spectrum of the problem (1) starts from $\sigma_0 = \pi^2$ (sometimes it is called cut-off frequency). Thus the solution is unique. By using variational methods and theory of self-adjoint operators one can prove

Theorem 1. Eigenoscillations always exist independently of geometrical parameters of the structure.

Theorem 2. The number of eigenvalues below cut-off of SP, *K,* satisfies the inequalities:

if *b* is integer then *max{1, [b]-1}≤ K ≤max{1, [b]}*;

if *b* is not integer then *max{1, [b]}≤ K ≤max{1, [b]+1}*,

where *[b]* is the integer part of the number *b*.

In the proof, the approach based on the "Dirichlet-Neumenn bracket" [3] is used.

NUMERICAL INVESTIGATION

The next linear infinite set (3) for the coefficients of solution's expansion in domain *Ω∩ {x≥0.5}* is obtained by the mode-matching method:

$$\sum_{m=0}^{+\infty}\sum_{n=0}^{+\infty} a_{m,n}\left(\frac{e^{b\alpha/2}}{\alpha_1-\alpha}+(-1)^l\frac{e^{-b\alpha/2}}{\alpha_1+\alpha}\right)\left(\frac{1}{(2m_1+1)^2-(2m)^2}+\frac{1}{(2n_1+1)^2-(2n)^2}\right)=0 \quad \forall m_1,n_1, \tag{3}$$

where *l* even (odd) corresponds to the even (odd) oscillation in variable *x*,

$$\alpha = \alpha\,(m,n) = \sqrt{\pi^2(n^2+m^2)-\lambda^2}\,, \alpha_1 = \alpha\,(2m_1+1, 2n_1+1).$$

This set is investigated numerically with two ways of truncation:

1) equal truncation of the upper index in every sum (for *0≤m₁, n₁≤ N*):

$$\sum_{m=0}^{N}\sum_{n=0}^{N} a_{m,n}\left(\frac{e^{b\alpha/2}}{\alpha_1-\alpha}+(-1)^l\frac{e^{-b\alpha/2}}{\alpha_1+\alpha}\right)\left(\frac{1}{(2m_1+1)^2-(2m)^2}+\frac{1}{(2n_1+1)^2-(2n)^2}\right)=0; \tag{4}$$

2) using Cantor's numeration of the pair of numbers (see notations in [4]), the double sum in (3) simplifies to a single sum and then the latter is truncated (for *0≤k₁≤K*):

$$\sum_{k=0}^{K} a_k\left(\frac{e^{b\alpha/2}}{\alpha_1-\alpha}+(-1)^l\frac{e^{-b\alpha/2}}{\alpha_1+\alpha}\right)\left(\frac{1}{(2m_1+1)^2-(2l(k))^2}+\frac{1}{(2n_1+1)^2-(2r(k))^2}\right)=0, \tag{5}$$

where $\alpha = \alpha\big(l(k),r(k)\big) = \sqrt{\pi^2\big(l(k)^2+r(k)^2\big)-\lambda^2}, \alpha_1 = \alpha\big(l(k_1),r(k_1)\big).$

Based on the above, approximate formulas for the eigenvalues are obtained (6a for the even, 6b for the odd oscillations):

$$tg\left(\frac{\lambda b}{2}\right) = \frac{\sqrt{2\pi^2-\lambda^2}}{\lambda} \tag{6a}$$

$$tg\left(\frac{\lambda b}{2}\right) = \frac{-\lambda}{\sqrt{2\pi^2-\lambda^2}} \tag{6b}$$

From formulas (6a) and (6b), a formula for the relation between the even and odd oscillations corresponding to the eigenvalue λ is obtained:

$$b_{even} - b_{odd} = \frac{\pi\,(2k+1)}{\lambda}, \tag{7}$$

where b_{even} and b_{odd} are the lengths of cross for the even and odd oscillations respectively, $k \in Z^+$.

a)

b)
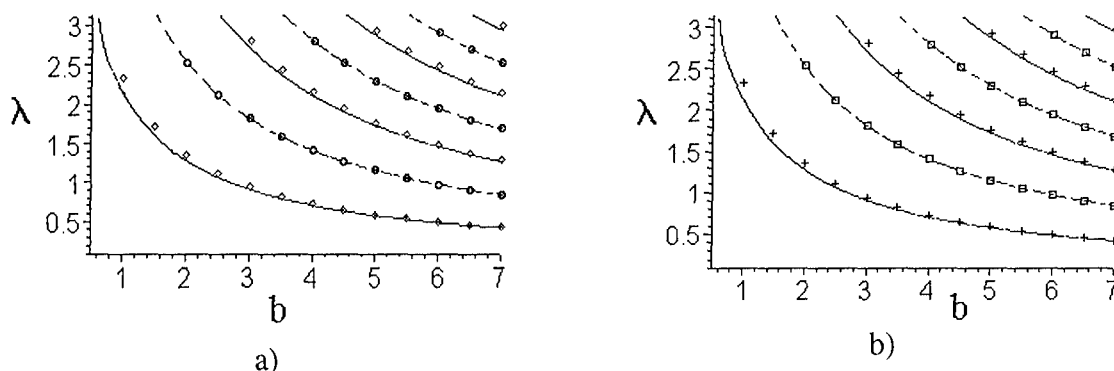
Fig. 2. Variation of the eigenvalue λ with the cross-length b. The solid line is the approximate relation (6a), and the dashed line is the approximate relation (6b). In Figure 2a, dependences of eigenvalues versus b from the set (4) with $N=2$ are also plotted, where diamonds and circles correspond to even and odd cases, respectively. In Fig. 2b, dependences of eigenvalues versus b from the set (5) with $K=9$ are plotted, where crosses and squares correspond to even and odd cases, respectively.

As we can see in Figure 2, there is a good matching between two different ways of calculation. Computations for larger values of N and K do not change this situation, because the difference between them is very small.

RESULTS

1. It has been proven that eigenoscillations always exist.

2. It has been found the number of modes of oscillation.

3. It has been found the approximate formulas for eigenfrequencies, and on its basis the formula for the relation between even and odd modes of oscillation has been obtained.

4. The dependences of the eigenvalues versus the length of cross for even and odd modes of oscillation have been obtained in two ways.

5. Numerical methods of calculation of eigen frequencies have been developed in the three-dimensional case.

ACKNOWLEDGEMENT

REFERENCES

[1] S.V. Sukhinin, S.P. Bardakhanov. Eolian tones of the plate in a channel, *Journal of Applied Mechanics and Technical Physics,* Vol. 39, No. 2, 1998.

[2] Cumpsty, D.S.Whitead The excitation of Acoustic Resonance by Vortex Shedding, *Journal of Sound and Vibration,* V. 18, N.3, p.353-369.

[3] M. Reed, B. Simon. *Methods of Modern Mathematical Physics.* Mir, 1977 (Russian translation).

[4] A.I.Maltsev. *Algorithms and Recursive Functions,* Moscow, Nauka, 1965 (in Russian).

SPECTRAL PERFORMANCES OF A NON-ISOTROPIC DIELECTRIC RESONATOR WITH IMPERFECT CONDUCTING END WALLS

Y.V. Prokopenko, and Y.F. Filippov

Institute of Radiophysics and Electronics, National Academy of Sciences of Ukraine
12 ul. Akademika Proskury, Kharkov, 61085, Ukraine
e-mail: Prokopen@ire.kharkov.ua, Fil@ire.kharkov.ua

ABSTRACT

High Q-factor oscillations in a longitudinal anisotropic dielectric resonator with imperfect conducting end walls are considered. Using an integral equation, which was derived by the authors, the spectral characteristics of such oscillations are studied.

INTRODUCTION

As a rule, open cylindrical resonators exited at the lowest oscillation modes and made of a material with a large dielectric permittivity are applied to produce stable microwave generators and filters. Recently,dielectric resonators with small dielectric permeabilities are widely applied. They are excited at higher oscillation modes, that are characterized by large values of azimuth indexes. The formed waves are incident on a lateral area at very small angles, as a result, a very small part of energy goes out the resonator. Such oscillations are known as "whispering gallery" modes. The usage of anisotropic materials, such as uniaxial single-crystals of quartz, ruby, sapphire, having small dielectric losses (not more than 5×10^{-5}), allows to increase considerably the Q-factor and apply them in devices of a millimetre and optical wave range. These oscillations are also used to study the parameters of high-temperature superconductors. Analysing the resonance oscillation spectrum of an anisotropic resonator, it is possible to determine the components of dielectric permittivity tensor of crystals. In papers $[1-2]$, spectral characteristics of resonators with perfectly conducting end-walls were investigated. The imperfect conductivity of the latter can essentially influence the spectral property of resonance oscillations. The restriction of a resonator by end high-temperature superconducting films has allowed measurements in a low-frequency microwave range of small absolute values of their surface resistance. In $[3-4]$, using power reasons, the influence of imperfect conductivity of end-walls was studied theoretically.

INTEGRAL EQUATION. FIELD CHARACTERISTICS OF A DIELECTRIC RESONATOR

A cylindrical dielectric resonator limited from two sides by identical imperfect conducting end-walls and made of an anisotropic uniaxial crystal, is considered in this paper. The axes of an anisotropy of crystal are parallel to its geometric axes. The electrical parameters of the resonator are characterized by a dielectric permittivity tensor $\hat{\varepsilon}_d$. The spectral characteristics of oscillations are determined by solving the integral equation

$$(\omega - \omega_q^*)\int_v (\vec{H}\vec{H}_q^* + \vec{E}\hat{\varepsilon}(r)\vec{E}_q^*)dV = i\frac{c^2}{2\pi}\varsigma\int_S [\vec{v}[\vec{v},\vec{H}]]\vec{H}_q^* dS . \tag{1}$$

Here, the left-hand integration is carried out over the whole volume v, and the right-hand one over a surface of end-planes S, characterized by a surface impedance ζ; $\hat{\varepsilon}(r) = \hat{\varepsilon}_d$ inside and $\hat{\varepsilon}(r) = 1$ outside the resonator; the sign * is for the complex conjugation; $\omega, \vec{H}, \vec{E}$ are frequency and fields of resonance oscillations in a resonator with imperfect conducting end-planes, and $\omega_q, \vec{H}_q, \vec{E}_q$ - with ideally conducting; $\vec{v}$ is the basis vector of axial resonator axes.

In a resonator with ideally conducting end-walls, independent EH and HE oscillations exist with fields $\vec{H}_q, \vec{E}_q$ expressed through the potential functions for EH oscillations

$$U_q = A_q R_H(r) \begin{bmatrix} \cos n\varphi \sin k_z z \\ \sin n\varphi \cos k_z z \end{bmatrix},$$

$$\text{where } R_H(r) = \begin{cases} J_n(\chi_H r), & r \le r_0 \\ \dfrac{\chi_H^2}{\chi_0^2} \dfrac{J_n(\chi_H r_0)}{H_n^{(1)}(\chi_0 r_0)} H_n^{(1)}(\chi_0 r), & r \ge r_0 \end{cases} ;$$

$$V_q = B_q R_E(r) \begin{bmatrix} \sin n\varphi \cos k_z z \\ \cos n\varphi \sin k_z z \end{bmatrix},$$

$$\text{where } R_E(r) = \begin{cases} J_n(\chi_E r), & r \le r_0 \\ \dfrac{\chi_H^2}{\chi_0^2} \dfrac{J_n(\chi_E r_0)}{H_n^{(1)}(\chi_0 r_0)} H_n^{(1)}(\chi_0 r), & r \ge r_0 \end{cases} -$$

for HE oscillations. Here, q stands for a triple index nms - azimuth, radial and axial indexes, respectively, and the resonance frequencies are determined by the equation

$$(\alpha_H - \alpha_0)(\varepsilon_{zz}\alpha_E - \alpha_0) = \frac{nkk_z(1 - \varepsilon_{xx})}{(\chi_h \chi_e)^2 r_0^2},$$

where $\chi_H = \sqrt{\varepsilon_{xx} k^2 - k_z^2}$, $\chi_E = \sqrt{\dfrac{\varepsilon_{zz}}{\varepsilon_{xx}}(\varepsilon_{xx} k^2 - k_z^2)}$ are the radial components of wave

vectors of EH and HE oscillations; $k_z = \dfrac{s\pi}{2l}$, $2l$ and r_0 are height and radius of a resonator, $s = 0;1;2...$; ε_{zz} and ε_{xx} is a component of a dielectric permittivity tensor in parallel and diametrical directions to the axes of uniaxial crystal;

$$\alpha_j = \frac{J_n'(\chi_j r_0)}{\chi_j r_0 J_n(\chi_j r_0)} \quad ; \quad \alpha_0 = \frac{H_n'(\chi_0 r_0)}{\chi_0 r_0 H_n(\chi_0 r_0)}.$$

The index j has values H and E; $J_n(x)$, $H_n^{(1)}(x)$ are the Bessel and Hankel cylindrical functions of the first kind.

The fields of resonance oscillations are orthogonal to a continuous spectrum and satisfy the orthogonality condition

$$\int_v (\vec{H}_p^* \vec{H}_q + \vec{E}_p^* \hat{\varepsilon} \vec{E}_q) dV = 2N_p \delta_{pq},$$

where δ_{pq} is the Kronecker symbol, and $N_p = \int_v \vec{H}_p \vec{H}_p^* dV = \int_v \vec{E}_p^* \hat{\varepsilon} \vec{E}_p dV$ is a norm for p's

oscillation.

For both axial and azimuth-homogeneous oscillations ($k_z = n = 0$) it is characteristic, that in the case of EH oscillations the E_z component of the field is equal to zero, and their resonant frequencies are determined by the equation $\alpha_H = \alpha_0$, at HE oscillations $H_z = 0$, the resonant frequencies are determined from the equation $\alpha_E = \varepsilon_{zz}\alpha_0$. At $k_z \neq 0$, $n \neq 0$ all of these oscillations have all non-zero field components. In fact, the oscillations with parameters $H_z \gg E_z$ for EH oscillations and $E_z \gg H_z$ for HE oscillations are selected by an adequate methods of generation.

In a resonator with imperfect conducting end-walls the fields $\vec{E}, \vec{H}$ are described through the potential functions U and V. The inter-mode interaction occurs if frequencies coincide between HE and EH oscillations. Assuming that the frequency degeneracy is absent, we can present the solution of equation (1) as

$$U = \sum_q \beta_{Hq} U_q$$

for EH oscillations and

$$V = \sum_q \beta_{Eq} V_q$$

for HE oscillations, where β_{Hq} β_{Eq} are the expansion factors. Using expressions for fields and integrating over the space coordinates, we obtain an expression defining the displacement of resonance frequency under the influence of imperfect conductivity of end-walls.

CONCLUSION

The obtained relations allow to determine a surface impedance of end-walls using the experimentally measured frequencies and basic Q-factors of resonance oscillations of a dielectric resonator with imperfect conducting walls.

REFERENCES

[1] Kobayashi Y., Tanaka S. IEEE Trans., 1980, Vol. MMT-28, no.10, P.1077-1085.
[2] Egorov V.N., Maltseva I.N. Electronic technique. Ser.1. Microwave electronics, 1984, Vol.1, P.3-8. (in Russian).
[3] Krupka J., Derzakou'sky K., Abramowicz A. IEEE Trans., 1999, Vol. MMT-47, No.6, P.752-759.
[4] Prokopenko Yu.V., Filippov Yu.F., Cherpak N.T. Radiophysics and electronics. IRE NAS of Ukraine, 1999, Vol.4, No2, P.50-54. (in Russian).

TWO-DIMENSIONAL BRAGG RESONATOR WITH NONPERIODIC RADIAL AND ANGULAR PERTURBATION OF PARAMETERS

V. F. Borulko, and Vladimir E. Ivanilov

Department of Radiophysics, Dniepropetrovsk State University, 13 Naukova St.,
Dniepropetrovsk, 49050, Ukraine.
Tel: 38 056 7254592, E-mail: dsu-microwave@fm.com.ua

ABSTRACT

Reflection and angular-mode transformation of electromagnetic waves propagating in medium with small two-dimensional quasi-periodic inhomogeneity are theoretically considered. Using a complex form of the asymptotic method of Krylov, Bogoliubov and Mitropolsky, expressions for coupling coefficients of propagating waves are derived. Existence of "Brewster radius" in Bragg phenomenon is discovered for the case of TE waves in a medium with periodic perturbation of permeability. Radial distributions of complex amplitudes are numerically computed.

INTRODUCTION

Attention to the Bragg structures is to be explained by the variety of physical effects that can be observed in them [1], i.e. wave reflection, mode conversion, coupling of surface and space waves. Additional variety of effects occurs if parameter perturbation becomes non-periodic [2].

In present work, two-dimensional Bragg structure with nonperiodically inhomogeneous permittivity and permeability is considered. The permittivity and permeability of medium are assumed to be presented in the form of a sum of spatial nonperiodically oscillating harmonics of perturbation. The amplitude and wavenumber of each harmonic smoothly vary along radial coordinate. The perturbations as functions of the angular coordinate are expressed in the form of the Fourier expansion. In this case, the Floquet method [1] is not applicable because of nonperiodicity of the structure and traditional coupled-waves method [1] is failed near cut-off radii. Approximate solutions describing Bragg reflection and conversion of angular mode are found by a modified asymptotic method of Krylov, Bogoliubov and Mitropolsky (KBM) [3]. The main feature of the proposed approach is the usage of the Hankel functions in zero-order approximation instead of exponential ones. This allowed us to overcome the problem of cut-off radii.

METHOD OF ANALYSIS

We consider a two-dimensional waveguiding structure nonperiodically inhomogeneous along radial and angular coordinates. Permittivity and permeability are presented in the form of a sum of spatially oscillated harmonics of perturbation as follows:

$$\varepsilon = \varepsilon(\rho, \varphi) = \varepsilon_{00} + \beta \sum_{j,s} \varepsilon_{js} (\beta \rho) \exp[i \psi_j(\rho) + i s \varphi],$$

$$\mu = \mu(\rho, \varphi) = \mu_{00} + \beta \sum_{j,s} \mu_{js} (\beta \rho) \exp[i \psi_j(\rho) + i s \varphi],$$

$$\tag{1}$$

where $\psi_j(\rho) = \int \chi_j(\beta \rho) d\rho$ is the longitudinal phase of perturbation harmonic, amplitude ε_{js} and μ_{js} and wavenumber χ_j of each harmonic smoothly vary along the radial coordinate. We

suppose that smallness of perturbation amplitudes and smoothness of parameter variation are determined by the same small parameter β [3]. Simultaneously with radial coordinate ρ, we introduce "smooth" scale $\zeta=\beta\rho$. For the case of $\partial/\partial z \equiv 0$ and *TE* waves all field components can be expressed in terms of E_z. We introduce the potential function $\Pi(\rho,\varphi)$ by a relation $E_z = \rho^{-1/2}\Pi(\rho,\varphi)$. For $\Pi(\rho,\varphi)$ the following differential equation is obtained:

$$\frac{\partial^2\Pi}{\partial\rho^2} + \frac{\partial^2\Pi}{\rho^2\partial\varphi^2} + \left[k_0^2\varepsilon(\rho,\varphi)\mu(\rho,\varphi) + \frac{1}{4\rho^2}\right]\Pi - \frac{1}{\mu}\frac{\partial\mu}{\partial\rho}\left(\frac{\Pi}{2\rho} - \frac{\partial\Pi}{\partial\rho}\right) - \frac{1}{\mu\rho^2}\frac{\partial\mu}{\partial\varphi}\frac{\partial\Pi}{\partial\varphi} = 0., \quad (2)$$

If $\beta = 0$, a solution of the unperturbed differential equation is presented as a sum of divergent and/or convergent cylindrical waves

$$\Pi(\rho,\varphi) = \sum_m a_m \rho^{1/2} H_{n(m)}^{(2)}(k_m\rho)\exp[in(m)\varphi] = \sum_m a_m \exp[i\theta_m(\rho) + in(m)\varphi], \quad (3)$$

where $H_{n(m)}(t)$ are the Hankel functions, n (1) and $n(2)$ are angular indices of coupling waves, $\theta_m(\rho)$ is complex space phase and $k_m = \pm k_0\sqrt{\varepsilon_{00}}$ are the unperturbed wavenumbers (sign "plus" corresponds to divergent waves, sign "minus" corresponds to convergent waves). In contradistinction to traditional Bragg structures [1,2] in the considered task unperturbed radial wavenumber h_m is not constant and real and for divergent waves it is defined in terms of the cylindrical functions [4]. At fixed small β there is such a value of the radial coordinate $\rho_0 = \rho_0[\beta, n(m)]$, that for $\rho > \rho_0$ values h_m and $k_{00}^2 - [n^2(m) - 1/4]/\rho^2$ can be considered as smoothly varying along ρ.

A solution of (2) is sought as an asymptotic series on degrees of a parameter β

$$\Pi(\rho,\varphi) = \sum_{m=1}^{2} a_m \exp[i\theta_m(\rho) + in(m)\varphi] + \beta u_1(a,\theta,\psi,\zeta,\varphi) + \beta^2 u_2(a,\theta,\psi,\zeta,\varphi) + ..., \quad (4)$$

where u_q $(q = 1,2,...)$ are sought functions, a_m are amplitudes of the cylindrical waves propagating in the waveguiding structure. The functions exp $(i\theta_m)$ strictly satisfy the unperturbed equation and are defined by (3).

Bragg wave coupling occurs when the difference of wavenumbers of propagating waves is close to the wavenumber of one of the spatial perturbation harmonics ($\eta_m = h_{3-m} - h_m - \chi_{p(m)}$ are wavenumber mismatches). A solution suitable near a space parametrical resonance is searched with the aid of the complex form [2] of the asymptotic method of Krylov, Bogoliubov and Mitropolsky (KBM) [3]. The complex amplitudes a_1 and a_2 of cylindrical waves are supposed to be functions of ρ and satisfy to the following equations [2]:

$$\frac{da_m}{d\rho} = \beta B_m^{(1)}(a,\zeta,\alpha_m) + \beta^2 B_m^{(2)}(a,\zeta,\alpha_m) + ..., \quad (m = 1,2) \quad (5)$$

where $\alpha_m = \theta_m - \theta_{3-m} - \psi_{p(m)}$ are phase mismatches from a resonance, $B_m^{(q)}$ $(q = 1,2,...)$ are functions chosen from the condition of absence of infinitely growing members in u_q when $\rho \to \infty$ and $\eta \to 0$. Substituting expansion (4) into (2) using (5) and equating the members with identical smallness order, we get succession of equations for u_q. In each smallness order we search solutions under "frozen" a_n and ζ. They must be valid for both small values of η and not small ones. To ensure single-valued determination of $B_m^{(q)}$ for not small η we demand absence in u_q resonance addends proportional $\exp(i\theta_m)$ and "potentially" resonance addends proportional to exp $(i\theta_m - i\alpha_m)$. The main distinction of presented modified version of KBM method from traditional one [3] is using the Hankel functions in zero-order approximation

instead of exponential functions. This allows us to overcome the problem of cut-off radii and widen the area of validity of asymptotic method.

As a first approximation on β we have following inhomogeneous differential equation for u_1:

$$\frac{\partial^2 u_1}{\partial \rho^2} + \frac{\partial^2 u_1}{\rho^2 \partial \varphi^2} + \left[k_{00}^2 + \frac{1}{4\rho^2}\right]u_1 + \sum_{m=1}^{2}\left(-2ih_m B_m^{(1)} + \eta_m \frac{\partial B_m^{(1)}}{\partial \alpha_m}\right)\exp\left[i\theta_m(\rho) + in(m)\varphi\right] +$$

$$+ \sum_{m=1}^{2} a_m \sum_{j,s} D_{mjs} \exp\left[i\theta_m + in(m)\varphi + i\psi_j + is\varphi\right] = 0,$$
(6)

where $D_{mjs} = k_{00}^2 \varepsilon_{j,s}/\varepsilon_{00} + \mu_{j,s}/\mu_{00}\{k_{00}^2 - \chi_j[h_m - i/(2\rho)] + sn(m)/\rho^2\}$.

Taking into account that $\theta_m - \alpha_m = \theta_{3-m} + \psi_{p(m)}$ we find $B_m^{(1)}$. In the first approximation on β the following system of the linear differential equations for amplitudes a_1 and a_2 is obtained:

$$\frac{da_m}{d\rho} = \beta a_{3-m} G_m \exp(-i\alpha_m), \quad (m = 1, 2)$$
(7)

where $G_m = -iD_{3-m,p(m),n(m)-n(3-m)}/(2h_m + \eta_m)$. Parameters G_1 and G_2 describe spatial coupling of the waves propagating in the inhomogeneous medium. If perturbation is homogeneous in the angular direction, only waves with the same angular numbers and opposite propagation directions can be coupled and Bragg reflection can be observed. If coupled waves have the same direction of propagation, a resonance conversion of mode occurs. If the angular numbers and propagation directions are different, there is a combination of the reflection and the mode conversion in considered waveguiding structure. In two last cases the resonance conditions must be satisfied for both radial and angular wavenumbers. Because the value of longitudinal wavenumber is not constant and real, the process of Bragg transformation is not periodic even if perturbation wavenumber and amplitude are constant. For the case of a periodic perturbation of the permeability value of G_m becomes close to zero at some value of ρ. Similar "Brewster radius" can be observed also for TM waves and a periodic perturbation of permittivity. Specific type of Bragg resonator is formed near these radii.

CONCLUSIONS

Combination of radial and angular perturbation of the filling provides a reflection or mode conversion for waves with different angular indices. A modification of the asymptotic method of Krylov, Bogoliubov and Mitropolsky by using the Hankel functions widens its possibilities. The found solution can be used to investigate resonator properties of waveguiding structures filled with inhomogeneous medium. The obtained results can be useful for designing frequency and angular selective reflectors and resonators.

REFERENCES

[1] C. Elachi, "Waves in active and passive periodic structures: A review" *Proceedings of the IEEE*. Vol. 64, No. 12, pp. 1666-1698, 1976,
[2] V. F. Borulko, "Polarization and mode conversions in nonperiodically corrugated waveguides with a gyrotropic filling", *Proc. of the 1995 URSI International Symposium on electromagnetic Theory*, St. Petersburg, Russia, May 23-26, 1995, pp. 729-731.
[3] N. N. Bogoliubov, Yu. A.Mitropolsky, *Asymptotic Methods in the Theory of Nonlinear Oscillations*. New York: Gordon and Breach Science Publ., 1961.
[4] M. Abramovitz and I.Stegun *Handbook of Mathematical Functions*. National Bureau of Standards, 1964.

COMPLEX WAVES IN PLANAR SPIRAL WITH TREE-LAYERED DIELECTRIC

K.P.Yatzuk

Kharkov National University, 4 Svobody Sq., Kharkov, 61077, Ukraine

tel. (+380)-572-45-71-33, e-mail: Ludmila.P.Yatsuk@univer.kharkov.ua

ABSTRACT

A system consisting of three-layered dielectric with semi-transparent film in form of a plane logarithmic spiral between two layers and metallic screen on one side of system is considered. A dispersion equation for symmetric waves was obtained and computations were curried out for various system parameters and dielectric permittivities. Proper and improper slow waves were found and influence of the system parameters on their existence was determined.

INTRODUCTION

It is known [1] that complex waves (CW) can exist in layered dielectric or in metal-dielectric waveguides for some system parameters in some frequency band. The expression «complex» means that a wave number is complex for ideal system parameters. The complex waves can be proper, improper, fast or slow. They can exist both in open or closed waveguides as well. The improper complex waves exist in open systems. They do not satisfy the radiation condition, are called «leaky waves» and have a high phase velocity. The slow improper complex waves were also observed in open systems in wide frequency band. The introduction of thin dissipative film in layered dielectric causes the coupling between waves of various polarization and, as a result, a great variation of CW characteristics behavior. The waves became proper in some frequency band, etc. This was observed only for a thin film. But the literature presents no data about the existence of CW in layered dielectrics with an anisotropic semi-transparent film. So, we investigated a system consisting of three-layered dielectric with a film in form of plane logarithmic spiral. The aim of such study is to find the waves with various physical nature.

CONSIDERATION

The system under consideration consists of two planar dielectric layers which thickness are a, d and dielectric permittivities $\varepsilon_3, \varepsilon_2$, respectively, and semi-infinite dielectric area with permittivity ε_1. The plane logarithmic spiral is situated between the first and second layers. The whole system is situated on a grounded screen. The spiral is described by the curve $\rho = \rho_0 \exp(u / \varphi)$, where ρ, φ, z are cylindrical coordinates, ρ_0 is starting spiral radius, $u = ctg\psi$ is spiral parameter, ψ is the twirl angle of the spiral.

We used the following approximation. 1) All dielectrics are ideal. 2) The spiral is assumed as an anisotropy sheet model. 3) The spiral and screen are perfectly conducting, the time dependence is $\exp(i\omega t)$. 4) We assume that only symmetric waves exist in the spiral.

The mode matching method has been used for the problem solution. There are three regions $I - d < z < \infty, \varepsilon = \varepsilon_1$; $II - 0 < z < d, \varepsilon = \varepsilon_2$, $III - -a < z < 0, \varepsilon = \varepsilon_3$, The spiral and screen ones are situated at $z = 0, -a$, respectively. The fields in each region are expressed using the electric and magnetic Hertz vectors $\vec{A}^{e,m}\left(0, 0, A_{zj}^{e,m}\right)$, where j is the region number. Potentials are various for each region and expressed as follows: for j=1 $A_{z1}^{e,m} = N^{e,m} H_0^{(2)}(\gamma\rho)e^{-ip_1 z}$, for j=2,3 $A_{zj}^{e,m} = H_0^{(2)}(\gamma\rho)(F_j^{e,m} e^{-ip_j z} + G_j^{e,m} e^{ip_j z})$, where $H_0^{(2)}(\gamma\rho)$ is the Hankel function, γ is the

longitudinal (radial) wave number, p_j is the transverse wave number, $p_j = \sqrt{k^2 \varepsilon_j - \gamma^2}$,

$k = \omega / c$ is a wave number in free space, $N_1^{e,m}, F_{2,3}^{e,m}, G_{2,3}^{e,m}$ are unknown coefficients.

The boundary conditions are formulated as conjugate conditions at two dielectric boundaries, anisotropy sheet model on spiral and zero conditions on metal screen. Substituting the fields from each region into boundary conditions, we obtain the algebraic expressions for unknown coefficients and dispersion equation in the form

$$\varepsilon_2 k^2 u^2 R_2 A + B p_2 M_4 = 0,\tag{1}$$

where

$$A = A_0 M_4 p_2 \varepsilon_3 / (p_3 \varepsilon_2) - M_4, \quad B = p_3 A_0 R_2 - p_2 R_1,$$
$$A_0 = [\exp(2p_3 a) + 1] / [\exp(2p_3 a) - 1],$$
$$P^- = p_2 - p_1, \quad P^+ = p_2 + p_1, \quad S_1 = \exp(2p_2 d),$$
$$R_{1,2} = P^- \pm S_1 P^+, \quad M_{1,2} = \varepsilon_1 p_2 \mp \varepsilon_2 p_1, \quad M_{3,4} = M_1 \pm S_1 M_2.$$

We assume that in dispersion equation (1) the radial wave number can be complex $\gamma = \gamma' + i\gamma''$. So, we found the complex roots by means of the computer program. The computations were fulfilled for various a, d, u, ε_j in waveband 6-60cm. We obtained the following results. 1) For the case $\varepsilon_1 = \varepsilon_2 = \varepsilon_3 = 1$ the slowing down (SD) of the wave is determined by the spiral parameter u in the same way as for usual pure surface wave. 2) In the case of substrate or superstrate presence $(\varepsilon_1 = 1, \varepsilon_2 > 1, \varepsilon_3 > 1)$ we also have not found the complex waves. 3) The complex waves occur if three-layered dielectric exists. And what is more, they exist if the thickness of the air gap between the spiral and semi-infinite area is small or the superstrate thickness is small and $\varepsilon_2 < \varepsilon_1$. The calculation results are:

A) Dispersion curves can have two parts: one with $\gamma'' = 0$ and normal dispersion (usual surface wave), another one with $\gamma'' < 0$ and anomalous dispersion (this is improper complex wave), but both of them are slow waves. B) The complex waves occur in case of a small wave-length λ for small ε_1 and in the case of large wave-length for larger ε_1. C) The increasing of ε_1 causes the increase of the surface waves SD, but a decrease of the complex waves SD. D) The increasing of the substrate permittivity ε_3 causes the increasing of the surface and the complex waves SD as well. E) The increasing of the spiral parameter u causes the complex wave arise in a larger wave-length.

CONCLUSION
It was found that the improper slow waves in layered dielectric with semi-transparent film occur in the case of small gap between the spiral and semi-infinite dielectric space. The frequency band of these waves existence depends on the system parameters and dielectric permittivities. These results can be used in designing of applicators for irradiation of live organisms.

REERENCE
[1] G.I.Veselov, S.B.Raevsky Layered metal-dielectric waveguides.-M.:-Radio and connect. 1988.-247p.(in Russian).

GRATINGS
AND
FREQUENCY-SELECTIVE
SURFACES

DIFFRACTION BY A MULTILAYER-COATED BISINUSOIDAL GRATING

Y. Okuno*, T. Matsuda**, and M. Kinoshita*

* Department of Electrical and Computer Engineering, KumamotoUniversity, Kumamoto 860-8555, Japan okuno@gpo.kumamoto-u.ac.jp

** Kumamoto National College of Technology, Nishigoshi 861-1102, Japan

Diffraction from a multilayer-coated bisinusoidal grating is analyzed by Yasuura's mode-matching method. The diffracted fields over the coating, inside the layers, and below the metal surface are represented in terms of finite modal expansions consisting of vector modal functions with unknown coefficients. Since the functions satisfy the vector wave equation and the periodicity and radiation condition, the coefficients are determined so that the representations meet the boundary condition in the least-squares sense. In the present problem where the geometry has several boundaries that are corrugated in two directions, however, the size of the least-squares problem becomes so large that we face a trouble of memory deficiency in handling the problem on a computer. We, hence, employ the technique of sequential accumulation in solving the problem, the technique which considerably decreases the memory demand and enables us to solve the problem on a small-sized computer.

INTRODUCTION

We investigate the problem of plane-wave diffraction by a multilayer-coated bisinusoidal grating which is a stack of dielectric thin films over a metal grating. Both the films and the grating are periodically corrugated in two directions. In the numerical analysis based on the Yasuura method [1] we solve a least-squares problem that finds modal coefficients in each region: the free space over the grating; inside the layers; and in the metal grating.

When the number of modal functions in each region or the number of layers is increased, the size of the least-squares problem also increases considerably. This causes the problem of huge requirement of computer storage. Apparently there is a minimum number of modal functions to ensure a desired accuracy of solutions. Hence, if we solve the least-squares problem by a conventional algorithm, the number of layers must be limited strongly.

We, hence, combine a technique called sequential accumulation [2] with the QR decomposition algorithm in solving the least-squares problem. This reduces the storage requirement in the numerical computation. In addition, taking the fact that the Jacobian matrix in the problem has a band structure into account, we can attain further reduction of storage demand and shortening of computation time.

FORMULATION AND METHOD OF SOLUTION

We consider a stack of surfaces S_q ($q = 1, 2, ..., Q$) accumulating in the Z-direction. Each surface is modulated sinusoidally in the X- and Y-direction with a common period d. The qth surafce is governed by $z - H_q = \zeta(x, y) = (h/4) [\sin(2\pi x/d) + \sin(2\pi y/d)]$, where H_q is the mean height of the qth surface. The region V_0 above S_1 is a vacuum; the region V_q between S_q and S_{q+1} (q = 1, 2, ..., Q-1) is filled with a dielectric whose refractive index n_q is real; and the region V_Q below S_Q is a metal with a complex index n_Q.

Let an incident plane wave be $\mathbf{E}^i(\mathbf{r}) = \mathbf{e}_0 \exp(i k_0 \cdot \mathbf{r})$ where $\mathbf{k}_0 = (\alpha, \beta, -\gamma) = (k \sin \theta \cos \phi, k \sin \theta \sin \phi, -k \cos \theta)$ with k being the free space wave-number. The $\mathbf{e}_0$ is a unit vector, which can be decomposed into the TE (the electric field is perpendicular to the plane of incidence) and TM (magnetic field perpendicular) component: $\mathbf{e}_0 = \mathbf{e}_0^{TE} \cos \delta + \mathbf{e}_0^{TM} \sin \delta$, where $\mathbf{e}_0^{TE} = \mathbf{k}_0 \times \mathbf{i}_Z / | \mathbf{k}_0 \times \mathbf{i}_Z |$ and $\mathbf{e}_0^{TM} = \mathbf{e}_0^{TE} \times \mathbf{k}_0 / | \mathbf{e}_0^{TE} \times \mathbf{k}_0 |$ are unit vectors in the TE and TM direction. Thus the incident field is characterized by the three angles θ, ϕ, and δ.

We denote the diffracted fields in each region by $\mathbf{E}_q^d(\mathbf{r})$ and $\mathbf{H}_q^d(\mathbf{r})$ ($q = 0, 1, ..., Q$). They satisfy (i) the Helmholtz equation in each region; (ii) the periodicity condition in the X- and Y-

direction; (iii) the radiation condition for $q = 0$ and Q; and (iv) the boundary condition that the tangential components of the total electric and magnetic field are continuous across S_q.

To find the diffracted field in each region in terms of a finite summation of vector modal functions, we first define the scalar modal functions, which are the separated solutions in each region satisfying the periodicity condition:

$$\varphi_{qmn}{}^\pm(\mathbf{r}) = \exp(\,i\mathbf{k}_{qmn}{}^\pm \cdot \mathbf{r}\,) \quad (q = 0, 1, \ldots, Q; m, n = 0, \pm1, \pm2, \ldots). \tag{1}$$

Here, $\mathbf{k}_{qmn}{}^\pm = (\alpha_m, \beta_n, \pm\gamma_{qmn})$ is defined by $\alpha_m = \alpha + 2m\pi/d$, $\beta_n = \beta + 2n\pi/d$, and $\gamma_{qmn}{}^2 = (n_q k)^2 - \alpha_m{}^2 - \beta_n{}^2$, $\mathrm{Re}(\gamma_{qmn}) \geq 0$, and $\mathrm{Im}(\gamma_{qmn}) \geq 0$. Note that the superscripts $+$ and $-$, respectively, mean an up- and down-going wave. Note also that we need only up-going waves in V_0 and down-going waves in V_Q because of the radiation condition.

Next we construct TE and TM vector modal functions by

$$\varphi_{qmn}{}^{TE\pm} = \mathbf{e}_{qmn}{}^{TE\pm}\,\varphi_{qmn}{}^\pm(\mathbf{r}), \quad \mathbf{e}_{qmn}{}^{TE\pm} = \mathbf{k}_{qmn}{}^\pm \times \mathbf{i}_Z\,/\,|\,\mathbf{k}_{qmn}{}^\pm \times \mathbf{i}_Z\,| \tag{2}$$

and

$$\varphi_{qmn}{}^{TM\pm} = \mathbf{e}_{qmn}{}^{TM\pm}\,\varphi_{qmn}{}^\pm(\mathbf{r}), \quad \mathbf{e}_{qmn}{}^{TM\pm} = \mathbf{e}_{qmn}{}^{TE\pm} \times \mathbf{k}_{qmn}{}^\pm\,/\,|\,\mathbf{e}_{qmn}{}^{TE\pm} \times \mathbf{k}_{qmn}{}^\pm\,|\,. \tag{3}$$

The TE and TM are defined with respect to the plane of propagation.

An approximation to $\mathbf{E}_q{}^d(\mathbf{r})$ is given by

$$\mathbf{E}_{qN}{}^d(\mathbf{r}) = \Sigma_{p=TE, TM}\,\Sigma_{d=+, -}\,\Sigma_{m,n=-N}{}^N\,A_{qmn}{}^{pd}(N)\,\varphi_{qmn}{}^{pd}(\mathbf{r}), \tag{4}$$

where $A_{qmn}{}^{pd}(N)$'s are unknown coefficients to be determined by the boundary condition. Note that: $d = +$ alone in V_0 and $d = -$ in V_Q because of the radiation condition.

The coefficients are determined so that the $\mathbf{E}_{qN}{}^d(\mathbf{r})$ and accompanying magnetic fields satisfy the boundary condition in the mean-squares sense. To do this, we first define the mean-square error on the boundary

$$I_N = \int |\,\mathbf{v} \times [\mathbf{E}_{0N}{}^d + \mathbf{E}^i - \mathbf{E}_{1N}{}^d]\,|^2\,dS + w^2\!\int |\,\mathbf{v} \times [\mathbf{H}_{0N}{}^d + \mathbf{H}^i - \mathbf{H}_{1N}{}^d]\,|^2\,dS$$
$$+ \Sigma_{q=2}{}^Q\,\{\;\int |\,\mathbf{v} \times [\mathbf{E}_{q-1, N}{}^d - \mathbf{E}_{qN}{}^d]\,|^2\,dS + w^2\!\int |\,\mathbf{v} \times [\mathbf{H}_{q-1, N}{}^d - \mathbf{H}_{qN}{}^d]\,|^2\,dS, \tag{5}$$

where the range of integration is a unit cell on each surface and w is a weight having an impedance dimension. Then, we locate $J{\times}J$ sampling points $(x_i,\ y_j,\ \zeta(x_i,\ y_j) + H_q)$ on the unit cell, where $x_i = id/J$ ($i = 1, 2, \ldots, J$) and $y_j = jd/J$. The number of divisions is given by $J = 2M = 2(2N + 1)$, i.e., twice as many as the number of modal truncation. Thus we have a discretized form of I_N:

$$I_N \cong I_{NJ} = \|\,\Phi\mathbf{A} - \mathbf{b}\,\|^2. \tag{6}$$

Here, $\mathbf{A}$ is a $4M^2Q$-dimensional column vector whose elements are the unknown modal coefficients; and $\mathbf{b}$ is a $24M^2Q$-dimensional column vector consisting of sampled values of $-\mathbf{v}{\times}\mathbf{E}^i$ and $-w\mathbf{v}{\times}\mathbf{H}^i$. The Jacobian matrix Φ has a band structure that

$$\Phi = \begin{bmatrix} \Phi_{00} & \Phi_{01} & \cdots & 0 \\ 0 & \Phi_{11} & \cdots & 0 \\ \vdots & \vdots & & \vdots \\ 0 & 0 & \cdots & \Phi_{Q-1,Q} \end{bmatrix}. \tag{7}$$

The elements of the $24M^2 \times 2M^2$ sub-matrix Φ_{00} are sampled values of $\mathbf{v} \times \varphi_{0mn}{}^{TE+}$, $\mathbf{v} \times \varphi_{0mn}{}^{TM+}$, and the accompanying magnetic fields. Other sub-matrices (Φ_{qq} and $\Phi_{q\,q+1}$) are defined similarly and the size of the sub-matrices are $24M^2 \times 4M^2$ excepting $\Phi_{Q-1\,Q}$ whose size is $24M^2 \times 2M^2$ as well as Φ_{00}. Hence, the size of the Jacobian is $24M^2Q \times 4M^2Q$.

QR DECOMPOSITION WITH SEQUENTIAL ACCUMULATION

The QR decomposition algorithm is known widely as an effective method for solving a least-squares problem: The Jacobian is decomposed into a product of a unitary matrix Q and an

upper triangular matrix R; and the solution is given by solving **RA = Q*b**. If the Jacobian is full rank, there is no essential difficulty in this procedure. Even if this is the case, increment of Q and/or M causes a serious problem of the lack of computer storage. For example, if we set $M = 11$ ($N = 5$: quite few) and $Q = 5$ (the number of coating layers is 4), then the matrix size is 13,420 × 2420, which is beyond the capacity of a desktop computer.

This difficulty can be removed by the use of the sequential accumulation. We first decompose Φ and **b** into Q segments as

$$\Phi = \begin{bmatrix} \Phi^{(1)} \\ \vdots \\ \Phi^{(Q)} \end{bmatrix}, \quad \mathbf{b} = \begin{bmatrix} b^{(1)} \\ \vdots \\ b^{(Q)} \end{bmatrix}. \tag{8}$$

Here, $\Phi^{(q)} = (0 \cdots 0 \; \Phi_{qq} \; \Phi_{q\,q+1} \; 0 \cdots 0)$ are $24M^2 \times 4M^2 Q$ (actually $24M^2 \times 4M^2$) matrices, and $b^{(q)}$ are corresponding parts of the driving vector **b**. Decomposing the first segment, we obtain

$$Q^{(1)*}\begin{bmatrix} \Phi^{(1)} & b^{(1)} \end{bmatrix} = \begin{bmatrix} R^{(1)} & g^{(1)} \\ 0 & e^{(1)} \end{bmatrix}. \tag{9}$$

Appending the segment $[\Phi^{(2)} \; b^{(2)}]$ to $[R^{(1)} \; g^{(1)}]$ and decomposing the result, we have

$$Q^{(2)*}\begin{bmatrix} R^{(1)} & g^{(1)} \\ \Phi^{(2)} & b^{(2)} \end{bmatrix} = \begin{bmatrix} R^{(2)} & g^{(2)} \\ 0 & e^{(2)} \end{bmatrix}. \tag{10}$$

Repeating the same procedure Q times, we finally obtain

$$Q^{(Q)*}\begin{bmatrix} R^{(Q-1)} & g^{(Q-1)} \\ \Phi^{(Q)} & b^{(Q)} \end{bmatrix} = \begin{bmatrix} R^{(Q)} & g^{(Q)} \\ 0 & e^{(Q)} \end{bmatrix}. \tag{11}$$

The solution is obtained by solving

$$R^{(Q)}\mathbf{A} = g^{(Q)} \tag{12}$$

and the mean-square error is given by $I_{NJ} = [\, e^{(Q)} \,]^2$.

NUMERICAL RESULTS

Here we show some numerical results that prove the effectiveness of the present algorithm. The diffraction of a plane wave by a coated silver grating is taken as an example. Because of the limitation in space, we confine ourselves to comparison of the methods of solution: the conventional QR decomposition (C-QRD) and the QR decomposition with the sequential accumulation (SA-QRD).

Setting $Q = 3$, we examined the size of required memory for $M = 7, 9$, and 11. In C-QRD they are 33 and 55 MB for $M = 7$ and 9; but the computation for $M = 11$ could not be executed on a desktop computer with a 64 MB memory. While in SA-QRD the memory size are 10, 29, and 45 MB. There is a complete agreement between the solutions obtained by the two methods while C-QRD works. Further, the memory demand in SA-QRD, in contrast to that of C-QRD, almost does not depend on Q. This means that we can handle the problem with many layers at the cost of CPU time increment alone.

The CPU time also is reduced by the use of sequential accumulation. For example, for $Q = 2$ and $M = 4$, C-QRD and SA-QRD, respectively, need 642 s and 474 s to obtain the solution.

REFERENCES

[1] Y. Okuno and H. Ikuno, The Yasuura method for solving boundary-value problems of the Helmholtz equation in homogeneous media, *Radiotekhnika i Elektronika*, **37**, 10, 1744-1763, 1992 (translated into Russian by Yu. Eremin).

[2] C.L. Lawson and R.J. Hanson, *Solving Least Squares Problems*, Prentice-Hall, Englewood Cliffs, 1974.

AN ANALYTICAL TECHNIQUE FOR MODELING OF WAVE PROPAGATION IN PERIODIC STRUCTURES

Svetlana Volkova and Valery Pilipchuk
Department of Mathematics
State Chemistry and Technology University
Gagarin Ave., 8, Dnepropetrovsk 49005, Ukraine
e-mail: s.volkova@mailexcite.com

ABSTRACT

Nonlinear systems under periodic pulsed excitation are considered. Solutions of the differential equations of motion are represented in a special form with contains a standard pair of non-smooth periodic functions and possesses a convenient structure.

INTRODUCTION

A problem of the stationary wave propagation in a periodic structure can be reduced to the analysis of differential equations with periodic coefficients. Periodic structures with localized singularities (inserts) are widely employed in various optical and electromagnetic systems. The localized singularities are customarily simulated by using one of two methods: by subjecting the variables to be determined to additional conditions in the neighborhoods of the points of localization of the inserts [1] or by introducing singular terms of the Dirac function type into the equations. The principal merit of the first approach is the fact that the differential equations describing the system are the same as when no singularities are present. However, there equations are treated separately in each of the spatial intervals between the inserts, and hence, instead of a single set, a whole sequence of sets are analyzed. The second method yields a single set of equations over the whole spatial domain without introducing the above-mentioned conditions imposed on the variables. However, to be correct, the analysis should be carried out within the framework of the theory of distributions [2] that requires additional mathematical proofs in non-linear cases. A method is presented in this paper that enables one, on the one hand, to eliminate the singular terms in the equations and, on the other hand, to obtain solutions by analyzing a boundary-value problem on a standard interval, in the form of a single analytic expression over the whole spatial interval [3-6]. The technique is based on a special representation for a periodic solution using a pair of (non-smooth) functions that have relatively simple forms associated with the translation and reflection subgroups in the group of Euclidean motions. These functions are termed the saw-tooth sine and right-angled cosine respectively. The mechanical model that generates these functions is the vibration-impact oscillator moving with constant velocity between two rigid barriers. The representation includes the two components and possesses an algebraic structure. This essentially simplifies all analytical transformations with equations.

NON-SMOOTH TRANSFORMATION OF TIME

Ours system modeling with localized temporal singularities will be based on the fact that any periodic function $x(t)$ with period T=4 can be represented in the form

$$x(t) = X(\tau) + Y(\tau)e, \quad \{t \rightarrow \tau\}, \tag{1}$$

where $\tau = \tau(t;\Theta)$ is the saw-tooth piecewise-smooth function of argument ζ,
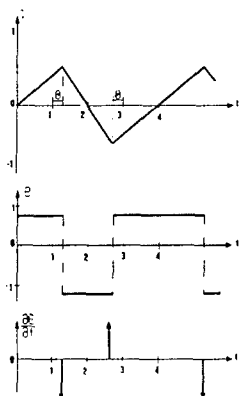
$$\tau(\zeta) = \begin{cases} \zeta, & -1 \le \zeta \le 1, \\ -\zeta + 2, & 1 \le \zeta \le 3, \end{cases}$$

$$\tau(\zeta) = \tau(\zeta + 4), \forall \zeta.$$

$$e = e(t;\Theta) = \frac{\partial \tau(t;\Theta)}{\partial t},$$

Θ *(-1< Θ <1)* is a parameter which characterizes the slope of the "saw" (Fig.1). If $\Theta \neq 0$, function $\tau(t;\Theta)$ is not symmetrical, pulses act two by two. If $\Theta = 0$, the function $\tau(t;\Theta)$ is symmetrical, and pulses act through the equal gap of time.

Fig.1.

FORMULATION OF THE PROBLEM

Many problems of nonlinear optoelectronics and electromagnetics are reduced to the following equation

$$\left(\frac{1}{c^2}\frac{\partial^2}{\partial t^2} - \frac{\partial^2}{\partial y^2}\right)\psi(y,t) + T\psi(y,t) + \beta\psi(y,t)^3 = 0, \tag{2}$$

where c is the velocity of wave. The function ψ depends on the spatial coordinates and time t. Suppose that

$$\psi(y,t) = x(t)\cos(\omega y + \varphi), \tag{3}$$

where ω is the frequency, φ is the initial phase.
Substitute expression (3) in (2). By using Galerkin's method we obtain a nonlinear differential equation of the second order (the Duffing equation) with periodic pulsed excitation:

$$\ddot{x} + \left[p + q\frac{\partial e(t;\Theta)}{\partial t}\right]\dot{x} + \varepsilon x^3 = 0, \tag{4}$$

where $\dot{x} \equiv \dfrac{dx}{dt}$, p and q are the parameters, ε is the parameter of nonlinearity.
The following problem will be studied:

◆ for $\Theta=0$, obtain an asymptotic solution,
◆ for $\Theta \neq 0$, obtain an exact solution in elliptical functions. In this case, the y- component is zero,
◆ for large values of the nonlinearity ε, solve the equation by numerical-analytical method.

ANALYTICAL STUDY

Non-vanishing solution of (4) is build in the way borrowed from [1]. Obtain differential equation system

$$(1-\Theta^2)X'' - 2\Theta Y'' + (1-\Theta^2)^2 pX = -\varepsilon(1-\Theta^2)^2 R_f$$

$$(1+3\Theta^2)Y'' - 2\Theta X'' + (1-\Theta^2)^2 pY = -\varepsilon(1-\Theta^2)^2 I_f \qquad (5)$$

with the boundary conditions

$$(X'+qX)\big/_{\tau=\pm I} = [2\Theta Y' + \Theta^2(X'+qX)]\big/_{\tau=\pm I}$$

$$Y\big/_{\tau=\pm I} = 0 \qquad (6)$$

The set (5)-(6) does not contain singular terms. This is its main advantage. Pulsed influence reveals itself in the boundary conditions with parameter q. Under q=0, pulsed excitation does not act to the system.

CONCLUSIONS

A standard pair of non-smooth periodic functions which join small sections of the solution (in the intervals between the pulses) into a single analytic expression over the whole time interval plays an important role in the proposed method.

REFERENCES

[1] Samoilenko A.M., Perestyk N.A. *Differential Equations with Pulsed Excitation*, Vihcha Shkola, Kiev, 1987.

[2] Vladimirov V.S. *Equations of Mathematical Physics*. Nauka, Moscow, 1967.

[3] Pilipchuk V.N. A transformation of vibrating systems based on a nonsmooth periodic pair of functions. *Doklady Akademii Nauk UkrSSR*, A(4), 1988, pp. 37-40.

[4] Pilipchuk V.N. Calculation of mechanical systems with pulsed excitation. *J. Appl. Maths Mechs*, Vol. 60, No. 2, pp. 217-226, 1996.

[5] Pilipchuk V.N., Vakakis A.F. and Azeez M.A.F. Study of a class of sub-harmonic motions using a nonsmooth temporal transformation (NSTT). *Physica D*, vol. 100, 1997, pp. 145 – 164.

[6] Pilipchuk V.N. and Vakakis A.F. Study of the oscillators on a nonlinearly supported string a nonsmooth transformation. *Journal of Vibration and Acoustics*. Vol.120, No. 2, 1998, pp.434-440.

PROBLEM OF PLANE ELECTROMAGNETIC WAVE DIFFRACTION BY MULTIELEMENT GRATING IMBEDDED IN A HALF-SPACE

Z. T. Nazarchuk, O. I. Ovsyanikov and T. D. Senyk

Karpenko Physico-Mechanical Institute, National Academy of Science of Ukraine
5 Naukova St., Lviv, 79601 Ukraine. E-mail: star@ipm.lviv.ua

ABSTRACT

The problem of the plane electromagnetic wave diffraction by a multielement grating which is imbedded in a half-space is considered. A system of singular integral equations is obtained by satisfying the necessary boundary conditions. The numerical results describing the resonance characteristics of the cascaded grating imbedded into a half-space are presented in the paper.

STATEMENT OF THE PROBLEM

Our goal was to investigate the diffraction of plane electromagnetic wave with an oblique angle of incidence by a multielement grating with arbitrary-shaped elements imbedded into a half-space. We considered the next problem: let each period d of the grating contain a boundary (contour L_0) which separate the media: the upper S_1 ($\chi_1 = \omega\sqrt{\varepsilon_1\mu_1}$) and lower S_2 ($\chi_2 = \omega\sqrt{\varepsilon_2\mu_2}$). The lower half-space contains N perfectly conducting screens with contours L_i (Fig.1). The source of primary electromagnetic field E^* (*TM*-polarized plane electromagnetic wave with $\exp(-i\omega t)$ time factor) is located in S_1.
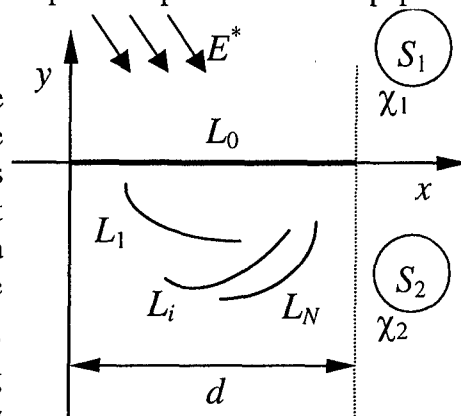
Fig.1. Geometry of the problem.

The sought for potential of the field E can be found from the next boundary problem: to solve the Helmholtz equation $\Delta E + \chi^2 E = 0$ which satisfies the following conditions:

– junction conditions on contour L_0 ($z = x + iy$):

$$E_1(z)\Big|_{L_0} = E_2(z)\Big|_{L_0} \; ; \; \frac{1}{\mu_1}\frac{\partial}{\partial n}E_1(z)\Big|_{L_0} = \frac{1}{\mu_2}\frac{\partial}{\partial n}E_2(z)\Big|_{L_0} \; , \; E_{1,2}(z) \stackrel{\text{def}}{=} E(z)\Big|_{z \in S_{1,2}} \; ; \qquad (1)$$

– boundary condition on contours L_i:

$$E_2(z)\Big|_{L_i} = 0 \, , \, i = \overline{1,N} \, ; \qquad (2)$$

– Sommerfeld's radiation conditions and Meixner's edge condition at the screen L_i ribs.

SYSTEM OF SINGULAR INTEGRAL EQUATIONS

The satisfying of the junction conditions (1) leads to the next integral equations:

$$\int_{L_0} \left(j_1^0(s)G_2(\vec{r}) - j_2^0(s)G_1(\vec{r}) \right)ds - \sum_{i=1}^{N}\int_{L_i} j_i(s)G_2(\vec{r})ds = -E^*(z), \; z \in L_0 . \qquad (3)$$

$$\frac{\pi}{\mu_2}j_2^0(z) + \frac{\pi}{\mu_1}j_1^0 - \int_{L_0}\left(\frac{j_2^0(s)}{\mu_2}\frac{\partial}{\partial n_0}G_2(\vec{r}) - \frac{j_1^0(s)}{\mu_1}\frac{\partial}{\partial n_0}G_1(\vec{r}) \right)ds -$$

$$-\frac{1}{\mu_2}\sum_{i=1}^{N}\int_{L_k} j_i(s)\frac{\partial}{\partial n_0}G_2(\vec{r})ds = -\frac{1}{\mu_1}\frac{\partial}{\partial n_0}E_0^*(z). \tag{4}$$

The satisfying of the boundary condition leads to the last integral equation of the desired ones:

$$\int_{L_0} j_2^0(s)G_2(\vec{r})ds + \sum_{i=1}^{N}\int_{L_i} j_i(s)G_2(\vec{r})ds = 0, \quad z\in L_i, \ i=\overline{1,N}. \tag{5}$$

Here $G^{1,2}(\vec{r})=G(\vec{r})\Big|_{\chi=\chi_{1,2}}$ is the Green's function which should be calculated by a special algorithm [1].

Thus, we obtained a system of $N+2$ integral equations for $N+2$ unknowns $j_{1,2}^0$, j_i, $i=\overline{1,N}$.

SYSTEM OF LINEAR ALGEBRAIC EQUATIONS

After normalization of the system (3)-(5) and by applying the specially constructed quadrature formulae [2] to its singular elements, the ordinary Gauss-type ones and to the non-singular elements, we obtained the system of linear algebraic equations:

$$\sum_{k=1}^{n}\Big\{q_0^1(\xi_k)[-B(\xi_k,\xi_l)-R_1(\xi_k,\xi_l)]+q_0^2(\xi_k)[B(\xi_k,\xi_l)+R_2(\xi_k,\xi_l)]+$$

$$+\sum_{i=1}^{N}q_i(\xi_k)K_2^i(\xi_k,\xi_l)\Big\} = -\frac{n}{\pi}E^*(\xi_l), \quad t_0(\xi_l)\in L_0, \ l=\overline{1,n}; \tag{6}$$

$$\sum_{k=1}^{n}\Big\{q_0^1(\xi_k)A_1(\xi_k,\xi_l)+q_0^2(\xi_k)A_2(\xi_k,\xi_l)+$$

$$+\frac{1}{\mu_2}\sum_{i=1}^{N}q_i(\xi_k)P_2^i(\xi_k,\xi_l)\Big\} = -\frac{n}{\pi}\frac{|t_0'(\xi_l)|}{\mu_1}\frac{\partial}{\partial n_0}E^*(\xi_l), \quad t_0(\xi_l)\in L_0, \ l=\overline{1,n}; \tag{7}$$

$$\sum_{k=1}^{n}\Big\{q_0^1(\xi_k)K_2(\xi_k,\xi_l)+q_i(\xi_k)[B(\xi_k,\xi_l)+R_2^i(\xi_k,\xi_l)]+$$

$$+\sum_{\substack{m=1\\m\neq i}}^{N}q_m(\xi_k)K_2^m(\xi_k,\xi_l)\Big\} = 0, \quad t_0(\xi_l)\in L_i, \ i=\overline{1,N}, \ l=\overline{1,n}. \tag{8}$$

Here:

$$R_{1,2}(\tau,\tau_0)=H_{1,2}(\tau,\tau_0)+\ln|\tau-\tau_0|+S_{1,2}(\tau,\tau_0), \quad \tau\neq\tau_0, \ t(\tau)\in L_0,$$

$$K_2(\tau,\tau_0)=H_2(\tau,\tau_0)+S_2(\tau,\tau_0), \quad t(\tau)\in L_0,$$

$$P_{1,2}(\tau,\tau_0)=H_{1,2}^{\partial}(\tau,\tau_0)+S_{1,2}^{\partial}(\tau,\tau_0), \quad \tau\neq\tau_0, \ t(\tau)\in L_0,$$

$$B(\xi_k,\xi_l)=\ln 2+2\sum_{m=1}^{n-1}\frac{1}{m}T_m(\xi_k)T_m(\xi_l),$$

$$A_{1,2}(\xi_k,\xi_l)=\frac{n}{\mu_{1,2}}\delta_{kl}-\frac{1}{\mu_{1,2}}P_{1,2}(\xi_k,\xi_l), \tag{9}$$

$$\xi_k=\cos\left(\frac{2k-1}{2n}\pi\right), k=\overline{1,n}, \ T_m(\tau)=\cos(m\arccos\tau).$$

The super-index i denotes $t(\tau) \in L_i$, $\vec{E}^{\,i}$. The expressions (9) in the case of geometric singularity ($\tau = \tau_0$ for the same contour) should be calculated by special formulae.

NUMERICAL RESULTS

The software in Visual FORTRAN 6.0 programming language has been developed and some numerical results for the far field approximation have been obtained for the cascaded grating imbedded into a half-space. The grating elements have been treated as parabolic arcs:

$$t_k(\tau) = a(\tau + i\varepsilon(1 - \tau^2)) + ih(k-1) - ih_0, \quad \tau = [-1;1], \varepsilon = b/a, k = 1,2; \qquad (10)$$

where h_0 is the imbedding depth; h is the distance between layers; ε is the arc curvature (Fig. 2). Fig.3 shows the "incident angle β – imbedding depth h_0" dependencies (β runs through $2°...88°$; h_0 runs through $0.05...1.00$) in 3-D and topographic forms for different screens curvatures.
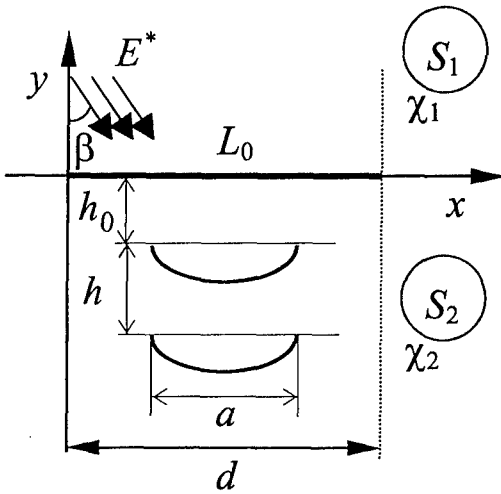
Fig. 2. The cascaded grating
imbedded into a half-space

$\varepsilon = 0.0$

$\varepsilon = 0.25$

$\varepsilon = 0.5$
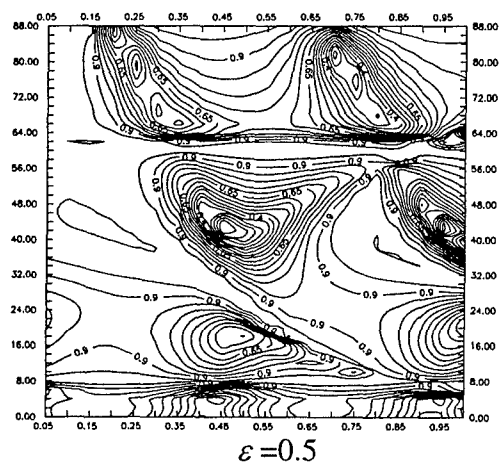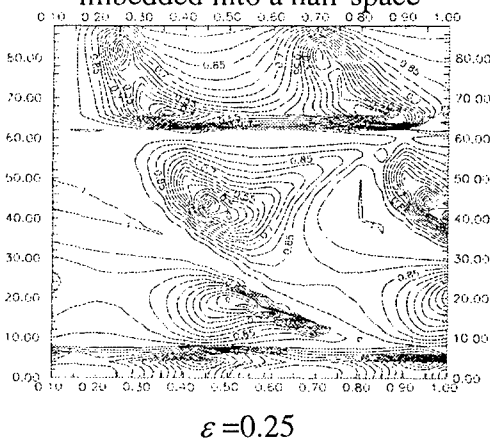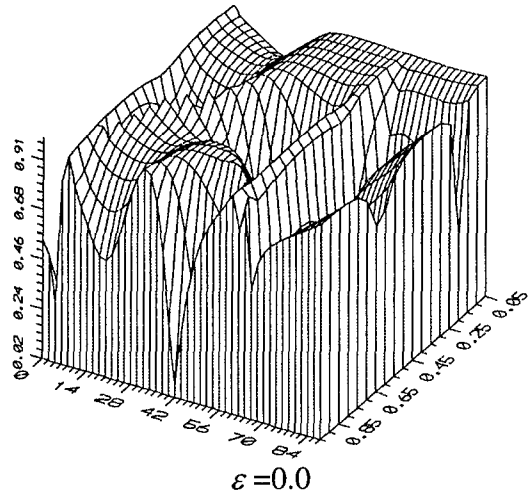
Fig. 3. The grating parameters: $\chi_1 = \pi$, $\chi_2 = 2\pi$, $a=0.5$, $h=1.0$, $d=1.0$.

REFERENCES

[1] Z.Nazarchuk, O.Ovsyannikov, T.Senyk Interpolation method for evaluation of periodic Green function in the problem of diffraction. Radiophysics and Radioastronomy. V.1, 1996, pp.32–36.
[2] V.V.Panasyuk, M.P.Savruk, Z.T.Nazarchuk Method of singular integral equations in the two-dimensional diffraction problems. Kiev: Naukova dumka, 1984. – 344 p. (In Russian).

ELECTROMAGNETIC WAVE SCATTERING BY A DOUBLY-PERIODIC MAGNETODIELECTRIC LAYER

Natalia V. Sidorchuk and Vladimir V. Yachin

Institute of Radio Astronomy, National Academy of Sciences of Ukraine
4, Krasnoznamennaya str., 61002, Kharkov, Ukraine
email: yachin@rian.kharkov.ua

ABSTRACT

The problem of electromagnetic wave scattering by a double-periodic magneto-dielectric layer is solved by the new method based on the rigorous integro-differential equations. The Galerkin method is applied to reduce these equations to a set of second-order differential ones with constant coefficients in functionals. The general moments of the solution are given. Scattering by some magnetodielectric structures including perfectly conducting ones are studied. Numerical results for transmission and reflection coefficients are presented.

INTRODUCTION

3-D models are best matched to the real scattering process. Basically, the 3-D scattering problems were investigated to study the properties of composite structures with double-periodic inserts made from perfect metal, for the problem of designing electromagnetic wave absorbers based on the double-periodic lossy structures and for the vector problems of scattering by so-called photonic crystal.

In this paper, a vector problem of the wave scattering by a double-periodic layer composed of magnetodielectric parallelepipeds is solved. This paper is conceptually analogous to paper [1] devoted to the scattering by single-periodic layers and it is an extension of paper [2], where double-periodic gratings were investigated with the use of the volume integral equations.
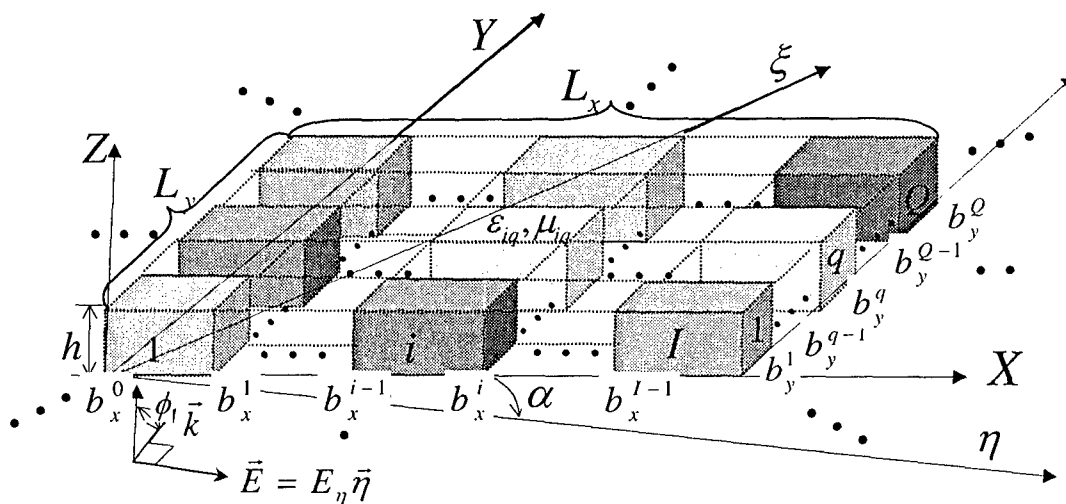
Figure 1 Geometry of the scattering problem

METHOD

Formulation of the problem is as follows: from the half-space z<0, a linearly-polarized plane electromagnetic wave is incident at an arbitrary angle φ on the double-periodic infinite layer (Fig.1). We suppose that the incident wave is TE-polarized and α is the angle between the x axis and the electric field vector $\vec{E}$ lying in the plane of the layer. The layer consists of rectangular parallelepipeds of arbitrary sizes along the x axis and the y axis, L_x and L_y are periodicities of the layer in the x and y direction, respectively. The parallelepipeds are characterized by the complex relative permittivity ε and permeability μ and have the thickness h. We consider the field components in the (η, ξ, z) coordinate system connected with the incident field polarization and rotated at the angle α about the (x, y, z) coordinate system. We have to obtain the transmitted and reflected fields in the immediate vicinity of the layer.

Integral equations [3] can be transformed to the equations for the field components in the scalar form:

$$E_\eta(r) = E_{0\eta}(r)e^{i(k_\xi\xi+k_z z)} + \frac{1}{4\pi}\left\{(k^2+\frac{\partial^2}{\partial\eta^2})\int_V[\varepsilon(r')-1]E_\eta(r')G(r,r')dr' + \right.$$

$$\left.+\frac{\partial^2}{\partial\eta\partial\xi}\int_V[\varepsilon(r')-1]E_\xi(r')G(r,r')dr'+\frac{\partial^2}{\partial\eta\partial z}\int_V[\varepsilon(r')-1]E_z(r')G(r,r')dr'\right\}+ \qquad (1)$$

$$+\frac{ik}{4\pi}\left\{\frac{\partial}{\partial\xi}\int_V[\mu(r')-1]H_z(r')G(r,r')dr'-\frac{\partial}{\partial z}\int_V[\mu(r')-1]H_\xi(r')G(r,r')dr'\right\},$$

Here the Green's function is presented in the integral form, V is the scatterer volume, i.e. the layer. For the other field components, $E_\xi, E_z, H_\eta, H_\xi, H_z$, equations can be written in a similar manner.

For each period segment numbered (k,l) we can write the notations $b_x^{k-1}<x_k'<b_x^k$, $b_y^{l-1}<y_l'<b_y^l$, $\varepsilon(r_{kl}')=\varepsilon_{kl}$, $\mu(r_{kl}')=\mu_{kl}$.

Following the algorithm given in [2] we present the field in each period segment as an expansion in terms of the spatial harmonics and act on the equation for these fields by the linear operator

$$\hat{A}_{pq}^{kl}F(x',y',z') = \frac{1}{L_xL_y}\int_{b_x^{k-1}}^{b_x^k}\int_{b_y^{l-1}}^{b_y^l}(\varepsilon-1)e^{-i(k_x+\frac{2\pi p}{L_x})x'}e^{-i(k_y+\frac{2\pi q}{L_y})y'}F(x',y',z')dx'dy'.$$

Thus, we can obtain the set of linear differential equations for the field functionals. By summing these equations over all segments we can express the fields and field functionals for individual segment through the ones for another segment, e.g.:

$$E_{\eta pq}^{kl} = \frac{\varepsilon_{k'l'}(\varepsilon_{kl}-1)}{\varepsilon_{kl}(\varepsilon_{k'l'}-1)}(ax_{p-r}^k ay_{q-s}^l)(ax_{p-r}^{k'} ay_{q-s}^{l'})^{-1}E_{\eta pq}^{k'l'},$$

where

$$ax_p^k = \frac{1}{L_x}\int_{b_x^{k-1}}^{b_x^k}e^{-ix\frac{2\pi p}{L_x}}dx, \quad ay_q^l = \frac{1}{L_y}\int_{b_y^{l-1}}^{b_y^l}e^{-ix\frac{2\pi q}{L_x}}dy,$$

Next we solve the equation set for the field functionals and thus for the field components (the procedure in paper[2]). Using the extinction theorem at the last stage we obtain coefficients C_j

and the expressions for the scattered fields. To take an example, for the transmitted E-components

$$E_\eta^t(\eta,\xi,z) = \frac{1}{4}\sum_m\sum_p \frac{e^{i(\psi_{mp}\eta + \theta_{mp}\xi + \chi_{mp}(z-h))}}{\chi_{mp}} \sum_j C_j e^{\lambda_j h}(\lambda_j + i\chi_{mp})\{(1-\psi_{mp}^2)W1_{mp} -$$

$$-\psi_{mp}\theta_{mp}W2_{mp} - \theta_{mp}W5_{mp} + \chi_{mp}W4_{mp} - \psi_{mp}\chi_{mp}W6_{mp}\},$$

where

$$\psi_{mp} = (k_x + \frac{2\pi m}{L_x})\cos\alpha + (k_y + \frac{2\pi p}{L_y})\sin\alpha, \; \theta_{mp} = -(k_x + \frac{2\pi m}{L_x})\sin\alpha + (k_y + \frac{2\pi p}{L_y})\cos\alpha,$$

$$\chi_{mp} = \sqrt{k^2 - \psi_{mp}^2 - \theta_{mp}^2},$$

a)   b)
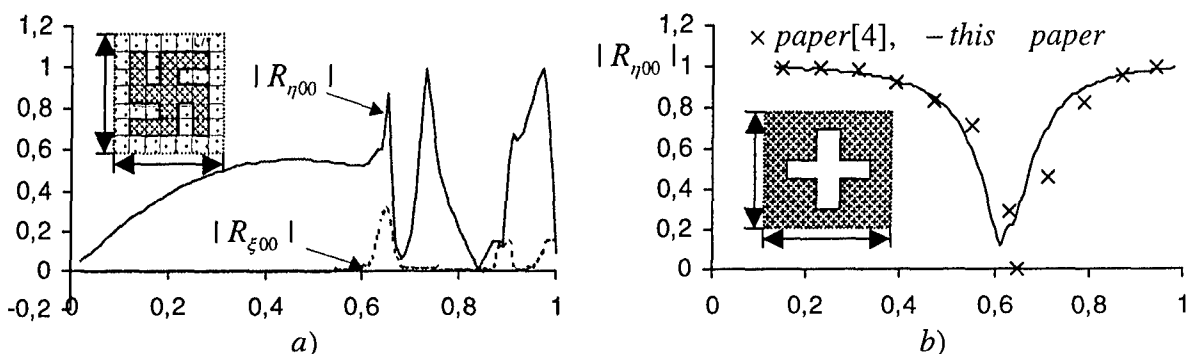
Figure 2. Reflection coefficient versus frequency parameter L/λ when a normally incident plane wave illuminates a structure with parameters: $\{ L_x = L_y = 1,\ \alpha = 0,\ \varphi = 0.001^o \}$; for

a)$\{ \mu = 1,\ \varepsilon_{swastic} = 10,\ \varepsilon_{slab} = 2,\ h = 0.3L \}$; for b) $\{ \varepsilon = 250 + 2500000i,\ \mu = 1/\varepsilon,$

$h = 0.001 \}$

λ are the eigen values and $W1,...,W6$ are the corresponding eigen vectors of the structure.

The considerations are illustrated by two graphics. In Fig. 2(b) the reflection coefficient of the magnetodielectric periodic layer closely approximating the perfectly conducting cross-perforated screen is shown, and the data are compared with results of paper [4]. In Fig. 2(a) the reflection coefficient of the structure composed of periodically disposed dielectric swastikas in a dielectric slab is shown as well.

REFERENCES

[1] N.A.Khizhnyak, N.V.Ryazantseva and V.V.Yachin, The scattering of electromagnetic waves by a periodic magnetodielectric layer, Journal of Electromagnetic Waves and Applications, vol.10, No.5, 1996 , pp. 731-739.

[2] V.V.Yachin and N.V.Ryazantseva, The scattering of electromagnetic waves by rectangular-cell double-periodic magnetodielectric gratings, Microwave and Optical Technology Letters, vol.23, No. 3, 1999, pp.177-183.

[3] N. A. Khizhnyak, Green's function of Maxwell's equations for inhomogenious media, Soviet Phys.-Technical Phys., Physics, vol. 28, No. 7, 1958, pp.1592-1609. (original Russian pagination).

[4] B. J. Rubin and H. L. Bertony, Reflection from a periodically plane using a subsectional current approximation, vol. AP-31, No.6, 1983, pp.829-836.

SCATTERING OF ELECTROMAGNETIC WAVES BY DIELECTRIC GRATINGS WITH ELLIPTICALLY LAYERED MEDIA

Tsuneki YAMASAKI, Takashi HINATA, and Toshio HOSONO

Department of Electrical Engineering, College of Science and Technology, Nihon University
Tel.: +81-3-3259-0771, Fax.:+81-3-3259-0783, E-mail: yamasaki@ele.cst.nihon-u.ac.jp

1. Introduction

Dielectric gratings have found applications in various areas such as integrated optics[1] and acousto-optics, optical filters, and holography. Recently, the refractive index can easily be controlled to make the periodic structures such as fiber grating and photonic crystal waveguide by the development of manufacturing technology of optical devices. Thus, the scattering and guiding problems of the inhomogeneous gratings have been considerable interest, and many analytical and numerical methods which are applicable to the dielectric gratings having an arbitrarily periodic structures have been proposed.

In this paper, the scattering of electromagnetic waves by dielectric gratings with elliptically layered media are analyzed using the combination of improved Fourier series expansion method[2] and the multilayer method[3].

Numerical results are given for the transmitted scattered characteristics for the case of incident angle and frequency by dielectric gratings whose shape of grating is an elliptic cylinder, and whose interior distribution of permittivity is an elliptically layered medium for both TM and TE waves. The influences of the incident angle and frequency of the transmitted power are compared between circular cylinder and elliptic cylinder.

2. Method of Analysis

We consider the dielectric grating with elliptically layered media as shown in Fig.1(a). The grating is uniform in the y-direction and the permittivity $\varepsilon(x,z)$ is an arbitrary periodic function of z with period p. Fig.1(a) shows the configuration whose shape of the grating is an elliptic cylinder with the cross section of $a \times d/2$, and whose interior distribution of permittivity $\varepsilon(x,z)$ is elliptically layered medium. The permeability is assumed to be μ_0. The time dependence is $\exp(-i\omega t)$ and suppressed throughout. In the formulation, the TM (the magnetic field has only the y-component) case is discussed. For the TE (the electric field has only the y-component) case, only numerical results are presented. When the plane wave is assumed to be incident from $x > 0$ at the angle θ_0, the magnetic fields in the regions $S_1 (x \geq 0)$ and $S_3 (x \leq -d)$ are expressed[2] as

$$S_1(x \geq 0) \; : \quad H_y^{(1)} = e^{ik_1(z\sin\theta_0 - x\cos\theta_0)} + e^{ik_1 z \sin\theta_0} \sum_{n=-N}^{N} r_n^{(1)} e^{i(k_n^{(1)} x + 2\pi nz/p)} , \tag{1}$$

$$S_2(-d < x < 0) \; : \quad H_y^{(l,2)} = \sum_{\nu=1}^{2N+1} \left[A_\nu^{(l)} e^{ik_\nu^{(l)}\{x+(l-1)d_\Delta\}} + B_\nu^{(l)} e^{ik_\nu^{(l)}(x+ld_\Delta)} \right] e^{ik_1 z \sin\theta_0} \sum_{n=-N}^{N} u_{\nu,n}^{(l)} e^{i2\pi nz/p} \tag{2}$$
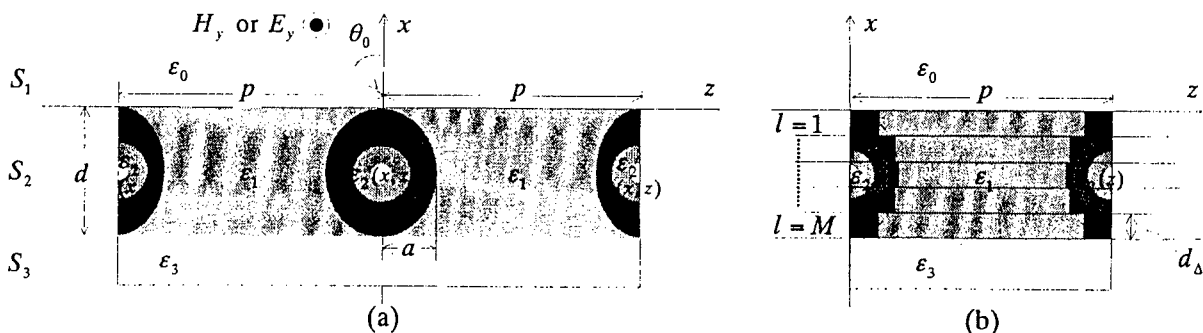
Fig.1 Structure of the dielectric grating with elliptically layered media. (a) Coordinate system, (b) Approximated inhomogeneous layers.

$$\underline{S_3(x \leq -d)} \quad : \quad H_y^{(3)} = e^{ik_1 z \sin\theta_0} \sum_{n=-N}^{N} t_n^{(3)} e^{-i\left\{ k_n^{(3)}(x+d) - 2\pi nz/p \right\}} \ , \tag{3}$$

$$k_n^{(j)} \triangleq \sqrt{k_0^2 \varepsilon_j / \varepsilon_0 - \left(k_1 \sin\theta_0 + 2\pi n/p\right)^2} \ ; \ k_1 \triangleq \omega \sqrt{\varepsilon_1 \mu_0} \ , \ k_0 \triangleq 2\pi/\lambda \ , \ d_\Delta = d/M \ , \ l = 1 \sim M$$

where λ is the wavelength in free space, $h^{(l)}$ is the propagation constant in the x-direction and $r_n^{(1)}$, $A_v^{(l)}$, $B_v^{(l)}$ and $t_n^{(3)}$ are unknown coefficients to be determined from boundary conditions. $h^{(l)}$ must satisfy the following eigenvalue equation[2]

$$\Lambda_1 \mathbf{U}^{(l)} = \left\{ h^{(l)} \right\}^2 \Lambda_2 \mathbf{U}^{(l)} \ ; \ \Lambda_1 \triangleq \left[\eta_{m,n}^{(l)} \right], \ \Lambda_2 \triangleq \left[\zeta_{m,n}^{(l)} \right], \ l = 1 \sim M \ , \tag{4}$$

where

$$\mathbf{U}^{(l)} \triangleq \left[u_{-N}^{(l)}, \cdots, u_0^{(l)}, \cdots u_N^{(l)} \right]^T , \ T \ : \ \text{transpose}, \ \varepsilon^{(l)}(z) \triangleq f^{(l)}(z)/g^{(l)}(z) \ ,$$

$$\zeta_{n,m}^{(l)} \triangleq k_0^2 \xi_{n,m}^{(l)} - \gamma_n^{(l)} \left\{ \gamma_n^{(l)} \eta_{n,m}^{(l)} + 2\pi (n-m) \eta_{n,m}^{(l)} / p - \varphi_{n,m}^{(l)} \right\},$$

$$\eta_{n,m}^{(l)} \triangleq \frac{1}{p} \int_0^P \left\{ f^{(l)}(z) g^{(l)}(z) \right\} e^{i2\pi(n-m)z/p} dz \ , \ \varphi_{n,m}^{(l)} \triangleq \frac{2i}{p} \int_0^P \left\{ f^{(l)}(z) \frac{d\left\{ g^{(l)}(z) \right\}}{dz} \right\} e^{i2\pi(n-m)z/p} dz \ ,$$

$$\xi_{n,m}^{(l)} \triangleq \frac{1}{p} \int_0^P \left\{ f^{(l)}(z) \right\}^2 e^{i2\pi(n-m)z/p} dz \ , \ \gamma_n^{(l)} \triangleq \left(k_1 \sin\theta_0 + 2\pi n/p\right), \ m,n = \left(-N, \cdots, 0, \cdots N\right).$$

In inhomogeneous grating region S_2 $(-d < x < 0)$, the elliptic cylinder is divided into thin layers $d_\Delta (= d/M)$, as shown in Fig.1(b). The dielectric distribution of thin layer is approximated to step index profile $\varepsilon^{(l)}(z)[\triangleq \varepsilon((l+0.5)d_\Delta, z); l = 1 \sim M]$. Therefore, $f^{(l)}(z)$ or $g^{(l)}(z)$ contain discontinuity such as the step function, $(n-m)\eta_{n,m}^{(l)}$ does not converge, because $\eta_{n,m}^{(l)}$ is $O(1/|n-m|; n \neq m)$ as $|n-m| \to \infty$ [$|\eta_{n,m}^{(l)}|$ is less than $K/|n-m|$, where K is independent of $|n-m|$], so that the solution of the Eq.(4) also does not converge to the correct value. To solve this difficulty, the function containing the discontinuity is approximated by a Fourier series of N_f terms[4]. We have experienced that $N = 1.5N_f$ is sufficient when N_f is related to the modal truncation number N[4].

From the boundary conditions at $x = 0$, $x = -l \cdot d_\Delta$ $(l = 1 \sim M - 1)$, and $x = -d$, we get the following homogeneous matrix equation in regard to $A^{(M)}$ by matrix algebra[5].

$$\mathbf{W} \cdot \mathbf{A}^{(M)} = \mathbf{F}, \quad \mathbf{W} \triangleq \left[\mathbf{Q}_1 \mathbf{S}_1 + \mathbf{Q}_2 \mathbf{S}_3 - \left(\mathbf{Q}_1 \mathbf{S}_2 + \mathbf{Q}_2 \mathbf{S}_4 \right) \mathbf{Q}_4^{-1} \mathbf{Q}_3 \right], \tag{5}$$

where the elements of matrix $\mathbf{W}$ and $\mathbf{F}$ are obtained by reference[5]
The mode power transmission coefficients $|T_n^{(TM)}|^2$ is given by

$$|T_n^{(TM)}|^2 \triangleq \varepsilon_1 \operatorname{Re}\left\{ k_n^{(3)} \right\} |t_n^{(3)}|^2 / \left(\varepsilon_3 k_0^{(1)} \right), \tag{6}$$

where superscript (TM) indicates TM wave case.

3. Numerical Analysis

We consider the following structure of grating:
(1) Grating shape ; elliptic cylinder

$$[(x+d/2)/(d/2)]^2 + (z/a)^2 = 1 \tag{7}$$

(2) Distribution of permittivity $\varepsilon(x,z)$; elliptically layered media

$$\varepsilon(x,z) \triangleq \begin{cases} \varepsilon_2[1 - b\{(2(x+d/2)/d)^2 + (z/a)^2\}] \ ; b = 1 - \varepsilon_1/\varepsilon_2 \ : \text{inside of elliptic cylinder} \\ \varepsilon_1 \qquad : \text{outside of elliptic cylinder} \end{cases} \tag{8}$$

For the above case, we put $g^{(l)}(z) = 1$ and $f^{(l)}(z) = \varepsilon(x,z)$, and the values of parameters chosen are $\varepsilon_1 = \varepsilon_3 = \varepsilon_0$, $\varepsilon_2/\varepsilon_0 = 3$ and $d/p = 2/3$. For the TM wave, the results to check the validity of our method are computed with $N = 9$ $(N_f = 6)$ and $M = 30$. For the TE wave, the results are computed with $N = 10$ and $M = 20$. In this case, the relative error are less than about 0.1% and the energy error is less than about 10^{-3} for both TM and TE waves.

Figures 2(a) and 2(b) show $|T_0^{(TM)}|^2$ and $|T_0^{(TE)}|^2$ for various values of incident angle θ_0 at $2a/d = 0.8, 1.0$ and 1.2 for $p/\lambda = 1.0$. The case of circular cylinder is $2a/d = 1.0$. From in Figs.2(a), the effect of grating shape is seen clearly at the minimum of coupling resonance $|T_n^{(TM)}|^2 \cong 0$, and it

moves toward larger θ_0 as $2a/d$ increases. On the other hand, for TE case, $|T_0^{(TE)}|^2$ has a symmetric shape around $\theta_0 = 30°$. Therefore, we note that the θ_0 dependence at coupling resonance is more significant for the TE case than for the TM case. It is interest the peak of $|T_0^{(TE)}|^2$ at $2a/d = 1.0$ moves toward at $\theta_0 \cong 90°$.

Figures 3(a) and 3(b) show $|T_0^{(TM)}|^2$ and $|T_0^{(TE)}|^2$ for various values of normalized frequency (p/λ) at $\theta_0 = 30°$ with the same parameters as in Fig.2. Comparing the TM case with the TE case, we note that the characteristic tendencies for the effect of grating shape are approximately same at $p/\lambda < 0.7$, but for about $p/\lambda > 0.7$, the effect of the grating shape is more significant for TE case.

4. Conclusions

In this paper, we have analyzed the scattering of electromagnetic waves by dielectric gratings with elliptically layered media using improved Fourier series expansion method and multilayer method. Numerical results are given for the transmitted scattered characteristics for the case of incident angle and frequency for both TM and TE cases. The influences of the incident angle, and the frequency on the transmitted power for grating shape are discussed. Finally, the authors would like to thank Mr. Ryuji Terada at graduate student of Nihon University for help with drawing graphics in this work.
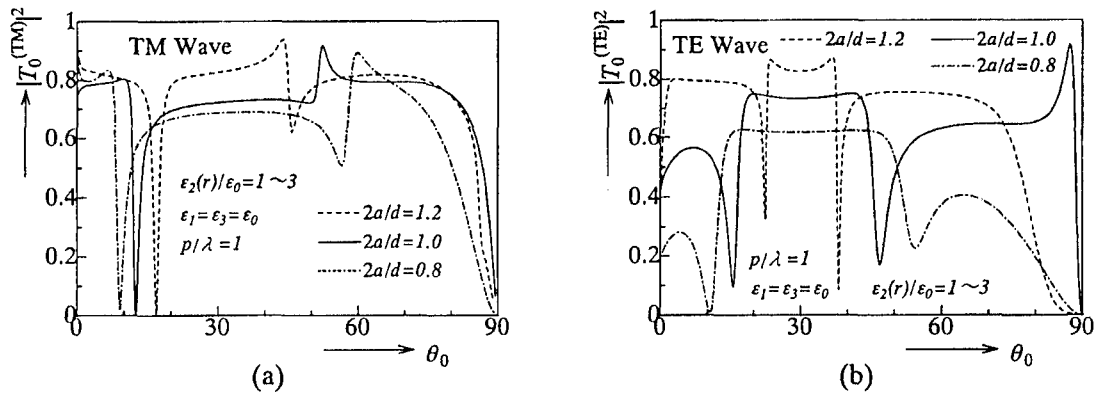
Fig.2 $|T_0^{(TM)}|^2$ and $|T_0^{(TE)}|^2$ versus θ_0. (a) TM wave, (b) TE wave.
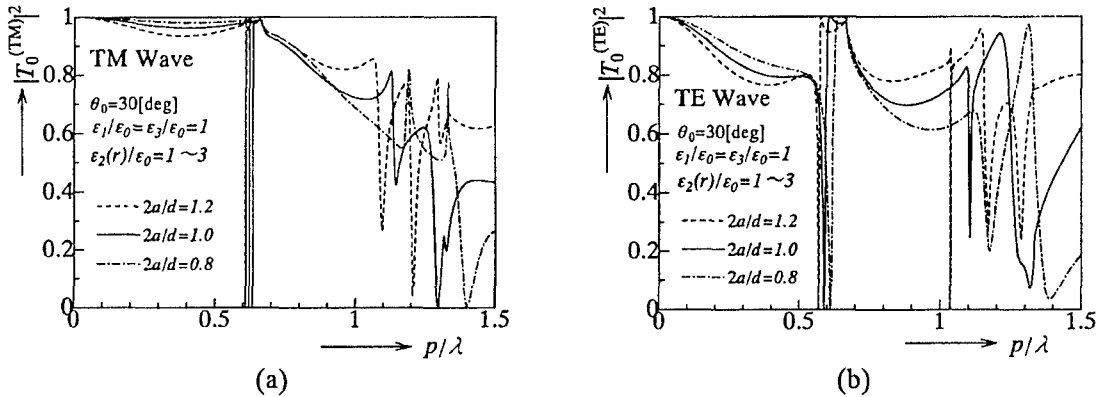
Fig.3 $|T_0^{(TM)}|^2$ and $|T_0^{(TE)}|^2$ versus p/λ. (a) TM wave, (b) TE wave.

References

[1] *Tamir, T., ed.,* Integrated Optics. Springer-Verlag, - p.110-118, 1979.

[2] *Yamasaki, T., Tanaka, T., Hinata, T. and Hosono, T.,* Analysis of Electromagnetic Fields Inhomogeneous Dielectric Gratings with Periodic Surface Relief, Radio Science, Vol.31, No.6, pp.1931-1939, 1996.

[3] *Yamasaki, T., Hosono, T. and Kong, J. A.,* Propagation characteristics of dielectric waveguides with periodic surface-relief, IEICE Trans., in Japan., Vol.E74, No.9. p.2839-2847, 1991.

[4] *Yamasaki, T., Hinata, T. and Hosono, T.,* Electromagnetic field analysis of planar gratings with periodic distribution of dielectric constant, IECE Trans. in Japan., Vol.J69-B, No.1. p.125-132, 1985 (in Japanese). [translated Scripta Technica, INC., Vol.69, April. p.75-84, 1986.]

[5] *Yamasaki, T., Hinata T., and Hosono T.,* Scattering of Electromagnetic Waves by Columnar Dielectric Grating with Inhomogeneous Media, Tech. Rep. Electromagnetic Theory, I.E.E., Japan, Vol. EMT-99-114. p.45-50, 1999 (in Japanese).

RESONANCE EFFECTS FOR THE DIFFRACTION BY HIGH REFLECTING GRATINGS IN THE DOUBLE RESONANCES CASE

N. A. Balakhonova, A. V. Kats, I. S. Spevak

Kharkiv Military University, P.O. Box 8847,
61002 Kharkiv, Ukraine, e-mail avkats@akfirst.kharkiv.com
Natasha.Balakhonova@ukrpost.net

The light diffraction by high reflecting grating is under is considered under the double resonance conditions. This means that two diffracted spectra are grazing waves, i.e., condition $\left|\vec{k}_t + m\vec{g}\right| \approx k$ is fulfilled for two integers $m = r, r'$ simultaneously. Here $\vec{g}$ is the grating wavevector, $d = 2\pi/g$ is its period, $\vec{k}_t$ presents tangential component of the incident wave wavevector. In the simplest geometry case (the plane of incidence is perpendicular to the grating groove) double resonances arise near the 'magic' angles of incidence, $\theta_{mag} = \arcsin\left(\left|r + r'\right|/\left|r\right| + \left|r'\right|\right)$, integers r and r' are of opposite sign. The structure of the double resonance strongly depends on the 'resonance' Fourier amplitudes, ζ_r, $\zeta_{r'}$ of the grating, and on the 'inter-resonance' harmonics, $\zeta_{\pm(r-r')}$. The latter causes interaction between resonance waves via the first order scattering process [1–3].

GENERAL SETUP

Let a plane monochromatic p-polarized electromagnetic wave

$$\vec{H}^i(\vec{r},t) = \vec{e}_y H \exp\left[i(\vec{k}\vec{r} - \omega t)\right] \tag{1}$$

is incident on the surface $z = \zeta(x) = \sum \zeta_m \exp(imgx)$. Here $\vec{k} = (k_x, 0, k_z)$ is the wave vector of the incident wave, H presents the amplitude of the magnetic field. The total field $\vec{H}$ above the surface (in the framework of Rayleigh hypothesis) may be presented as a sum of the incident wave (1) and scattered outgoing ones:

$$\vec{H}' = \vec{e}_y \sum_{m=-\infty}^{\infty} H_m \exp\left[i(k_{mx}x + k_{mz}z - \omega t)\right], \tag{2}$$

where $k_{mx} = k_x + mg$, $k_{mz} = -\sqrt{k^2 - k_{mx}^2}$, $k = \dfrac{\omega}{c}$, $\mathrm{Re}(k_{mz})$, $\mathrm{Im}(k_{mz}) \le 0$, $k_x = k\sin\theta$, θ is the angle of incidence. Assuming the surface impedance $\xi = \xi' + i\xi''$, ($\xi' > 0$, $\xi'' < 0$) to be small, $|\xi| \ll 1$, and making use of the impedance boundary conditions at the surface $z = \zeta$, one arrives to the infinite set of linear equations for the amplitudes H_m. One can present the solution of these equations in explicit form as the ratios of power series in the grating Fourier amplitudes ζ_m, cf. [1–3]. For instance, in the main approximation the normalized amplitudes $h_n = H_n/H$ of the resonance and specular reflected waves are

$$h_r = \left(V_r M_{r'r'} - V_{r'} M_{rr'}\right)/D, \qquad h_0 = R_0 + i\sum_r r v_{\bar{r}} h_r, \tag{3}$$

$R_0 = \left(\beta_0 - \xi\right)/\left(\beta_0 + \xi\right)$ presents Fresnel reflection coefficient, and

$$D = M_{rr} M_{r'r'} - M_{rr'} M_{r'r}, \qquad V_r = 2ir\beta_0 v_r/b_0 + O\left(v^2\right) + O(\xi v),$$

$$M_{rr'} = b_r \delta_{r,r'} + \mathrm{sgn}(r)\left(r - r'\right)v_{r-r'} + \sum_N (N - r)(N - r')v_{r-N} v_{N-r'}/b_N + O\left(v^3\right) + O\left(\xi v^2\right).$$
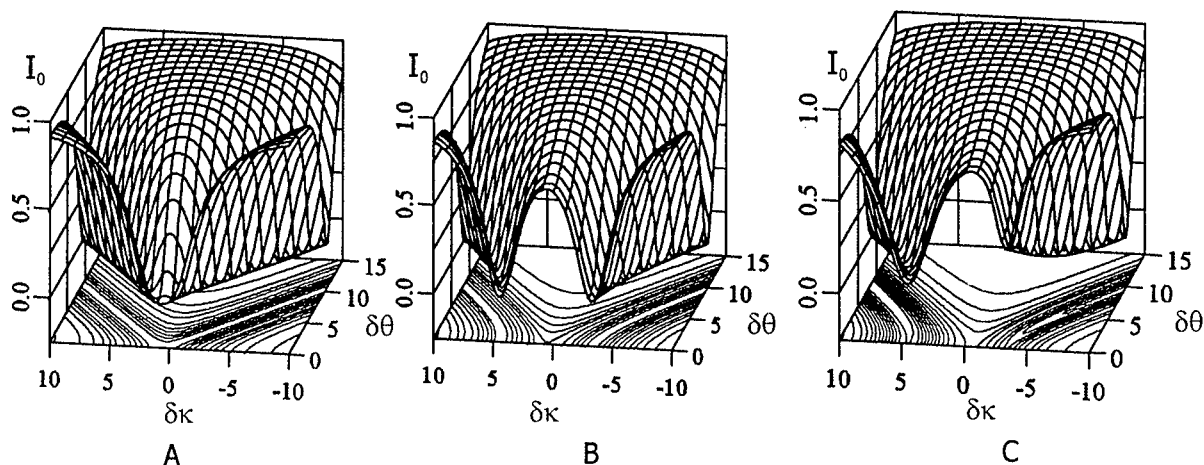
Fig. 2. Plots I_0 against $\delta\kappa$ and $\delta\theta$ for the gratings with $w_1 = 1$ and $w_2 = 0.5$, $\gamma = \pi/2$ (A); $w_2 = 2$, $\gamma = \pi/2$ (B); $w_2 = 2$, $\gamma = \pi/4$ (C).

Here $\beta_n = -k_{nz}/k$, $b_n = \beta_n + \xi$, $\nu_n = g\zeta_n$, $\overline{n} = -n$, index N corresponds to nonresonance spectra.

CLOSE TO NORMAL INCIDENCE

The explicit form of the solution (3) allows carrying out complete examination of the double resonance diffraction. Moreover, in the close vicinity of the resonance extrema it may be done analytically. Let us present here, for instance, the case of double resonance for close to normal incidence. Let the normalized wavenumber of the grating $\kappa = g/k$ be close to the value

$K = \sqrt{1 + (\xi'')^2}$, $\kappa = K + \Delta\kappa$, $\Delta\kappa \ll 1$ (the values $\kappa = K$, $\theta = 0$ correspond to the position of the resonance extrema for infinitesimal grating height). Expanding normalized z-components of the resonance spectra wavenumbers, $\beta_{\pm 1}$, in θ and $\Delta\kappa$ with first order terms accuracy (in other terms of (3) it is sufficient to put $\theta = 0$, $\Delta\kappa = 0$), one obtains simplified expressions, cf. [3-4]. For instance, for the specular reflected wave we have

$$h_0 = \frac{1 - 2w_1^2 - \left(\delta\kappa - w_1^2/\sqrt{3}\right)^2 + \delta\theta^2 + 4w_2^2 + 2i\left(\delta\kappa - w_1^2/\sqrt{3}\right)\left(1 - w_1^2\right) - 4iw_1^2 w_2 \cos\gamma}{1 + 2w_1^2 - \left(\delta\kappa - w_1^2/\sqrt{3}\right)^2 + \delta\theta^2 + 4w_2^2 + 2i\left(\delta\kappa - w_1^2/\sqrt{3}\right)\left(1 + w_1^2\right) + 4iw_1^2 w_2 \cos\gamma}. \quad (4)$$

For simplicity, we presented the result for biharmonic grating (the role of high order grating Fourier amplitudes consists in the shift and broadening of the resonance, but these amplitudes do not influence essentially the double resonance structure). Here the grating amplitudes
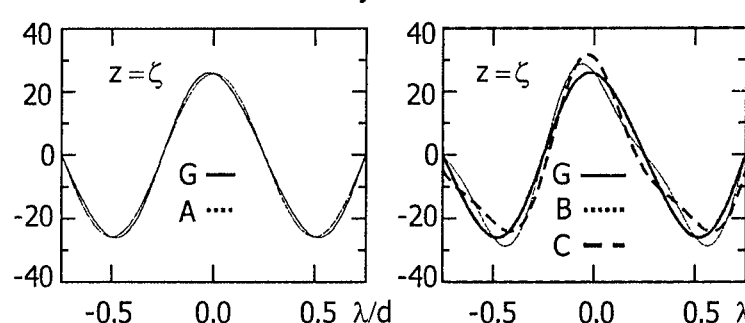
Fig. 1. The difference between the pure harmonic grating with $w_1 = 1$, (G), and the gratings (A), (B), (C) of Fig. 1 for the Au ($\lambda = 632.8$ nm, $\varepsilon = -10 + 1.5i$).

$\nu_{\pm 1} = \sqrt{\xi'} w_1 e^{\pm i\psi_1}$,

$\nu_{\pm 2} = \xi' w_2 e^{\pm i\psi_2}$, and

$\delta\theta = \theta B$, $\delta\kappa = \Delta\kappa B$,

$B = K/(|\xi''|\xi')$, $\gamma = 2\psi_1 - \psi_2$.

Note that h_0 depends on the renormalized grating amplitudes w_1 and w_2, and renormalized variables $\delta\theta$ and $\delta\kappa$ and in these terms presents universal result that does not depend on the impedance of the boundary. The latter determines only the scaling factor

$B \gg 1$. Note also that the scaling factor for the second harmonic (ξ') is much smaller than for the first harmonic ($\sqrt{\xi'}$). This means that the second harmonic affects the resonance essentially if its magnitude is small in comparison with the first harmonic amplitude, $|v_2| \ll |v_1|$. This limiting case is of special interest.

Examination of the representation (4) enables one to find all features of the double resonance diffraction analytically; in particular, one can define parameters of the grating corresponding to the total suppression of specular reflection (TSSR), Ref. [5]. For the harmonic grating ($w_2 = 0$) with small amplitude, $w_1 \leq 1/\sqrt{2}$, the intensity $I_0 = |h_0|^2$ possesses minimal value at the point $\delta\theta = 0$, $\delta\kappa = w_1^2/\sqrt{3}$. With w_1 increasing, the minimal value decreases and tends to zero if $w_1 = 1/\sqrt{2}$. For $w_1 > 1/\sqrt{2}$, $w_1 \neq 1$ this point becomes a saddle one, zero value of I_0 corresponds to the point $\delta\theta = \sqrt{2w_1^2 - 1}$, $\delta\kappa = w_1^2/\sqrt{3}$. The special case presents $w_1 = 1$. TSSR for this grating exists for one-parametric set of parameters, namely, at hyperbolas $\delta\kappa = 1/\sqrt{3} \pm \sqrt{\delta\theta^2 - 1}$. Note that the surface $I_0(\delta\theta, \delta\kappa)$ is symmetrical relative to the plane $\delta\kappa = w_1^2/\sqrt{3}$. This property takes place also for non-harmonic grating ($w_2 \neq 0$) if $\cos\gamma = 0$.

In the case $w_1 = 1$, $\cos\gamma = 0$, and $w_2 \neq 0$, TSSR exists at the modified hyperbolas $\delta\kappa = \pm\sqrt{4w_2^2 - 1 + \delta\theta^2} + 1/\sqrt{3}$, cf. Fig. 1, (B). For the special magnitude of the second harmonic, $w_2 = 0.5$, the hyperbolas transform to two intersecting straight lines. The point of the intersection, $\delta\theta = 0$, $\delta\kappa = 1/\sqrt{3}$, corresponds to the extremely wide I_0 minimum, Fig. 1, (A). For the phase shift, $\gamma \neq \pm\pi/2$ the exact TSSR is impossible, but there exists regions corresponding to rather small I_0 values, cf. Fig. 1, (C).

CONCLUSION

The results presented show high efficiency of the modified perturbation method [1-4] in the analysis of the resonance diffraction. In spite of simplicity, they are in a very good correspondence with existing experimental data [6]. Moreover, the simplicity enables one to find the cases of special interest both for further experimental investigations and for solving the problem of high-accuracy measurements of gratings and media parameters, and for designing the unique optical devices.

REFERENCES

[1] Kats A.V., Pavitskii P. D., Spevak I.S., Izv Vuzov Radiofizika. 1992. V. 35, № 3-4. pp. 234 - 245. (in Russian).
[2] Kats A.V., Pavitskii P. D., Spevak I.S. // Zh. Eksperimentalnaya i Teoeticheskaya Fizika, 1994. V. 105, № 1. pp. 79 - 93. (in Russian).
[3] Kats A.V., Spevak I.S. Diffraction of the electromagnetic waves. Kharkiv: KMU, 1998. 178 p. (in Ukrainian).
[4] Balakhonova N.A., Kats A.A., Kats A.V., Spevak I.S., Radiotechnika, 1999. N. 110, P. 170-175 (in Russian).
[5] Hutley M.C., Maystre D., Opt. Commun. 1976. V. 19. N 3. P. 431-436.
[6] Nash D.J., Cotter N.P.K. et al., J. Mod. Optics. 1995. V. 42, N. 1, P. 243-248.

THE DIFFRACTION OF THE NORMALLY INCIDENT PLANE WAVE BY A GRATING OVER A CHIRAL MEDIUM

Sergey B. Panin and Anatoly Y. Poyedinchuk

Institute of Radiophysics and Electronics, National Academy of Sciences of Ukraine
12 Academika Proskury Str., Kharkov, 61085, Ukraine. Tel.: +38(0572)-448319; 448556
FAX: +38(0572)-441105, E-mail: panin; chuk@ire.kharkov.ua

A rigorous solution was sought at normal incidence of a plane electromagnetic wave on a planar strip grating placed over a chiral medium. The approach consists in drawing up the coupled systems of dual series functional equations for the Fourier coefficients describing the field in the chiral medium and in the following application of the analytical regularization procedure based on the Riemann-Hilbert boundary-value problem method.

The present development of UHF-techniques is characterized by the widespread application of the composite materials, thereat the perspectives of the chiral media use is particularly interested [1].

1. Let the XOY plane separate chiral (z<0) and nonchiral (z>0) media. A simply periodic grating composed by infinitely thin and perfectly conducting strips extending infinitely along the OX axis lies in a plane z=h>0. The strip separation is d, the grating period is l.

A plane electromagnetic wave $\mathbf{E}^i = \mathbf{E}_0 \exp(-ikz)$, $\mathbf{H}^i = \mathbf{H}_0 \exp(-ikz)$ (let $\mathbf{E}_o = (\tilde{e}, 0, 0)$; $\mathbf{H}_o = (\tilde{h}, 0, 0)$ where $\tilde{e}, \tilde{h} \in C$) are normally incident on the grating from z>h. The time dependence assumed to be $\exp(-i\omega t)$ is dropped. The diffracted field is to be found.

2. An isotropic chiral medium is described by the following constitutive relations [1]

$$\mathbf{D} = \varepsilon_0 \varepsilon \mathbf{E} + i\gamma \sqrt{\varepsilon_0 \mu_0} \mathbf{H}, \quad \mathbf{B} = \mu_0 \mu \mathbf{H} - i\gamma \sqrt{\varepsilon_0 \mu_0} \mathbf{E}, \qquad (1)$$

where ε_2 and μ_2 is, respectively, the permittivity and permeability, γ represents the chirality parameter which characterizes the magnetic-electric interaction.

Taking into account that the incident field does not depend on the x-coordinate and the grating is uniform and extends infinitely along the OX axis, the sought field will not have any x variations. So the considered problem is two-dimensional. For this problem, (1) yield the following relationships governing the field in a homogeneous chiral medium

$$\Delta_{yz} u^{\pm} + k^{\pm 2} u^{\pm} = 0,$$

$$E_x^{\pm} = u^{\pm}(y, z), \quad E_y^{\pm} = \mp \frac{1}{k^{\pm}} \frac{\partial u^{\pm}}{\partial z}, \quad E_z^{\pm} = \pm \frac{1}{k^{\pm}} \frac{\partial u^{\pm}}{\partial y}, \quad \mathbf{E} = \mathbf{E}^+ + \mathbf{E}^-, \quad \mathbf{H} = \mathbf{H}^+ + \mathbf{H}^- = -i \frac{1}{\rho_2} (\mathbf{E}^+ - \mathbf{E}^-),$$

where $k^{\pm} = -k_2(1 \pm \eta), k_2 = \omega \sqrt{\varepsilon_0 \varepsilon_2 \mu_0 \mu_2}, \eta = \gamma / \sqrt{\varepsilon_2 \mu_2}, \rho_2 = \sqrt{\mu_0 \mu_2 / \varepsilon_0 \varepsilon_2}$. So the electric field is described by the sum of the so called "wave" fields $\mathbf{E}^{\pm}$ and $E_x^{\pm}$ is that through which all the rest field components can be presented.

It is worth noting that notwithstanding the problem is two-dimensional, all the components of the fields are kept. Thus the vector problem is considered.

3. The sought physical solution has to fit the following conditions: Maxwell's equations; radiation condition at infinity; boundary conditions; periodicity condition; finiteness of the field energy. In this formulation, the problem solution exists and is unique.

Let us seek the solution in the form of the Fourier series expansion. Using the boundary conditions on the $z=0$, $z=h$ surfaces one can obtain the two systems of functional equations:

$$\begin{cases} \sum_{\substack{n=-\infty \\ (n\neq 0)}}^{n=+\infty} X_n |n| \exp(in\varphi) = F, & |\varphi| < \delta \\ \sum_{n=-\infty}^{n=+\infty} X_n \exp(in\varphi) = 0, & \delta < |\varphi| \le \pi \end{cases} \qquad \begin{cases} \sum_{n=-\infty}^{n=+\infty} Y_n \exp(in\varphi) = 0, & |\varphi| < \delta \\ \sum_{\substack{n=-\infty \\ (n\neq 0)}}^{n=+\infty} Y_n |n| \exp(in\varphi) = \widetilde{F}, & \delta < |\varphi| \le \pi \end{cases} \qquad (2)$$

where $\varphi = 2\pi y/l, \delta = \pi d/l$ and $F(X,Y)$, $\widetilde{F}(X,Y)$; $X(x,y)$, $Y(x,y)$ are determined by analogy with [3]; x_n, y_n are the Fourier coefficients describing the field in the chiral medium and give all the unknown values. Coupled systems (2) of dual series equations with the trigonometric kernels are systems of the first kind. These systems are ill-conditioned and do not allow developing an efficient numerical algorithm. The analytical regularization can help us to get rid of this ill-conditioning and arrive at the form admitting efficient numerical and analytical treatment [2].

4. It was proved that these systems can be simplified by the method of Rieman-Hilbert boundary value problem. Applying this method to each system individually we arrive at the following infinite system of linear inhomogeneous algebraic equations:

$$\begin{cases} X_m = \sum_{n=-\infty}^{n=+\infty} V_{mn}(u)\{\alpha_n X_n + \beta_n Y_n\} + b_m, \\ Y_m = \sum_{n=-\infty}^{n=+\infty} \widetilde{V}_{mn}(\widetilde{u})\{\widetilde{\alpha}_n X_n + \widetilde{\beta}_n Y_n\} + \widetilde{b}_m, \end{cases} \quad m = 0,\pm 1,\dots \qquad (3)$$

$$b_0 = 2i\chi_1 W_0(u)\left(\widetilde{e}\exp(-ik_1 h) + \frac{2i\widetilde{h}A_0 v_2}{T_o^+}\exp(ik_1 h)\right), b_m = -2i\chi_1 V_{no}(u)\left(\widetilde{e}\exp(-ik_1 h) + \frac{2i\widetilde{h}A_0 v_2}{T_o^+}\exp(ik_1 h)\right),$$

$$\widetilde{b}_0 = -2\rho_2 \widetilde{h}\chi_1 W_0(\widetilde{u})\left(\exp(-ik_1 h) + \frac{T_o^-}{T_o^+}\exp(ik_1 h)\right), \widetilde{b}_m = 2\rho_2 \widetilde{h}\chi_1 \widetilde{V}_{no}(\widetilde{u})\left(\exp(-ik_1 h) + \frac{T_o^-}{T_o^+}\exp(ik_1 h)\right),$$

where all the unknown values can be found in [3]. The asymptotic estimates $\widetilde{\alpha}_n, \widetilde{\beta}_n$ $\sim const|n|\exp(-\xi|n|)$; α_n, $\widetilde{\beta}_n \sim const/|n|$ and the $V_{nn}, \widetilde{V}_{nn}$ behavior at $|m|, |n| \to \infty$ allow one to say that (3) is the Fredholm system of the second kind. Using this system, various diffraction values can be calculated by the reduction method in any necessary accuracy. Having chosen the smallness parameter an analytical solution can be found by the method of successive approximations.

5. For example, seek the reflection coefficients. Let the coefficients a_o^x and a_o^y determine the reflection ($z > h$) of the x- and y- electric field components, which establish, respectively, the grating-period averaged field in E- and H-polarizations. It is supposed, that the incident field has the only polarization $\widetilde{e} = 1, \widetilde{h} = 0$. The reflection coefficients magnitudes $|a_0^x|$ and $|a_0^y|$ as a function of $\chi = l/\lambda_0$ indicating the excitation field frequency are plotted in Fig.1,2.

The $|a_0^x|, |a_0^y|$ as a functional of the chirality parameter η are plotted in Fig.3:
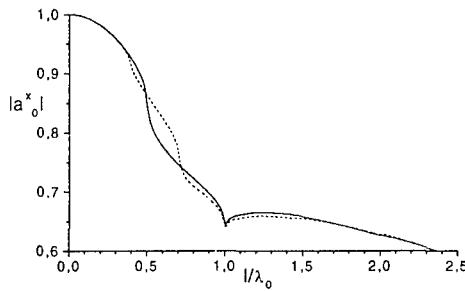
Fig. 1. Reflection coefficient $|a_0^x|$ versus frequency $1/\lambda_0$: $\varepsilon_1 = 1$; $\mu_1 = 1$; $\mu_2 = 1$; $d/l = 0.5$; $h/l = 0.05$. Solid curves correspond to $\eta = 0$, $\varepsilon_2 = 4$; the dash curve corresponds to $\eta = 0.3$.
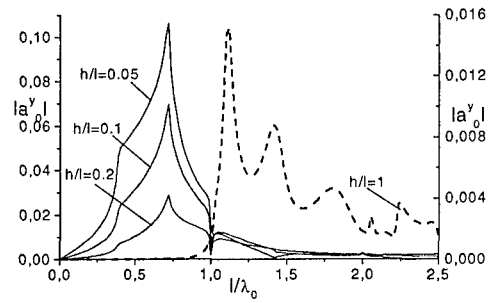
Fig.2. Reflection coefficient $|a_0^y|$ versus frequency $1/\lambda_0$ for different h/l. Solid curves correspond to the left axis, dotted line to the right axis: $\varepsilon_1 = 1; \mu_1 = 1; \varepsilon_2 = 4; \mu_2 = 1; \eta = 0.3; d/l = 0.5$.
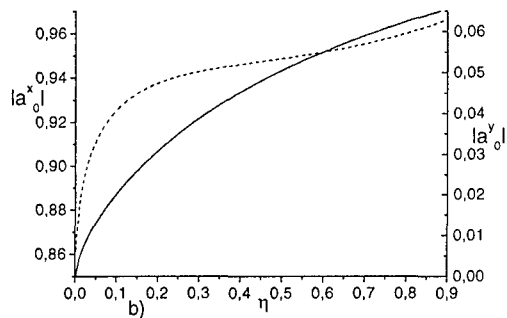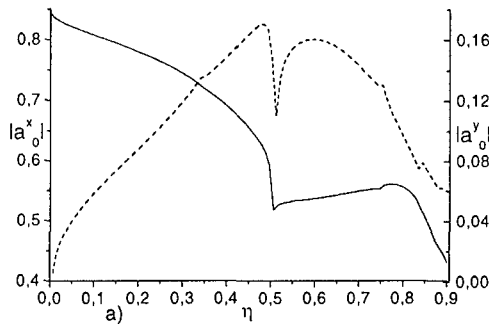
Fig.3. Reflection coefficients $|a_0^x|$ (solid line, left axis) and $|a_0^y|$ (dash line, right axis) versus chirality parameter η at $\chi = 0.71$ (a) and $\chi = 0.38$ (b): $\varepsilon_1 = 1; \mu_1 = 1; \varepsilon_2 = 4; \mu_2 = 1; d/l = 0.5; h/l = 0.05$. The obtained solution describe the field in two polarization states, while the incident wave has single polarization. The appearance of additional polarization is attributed to the fact that the chiral medium eigenwaves represent circularly polarized waves produced by the superposition of E-and H-polarized fields.

The given approach permits to consider the following problems: the wave oblique incidence; the involvement of optional layers, the more complicated grating geometry, etc.

REFERENCES

[1] Tretecov S.A. Electrodynamics of complex media, chiral, bi-isotropic, and some bianisotropic materials //Radiotechnika i Elektronika, Vol.39, №10, p.1457-1470, 1994. (In Russian)

[2] Poyedinchuk A.Ye., Sirenko Yu.K., Shestopalov V.P., Tuchkin Yu.A. "New solution method of direct and inverse problems in diffraction theory." Kharkov: Pub.KhSU, p.285, 1997. (In Russian)

[3] Panin S.B., Poyedinchuk A.Ye. The solution method of the vector problem of the electromagnetic wave diffraction by one-dimensional periodic grating with chiral medium // Dopovidi Nacionalnoy Akademii nauk Ukrainy.-Series A.-2000.- №3.- p.85-89. (In Russian)

THE VORTEX LATTICE METHOD IN THE ELECTROMAGNETIC WAVE DIFFRACTION ON THE METHOD GRADING WITH GYROTROPIC LAYER

Y.V. Gandel and V.V. Khoroshun

Kharkov National University
Dept. of Mathematics and Mechanics
4, Svoboda square, Kharkiv, 61077, Ukraine
Tel. 8-0572-457202. E-mail: gandel@ilt.kharkiv.ua

ABSTRACT

A mathematical model of diffraction of plane linear polarized monochromatic wave on the band grating located on the one side of the planar gyrotropic layer is suggested. It is based on the reducing of the problem under consideration in its exact formulation to a singular integral equation and its numerical solution by the method of discrete singularities.

This approach is interesting both by the possibility of the discretization of the considered problem by the direct numerical method and its possibility to be extended to the corresponding problem with a multielement grating.
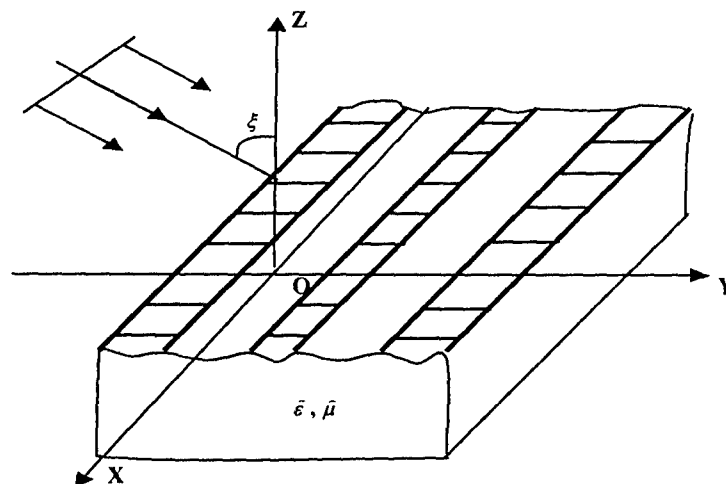
Denote by Ω_1 and Ω_3 the half-spaces $z > 0$ and $z < -a$, respectively; also let Ω_2 be the layer $-a < z < 0$.

The domain Ω_2 is occupied by a gyrotropic layer of thickness a with the tensors of dielectric and magnetic permittivity [1,2]

$$\hat{\varepsilon} = \begin{bmatrix} \varepsilon_{11} & 0 & 0 \\ 0 & \varepsilon & -i\varepsilon_a \\ 0 & i\varepsilon_a & \varepsilon \end{bmatrix}, \qquad \hat{\mu} = \begin{bmatrix} \mu_{11} & 0 & 0 \\ 0 & \mu & -i\mu_a \\ 0 & i\mu_a & \mu \end{bmatrix}.$$

Infinitely thin and ideally conducing grating with a period l and the thickness of aperture d is on the upper base of the layer.

The half-spaces Ω_1 (above the gyrotropic layer) and Ω_3 (under that) are occupied by gomogeneous isotropic magneto-dielectrics with parameters ε_1, μ_1 and ε_3, μ_3, respectively. Plane monochromatic E-polarized (with an angle ς to the normal to the plane of the grating) wave having only one non-zero component of the electric field of the form $e^{-i\varpi t} E_x^0$, where

$$E_x^0 = e^{-i\gamma_{01} z} e^{i h_0 y}, \quad \gamma_{01} = \sqrt{k_0^2 n_1^2 - \sin^2 \varsigma}, \quad \gamma_{01} > 0; \quad h_0 = k_0 n_1 \sin \varsigma, \quad k_0 = \frac{\varpi}{c}, \quad n_1 = \sqrt{\varepsilon_1 \mu_1},$$

is incident on the grating from the upper half-space.

We consider the case when the complete electromagnetic field has the form

$$e^{-i\varpi t}(E_x(y,z),0,0), \quad e^{-i\varpi t}(0,H_y(y,z),H_z(y,z)),$$

and as it follows from the Maxwell equations, H_y and H_z can be represented with the help of E_x, in particular,

$$H_y = \frac{1}{ik_0}\left\{M\frac{\partial E_x}{\partial z} + iK\frac{\partial E_x}{\partial y}\right\}, \text{ where } M = \frac{\mu}{\mu^2 - \mu_a^2}, \quad K = -\frac{\mu_a}{\mu^2 - \mu_a^2}.$$

Here we use the notations of [5]. For non-gyrotropic media, $K=0$.

We seek the unique non-zero component of the electric field that satisfies the Maxwell equations in the form:

in the domain Ω_1
$$E_{x1} = e^{-i\gamma_{01} z} e^{i h_0 y} + \sum_{n=-\infty}^{\infty} a_n e^{i\gamma_{n1} z} e^{i h_n y}, \quad z > 0$$

in the domain Ω_2
$$E_{x2} = \sum_{n=-\infty}^{\infty}\left(b_n e^{-i\gamma_{n2} z} + c_n e^{i\gamma_{n2}(z+a)}\right) e^{i h_n y}, \quad -a < z < 0$$

in the domain Ω_3
$$E_{x3} = \sum_{n=-\infty}^{\infty} d_n e^{-i\gamma_{n3}(z+a)} e^{i h_n y}, \quad z < -a,$$

where $\gamma_{nj} = \sqrt{k_0^2 n_3^2 - h_n^2}, \quad j=1,3; \quad \gamma_{n2} = \sqrt{k_0^2 \varepsilon_{11}\mu_\perp - h_n^2}, \quad \mu_\perp = M^{-1}; \quad \operatorname{Re}\gamma_{nj} \geq 0,$ $\operatorname{Im}\gamma_{nj} \leq 0, \quad j=1,2,3;$ in accordance to the Snell law $h_{n1} = h_{n2} = h_{n3} = h_n,$

where $h_{nj} = k_0 n_j \sin\varsigma + \frac{2\pi n}{l}, \quad j=1,2,3, \quad n_j$ is the refraction coefficient of the media.

Further, using the boundary conditions on the boundaries of the media for the tangential components of the electric field E_x and magnetic field H_y and expressing coefficients b_n, c_n and d_n in the representations of the field by a_n one comes to the dual summator equations in the dimensionless coordinates $\varphi = \frac{2\pi}{l} y; \quad \theta = \frac{\pi}{l} d$

$$1 + a_0 + \sum_{\substack{n=-\infty \\ n\neq 0}}^{\infty} a_n e^{in\varphi} = 0, \quad \theta \leq |\varphi| \leq \pi \tag{SH}$$

$$(B + D_0)a_0 + \sum_{\substack{n=-\infty \\ n\neq 0}}^{\infty}\left\{in + Ai\frac{|n|}{n} + B + D_n\right\}e^{in\varphi} = f(\varphi), \quad |\varphi| < \theta,$$

where $A, B, D_n, n \in Z$ are known where $D_n = O\left(\frac{1}{n^2}\right), n \to \infty.$

The limiting cases of the problem under consideration were researched in [3,4,5].

Using the method [6] developed by one of the authors of the paper, we introduce a new unknown function

$$F(\varphi) = \sum_{n=-\infty}^{\infty} i n a_n e^{in\varphi},$$

that, as follows from (SH), has the following properties

$$F(\varphi) = 0, \ \theta \le |\varphi| \le \pi;$$ (AC)

$$\int_{-\theta}^{\theta} F(\psi) d\psi = 0;$$

and by the conditions on the edge we seek $F(\varphi)$ in the form

$$F(\varphi) = \frac{V(\varphi)}{\sqrt{\theta^2 - \varphi^2}}, \ |\varphi| < \theta$$

where $V(\varphi)$ is a bounded function.

It is shown that $F(\varphi)$, $|\varphi| < \theta$ satisfies a singular integral equation of the second kind

$$F(\varphi) + A \int_{-\theta}^{\theta} \frac{F(\psi) d\psi}{\psi - \varphi} + B \int_{-\theta}^{\varphi} F(\psi) d\psi + \int_{-\theta}^{\theta} Q(\varphi, \psi) F(\psi) d\psi = f(\varphi), \ |\varphi| < \theta,$$ (SE)

where for constants A, B and smooth functions $Q(\varphi, \psi)$, $|\varphi| \le \theta$, $|\psi| \le \theta$; $f(\varphi)$, $|\varphi| \le \theta$ the explicit expressions are found.

The discretization of (SE) with additional condition (ac) was done via discrete singularity method [6,7,4] with the help of the interpolation with the Chebyshev points.

The used method can also be applied to the numerical solution of the problem with multielement grating with m bands on a period.

In this case the problem is reduced to the analogous singular integral equation on the system of m intervals with m additional conditions.

REFERENCES

[1] B. Laks, K. Button. Super-high-frequency ferrites of ferrimagnetics.– M.: Mir, 1965.–675pp.

[2] V.L. Ginsburg. Electromagnetic wave propagation in plasma.M.: Nauka, 1967.–683pp. (in Russian).

[3] Y.V. Gandel, V.V. Khoroshun. Singular integral equations of the problem of electromagnetic wave diffraction by a grating with a cross-magnetized ferrite // Theses of the VI-th International Symposium "Methods of Discrete Features in the Problems of Mathematical Physics", B.I.–Kharkov,1993.–P.123-124. (in Russian).

[4] Y.V. Gandel, V.A. Strelchenko. Mathematical Model for Numerical Analysis of Electromagnetic Wave Diffraction by Gratings in the Boundary Plane Vacuum-Ferrite // Integral Transforms and their Application in the Boundary-Value Problems.–Coll. papers.–Kyiv: Institute of Mathematics, NAS of Ukraine,1996.–Vol.12.– P.34-41. (in Russian).

[5] Y.V. Gandel, A.V. Litvinov, V.V. Khoroshun. Solution of the Problem of Electromagnetic Wave Diffraction by a Strip Grating with a Cross-Magnetized Bigyrotropic Medium // Proceedings on the IX-th Intl. Symp. "Methods of Discrete Features in the Problems of Mathematical Physics"– Orel, 2000.–P. 128-132. (in Russian).

[6] Gandel Yu.V. Method of discrete singularities in electrodynamic problems. Questions of cybernetics, VK-124, Moscow, 1986, pp. 166-183 (in Russian).

[7] Lifanov I.K. Singular integral equations and discrete vortices. Utrecht, the Netherlands; Tokyo, Japan, 1996, 475p.

INVERSE

AND

SYNTHESIS PROBLEMS

SOLUTIOIN OF THE DIRECT AND INVERSE PROBLEMS OF THE WAVE REFLECTION FROM THE WAVEGUIDE FRAGMENT FILLED WITH A LOSSY DIELECTRIC

S. V. Buharov

Radiophysics Dept., Dnepropetrovsk State University
13 Naukovy lane, Dnepropetrovsk, 49050, Ukraine
Phone: (0562) 43-36-30, e-mail: buser@ap1.net-rff.dsu.dp.ua

ABSTRACT

In this paper various math method application for solving the transcendential equation system

$$\begin{cases} f1(a,b) - A = 0 \\ f2(a,b) - B = 0 \end{cases} \text{ is considered.}$$

This system appears when a problem of determination of the complex permittivity from the known coefficient of reflection from the short ended rectangular waveguide fragment filled with a lossy dielectric is solved.

Different types of the direct problem formulation which determine the variety of functions $f1(a,b)$, $f2(a,b)$ are considered.

The comparison of the obtained results in dependence on the direct problem formulation is presented.

INTRODUCTION

A waveguide method of the complex permittivity measurement is based on the interaction between electromagnetic wave directed by the transmission line and researched substance.

A rectangular waveguide fragment is filled with a substance under the test. Information about the complex reflection coefficient (or waveguide fragment impedance) is obtained by the measuring device which is turned on to the other end of the waveguide.[1]

The H_{10} wave is used for measurement.

The direct problem

The 1-st formulation uses the transmission line theory. In this case

$$z_S = z_1 \cdot th(\gamma \cdot d); \quad \gamma = \alpha + i \cdot \beta = i \cdot \frac{2\pi f}{c} \cdot \sqrt{\varepsilon - (c/2af)^2}; \quad R = \frac{z_0 - z_S}{z_0 + z_S};$$

$$R = \frac{\sqrt{\varepsilon - \left(\frac{c}{2af}\right)^2} - \sqrt{1 - \left(\frac{c}{2af}\right)^2} * th(\gamma d)}{\sqrt{\varepsilon - \left(\frac{c}{2af}\right)^2} + \sqrt{1 - \left(\frac{c}{2af}\right)^2} * th(\gamma d)} \tag{1}$$

The 2-nd formulation uses the partial wave conception. In this case, the reflected wave is considered as a superposition of waves after numerous reflections from different waveguide regions boundaries. The H_{10} wave can be considered as a sum of two TEM waves (incident on and reflected from the narrow wall). This approach is illustrated in Fig 1.
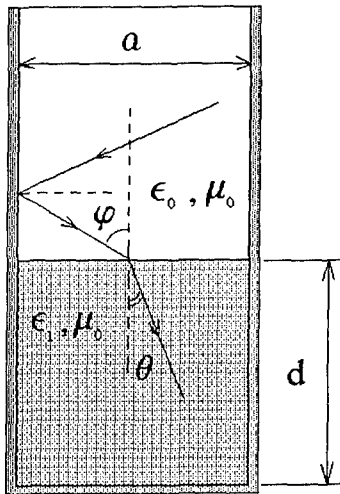
Fig.1 The wave approach

When the TEM wave is incident on the lossy dielectric surface [2] at an angle φ, the reflection coefficient is

$$R_{01} = \frac{W_1 \cos\varphi - W_0 \cos\theta}{W_1 \cos\varphi + W_0 \cos\theta};$$

$$tg\theta = \frac{k_0 \cdot \sin\varphi}{\mathrm{Re}\left(\sqrt{k_1^2 - k_0^2 \cdot \sin^2\varphi}\right)};$$

Taking into account the boundary conditions on the waveguide walls we obtain

$$R_{01} = \frac{\sqrt{1 - (c/2af)^2} - \sqrt{\varepsilon} \cdot \cos\theta}{\sqrt{1 - (c/2af)^2} + \sqrt{\varepsilon} \cdot \cos\theta}$$

Taking into account the enormous reflections from the short end and the dielectric boundary [3] we obtain $R = \dfrac{R_{01} - \exp\left(-i \cdot 4\pi f d\sqrt{\varepsilon}\cos\theta/c\right)}{1 - R_{01} \cdot \exp\left(-i \cdot 4\pi f d\sqrt{\varepsilon}\cos\theta/c\right)}$ (2)

Comparison of the obtained results for coal powder with $\varepsilon = 5 - 0.2 \cdot i$ is shown in Fig.3, and Fig.4.
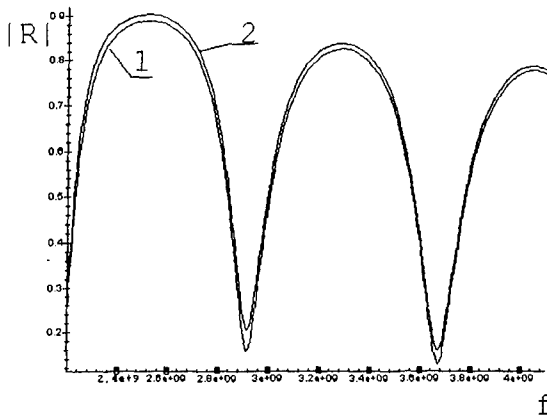
Fig.2 The absolute value of the reflection coefficient
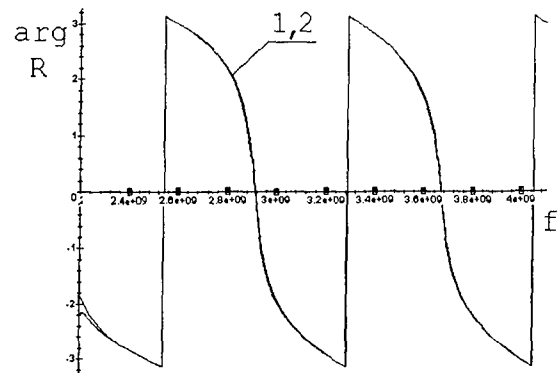
Fig.3 The phase angle of the reflection coefficient

The inverse problem

The inverse problem consists in the determination of the complex permittivity from the known reflection coefficient.

The 1-st formulation. From (1) we obtain the following equations

$$\frac{th(\gamma d)}{\gamma d} = A + iB; \quad \text{A and B are constants;} \quad \gamma d = a + ib,$$

$$\frac{a \cdot sh(2a) + b \cdot \sin(2b)}{(a^2 + b^2) \cdot [ch(2a) + \cos(2b)]} - A = 0, \qquad \frac{a \cdot \sin(2b) - b \cdot sh(2a)}{(a^2 + b^2) \cdot [ch(2a) + \cos(2b)]} - B = 0$$

There are some methods of the similar system solving. The following methods were used: The Newton method:

$$a_{n+1} = a_n - \frac{f1(a_n,b_n) \cdot \dfrac{\partial f2(a_n,b_n)}{\partial b} - f2(a_n,b_n) \cdot \dfrac{\partial f1(a_n,b_n)}{\partial b}}{\dfrac{\partial f1(a_n,b_n)}{\partial a} \cdot \dfrac{\partial f2(a_n,b_n)}{\partial b} - \dfrac{\partial f1(a_n,b_n)}{\partial b} \cdot \dfrac{\partial f2(a_n,b_n)}{\partial a}}$$

$$b_{n+1} = b_n - \frac{f2(a_n,b_n) \cdot \dfrac{\partial f1(a_n,b_n)}{\partial a} - f1(a_n,b_n) \cdot \dfrac{\partial f2(a_n,b_n)}{\partial a}}{\dfrac{\partial f1(a_n,b_n)}{\partial a} \cdot \dfrac{\partial f2(a_n,b_n)}{\partial b} - \dfrac{\partial f1(a_n,b_n)}{\partial b} \cdot \dfrac{\partial f2(a_n,b_n)}{\partial a}}$$

The optimisation approach: The problem of solving the system of equations is transformed into the problem of two variable function

$$F(a,b) = (f1(a,b) - A)^2 + (f2(a,b) - B)^2$$ minimum searching. The descent method with the alternation step was used. .

The extension by the parameter [4]. Parameter t is introduced into the initial system thus when t=0 the solution can be obtained easily: $\dfrac{th(\gamma d)}{\gamma d} - A - iB = 0$. Then assuming that $a = a(t)$, and $b = b(t)$, the following system of the differential equations is solved by the numerical methods

$$\frac{da}{dt} = \frac{-B \cdot \dfrac{\partial f1}{\partial b}}{\dfrac{\partial f1}{\partial a} \cdot \dfrac{\partial f2}{\partial b} - \dfrac{\partial f1}{\partial b} \cdot \dfrac{\partial f2}{\partial a}} ; \qquad \frac{db}{dt} = \frac{B \cdot \dfrac{\partial f1}{\partial a}}{\dfrac{\partial f1}{\partial a} \cdot \dfrac{\partial f2}{\partial b} - \dfrac{\partial f1}{\partial b} \cdot \dfrac{\partial f2}{\partial a}} ;$$

The solution of the initial system is obtained if $t = 1$.

The obtained results for several substances are listed in the following table .

	The 1-st formulation			The 2-nd
	Newton method	Optimisation	Extension	Optimisation
Toluene	e'=2.375 e''=0.0178	e'=2.368 e''=0.0183	e'=2.64 e''=0.02	e'=2.397 e''=0.022
Ethanol	e'=35.7 e''=4.1	e'=35.7 e''=4.1	e'=35.85 e''=3.91	e'=33.65 e''=1.32

REFERENCES

[1] A.A. Brandt, Investigation of dielectrics at super-high frequencies, M.: Fizmatgiz, 1963, 404pp.

[2] V.V. Nikolski, T.I. Nikolskaya, Electromagnetics and wave propagation, M.: Nauka, 1989, 544pp.

[3] V.F. Borulko, O.O. Drobakhin, I.V. Slavin, Multi-frequency microwave non-destructive measurements of the parameters of layered dielectrics, Dnepropetrovsk, Izd. DGU, 1992, 120pp.

[4] D.F. Davidenko. On the approximate solution of non-linear equation sets, Ukrainian Mathematical Journal, V.5, No.2, 1953.

AN ANALYTICAL NUMERICAL SOLUTION METHOD
OF THE REFRACTION INVERSE PROBLEMS

G.A. Alekseev, A.P. Kusaykin, and A.Y. Poyedinchuk
Usikov Institute of Radiophysics and Electronics of NASU

ABSTRACT

An analytical numerical method with the usage of ground measurements of the refraction angle is suggested for reconstructing the refractive index profile of spherical layered tropospheric environments. In this method, the original refraction inverse problem is reduced to the integral equation of the first kind with the self-adjoint positive definite compact operator. A numerical algorithm of solving this equation has been developed on the basis of the Lavrent'ev α-regularization method and tested on standard and biexponential tropospheric models.

From different methods for diagnosing radio-wave propagation conditions of the earth troposphere, we decided on the analysis of the interference structure of a signal when sent by a space-borne SHF transmitter over sea and recorded with an earth-detached receiver while the signal source moves close to the radiohorizon, as if it was in "radiosetting" [1]. No less then seven of ten observations of the signal interference structure correspond to the radio-wave propagation under subcritical refraction and with the reflection layers absent (normal "radiosetting"). This enables us to calculate the refraction angle from the shift of the interference minima depending on the radiosource apparent elevation (refraction direct problem). When in geometrical optical terms, the refraction direct problem admits of setting up the inverse problem consisting in the reconstruction of the refractive index of the earth troposphere from the elevation dependence of the refraction angle along the path from the space-borne transmitter to the ground-based observer. Solution of this problem would be a contribution toward the end of the operative determination of radio-wave propagation characteristics (first of all, radiohorizon distance) along desired intratropospheric paths to more reliability than it follows from the earth effective radius concept.

In geometrical optical terms and under the assumption that the earth troposphere is spherical layered, the refraction inverse problem, or problem of the reconstruction of earth troposphere refractive index profile $n(r)$ in terms of ground-measured refraction angle ξ at a radiosource positive apparent elevation ε is formulated as follows

$$\xi(\varepsilon) = -p \int_a^{a+h_s} \frac{n'(r)dr}{n(r)\sqrt{n^2(r)r^2 - p^2}}, \tag{1}$$

where $p = n_0 a \cos(\varepsilon)$ is the beam aiming parameter ($n_0 = n(a)$, a is the earth radius) and h_s is the height of the space-borne radiosource.

Given $\xi(\varepsilon)$ function, (1) is a nonlinear integral equation for $n(r)$, and by the change of variable $u = [r^2 n^2(r) - n_0^2 a^2][(a+h_s)^2 n^2(a+h_s) - n_0^2 a^2]^{-1/2}$ it is transformed to the linear integral equation

$$\xi(\varepsilon) = -p \int_0^1 \frac{\cos(\varepsilon)F(u)du}{\sqrt{u^2 c^2 + \sin^2(\varepsilon)}} \tag{2}$$

for a new unknown function F(u) which is associated with n(r) profile via the parametric relations

$$
\begin{cases}
n(u) = n_0 \exp\left(-\int_0^u F(u)du \right), \\
r(u) = n_0 a\left(u^2 c^2 + 1\right)^{1/2} / n(u)
\end{cases}
\tag{3}
$$

where $c = [(a+h_s)^2 n^2 (a+h_s) - n_0^2 a^2]^{1/2} / n_0 a$.

A straightforward discretization of (2), i.e. the transformation of the integral with proper quadrature formulae gives the ill-conditioned system of linear algebraic equations (SLAE) whose computer solution is sensitive to any small variations of the SLAE matrix and the right-hand side. Besides, as seen from (2), the functions from the range of the considered integral operator are indefinitely differentiable. Hence, when experimentally obtained, function $\xi(\varepsilon)$ may have no derivatives at some ε. In this case, equation (2) does not have solution in classical sense.

The aforesaid makes us refine the refraction inverse problem formulation. Let instead of exact $\xi(\varepsilon) = \xi_e(\varepsilon)$, its approximation $\xi_a(\varepsilon)$ be known and

$$
\int_{\varepsilon_1}^{\varepsilon_2} \left| \xi_a(\varepsilon) - \xi_e(\varepsilon) \right|^2 d\varepsilon \le \delta_\xi^2 \ ,
$$

where δ_ξ is the upper bound of the refraction angle measuring accuracy. Given input data $\xi_a(\varepsilon)$, $\varepsilon \in [\varepsilon_1, \varepsilon_2]$, the problem reduces to finding such an approximate solution $F_A(u)$ of (2) that is stable to relatively small $\xi_a(\varepsilon)$ variations and converges in the norm of space $L_2([0,1])$ toward the exact solution $F_E(u)$ as $\delta_\xi \to 0$ [2].

The trouble with the interferometric method for measuring refraction angle is large error δ_ξ and ε discreteness which is caused by the interference minima determination. To escape the discreteness, we reduce the initial equation (2) to the integral equation whose right-hand side represents an indefinitely differentiable function. To this end, rewrite (2) as

$$
f(\varepsilon) = \xi(\varepsilon)\sqrt{tg\varepsilon} = \int_0^1 \frac{\sqrt{0.5\sin(2\varepsilon)}F(u)du}{\sqrt{u^2 c^2 + \sin^2(\varepsilon)}} \equiv KF(\varepsilon)
\tag{4}
$$

and introduce an integral operator K^*: $L_2([\varepsilon_1,\varepsilon_2]) \to L_2([0,1])$ of the form

$$
K^* f(\upsilon) = \int_{\varepsilon_1}^{\varepsilon_2} \frac{\sqrt{0.5\sin(2\varepsilon)}f(\varepsilon)d\varepsilon}{\sqrt{\upsilon^2 c^2 + \sin^2(\varepsilon)}} \ .
\tag{5}
$$

Evidently, the equation $K^* f = 0$ possesses only a trivial solution. Acting on both sides of (4) by operator K^* yields

$$
AF \equiv \int_0^1 A(\upsilon, u)F(u)du = \Phi(\upsilon),
\tag{6}
$$

where

$$\Phi(\upsilon) = \int_{\varepsilon_1}^{\varepsilon_2} \frac{\xi(\varepsilon)\sin(\varepsilon)d\varepsilon}{\sqrt{\upsilon^2 c^2 + \sin^2(\varepsilon)}} , \quad A(\upsilon,u) = \ln\frac{\sqrt{a^2+\upsilon^2}+\sqrt{a^2+u^2}}{\sqrt{b^2+\upsilon^2}+\sqrt{b^2+u^2}} , \quad a = \sin(\varepsilon_2)/c, \text{ and } b = \sin(\varepsilon_1)/c.$$

A direct calculation reveals that operator A: $L_2([\varepsilon_1,\varepsilon_2]) \to L_2([0,1])$ given by the left-hand side of (6) is self-adjoint and positive definite.

Compared to (2), equation (6) offers the following benefits:

- function $\Phi(\upsilon)$ with the weight function given by the kernel of operator K^* somewhat smoothes the refraction angle measuring error on interval $[\varepsilon_1,\varepsilon_2]$, so it acts as a filter;

- with the interferometric method in which the refraction angle is discretely measured, the employment of operator K^* provides the indefinitely differentiable function suitable for the numerical work;

- for approximate solution, equation (6) admits the Lavrent'ev α-regularization method [3] in which the aim is to convert (6) to the Fredholm equation of the second kind

where $\alpha > 0$ is the regularization parameter.

$$\alpha F_A(u) + \int_0^1 A(u,\upsilon)F_A(\upsilon)d\upsilon = \Phi(u) , \tag{7}$$

As shown in [3], the solution of (7) is insensitive to small in the $L_2([0,1])$ norm perturbations ($\|\Phi-\Phi_\delta\| < \delta$) of the right-hand side. And as $\delta,\alpha \to 0$ with $\delta/\alpha \to 0$, it converges in the $L_2([0,1])$ norm toward the solution of (6) to be readily obtained by the numerical methods.

The computer modeling has shown that the suggested method of the refraction inverse problem numerical solution based on the conversion of the refraction integral equation into the equation with a self-adjoint positive definite operator with the following employment of the Lavrent'ev α-regularization method is capable of reconstructing the earth troposphere refractive index profile from the elevation dependence of the refraction angle with high potential accuracy 0.3N units.

Being determined by the refraction angle measuring accuracy, which in the interferometric method is of order 0.1°, the reconstructing accuracy reaches 20N units and permits a large-scale prediction of the refractive index profile.

REFERENCES (all in Russian)

[1] I.D. Gontar', I.S. Turgenev, V.B. Sinitskiy, and S.I. Shirmanova. Experimental research of interferometric method for diagnosing radio-wave propagation conditions under radio-wave exposure from a space-borne satellite. Pre-print # 385 IRE AN UkSSR, Kharkiv, 1989, 17 p.
[2] A.N. Tikhonov and V.Ya. Arsenin. Solution methods of ill-posed problems. Moscow: Nauka, 1986, 287 p.
[3] M.M. Lavrent'ev, V.G. Romanov, and S.P. Shishatskiy. Ill-posed problems in mathematical physics and analysis. Moscow: Nauka, 1980, 288 p.

SOLUTION OF LIGHTNING INTENSITY DISTANCE DISTRIBUTION RECONSTRUCTION PROBLEM BY USING THE SCHUMANN RESONANCE SIGNAL

A.V. Shvets

Institute of Radiophysics and Electronics, National Academy of Sciences of Ukraine
12 Ak. Proskury St., Kharkov, 61085, Ukraine; E-mail: larisa.nipi@ugp.viaduk.net

The inverse problem solution for revealing total worldwide lightning intensity and its distance distribution based on decomposition of average background Schumann Resonance (SR) spectra is considered. The developed one–site technique can be applied without invoking any preliminary knowledge about spatial structure of the world thunderstorm activity. The technique allows reducing the influence of additive interference occurring in experimental measurements. Apart from average electric and magnetic field power spectra for the inverse problem solution it is suggested to use their linear combinations emphasizing distance dependence and basic SR peaks. The influence of errors in source spectra and propagation parameters on recovered lightning intensity and its distance profile has been studied numerically.

Radio waves in the lower end of ELF band propagating within the Earth-ionosphere waveguide exhibit a very low attenuation. In the result of interference between radio waves repeatedly passing the globe circumference, a phenomenon known as Schumann Resonance (SR) is observed in spectra of natural electromagnetic emissions. SR are excited by lightning discharges and carry information both on sources and propagation parameters determined by the lower ionosphere properties [1]. SR are considered also as electromagnetic background for a problem of extracting signals of emissions e.g. of seismic or cosmic origin.

Interest to the study of the SR was recommenced last years by Williams [2] who suggested an idea of a global tropical Earth thermometer based on SR measurement from a single receiving station. Apart from total level of worldwide lightning intensity and then average tropical temperature SRs also carry information on spatial distribution of sources over the Earth surface. This information is useful for study of spatial dynamics of global lightning. An account for distances to sources inhomogeneously distributed over the globe is necessary for a correct estimation of the total lightning intensity by SR observations.

A simplified consideration employing a point source model placed on the Earth surface at some distance from an observer determines two characteristic ranges. The first is the globe circumference that determines basic SR frequencies. The second is a difference between direct and passed trough the antipodal to an observer point path lengths. Direct and antipodal waves come to an observation point with the phase difference determined by the source-observer range and interfere "pure" SR producing a distance signature in field spectra.

Fig. 1. Shaded relieves of distance-frequency dependencies for electric and magnetic field amplitude squared.

Such distance signatures are observed as quasi-hyperbolic structures in shaded relieves shown in Fig.1 representing the frequency–distance dependencies of electric and magnetic field amplitudes squared .

These spectral features are employed by various methods of distance detection to discharges producing so-called Q-bursts in ELF signal [3,4]. Q-bursts amplitudes exceed background level by few times

and can be analyzed as isolated events.

More sophisticated situation occurs with the analysis of background SR signal formed by totality of lightning discharges happening on the Earth [5-8]. In this case a simplified model which implies three world thunderstorm continental centers placed in Asia, Africa and South America is employed. But still essential problems remain with determination of parameters of this model such as effective sizes of the world thunderstorm centers and dynamics of redistribution of activity between them from experimental SR data.

We propose a new technique for solving the inverse problem for decomposition of distance distribution of the world thunderstorm activity from average SR spectra. The solution is based on supposition on incoherent summing of pulse energies produced by totality of lightning discharges forming SR background signal at input of a receiver. We suppose also spherical symmetry of the Earth-ionosphere waveguide. In this case the next similar equations for electric and full magnetic field amplitudes squared can be written:

$$\left|E_r\left(\omega\right)\right|^2 = \overline{m\left(\omega\right)} \cdot \sum_{i=1}^{N} S_i \left|e\left(\omega,D_i\right)\right|^2 \tag{1}$$

$$\left|H_\varphi\left(\omega\right)\right|^2 = \left|H_x\left(\omega\right)\right|^2 + \left|H_y\left(\omega\right)\right|^2 = \overline{m\left(\omega\right)} \cdot \sum_{i=1}^{N} S_i \left|h\left(\omega,D_i\right)\right|^2 \tag{2}$$

where S_i is an effective number of discharges with mean dipole current moment squared $\overline{m(\omega)}$ occurred within i^{th} distance interval, $e(\omega,D_i)$, $h(\omega,D_i)$ are frequency responses of the Earth-ionosphere waveguide on vertical lightning discharge with unit current dipole moment placed at the distance D_i from a receiver.

Equations (1), (2) represent expansions of average spectra by series of non-orthogonal base functions $|e(\omega,D_i)|^2$ and $|h(\omega,D_i)|^2$ and solutions of these ill-posed problems can be obtained in terms of regularized least squares method. To improve conditionality of the linear equation systems obtained we can require base functions to be closer to orthogonality. For this aim we constructed the next linear combination of electric and magnetic field amplitudes squared, emphasizing the distance signature as is seen from Fig. 2:

$$g^-(\omega,D,\gamma) = \left|e(\omega,D)\right|^2 - \gamma\left|h(\omega,D)\right|^2, \tag{3}$$

where $\gamma \cong 530$ is fitted to commensurate electric and magnetic components. Another function:

$$g^+(\omega,D,\gamma) = \left|e(\omega,D)\right|^2 + \gamma\left|h(\omega,D)\right|^2, \tag{4}$$

vise versa, suppresses distance signature and emphasizes basic SR peaks. This property of $g^+(\omega,D)$ can be used for solving the inverse problem for propagation parameters determination.

Inevitable for experimental measurements interference from pulse static and induction fields radiated by nearest lightning discharges, atmospheric (wind and rain or snow) and microseisms influencing field sensors being situated in the Earth's magnetic field and fair weather electric field frequently spoil acquired data. Such interference is observed usually as ascent of lower frequencies in measured spectra. To compensate these noises and extend data ensemble admissible for analysis, a set of functions of $1/f^n$ - type ($n=1,2..$) is added to system of base func-

Fig. 2. Shaded relieves of $g^-(\omega,D)$ and $g^+(\omega,D)$ in distance-frequency coordinates.

tions.

Base functions describing spectra of emissions of possibly seismic or cosmic origin falling into the SR frequency range might be added for their detection on the SR background. Results of reconstruction of model mean spectra superposed with low frequency noise shown in Fig. 3 demonstrate advantages of the proposed technique for separation of interference.

The results of this study are summarized below.

1. A one–site technique for recovering of a total level and distance profile of the global lightning activity based on decomposition of average field spectra of the natural SR electromagnetic background has been developed and tested by numerical simulation.

2. The technique allows reducing the influence of different types additive noises occurring in experimental measurements, extending data ensemble acceptable for analysis.

3. Together with the average power, electric and magnetic field spectra for the inverse problem solution is suggested, using their difference and sum that emphasize distance dependence and basic SR peaks, respectively.

4. The influence of errors in model average source and propagation parameters on recovered values of total lightning intensity and its distance profile have been studied numerically.

Fig. 3. Lightning distance profile reconstruction by model average SR spectra interfered with $1/f^n$–type additive noise.

REFERENCES

[1] Wait J. R., 1970. Electromagnetic Waves in Stratified Media. Pergamon Press, Oxford.

[2] Williams, E. R, 1992. The Schumann Resonance: A global tropical thermometer, Science, 256, 1184.

[3] Ishaq M., and Jones D. Ll., 1977. Method of obtaining radiowave propagation parameters for the Earth-ionosphere duct at ELF. Electronic Letters 13, 254-255.

[4] Nickolaenko A.P. and Kudintseva I.G., 1994. A modified technique to locate the sources of ELF transient events. Journal of Atmospheric and Terrestrial Physics 56, 1493-1498.

[5] Nickolaenko A. P., Hayakawa M., and Hobara Y., 1996. Temporal variations of the global lightning activity deduced from the Schumann resonance data, Journal of Atmospheric and Terrestrial Physics 58, 1699-11709.

[6] Heckman, S.J., E. Williams, and R. Boldi, 1998. Total global lightning inferred from Schumann resonance measurements, J. Geophys. Res., 103, 31775-31779.

[7] Belyaev, G.G., A. Yu. Schekotov, A. V. Shvets, A. P. Nickolaenko, 1999. Schumann resonances observed using Poynting vector spectra. J. Atmos. Solar-Terr. Phys., 61, 751-763.

[8] Shvets A.V., 1999. Distance estimation to the world thunderstorm centres by measurement of the Schumann resonance background. XXVIth General Assembly URSI, Univ. of Toronto, Toronto, Ontario, Canada, August 13-21, 1999, Abstracts, p. 297.

NEAR-FIELD EFFECTS IN THERMAL RADIO EMISSION[1]

Gaikovich K.P., Reznik A.N., Vaks V.L.

Institute for Physics of Microstructures RAS, GSP-105, Nizhny Novgorod, 603600, Russia

Phone: 8312 327920, Fax: 8312 675553, E-mail: gai@ipm.sci-nnov.ru

ABSTRACT

Our research is related with a new idea in the area of subsurface radiometry. This idea is based on a specific character of the quasi-stationary part of a thermal emission field (evanescent modes at interface). It is formed in media in another way in comparison with the wave (propagating) component. At first, the problem of the detection of the quasi-stationary field near the media surface has been formulated by S.M.Rytov (see, for example [1]), where it was shown that the energy density of this component enhances drastically with the decreasing of the distance above the surface whereas the energy density of the wave component is unchanged in the whole space. But till the present time this problem remained experimentally unsolved. The difficulty of these measurements is related to the strong influence of the media on antenna parameters, because the quasi-stationary field could be measured only at a small distance above the surface and only using electrically-small antennas (much less than wavelength in a medium) [2]. The theoretical analysis [2] shows that the effective depth of the formation of quasi-stationary component depends on the height of antenna above the surface of a medium and on the antenna size. At the surface, this skin-depth could be very small (for small antennas); it increases with the antenna height, and at the height comparable to wavelength in the medium it converges to skin-depth for the wave component of thermal emission. So, it is possible to discover the influence of the quasi-stationary field by measurements of the temperature-stratified medium using for the calibration the same medium at two different constant temperatures. Two near-field effects could be detected: (i) the effective radiobrightness dependence on the height of the small antenna and (ii) radiobrightness dependence on the aperture size at small distance above the surface. These effects lead to new one-wavelength methods of non-invasive temperature sounding of absorbing media, such as water and living tissue [3].

THE INTEGRAL EQUATION AND EFFECTIVE RADIOBRIGHTNESS

The well-known solution of the emission transfer equation for radiobrightness is inapplicable for the case of quasi-stationary field measurements. The solution of this problem of electrodynamics has been obtained in [2] on the base of wave approach, and the expression for the effective radiobrightness temperature at given wavelength λ could be written in compact form as:

$$T_b(h,D) = \int_{-\infty}^{0} T(z)K(h,D,z)dz, \tag{1}$$

where h is the height of antenna above the surface of the half-space, D is the effective antenna diameter. It is possible to represent the kernel K of (2) as a sum of quasi-stationary field and wave field parts. The quasi-stationary component dominates, if $D \ll \lambda$ and $h \ll \lambda$. In this case the depth of layer which gives the main contribution in the value of measured thermal

---

emission in (2) (the effective depth of radiobrightness formation) $d_{eff} = \left| \int_{-\infty}^{0} zK(h,D,Z)dz \right|$ is much less than the absorption skin-depth $d_{sk} = 1/\gamma$ (γ is the absorption coefficient). The wave field component dominates if $D \geq \lambda$ and $h \geq \lambda$, and $d_{eff} \to d_{sk}$. In any case because of near-field effect d_{eff} should be less than d_{sk}. Integral equation (1) has been applied in [3] for near-field effect calculations and for the statement and numerical simulation of the inverse problems of the temperature profile retrieval from the known dependence $T_b(D)$ or $T_b(h)$. It is used below for the comparison with the experimental results.

MEASUREMENTS. NEAR-FIELD EFFECTS

The measurements have been carried out using the high-sensitivity (0.05 K) radiometer at the frequency of 950 MHz with the spectral band 200 MHz. On the first stage of measurements, we use the temperature-stratified water as a media with well-known dielectric parameters. A special device has been worked out to create a stationary linear temperature profile in the water with the large gradient $dT/dz \cong 2.5$ K/cm and to manage the precise height h of the antenna above the water surface. The main technical problem was to develop the electrically-small antenna with high enough efficiency. The first examples of the stripline planar dipole antennas with the effective size about 1 cm have been developed [4] and applied in experiments. These copper antennas include the resonant circuit to achieve the antenna-water matching. In [4] the reflection coefficient R, efficiency η and sensitivity dT_b of the developed dipole antennas have been investigated. These parameters appeared practically independent on the temperature and the salinity of water in radiometer frequency band. The achieved antenna parameters permit to solve the main problem, i.e. to detect both the above mentioned effects at large temperature gradients in the temperature-stratified water.

Measurements have been carried out for the temperature-stratified water at three different values of salinity: $S = 0$, $1.8 \cdot 10^{-3}$ and $5.0 \cdot 10^{-3}$ g/cm^3. At the water salinity $S = 1.8$ g/litre the skin-depth at the given frequency is temperature independent and the medium can be considered as a homogeneous dielectric. The results for the first two values of salinity are shown in Fig.1,2. The measured temperature profile in the water is given in Fig.3. At $S = 0$ the temperature $T(z = -d)$ at the skin-depth was used to calculate the dielectric parameters.
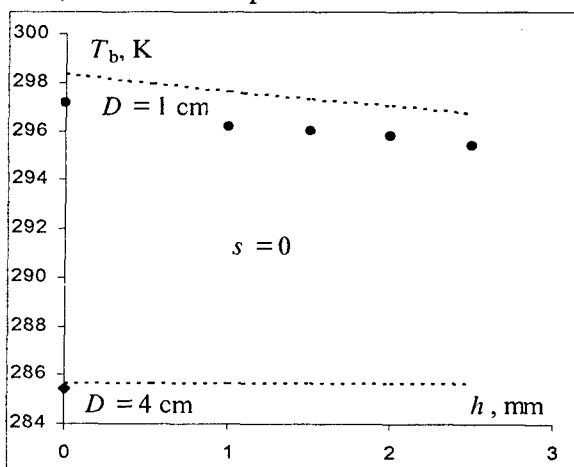
Fig.1. Measured dependence of radiobrightness on the antenna height at antenna sizes $D = 1$cm and $D = 4$ cm for the distilled (deionized) water ($S=0$). Circles-measurements, dashed line – calculation.
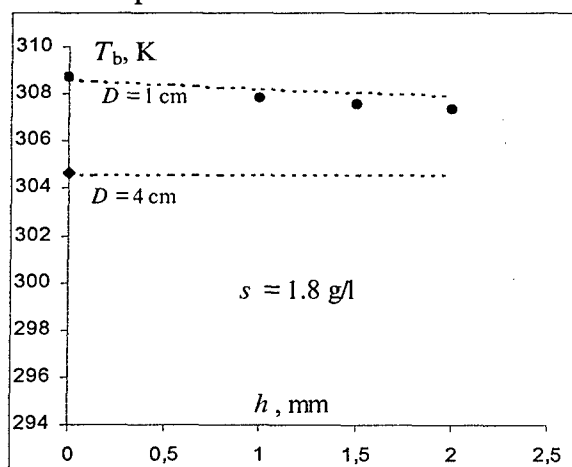
Fig.2. The same as in Fig.1, but at water salinity $S = 1.8 \cdot 10^{-3}$.

One can see in Fig.1,2 that the measurements and the results of calculation of T_b from the integral (1) are in a very good agreement. So, the dependencies of radiobrightness on the antenna height and size are successfully detected. More strong effects have been observed in distilled water, but in this case the dielectric parameters are temperature-dependent and it is difficult to get a high accuracy.

The calculated and the measured dependence of the effective depth d_{eff} of radiobrightness formation on water salinity at contact measurements ($h = 0$) along with the same dependence for the absorption skin-depth d_{sk} is presented in Fig.4. The well-detected difference between d_{eff} and d_{sk} is a demonstration of the near-field effect.
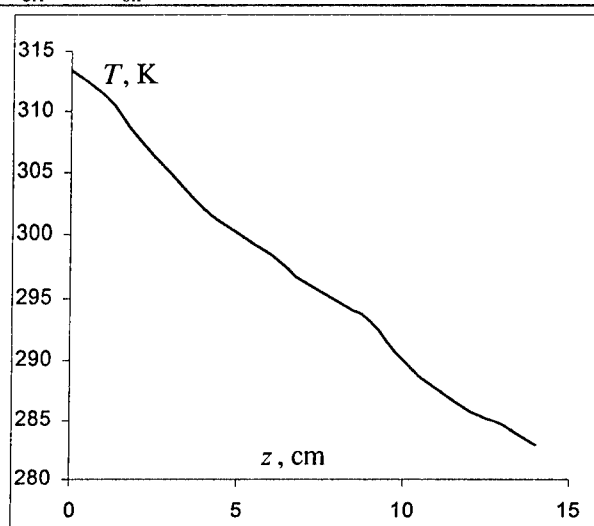
Fig.3. Temperature profile in water.
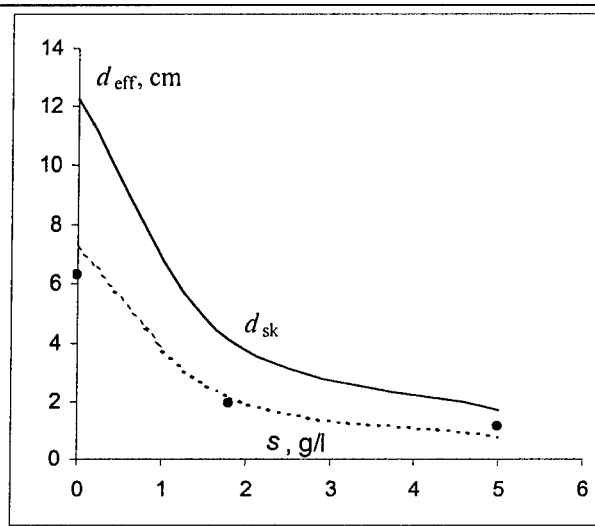
Fig.4. Measured (circles) and calculated (dashed) dependence of the effective depth of radiobrightness formation on water salinity. Solid line – calculated dependence of the absorption skin-depth.

METHODS OF SUBSURFACE RADIOTHERMOMETRY

It is possible to use the dependencies $T_b(h)$ and $T_b(D)$ for the retrieval of the temperature profile $T(z)$ from the solution of the integral equation (1). This possibility has been theoretically studied in [3] on the basis of numerical modeling of retrieval from the solution of ill-posed Fredholm integral equation of the 1-st kind (1) using the Tichonoff method. The first examples of the temperature retrieval by $T_b(D)$ are obtained. To use the height dependence $T_b(h)$ for temperature diagnostic it is necessary to work out the tunable antenna for matching at arbitrary height level h (in our measurements the antenna was matched for $h = 0$ only).

REFERENCES

[1] Rytov S.M. Introduction in the statistical radiophysics. Moscow, Nauka, 1966 (in Russian).
[2] Reznik A.N. Quasi-stationary field of thermal radiation in the theory of contact radiothermometry. Radiophysics and Quantum Electronics, 1991, v.34, No.5, pp.429-435.
[3] Gaikovich K.P., Reznik A.N. Near-field subsurface radiothermometry. 8th International Crimean Conference "Microwave & Telecommunication Technology" CriMiCo-98 (14-17 Sept. 1998, Sevastopol State Technical University, Crimea, Ukraine), Sevastopol: Weber Co., 1998, v.2, pp.629-630.
[4] Yurasova N.V., Gaikovich K.P., Reznik A.N., Vaks V.L. Antennas for Near-Field Radiothermometry. The present issue.

MATCHING OF THE NORMALLY INCIDENT H-POLARIZED PLANE WAVE WITH A LAYERED HALF-SPACE

Viktor Naidenko[1], and Elena Guseva[2]

[1] Kyiv State University of Trade and Economics, 19 Kioto street, Kyiv, 02156, Ukraine
[2] National Technical University of Ukraine «Kyiv Polytechnic Institute», 37 Prospect Peremogy, Kyiv, 03056, Ukraine

The plane $z=0$ divides the whole volume into two regions 1 and 2 (Fig. 1). An emitter from region 1 forms a plane unit wave with components H_y, E_x, which is normally incident on a stratified half-space (SH). Planes $x=0, \pm a, \ldots, x=\pm a/2$ are electrical walls. It conforms to the zero phase shift on a structure spacing in the x-direction of the SH [1]. Permittivity of region 2 strata is considered to be a diagonal tensor with components ε_x, ε_y, ε_z. The dependence on t is $exp(j\omega t)$.

Fields in region 1 are represented as a sum of incident and reflected waves

Fig.1

$$H_{y1} = e^{-i\Gamma_0 z} + R_0 e^{j\Gamma_0 z} + \sum_{n=1}^{\infty} R_n \cos(2\pi n x / a) e^{j\Gamma_n z},$$

$$\omega\varepsilon_0\varepsilon_{x1}E_x = \Gamma_0\left(e^{-i\Gamma_0 z} - R_0 e^{i\Gamma_0 z}\right) - \sum_{n=1}^{\infty} R_n\Gamma_n \cos(2\pi n x / a) e^{j\Gamma_n z},$$

where $\Gamma_n^2 = \varepsilon_{x1}[k^2 - (2\pi n / a)^2 / \varepsilon_{z1}]$, R_n - amplitudes of reflected waves, $n = 0, 1, \ldots$.

Region 2 is divided into two subregions 2.1 and 2.2, separated by the boundary $x=\pm t/2$ within the limits of one period of the SH. Fields in region 2 are represented as a sum of transmitted waves

$$H_{y2} = \sum_{m=1}^{\infty} B_m \Psi_m(x) e^{-j\gamma_m z}, \quad \omega\varepsilon_0 E_{x2} = \sum_{m=1}^{\infty} B_m \gamma_m \Psi_m^\varepsilon(x) e^{-j\gamma_m z},$$

where γ_m is determined, as follows from the wave equations, by one of the equalities

$$\gamma_m^2 = k^2\varepsilon_{x2.1} - q_m^2\varepsilon_{x2.1} / \varepsilon_{z2.1} = k^2\varepsilon_{x2.2} - h_m^2\varepsilon_{x2.2} / \varepsilon_{z2.2},$$

$$\Psi_m = \begin{cases} \cos 2v_m x/t, & x \leq t/2, \\ \dfrac{\cos v_m}{\cos u_m}\cos u_m(2x-a)/l, & t/2 \leq x \leq a/2, \end{cases} \qquad \Psi_m^\varepsilon = \begin{cases} \dfrac{1}{\varepsilon_{x2.2}}\cos 2v_m x/t, & x \leq t/2, \\ \dfrac{\cos v_m}{\varepsilon_{x2.1}\cos u_m}\cos u_m(2x-a)/l, & t/2 \leq x \leq a/2. \end{cases}$$

Other parameters are known, u_m and v_m is derived from the equations

$$\varepsilon_{z2.2}u_m \mathrm{tg}u_m = (l/t)\varepsilon_{z2.1}v_m \mathrm{tg}v_m, \quad u_m^2 = (\varepsilon_{z2.1}/\varepsilon_{x2.1})(l/t)^2[v_m^2\varepsilon_{x2.2}/\varepsilon_{z2.2} - (kt/2)^2(\varepsilon_{x2.2} - \varepsilon_{x2.1})].$$

On the region 1 and 2 boundary $z=0$ the boundary conditions should be satisfied

$$H_{y1} = H_{y2}\big|_{z=0}, \quad E_{x1} = E_{x2}\big|_{z=0}.$$

Substituting field expressions into these conditions, one gets a system of functional equations:

$$\begin{cases} 1 + R_0 + \displaystyle\sum_{n=1}^{\infty} R_n \cos\frac{2\pi n x}{a} = \sum_{m=1}^{\infty} B_m \Psi_m(x), & (1a) \\[4mm] \dfrac{\Gamma_0}{\varepsilon_{x1}}(1 - R_0) - \dfrac{1}{\varepsilon_{x1}}\displaystyle\sum_{n=1}^{\infty} R_n\Gamma_n \cos\frac{2\pi n x}{a} = \sum_{m=1}^{\infty} B_m \gamma_m \Psi_m^\varepsilon(x). & (1b) \end{cases}$$

This system can be reduced to the system of linear algebraic equations (SLAE) of the first or second kind for R_n or B_m. In order to do this, every equation (1) is multiplied by a system of the same or different functions that are full and orthogonal on interval $0 \leq x \leq a/2$ and integrated with respect to x between 0 and $a/2$ (the task is even about plane $x = 0$). In the given problem the
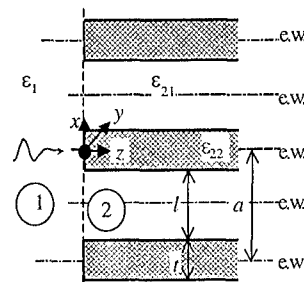
system of functions $\{\cos(2\pi qx/a)\}\big|_{q=0}^{\infty}$ with weight 1, $\{\Psi_q(x)\}\big|_{q=1}^{\infty}$ with weight $1/\varepsilon_x$ and $\{\Psi_q^\varepsilon(x)\}\big|_{q=1}^{\infty}$ with weight ε_x are full and orthogonal on interval $0 \leq x \leq a/2$. Hereinafter one needs the following integrals

$$\frac{4}{a}\int_0^{a/2}\cos(2\pi nx/a)\cos(2\pi qx/a)dx = \begin{cases} 2, & n=q=0, \\ 1, & n=q\neq 0, \\ 0, & n\neq q, \end{cases} \quad J_{mn}=\frac{4}{a}\int_0^{a/2}\cos\frac{2\pi nx}{a}\Psi_m(x)dx,$$

$$\frac{4}{a}\int_0^{a/2}\Psi_m(x)\Psi_q^\varepsilon(x)dx = \frac{4}{a}\int_0^{a/2}\Psi_q(x)\Psi_m^\varepsilon(x)dx = \begin{cases} I_m, & m=q, \\ 0, & m\neq q, \end{cases}, \quad J_{mn}^\varepsilon=\frac{4}{a}\int_0^{a/2}\cos\frac{2\pi nx}{a}\Psi_m^\varepsilon(x)dx.$$

Applying the system of functions $\{\cos(2\pi qx/a)\}\big|_{q=0}^{\infty}$ to (1), one gets the following SLAE:

$$\begin{cases} \Delta_n(\delta_{n0}+R_n)=\sum_{m=1}^{\infty}B_m J_{mn}, & n=0,.... \\ \Delta_n(\delta_{n0}-R_n)=\dfrac{\varepsilon_{x1}}{\Gamma_n}\sum_{m=1}^{\infty}B_m\gamma_m J_{mn}, & n=0,... \end{cases} \quad \Delta_n=\begin{cases} 2, & n=0, \\ 1, & n\neq 0, \end{cases} \quad \delta_{nq}=\begin{cases} 1, & n=q, \\ 0, & n\neq q. \end{cases} \quad (2)$$

Eliminating from SLAE (2) R_0 and R_n, one gets a system of the first kind for B_m:

$$\left\{\sum_{m=1}^{\infty}B_m J_{mn}\left(1+\varepsilon_{x1}\gamma_m/\Gamma_n\right)=4\delta_{n0}\right., \tag{3}$$

SLAE (3) being solved, amplitudes R_n is derived from one of subsystems (2).

Applying system of functions $\{\Psi_q^\varepsilon(x)\}\big|_{q=1}^{\infty}$ to (1a) and $\{\Psi_q(x)\}\big|_{q=1}^{\infty}$ – to (1b), one gets

$$\begin{cases} J_{m0}^\varepsilon+\sum_{n=0}^{\infty}R_n J_{mn}^\varepsilon=B_m I_m, & m=1,... \\ \Gamma_0 J_{m0}-\sum_{n=0}^{\infty}R_n\Gamma_n J_{mn}=B_m\gamma_m I_m\varepsilon_{x1}, & m=1,... \end{cases} \tag{4}$$

B_m can be eliminated from this SLAE. One gets SLAE of the first kind for R_n:

$$\sum_{n=0}^{\infty}R_n\left(J_{mn}^\varepsilon\varepsilon_{x1}+J_{mn}\Gamma_n/\gamma_m\right)=J_{m0}\Gamma_0/\gamma_m-J_{mn}^\varepsilon\varepsilon_{x1}, \quad m=1,... \tag{5}$$

Applying system $\{\cos(2\pi qx/a)\}\big|_{q=0}^{\infty}$ to (1a) and $\{\Psi_q(x)\}\big|_{q=1}^{\infty}$ – to (1b), one gets SLAE

$$\begin{cases} \Delta_n(\delta_{n0}+R_n)=\sum_{m=1}^{\infty}B_m J_{mn}, & n=0,.... \\ B_m\gamma_m I_m\varepsilon_{x1}=\Gamma_0 J_{m0}-\sum_{n=0}^{\infty}\Gamma_n R_n J_{mn}, & m=1,.... \end{cases} \tag{6}$$

SLAE of the second kind for B_m or R_n can be derived by eliminating R_n or B_m from (6):

$$\sum_{q=1}^{\infty}B_q\left(\delta_{mq}\gamma_m I_m\varepsilon_{x1}+\sum_{n=0}^{\infty}\Gamma_n J_{mn}J_{qn}/\Delta_n\right)=2\Gamma_0 J_{m0}, \quad m=1,... \tag{7}$$

$$\sum_{q=0}^{\infty}R_q\left(\delta_{nq}\Delta_n\varepsilon_{x1}+\Gamma_q\sum_{m=1}^{\infty}J_{mn}J_{mq}/(\gamma_m I_m)\right)=\Gamma_0\sum_{m=1}^{\infty}J_{mn}J_{m0}/(\gamma_m I_m)-2\delta_{n0}\varepsilon_{x1}, \quad n=0,... \tag{8}$$

Applying system $\{\Psi_q^\varepsilon(x)\}\big|_{q=1}^{\infty}$ to (1a) and $\{\cos(2\pi qx/a)\}\big|_{q=0}^{\infty}$ – to (1b), one gets SLAE

$$\begin{cases} J^{\varepsilon}_{m0} + \sum_{n=0}^{\infty} R_n J^{\varepsilon}_{mn} = B_m I_m, & m = 1,... \\ \Delta_n \left(\delta_{n0} - R_n \right) \Gamma_n = \varepsilon_{x1} \sum_{m-1}^{\infty} B_m \gamma_m I_m, & n = 0,... \end{cases} \qquad (9)$$

Eliminating amplitudes R_n or B_m from (9), one gets SLAE of the second kind for B_m or R_n

$$\sum_{q=1}^{\infty} B_q \left(\delta_{mq} I_m + \varepsilon_{x1} \gamma_q \sum_{n=0}^{\infty} J^{\varepsilon}_{mn} J^{\varepsilon}_{qn} / (\Delta_n \Gamma_n) \right) = 2 J^{\varepsilon}_{m0}, \quad m = 1,... \qquad (10)$$

$$\sum_{q=0}^{\infty} R_q \left(\delta_{nq} \Delta_n \Gamma_n + \varepsilon_{x1} \sum_{m=1}^{\infty} \gamma_m J^{\varepsilon}_{mn} J^{\varepsilon}_{mq} / I_m \right) = 2 \delta_{n0} \Gamma_n - \varepsilon_{x1} \sum_{m=1}^{\infty} \gamma_m J^{\varepsilon}_{mn} J^{\varepsilon}_{m0} / I_m, \quad n = 0,... \qquad (11)$$

Comparison of the obtained systems of the second kind shows that SLAE (8) and (10) are the best from the point of view of convergence of the coefficients of unknown amplitudes.

The presented results of computations are obtained by SLAE (8). The data in table 1 allow to make conclusions about the accuracy of calculations as a function of SLAE order M, relative permittivity ε' ($\varepsilon'_{x2.2} = \varepsilon'_{z2.2} = \varepsilon'$, $\varepsilon'_{x2.2} = \varepsilon'_{z2.2} = 1$) and thickness t/a, (l/a = const).
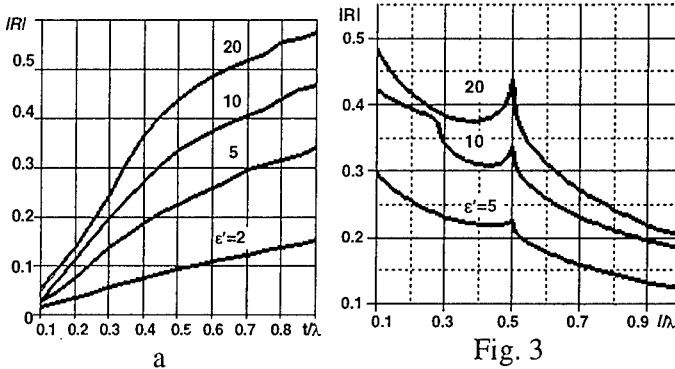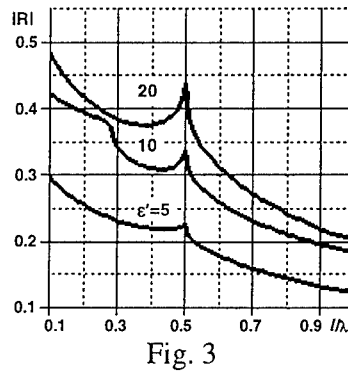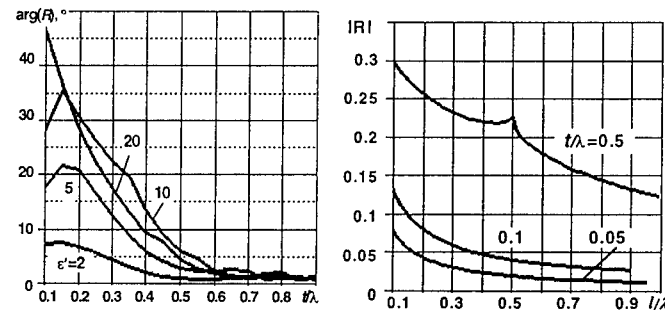
Table 1

ε'	value	$M=5$	$M=10$	$M=20$	$M=4$
2	$|R_0|$	0.033964	0.033965	0.033965	0.0339
	arg(R_0), º	4.81338	4.91077	4.93382	4.937
6	$|R_0|$	0.059584	0.059587	0.059589	0.0595
	arg(R_0), º	11.5367	11.8328	11.9055	11.91
10	$|R_0|$	0.063381	0.063360	0.063366	0.0633
	arg(R_0), º	14.7730	15.1788	15.2768	15.28
2	$|R_0|$	0.13577	0.13578	0.13578	0.1357
	arg(R_0), º	1.94421	1.96517	1.97255	1.974
3 5	$|R_0|$	0.29841	0.29841	0.29844	0.298
	arg(R_0), º	7.42772	7.4624	7.47427	7.478
10	$|R_0|$	0.39326	0.39302	0.39301	0.393
	arg(R_0), º	3.01915	3.05608	3.07333	3.080

Fig. 2

a

b

Fig. 3

Fig. 4

Reflectance magnitude $|R_0|$ and phase $arg(R_0)$ (further index 0 is omitted) as functions of ε' and relative dimensions a/λ, t/λ, l/λ are computed. With every next higher mode, new points of inflection appear on curves. Fig. 2 shows $|R|$ and $arg(R)$ as a function of t/λ for several values of ε' ($a/\lambda = 1$). Fig. 3 shows $|R|$ as a plot of l/λ for several values of ε' ($t/\lambda = 0.5$). Fig. 4 shows the dependency of $|R|$ from l/λ for several values of t/λ ($\varepsilon' = 5$).

REFERENCES
[1] Axial - symmetric periodic structures and resonators / V. I. Naidenko, F. F. Dubrovka – Kiev, Vyshcha shkola, 1985. - 224c. (in Russian).

NEAR-FIELD AND FAR-FIELD IMAGE RECONSTRUCTION FOR AN IMPERFECTLY CONDUCTING CYLINDER

Wei-Ting Chen and Chien-Ching Chiu
Electrical Engineering Department, Tamkang University
Tamsui, Taiwan, R.O.C.

ABSTRACT

Comparison of image reconstruction by using near-field and far-field data for an imperfectly conducting cylinder is investigated. A conducting cylinder of unknown shape and conductivity scatters the incident wave in free space and the scattered near and far fields are measured. By using measured fields, the imaging problem is reformulated into an optimization problem and solved by the genetic algorithm. Numerical results show that the convergence speed and final reconstructed results by using near-field data are better than those obtained by using far-field data. Finally, it is worth noting that the present work provides not only comparative information but also quantitative information.

INTRODUCTION

The electromagnetic inverse scattering problem of conductors has been a subject of considerable importance in remote sensing and noninvasive measurement. In the past twenty years, many rigorous methods have been developed to solve the exact equation. However, inverse problem of this type are difficult to solve because they are ill-posed and nonlinear. As a result, many inverse problems are reformulated as optimization problems. General speaking, two main kinds of approaches have been developed. The first is based on gradient search approach such as the Newton-Kantorovitch method [1], [2], the Levenberg-Marguart algorithm [3]. Since these approaches apply the gradient search method to find the extreme of the cost function. This method is highly dependent on the initial guess and tends to get trapped in a local extreme. In contrast, the second approach is based on the genetic algorithm [4], [5]. The genetic algorithm is a well known algorithm that uses the stochastic random choice to search through a coding of a parameter space. Compared to gradient search optimization techniques, the genetic algorithm is less prone to convergence to a local minimum, which in turn renders it an ideal candidate for global optimization.

In this paper, comparison of image reconstruction by using near-field and far-field data for an imperfectly conducting cylinder is presented. The genetic algorithm is used to reconstruct the shape and conductivity of a scatterer.

THEORETICAL FORMULATION

Let us consider an imperfectly conducting cylinder with cross section described in polar coordinates in the xy plane by the equation $\rho = F(\theta)$ located in free space. An incident plane wave whose electric field vector is parallel to the z axis is illuminated upon the metallic cylinder. By using the induced current concept, the scattered field can be expressed as the integral of the two-dimensional Green functions multiply the induced surface current density, which is proportional to the normal derivative of the electric field on the conductor surface [2], [4]. Besides, for an imperfectly conducting scatterer with finite conductivity, the boundary condition can be approximated by assuming that the total tangential electric field on the scatterer surface is related to surface current density through a surface impedance [2]. As a

result, for the direct problem, given the shape and the conductivity of the object, we can use the boundary condition to solve the surface current density, then calculate the scattered field by using the Green function. Let us consider the following inverse problem: given the scattered field, determine the shape and the conductivity of the object. The genetic algorithm is used to minimize the root mean square error of the measured scattered field and the calculated scattered field, through three genetic operators: reproduction, crossover and mutation. When the root mean square error changes by less than 1% in two successive generations, the genetic algorithm will be terminated and a solution is then obtained, i.e., the shape and the conductivity is obtained.

NUMERICAL RESULTS

By a numerical simulation we compare the image reconstruction by using near-field and far-field data. Let us consider an imperfectly conducting cylinder in free space and a plane wave of unit amplitude incident upon the object. The frequency of the incident wave is chosen to be 3 GHz. In our calculation three examples are considered. To reconstruct the shape and conductivity of the cylinder, the object is illuminated by four incident waves with incident angles $\phi = 0°$, $90°$, $180°$, and $270°$, and eight measurement points is taken on a circle of radius R' at equal spacing. In our cases, R' is chosen much smaller than or larger than $2D'^2/\lambda$, corresponding to the near-field or far-field measurement, where D' is the largest dimension of the scatterer. Here R'=0.06m for near-field measurement and R'=7m for far-field measurement. The number of unknowns is set to 10, to save computing time. The population size is chosen as 300. The search range for unknown coefficient of the shape function is chosen to be from 0 to 0.1. The search range for unknown conductivity is chosen from 3×10^7 to 7×10^7. The extreme value of the coefficient of the shape function and conductivity can be determined by the prior knowledge of the objects. The crossover probability and mutation probability are set to be 0.8 and 0.04 respectively.

In the first example, the shape function is chosen to be

$$F(\theta) = (0.02 + 0.004 \sin 2\theta + 0.008 \sin 3\theta) \text{ m}$$

with copper material ($\sigma = 5.8 \times 10^7$ s/m). The reconstructed relative root mean square error for the shape and conductivity (ES and EC) by using the near-field and far-field data are plotted in Fig. 1. Here the shape function is also plotted for reference.

Fig. 1 Shape function errors and conductivity errors for example 1 in each generation by using near-field and far-field data

From Fig. 1, it is clear the convergence speed and final rms error by using the near-field data are better than those obtained by using far-field data. The final rms errors for conductivity by

using the near-field and far-field data are 1.7×10^{-2} and 2.4×10^{-2} respectively. Note that the convergence is achieved at the 130th generation by near-field measurement. However, for far-field measurement, the convergence is not achieved until the generation is 200. This is due to the fact that the kernel of integral for far-field measurement is more smooth (less singular) than that for near-field measurement. As a result, the near-field measurement is less illposed than the far-field measurement.

Fig. 2 Shape function errors and conductivity errors for the example 2 in each generation by using near-field and far-field data

In the second example, we selected the peanut shape function $F(\theta) = (0.026 + 0.009 \cos 2\theta)\,\mathrm{m}$ with silver material ($\sigma = 6.17 \times 10^{7}$ s/m). The purpose of this example is to show that different shape and conductivity has similar results. Reconstructed results are shown in Fig. 2.

CONCLUSIONS

We have compared the image reconstruction results for an imperfectly conducting cylinder by using near-field and far-field data. It is found that the reconstructed results for near-field measurement are better than those obtained by the far-field measurement. The can be explained by the fact that the near-field measurement is less illposed than the far field measurement. Finally, it is worth noting that in these cases the present work provides not only comparative information but also quantitative information.

REFERENCES

[1]   A. Roger, "Newton-Kantorovitch algorithm applied to an electromagnetic inverse problem," IEEE Trans. Antennas Propagat., vol. 29, pp. 232-238, 1981.

[2]   C. C. Chiu and Y. W. Kiang, "Electromagnetic imaging for an imperfectly conducting cylinders," IEEE Trans. Microwave Theory Tech., vol. 39, pp. 1632-1639, Sept. 1991.

[3]   F. Hettlich, "Two methods for solving an inverse conductive   scattering problem," Inverse Problems, vol. 10, pp. 375-385, 1994.

[4]   C. C. Chiu and P. T. Liu, "Image reconstruction of a perfectly conducting cylinder by the genetic algorithm," IEE Proc.-Micro. Antennas Propagat., vol. 143, pp.249-253, June 1996.

[5]   Z. Q. Meng, T. Takenaka and T. Tanaka, "Image reconstruction of   two-dimensional impenetrable objects using genetic algorithm," Journal of Electromagnetic Waves and Application, vol. 13, pp. 95- 118, 1999.

SHEET CURRENTS RETRIEVAL IN HIGH-T_C SUPERCONDUCTOR FILMS[1]

A.V. Zhilin, K.P. Gaikovich, Y.N. Nozdrin, and A.N. Reznik

Institute for Physics of Microstructures RAS, GSP-105, Nizhny Novgorod, 603600, Russia

Phone: 8312 327920, Fax: 8312 675553, E-mail: gai@ipm.sci-nnov.ru

ABSTRACT

Investigations of 2-D sheet current distributions based on measurements of magnetic field above the type-II high-temperature superconductor (HTSC) YBaCuO films in a remanent magnetization state have been carried out. Using the Biot-Savart law and continuity equation, integral equations (of the 2-D convolution type) for two components of the current have been obtained. These equations have been solved on the basis of Tikhonov's method of generalized discrepancy. Sheet current pattern in superconductors has been retrieved as well as the magnetic field distribution on the film surface. The current peculiarities related to the laser pulse effect have been retrieved from measurements. A new physical effect of the redistribution of currents after the laser pulse impact without the change of the total vortices number has been observed.

MEASUREMENTS

The method of measuring the perpendicular component of magnetic field $H_z(x,y)$ at arbitrary height level z above the film surface uses a Hall scanning probe. A normally-directed external magnetic field was generated by a solenoid coil, which is cooled with liquid nitrogen and produces a maximum field of 500 gauss. The magnetic field increases linearly up to its maximum value during 20 seconds, and then decreases in the same way down to zero value. Thin film (about 0.1 μm) with a diameter of 20 mm was chosen for measurements. A Hall probe with the sizes 100 x 50 μm in the x-y plane and 10 μm in the z-direction was applied in experiments. The height z of measurements was chosen in 200-300 μm interval to ensure non-invasive conditions. The lateral resolution of measurements (pixel size) was chosen 250 μm (comparable with the Hall probe size). The time of the one-pixel integration was 0.25 s at the integration time constant $\tau_0 = 1$s. The noise level was about 0.1 gauss, and it was uncorrelated at the adjacent pixels.

INVERSE PROBLEMS

The integral equations (of the 2-D convolution type) for two components of current for the inverse problem formulation have been obtained in [1] using the Biot-Savart law and the continuity equation:

$$H_z(x,y,z) = \frac{1}{c}\iint j_x(x',y') \frac{Y\left[z^2(X^2+Y^2+2z^2)-X^2(X^2+Y^2)\right]}{(X^2+Y^2+z^2)^{3/2}\left(X^2+z^2\right)^2} dx'dy', \qquad (1)$$

$$H_z(x,y,z) = -\frac{1}{c}\iint j_y(x',y') \frac{X\left[z^2(X^2+Y^2+2z^2)-Y^2(X^2+Y^2)\right]}{(X^2+Y^2+z^2)^{3/2}\left(Y^2+z^2\right)^2} dx'dy', \qquad (2)$$

where j_x, j_y are the components of the sheet current $\vec{j}$, $X = x\text{-}x'$, $Y = y\text{-}y'$. Deconvolution of (3) and (4) yields a solution of the inverse problem of 2-D current pattern retrieval from a 2-D magnetic-field distribution measured in the x–y plane at some arbitrary vertical distance z. Special regularization methods should be applied in this case. Convolution equations (3) and (4) have been solved by using Tikhonov's method of generalized discrepancy [1]. Our numerical simulation gave the following results. The *rms* of random errors of retrieval related to the random "data" noise with the *rms* of 0.1 gauss changes from 0.1 A/cm for the low current values (about 2 A/cm) up to 0.5 A/cm for the strong currents (about 20 A/cm).

To reduce the measurements time to about 3 hours instead of 48 hours, the retrieval of the true magnetic field $H(t)$ from the measured time dependence $H_m(t)$ has been carried out from the deconvolution of the equation

$$H_m(t) = \frac{1}{\tau_0} \int_{-\infty}^{t} H(\tau)\, e^{-\frac{t-\tau}{\tau_0}}\, d\tau, \tag{3}$$

where τ_0 is the integration time constant. The equation (2) has the exact solution

$$H(t) = H_m(t) + \tau_0 \frac{dH}{dt}(t), \tag{4}$$

but this solution of ill-posed equation (2) has a property to amplify the random noise. To solve the problem, the Tikhonov method for the initial convolution equation (2) has been used as a preliminary data processing shown in Figs.1, 2.
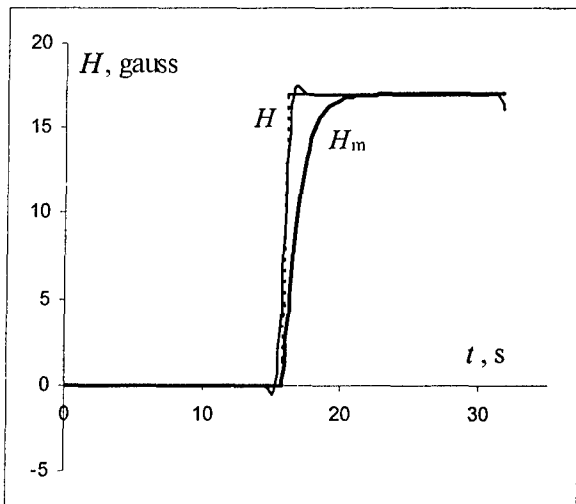
Fig.1. Numerical simulation. Retrieval of the step-function.
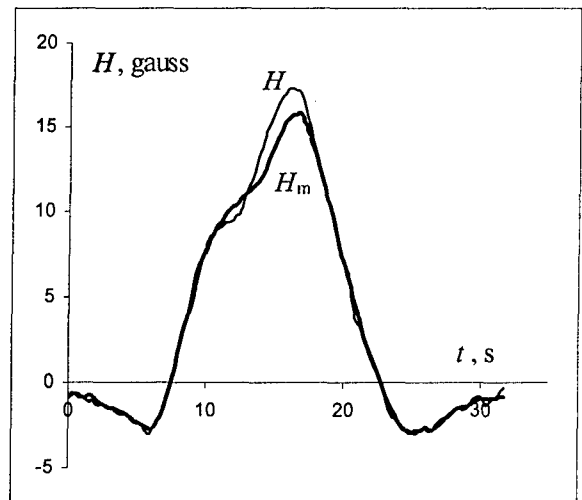
Fig.2. Retrieval of the measured magnetic field.

EFFECT OF LASER PULSE IRRADIATION

In Fig.1, initial state of the magnetic field of a circular disk film with a diameter of 20 mm after the above magnetization process is shown (height of measurement was $z = 225\ \mu m$). The current perturbation due to a laser pulse (with the beam footprint of 2 mm at the power density about 10 kW/cm^2) leads to a new distribution of currents and, hence, to a new

magnetic field distribution shown in Fig.2. The pulse duration $\tau = 10^{-7}$ s was chosen comparable to the time of film-substrate heat exchange.
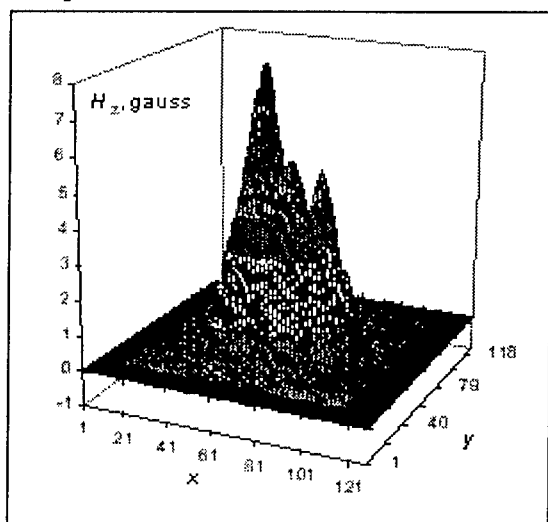
Fig.3. Initial magnetic field at $z = 250$ μm.
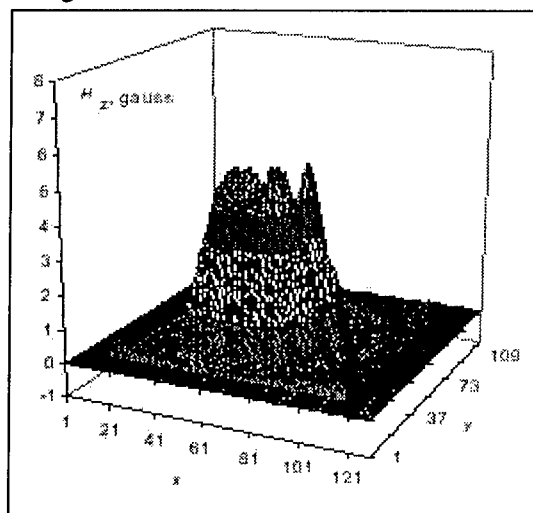
Fig.4. After a laser pulse.

The retrieved current patterns before and after laser pulse are presented in Figs.5, 6. One can see that the strong counterclockwise current rotation region near the center of the film (Fig.6) has disappeared. The magnetic field distributions before and after the laser pulse were calculated using the retrieved currents. The most unexpected result is that the mean (over the film surface) value of the change of the surface magnetic field is equal to zero within the limits of measurement error (see in Fig.7). It means that in the considered case the laser pulse redistributes the currents significantly without a change in the total number of current vortices in the film. So, the well-known Bean theory appears inapplicable in this case.
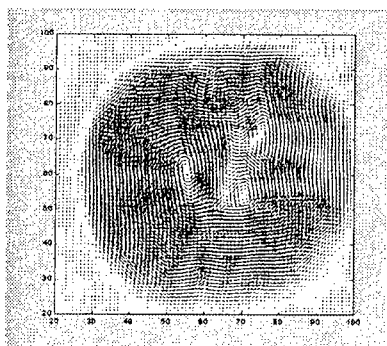
Fig.5. Initial currents.
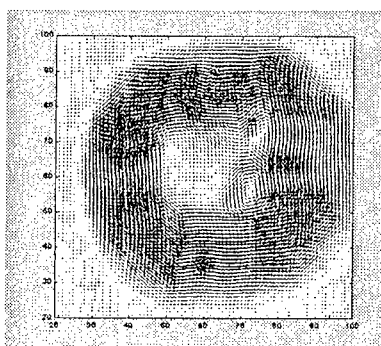
Fig.6. After a laser pulse.
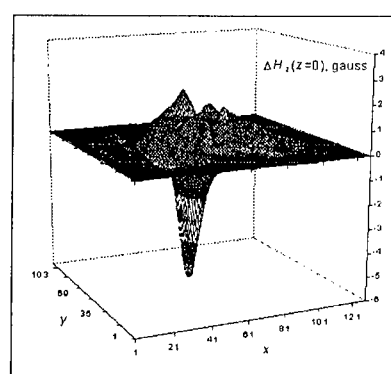
Fig.7. Calculated change of the surface magnetic field because of the laser pulse.

Thus, this effect gives a possibility to change the magnetization in the HTSC films by using the optical emission. Besides, it enables one to switch or to change the polarization of the optical signal reflected from the film (by the same transmitted signal) using a magneto-optical coating of the film.

REFERENCES

[1] Gaikovich K.P., Nozdrin Yu.N., Reznik A.N., Zhilin A.V. Determination of sheet current patterns of HTSC films fixed in a magnetic field by measurements of magnetic field. XII German–Russian–Ukrainian Seminar on High Temperature Superconductivity (25-29 October, 1999, Kiev, Ukraine), 1999, Kiev: V.N.Bakul Institut for Superhard Materials of National Academy of the Ukraine, p.86.

SYNTHESIS OF A WAVEGUIDE ARRAY WITH DUE REGARD FOR THE MUTUAL COUPLING OF RADIATORS

M. I. Andriychuk, and P. O. Savenko

Institute of Applied Problems of Mechanics & Mathematics of NASU

3"B" Naukova St., Lvov, 79601, Ukraine

Phone: +380 322 65-19-79, e-mail: andr@iapmm.lviv.ua

ABSTRACT

The approach for solving the nonlinear synthesis problems of radiating systems according to the prescribed amplitude radiation pattern with due regard for the mutual coupling of separate radiators is proposed by an example of synthesis of a linear waveguide array. The variational statement of the problem is considered. The goal functional takes into account both the mean-square deviation of modules of the prescribed and synthesized radiation patterns and restriction on a norm of the excitation sources. The investigation of the problem solutions and their numerical determination is based on a research of solutions of the Euler equation of the used functional. This equation is a nonlinear integral equation of the Hammerstein type. Algorithms of the direct minimization of functional by gradient methods are also constructed.

THE PROBLEM STATEMENT

The considered two-dimensional waveguide array present the system of $N = 2M + 1$ plane semiinfinite waveguides of width l located equidistantly at the distance d. The boundaries of waveguides and the boundary of the half-space are perfectly conducting. It is supposed that in this system of waveguides an H- polarized electromagnetic wave $\left(\vec{H} = \{0, H_y, 0\}, \vec{E} = \{E_x, 0, E_z\} \right)$ is propagating. In this case components $\vec{E}$ of the electrical field are expressed through H_y as follows: $E_x = \dfrac{i}{\omega\varepsilon} \dfrac{\partial H_y(x,z)}{\partial z}$,

$E_z = \dfrac{i}{\omega\varepsilon} \dfrac{\partial H_y(x,z)}{\partial x}$. Electromagnetic field at any point of space can be calculated, if the

distribution functions of the fields in the apertures of the waveguides $J_n(\varsigma) = \dfrac{\partial H_{y_n}(0,\varsigma)}{\partial x}$,

$\left(n = \overline{-M, M} \right)$ are known. If the nth waveguide is exited by a normal wave with a unit amplitude, the problem of determination of the functions $J_n^{(m)}(\varsigma)$ with due regard for the mutual coupling is reduced to solution of a system of linear integral equations [1]:

$$\int_{-l/2}^{l/2} I_p^{(m)}(\zeta) M_p(\eta,\zeta)d\zeta + \sum_{j=-M}^{M} \int_{-l/2}^{l/2} I_j^{(m)}(\zeta) M_{jp}(\eta,\zeta)d\zeta = -F_{mp}(\eta) \quad (p = -M \div M), \quad (1)$$

where

$$M_p(\eta,\zeta) = \frac{i}{kl} + \frac{2i}{l} \sum_{n=1}^{\infty} \frac{1}{\mu_n} \cos\frac{n\pi\eta}{l} \cos\frac{n\pi\zeta}{l}, \quad (2)$$

$$M_{jp}(\eta,\zeta) = \frac{i}{2} H_0^{(1)}(k \mid \eta - \zeta + (p-j)d \mid), \quad (3)$$

$$F_{mp}(\eta) = \begin{cases} 0, p \neq m \\ 2\cos\dfrac{n_0\pi}{l}\eta, p = m \end{cases}. \tag{4}$$

The radiation pattern (RP) of array, in accordance with the solution of (1), can be presented as

$$f(\xi) = A\vec{a} \equiv \sum_{m=-M}^{M} a_m f_m(\xi), \tag{5}$$

where $f_m(\xi) = \sum\limits_{j=-M}^{M} e^{ikjd\xi} \int\limits_{-l/2}^{l/2} I_j^{(m)}(t)e^{ikt\xi}dt$ is RP of the m th radiator in the case of its

excitation by the normal wave with a unit amplitude, a_m are the complex factors which characterize the excitation of the array elements, k is the wavenumber.

THE METHOD OF SOLUTION

We formulate the synthesis problem according to the prescribed amplitude RP $F(\xi)$ of the waveguide array as a minimization problem of the smoothing functional [2]:

$$\sigma_\alpha(\vec{a}) = \left\| F - |f| \right\|_{H_f}^2 + \alpha\|\vec{a}\|_2^2 \equiv \left\| F - |A\vec{a}| \right\|_{H_f}^2 + \alpha\|\vec{a}\|_2^2. \tag{6}$$

We obtain the following Euler equation

$$\alpha\vec{a} = A^*Af + A^*\left(Fe^{-i\arg f}\right) \tag{7}$$

from a condition of vanishing of the Gateaux derivative of σ_α.

For the analysis of quantitative and qualitative properties of existing solutions it is reasonable to use an equation equivalent to (7) with respect to the synthesized RP f:

$$\alpha f = AA^*f + AA^*\left(Fe^{i\arg f}\right). \tag{8}$$

In the extended form the equation (8) has the following form

$$\alpha f(\xi) + \int\limits_{-\pi/2}^{\pi/2} K(\xi,\xi')f(\xi')d\xi' = \int\limits_{-\pi/2}^{\pi/2} K(\xi,\xi')F(\xi')e^{i\arg f(\xi')}d\xi', \tag{9}$$

where the kernel function is $K(\xi,\xi') = \sum\limits_{n=-M}^{M} f_n(\xi)\overline{f_n(\xi')}$, which is degenerate and positive,

and by virtue of the condition $f_{-m}(\xi) = f_m(\xi)$ it is real.

We write the equation (7) for a numerical determination of solutions as follows

$$\alpha a_n + \sum_{m=-M}^{M} d_{nm}a_m = b_n(\vec{a}) \quad \left(n = -\overline{M,M}\right), \tag{10}$$

where

$$d_{nm} = \int\limits_{-\pi/2}^{\pi/2} f_n(\xi)\overline{f_m(\xi)}d\xi, \qquad b_n(\vec{a}) = \int\limits_{-\pi/2}^{\pi/2} F(\xi)e^{i\arg f(\xi)}\overline{f_n(\xi)}d\xi. \tag{11}$$

The solution of (10) is calculated using the iterative process

$$\alpha a_n^{(p+1)} + \sum_{m=-M}^{M} d_{nm}a_m^{(p+1)} = b_n(\vec{a}^{(p)}), \quad \left(n = -\overline{M,M}\right), \tag{12}$$

built by an implicit scheme of the method of successive approximations. Here, $p = 0,1,2,...$ is the number of iteration. Thus, on each step of iteration the system of linear algebraic equations with the matrix $(\alpha E + D)$, where E is the unit matrix is solved. From functional

entry of the equation (10), it follows that matrix D is positively semi-defined. In accordance with [3] $\left\|(\alpha E + D)^{-1}\right\| \le 1$ for arbitrary $\alpha > 0$. Inverting the matrix $(\alpha E + D)$ once, we can reduce the iterative process (12) to the form

$$a_n^{(p+1)} = (\alpha E + D)^{-1} \bar{b}_n(\bar{a}^{(p)}), \quad (p = 0,1,2,\dots). \tag{13}$$

The theorem of local convergence of the iterative processes (12), (13) is proved.

We mark some properties of solutions of equation (9):

1. If $f(\xi)$ is a solution of (9), then complex conjugate function $\overline{f(\xi)}$ is also a solution of (9).

2. If $f(\xi)$ is a solution of (9), then $e^{i\gamma} f(\xi)$, where γ is an arbitrary real constant, is also a solution of (9).

3. Linear and nonlinear operators in (9) are invariant with respect to the properties of parity of the phase RP, $\arg f(\xi)$, by virtue of symmetry of the system of radiators in the case of symmetrically prescribed RP $F(\xi)$.

The last property enables one to carry out an investigation of solutions of equation (8) separately in the classes of even and odd phase RPs.

Equation (8) may have non-unique solution and these solutions can branch depending on the value of parameter $C = Mc = Mkd$ characterizing electrical size of array.

Algorithms of direct numerical minimization of the functional $\sigma_\alpha(\bar{a})$ by the method of conjugate gradients [4] have been also constructed.

CONCLUSIONS

Computer codes for solving the problems of synthesis of a wavegiude array according to the prescribed amplitude RP by using the proposed approach have been developed. These codes enable one to realize numerical simulation of the wavegiude arrays of various types in a wide range of variation of their geometrical and electro-physical parameters. In the presentation, the examples of synthesis of narrow one- and two-beam RPs will be presented.

In summary, we mark, that the mentioned above solution technique of the nonlinear synthesis problem of a waveguide array can be simply generalized for the synthesis problems of the other types of arrays with due regard of the mutual coupling of separate elements.

REFERENCES

[1] I. V. Skorokhvatova "The synthesis problem of waveguide array with due regard for the mutual coupling of elements", *Numerical Methods of Electrodynamics,* Moscow, Moscow State University, 1977, pp. 79-91 (in Russian).

[2] M. I. Andriychuk, N. N. Voitovich, P. A. Savenko, V. P. Tkachuk, *Antenna synthesis according to the amplitude radiation pattern. Numerical methods and algorithms.* Kiev, Naukova Dumka, 1993 (in Russian).

[3] G. I. Marchuk, *Methods of Mathematical Analysis,* Moscow, Science, 1977 (in Russian).

[4] E. Polak, *Computational Methods in Optimization. A Unified Approach.* New York, London, Academic Press, 1971.

REGULARIZED IMAGE RECONSTRUCTION
IN THE ELECTROMAGNETIC GEOTOMOGRAPHY
THROUGH THE USE OF THE WIENER FILTER

Andrzej Prałat, and Rafał Zdunek
Institute of Telecommunication and Acoustics,
Wroclaw University of Technology
Wybrzeże Wyspiańskiego 27, 50 – 370 Wrocław, Poland
e – mail: pralat@zue.ita.pwr.wroc.pl, rafal@zue.ita.pwr.wroc.pl

ABSTRACT

A method of regularization of the reconstructed image in electromagnetic geotomography is proposed. The Wiener filter for attenuating noise disturbance in reconstructed images is used with the Landweber iterations. The results of the reconstruction from measured data both with and without filtration are shown. The efficiency of the proposed regularization technique is discussed.

INTRODUCTION

Electromagnetic geotomography [1] makes it possible to investigate a distribution of the attenuation coefficient of electromagnetic waves inside a given earth section, usually between two bore-holes.

Measurement data may be obtained by measuring the attenuation of the electromagnetic field strength along conventional rays, which are chosen in such a way as to cover the investigated area. Each ray may be described by a linear equation and, therefore, the set of linear equations matches the investigated area.

The problems of reconstructing the image of the electromagnetic wave attenuation coefficient are related to the problems of solving a set of linear equations. This apparently easy-to-use set of equations has many disadvantageous features: it is ill-conditioned, has not one solution and its coefficient matrix is very sparse and very large. Because of this, many easy methods of solving linear equations cannot be used with this set.

Measurement errors of any kind make the set of equations inconsistent. Moreover, ill-conditioning means that the reconstructed image is affected by inaccurate data. This leads us to the question of how to choose the right solution to this set of equations.

Regularization is a technique which deals with the solving of such a problem. It is usually a compromise between the solution which corresponds most closely to the result of the reconstruction from data with interference and an *a priori* solution, often adopted by default on the basis of measurements obtained using different methods. One of the many methods of regularization [2] is a filtration of the reconstructed image.

There are also a lot of image reconstruction methods that may be used. Iteration methods, based on the Landweber iterations, are the most commonly-used methods. Through some modifications of the Landweber iterations, especially the implementation of the regularization method, the right reconstruction method may be found.

The SIRT algorithm based on the Landweber iterations has been described in this paper. Then, the method of usage of the Wiener adaptive filter in the Landweber scheme was described. The results of reconstruction by means of the SIRT algorithm of the least squares, both with and without using the Wiener filter, were shown. Measurement data of the

attenuation of the electromagnetic field strength in the earth were used in the reconstruction. The efficiency of this regularization method was discussed.

PROPOSED METHOD OF REGULARIZATION IN ELECTROMAGNETIC GEOTOMOGRAPHY

The Landweber [3] iteration scheme is used in many iteration methods of solving the sets of linear equations. In this scheme, the image vector X^{q+1} is updated in the current iteration step q. This is shown by the following formula:

$$X^{q+1} = X^q + \alpha^q \cdot A^T \cdot \left(Y - A \cdot X^q\right) \qquad (1)$$

where A is the coefficient matrix and Y is the measurement vector.

The oldest method based on the Landweber iteration scheme representative is the Richardson algorithm, also called the SIRT algorithm of the least squares. In this method, the coefficient α^q does not change during succeeding iteration steps. Its value only defines a radius of convergence of iteration process.

In the SIRT algorithm, no additional *a priori* information was introduced concerning the distribution of pixel values in the image. Thus, the iteration process is convergent to an accurate solution, i.e. the one which faithfully corresponds to the measurement data. Unfortunately, the real data are corrupted by measurement errors and the image reconstructed "accurately" may be strongly degraded, mainly because the system of equations is ill-conditioned and its matrix of coefficients is sparse. Measurement errors show white Gaussian noise. Therefore, interference shown by the reconstructed image is also a form of noise, i.e. "salt and pepper" effect may be seen.

One of the most effective tools for attenuating this effect is the Wiener adaptive filter which is used in many applications of image processing. Therefore, it seems reasonable to improve the process of reconstruction through the use of appropriate filtration of the reconstructed image used in the process of iteration.

The typical Wiener filter from the MATLAB "Image Processing" toolbox [4] was used for this purpose. It is designed to filter noise disturbances from the 2-dimentional image consisting of pixels. The adaptive Wiener method is based on statistical estimation of the local mean and variance from the local neighbourhood of each pixel. The size of this neighbourhood can be defined in different ways, but here it is limited to the nearest neighbourhood because of the small size of the filtered image. Used filters also have the ability to force the filtration of a given noise power. On the basis of many tests of reconstruction of an original image and reconstruction from real data, it may be stated that the best results can be obtained if the level of noise is equal to 0.001.

The different ways of using the Wiener filter in the Landweber iteration scheme were investigated. The best results were obtained when the reconstructed image was filtered at every 5th step of the iterations. At the appropriate step of the iterations, the image vector X was transformed to an image matrix whose elements strictly correspond to the pixels of the image. In order to improve the filtration of pixels on the edges of the reconstructed area, the image matrix was expanded by additional edge elements (edge pixels) to which the mean value (the value of the background) of the reconstructed image was attributed. The expanded image was filtered and then the appropriate part of the image matrix was re-transformed to the image vector X and the process of iteration was gone on.

RECONSTRUCTION RESULTS

Measurement data of the attenuation of the electromagnetic field strength in the earth were used for the reconstruction. These measurements were carried out in Upper Silesia in southern Poland. The result of the reconstruction presented in Fig. 1a was obtained by using the SIRT algorithm without filtration. However, in Fig. 1b it is shown after using filtration.
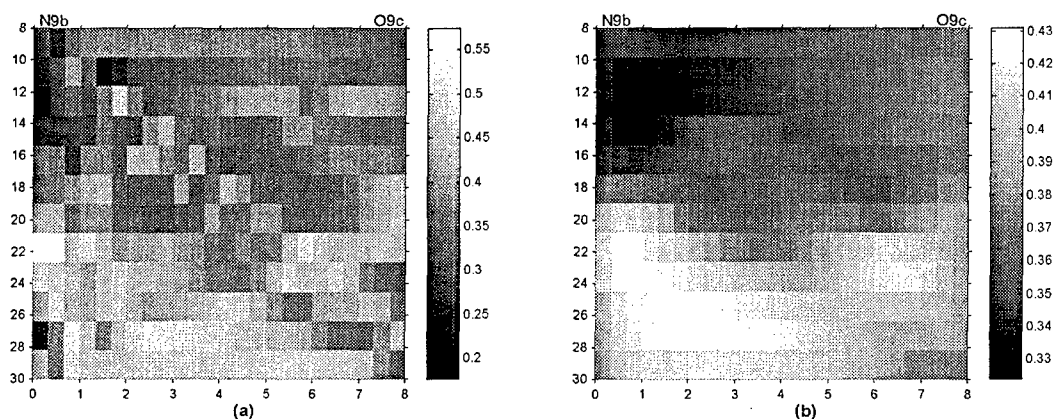
Fig. 1. The result of reconstruction by means of the SIRT algorithm:
a)   without filtration
b)   after implementing filtration

CONCLUSIONS

Regularization through the use of the Wiener filter used in the Landweber iterations allows considerable attenuation of the reconstructed image disturbance (the "salt and pepper" effect). The image presented in Fig. 1b is smoother than the image in Fig. 1a. For the reconstruction of geotomographical images, it is assumed that the attenuation coefficient does not change abruptly. Thus, a smooth reconstructed image is desirable. In many iterative reconstruction methods, regularization by means of interrupting the process of iteration earlier is used. When the Wiener filter was used, it was noticed that the convergent solution was already obtained after a few iterations and the reconstructed image did not change considerably during further iterations. Therefore, an acceleration of the reconstruction process was obtained.
Summing up, the usage of the Wiener filter in the reconstruction process enhances the results of the reconstruction. Moreover, this method can be applied in many areas of tomography.

REFERENCES

[1]   A. Prałat, R. Zdunek, The Use of Electromagnetic Geotomography for The Investigation of Mining Damage Areas, *Publs. Inst. Geophys. Pol. Acad. Sc.*, M-22 (310), 1999, pp. 301–311.
[2]   G. Demoment, Image Reconstruction and Restoration: Overview of Common Estimation Structures and Problems, *IEEE Trans. on Acoustics, Speech and Signal Processing*, Vol. 37, No. 12, December 1989, pp. 2024 – 2036.
[3]   N. H. Clinthorne, T. S. Pan, P. Ch. Chiao, W. L. Rogers, J. A. Stamos, Preconditioning Methods for Improved Convergence Rates in Iterative Reconstruction, *IEEE Trans. on Medical Imaging*, Vol. 12, No. 1, March 1993, pp. 78 – 83.
[4]   Image Processing Toolbox for MATLAB 5.2

TOLERANCE OF THE SOLUTION TO THE PROBLEM OF A BURIED WAVEGUIDE SYNTHESIS

N.E.Nikolaev, and V.V.Shevchenko
Russian Peoples' Friendship University
Mikluho-Maklaya, 6, Moscow,117198, Russia
E-mail: nnikolaev@sci.pfu.edu.ru

ABSTRACT

The problem of finding the permittivity profile of graded-index single-mode planar waveguide after the given mode parameters is considered. For solving this inverse problem some universal mathematical model of profile is implemented. It has the form of a double truncated exponential-power function. Each set of function parameters corresponds to a particular distribution of permittivity in the waveguide. Multiply repeated numerical solution of direct problem by special algorithm using the least-square method enables to select the function parameters for a certain set of mode parameters. For solving the inverse problem a knowledge of the propagation constants is required. Exact reconstruction of the waveguide parameters can be obtained by using four criteria. Nevertheless, there are always some errors in determination of the propagation constants. The tolerance of the solution to these errors is investigated.

1.   For describing the permittivity profile in a waveguide, the authors propose a reasonably universal function [1, 2]. It has the following form:

$$\varepsilon(y) = \varepsilon_g [1 - 2\Delta_j f_j(y)], \tag{1}$$

where
$$f_j = \left\{ \frac{1 - exp\, q_j \varphi_j(y)}{1 - exp\, q_j} \right\}^{p_j}, \tag{2}$$

j=1, when $0 \le y \le r$; j=2, when $r \le y \le 1$,

$$\Delta_1 = \frac{\varepsilon_g - \varepsilon_b}{2\varepsilon_g} \ , \ \Delta_2 = \frac{\varepsilon_g - \varepsilon_s}{2\varepsilon_g} \ , \ \varphi_1 = 1 - \frac{y}{r} \ , \ \varphi_2 = 1 - \frac{1-y}{1-r} \tag{3}$$

Here $\varepsilon(y) = \varepsilon_b$, if y=0 ; $\varepsilon(y) = \varepsilon_g$, if y=r ; $\varepsilon(y) = \varepsilon_s$, if y=1 .

This model can be used for the studies of the waveguides of vastly different types. The process of solving the direct problem becomes easier when compared with other methods, such as, for example, the WKB-method [3-6]. Besides, those methods cannot be used in the case of a single-mode waveguide. The usage of the Shift Formula Method (SFM) [7] makes such a solution possible.

The SFM is based on the representation of permittivity profile using the double truncated exponential-power function (1). This method is convenient to solve direct problem for a single-mode waveguide. Besides, it performs very well in solving the inverse problem [2, 8]. The advantage of SFM over other methods lies in the fact that it uses the mathematical model (1) to represent the permittivity profile of a waveguide.

According to this model the permittivity distribution in the waveguide is determined by 9 parameters. Usually some of them can be specified beforehand considering the implantation process of fabricating the buried waveguides [9]. So the problem of profile reconstruction reduces to finding the parameters p_1, q_1, p_2, q_2 (see formula (1)). The form of the profile can be easily changed by setting the values of these four parameters. Over methods (for example, method of stratification) require much more parameters to describe the profile. The direct problem consists in finding the values of cut-off frequencies and dispersion characteristics of the waveguide with the known profile. In this case methods differ slightly, because one needs to describe the profile only once. However, the situation changes drastically when solving the inverse problem. The aim of the inverse problem consists just in finding the permittivity profile. In this case it is much more easy to find no more than four parameters. Besides, it needs less time.

2. The process of a waveguide profile reconstruction consists of several steps [2]. Firstly, it should be noted that to solve the problem one has to know two values of propagation constants within the limits of single-mode operating regime, i.e. it is suggested that for some waveguide the normalized propagation constants B_1, B_2 at two normalized frequencies V_1, V_2 [10] are known. Then some arbitrary profile parameters p, q are chosen. For the waveguide with such parameters the propagation constants are calculated at two frequencies V_1, V_2. Then they are compared with propagation constants B_1, B_2 of the studied waveguide. The difference between the values of propagation constants are estimated using several criteria. The first one is the least-square method, the second is the closeness of the values $(B_1 - B_2)/(V_2 - V_1)$ calculated for the modes of both waveguides.

These operations are repeated many times till both criteria become close with some preset accuracy.

Such a process was described in [2], and it yielded good accuracy in the selection of profile parameters. The application of two criteria enables one to find a waveguide which has the same propagation constants B_1, B_2 as the studied waveguide.

The main demerit of such a process lies in the fact that the found waveguide is not unique: there are many waveguides having the same normalized propagation constants B_1, B_2 at two normalized frequencies V_1, V_2.

3. In order to reduce the number of the waveguides with the same propagation constants, two more criteria were implemented. These criteria are the following: the closeness of the tangents to dispersion curve at two normalized frequencies V_1, V_2 for the studied waveguide and the waveguide under consideration.

Simultaneous application of all four criteria allows to find the parameters p_1, q_1, p_2, q_2 that characterise some waveguide. The important thing to state is that the found waveguide is the only one which satisfies all four criteria.

At the very beginning of the process the studied waveguide was not chosen arbitrary. In order to test, at the end of the process, what profile parameters have been found, the normalised propagation constants B_1, B_2 were calculated for the waveguide with preset parameters.

It is significant to note that the profile parameters of the waveguide found at the process coincide with preset parameters. It means that the process has resulted in exact reconstruction of the waveguide profile.

Figure 1. illustrates the obtained result. Here, the curves show the correspondence between parameters q_1 and q_2 for some correlation between parameters p_1 and p_2 --- at the figure symbol α_p means: $\alpha_p = arctg(p_2 / p_1)$. The curves (a) were obtained using only two criteria [2, 8]. The curves (b) and (c) are the result of application of two more criteria. One can see that the curves (b) and (c) intersect at the point which corresponds to the unique

correlation between all four parameters p_1, q_1, p_2, q_2. At the figure these parameters are: $q_1 =$ -3.0, $q_2 = -2.0$, $p_1 = p_2 = 4.0$; and they coincide with the preset parameters.

4. It is important to study the tolerance of the solution. On this question some notes can be made. The normalized propagation constants B_1, B_2 serve as the basis values for finding the profile parameters. However, they can be determined with some mistakes. In order to test the influence of these mistakes on the values of profile parameters found at the process, some analysis was held. The essence of it is as follows. It was supposed that the propagation constants B_1, B_2 were not determined exactly, i.e. instead of exact values the values with some deviation were used. Then the obtained parameters were compared with the parameters obtained from the exact values of propagation constants. The conclusion is the following: the mistakes in determining the values of propagation constants have some influence on the resulting parameters, but it is not considerable.
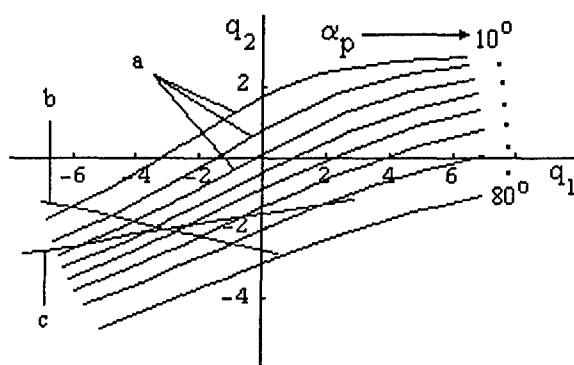
Figure 1.

The same studies were held on the influence of mistakes in determining the values ε_h, ε_g, ε_s, r. They showed the same thing as for mistakes in determining the propagation constants, i.e. these mistakes must be taken into account only if they are considerable.

References

[1] N.E.Nikolaev, V.V.Shevchenko, *Radiotekhnika i Elektronika*, 1997, v.42, No.8, p.901 (in Russian).

[2] N.E.Nikolaev, V.V.Shevchenko, *MMET'98 Proceedings*, Kharkov, 1998.

[3] D.Marcuse, *IEEE J.Quantum Electr.*, 1973, v.QE-9, No.10, p.1000.

[4] J.Janta, J.Ctyroky, *Optics Comm.*, 1978, v.25, No.1, p.49.

[5] J.M.White, P.F.Heidrich, *Appl. Opt.*, 1976, v.15, No.1, p.151.

[6] L.M.Andrushko, Dielectric Inhomogeneous Waveguides of Optical Range, Kiev: Tekhnika, 1983.

[7] N.Espinosa-Ortiz, V.V.Shevchenko, *Radiotekhnika i Elektronika*, 1994, v.39, No.3, p.39 (in Russian).

[8] N.E.Nikolaev, V.V.Shevchenko, *Radiotekhnika i Elektronika*, 1998, v.43, No.6, p.703 (in Russian).

[9] M.L.Von Bibra, A.Roberts, *J.Lightwave Techn.*, 1997, v.15, No.9, p.1695.

[10] T.Tamir, Guided-Wave Optoelectronics, Springer-Verlag Berlin Heidelberg,1988.

ABOUT PERMITTIVITY PROFILES HAVING JOINT ANALYTIC SOLUTIONS
FOR HORIZONTALLY AND VERTICALLY POLARIZED WAVES

Mironov V.L., Komarov S.A., and Sukovatov Y.A.

Department of Physics, Altai State University,
Dimitrov Street, 66, Barnaul, 656099, Russia
E-mail: klesch@phys.dcn-asu.ru

Theoretical study of polarization properties of scattered microwave signals depending on vertical variations of soil moisture content is of great interest [1]. Distribution of moisture in soil can be different: the upper layer is dry and the lower is wet and vice versa, other details of the distribution are also of interest. Naturally the question arises: what information about the distribution of moisture in soil can be obtained using microwave polarization measurements? Permittivity of soil varies with variations of moisture content. For studying this problem we must solve problems of microwave scatter from terrains with different permittivity profiles. In [1], numerical solutions of equations for horizontally polarized electromagnetic waves (H-waves) and vertically polarized waves (V-waves) in the region of variation of the permittivity were used. However, analytic solutions of the problems are also of interest, since they allow more readily to study the dependence of solution from parameters. Analytic solutions for H-waves for exponential permittivity profile were presented in [2]. Equations for H- and V-waves are different. Usually (for a particular permittivity profile) we have an analytic solution for H-waves and no such a solution for V-waves.

In the present paper we consider two model permittivity profiles for which we obtain joint analytic solutions for H- and V-waves: hyperbolic and square hyperbolic profiles. For the case of hyperbolic profile solutions for H- and V-waves are confluent hypergeometric functions with the integral second indices. For the case of square hyperbolic profile we have confluent hypergeometric functions with non-integral second indices. The first profile can model transition layer, and the second - region with the permittivity maximum. Solutions obtained can be used for testing of computer programs, for modelling of soil moisture distribution influence on the polarization properties of scattered microwave signals.

Let us divide all the system into three regions:

$$region1. : z > 0 \varepsilon(z) = 1 \tag{1}$$

$$region2. : -d \leq z \leq < 0 \varepsilon(z) = \frac{\varepsilon_1 \varepsilon_2}{(\varepsilon_2 - \varepsilon_1)(z/d) + \varepsilon_2} \tag{2}$$

$$region3. : z \leq -d \varepsilon(z) = \varepsilon_2 \tag{3}$$

For the region 2 we have the following equation for v-waves:

$$\frac{d^2 H_y}{dz^2} - \frac{\varepsilon' dH_y}{\varepsilon dz} + \left(\frac{\varpi^2}{c^2} \varepsilon(z) - K_x^2 \right) H_y = 0 \tag{4}$$

Its solution is:

$$H_y = C_1 e^{K_x \tau / k} F(\alpha_v, 1, \eta) + C_2 e^{K_x \tau / k} G(\alpha_v, 1, \eta) \tag{5}$$

where $\alpha_v = 1/2 - \dfrac{\varpi^2 \varepsilon_0}{2c^2 k K_x}$, $\varepsilon_0 = \varepsilon_1 \varepsilon_2$, $k = \Delta / d$, $\Delta \varepsilon = \varepsilon_2 - \varepsilon_1$, K_x is the x-component of

the wave vector, ω is the frequency, $c^2 = (\varepsilon_0 \mu)^{-1}$, $\tau = kz + \varepsilon_2$, $\eta = 2K_x \tau / k$.

Equation for H-waves is

$$d^2 E_y / dz^2 + (\varpi^2 / c^2 \varepsilon(z) - K_x^2) E_y = 0 \tag{6}$$

and has the following solution:

$$E_y = C_1 e^{K_x \tau / k} F(\alpha_h, 0, \eta) + C_2 e^{K_x \tau / k} G(\alpha_h, 0, \eta) \tag{7}$$

where $\alpha_h = -\dfrac{\varpi^2 \varepsilon_0}{2c^2 k K_x}$.   Using boundary conditions $E_t = const$, $H_t = const$ we can

determine 5 constants for solution of the equations in all three regions and find the reflection coefficient for H- and V-waves:

$$R_{v,h} = \frac{1 + N_{v,h}}{1 - N_{v,h}} \tag{8}$$

where

$$N_{v,h} = (-2K_x / i\varepsilon_1 K_{z1}) \frac{L_F\left(-F_{v,h}(0)/2 + \dfrac{\partial F_{v,h}(0)}{\partial \eta}\right) - L_G\left(-G_{v,h}(0)/2 + \dfrac{\partial G_{v,h}(0)}{\partial \eta}\right)}{L_F F_{v,h}(0) - L_G G_{v,h}(0)} \tag{9}$$

where

$$L_F = (iK_{z3} - K_x) F_{v,h}(-d) + \frac{\partial F_{v,h}(-d)}{\partial \eta} 2K_x \tag{10}$$

$$L_G = (iK_{z3} - K_x) G_{v,h}(-d) + \frac{\partial G_{v,h}(-d)}{\partial \eta} 2K_x \tag{11}$$

here $F_{v,h}(-d) = F_{v,h}(\alpha_{v,h}, \gamma_{v,h}, z = -d)$ and so on, $K_{z3} = \sqrt{\varpi^2 \varepsilon_2 / c^2 - K_x^2}$.

From equation (14) we can find the dependence of the reflection coefficient on the angle of the incidence having fixed 3 parameters of the non-uniform layer ε_1, ε_2 and d. If the permitivity increases (decreases) with $-z$ we have $\varepsilon_2 > \varepsilon_1 (\varepsilon_1 > \varepsilon_2)$. Hypergeometric functions in (14) are different for H- and V-waves. So we have different angular dependence of the reflection coefficient for these waves. Thus, using details of the angular dependence of the reflection coefficient we can, as the matter of principle, determine relations between 3 parameters of the non-uniform permittivity layer.

Similar solutions are obtained for the layer $\varepsilon(z) = \varepsilon_0 / (kz + \beta)^2$.

REFERENCES

[1] S.A. Komarov, and A.I. Yakushev, Radiotechnics and electronics, V.34, No.6, 1998, pp.650-656. (In Russian).
[2] V.V. Bogorodsky, A.I. Kozlov and L.T. Tuchkov. Radiothermal emission from terrain, Leningrad, Hydrometeoizdat, 1977. (In Russian).

IMAGING OF "ILLUMINATED" PART OF SMOOTH CONVEX PERFECTLY CONDUCTING SURFACE FROM FULL POLARIZATION RECEIVER DATA

A.V. Muzychenko

Kharkov Military University, Kharkov, Ukraine

ABSTRACT

The technique of imaging of "illuminated" part of convex perfectly conducting electrically large object is proposed. The technique is based on a relationship between the scatterer geometry and high-frequency approximation of its transient characteristic.

INTRODUCTION

For consideration of a number of applied problems there is a need to determine the scatterer geometrical shape from radar information. In this paper, a technique of imaging of "illuminated" part of a convex perfectly conducting electrically large object is proposed. This technique is based on a relationship between the object geometry and its transient characteristic (TC). From full polarization receiver data it is possible to determine principal curvatures of the object surface at the bright point. This information allows us to build a fitted paraboloid with vertex at the bright point. This paraboloid is taken as initial approximation of object surface near the bright point. Then a series of steps in time is carried out. On each step at first the imaged surface is approximated by mentioned surface and then it is improved with a correction determined from the difference between the values of real TC and TC calculated from already imaged surface part. The procedure is continued till moment when the boundary of "illuminated" part is reached.

DETERMINATION OF PRINCIPAL CURVATURES AT THE BRIGHT POINT

Obtaining of principal curvatures and principal directions at the bright point is based on the iterations of Fock's equation. The technique developed in [1] enables us to evaluate two terms of beam series in the general bistatic case. For magnetic vector of diffracted field one can obtain:

$$\vec{H}(t) = \vec{A}_0 \Omega_0(t - t_0) + \vec{A}_1 \Omega_1(t - t_0),$$

where function $\Omega_0(t)$ describes time structure of sounding signal, $\Omega_1(t) = \int_0^t \Omega_0(\tau) d\tau$, $\vec{A}_0$, $\vec{A}_1$ are the vector coefficients of factorization that in the special case of monostatic radar system can be written as:

$$\vec{A}_0 = \frac{1}{2d\sqrt{\kappa_1 \kappa_2}} \vec{p}^0, \quad \vec{A}_1 = \frac{1}{4d\sqrt{\kappa_1 \kappa_2}} \left[-\vec{\tau}_1(\kappa_2 - \kappa_1)\cos\beta + \vec{\tau}_1(\kappa_2 - \kappa_1)\sin\beta - \frac{\vec{p}^0}{2}(\kappa_2 + \kappa_1) \right],$$

where d is distance to object, κ_1, κ_2 are principal curvatures at bright point, $\vec{\tau}_1, \vec{\tau}_2$ are unit vectors of principal directions at bright point, $\vec{p}^0$ is the unit vector of polarization corresponding to the direction of magnetic field vector of the sounding wave, β is the angle between the unit vectors $\vec{p}^0$ and $\vec{\tau}_1$, $(0 \le \beta \le \pi)$.

However, taking into account the type of the $\vec{A}_0$ and $\vec{A}_1$ coefficient vector dependence for finding the surface parameters κ_1, κ_2 and β, it is necessary to receive the signals on two orthogonal polarizations, $\vec{p}^0$ и $\vec{p}_\perp^0$. After discretization and some transformations it is possible to obtain the expression for κ_1, κ_2 and β.

ALGORITHM OF IMAGING OF "ILLUMINATED" OBJECT SURFACE PART

Imaging of surface is performed in the coordinate system related to the object. Its center is located at the bright point, z axis coincides with the sounding direction. Time of wave propagation and longitudinal coordinate in light meters are counted along the z-axis. The x- and y-axes form a right-hand triplet of orthogonal vectors with the z-axis. These vectors are directed along the principal axes of surface at the bright point. The imaged surface is described by polar coordinates ρ, φ in each time section $z = t$.

Suppose that unknown surface near the bright point is approximated well by a fitted paraboloid with equation $z = ax^2 + by^2$, where a and b are principal curvatures at the bright point. Denote the contour that terminates this paraboloid at $z = t_0$ as Γ_{t_0}. At each point of this contour the normal unit vector to the paraboloidal surface $\vec{n}_0(\varphi)$ and unit vector of the tangent to Γ_{t_0} contour $\vec{\tau}_0(\varphi)$ are determined. The vector $\vec{p}$ is built from these vectors as $\vec{p} = \vec{n}_0 \times \vec{\tau}_0$. Then straight lines with directing vectors $\vec{p}$ are built till crossing the plane $z = t_0 + \Delta t$. The set of points of crossing of these lines with the plane $z = t_0 + \Delta t$ forms contour $\Gamma_{t_0 + \Delta t}$. However, actual values of $\rho(\varphi, t_0 + \Delta t)$ function will differ from the calculated ones. To take into account corrections, the $\alpha(\varphi)$ function is introduced which modifies the $\vec{p}$ vector as $\vec{p}_1 = \vec{p} + \alpha(\varphi)(\vec{p} \times \vec{\tau}_0)$.

In [2] it has been shown that projection of perfectly conducting object TC onto the direction perpendicular to sounding direction in the physical-optics approximation may be represented as a contour integral: $\Psi(t) = \vec{R}^0 \int_{\Gamma_t} \vec{f}(\vec{n}) dl$,

where $\vec{R}^0$ is the unit vector of sounding direction, $\vec{f}(\vec{n}) = \dfrac{\vec{n}}{\sqrt{1 - (\vec{R}^0 \cdot \vec{n})^2}}$, $\vec{n}$ is the unit vectors of outer normal to scatterer surface at points of Γ_t contour.

Taking into account this correction, the expression for TC at the moment $t_0 + \Delta t$ can be written as:

$$\Psi_i(t_0 + \Delta t) = \int_0^{2\pi} \alpha(\varphi)\Phi(\varphi)d\varphi + \Psi^0(t + \Delta t), \qquad (2)$$

where $\Psi_i(t_0 + \Delta t)$ is the value of the TC projection on the direction of the i-th polarization of receiving antenna, $\Phi(\varphi)$ is the function determined from the parameters of improved surface,

$$\Psi^0(t_0 + \Delta t) = \vec{R}^0 \int_0^{2\pi} \frac{\vec{n}_0(\varphi, t_0 + \Delta t)}{\sqrt{1 - (\vec{R}^0 \cdot \vec{n}_0(\varphi, t_0 + \Delta t))^2}} \sqrt{\rho^2(\varphi, t_0 + \Delta t) + \rho_\varphi^2(\varphi, t_0 + \Delta t)} d\varphi, \quad \rho_\varphi \text{ is the}$$

angular derivative of the radius-vector ρ.

Thus for determining a correction we have the equation: $\int_0^{2\pi} \alpha(\varphi)\Phi(\varphi)d\varphi = \Delta\Psi_i$,

where $\Delta\Psi_i = \Psi_i - \Psi^0$. This equation has an infinite set of solutions. However, taking into account smoothing character and small value of $\alpha(\varphi)$ function, we shall find a solution with the minimum norm. It can be written, in the case of metric C, as $\alpha_0(\varphi) = \dfrac{\Delta\Psi_i \operatorname{sgn}\Phi(\varphi)}{\int_0^{2\pi}|\Phi(\varphi)|d\varphi}$ and

in the case of L_2-metric as $\alpha_0(\varphi) = \dfrac{\Delta\Psi_i\Phi(\varphi)}{\int_0^{2\pi}\Phi^2(\varphi)d\varphi}$.

Moreover, this value is chosen as $\alpha_0(\varphi)$ for which $|\Delta\Psi_i|$ is the smallest.

After finding the improved $\bar{p}$ vector we build new ruled surface with generating rays parallel to the $\bar{p}$ vector and then find points of crossing of this surface with the plane $z = t_0 + \Delta t$. So, the contour $\Gamma_{t_0+\Delta t}$ is corrected. After that the next iteration in the contour $\Gamma_{t_0+\Delta t}$ improving is carried out. This procedure is performed until the value of the difference $|\Delta\Psi_i|$ is greater than any small ε specified before. Then the next step in time is carried out and contour $\Gamma_{t_0+2\Delta t}$ is determined. This contour is improved as it has been described above.

The procedure of surface imaging is continued till the moment when the boundary of "illuminated" part is reached.

For testing the algorithm, the imaging of "illuminated" parts of several simple surfaces sounded along one of the axes of symmetry was carried out. In Figures 1 and 2, the results of imaging for a sphere with radius of 3 m (Fig. 1) and an ellipsoid with semi-axes of 3, 2 and 1m at the sounding along the smallest semi-axis (Fig. 2) are presented.
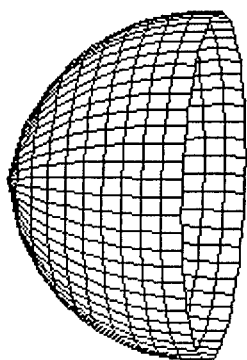
Fig.1   Fig.2

REFERENCES

[1] A.Y.Povzner, I.V.Sukharevsky, «About finding of asymptotic of short waves diffraction problems solutions». *J. Comput. Maths. and Math. Physics*. 1961, vol.1, №2 p.224-245 (in Russian).

[2] O. I. Sukharevsky, V. A. Vasilets, "Impulse characteristics of smooth objects in bystatic case", *J. Electromagnetic Waves and Applications*, 1996. - Vol.10 – p.1613-1622.

ABOUT ONE METHOD OF SOLUTION
OF THE SYNTHESIS PROBLEMS OF RADIATING SYSTEMS
AFTER THE GIVEN POWER DIRECTIVITY PATTERN

P.O. Savenko

Pidstryhach Institute for Applied Problems of Mechanics and Mathematics,
National Academy of Sciences of Ukraine,
3-B, Naukova Str., 79000 Lviv-MSP, Ukraine
E-mail: savenko@iapmm.lviv.ua

ABSTRACT

A numerical solution method of the synthesis problems of radiating systems after the given power directivity pattern (DP) is presented. On the operational level the variational statement of the problems that takes into account a mean-square discrepancy between the given and synthesized DPs, and also weighed restriction on norm the extrinsic sources of excitation is considered. The existence theorems of quasi-solutions are proved. It is shown that the problem has nonunique solution. Numerical algorithms of their determining are built and discussed.

STATEMENT OF THE SYNTHESIS PROBLEM, EXISTENCE OF QUASI-SOLUTIONS

As known [1], a problem of excitation of electromagnetic field in the unlimited homogeneous isotropic space by the driving sources, which are localized in some domain $\overline{V} \in R^3$ and vary in time as $e^{i\omega t}$ (here, ω is the frequency of oscillations) is reduced to the set of the Maxwell equations with respect to the vectors E, H of the complex amplitudes of electrical and magnetic field. Asymptotic of solutions of this set for $r \to \infty$ in the spherical coordinate system has the following form:

$$E(r, \vartheta, \varphi) = -i\omega\mu \frac{e^{-ikr}}{4\pi r}\left\{0, f_\vartheta(\vartheta, \varphi), f_\varphi(\vartheta, \varphi)\right\},$$

$$H(r, \vartheta, \varphi) = ik \frac{e^{-ikr}}{4\pi r}\left\{0, f_\varphi(\vartheta, \varphi), -f_\vartheta(\vartheta, \varphi)\right\}, \qquad (1)$$

where $f_\vartheta(\vartheta, \varphi)$, $f_\varphi(\vartheta, \varphi)$ are components of the vector field DP of radiating system. Abstracting from a concrete type of radiating system, the functions $f_\vartheta(\vartheta, \varphi)$, $f_\varphi(\vartheta, \varphi)$ can be represented with the aid of linear operator $A = \{A_\vartheta, A_\varphi\}$:

$$f = AI \qquad \left(f_\nu = A_\nu I, \quad \nu = \vartheta, \varphi\right), \qquad (2)$$

which acts from the complex Gilbert space $H_I = L^2[\overline{V}] \oplus L^2[\overline{V}] \oplus L^2[\overline{V}]$ of square integrable vector-valued functions $I = \{I_x, I_y, I_z\} \in H_I$ into the complex space of the vector-valued continuous on the compact $\overline{\Omega} \in R^2$ (or $\overline{\Omega} \in R^1$) functions of real arguments $C_f^{[2]} = C[\overline{\Omega}] \oplus C[\overline{\Omega}]$. The form and the properties of operators A_ν depend on the type and geometry of radiating system. The power DP of the radiating system is determined by the expression

$$N(\vartheta, \varphi) = |f(\vartheta, \varphi)|^2 = |f_\vartheta(\vartheta, \varphi)|^2 + |f_\varphi(\vartheta, \varphi)|^2. \qquad (3)$$

In the elementary aspect, this problem can be formulated as a problem of determination of solutions to the nonlinear operational equation of the first kind

$$\left|AI\right|^2 \equiv \left|A_\vartheta I\right|^2 + \left|A_\varphi I\right|^2 = N_0, \tag{4}$$

where $N_0(\vartheta, \varphi)$ is a real nonnegative continuous on the compact $\overline{\Omega} \in R^2$ (or $\overline{\Omega} \in R^1$) function, which cannot belong to the space of values of nonlinear operator $\left|AI\right|^2$. The problem (4) is essentially ill-posed [2]. In view of this, the problem of determination of quasi-solutions to equation (4), as a problem of minimization of a functional is formulated as

$$\sigma_\beta(I) = \left\| N_0 - \left|AI\right|^2 \right\|_{H_f}^2 + \beta \left\| I \right\|_{H_I}^4 \equiv \left\| N_0 - \left|f\right|^2 \right\|_{H_f}^2 + \beta \left\| I \right\|_{H_I}^4 \tag{5}$$

in the space H_I, where $\beta > 0$ is a real weight parameter.

Theorem 1. Suppose that *a linear operator A injectively maps the space H_I into $C_f^{[2]}$ and is completely continuous, $N_0(\vartheta, \varphi)$ is a given non-negative continuous on $\overline{\Omega}$ function, and $\max_{(\vartheta, \varphi) \in \overline{\Omega}} N_0(\vartheta, \varphi) = 1$. Then in H_I at any value β $(0 < \beta < +\infty)$ there exists only one point of absolute minimum of the functional $\sigma_\beta(I)$, and from any minimizing sequence it is possible to select a subsequence converging weakly to one of the points of absolute minimum.*

Since $H_I = L^2[\overline{V}] \oplus L^2[\overline{V}] \oplus L^2[\overline{V}]$ is a reflexive Banach space, to prove the theorem it is enough to show [3] the realization of the following conditions: 1) $\sigma_\beta(I)$ is a semicontinuous lower functional; 2) $- \lim_{\|I\|_{H_I} \to \infty} \sigma_\beta(I) = +\infty$.

2. The Euler equation of functional σ_β. For a numerical determination of valleys and study of their qualitative characteristics, we shall use the Euler equation, which is determined from the necessary condition for a functional minimum [3] $D\sigma_\beta(I, \psi) \equiv 0$:

$$I = \frac{2}{\beta v} A^*(N_0 \cdot AI) - \frac{2}{\beta v} A^*\left(\left|AI\right|^2 \cdot AI\right) \qquad (v = \|I\|_{H_I}^2) \tag{6}$$

in the space H_I. The equation obtained is a nonlinear operational equation of the Hammerstein type. Acting on both parts of equality (6) by the operator A and taking into account that A realizes an injective mapping from H_I into $C_f^{[2]}$, we obtain an equivalent to (6) equation with respect to the synthesized DP in the space $C_f^{[2]}$:

$$f = B(f) \equiv \frac{2}{\beta v} AA^*(N_0 \cdot f) - \frac{2}{\beta v} AA^*\left(\left|f\right|^2 \cdot f\right). \tag{7}$$

Corollary 1. *Since the functional σ_β is differentiable in the Gateaux sense on H_I, it has only one valley and posses the m-property (the valley is an interior point of some convex set, inhering H_I), the equation (6) in the space H_I and equation (7) in the space H_f have, at least, one solution each.*

Lemma 1. *Under conditions of the theorem 1, for limited values of parameters β, v: $0 < \beta v < +\infty$ $B(f)$ is a completely continuous operator in space $C_f^{[2]}$.*

Corollary 2. *Since for the elements of relatively compact subset of normed space the strong and weak convergence coincide* [4], *then from the theorem 1 and lemma 1 it follows that, if* $\{I_n\}$ *is a minimizing sequence of functional* $\sigma_\beta(I)$, *which weakly converges to a valley* I_*, *then the sequence* $\{f_n = AI_n\} \in C_f^{[2]}$ *converges uniformly in* $C_f^{[2]}$ *to* $f_* = AI_*$.

3. Numerical solution of the problem

The equations (6), (7) are solved numerically by the method of successive approximation. The iterative process is built as follows:

$$I_{n+1} = \frac{1}{\beta v_n} A^*(N_0 \cdot f_n) - \frac{1}{\beta v_n} A^*(|f_n|^2 \cdot f_n), \quad f_{n+1} = AI_{n+1} \quad (n = 0,1,2,...).(8)$$

Parameter v_n on each step of iteration is determined by the formula

$$v_n = \exp\left(\frac{2}{3}\ln\left(\|\Phi(I_n)\|_{H_I} / \beta\right)\right), \text{ where } \Phi(I_n) = A^*\left(N_0 - |AI_n|^2\right) \cdot AI_n \equiv A^*\left(N_0 - |f_n|^2\right) \cdot f_n.$$

For the convergence of sequential approximations (8) it is enough to show [5] the fulfillment of the following two conditions: 1). The operator $B(f)$ (Eq. (7)) transforms some closed convex set $W_d = \{f : \|f - f_*\| \le d < 1\}$ of the Banach space $C_f^{[2]}$ into itself. 2). The operator $B(f)$ is differentiable at each point of the set W_d in the Frechet sense and $\sup_{f \in W_d} \|B'(f)\|_C = \delta < 1$.

The fulfillment of the condition 1) approves

Lemma 2. *If* $\{f_*, v\}$ *is a solution of the equation* (7), $\beta v \ge \|AA^*\|$, $\|N_0\|_C = 1$, *then the operator* $B(f)$ *transforms a full-sphere* $W_d \subset C_f^{[2]}$ *into itself.*

The condition 2) substantially depends on the type of radiating system and form of the operators A, A^*. Its fulfillment by an example of a problem of synthesis of a flat rectangular antenna array is easy to show.

A numerical example of the synthesis of rectangular array consisting from 11×11 radiators, placed in the plane XOY, will be presented.

CONCLUSION

In summary, we shall note that iterative process (8) can be simply generalized to the synthesis of various types of radiating systems. For this purpose it is necessary to determine the type and properties of the operator A, which with required accuracy characterizes DP of radiating system. Thus only conditions of convergence of iterative process are depended on the properties of the operators A and A^*.

REFERENCES

[1] Markov, G.T., Sazonov, D.M. *Antennas*, Energiya Publ, Moscow, 1975 (in Russian).

[2] Tichonov, A.N., Arsenin, B.Y. *Methods of Solution of Incorrect Problems*, Nauka Publ, Moscow, 1979 (in Russian).

[3] Vainberg, M.M. V*ariational Method and Method of Monotone Operators*, Moscow, Nauka Publ, 1972 (in Russian).

[4] Vainberg, M.M., *Functional Analysis*,. Moscow, Nauka Publ., 1979 (in Russian) .

[5] Kantorovich, G.P., Akilov, L.V. , *Functional Analysis*, Moscow, Nauka Publ., 1977 (in Russian).

APPLICATION OF PONTRYAGIN'S PRINCIPLE OF MAXIMUM TO THE INVERSE PROBLEMS OF SCATTERING

D.O. Batrakov, and M.M. Tarasov.

Chair of Theoretical Radiophysics, Radiophysical Dept.,
Kharkov National University, Svobody Sq. 4, 310077, Kharkov-77, Ukraine.
tel. 8- (0572) -45-7257, E-mail: Dmitry. O.Batrakov @univer. Kharkov. UA

ABSTRACT

We are concerned with the practical application of a new approach to the inverse problems of electromagnetic wave scattering. Our main goal is retrieval of an unknown permittivity distribution. Within the framework of such a statement the problem is reduced to minimization of some smoothing functional. Further minimization is carried out with the use of Pontryagin's principle of maximum, instead of approaches which are based on the Newton-Kantorovich iterative technique and Euler's equations.

PROBLEM STATEMENT

Suppose that it is required to estimate (i.e., to find approximately) a distribution of $\varepsilon(z)$ in the structure shown in Fig. 1. Inhomogeneous only by coordinate z layer lays on a homogeneous substrate, whose permittivity is supposed to be known and equal ε_c. Investigated layer lies between the planes $z = -H$ and $z = 0$. Thus, layer's thickness is supposed to be known and equal H. The upper half space is supposed to be a free one.
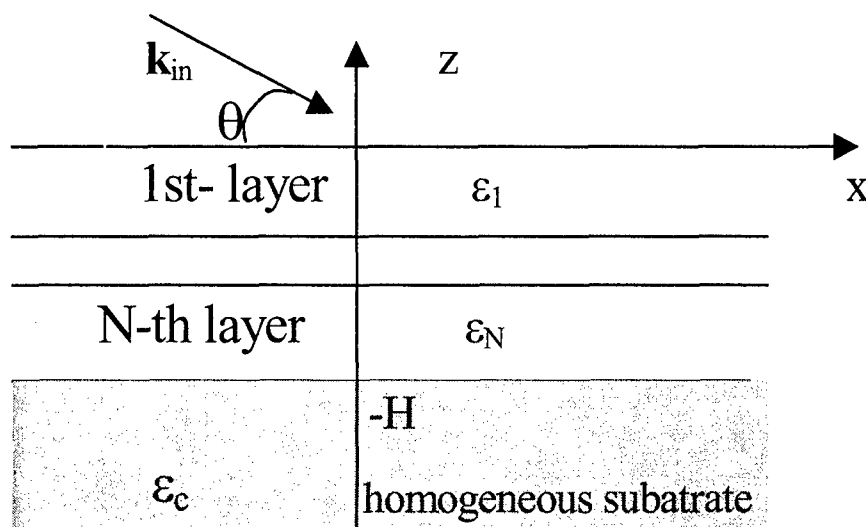
Fig.1.

Besides, anisotropy and dispersion are neglected, and ε *(z)* does not depend on x and *y*. Permeability everywhere is supposed to be equal 1.
To obtain the information about electromagnetic properties of investigated structure it is irradiated with a known electromagnetic field and some properties of the scattered field are measured. The sources of monochromatic (~*exp (-iω t)*) waves are located within the free half-space either at a finite distance from the layer or at infinity. They generate a primary

electromagnetic wave with complex amplitude $\vec{E}_0(\vec{r})$. This wave is scattered by the layer and generates internal and scattered fields.

In our investigation, it is considered an important from the practical viewpoint case when experimentally registered quantity is the power of the scattered field instead of the earlier discussed case when the complex amplitude was registered.

Thus, suppose that we know, from N experiments, the corresponding values of informative parameter a_k, k=1, 2..., N. Besides, it is supposed that we know the permittivity profile of $\varepsilon aux(z)$ of some auxiliary planar layered structure, which occupies the same volume that the probed structure and lies on the same homogeneouss substrate with ε_c. It is supposed that the unknown profile in some sense differs little from $\varepsilon aux(z)$.

As described earlier [1], one can obtain the following approximate equation for $\vec{E}_{aux}(z')$:

$$\vec{E}(z) \approx \vec{E}_{aux}(z) + \int\limits_{-D}^{0} G_e(z,z')\vec{E}_{aux}(z')\eta(z')dz' \tag{1}$$

Here, the unknown function is:

$$\eta(z) \equiv \varepsilon(z) - \varepsilon_{aux}(z). \tag{2}$$

Introduce the notations as

$$h_k = \vec{E}_k(z),\ g_k = \vec{E}_{aux}^{(k)}(z),\ \int\limits_{-H}^{0} G_e(z,z')\vec{E}_{aux}^{(k)}(z')\eta(z')dz' = \int\limits_{-H}^{0} L_k(z')\eta(z')dz', \tag{3}$$

Then the relation (1) takes the form as

$$h_k \approx g_k + \int\limits_{-D}^{0} L_k(z)\eta(z)dz; \tag{4}$$

As it was shown earlier the problem of solving (4) may be reduced to the minimization of a corresponding smoothing functional:

$$\Phi = \Phi[X(z),\eta(z)] = \int\limits_{a}^{b} F(X(z),\eta(z),z)dz. \tag{5}$$

Here, X (z) is some vector function satisfying to the vector differential equation (i.e., to a set of scalar equations)

$$\frac{dX}{dz} = f(X(z),\eta(z),z) \tag{6}$$

As it was shown in [2,3], it is possible to introduce an auxiliary vector function $\Psi(z)$, which is called conjugate to X (z), and also Hamilton's function

$$H[X(z),\Psi(z),\eta(z),z] = -F + \sum\limits_{k=1}^{N} \psi_k(z)f_k(X(z),\eta(z),z) \tag{7}$$

Thus the vector function $\Psi(z)$ satisfies so-called conjugate set of equations:

$$\frac{d\Psi}{dz} = -\frac{\partial H}{\partial X} \Leftrightarrow \frac{d\psi_k}{dz} = -\frac{\partial H}{\partial x_k},\ k = 1,2,...,N. \tag{8}$$

Pontryagin's principle of maximum [1,2] states that the function $\eta(z)$ supplies a minimum to a functional (5) in the only case when it supplies a maximum to Hamilton's function (7). Hence, to find the unknown function $\varepsilon(z)$ it is necessary to make the following steps:
1) Proceed from set (6) and form a functional (5) to find Hamilton's function by the formula (7).

2) Find the derivative of Hamilton's function (7) on x_k, k=1, 2, ...,N and obtain conjugate set (8).

3) Find analytically, from the condition $\dfrac{\partial H}{\partial \eta} = 0$, a required "optimum guidance"

$$\eta_{opt}(z) = \eta_{opt}\big(X(z),\Psi(z),z\big) \tag{9}$$

4) Substitute (9) into the basic and conjugate sets of differential equations (6), (8) and, thus, obtain a closed form of the set of equations for X(z) and Ψ(z):

$$\begin{cases} \dfrac{dx_k}{dz} = f_k\big(X(z), \eta_{opt}(X(z),\Psi(z),z),z\big) \quad k=1,2,...,N; \\[3mm] \dfrac{d\psi_k}{dz} = -\dfrac{\partial H\big(X(z),\Psi(z),\eta_{opt}(X(z),\Psi(z),z),z\big)}{\partial x_k}; \end{cases} \tag{10}$$

5). Solve the boundary-value problem for set (10) numerically and substitute the obtained vector functions *X (z)* and Ψ(z) into (9). Find the "optimum guidance" η_{opt}(z) and finally obtain ε(z) from (2).

CONCLUSION

Thus, the proposed numerical algorithm is an efficient tool for solving the one-dimensional inverse scattering problems that occur in a variety of contexts [1]. Its performance will be demonstrated via the results of several numerical experiments.

REFERENSES

[1]   Batrakov D.O. Development of physical models according to a problem of remote sensing of inhomogeneous media. – *Doctor of Sciences Thesis*, Kharkov, 1995 (in Russain).
[2] Pontryagin L.S., Boltyansky V.G., Gamkrelidze R.V., Mischenko E.F. *Mathematical Theory of Optimal Processes*, Moscow, Nauka Publ., 1983 (in Russian).
[3] Moiseev N.N. *Numerical Methods in the Theory of Optimal Systems,* Moscow, Nauka Publ., 1971 (in Russian).

IONOSPHERIC

ELECTROMAGNETICS

STRONG MESOSPHERIC ELECTRIC FIELDS AND TROPOSPHERE-MESOSPHERE COUPLING

Sergey I. Martynenko

V. Karazin Kharkiv National University, Kharkiv, Ukraine

E-mail: Sergey.I.Martynenko@univer.kharkov.ua

ABSTRACT

A new mechanism of the electron relaxation cooling in the mesosphere due to disturbances in tropospheric conductivity is discussed.

INTRODUCTION

The study of electrical coupling between the troposphere and the mesosphere is an important problem related to atmospheric electrodynamics [1]. Observations have revealed strong electric fields up to 10 V/m (see, for example, [2, 3]), which suggests that the mesosphere should not be treated as a passive element but as an active one in the atmospheric circuit. The occurrence of transient optical emissions in the mesosphere and lower ionosphere called sprites also supports the concept of strong mesospheric electric fields (see, for example, the recent review [4]). All this requires a search for new electrodynamic mechanisms for the effects of disturbances in tropospheric conductivity on the state of the lower ionosphere; one such mechanism has been discussed in [5, 6] where it has been found that the subionospheric VLF propagation anomaly is related to earthquakes and nuclear accidents. In this paper, troposphere-mesosphere coupling features are considered in the case when the effect of strong mesospheric electric fields are allowed for, and electron relaxation cooling in the mesosphere due to disturbances in the tropospheric conductivity is discussed. The effects of these processes on the ionospheric conductivity are considered.

THE TROPOSPHERE-MESOSPHERE ELECTRIC CIRCUIT

The electrodynamic troposphere-ionosphere coupling is treated using the following model of a troposphere-mesosphere electric circuit which consists of a localized or global-scale powerful source of the mesospheric current $j_m \sim 10^{-8} - 10^{-9}$ A/m^2, a local near-ground (or troposphere-stratosphere) resistance R_t, a local mesospheric load resistance R_m for the mesospheric source, and the resistance of the global atmospheric layer between the ground and the lower boundary of the ionosphere $R_a \approx 200$ Ohm. Since the electric current discharge density in the global capacitor $j_a \sim 10^{-12}$ A/m^2 under undisturbed conditions (fair-weather current, see, for example, [7]), and $j_a \sim 10^{-12}$, the j_a can be neglected. Also during undisturbed conditions, $R_t \gg R_m \gg R_a$. Then during undisturbed conditions, the integral mesospheric source loading is $R = R_m R_t / (R_m + R_t) \approx R_m$, i.e., the electrical troposphere-mesosphere coupling does not appear.

During disturbed conditions, the resistance R_t can decrease by an order of magnitude and more due to, for example, an increase in the level of near-earth radiation in the vicinity of strong earthquakes or during accidents at nuclear plants with the emission of radioactive materials (see, for example, [5, 6]). As a consequence, the ratio between R_t and R_m changes, which leads to a change in R. For example, a decrease in R_t of up to two orders of magnitude results in the inequality $R_t << R_m$, and $R \approx R_t$. Then, the potential difference U in the mesosphere, which depends on the strong electric field intensity E, becomes dependable on R_t. Because of an increase in the tropospheric conductivity, the decrease in R and R_t, in turn, results in a corresponding decrease in E and the electron temperature T_e in the mesosphere: the ionospheric electron cooling "law" under the influence of disturbances in tropospheric conductivity when strong mesospheric electric fields occur. Thus, strong mesospheric electric fields result in a new additional electrodynamic troposphere-mesosphere coupling during disturbed conditions.

DISTURBANCES IN LOWER IONOSPHERE PARAMETERS

To estimate the effect of the decrease in the mesospheric electric field intensity E on changes in lower ionosphere parameters, we have used the well known system of equations, the energy balance equation (in terms of the electron temperature T_e), the two continuity equations in the electron density N and the positive-ion density N^+ in the stratified inhomogeneous weakly-ionized plasma, and the condition of quasi-neutrality. The initial values of T_e were taken as the solutions to the above equations in quasi-steady state (E=1–10 V/m, z=60–75 km, daytime conditions) when there occur strong electric fields in the mesosphere and conductivity disturbances are absent in the troposphere.

Numerical simulations for highly disturbed tropospheric conditions, $R_t << R_m$, show that, for example, at z=60 km decreases of $\Delta E_1 = 1$ V/m and $\Delta E_2 = 10$ V/m in mesospheric electric field intensity result in decreases of a factor of 2.3 and 12, respectively, in T_e. Again, this causes the corresponding decrease in the effective electron collision frequency ν_e by a factor of 2 and 8, as well as an increase in the electron number density N by a factor of 1.1 for $\Delta E_1 = 1$ V/m and in a decrease by a factor of 2 for $\Delta E_2 = 10$ V/m. As a result, the low-frequency electron conductivity at the mesospheric heights increases, which results in a decrease in the low-frequency electron conductivity contours by approximately $\Delta z_1 \leq 5$ km and $\Delta z_2 \leq 10$ km, respectively.

Numerical simulations show that the resulting decrease in the effective electron collision frequency ν_e plays the key role. A similar lowering of the lower boundary of the ionosphere was observed, for example, in [5, 6] in VLF signals propagated over nuclear plants during accidents with the emission of radioactive materials into the atmosphere.

DISCUSSION AND CONCLUSIONS

Thus, strong electric fields occurring naturally in the mesosphere can result in new troposphere-ionosphere electromagnetic links, the manifestations of which are observed most clearly during strong disturbances of different nature in atmospheric conductivity. The atmosphere can be affected by strong earthquakes, volcano eruptions, rocket launch (see, for example, [8, 9]), accidents at nuclear plants with the discharge of radioactive materials, and other natural and anthropogenic disturbances.

Under such conditions, a decrease in the strong mesospheric electric field intensity is to be expected, and as a consequence, a relaxation electron cooling at the mesospheric heights and essential conductivity changes in the ionospheric D region occur. The latter enables radio wave techniques to be used for remotely probing these poorly understood physical processes.

REFERENCES

[1] Coupling, energetic and dynamics of atmospheric regions: CEDAR Phase III. Executive summary.– Bolder, CO: Philip Tobias Enterprises, 1996. 40 p.

[2] Goldberg, R. A. Middle atmospheric electrodynamics: status and future // J. Atmos. Terr. Phys.– 1984.– Vol. 46, No. 11.– Pp. 1083–1101.

[3] Martynenko, S. I., V. T. Rozumenko, A. M. Tsymbal, O. F. Tyrnov, and A. M. Gokov. Mesospheric electric field measurements with a partial reflection radar // J. Atmos. Electricity.– 1999.– Vol. 19, No. 2.– Pp. 81–86.

[4] Rodger, C. J. Red sprites, upward lightning, and VLF perturbations // Rev. Geophys.– 1999.– Vol. 37, No. 3.– Pp. 317–336.

[5] Martynenko, S. I., I. M. Fuks, and R. S. Shubova. Ionospheric electric-field influence on the parameters of VLF signals connected with nuclear accidents and earthquakes // J. Atmos. Electricity.– 1996. –Vol. 16, No. 3. Pp. 259–269.

[6] Fuks, I. M., R. S. Shubova, and S. I. Martynenko. Lower ionosphere response to conductivity variations of the near-earth atmosphere // J. Atmos. Solar-Terr. Phys.– 1997.– Vol. 59, No. 9.– Pp. 961–965.

[7] Bering E. A., A. A. Few, J. R. Benbrook. The global electric circuit // Phys. Today.– 1998. – Oct.– Pp. 24–30.

[8] Rauscher, E. A., W. L Van Bise. The relationship of extremely low frequency electromagnetic and magnetic fields associated with seismic and volcanic natural activity and artificial ionospheric disturbances // Atmospheric and ionospheric electromagnetic phenomena associated with earthquakes.– Tokyo: TERRAPUB, 1999.– Pp. 459–487.

[9] Hardy D. A., D. E. Hastings, D. R. Rivas, W. J. Burke, D. L. Cooke, L. C. Gentile. Beam arc distributions of shuttle pickup ions and their instabilities // J. Geophys. Res.– 1996.– Vol. 101, No. A9.– Pp. 19,629–19,647.

THE ATTENUATION OF A SPECULAR COMPONENT OF HF SIGNALS FROM THE VERTICAL SOUNDING OF IONOSPHERE

P.F. Denisenko, G.I. Kuleshov, and A.I. Skazik

Institute of Physics, Rostov State University

194 Stachky Ave., 344104 Rostov-on-Don, Russia

Phone: +7-8632-280985, Fax: : +7-8632-285044, e-mail: denis@ip.rsu.ru

ABSTRACT

The turbidity of the ionosphere for a passing electromagnetic radiation is described by the signal-to-noise ratio $\beta^2 = I_0 / \langle I_s \rangle$, which is the ratio of specular I_0 to $\langle I_s \rangle$ ensemble average scattered components of the wave field. The main method of β^2 value estimation used now is the approximation of experimentally obtained amplitude distribution laws of the reflected by the ionosphere waves with the aid of certain theoretical model. However, the same data, obtained from vertical F-region sounding, are described well enough by different models and lead to different β^2 values that differ by several orders [1].

In this paper, a new method for β^2 value obtaining is proposed. No assumptions about the amplitude distribution law of the waves reflected by the ionosphere are required. This method leads to a correct estimation of the attenuation L_s of specular component of the wave field, coupled with β^2 by the proportion $L_s = \ln\left((1 + \beta^2) / \beta^2 \right)$.

THEORETICAL CONSIDERATION

The mean powers in specular and scattered components are denoted as $I_c = \sum_{k=1}^{m} E_{0k}^2$, $\langle I_s \rangle = \langle E_s^2 \rangle$. Electron-ion and electron-molecular collisions lead to an absorption of both specular and scattered components of the field. Path lengths of scattered waves are greater than those of the specular components. A small angle scattering θ takes place in the ionosphere [2] (forward scattering) which leads to a relatively small change in path length of the order $\left[\sqrt{l^2 + (l\theta)^2} - l \right] / l = \theta^2/2 \ll 1$, where l is the path length of a specular wave. That is why the difference in absorption L_v of specular and scattered components due to collisions

is neglected. Then, the full mean power in the reflected wave $I = I_c + \langle I_s \rangle$ can be rewritten as $I = I_0 \exp(-L_v)$, where I_0 is the power of the wave incident on the ionosphere. The power in specular component decreases as $I_c = I_0 \exp(-L_v - L_s)$. This yields in

$$\gamma^2 = \beta^2 / (1 + \beta^2) = \exp(-L_s), \ \gamma^2 = I_c / I, \ \beta^2 = I_c / \langle I_s \rangle. \tag{1}$$

That is why it is necessary to estimate either L_s, or specular component to obtain the power ratio γ^2, or the signal to noise ratio β^2.

The quadrature component of the signal as a function of time can be written as

$$E(t) = \sum_{k=1}^{m} E_{0k} \cos(\Omega_k t + \varphi_{0k}) + E_s(t) \cos \varphi_s(t), \tag{2}$$

where the first item is a superposition of m specular components with amplitudes E_{0k}, phases φ_{0k}, Ω_k is the Doppler frequency shift of the specular component, E_s and φ_s are accidental amplitude and phase of superimposed scattered waves respectively. (2) can be rewritten as

$$E(t) = \sum_{k=1}^{m} (-a_k \sin \Omega_k t + b_k \cos \Omega_k t) + \varepsilon_s(t), \tag{3}$$

where $a_k = E_{0k} \sin \varphi_{0k}$, $b_k = E_{0k} \cos \varphi_{0k}$, $\varepsilon_s(t) = E_s(t) \cos \varphi_s(t)$. For discontinuous time t_i, $i = 1, 2, ..., n$, $n > 2m$ (3) yields in

$$\vec{E} = \hat{A} \vec{a} + \vec{\varepsilon}_s, \tag{4}$$

where $\vec{E}^T = [E(t_1), E(t_2), ..., E(t_n)]$, $\vec{\varepsilon}_s^T = [\varepsilon_s(t_1), \varepsilon_s(t_2), ..., \varepsilon_s(t_n)]$, $\vec{a}^T = (a_1..., a_m, b_1,..., b_m)$; $A_{k,i} = -\sin \Omega_k t_i$, $A_{m+k,i} = \cos \Omega_k t_i$ are the elements of $\hat{A}$ matrix.; the upper 'T' index means transposition. ε_s can be treated as an error vector with the zero mean and r.m.s. $\sigma_s^2 = \langle \vec{\varepsilon}_s^2(t_i) \rangle = \langle E_s^2 \rangle / 2$ elements. System (4) is solved using the Least Squares Method (LSM) by minimizing the following equation [3]

$$\Phi(a) = (\vec{E} - \hat{A}\vec{a})^T \hat{W} (\vec{E} - \hat{A}\vec{a}), \tag{5}$$

where $\hat{W}$ is considered as an identity matrix if the samples are obtained from the correlation. This leads to an LSM estimation:

$$\vec{a} = \hat{B}^{-1} \vec{E}, \ \hat{B} = \hat{A}^T \hat{A}. \tag{6}$$

Using (6), we have: $I_c = E_c^2 = \sum_{k=1}^{m}\left(a_k^2 + b_k^2\right)$, and from (5) $\langle I_s \rangle = \langle E_s^2 \rangle = 2\sigma_s^2 = 2\Phi/(n - 2m)$.

These equations allow us to obtain all necessary estimations (1).

EXPERIMENTAL RESULTS

The method for estimating the β^2, L_s parameters described above was tested on experimental data obtained in Rostov ($47°13'N$, $39°14'E$) from the November 17 to 19, 1997 with the help of a "Parus" ion-sonde at different time of the day and on different frequencies using o- and x-waves reflected from the F-region. Measurement duration of the time series of in-phase and quadrature components was 180-200 sec, sampling time $\Delta t = 0,5$ sec. It turned out, that in most cases $\beta^2 < 1$. It is seen from Fig.1. The X-axis corresponds to the values of β^2, the y-axis – to the probability that β^2 belongs to the given interval. The histogram uses the data of processing 59 samples. It is shown that the most probable values of β^2 lie between 0.2 and 0.35. Predominance of scattered component in the reflected signal witness of multifold scattering in the F–region. This scattering leads to noticeable values of attenuation L_s . This is a reliable base for the development of a new method for spectra of irregularities in electron density estimating.
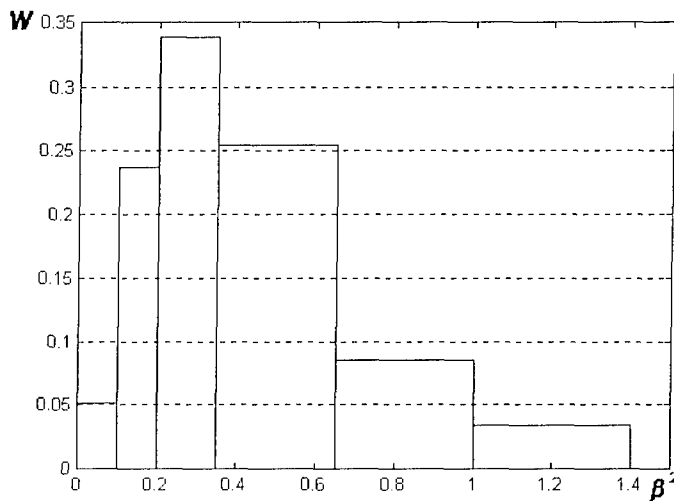
Figure 1

REFERENCES

[1] P.F. Denisenko, V.V. Sotsky, Y.N. Faer. Probability density description of the amplitudes of decameter signals vertically reflected by the F-region of the ionosphere // Geomagnetism and aeronomy. 1993. Vol. 33. No 1. p. 169.

[2] Y.L. Alpert. Distribution of electromagnetic waves and the ionosphere. M.: Nauka, 1972.

[3] Hudson D. J. Lectures on Elementary Statistics and Probability. M.: Mir, 1970.

CALCULATION OF THE UPPER ATMOSPHERE DYNAMIC CHARACTERISTICS FROM IONOSPHERIC DATA

Vitaly I.Taran, Dmitry A.Dzyubanov, Yelena I.Grigorenko and Valeri N.Lysenko

Institute of Ionosphere of National Academy of Sciences
and Ministry of Education and Science of Ukraine, Kharkov, Ukraine
E-mail: iion@kpi.kharkov.ua

ABSTRACT
Calculation of the thermospheric wind vertical component is discussed. Measured values of the vertical plasma drift velocity, charged particles temperature and parameters of electron density profile are used in calculations.

UPPER ATMOSPHERE DYNAMIC PROCESSES
The method of incoherent scattering is the most informative radiophysical method of near space investigations. By this method such ionospheric parameters as electron density Ne, electron and ion temperatures (Te and Ti), plasma drift velocity, etc. can be determined. However, ionosphere is a part of the upper neutral atmosphere and it is naturally influenced by the latter. In particular, at the F-region height ionospheric plasma is dragged by thermospheric winds, and the formation of the electron density profile is carried out in the moving substance flow [1]. Naturally, thermospheric winds effect essentially the electron density vertical distribution. As ionospheric plasma is pierced by geomagnetic field, thermospheric winds force it to move along the geomagnetic field lines and depending on the movement direction the plasma can get lower into the high recombination rate region or to drift out of it. From the other hand, analyzing electron density distribution taking into account the main physical processes which determine this distribution one can estimate certain characteristics of thermospheric wind. In particular, thermospheric wind vertical component can be calculated using measured plasma vertical drift velocity. Unknown quantity can be found from the electron density profile calculation by solving a continuity equation.

CALCULATIONS
If only vertical component of main ionospheric process will be taken into account, the continuity equation in the diffusion approximation can be presented as [1]:

$$\frac{\partial N_i}{\partial t} = \frac{\partial}{\partial z}\left[D_{in} \sin^2 I \left(\frac{\partial N_i}{\partial Z} + A N_i \right) - w N_i \right] - \beta N_i + q .$$

Here, D_{in}-ion O^+ diffusion rate,

$$A = \frac{T_e}{N_e T_i}\frac{\partial N_e}{\partial z} + \frac{m_i g}{K T_i} + \frac{1}{T_i}\frac{\partial (T_e + T_i)}{\partial z},$$

$$N_e = \left[O^+ \right] + \left[NO^+ \right] + \left[O_2^+ \right]$$

$w = v_{nx} \sin I \cos I \cos D - v_{ny} \sin I \cos I \sin D$ is the vertical component of the plasma drift caused by the thermospheric wind, v_{nx}, v_{ny} are the longitudinal and latitudinal components of the thermospheric wind velocity (positive component of longitudinal component is oriented to the North, and latitudinal one to the East), I and D are the inclination

and declination of geomagnetic field, respectively, β is the linear recombination rate, q is the ion O^+ production rate. To solve the equation, the data measured are used. Experimental values of T_e и T_i were used to calculate recombination and diffusion processes. To control the w calculations, Ne height maximum values were used.

In the analysis, the date 07.07.99 was chosen. In Figs.1 and 2, the vertical component of plasma velocity at 300 km and Ne maximum height are presented.
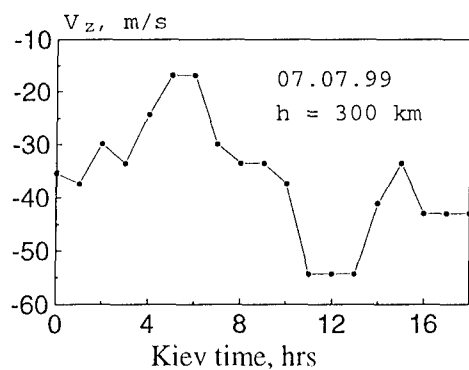
Fig. 1
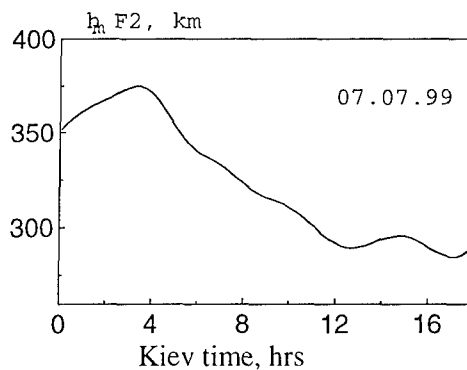
Fig. 2

Calculation results and some initial values are presented in Table 1.

Table 1.

Time , hrs	10	12	14	16
h^mF2, km	310	295	292	289
lgN_e	5.97	5.9	5.85	5.83
V_z, m/sec	-37	-50	-40	-45
w, m/sec	-22	-44	-36	-42

The w value obtained differs from the values calculated for the summer season of high solar activity (these are 0 - 5 m/sec) [2]. This indicates to the difference in the circulation patterns of the present season which is in accordance with the middle of solar activity. Besides, increasing of downward velocity w is observed in afternoon hours. It is connected to the fact that geomagnetic field declination in Kharkov is about 10°. So, in the afternoon period the conditions for carrying the plasma by the neutral atmosphere along geomagnetic field are more favorable.

REFERENCES
[1] G.S.Ivanov-Kholodny, A.V. Michailov. *Ionosphere State Prediction*. Leningrad: Gidrometeoizdat, 1980 (in Russian).
[2] D.A.Dzyubanov, G.I.Ostrovsky and A.V.Michailov. Atomic oxygen longitudinal variations in the thermosphere calculated from ionospheric data, *Geomagnetism and Aeronomy*, 1984, Vol. 24, N 1, p.69-72 (in Russian).

AN ANALYSIS OF THE PLASMA STABILITY IN THE UPPER IONOSPHERE

Vsevolod B. Ivanov and Maxim V. Tolstikov

Irkutsk State University

20 Ul. Gagarina, Irkutsk, 664003, Russia
E-mail: ivb@ivb.baikal.ru

ABSTRACT

The authors of [1] demonstrated a possible spatial enhancement of plasma density irregularities as they propagate through the topside ionosphere. The concerned phenomenon was analyzed on the basis of the numerical solution of the equation describing the evolution of small disturbances of a quasiwave origin. It is of interest to carry out an analytical treatment of this phenomenon, not based on computational methods. This paper presents the results of such a treatment.

INTRODUCTION

The cited reference gives the equation defining the dynamics of weak plasma density fluctuations under the assumption of the ambipolar motion of charged particles along geomagnetic field lines:

$$\frac{d^2n}{dz^2} - \frac{dn}{dx}\left(\frac{1}{H_p} + \frac{1}{H}\frac{\upsilon}{\upsilon+i\omega} + \frac{i\omega V}{c^2}\right) + n\left[\left(\frac{1}{HH_p} + \frac{i\omega V}{c^2 H}\right)\frac{\upsilon}{\upsilon+i\omega} - \frac{i\omega V' + (\beta+i\omega)(\upsilon+i\omega)}{c^2}\right] = 0 \quad (1)$$

The relationship was obtained from linearized equations of motion and continuity for electron-ion gas on the assumption about the harmonic character of time variations with frequency ... Allowance is made for the main processes governing the dynamics of ionospheric plasma in mid-latitudes under conditions of the upper most (above the F2-region maximum) ionosphere. Of fundamental importance is to take into account the inertia (time derivative) in the equation of motion. The movement of charges along the direction Z of the external magnetic field is considered, which was thought to be close to a vertical one. In the above equation, H is the height scale of the main component of the neutral atmosphere, atomic oxygen; Hp is the plasma height scale, υ is the collision frequency of ions with neutral atoms, V is the hydrodynamic plasma velocity (vertical component), V'=dV/dz, c is the ion sound velocity, and β is the linear recombination coefficient for the ions of the ionospheric F-region.

Background plasma is a priori treated as strongly inhomogeneous, i.e. the size of disturbances can be comparable with the scale of variation of ionospheric parameters. In such a situation, analytical methods of investigating the above equation are, strictly speaking, not correct. Nevertheless, we have made such an attempt, bearing in mind that the qualitative aspect of the characteristics identified will remain valid.

RESULTS

First, an analysis was made of the dispersion equation that follows from the basic relationship. To obtain the dispersion relation in the above equation it is necessary to use, instead of the differention, the multiplication by **ik**, where **k** is the wave number of disturbances. As a result, we get a quadratic algebraic equation relating the frequency and the wave number of the oscillations in terms of background ionospheric parameters. The equation is rather unwieldy, and

is not reproduced here; however, it can be easily solved by using systems of symbolic mathematics.

In the propagation problem, the frequency should be considered as a real positive quantity, and the equation should be solved for a complex wave number whose real part defines the wavelength, and its imaginary part is the damping or enhancement coefficient in space. Two roots of the quadratic equation correspond to two waves with oppositely directed phase velocities. As ionospheric parameters, use was made of the data obtained from a numerical ionospheric model. It should be noted that in the height range under consideration these parameters undergo very strong changes, and, for that reason, it is convenient to illustrate results of calculations in the form of plots of height dependencies of the wave number and of the damping-enhancement coefficient at fixed values of the frequency.
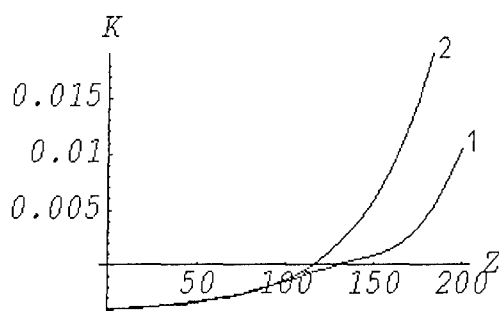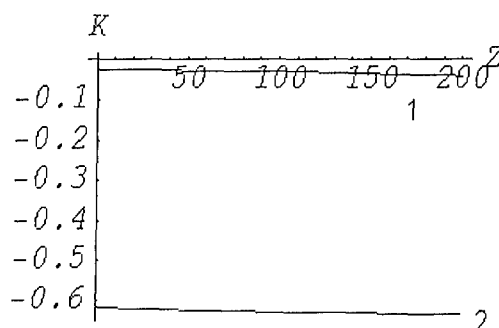
Fig. 1a   Fig. 1b

Figure 1a presents the plot of the imaginary part of the wave number versus the height Z (down from 600 km) for the frequencies of 1-0.04 s^{-1} and 2 - 0.7 s^{-1} for the branch of the oscillations, having a negative phase velocity, calculated for typical conditions of the nightside mid-latitude ionosphere. Fig.1b illustrates analogous dependencies for the real part of the wave number. The height variation of **Re k** and **Im k** is plotted for the range from 600 to 400 km above the ground. Since the typical scale of variation of ionospheric parameters H is in this case about 40 km, the value of **Re(Hk)** in the calculations presented, even if not much larger than unity, somewhat approaches the validity condition of a weakly inhomogeneous medium when analysis of the dispersion relation is adequate.

It is evident from the plots presented that the quasiwave disturbances propagating with a negative phase velocity are increasing spatially in a certain height range. The negative phase velocity corresponds to the direction opposite the axis Z. In this case the axis Z is directed from top to bottom and zero correspond to 600 km . The other branch of the oscillations, having a positive phase velocity, must be excluded from consideration because in this setting of the problem it appears to be increasing spatially at all altitudes, which is unfeasible physically.

What is the reason for the build-up of the oscillations? The answer to this question follows from the fact that for the dayside ionospheric conditions calculations show that the oscillations are damped ones. The main qualitative difference of the nightside upper ionosphere from the dayside ionosphere is that the vertical hydrodynamic plasma velocity at night is directed from top to bottom, whereas in dayside conditions the velocity is oppositely directed. Thus the decisive factors that are responsible for the spatial enhancement of the weaves include the presence of the downward directed background plasma velocity, and variations of ionospheric parameters with the height, plasma inhomogeneity. When considering stability problems, the presence of the above factors leads to the build-up of small initial disturbances with the time. In the propagation problem, this leads to an enhancement of the wave amplitude in space.

An alternative approach to an analytical treatment of the problem involves attempts to obtain the solution of the input equation in the geometrical optics approximation. It should be noted that

here, as in the case of the method of the dispersion relation, some reservations remain that are associated with the limitations of a weak inhomogeneity of the medium. We have to state again that we operate at the validity limit of the main approximations. And again we emphasize the qualitative character of results obtained.

Through substitution of variables the initial equation is brought to a canonical from of the Helmholtz equation - the first derivative is excluded. Next, a standard procedure is used to obtain the solution in the geometrical optics approximation. Results of calculations are presented in Fig.2. The figure show a "snapshot" of the wave number in the form of a height dependence of the density disturbance.
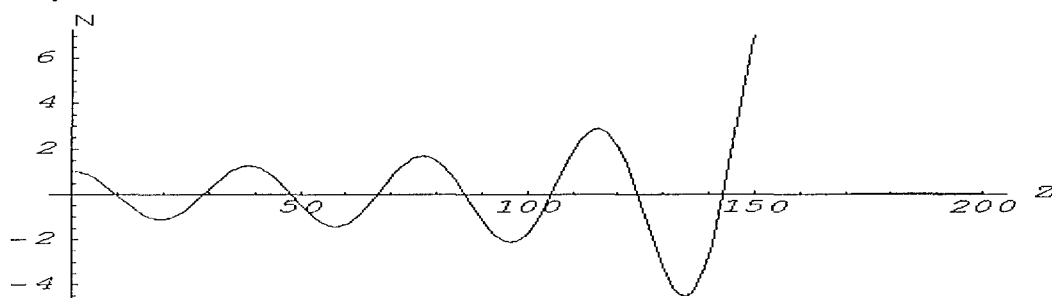
Fig. 2

One can see that there occurs an enhancement of disturbances with the decreasing height. At still lower altitudes the enhancement of the waves formally becomes increasingly more intense. Furthermore, the validity conditions of the geometrical optics approximation are obviously violated, and the result of calculations ceases to be adequate to the real situation.

The results presented in this study are, we believe, serious theoretical arguments in favor of the hypothesis of the existence of a region of intense plasma density fluctuations of the upper ionosphere in middle and moderately high latitudes at night. It is our hope that these arguments will provide further impetus to experimental investigations to detect such a region, with the use of incoherent scatter radars in particular.

ACKNOWLEDGMENTS

REFERENCES

1. V.B. Ivanov, V.M. Polyakov, Izvestiya Vuzov. Radiofizika, 1998, V. XLI, No.4, p. 432-437

APPLICATION OF THE HURST EXPONENT IN THE ANALYSIS OF NATURAL ELF ELECTROMAGENTIC NOISE

A.P. Nickolaenko

Usikov Institute of Radio-Physics and Electronics
Ukrainian National Academy of Sciences,
Kharkov 61085, 12, Acad. Proskury st., Ukraine,
sasha@vlf.kharkov.ua, sasha@ire.kharkov.ua

ABSTRACT

We apply the R/S analyses to determine the Hurst exponent for the natural electromagnetic radio signal in the extremely low frequency (ELF) band. The Hurst exponent is used for classification of random and chaotic signals. We present the results of R/S analyses for the natural ELF radio noise and for quasi-random successions generated by a computer.

WHAT IS THE R/S ANALYSIS?

Properties of natural stochastic signals reflect their origin, namely, noise or dynamic chaos. The R/S analyses was suggested in mathematics to resolve the signals and to establish what we have to deal with: the random noise or dynamic chaos [1]. The Hurst exponent has links with the spectral index: $\beta = 2Hu - 1$.

First, we introduce the procedure formally. Suppose we have a random series of the data flow: $x(t_K) = x_K$, where $K \in [1; M]$. Then, the Hurst exponent (Hu) is defined by the following formula:

$$\left(\frac{R_N}{S_N}\right)_{AV} = (N)^{Hu} \tag{1}$$

Here N is the current length of the data sample, and R_N is the current range of random variable found from

$$R_N = (x_{\max}) - (x_{\min}) \tag{2}$$

while its standard deviation (the RMS value) and the mean value are found from

$$S_N = \left[\frac{1}{N-1}\sum_{K=1}^{N}(x_K - \bar{x}_N)^2\right]^{\frac{1}{2}} \tag{3}$$

$$\bar{x}_N = \frac{1}{N}\sum_{K=1}^{N}x_K \tag{4}$$

How to obtain the Hurst exponent from the data set? We consider for simplicity that the full number of data points satisfies the binary condition $M = 2^L$. Then, we divide the data set into two parts ($N = M/2$) and compute the R_N and S_N values for each part. Then, we find their R/S ratio for the given N:

$$Y_N = R_N / S_N \tag{5}$$

and average it

$$Z_N = \left\langle \frac{R_N}{S_N} \right\rangle \qquad (6)$$

Here, the angular brackets denote averaging over the ensemble.

Then, we break the series into four parts, obtaining a new length of data ($N = \frac{M}{4}$) and the computational procedure is repeated once again resulting in a new averaged R/S ratio Z_N, etc. Finally, we arrive to the elementary data slice containing two elements, $N = 2$. In this case, see equations (2-4), $R_2 = \sqrt{2} \cdot S_2$, so that 'initial' R/S ratio is

$$Z_2 = \left\langle \frac{R_2}{S_2} \right\rangle = \sqrt{2} \qquad (7)$$

The logarithm of current values of the R/S ratio $\log_2(Z_N)$ is plotted against $I = \log_2(N) \in \left[1; \frac{L}{2}\right]$, and the best fit straight line gives the Hu value (1).

Fig. 1. General properties of the $Z(N)$ curves.
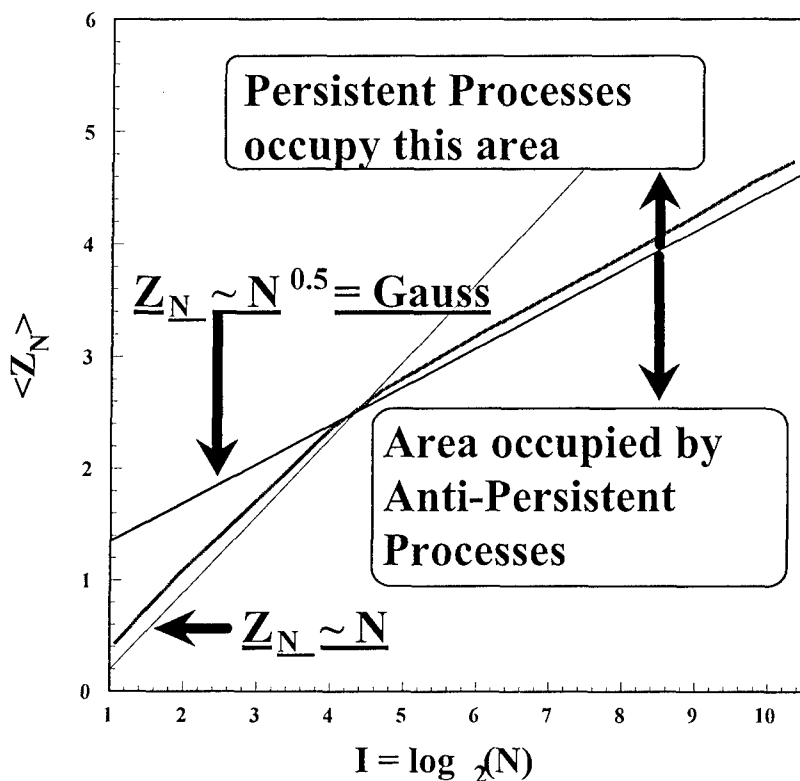
The $\frac{R}{S}$ curves and the HURST exponent have the following general properties. The exponent describes the nature of 'randomness' of the data. When we treat the Gaussian white noise, the tilt of the plot equals $Hu = 0.5$. Indeed, the RMS value equals for a long enough sample of normal noise [2]: $S_N^{Gauss} \rightarrow const$, $N \gg 1$. While its range increases as $R_N^{Gauss} \approx \sqrt{N}$. Hence, $Z_N^{Gauss} \approx \sqrt{N}$ and $Hu = 0.5$ for $N \gg 1$.

Normal processes of short duration are characterized by $Hu \cong 1$. So, the normal noise has the higher tilts at lower N, which are then reduced approaching the 0,5 stationary value (see Fig.1). The line of $Hu = 0.5$ tilt divides the noise into two types:

•When $Hu \in \left[0.5; 1.0\right]$ we say that the process contains persistence: its current value depends on the previous ones or on the pre-history.

•When $Hu \in \left[0.0; 0.5\right]$ we regard the process as anti-persistent one (with no 'memory').

For the most of natural processes, the tilt corresponds to $Hu \in \left[0.7; 0.8\right]$. General behavior of the Hurst exponent is illustrated in Fig. 1.

For short duration of the data samples, the $Z(N)$ curve for the normal noise grows as N. With an increase of the sample size, the growth becomes proportional to $\sqrt{N}$ that is the stationary Gaussian noise. The random process is regarded as a persistent one when its $Z(N)$ curve is found above the $\sqrt{N}$ dependence, and it is called the anti-persistent process when it lies below this line.

APPLICATIONS OF THE R/S ANALYSIS TO SYNTHESIZED AND NATURAL SIGNALS

We have computed the quasi-random successions of numbers with the uniform exponential and normal distributions [3]. The normal deviates were generated using the Matlab 5.0 software as well. The R/S analyses of computer generated numbers showed a peculiar behavior. In particular, the Gaussian variance does not demonstrate the expected $\sqrt{N}$. Unknown drawbacks of the algorithm?

We processed also the ELF radio signals recorded with two orthogonal horizontal magnetic antennas in the frequency range of Schumann resonance (a courtesy of Dr. C. Price, from Tel Avai University). Processing showed that stabilization occurs of the RMS values over an 'inertia' interval $I \in [7-12]$. Simultaneously, the signal range R becomes saturated when $I \geq 12$. This is probably caused by the finite dynamic range of the equipment. As a result, the Hurst exponent equals ¼ over inertia interval starting from the 'knee' area $I \in [2, 3]$.

It looks like the knee position depends on the pulse rate in natural ELF radio noise. When the pulse rate grows, the inertia interval starts from lower values of I, and the whole line of 1/4 slope shifts downward. The $Hu = 0.25$ value indicates that the Schumann resonance signal is an anti-persistent noise. Hence, there is no interaction between individual pulses arriving from worldwide lightning strokes.

CONCLUSION

1. Behavior of the Hurst exponent for the synthesized random Gaussian variable may indicate unknown drawbacks in the commonly used computational procedure.

2. Natural Schumann resonance signal is an anti-persistent noise. This rigorously proves independence of individual lightning stokes.

3. Diurnal variations of the Hurst exponent may be a replica of daily changes in the global lightning rate.

REFERENCE

[1] Turcotte, D.L., *Fractals and Chaos in Geology and Geophysics*, Second edition, Cambridge University Press, Cambridge, 1997, pp. 159-162.

[2] Rytov, S. M., *Introduction to Statistical Radio Physics, Part 1: Random Processes*, Moscow, Nauka, 1976, pp. 204-210 (in Russian).

[3] W.H. Press, S.A. Teukolsky, W.T. Vetterling, Brian P. Flannery, *Numerical Recipes in FORTRAN*, Second ed., Cambridge Univ. Press, 1992. p 271.

ACCELERATING THE CONVERGENCE OF THE TIME DOMAIN SOLUTION FOR A NATURAL ELF PULSE

A.P. Nickolaenko

Usikov Institute of Radio Physics and Electronics
Ukrainian National Academy of Sciences,
Kharkov 61085, 12, Acad. Proskury st., Ukraine,
sasha@vlf.kharkov.ua, sasha@ire.kharkov.ua

L.M. Rabinowicz

Radioastronomical Institute, Ukrainian National Academy of Sciences
Kharkov, Ukraine

ABSTRACT

We present a compact analytical time domain solution for the ELF electromagnetic wave propagating in the Earth ionosphere cavity. The workability of the formula obtained is demonstrated by computations of the pulse waveforms originating from a point vertical electric source.

INTRODUCTION

The extremely low frequency (ELF) wave propagates within the spherical cavity formed by the Earth and lower ionosphere as the TEM mode. The cavity acts as a radio filter, therefore, an initially short pulse arrives to a remote observer as a spheric radio wave having a sharp onset succeed by a low frequency tail. First, we construct an analytical time-domain solution for such a pulsed wave traveling in the spherical Earth-ionosphere cavity, then, we obtain a compact form for the time-domain presentation.

MODEL

Consider the point vertical electric dipole as the source of the radio wave. The current moment of the source is a delta-pulse in the time domain $M_C(t) = M_0 \cdot \delta(t)$. We use the polar spherical coordinate system $\{r, \theta, \varphi\}$ with the origin at the center of the Earth and the $\theta = 0$ axis pointing to the source.

The time domain fields are found as the Fourier transform (a contour integral) of the zonal harmonic series representation. The final result is the sum of residuals over the poles found from the following equation

$$n(n+1) - v(\omega)\left[v(\omega) + 1\right] = 0 \qquad (1)$$

We use the linear heuristic frequency dependence of the propagation constant $v(\omega) = A\omega + B$ that corresponds to the experimentally observed Schumann resonance frequencies of 8, 14, 20, etc., Hz when $A = \dfrac{1}{12\pi} - \dfrac{i}{200\pi}$ and $B = -\dfrac{1}{3}$. The time domain fields are:

$$E(t) = 2E_A \operatorname{Re}\left\{\sum_{n=1}^{\infty} \frac{n(n+1)P_n(x)}{n-B} \exp\left(it\frac{n-B}{A}\right)\right\}$$

$$E_A = \frac{M_0}{4\pi h a^2 \varepsilon} \qquad (2)$$

$$H(t) = 2H_A \operatorname{Im}\left\{\frac{1}{A}\sum_{n=1}^{\infty} \exp\left(it\frac{n-B}{A}\right) P_n^1(x)\right\}$$

$$H_A = \frac{M_0}{4\pi h a c^2} \qquad (3)$$

Here h is the effective height of the ionosphere, a is the Earth radius, ε is the permittivity of vacuum, $P_n(x)$ and $P_n^1(x)$ are the Legendre and associated Legendre polynomials, $x = \cos\theta$. Terms in the time series contain the exponentially decaying factor that is unity when $t = 0$. Hence, the series (2) and (3) diverge at the source point $x = 1$ for $t = 0$. They converge anywhere uniformly and absolutely for $t > 0$, including the source point.

ACCELERATING CONVERGENCE

We use the generating function of the Legendre polynomials to accelerate the convergence of time-domain series (2) and (3):

$$R_0(g,x) = \sum_{n=0}^{\infty} g^n P_n(x) = \frac{1}{\left(1 - 2gx + g^2\right)^{\frac{1}{2}}} \qquad \text{with} \quad g = \exp\left(i\frac{t}{A}\right) \quad (4)$$

Final expressions are of the form:

$$E(t) = \operatorname{Re}\left\{E_A g^{-B}\left[R_{-1} + B(R_0 - 1) + B(B+1)\left(\frac{R_1 - g}{g}\right) + B(B+1)^2\sum_{n=1}^{\infty}\frac{g^n P_n(x)}{(n+1)(n-B)}\right]\right\} \qquad (5)$$

$$H(t) = \operatorname{Im}\left\{\frac{H_A}{A}\frac{g^{(1-B)}\left(1-x^2\right)^{\frac{1}{2}}}{\left(1-2xg+g^2\right)^{\frac{3}{2}}}\right\} \qquad (6)$$

In case of direct proportionality, namely, $B = 0$ and $A \neq 0$, the formulas become very simple:

$$E(t) = \operatorname{Re}\left\{\frac{E_A(1-xg)}{\left(1-2xg+g^2\right)^{\frac{3}{2}}} - 1\right\} \qquad (7)$$

$$H(t) = \operatorname{Im}\left\{\frac{H_A}{A}\frac{g\left(1-x^2\right)^{\frac{1}{2}}}{\left(1-2xg+g^2\right)^{\frac{3}{2}}}\right\} \qquad (8)$$

RESULTS AND DISCUSSION

Computed waveforms for the magnetic pulses are shown in Fig. 1 for the source-observer distances of 5000, 10000 and 15000 *km* (1000 *km* = 1 *Mm*). Time is shown along the horizontal axis in *ms*. Pulse amplitude is depicted in arbitrary units on the ordinate. One may see an increase in the pulse delay with the distance. Antipodal and round-the-world waves are clearly seen in the plots (shown with arrows).

Horizontal Magnetic Field Component
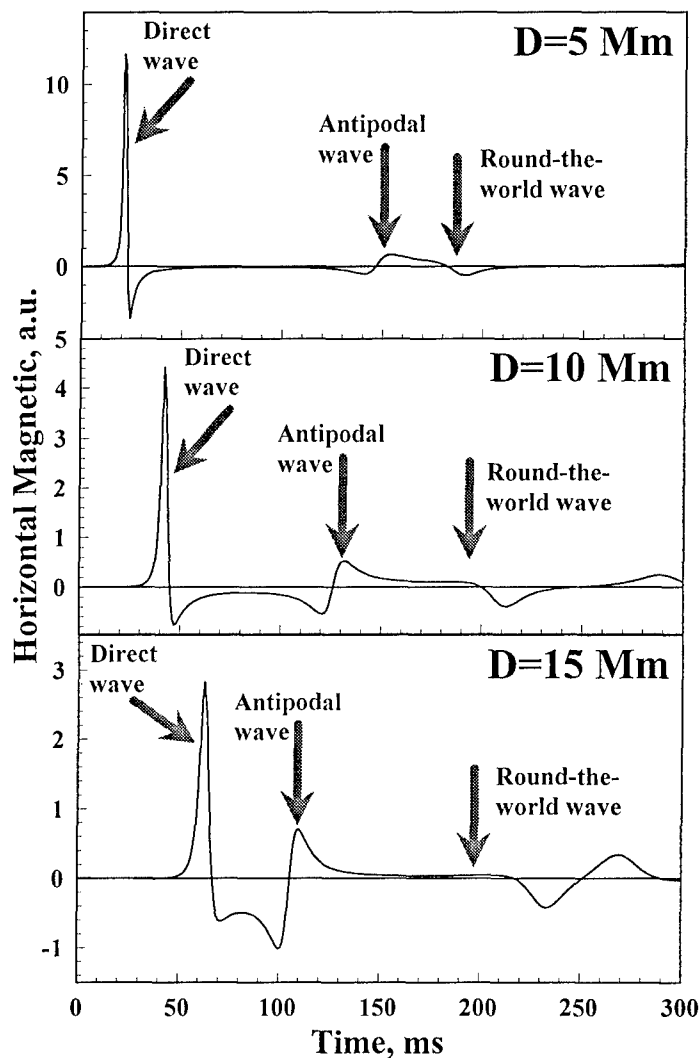
Fig. 1. $H(t)$ waveforms at 5, 10 and 15 *Mm* distances from the lightning stroke. Arrows denote the direct, antipodal and round-the-world waves. The 'square' form of $H(t)$ appears due to negative onset of antipodal pulse.

CONCLUSION

The main results are as follows:

1. We obtained a compact analytical time-domain solution for both ELF field components in the spherical Earth-ionosphere cavity.

2. We derived an exact presentation for the linear $v(\omega)$ dependence.

3. Formulae become very compact when $v(\omega)$ is directly proportional to the frequency.

4. All specific features of the ELF radio pulses are pertinent to the compact solutions.

ON THE SCHEME FOR SEEKING THE SOLUTION TO A SYSTEM OF MAXWELL'S EQUATIONS IN A SPHERICALLY SYMMETRIC MODEL OF THE EARTH-IONOSPHERE WAVEGUIDE

Victor N.Popov

Institute of Solar-Terrestrial Physics SD RAS
P.O.Box 4026, Irkutsk, 664033, Russia
E-mail: rp@iszf.irk.ru

A classical scheme for solving the boundary-value problem for a system of Maxwell's equations in a spherically stratified model of the Earth-ionosphere waveguide has been known since the beginning of this century, and implies the following. The elementary electric or magnetic dipoles are usually assumed as emitters. In each of these cases the Hertz potentials are introduced, which satisfy partial differential equations with separable variables. Solutions to this equations are sought either in the form of a series in terms of eigenfunctions of the angular operator (series of zonal harmonics) or in the form of a series in terms of eigenfunctions of the radial operator (series of normal modes). The transition from one series to the other is accomplished through the Watson transformation.

Attempts to generalize this scheme to the case of more sophisticated waveguide and emitter models led the author to the conclusion that the scheme should be modified. To elucidate the essence of the problem, a very simple model is considered, in which the ionosphere represents a cold plasma layer of a finite thickness, the Earth is modeled by a perfectly conducting sphere, and the waveguide is excited by an azimuthally symmetric current that models the transmit antenna.

Unlike the classical scheme, we abandoned the idea of introducing any potentials, and formulated boundary-value problems for the components of fields. Furthermore, elementary (point) models of emitters are not considered. It is assumed that all current density components of the emitter are sufficiently smooth functions of spatial coordinates, which involves the assumption about the smoothness of the desired solution to the system of Maxwell equations. This assumption permits us to formulate mathematically correctly the boundary conditions at special points in a spherical coordinate system.

The objective of this paper is to devise a reasonably rigorous mathematical scheme for seeking the formal expressions for solving a system of Maxwell's equations. The presence of such expressions induces us to hope that some

properties of the determined solutions can be revealed by using rigorous mathematical methods.

In the model under consideration, the boundary-value problem for the system of Maxwell equations is reduced to two independent boundary-value problems

$$\left(L_y^m + L_\theta / y^2\right) y E_\varphi = \frac{4\pi}{i\omega} y j_{0\varphi}, \ (y \in (1, \infty), \theta \in (0, \pi)),$$

$$\lim_{y \to \infty}\left((y E_\varphi)'_y - ikay E_\varphi\right) = 0, \ \lim_{y \to 1} y E_\varphi = 0, \ \lim_{\theta \to 0, \pi} y E_\varphi = 0.$$

$$\left(L_y^e + L_\theta / y^2\right) y B_\varphi = \frac{4\pi}{i\omega} \frac{1}{ika}\left(\varepsilon \frac{\partial}{\partial y} \frac{y j_{0\theta}}{\varepsilon} - \frac{\partial j_{0r}}{\partial \theta}\right), \ (y \in (1, \infty), \theta \in (0, \pi)),$$

$$\lim_{y \to \infty}\left((y B_\varphi)'_y - ikay B_\varphi\right) = 0, \ \lim_{y \to 1}(y B_\varphi)'_y = 0, \ \lim_{\theta \to 0, \pi} y B_\varphi = 0.$$

Here $k = \omega / c, \ y = r / a,$ a is the radius of a perfectly conducting sphere, $j_{0r, \theta, \varphi}$ - are the current density components of the emitter, ε - is complex permittivity,

$$L_y^m = -\left(\frac{1}{ika}\frac{\partial}{\partial y}\right)^2 + \varepsilon, \ L_y^e = -\frac{\varepsilon}{ika}\frac{\partial}{\partial y}\frac{1}{\varepsilon}\frac{1}{ika}\frac{\partial}{\partial y} + \varepsilon, \ L_\theta = -\frac{1}{ika}\frac{\partial}{\partial \theta}\frac{1}{ika}\frac{1}{\sin\theta}\frac{\partial}{\partial \theta}\sin\theta.$$

The solution to the boundary-value problems must be sought in the open region. This mathematical statement is a consequence of physical considerations.

Solutions to the boundary-value problem for the φ components can be sought in the form of series in terms of eigenfunctions of one of the operators: radial or angular. This paper presents formal schemes for solving boundary-value problems by the former method.

We represent the problems for eigenvalues of radial operators as

$$y^2 L_y^{m,e} R_{ln}^{m,e} = \gamma_n^{m,e}(\gamma_n^{m,e} + 1 / ka) R_{ln}^{m,e}, \ (y \in (1, \infty)),$$

$$\lim_{y \to \infty}\left((R_{ln}^{m,e})'_y - ikaR_{ln}^{m,e}\right) = 0, \ \lim_{y \to 1} R_{ln}^m = 0, \ \lim_{y \to 1}(R_{ln}^e)'_y = 0.$$

Thus it has been possible to represent the inhomogeneous boundary-value problems for expansion coefficients of the components of fields in an identical form for both types of fields. The solutions of these problems are expressed in terms of associated Legendre functions of the form $P_{v_n}^{(1)}(\cos\theta)$, unlike the well-known solutions which involve Legendre functions of the form $P_{v_n}(\cos\theta)$.

The final expressions for the φ components of fields have the form

$$yE_\varphi(y,\theta) = -\frac{4\pi a}{c}ika\int\limits_1^\infty dy'\int\limits_0^\pi d\theta'\sin\theta'R_1^{m+}(y)H^m(\theta,\theta')R_1^m(y')y'\,j_{0\varphi}(y',\theta'),$$

$$yB_\varphi(y,\theta) = -\frac{4\pi a}{c}ika\int\limits_1^\infty dy'\int\limits_0^\pi d\theta'\{\left[R_1^{e+}(y)\frac{(\sin\theta'H^e(\theta,\theta'))_{\theta'}'}{ika}\widetilde{R}_1^e(y')\right]j_{0r}(y',\theta') +$$

$$+\sin\theta'\left[R_1^{e+}(y)H^e(\theta,\theta')R_2^e(y')\right]y'\,j_{0\theta}(y',\theta')\}.$$

Here $R_1^{m,e}(y)$ are infinite-dimensional columns of eigenfunctions of radial operators, $\widetilde{R}_1^e(y)$ are infinite-dimensional column of eigenfunction of conjugate operation $\widetilde{L}^e$,

$$R_2^e = -\frac{1}{ika}\frac{1}{\varepsilon}\frac{d\varepsilon\widetilde{R}_1^e}{dy},$$

the index "+" signifies the transposition operation, $H^{m,e}(\theta,\theta')$ are infinite-dimensional diagonal matrices whose elements are solutions of the equations

$$\frac{d}{d\theta}\frac{1}{\sin\theta}\frac{d}{d\theta}\sin\theta H_n^{m,e}(\theta,\theta') + v_n^{m,e}(v_n^{m,e}+1)H_n^{m,e}(\theta,\theta') = \frac{\delta(\theta-\theta')}{\sin\theta'},\ \theta,\theta'\in(0,\pi),\ v_n^{m,e} = ka\gamma_n^{m,e}.$$

It can be demonstrated that all components of fields may be expressed in terms of the Green's functions

$$G^{m,e}(y,\theta;y',\theta') = R_1^{m,e+}(y)H^{m,e}(\theta,\theta')\widetilde{R}_1^{m,e}(y')$$

and there derivation with respect to spatial variables. The resulting expressions for the components of fields are formally exact solutions of an inhomogeneous boundary-value problem for a system of Maxwell's equations. Mathematically, the method of reasoning which we are using in this paper has the character of plausible reasoning. Proving the assumptions made, specifying or modifying them should be the subject of a separate study.

THE ROLE OF EXCITED MOLECULAR IONS IN THE VARIATION OF THE E-LAYER PEAK HEIGHT CAUSED BY THE SOLAR ACTIVITY

Taras G. Zhivolup

Institute of Ionosphere of National Academy of Sciences
and Ministry of Education and Science of Ukraine, Kharkov, Ukraine
E-mail: iion@kpi.kharkov.ua

ABSTRACT

The data obtained by the Kharkov incoherent scatter radar show a monotonous linear decrease of the E-layer peak height (h_mE) in the transition from the low to medium solar activity. Such behavior of the E-layer peak height is accounted by the influence of the oscillation-excited ions O_2^+ on the h_mE variations depending on the level of solar activity. The theoretical dependences $h_mE(F_{10.7})$ are in a good agreement with the experimental data.

VARIATIONS OF THE E-LAYER PEAK HEIGHT WITH CHANGEABLE SOLAR ACTIVITY ACCORDING TO THE THEORY ALLOWING FOR THE EXCITED IONS

One of the basic problems in the E-layer theory is the behavior of its peak height h_mE depending on the level of solar activity. Now consider the influence of the oscillation-excited ions O_2^+ on the h_mE variations depending on the level of solar activity.

According to the theory allowing for the excited ions [1], the E-layer peak height is formed between the two levels: one which is associated with the maximum of on the ion-forming rate function h_q and the other related to the maximum concentration of excited ions O_2^+ at h_a.

Consider the h_a behavior as the solar activity increases. For this purpose let us make theoretical calculations of $h_a(F_{10.7})$ dependence using the expression [1]

$$\frac{d}{dh} lg(T) = \frac{d}{dh} lg \frac{n_e}{A + n\gamma},$$

(1)

where T is the atmospheric temperature, n is the natural particle concentrations, g is the rate of collision deactivation reaction A-is the probability of radioactive transition from the excited state to the basic one. We believe that T(h) and n(h) correspond to the Jacchia-71 model [2],and h_mE is located close to ha. Then

$$\frac{d}{dh} lg(n_e) = 0.$$

Using the diffusion equation for each atmospheric component n_i of the Jacchia-71 model we transform equation (1) in the following way:

$$\frac{dT}{dh} = \frac{\gamma}{A}\frac{g}{k}\rho, \qquad (2)$$

where g is the free fall acceleration, k is the Bolzman constant, r is the atmospheric density. This expression relates the atmospheric temperature gradient to its density and is the equation for determining ha-the peak height of the excited ions O_2^+.

Define the magnitude of the h_mE change in the transition from the solar activity minimum to its maximum. For this purpose using the relation (2) we obtain the $h_a(F_{10.7})$ dependences and determine the amount of the sudden change in h_q associated with a more rapid increase in the intensity of the line 102.6 nm as compared to the line 97.7 of solar radiation with increasing solar activity for each season.

The $h_a(F_{10.7})$ dependences were obtained from three values of ha estimated for each season to account for three definite values of the exosphere temperature T_∞ and the rate of collision de-activation reaction $\gamma=2*10^{-15}cm^3s^{-1}$.

In order to calculate the profiles $\rho(h)$ the modified Jacchia-71 models were utilized for summer, winter and equinox seasons. The estimated profiles $\rho(h)$ were corrected for the values of the Groves model [3] at 110 km in the 50^0 latitude for March, June, September and December. The amount of the jump h_q for all seasons was taken to be equal to 0.4H and assigned to the solar activity level $F_{10.7} = 207$ for March, $F_{10.7} = 200$ for June, $F_{10.7} = 215$ for September and $F_{10.7} = 202$ for December.

According to the calculation that were made in the transition from the low to high solar activity, the magnitude of h_mE decrease for March was 4.98 km, for June-5.47 km, for September-4.95 km and for December-3.25km. In this case ha shows a smooth linear decrease in the transition from low to high SA and the magnitude of its decrease is 1.44 km for March, 1.44-for June, 1.35-for September and 1.53 km for December.

The contribution of the sudden change h_q to the magnitude of decreasing h_mE is more significant as compared to the magnitude of the h_a drop.

COMPARISON BETWEEN THE THEORY ALLOWING FOR THE EXCITED IONS AND THE INCOHERENT SCATTER DATA
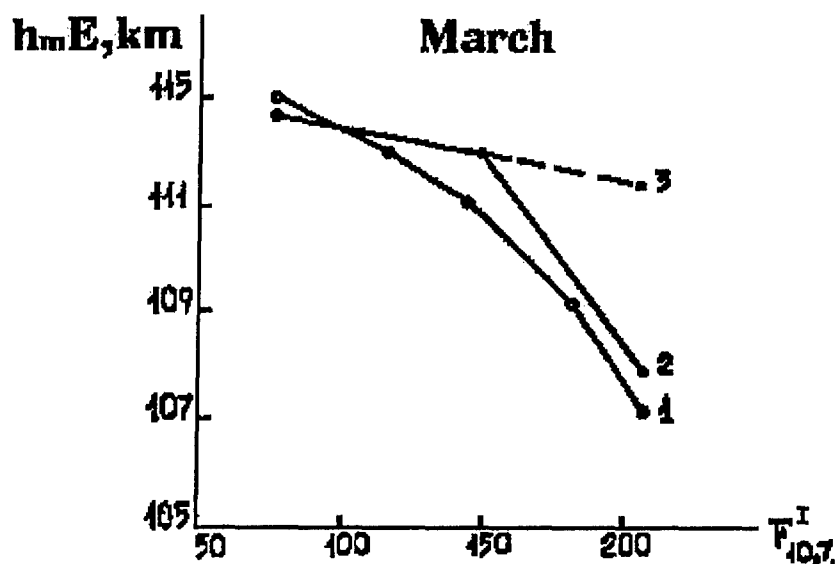
Fig. 1a
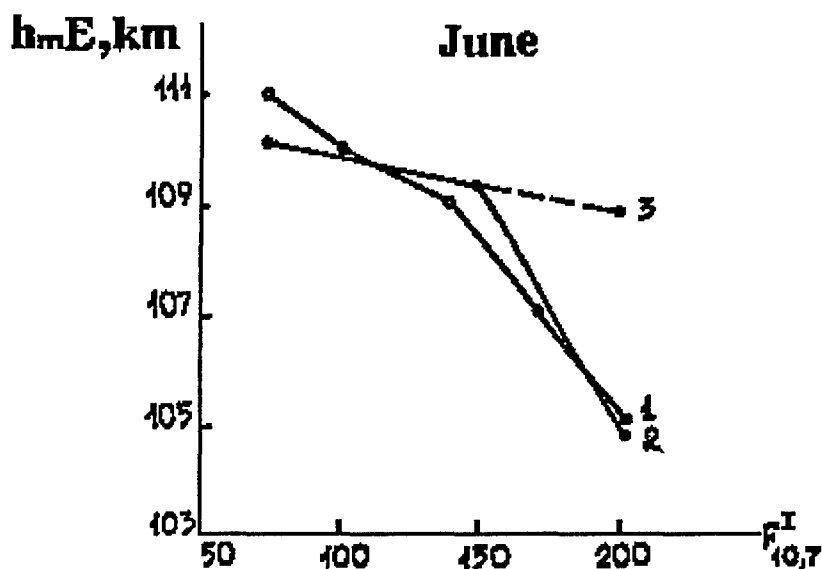
Fig.1b

Fig.1a, 1b. Comparison between the empirical afternoon dependences $h_mE(F_{10.7})$ (1) for March and June and the theoretical dependences (2) allowing for the sudden change in h_q in the transition from low to high solar activity; 3 – theoretical dependence $h_a(F_{10.7})$.

Fig.1a, 1b show the comparison between the theoretical dependences $h_mE(F_{10.7})$ and the empirical ones obtained from the incoherent scatter data for March, June, September and December.

It is seen that the theoretical dependences $h_mE(F_{10.7})$ are in a good agreement with the experimental data: the predicted and experimental relations $h_mE(F_{10.7})$ show the identical behavior (a slow monotonous h_mE decrease with increasing $F_{10.7}$= 73-150 and more abrupt drop in h_mE with $F_{10.7}$>150) and basically they differ from one another by less than 1 km. Thus, by considering the oscillation-excited ions it became possible to provide an insight into the monotonous linear decrease of the E-layer peak height in the transition from low to medium solar activity.

REFERENCES

[1] Antonova L.A., Ivanov-Kholodny G.S., Chertoprud V. Ye. E-layer aeronomy (registration of solar ultraviolet radiation variations and geomagnetic disturbances)/ M.: Janus, 1996. 168p.
[2] Jacchia L.G. Revised static models of the thermosphere and exosphere with empirical temperature profiles/ Spec. Rep.N 332. Smithson. Astrophys. Observ., Cambridge, Mass. 1971.
[3] Groves G.V. Seasonal and latitudinal models of atmospheric temperatures, pressure and density, 25 to 110/ Air Force Cambridge Labs., L.G. Harnison Field, Mass. 1970.

DISPLAYS OF POSSIBLE HARBIGERS OF EARTHQUAKES ON RECORDINGS OF VLF-SIGNALS DEPENDING ON THEIR CHARACTERISTICS

Natalia A. Kazakova, Anatoliy G. Kolesnik, and Boris M. Shinkevich

Siberian Physical Technical Institute , Tomsk, Russia
E-mail: Natalia@elefot.tsu.ru

INTRODUCTION

A complex of electromagnetic disturbances in a zone of preparation, as in the earth crust and in the environment precedes an earthquake. One of the methods of searching seismo-ionospheric effects in D-region is the radiograph of Earth - ionosphere wavequide by Very Low Frequency waves (VLF). Such research of parameters of the environment allows to obtain additional information about physical mechanisms of electromagnetic harbingers of earthquakes, and the solution of the given problem is directly connected to forecasting possible time intervals between the beginning of preparation and moment of the earthquake. The records of VLF-signals amplitude show abnormal variations of different intensity above the seismically active region before and after strong earthquakes. The validity of the dependence between the registered disturbances and earthquakes can be experimentally proven either by a statistical material based on the most general regularities, or by the presence of special characteristics in the signal, inherent to the specific process with the regard of geophysical conditions as a whole [1-4].

ANALIS OF EXPERIMENTAL DATA

This paper presents an analysis of the dynamics of behavior of VLF-signal amplitude on the radio link Tsusima – Tomsk (extension about 4000 km, 10.2 kHz) and the radio link Irkutsk-Tomsk (extension about 1300 km, 50 kHz) from February 20 to August 31, 1997. The data were obtained on a receiving-measuring complex of continuous monitoring of electromagnetic background of environment with the purpose to find in this dynamics the component induced by seismic processes in the regions adjoining to the tested route. The general characteristics of earthquake harbingers were specified on the basis of the abnormal features of the received signals. Possible electromagnetic harbingers were determined for the earthquakes occurring in the region nearby the route at the distance about ± 3500 km. During the period of research, in this region, 610 and 420 events with magnitude > 4.0 have taken place, respectively.

We have tried to define the dependences of the harbinger images on the characteristics of earthquakes and geleogeophysical conditions. The quantitative analysis of processed data (the recorded VLF-signal amplitude for the period under research) has shown that the temporary interval between the beginning of observation of harbinger images (t_{pert}) and the moment of earthquake (t_{quak}) $(t = t_{quak} - t_{pert})$ is more than *15 hours* both for earthquakes with depth more than *150 km*, which occurred at a distance from the tested VLF- radio link of more than *1500 km*, and for earthquakes with magnitude of more than *6*, which have taken place up to *1500 km* from VLF-radiolines. This dependence of temporary interval of earthquake harbinger image on the distance, depth and magnitude of earthquakes is shown in Fig.1. for radio link Tsusima-Tomsk and Fig.2 for radio link Irkutsk-Tomsk.
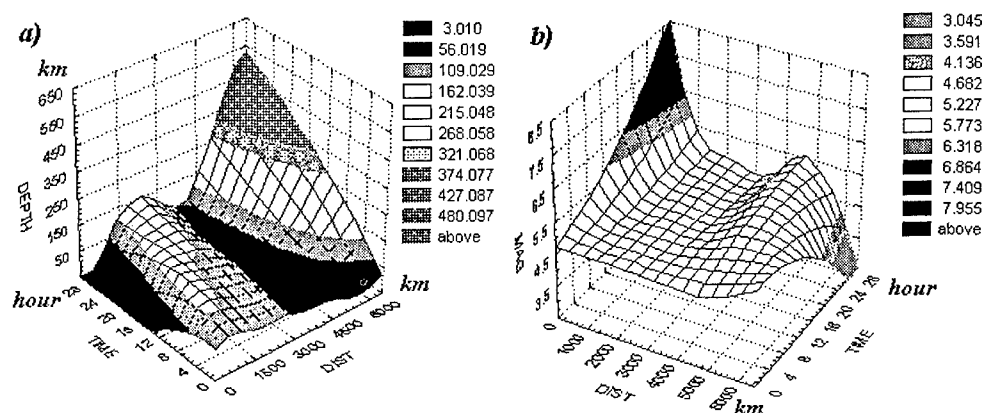
Fig. 1 The dependence of temporary interval of earthquake harbinger image on the distance, depth (a) and magnitude (b) for the radio link Tsusima-Tomsk

a) b)
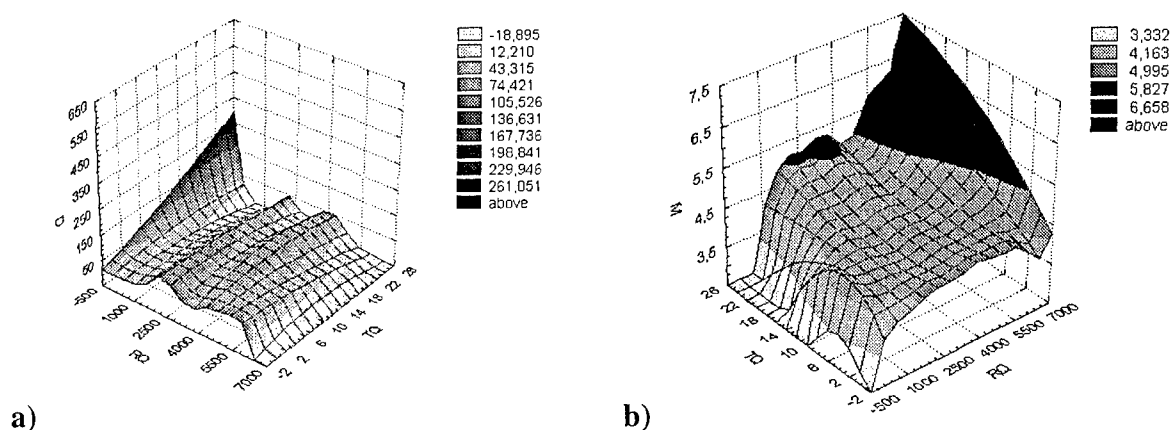
Fig. 2 The dependence of temporary interval of earthquake harbinger image on the distance, depth (a) and magnitude (b) for the radio link Irkutsk-Tomsk

A time interval between the earthquake preparation registered by the VLF-signal amplitudes and earthquake itself makes from 3 minutes to 15 hours. The statistical analysis of processed data (the VLF-signal amplitudes in the period of observation) has shown that 65 % and 57%, respectively, of all the events in this region have been displayed by the signals of the harbinger images.

REFERENCES

[1] M.B. Goxberg, V.A. Morgunov, O.A. Pokhotelov, Seismoelectromagnetic phenomenon - Moscow: N., 1988, 174p.

[2] M Hayakawa, O.A. Molchanov, T.Ondoh, E. Kawai // Journal of Atmospheric Electricity, -Vol.16, No 3, -1996, -p. 247-257.

[3] N.A. Kazakova, A.G. Kolesnik, B.M. Shinkevich Anomalous variation of VLF- signals amplitude with earthquakes preparing processes/ Izvestiya, Physics of the Solid Earth -2000, N 6, p.2-5

HF DOPPLER PROBING THE DISTURBANCES ORIGINATING IN THE IONOSPHERE FROM NATURAL AND ANTHROPOGENIC SOURCES

Leonid F. Chernogor, Leonid S. Kostrov, and Victor T. Rozumenko

V. Karazin Kharkiv National University, Kharkiv, Ukraine

E-mail: Leonid.F.Chernogor@univer.kharkov.ua

The measurements were made in 1995 to 2000 at two frequencies of 2.8 MHz and 3.0 MHz. The moving solar terminator generated detectable effects only in the absence of other disturbances in the ionosphere, and, first of all, in the absence of magnetic storms. The response to the dawn terminator commences immediately after the sunrise in the lower part of the ionospheric F-region where the probing radio waves are reflected (Fig. 1). The quasi-periodic oscillations of the Doppler shift f_D, with a 0.35±0.15-Hz amplitude lasted 30–40 min. Most frequently and clearly, the oscillations are observed with a $T \approx 20$ min period approximately in 30–60 min after the sunrise at F-region heights (i.e., approximately at the sunrise at the ground), and a constant f_D of 0.75±0,25 Hz follows and continued for ~1.5±0.5 hours. A quasi-periodic oscillation with $T \approx 10$–20 min is usually observed in this case.
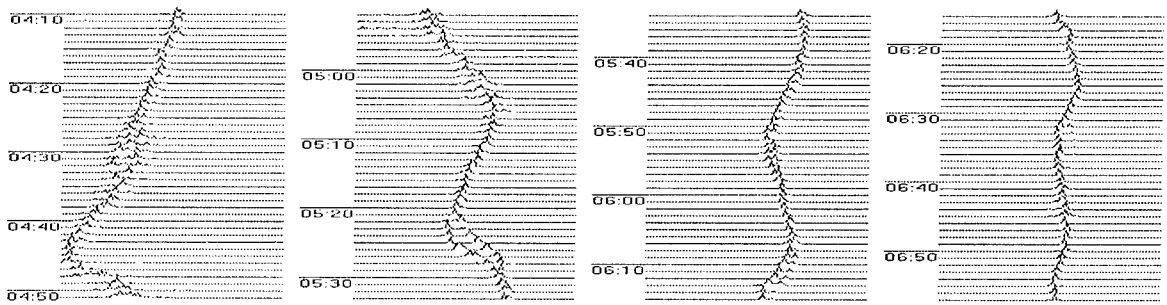
Fig. 1. Doppler spectra at 2.84 MHz on November 1, 1998. The f_D fluctuates between -1 Hz and +1.5 Hz. The sunrise time in the F region was at ~04:20, and at the ground near 05:30.

The response to the dusk terminator is similar (see Fig. 2), but there are some differences. Often, approximately 30 min before the sunset at the ground, a constant negative f_D of 0.7±0.2 Hz is observed during a 25±7-min interval. It is apparently associated with processes in the magnetically conjugate region. At sunset at the ground, the quasi-periodic oscillations follows with $T \approx 10$–20 min. Simultaneously, the constant component in the f_D increases up to 1 Hz. The duration of these processes can be 60±10 min. Finally, during the sunset in the lower part of the F-region, the quasi-periodic oscillations with 0.25±0.05-Hz amplitudes and 15–20-min periods ($T \approx 20$-min period dominates) enhance, and continued for 75±45 min. Simple models have been developed for the processes associated with the moving terminator.

The HF Doppler radar investigations of a variety of processes associated with rocket launches were performed over the same period of time. The observations have been analysed of thirty-two launches from different cosmodromes (Baikonur, Plesetsk, Cape Canaveral, Kourou, and others). At large distances (R~10 000 km), a response of the ionosphere to the launch of small rockets (such as Pegasus XL) has not been detected. At R~2000–3000 km, a response is readily detectable to the launch of a big and high-power rocket (such as Proton or
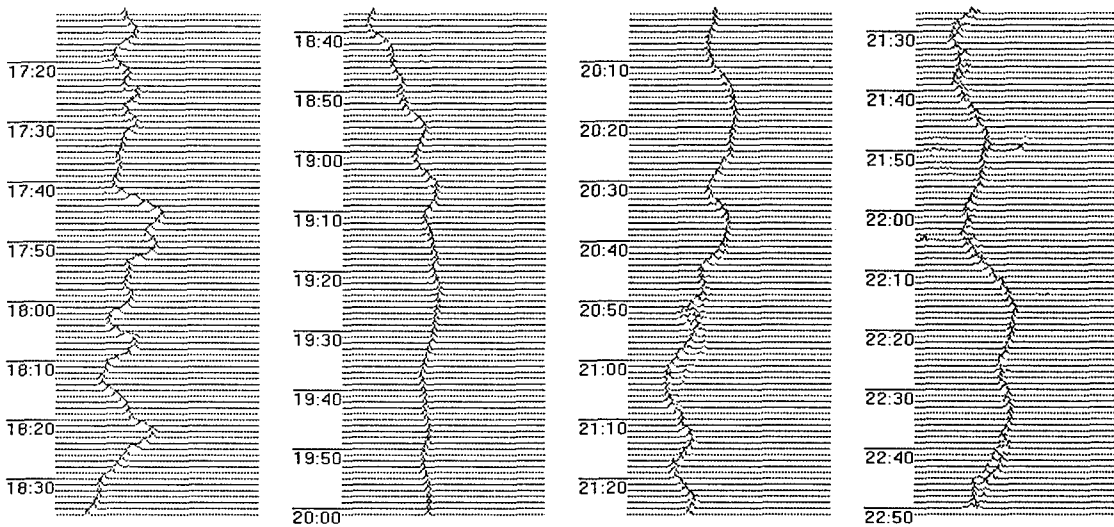
Fig. 2. Doppler spectra at 2.84 MHz on November 21, 1998. The sunset time at the ground was near 18:10, and in the F region near 19:00.

Arian). During Space Shuttle launch, perturbations are not detected immediately after the launch but follow with a delay of 50–60-min, which is apparently linked to the Shuttle orbital maneuvering system engine burns in the ionosphere.

Consider a few examples of several of these effects in detail.

The daytime Space Shuttle launch, $R \approx 10\ 000$ km, at 10:35 Kyiv time (Kyiv time is indicated everywhere in this paper) on December 4, 1998 (see Fig. 3). The day cannot be considered quiet. One hour before the liftoff, multiple propagation path signals were observed, and they continued till 11:00. From 11:25 to 12:00 and from 12:30 to 13:20, the number of multipath signals increased, and the quasi-periodic oscillations with 0.2–0.4-Hz amplitudes and a $T \approx 20$-min period appeared. After 13:00 the oscillations with $T \approx 10$ min prevailed.
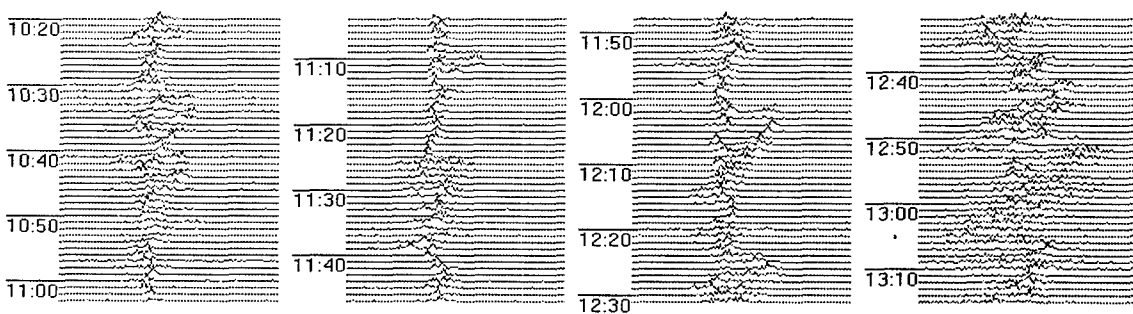
Fig. 3. Doppler spectra at 2.84 MHz on December 4, 1998, the day of the Shuttle Endeavour launch.

The night time Space Shuttle Discovery launch at 21:20 on October 29, 1998, (see Fig. 4). Sunset solar terminator effects were observed till 21:05. Over the 21:06–21:35 interval, a negative f_D was observed. Then it was changing not more than by 0.1 Hz till 22:20, and again after that instant of time up to 23:00, $\Delta f_D \approx -0.3$ Hz, and $T \approx 25$ min. After 23:00 the ionosphere remained quiet.
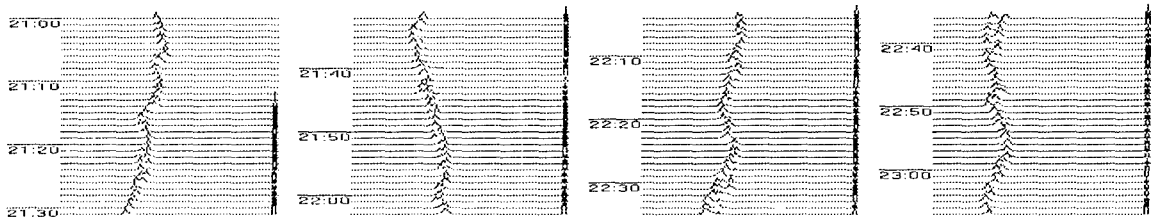
Fig. 4. Doppler spectra at 2.84 MHz on October 29, 1998, the day of the Shuttle Discovery launch.

The nighttime Proton launch, $R \sim 2\,500$ km, at 02:09 on March 3, 1999, (see Fig. 5). One hour before the launch, the ionosphere was quiet, and $f_D \leq 0.1$ Hz. From 02:10 to 02:55, quasi-periodic oscillations were observed with $f_D \leq 0.25$ Hz and $T \approx 10$ min. At 03:10 a moderate number of multipath signals happened with $f_D \approx -0.3$ Hz. Over the 03:30–04:15 interval, the number of multipath signals increased, $f_D \approx 0$ Hz; after 04:20 the $f_D \approx 0.3$–0.4 Hz, and the quasi-periodic perturbations with $T \approx 10$ min appeared. Clearly, the dawn solar terminator effects were observed after 03:30.
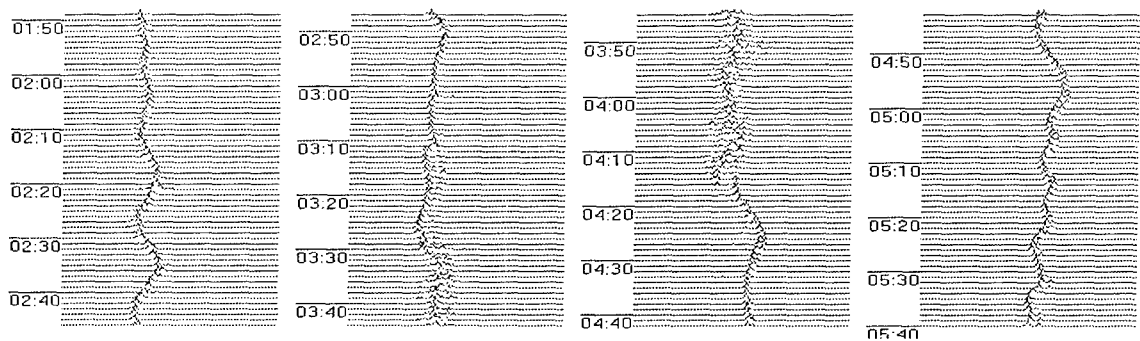
Fig. 5. Doppler spectra at 3.04 MHz on March 21, 1999, the day of the Proton space vehicle launch.

The night time Zenit-2 launch, $R \sim 2\,500$ km, at 23:29 on September 9, 1998, (see Fig. 6). A computer error caused a premature engine shutdown at the 272-nd second of the mission during the second stage burn. Approximately an hour before the launch, several multipath signals ($\Delta f_D \approx 0$ Hz) were observed. Over the 23:35–00:30 interval, $\Delta f_D \approx -0.5$ Hz, and the number of multipath signals increased. From 00:30 to 02:00, the ionosphere remained quiet.
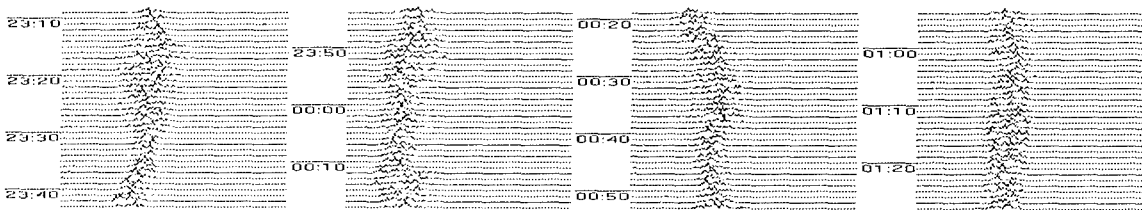
Fig. 6. Doppler spectra at 3.49 MHz on September 9, 1999, the day of the Zenit-2 rocket launch.

LARGE-SCALE DISTURBANCES ORIGINATING FROM REMOTE EARTHQUAKES IN THE PLASMA AT MESOSPHERIC HEIGHTS

A. M. Gokov, S. I. Martynenko, V. T. Rozumenko, and O. F. Tyrnov

National Kharkiv V. Karazin University, Kharkiv, Ukraine

E-mail: Oleg.F.Tyrnov @univer.kharkov.ua

ABSTRACT

The results are discussed of MF radar remote sensing of disturbances caused by strong earthquakes at great distances in the plasma at mesospheric heights, and a mechanism is advanced for the development of such large-scale disturbances in ionospheric plasma parameters, which is a large-scale mesospheric electric potential redistribution due to an increase in the atmospheric conductivity over a seismic region.

INTRODUCTION

The authors of [1] were the first who observed the development of large-scale ionospheric disturbances caused by a strong seismic activity for a few days and during the Chile May 22, 1960, earthquake with a magnitude of 9.6; the measurements were taken using a net of 18 MHz riometers in North America and spaced by thousands kilometers from each other. Among other things, increases in the signal amplitude by a factor of up to 2 over a background noise were observed to correlate with the seismic disturbances. Similar effects were observed before and during the January 17, 1995, Kobe earthquake with 7.2 magnitude [2]. In the latter case, two sequence of 22 MHz radio bursts were observed at a distance of 77 km from the epicenter. Such seismic phenomena have not found a satisfactory explanation yet.

In this paper, we present some observations of disturbances caused by remote earthquakes in the lower ionosphere, and discuss possible mechanisms of their development.

EXPERIMENTAL RESULTS

The lower ionosphere disturbance diagnostics at distances of up to a few thousand kilometers from strong earthquakes included records of $f=2$–3.5 MHz noise and 25 μs MF radar pulses scattered from the $z \sim 60 \sim 85$ km altitude region.

Fig. 1 represents time dependences of $R = A_-^2 / A_+^2$ obtained for different altitudes at the National Kharkiv V. Karazin University Radiophysical Observatory approximately 11,000 km away from a 5.7 magnitude earthquake which occurred at a 33 km depth near Western New Guinea, 3.37 S latitude and 135.1 E longitude, at 12:48:54 LT on March 20, 1995; the arrow marks the time of the earthquake. Here A_+^2 and A_-^2 are the ordinary and extraordinary, respectively, MF radar signal intensities averaged over successive 1-min intervals.

March 20, 1995
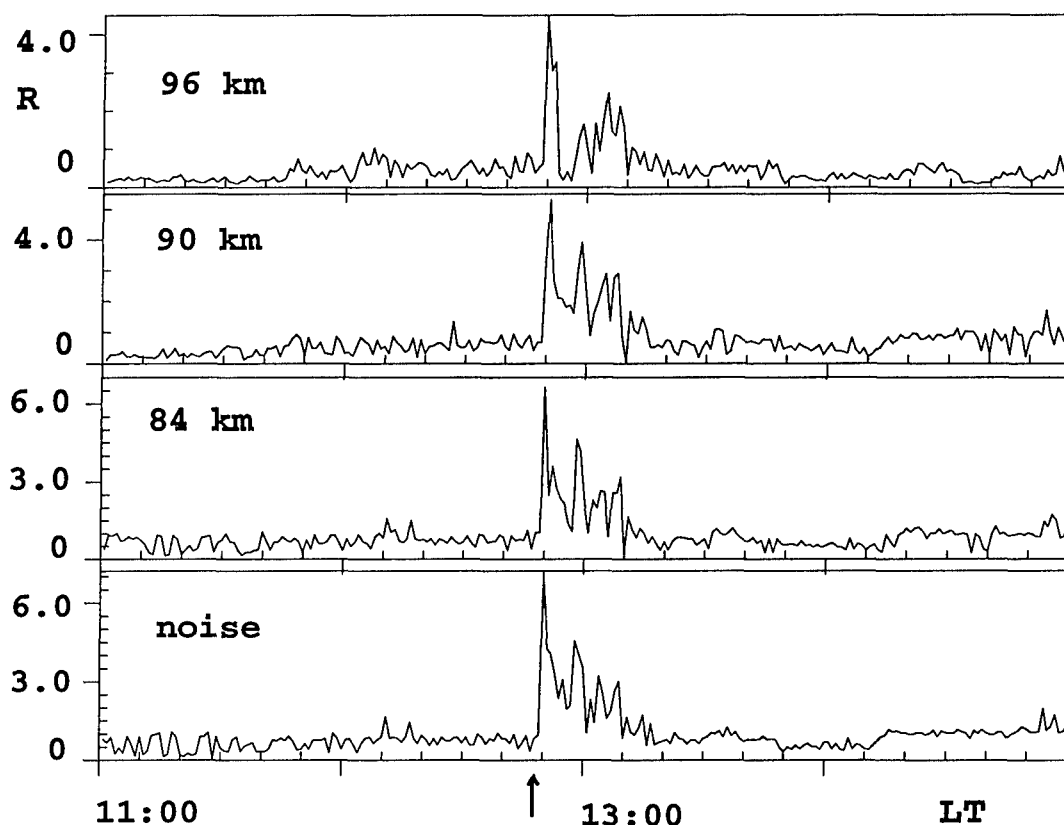
Figure 1. Time dependences of R for 2.3 MHz signals scattered from 84 km, 90 km, 96 km altitudes at Kharkiv during the March 20, 1995, West New Guinea earthquake; the time of earthquake is marked by the arrow.

The small characteristic time scale of the disturbance development (less than a few seconds) can indicate that the changes in MF radar signals were caused by the corresponding changes in the electron temperature A_-^2 and the effective collision frequency v_e in the ionospheric D region. The similarity between the dependences of R on time and height mean that the main ionospheric disturbance was localized below the 84-km altitude where the signal-to-noise ratio was low and prevented the detection of MF radar signals. As a whole, it is clearly seen that the remote earthquake caused a sharp increase in the value of R, which could result from a decrease in the total absorption of signals and noise below the 84-km altitude.

DISCUSSION

The detection of strong mesospheric electric fields at mesospheric heights (see, for example, [3, 4]) provides a new opportunity to explain electrodynamic interactions between the troposphere, the mesosphere, and the ionosphere. Thus, for example, the existence of such fields over a seismically active area makes possible the following mechanism. A big increase

(by one or two orders of magnitude) in the tropospheric conductivity over the seismic area results in a decrease in strong mesospheric electric field intensities due to troposphere-mesosphere electrical coupling (see, for example, [5, 6]). This causes a rapid decrease in T_e and v_e as well as the corresponding changes in mesospheric conductivity. The last effect results in rapid changes in radio propagation conditions in the lower ionosphere over the seismic area.

It should be noted that considerable changes in the mesospheric electric potential over a remote earthquake can result in a change in the difference in electric potential voltage between mesospheric potentials over the remote earthquake and over the observation site, which is equivalent to changes in mesospheric electric field intensities over the observation site. Therefore the development could also be expected of disturbances in the plasma at mesospheric heights. For the experiment depicted in Fig. 1, the remote earthquake should have decreased the large-scale difference in the electric potential voltage, which has resulted in a decrease of T_e, v_e, and the total absorption of the signals and noise below the 84-km altitude.

REFERENCES

[1] Warwick, J. W., C. Stoker, T. R. Mayer, Radio emission associated with rock fracture: Possible application to great Chilian earthquake of May 22, 1960, *J. Geophys. Res.*, 1982, Vol. 87, No. B4, pp. 2851–2859.
[2] Maeda, K., and N. Tokimasa, Decametric radiation at the time of the Hyogo-ken Nanbu earthquake near Kobe in 1995, *Geophys. Res. Lett.*, 1996, Vol. 23, No. 18, pp. 2433–2436.
[3] Goldberg, R. A., Middle atmospheric electrodynamics: status and future, *J. Atmos. Terr. Phys.*, 1984, Vol. 46, No. 11, pp. 1083–1101.
[4] Martynenko, S. I., V. T. Rozumenko, A. M. Tsymbal, O. F. Tyrnov, and A. M. Gokov, Mesospheric electric field measurements with a partial reflection radar, *J. Atmos. Electricity*, 1999, Vol. 19, No. 2, pp. 81–86.
[5] Martynenko, S. I., I. M. Fuks, and R. S. Shubova, Ionospheric electric-field influence on the parameters of VLF signals connected with nuclear accidents and earthquakes, *J. Atmos. Electricity*, 1996, Vol. 16, No. 3, pp. 259–269.
[6] Fuks, I. M., R. S. Shubova, and S. I. Martynenko, Lower ionosphere response to conductivity variations of the near-earth atmosphere, *J. Atmos. Solar-Terr. Phys*, 1997, Vol. 59, No. 9, pp. 961–965.

MATHEMATICAL MODEL OF THE MEASURING CHANNEL FOR IONOSPHERE PARAMETER DEFINITION BY THE INCOHERENT SCATTER RADAR TECNIQUE

Valeri N. Lysenko

Institute of Ionosphere of National Academy of Sciences
and Ministry of Education and Science of Ukraine, Kharkov, Ukraine
E-mail: iion@kpi.kharkov.ua

ABSTRACT

In the paper, the mathematical description of the measuring channel of the incoherent scatter radar (ISR) is proposed. As an example of application of the model, the distortions of altitude profiles of the normalized correlation functions (NCF) of scattering medium, electron density, electronic and ionic temperatures are calculated. The offered model can be applied to development of the measuring procedures of the ionospheric plasma parameters and of estimation of their accuracy.

THE GENERALIZED BLOCK DIAGRAM OF THE MEASURING CHANNEL

The IS radar technique is a very powerful tool for research of the ionosphere plasma characteristics, i.e. electronic density, ionic and electronic temperatures, ionic composition, etc. The special radar systems, the IS radars, are applied for the method realization. The generalized block diagram of the radar is shown in Fig.1. It includes the following structural units:

| RTD and TA | Medium of distribution | RRD and RA | Correlator | TNCF |
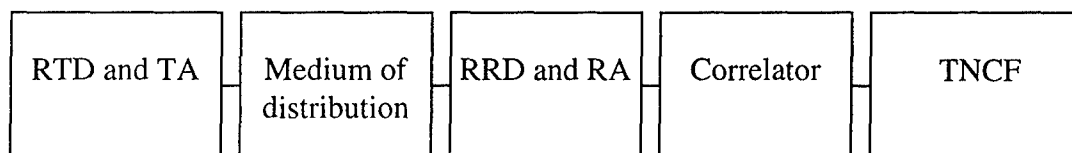
Fig. 1. The block diagram of the measuring channel

1. The transmitting antenna (TA); the radiotransmitting device (RTD), which is characterized by duration Tzi and shape U (t) of the sounding radio-frequency pulse enveloping.
2. Medium of distribution - ionosphere, which is described by the altitude dependence of the normalized correlation functions $\rho(h,\tau)$ on the thermal fluctuations of electron density.
3. The receiving antenna (RA); the radioreceiving device (RRD), which is characterized by impulse response of the receiving tract G(t) with duration t_s and nonuniformity of the noise power $\gamma(t)$.
4. The correlator, which is submitted by algorithm of an evaluation of the correlation function (CF) and performance (characteristic) of transformation of the analog-in-digital converter (ADC) g(s).
5. The transformer NCF (TNCF) in parameters of the ionospheric plasma, for example, in temperatures of ions T_i and electrons T_e (with performance $\eta[\rho(h,\tau),T_i,T_e]$, where h is the altitude, τ is the time of lag). TNCF represents a computer subprogram, which realizes calculation of temperatures by a least squares fitting of a theoretical NCF of a scattering medium to the measured function.

NONLINEAR TRANSFORMATIONS OF THE IS SIGNAL

The measuring system is rather composite with numerous, including nonlinear, signal transformations in it. To estimate the influence of systems of a radar and ionosphere on NCF of the IS signal and on temperatures T_i, T_e the following expressions for the power

$$P_s = \frac{1}{\sigma_n \sqrt{2\pi(1+q)}} \int_{-A}^{A} g^2(u)\exp[-\frac{u^2}{2\sigma_n^2(1+q)}]du - \frac{1}{\sigma_n\sqrt{2\pi}}\int_{-A}^{A}g^2(u)\exp[-\frac{u^2}{2\sigma_n^2}]du \qquad (1)$$

and correlation function

$$R_s = \frac{1}{2\pi\sigma_n^2(1+q)\sqrt{\left(1-r_{s+n}^2(\tau)\right)}}\int_{-A}^{A}\int_{-A}^{A}g(u)g(v)\exp[-\frac{u^2-2r_{s+n}(\tau)uv+u^2}{2\sigma_n^2(1+q)(1-r_{s+n}^2(\tau))}]dudv -$$

$$-\frac{1}{2\pi\sigma_n^2\sqrt{\left(1-r_n^2(\tau)\right)}}\int_{-A}^{A}\int_{-A}^{A}g(u)g(v)\exp[-\frac{u^2-2r_n(\tau)uv+v^2}{2\sigma_n^2(1-r_n^2(\tau))}]dudv \qquad (2)$$

were obtained. The equations (1) and (2) take into account the characteristics of transformation ADC, properties of a signal both noise and algorithm of operation of the correlator.

At a deduction of expressions (1) and (2) it was taken into account, that the signal can be described by the one-dimensional p (u, t) and two-dimensional p(u1, u2, t1, t2) gaussian elementary probability law [1]. Here g (u) =g (u,Δ,A), Δ is the step of quantization on a level; σ_n^2 is a variance of noise of the measuring channel; $q = P_s / <P_n>$; $<P_n> \sim \sigma_n^2$; (-A - +A) is the range of the entering voltages ADC; $r_n(\tau)$ is NCF of noise of the receiving channel; $r_{s+n}(t)$ is NCF of the signal plus noise; $P_s=P_s(t_a)$; $R_s=R_s(t_a,\tau)$; NCF $r_{s+n}(\tau) = [R_s(t_a,\tau) + R_n(t_a,\tau)]$ /$P_{norm}(t_a,t_a+\tau)$, $P_{norm}(t_a,t_a+\tau)$ are normalizing dividers; $t_a=2h_a/c$ is time of delay from forward front of sounding impulse; h_a is the altitude, for which NCF is determined; c is the velocity of light.

CF OF THE IS SIGNAL AT THE OUTPUT OF THE RECEIVING CHANNEL

Taking into account the structure of the IS signal [2] for the altitude (delay) profile $R_s(t_a,\tau)$ at a lag $\tau = \tau_k$, the expression for numerical calculation of correlation functions of a signal at the output of the receiving channel is obtained:

$$R_s(t_a,\tau) = C\int_{\frac{c(t_a+\tau-T_{zl}-t_s)}{2}}^{ct_a/2}R(h,0)\int_0^{t_s}U(t_a-v-2h/c)\gamma(t_a-v)G(v)\times$$

$$\times\int_0^{t_s}U(t_a+\tau-z-2h/c)\gamma(t_a+\tau-z)\rho_{TF}(v-z+\tau,h)G(z)dzdvdh \qquad (3)$$

Here C is the constant of radar, U (x) =0, at x > T_{zi} and x < 0.

CALCULATION OF ALTITUDE DEPENDING OF PARAMETERS OF IS SIGNAL

Figure 2 shows the initial profiles of ion and electron temperatures and normalized to a maximum value of the profile of the electron density. They are obtained from the model IRI-95. These dependences are used for calculating initial altitude dependences NCF $\rho(h,\tau,T_i,T_e)$ and the IS power $P_{in}(h)$. In the same figure, the "measured" altitude profiles of NCF of a scattering medium and normalized power $P_{out}(h)$ of the IS signal are shown which are obtained as a result of calculation of CF according to (3). Fig.2 shows the spectral power density, the normalized electron density $N_{e\,out}(h)$ and temperatures $T_{i\,out}(h)$ and $T_{e\,out}(h)$, which are calculated on the "measured" correlation functions. The transmitter pulse length Tzi=0.8ms. The impulse response of the receiver is the measured characteristic of the narrow-band filter with a transmission band 2.5 KHz. Parameter $\gamma(t)$ is equal to 1. As a result of calculation, the altitude profiles of values NCF and power corresponding to data were measured by the correlator at output of receiver device. The data is destruction due to the influence of the sounding transmitter impulse and very narrow-band filter. Next, the "measured" CFs must be processed in according to the algorithm that forms estimation of NCF and takes into account the characteristics of performances of equipment and the profile of measured power (for instance, it can be used in the procedure described in [3]).
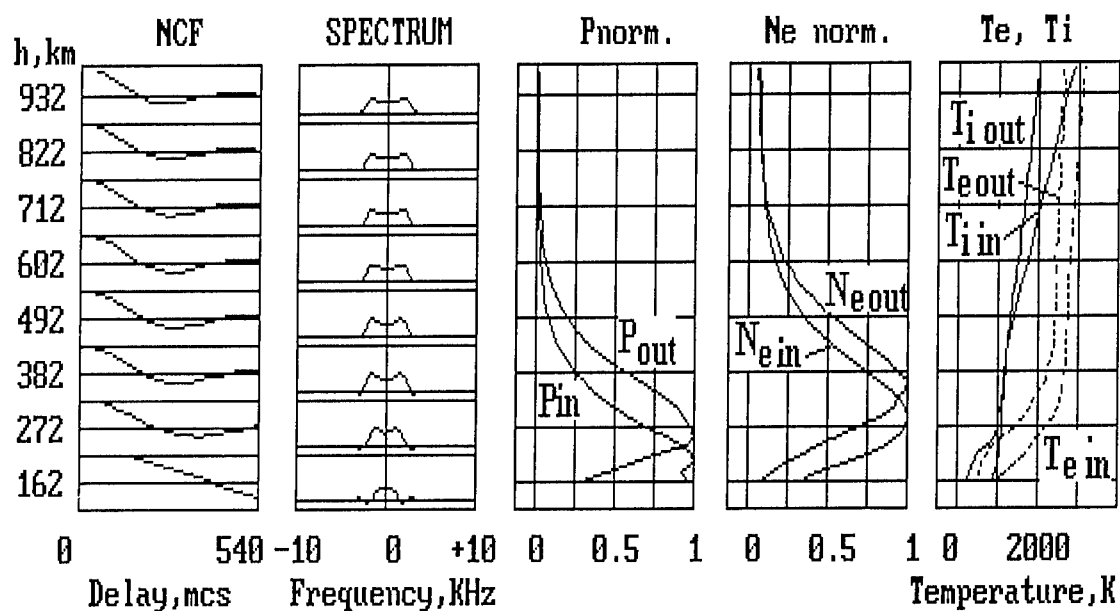
Fig. 2. Outcome of model operation of measurings of IS signal parameters.

REFERENCES

[1] V.I. Tihonov. A statistical radio engineering. M.: The Soviet radio, 1966, 678p.
[2] V.N. Lysenko. Dynamic distortions of the incoherent scatter signal //Ionosphere. The republican interdepartmental scientific and technical collection. 1991. Issue 1, p.p. 102-110.
[3] J.M. Holt, D.A. Rhoda, D. Tetenbaum and A.P. van Eyken. Optimal analysis of incoherent scatter radar data // Radio Science, Vol. 27, Number 3, 1992, p.p. 435-447.

SHORT-TERM FORECAST OF ATMOSPHERE ELECTRICAL CONDITION ON METEOROLOGICAL AND OPTICAL PARAMETERS

E.V. Ovcharenko, V.A. Donchenko, [*] V.T. Kalaida
Siberian Physical - Technical Institute, Tomsk, Russia
[*]Institute of Atmosphere Optics, Tomsk, Russia

ABSTRACT

This paper deals with the problem of interaction between the meteorological and electrical parameters of atmosphere. The method of the regression model making for nonstationary processes are presented. The model of electric field tension and meteorological parameters relationship permit to have the E consequences with the 8 per cent of remainder dispersion precision.

At present, the fact of the influence of meteorological processes on the characteristics of Atmosphere Electric Field (the tension of electric field and electroconductivity) is commonly known. A lot of experimental data have been accumulated in this scientific area. A lot of papers are devoted to the issues of the meteorological processes influence on the electric field tension and air conductivity. But often, this papers have a descriptive style.

A.X. Philipov [1] systematized the experimental data connected with the meteorological processes influence on the Atmosphere Electric Field. He has also made a table of the basic appropriations of the meteorological and electric parameters. And herein he picked out the most probable physical processes, which affect the electric field (under various meteorological conditions).

To specify the electrical and meteorological characteristics connection, it is necessary to obtain function or correlation dependencies. On the other hand, the problem of the electric field tension monitoring organization is associated with the necessity of building observation point network, or at least providing the meteorological network with electric field sensors. All this cause financial expenditure.

One of the ways of solving this problem is making of the relationship model between the electric field tension (EFT) and the standard observed meteorological parameters of the atmosphere.

The solution of this task is connected with some problems. First of all, it is a well known fact of feeble correlation between the EFT and such meteorological characteristics as temperature, humidity and pressure independently [2]. Secondly, the investigation of the day trend model area showed that the EFT is not a stationary process. Hence, the classical regression models, in particular square measure of proximity will be incorrect.

The possible variant of solving this problem may be in finding of alike dynamics of random processes, which will form a model. In this case it is possible to build of multi-factor (linear or nonlinear) regression model, which will be sufficiently reliable within the linear measure of proximity [3].

To carry out these investigations, at the automatic station [4], in May 1999 the synchronic measurements of all meteorological parameters and the EFT were organized. Using the received data, auto-correlation functions for each parameter were calculated. The calculation has shown that the moments when the auto-correlation function passes zero (the radius of auto-correlation) practically coincide and were equal to 7 hours. Proceeding from this, we can make a conclusion, that the dynamics of the processes involved into the model is identical and the terms of Kendall and Stuart are asserted. The multi-factor regression model was

constructed by "from ordinary to complex" scheme. First we investigated the possibility of linear model application.

It should be noted that the experimental series data of EFT, humidity, pressure and temperature have some peculiarities. All of the above-mentioned characteristics have a different in meanings variability range (for the EFT $E \sim \pm 1$ - 1000 V/m, $t \sim 1 \pm 30°C$, etc). Moreover, the measurement accuracy of each of these characteristics has different values, specified by the type of the devices used for measuring.

The dynamic ranges were unified in the following way. In the regression model, the standard deviations of the characteristics were taken into account (not an absolute values):

$$x_i = \frac{X_i - E(X_i)}{\sigma_i},$$
(1)

where x_i is the current value of the parameter, X_i is the process implementation, $E(X_i)$ is the mathematical expectation of the parameter, σ_i is the square root of the signal variance. Such normalization results in all the variables change within the range from 0 to 1. Hence, all dynamic ranges were equal.

Taking into account all the above mentioned facts, the following was done. In the first place, the linear set regression was verified:

$$y = \beta_0 + \beta_{11} x_1 + \dots + \beta_{1p} x_p + e,$$
(2)

where y is the Electric Field Tension, x_i is the meteorological parameter (the temperature, pressure and humidity in our case), $\beta_{ik} = \Lambda_{ik}/\Lambda_{ii}$, where $\Lambda_{ik} = (\lambda_{ik})^{-1}$ is the inverse covariation matrix, $\Lambda = E[X-E(X)][X-E(X)]^T$, where X is the row vector of observation data, $E(X)$ is the mathematical expectation of the parameter, T is transpose indicator, e is error (the remnant value in the regression model).

The covariation matrix (the matrix of the second moments) was calculated using the 30 days observation in May 1999. The time quantization of the signal was equal to 30 minutes. In the capacity of precision measure we used the difference between y and its regression estimation (i.e. remainder of variance):

$$D = \frac{1}{\Lambda_{ii}}.$$
(3)

The results of the calculation show that in this case the linear regression model can determine the reliable regression relationships between electric and meteorological parameters with the 10 -30% of deviation. In general, such accuracy is enough for the short term forecast of EFT on the basis of meteorological parameters data.

Table 1. *The results of using the linear regression model*

Duration of observation period, days	Confidence coefficient	Remnant dispersion of standard deviation
10	0.67	0.328
20	0.67	0.213
30	0.67	0.109

To specify this relationship, the nonlinear (polynomial) regression model was developed by using the following equation:

$$y = f(x_{1i}, \dots x_{pi}; \theta, \dots \theta_m) + e_i; i = 1 \dots n,$$
(4)

where $y(x_i, \theta_1, \theta_2, \theta_3)$ was introduced as the random values product of meteorological parameters x_k, $x_i \times x_j$. Since the series of the observation are rather short, we chose the binary relationships, i.e. three dimension polynom of the third order:

$$y = \sum_{i=0}^{n} \sum_{j=0}^{n} \sum_{k=0}^{n} \beta_{ijk} \cdot x_1^i x_2^j x_3^k, n = 2, i + j + k \le 2. \tag{5}$$

The result of using the nonlinear (polynomial) regression model is shown in Tab.2.

Table 2. *The result of using the nonlinear (polynomial) regression model*

Duration of observation period, days	Confidence coefficient	Remnant dispersion of standard deviation
10	0.67	0.221
20	0.67	0.159
30	0.67	0.082

It is natural that one month retrieval parameter values are not statistically significant, i.e. providing the necessary precision of the data obtained. But the above predicted arguments verify this conventional hypothesis. Hence, we can build a reliable multi - factor model, based on more long-term observation data, enabling us to obtain the value of EFT.

REFERENCES

[1] Philipov A.X Investigation of the electric and meteorological characteristics relationship. 1980. 335p

[2] Kobec V.P. Investigation of the atmosphere electric field. Ph.D. referat. Tomsk - 1998, 25p.

[3] Kendall M.J., Stuart A. Multi-order statistical analyses and time series. M.:Science, 679p.

[4] Panchenko M.V., Terpugova C.A., Belan B.D., etc. The metodical aspects of the plane nefelometer investigationof the troposphere aerosols in region. Optics of Atmosphere and Ocean 1994, V.7, N8, P.1022 - 1033 .

FUNCTION-THEORETIC

METHODS

A NEW NUMERICAL APPROACH TO ELECTROMAGNETICS: FINITE-ANALYTIC METHOD

Cuneyt Utku and Bahattin Turetken*

Technical University of Istanbul
Dept. of Electronics and Communication Eng.,
80626 Maslak, Istanbul, Turkey
Email: cuxu@ehb.itu.edu.tr

* TUBITAK-UEKAE
P.O.Box:21 41470 Gebze,Kocaeli, Turkey
Email: bahattin@mam.gov.tr

INTRODUCTION

Among the various methods used to solve differential equations, the finite differencing schemes are the easiest to implement, this feature usually being a trade-off for the accuracy of the solution. The finite-analytic (FA) method, which basically yields a simple but accurate finite differencing (FD) scheme has been utilized for solving heat transfer and fluid mechanics problems for sometime [1-2]. A general formulation for the FA method has been summarized and devised for the Helmholtz equation. A numerical example has been studied.

GENERAL FORMULATION

Assume that the analytic solution of a differential equation at any point of a local grid of n discrete points, can be expressed by a truncated series of suitable basis functions as,

$$f(\widetilde{x}_i) \cong \sum_{v=1}^{k-1} a_v A_v(\widetilde{x}_i), \quad i = 1,2,...,n \tag{1}$$

where $f(\widetilde{x}_i)$ is the solution of the differential equation, $\widetilde{x}_i : i = 1,..,n$ is a vector of m independent variables of spatial type, $A_v(\widetilde{x})$, $v = 1,2,...$ are the basis functions and a_v are the expansion coefficients. Eq. (1) yields n linear equations, one for each point of the local grid. For non-trivial solutions, the determinant of the system of linear equations of (1) must vanish,

$$\begin{vmatrix} f(\widetilde{x}_1) & f(\widetilde{x}_2) & \cdots & f(\widetilde{x}_{n-1}) & f(\widetilde{x}_n) \\ A_1(\widetilde{x}_1) & A_1(\widetilde{x}_2) & \cdots & A_1(\widetilde{x}_{n-1}) & A_1(\widetilde{x}_n) \\ \vdots & \vdots & \ddots & \vdots & \vdots \\ A_{n-1}(\widetilde{x}_1) & A_{n-1}(\widetilde{x}_2) & \cdots & A_{n-1}(\widetilde{x}_{n-1}) & A_{n-1}(\widetilde{x}_n) \end{vmatrix} = 0 \tag{2}$$

Expanding (2) with respect to the first row yields the FA representation of the related differential equation,

$$\sum_{i=1}^{n} (-1)^{i+1} M_i f(\widetilde{x}_i) = 0 \tag{3}$$

where M_i is the minor corresponding to the element $f(\widetilde{x}_i)$. Equations (2) and (3) are valid for the interior points of the solution domain. For the Cauchy boundary condition the following representation can be used in (3) for boundary points

$$\chi = \alpha f(\tilde{x}_b) + \beta f'(\tilde{x}_b) = \sum_{v=1}^{n-1} a_v \left[\alpha A_v(\tilde{x}_b) + \beta A'_v(\tilde{x}_b) \right] \tag{4}$$

where the prime is the derivative with respect to some variable and $\tilde{x}_b$ is a boundary point.

APPLICATION TO THE HELMHOLTZ EQUATION

Although different series representations in (1) can be used, the power series based FA representation is derived and used in this work for the two dimensional Helmholtz equation. A power series expansion for the solution of the Helmholtz equation can be written as

$$f(x,y) = \sum_{i=0}^{\infty} \sum_{j=0}^{i} c_{i,j} x^j y^{i-j} \tag{5}$$

where $c_{i,j}$ are the series coefficients. Substituting (5) in the Helmholtz equation will give the following recursion relation between the coefficients,

$$c_{i,j+2} = -\left((i-j)(i-j-1)c_{i,j} + \gamma^2 c_{i-2,j}\right) \big/ ((j+2)(j+1)) \tag{6}$$

where γ is the wavenumber. Thus upon using the recursion relation of (6) in (5) and arranging in terms of the unknown coefficients, one obtains the following as basis functions.

$$A_1(x,y) = 1 - \gamma^2 x^2 / 2 + \gamma^4 x^4 / 24 \;,\;\; A_2(x,y) = y - \gamma^2 x^2 y / 2 \;,\;\; A_3(x,y) = x - \gamma^2 x^3 / 6$$

$$A_4(x,y) = y^2 - x^2 - \gamma^2 x^2 y^2 / 2 + \gamma^2 x^4 / 6 \;,\;\; A_5(x,y) = xy - \gamma^2 x^3 y / 6 \tag{7}$$

$$A_6(x,y) = y^3 - 3x^2 y \;,\;\; A_7(x,y) = xy^2 - x^3 / 3 \;,\;\; A_8(x,y) = y^4 - 6x^2 y^2 + x^4$$

For a local grid of nine points one can write (2) by considering a point (i, j) as the origin of the local grid. Thus at the origin (i, j), $A_1(0,0) = 1, A_2(0,0) = A_3(0,0) = A_4(0,0) = A_5(0,0) = A_6(0,0) = A_7(0,0) = A_8(0,0) = 0$. Assigning for x and y in (7), the displacements from the origin. and noting that for the minors of reduced determinant

$$\begin{vmatrix} f_{i-1,j-1} & f_{i,j-1} & f_{i+1,j-1} & f_{i-1,j} & f_{i+1,j} & f_{i-1,j+1} & f_{i,j+1} & f_{i+1,j+1} \\ A_2(-w,-h) & A_2(0,-h) & A_2(w,-h) & A_2(-w,0) & A_2(w,0) & A_2(-w,h) & A_2(0,h) & A_2(w,h) \\ A_3(-w,-h) & A_3(0,-h) & A_3(w,-h) & A_3(-w,0) & A_3(w,0) & A_3(-w,h) & A_3(0,h) & A_3(w,h) \\ \vdots & \vdots & \vdots & \vdots & \vdots & \vdots & \vdots & \vdots \\ A_8(-w,-h) & A_8(0,-h) & A_8(w,-h) & A_8(-w,0) & A_8(w,0) & A_8(-w,h) & A_8(0,h) & A_8(w,h) \end{vmatrix} \tag{8}$$

$R_1 = R_3 = R_6 = R_8, R_2 = R_7, R_4 = R_5$ where $R_i : i = 1,2,...,8$ are the minors of the first row of (8) respectively and w and h are the displacements from the origin of the local grid in the x and y directions respectively. Thus the FA representation of (3) can be expressed as,

$$M_5 f_{i,j} = R_1 \left(f_{i-1,j-1} + f_{i+1,j-1} + f_{i-1,j+1} + f_{i+1,j+1} \right) - R_2 \left(f_{i,j-1} + f_{i,j+1} \right) - R_4 \left(f_{i-1,j} + f_{i+1,j} \right) \tag{9}$$

where M_5 is the minor of (2) corresponding to the element $f_{i,j}$. Furthermore if $w = h$ it can be shown that $R_2 = R_4$. The minors in (9) can be computed numerically. Assigning $\gamma = 0$ in (7) will yield the FA representations given in [3] for the Laplace equation.

NUMERICAL EXAMPLE

The FA representation (9) is used to calculate the scalar Green's function inside a rectangular waveguide satisfying Dirichlet boundary conditions and excited by a line source directed along the guide with both dimensions equal to the wavelength $\lambda = 1$ m. The difference between the numerical and the analytic results has been normalized by the analytic solution to give the normalized error pattern inside the guide's cross-section. The error patterns for the five-point (5P-FD), nine-point (9P-FD) and the FA schemes have been depicted in Fig. 1.
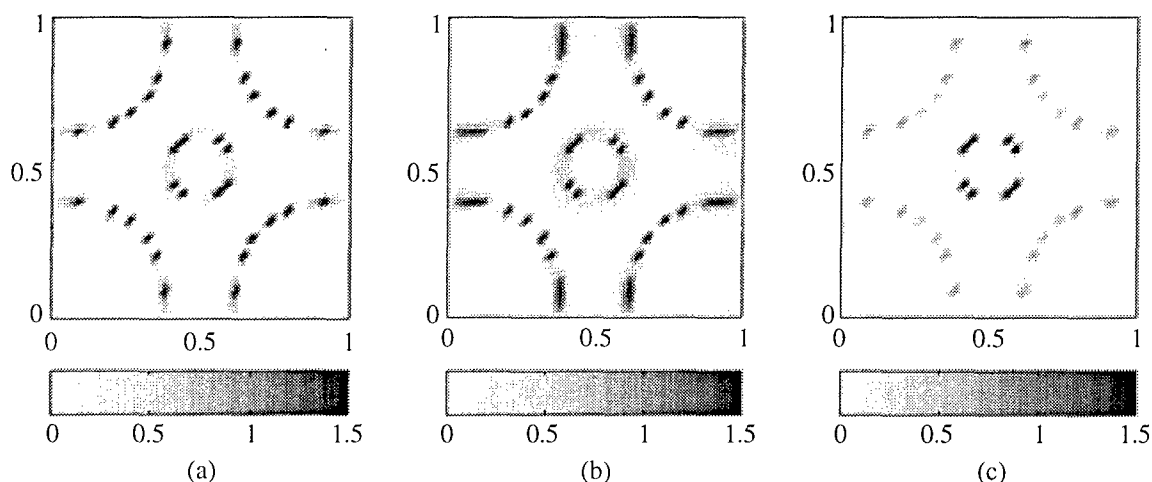

Fig. 1. Normalized error patterns for (a) 5P-FD (b) 9P-FD and (c) FA schemes

The system of equation for the whole grid has been solved by the conjugate gradient method. The 5P-FD scheme has converged with a relative residual of 0.00049 at 47 iterations, the 9P-FD scheme has converged with a relative residual of 0.00041 at 39 iterations and the FA scheme has converged with a relative residual of 0.00032 at 39 iterations. The FA scheme has shown the best over all performance.

CONCLUSION

A finite-analytic scheme, based on power series expansion, has been developed for the 2-D Helmholtz equation. The scheme developed here has proven to be better performing than the classical 5P-FD and 9P-FD schemes for the waveguide problem considered. Depending on the problem, different series expansions can be utilized for the FA scheme for higher accuracy giving the opportunity to develop a problem oriented FD scheme. Once the appropriate FA scheme has been developed one can use the resulting FD scheme to increase the accuracy and the efficiency of the solution without increasing the complexity of the FD scheme.

REFERENCES

[1] C.J. Chen, and P. Li, , "The finite analytic method for steady-state and unsteady heat transfer problems," 19th ASME/AIChE U.S. National Heat Transfer Conference, Orlando, FL, ASME Paper No. 80-HT-86, July 27-30, 1980.

[2] C.J. Chen. and H.C. Chen, "Finite analytic method for unsteady two dimensional Navier-Stokes equation," J. Comp. Phsy., vol. 53(2), pp. 209-226, 1984.

[3] F. Civan, "Practical implementation of the finite-analytic method," Appl. Math. Modelling, vol. 19, May, 1995.

ON AN APPLICATION OF THE KUMMER CONFLUENT HYPERGEOMETRIC FUNCTIONS

Georgi N. Georgiev[(1)], Tikhomir I. Stoyanov[(1)] and Mariana N. Georgieva-Grosse[(2)]

[(1)] Faculty of Mathematics and Informatics
University of Veliko Tirnovo "St. St. Cyril and Methodius"
BG-5000 Veliko Tirnovo, BULGARIA
E-mail: gngeorgiev@yahoo.com

[(2)] Meterstrasse 4/2, D-70839 Gerlingen, GERMANY
E-mail: Mariana.G@t-online.de

ABSTRACT

A lemma concerning an important property of the real zeros of Kummer func-tion is proved numerically. Based on it and on some known attributes of the latter, criteria for slow TE_{0n} modes propagation in a circular waveguide with azimuthally magnetized ferrite are drawn. The phase characteristics of the configuration for slow TE_{01} mode are presented.

INTRODUCTION

The complex Kummer confluent hypergeometric functions (CHFs) have been used to study normal TE_{0n} modes in the azimuthally magnetized circular ferrite waveguides [1-3]. The introduction of the real Kummer CHFs as wave functions for propagation, made here, reveals that slow TE_{0n} modes may also be transmitted in this class of structures in case of negative magnetization of the medium.

A PROPERTY OF THE REAL ZEROS OF KUMMER FUNCTION

Tricomi [4] has proved that if $\hat{a}, \hat{c}, \hat{x}$ are real, $\hat{x} > 0$ and $\hat{c} > 0$: i) The Kummer CHF $\Phi(\hat{a}, \hat{c}; \hat{x})$ [4] has real positive zeros only if $\hat{a} < 0$. ii) The number of zeros $l = abs[\hat{a}] + 1$ is finite, ($[\hat{a}]$ is the integer part of $\hat{a}$). iii) At the point $\hat{a} = [\hat{a}] = -n$, ($n \le l$ - a positive integer) a new zero appears.

Let $\hat{k} = \hat{a} - \hat{c}/2$ and $\hat{\varsigma}_{\hat{k},n}^{(\hat{c})}$ $(n = 1,2,...,l)$ be the consecutive zeros of Φ in $\hat{x}$ for specific $\hat{c}$. The numerical analysis shows that it holds $\lim\limits_{\hat{k} \to -(n-1)-\hat{c}/2} \hat{\varsigma}_{\hat{k},n}^{(\hat{c})} = +\infty$ and $\lim\limits_{\hat{k} \to -\infty} \hat{\varsigma}_{\hat{k},n}^{(\hat{c})} = 0$. Besides, it turns out that the products $\left|\hat{k}\right| \hat{\varsigma}_{\hat{k},n}^{(\hat{c})}$ are of special interest if $\left|\hat{k}\right|$ becomes very large (cf. Table 1). The numerical results permit to formulate the following Lemma.

Table 1. *Values of the first real positive zeros $\hat{\varsigma}_{\hat{k},1}^{(3)}$ of $\Phi(1.5 + \hat{k}, 3; \hat{x})$ and of the products $\left|\hat{k}\right| \hat{\varsigma}_{\hat{k},1}^{(3)}$ for large negative $\hat{k}$.*

$\hat{k}$	$\hat{\varsigma}_{\hat{k},1}^{(3)}$	$\left|\hat{k}\right| \hat{\varsigma}_{\hat{k},1}^{(3)}$	$\hat{k}$	$\hat{\varsigma}_{\hat{k},1}^{(3)}$	$\left|\hat{k}\right| \hat{\varsigma}_{\hat{k},1}^{(3)}$
-1000	0.0065936585	**6.5936585**	-10000	0.0006593654151	**6.593654151**
-2000	0.0032968276	**6.5936552**	-20000	0.0003296827058	**6.593654117**
-4000	0.0016484135	**6.5936543**	-40000	0.0001648413527	**6.593654109**
-6000	0.0010989423	**6.5936542**	-60000	0.0001098942351	**6.593654108**
-8000	0.00082420677	**6.5936541**	-80000	0.00008242067634	**6.593654107**
-10000	0.00065936541	**6.5936541**	-100000	0.00006593654107	**6.593654107**

Lemma 1: If $\hat{\varsigma}_{k,n}^{(\hat{c})}$ is the n th real positive zero of the Kummer CHF $\Phi(\hat{a},\hat{c};\hat{x})$ in case $\hat{a},\hat{c},\hat{x}$ - real, $\hat{x}>0$, $\hat{c}>0$, restricted and $\hat{k}=\hat{a}-\hat{c}/2$, the infinite sequence of numbers $\left\{\left|\hat{k}\right|\hat{\varsigma}_{k,n}^{(\hat{c})}\right\}$ is convergent for $\hat{k}\rightarrow-\infty$ and its limit $\hat{L}$ depends on $\hat{c}$ and n.

APPLICATION TO AZIMUTHALLY MAGNETIZED CIRCULAR FERRITE WAVEGUIDE ANALYSYS

The solution of propagation problem for slow TE_{0n} modes in a circular waveguide with ferrite, magnetized azimuthally to remanence by an infinitely thin central conductor yields the equation

$$\Phi(\hat{a},\hat{c};\hat{x}_0)=0 \tag{1}$$

The ferrite has a permeability tensor with off-diagonal element $\alpha = \gamma M_r / \omega$ (γ - gyromagnetic ratio, M_r - remanent magnetization, ω - angular frequency of the wave) and a scalar permit-tivity $\varepsilon = \varepsilon_0 \varepsilon_r$. In eqn. (1)

$\hat{a}=1.5+\hat{k}$, $\hat{c}=3$, $\hat{k}=\alpha\bar{\beta}/\left(2\bar{\beta}_2\right)$, $\bar{\beta}_2=\left[\bar{\beta}^2-\left(1-\alpha^2\right)\right]^{1/2}$, $\hat{x}_0=2\bar{\beta}_2\bar{r}_0$. The quantities $\bar{\beta}=\hat{\beta}/\left(\beta_0\sqrt{\varepsilon_r}\right)$, $\bar{\beta}_2=\hat{\beta}_2/\left(\beta_0\sqrt{\varepsilon_r}\right)$, $\bar{r}_0=\beta_0 r_0\sqrt{\varepsilon_r}$ are the phase constant, radial wavenumber and guide radius, normalized with the free space phase constant $\beta_0=\omega\sqrt{\varepsilon_0\mu_0}$ and relative permittivity ε_r. Eqn. (1) is satisfied if $\bar{\beta}_2 = \hat{\varsigma}_{k,n}^{(\hat{c})}/\left(2\bar{r}_0\right)$. A finite number n of slow TE_{0n} modes, equal to that of the zeros $\hat{\varsigma}_{k,n}^{(\hat{c})}$ of $\Phi(\hat{a},\hat{c};\hat{x}_0)$ for relevant $\hat{a}$ may be sustained for $\alpha<0$ only.

If σ is any of parameters α or $\bar{\beta}$, it satisfies a biquadratic equation with roots $\sigma_{1,2}$:

$$\sigma^4 - \left(1+\bar{\beta}_2^2\right)\sigma^2 + 4\bar{\beta}_2^2\hat{k}^2 = 0 \tag{2}$$

$$\sigma_{1,2}^2 = 0.5\left[\left(1+\bar{\beta}_2^2\right)\pm\sqrt{\left(1+\bar{\beta}_2^2\right)^2 - 4\times4\bar{\beta}_2^2\hat{k}^2}\right] \tag{3}$$

Denoting by $\left|\alpha_1\right|,\left|\alpha_2\right|$ and $\bar{\beta}_{(1)}$, $\bar{\beta}_{(2)}$ the roots of corresponding equations for α and $\bar{\beta}$, it may be shown that $\left|\alpha_1\right|=\bar{\beta}_{(2)}$, $\left|\alpha_2\right|=\bar{\beta}_{(1)}$. Thus, the phase curves $\bar{\beta}(\left|\alpha\right|)$ are symmetric with respect to the bisectrix of the right angle $\left|\alpha\right| 0 \bar{\beta}$. The numerical analysis shows that eqn. (3) has real solutions (the discriminant $\Delta = \left[\hat{\varsigma}_{k,n}^{(\hat{c})}\right]^2 - 8\bar{r}_0\,\hat{\varsigma}_{k,n}^{(\hat{c})}\left|\hat{k}\right| + 4\bar{r}_0^2 \geq 0$) in two regions:

i) $-(n-1)-c/2 > \hat{k} \geq \hat{k}_{\lim}^i(\bar{r}_0)$ and ii) $\hat{k}_{\lim}^{ii}(\bar{r}_0) \geq \hat{k} > -\infty$. Since $\lim\limits_{\hat{k}\rightarrow-(n-1)-c/2}\sigma_1 \rightarrow +\infty$ and $\lim\limits_{\hat{k}\rightarrow-(n-1)-c/2}\sigma_2 \rightarrow 2\left|\hat{k}\right|=2(n-1)+c$, the condition for propagation in the first one is $\left|\alpha\right| > 2(n-1)+c$ ($\left|\alpha\right|>3$ for TE_{01} mode) (case of strong anisotropy). Neglecting $\left[\hat{\varsigma}_{k,n}^{(\hat{c})}\right]^2$ in Δ when $\hat{k}\rightarrow-\infty$ and applying Lemma 1, the condition for propagation in the second region is obtained:
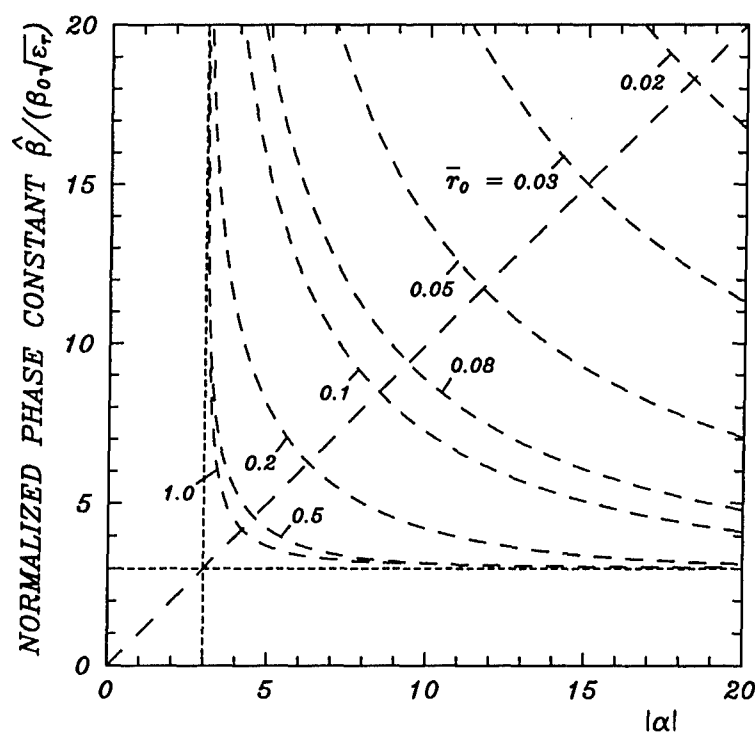
$$\bar{r}_0 \geq 2\hat{L}(\hat{c},n) \tag{5}$$

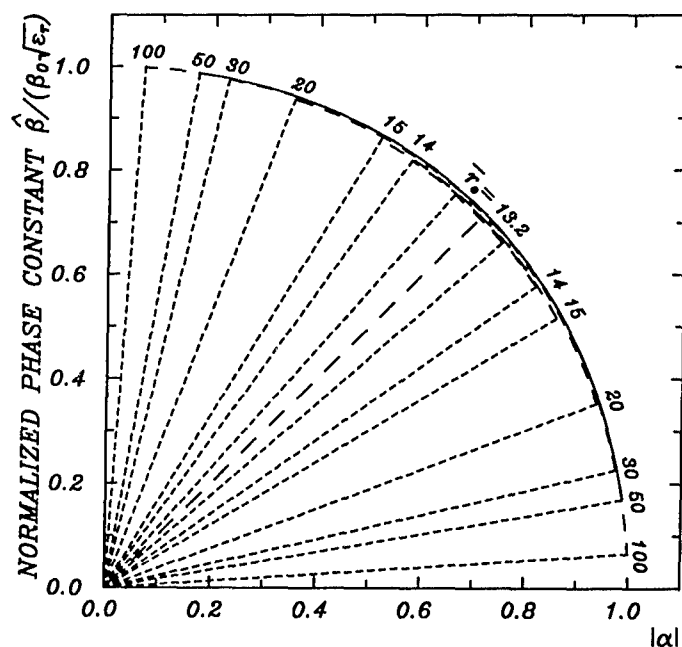**Fig.1.** $\overline{\beta}(|\alpha|)$ *curves of slow* TE_{01} *mode for*

Since $\lim\limits_{\substack{\hat{k}\to-\infty \\ \overline{r}_0\to+\infty}} \sigma_1 \to 1$ and

$\lim\limits_{\substack{\hat{k}\to-\infty \\ \overline{r}_0\to+\infty}} \sigma_2 \to 0$, it is equivalent

to $0<|\alpha|<1$ (case of weak anisotropy). The $\overline{\hat{\beta}}(|\alpha|)$ phase characteristics for TE_{01} mode in the two ranges are presented in Figs. 1, 2, respectively.

CONCLUSION

A property of the real zeros of Kummer CHFs is found out. Combined with know facts for the functions and their zeros, due to Tricomi, the main features of the slow TE_{0n} modes in a circular ferrite waveguide with azimuthal magnetization are determined: possibility for propagation in case of negative magnetization only in two areas, corresponding to weak and strong ferrite anisotropy.

REFERENCES

[1] J.Helszajn, *Ferrite Phase Shifters and Control Devices*, McGraw-Hill, London: K.P. Ivanov, G.N. Georgiev, "Azimuthally magnetized circular ferrite waveguides", chap. 14, pp. 262-288, 1989.

[2] A.A.P. Gibson, R. Sloan, L.E. Davis, D.K. Paul, "Double valued phase constants in gyrotropic waveguides", *IEE Proc., Part H, Microwaves, Antennas and Propa-gation*; vol. 138, pp. 258-260, June 1991.

Fig.2. $\overline{\hat{\beta}}(|\alpha|)$ *curves of slow* TE_{01} *mode for* $0<|\alpha|<1$.

[3] G.N. Georgiev, M.N. Georgieva-Grosse, "Formulae for differential phase shift computation in an azimuthally magnetized circular ferrite waveguide", *Millennium Conf. on Antennas and Propagation AP2000*, Davos, Switzerland, 9-14, Apr. 2000.

[4] F.G. Tricomi, *Fonctions Hypergéométrique Confluentes*, Gauthier-Villars, Paris, France, 1960.

A LAPLACE TRANSFORM TECHNIQUE FOR WEDGE SHAPED ISOREFRACTIVE REGIONS

V. Daniele, M. Gilli, and S. Grivet-Talocia

Dipartimento di Elettronica
Politecnico di Torino, Torino, Italy
e-mail: gilli@polito.it

Many techniques have been proposed for studying wedge shaped regions: among them it is important to mention the Malyuzhinets approach [1], which is based on the Sommerfeld representation. This technique yields an elegant formal procedure for solving difficult problems, like the diffraction by wedges with given surface impedances. However, even if the Sommerfeld integral is a valid ansatz for representing the solutions of the wave equation in angular regions, the Laplace transform appears to be a more valid representation, because of its solid mathematical foundation. Some authors [2, 3] have shown that the Laplace transform technique may be alternative with respect to the Malyuzhinets approach, even if in some cases it is not so simple and elegant.

In this paper we propose a new technique, based on the Laplace representations of the electromagnetic field, for solving isorefractive angular regions (Fig. 1) excited by an incident E-polarized plane wave in the z-direction. The technique can be briefly summarized as follows.
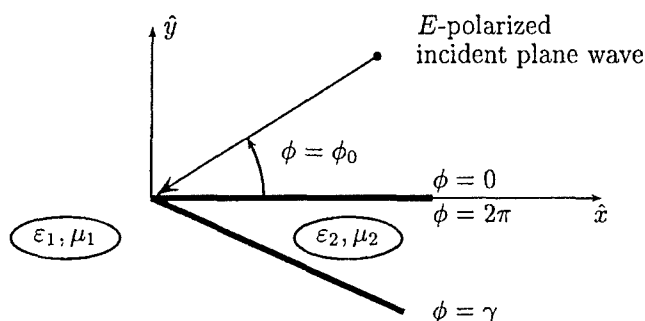
Figure 1: Geometry of the problem under investigation

By introducing the Laplace transform of the E_z and H_ρ components of the electromagnetic field

$$V(s, \phi) = \int_0^\infty E_z(\rho, \phi) \exp(-s\rho) d\rho \tag{1}$$

$$I(s, \phi) = \int_0^\infty H_\rho(\rho, \phi) \exp(-s\rho) d\rho \tag{2}$$

it is shown that in every angular homogeneous region the following representations hold

$$k \sin(w) V(s, \phi)|_{s=-jk\cos(w)} = A(w + \phi) + B(w - \phi) \tag{3}$$

$$Z I(s, \phi)|_{s=-jk\cos(w)} = A(w + \phi) - B(w - \phi) \tag{4}$$

where $k = \sqrt{\varepsilon_1 \mu_1} = \sqrt{\varepsilon_2 \mu_2}$ is the propagation constant of the isorefractive regions, $Z = 1/Y = \sqrt{\mu/\varepsilon}$ is the relevant impedance, and $A(w)$, $B(w)$ are suitable unknown functions.

By imposing the boundary conditions at the two interfaces $\phi = 0 - 2\pi$ and $\phi = \gamma$, the following system of linear difference equations is obtained

$$A_1(w) + B_1(w) = A_2(w + 2\pi) + B_2(w - 2\pi) \tag{5}$$

$$Y_1[A_1(w) - B_1(w)] = Y_2[A_2(w + 2\pi) - B_2(w - 2\pi)] \tag{6}$$

$$A_1(w + \gamma) + B_1(w - \gamma) = A_2(w + \gamma) + B_2(w - \gamma) \tag{7}$$

$$Y_1[A_1(w + \gamma) - B_1(w - \gamma)] = Y_2[A_2(w + \gamma) - B_2(w - \gamma)] \tag{8}$$

By multiplying both the sides of (5) by Y_2 and by summing and subtracting (6) from the resulting equation, we have

$$2Y_2 A_2(w + 2\pi) = (Y_2 + Y_1)A_1(w) + (Y_2 - Y_1)B_1(w) \tag{9}$$

$$2Y_2 B_2(w - 2\pi) = (Y_2 - Y_1)A_1(w) + (Y_2 + Y_1)B_1(w) \tag{10}$$

Then, the explicit solution with respect to A_2 and B_2 yields

$$A_2(w) = \frac{1 + Z_2 Y_1}{2} A_1(w - 2\pi) + \frac{1 - Z_2 Y_1}{2} B_1(w - 2\pi) \tag{11}$$

$$B_2(w) = \frac{1 - Z_2 Y_1}{2} A_1(w + 2\pi) + \frac{1 + Z_2 Y_1}{2} B_1(w + 2\pi) \tag{12}$$

Finally the substitution of expressions (11) and (12) into (7) and (8) allows to write the following homogeneous system, involving only the unknown functions $A_1(w)$ and $B_1(w)$

$$A_1(w + \gamma) + B_1(w - \gamma) = \frac{1 + Z_2 Y_1}{2} A_1(w + \gamma - 2\pi) + \frac{1 - Z_2 Y_1}{2} B_1(w + \gamma - 2\pi)$$

$$+ \frac{1 + Z_2 Y_1}{2} A_1(w - \gamma + 2\pi) + \frac{1 - Z_2 Y_1}{2} B_1(w - \gamma + 2\pi) \tag{13}$$

$$Y_1[A_1(w + \gamma) - B_1(w - \gamma)] = \frac{Y_1 + Y_2}{2} A_1(w + \gamma - 2\pi) + \frac{Y_2 - Y_1}{2} B_1(w + \gamma - 2\pi)$$

$$- \frac{Y_2 + Y_1}{2} A_1(w - \gamma + 2\pi) - \frac{Y_2 - Y_1}{2} B_1(w - \gamma + 2\pi) \tag{14}$$

At the interface $\phi = 0$, the longitudinal component of the electric and the magnetic fields can be written as the sum of the geometrical and the diffracted fields (E^d, H^d) as follows

$$E_z(\rho, 0) = A_0 \exp[jk\rho \cos(\phi_0)] + E_z^d(\rho) \tag{15}$$

$$H_\rho(\rho, 0) = Y_1 A_0 \sin(\phi_0) \exp[jk\rho \cos(\phi_0)] + H_\rho^d(\rho) \tag{16}$$

The corresponding Laplace Transforms $V(s, 0)$ and $I(s, 0)$ evaluated for $s = -jk\cos(w)$ take the

form

$$k \sin(w) V(s,0)\big|_{s=-jk\cos(w)} = k\sin(w) \int_0^\infty E_z(\rho,0)\exp(-s\rho)d\rho\bigg|_{s=-jk\cos(w)}$$

$$= \frac{j\sin(w)A_0}{\cos(w)+\cos(\phi_0)} + X(w)$$

$$I(s,0)\big|_{s=-jk\cos(w)} = \int_0^\infty H_\rho(\rho,0)\exp(-s\rho)d\rho\bigg|_{s=-jk\cos(w)}$$

$$= Y_1\bigg[\frac{j\sin(\phi_0)A_0}{\cos(w)+\cos(\phi_0)} + Y(w)\bigg]$$

(17)

where $X(w)$ and $Y(w)$ represent the Laplace Transforms (evaluated for $s = -jk\cos(\phi)$) of the diffracted electric and magnetic fields respectively, multiplied by Z_1.

Due to the boundary conditions at $\phi = 0$, equations (3) and (4) yield

$$\frac{j\sin(w)A_0}{\cos(w)+\cos(\phi_0)} + X(w) = A_1(w) + B_1(w)$$

$$\frac{j\sin(\phi_0)A_0}{\cos(w)+\cos(\phi_0)} + Y(w) = A_1(w) - B_1(w)$$

(18)

By deriving from (18) the explicit expressions of $A_1(w)$ and $B_1(w)$ in terms of $X(w)$ and $Y(w)$ and by substituting such expressions in (13) and (14), we obtain a difference equation system which involves only the two unknowns $X(w)$ and $Y(w)$.

The advantage of addressing this system instead of (13)-(14) is that, owing to physical considerations, it is readily derived that the unknowns $X(w)$ and $Y(w)$ do not exhibit poles in the strip of complex w plane, within the interval $0 \le Re(w) < 2\pi$. This allows to solve the system of difference equations containing $X(w)$ and $Y(w)$ by using the Fourier Transform approach introduced in [1]

$$\tilde{X}(\nu) = \mathcal{F}[X(w)] = \int_{-j\infty}^{j\infty} X(w)\exp(j\nu w)dw; \quad \tilde{Y}(\nu) = \mathcal{F}[Y(w)] = \int_{-j\infty}^{j\infty} Y(w)\exp(j\nu w)dw$$

(19)

that, owing to the pole location, satisfies the property

$$\mathcal{F}[X(w+w_0)] = \tilde{X}(\nu)\exp(-j\nu w_0); \quad \mathcal{F}[Y(w+w_0)] = \tilde{Y}(\nu)\exp(-j\nu w_0)$$

(20)

The mathematical derivation of the unknowns, first in the spectral and then in the natural domain, presents several details and some delicate aspects, that, for lack of space, cannot be discussed here. They will be outlined and dealt with during the conference presentation.

References

[1] G. D. Maliuzhinets, "Excitation, Reflection, and emission of surface waves from a wedge with given face impedances," *Sov. Phys. Dokl, Eng. Trans.*, vol. 3, pp. 752-755, 1958.

[2] A.S. Peters, "Water waves over sloping beaches and the solution of a mixed boundary value problem for $\nabla^2 f - k^2 f = 0$ in a sector," *Communications on pure and applied mathematics*, vol. 5, pp. 97-108, 1952.

[3] W. E. Williams, "Diffraction of an E-polarized plane by imperfectly conducting wedge," *Proc. R. Soc. Lond. A*, vol. 252, pp. 376-393, 1959

ONE GENERALISATION OF PROJECTIVE METHOD FOR THE WAVE DIFFRACTION PROBLEMS

I.V. Petrusenko*, and L.I. Chernish**

*Electronics Engineering Department, Gebze Institute of Technology,
Cayrova kampus, 41400 P.K. 141, Gebze/Kocaeli, Turkey, petrus@penta.gyte.edu.tr
**Radiophysics Department, Dniepropetrovsk State University,
Naukova lane, 13, Dniepropetrovsk – 50, 320625, Ukraine, lili@ap1.net-rff.dsu.dp.ua

ABSTRACT

For the canonical problem of electrodynamic analysis of waveguide step discontinuity new system of interlinked integral equations has been derived, which depends on some continuous parameter. Varying this parameter the matrix models corresponding to both well – known methods of partial regions and other possible techniques, for which a geometric interpretation is absent, are obtained. This approach makes it possible to compare the properties of matrix operators and effectiveness of some widely used methods of applied electrodynamics.

The projective methods take special place among the rigorous numerical – analytical methods of the wave diffraction theory. The usually used ones are the method of moments (MoM) and the mode – matching technique. In [1] on the basis of H. Shwartz' ideas the method of partial overlapping regions (OR) was proposed, which yielded another matrix operators [2]. But on this day the problems of correctness for matrix models obtained by MoM and effectiveness of OR – method are still open [3].

With this in mind, for the canonical problem of LM - wave diffraction on a step discontinuity in parallel – plate waveguide both new system of integral equations and matrix model have been obtained, which depend on some continuous parameter. Two particular values of this parameter correspond to MoM and OR – method, while a remaining part of its interval of definition suits the another possible techniques, for which it is difficult to make a geometrical interpretation. As result, this approach makes it possible to compare all of these methods analytically and numerically.

The problem under consideration is reduced to solution of the two – dimensional Helmholtz equation for scalar function $U(x,z)$ (E_y field component), which satisfies Dirichlet boundary condition on perfectly conducting metal walls. As usual, the whole domain of field determination is divided onto two semi – infinite uniform waveguides: (1) $x \in [0,b]$, $z \in (\infty,0]$; (2) $x \in [0,a]$, $z \in [0,\infty)$. Let also a field source is placed in first region and is absent in second one.

Taking into account the field continuity condition on the common boundary of partial regions $x \in (0,a)$, the sought solutions for each uniform waveguide can be expressed with the help of the second Green's formula in the form

$$\begin{cases} U_1(\bar{r}) = U_{inc}(\bar{r}) - \int_0^a \left\{ U_2(\bar{r}') \frac{\partial G_1}{\partial z'} \right\}_{z'=0} dx'; \\ U_2(\bar{r}) = \alpha \int_0^a \left\{ U_1(\bar{r}') \frac{\partial G_2}{\partial z'} \right\}_{z'=0} dx' - \beta \int_0^a \left\{ \tilde{G}_2 \frac{\partial U_1(\bar{r}')}{\partial z'} \right\}_{z'=0} dx'. \end{cases} \tag{1}$$

Here two new parameters are so related that $\alpha + \beta = 1$. The Green's functions satisfy the Dirichlet condition on the boundaries of the partial regions except $\widetilde{G}_2(\bar{r},\bar{r}')$, which satisfies the Neumann condition on the line $x \in (0,a)$.

As commonly in each subregion the sought solution is expanded into the eigenfunction series with unknown coefficients $R = \{R_n\}_{n=1}^\infty \in l_1$. After applying the Galerkin procedure a matrix equation

$$(I + D)R = f \qquad (2)$$

has been obtained. Here I is idem – factor and $f \in l_2$ is a source vector. As it has been found, the relation

$$D = 2\alpha A + (1 - 2\alpha)B \qquad (3)$$

takes place, where A is a matrix operator of the OR – method and B is a matrix operator of MoM. The principal part of last one contains a matrix operator C with elements

$$C_{mn} = \frac{2}{\pi}\sqrt{mn}\frac{\sin \pi\theta(m-n)}{m^2 - n^2}, \qquad (4)$$

where the parameter $\theta = \dfrac{a}{b} \in (0,1)$ is connected with geometry of the discontinuity. Only for pair of sequences $l_2 \to l_2$ operator C is bounded and by rough estimation

$$\|C\|_{l_2} \leq 1 + \max(\theta, 1 - \theta). \qquad (5)$$

Thus, a "continuous spectrum" of matrix models depending on the method's parameter $\alpha \in [0,1)$ was derived. In according with the interval of its variation the point $\alpha = 0$ corresponds to MoM and the point $\alpha = 0.5$ defines OR – method. The value $\alpha = 1$ is the particular case, for which the condition of field continuity on the common boundary of the partial regions is violated.

The properties of all these matrix models have been investigated analytically and numerically. The approximate solution of higher – order accuracy for dominant mode diffraction has been used, which had been found in [4] by semi – inversion method with the technique of asymptotic correction.

The typical results of computations are shown in Fig. 1, for which the truncation order of matrix operator is $N = 20$ and $M \in [6,14]$ means taking into account modes in second partial subregion.

From the calculations the conclusions follow:

  – relative error for absolute value of reflection coefficient $|R_1|$ does not exceed one percent for all methods up to $\alpha = 0.98$; at the same time a relative error for its phase is less than one third of percent;

  – there is a sufficiently narrow subinterval of method's parameter $\alpha = [0.484, 0.783]$, for which the complete coincidence of the calculated and test values is achieved in the one certain point depending on number of waveguide modes accounted; notice, the determination of test value had required considerably more analytical work and programming efforts;

  – the absolute minimum of condition number for truncated matrix corresponds to OR – method.
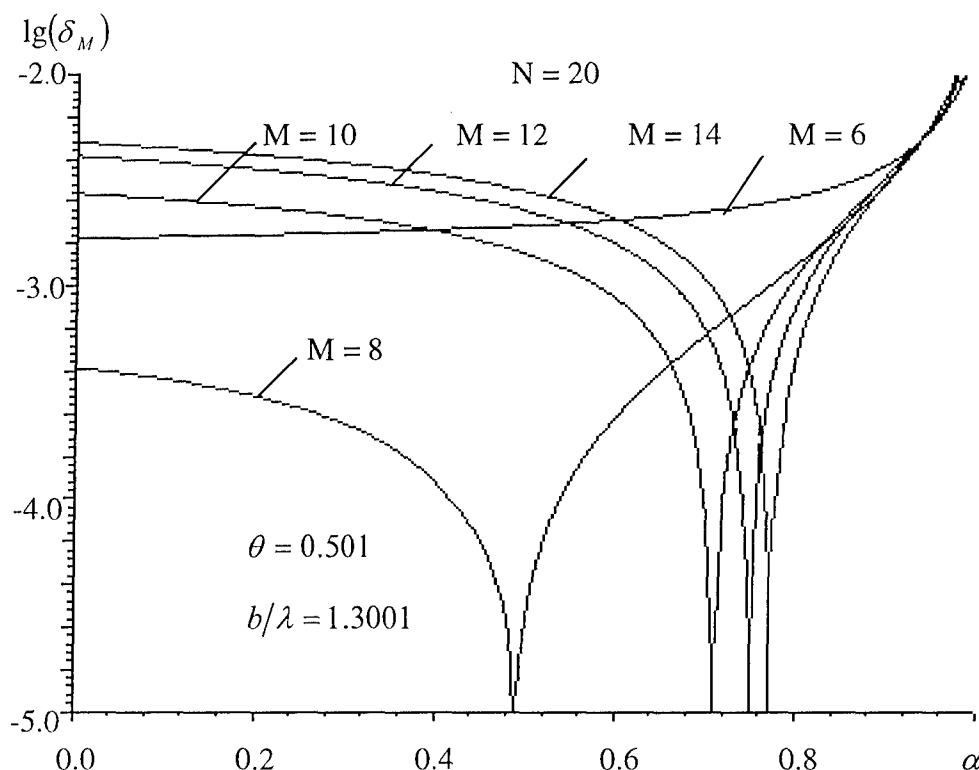
$\lg(\delta_M)$

Fig. 1. The magnitude of relative error for dominant mode reflection coefficient $|R_1|$
versus method's parameter for various number of modes in narrow waveguide

Thus, the technique proposed can be regarded as generalisation of method of moments and OR–method. It may be used for solving the wave diffraction problems effectively.

REFERENCES

[1] Prohoda I.G., Chumachenko V.P., "The method of partial overlapping regions for investigating complex waveguide – resonator systems", Izv. vuzov, Radiophysics, 1973, v. 16, N 10, p. 1578 – 1582.

[2] Chumachenko V.P., Petrusenko I.V., "Application of partial overlapping regions concept to solving of the electrodynamic two – dimensional problems", 1998, The Bulletin of Dniepropetrovsk State University, Physics. Radioelectronics, issue 3, p. 33 – 56.

[3] Petrusenko I.V., Dmitryuk S.G. "The method of the equivalent regularisation of the mode-matching technique equations", International Symposium "Physics and Engineering of Millimeter and Submillimeter Waves", 1994, 7-10 June, Kharkov, Ukraine, p. 13 –14.

[4] Kirilenko A.A., Senkevitch S.L., "Comparison of an efficiency of some algorithms for waveguide step discontinuities problems",IRE NANU,Preprint N204,Kharkov,1982, 32 p.

THE METHOD OF INTEGRATED AUXILIARY SOURCES FOR 3D DIFFRACTION PROBLEM SOLUTION

K. Tavzarashvili, A. Bijamov, R. Zaridze, and G. Bit-Babik
Department of Physics, Tbilisi State University, Georgia, E-mail: lae@resonan.ge

ABSTRACT

The application of the Method of Auxiliary Sources (MAS) for solving different types of Electromagnetics and particularly EMC related problems is presented. Recent improvements of MAS using the different types of Auxiliary Sources (AS) are demonstrated in several examples. These investigations have shown that the proper choice of the location and type of AS significantly reduce the total number of unknowns in the solved problems, improve the accuracy and convergence of the solution and lead to a highly efficient and fast solving algorithm.

INTRODUCTION

Despite the rapid development of computer technology solution of the modern Applied EM problems on Complex and Distributed Systems are restricted by the limited computational resources and the efficient and therefore the accurate numerical methods are in great demand. In the past few decades the MAS [1] has been proved to be an efficient tool for solving many EM problems including the EMC problems. The key idea of the MAS is to represent the unknown scattered field by a sum of fundamental solutions of appropriate wave equation – AS, whose radiating centers are located on an auxiliary surface shifted outside the area where the field is to be found.

It is well known that the efficiency of the MAS depends on several auxiliary parameters. The most crucial of these parameters is the distance between the auxiliary surface and the real surface of the scatterer. In some cases the auxiliary surface could not be moved far away from the real one (e.g. open, thin structures). To avoid this problem, the Integrated Auxiliary Sources (IAS) should be used. The IAS could use a current on auxiliary surface approximated, for example, by linear or sinusoidal functions; or represented by B-spline expansion.

Below, the different types of AS are presented and their applications for solving different kinds of problems are discussed.

DIFFERENT APPROACHES OF THE MAS

1. The AS represented by elementary dipoles can be used successfully in cases where they can be placed relatively deep inside the scatterer (or at reasonably far distance at both sides of the boundary surface for dielectric scatterers). The critical issue in this case is that the auxiliary surface that is formed by the AS should always surround the scattered field's singularity of the particular problem. If this condition is satisfied, then, generally, the better accuracy and convergence of solution occurs for bigger distances between auxiliary and real scatterer's surfaces. From physical point of view the mentioned condition means that the unknown scattered field expressed with the help of AS, which is analytical everywhere outside the auxiliary surface should coincide with the analytical continuation of the real scattered filed inside the scatterer. This becomes practically impossible if the singularity of the real scattered field appears outside the auxiliary surface and may lead to the divergence of the solution. If, however, the singularities of the particular problem is taken into account by some additional considerations, introducing, for example, some AS which describe exclusively these

singularities, then the convergence of the solution is significantly improved while the number of AS (number unknowns) can be sharply reduced.

As an example, consider a scattering of a point EM source field by a perfectly conducting sphere with aperture . (Benchmark problem geometry from [2]). The excitation is non-symmetrical (Fig. 1). This problem can be solved by MAS introducing some finite thickness for the given hollow sphere and distributing the set of AS inside this the wall of the sphere. However, because the thickness of the wall could not be taken very big in this model without significant changing of the initial problem conditions, the number of unknowns could be very big. Thus, we will construct the solution in different way.
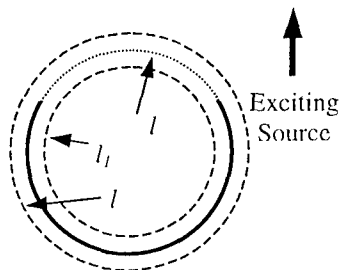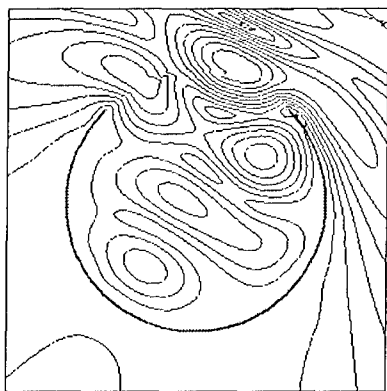
Fig. 1 Sphere with aperture

We introduce two regions: inside and outside the hollow sphere. The boundary l of these regions represents the same sphere but without aperture. Two sets of AS

$$U_n(\vec{r}) = \frac{e^{ik|\vec{r}_n - \vec{r}|}}{|\vec{r}_n - \vec{r}|}$$

are then introduced on the auxiliary surfaces l_1 and l_2 inside and outside of this auxiliary boundary. $\vec{r}_n$ is the point on the auxiliary surfaces, $\vec{r}$ is the observation point. The AS's located on the inner surface l_1 radiate a field outside the sphere and boundary l and the ones located on the surface l_2 radiate inside the sphere. Boundary condition for perfectly conducting bodies is used on the surface of the sphere from the both sides. On the auxiliary boundary the continuity of the total tangential magnetic and electric fields is enforced.

Fig. 2 Field distribution

This approach allows to locate the AS at sufficiently far distance from the surface where the boundary conditions are enforced. Additionally, to describe correctly the edge singularity of the scattered field which exist in this case near the border of the aperture, an auxiliary current that flows along this border can be added. This will add a fewer unknowns comparing to the total number of AS in the problem. In Fig. 2 the field distribution for the described problem is presented.

The above described approach of using the point-like AS was used for many applied electrodynamics problems including the investigation of electrostatic discharges. During the numerical modeling of electrostatic discharges the first step is the determination of the electrostatic filed near the discharging body. Using the Method of Auxiliary Sources this problem can be solved in a very efficient way [3].

2. In the case when the auxiliary surface could not be shifted far enough from the scatterer surface, the IAS can be used to reduce the number of unknowns that in case of conventional (dipole) type of AS would be very big for the same accuracy of the solution. Each IAS describes the radiation of a part of auxiliary surface and can be represented as the non-overlapped segments or parts of an auxiliary surface. On every such part, the IAS is presented by some function that approximates the current on it. The approximation can be linear, sinusoidal, B-spline or other that fits a particular problem in the best way form the viewpoint of efficiency, accuracy and simplicity. On the other hand, this approach is equivalent to the representation of the current on the AS and finding it by using the MoM algorithm and the
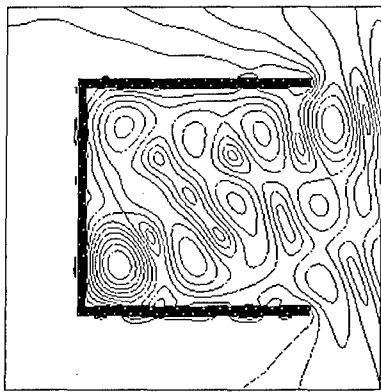
Fig. 3.
Cube with aperture and field in the middle cross-section.

functions representing IAS as the basis functions that are used to expand the unknown current in the MoM.

In Fig.3 the scattering by a hollow cube is demonstrated (geometry from [2]). The IAS in this case are represented by the wire segments with the sinusoidal $I = I_o \sin(kz - \alpha)e^{-i\omega t}$ distribution of current. These wires form a grid on the auxiliary surface. Obeying the boundary conditions in the number of points on the scatterer's surface, a system of linear algebraic equations is obtained. The unknowns are the current amplitudes in the nodes of the grid. In Fig.3 the filed distribution in the middle cross section of the hollow cube is presented. The side size of the cube is 0.3m, wavenumber k=42.0.
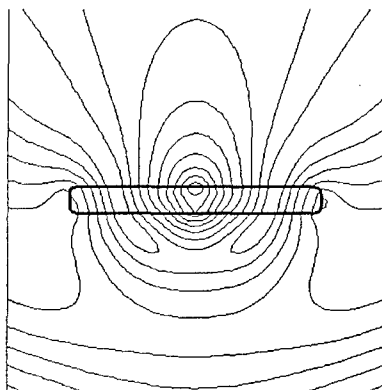
3. In case of thin dielectric or metallic structures the auxiliary current can be introduced on the whole auxiliary surface, not only in the grid points as in previous example. Suitable representation of the auxiliary current is made by dividing the auxiliary surface into patches (triangle or rectangular) and using the IAS as the source radiating from the particular patch. With this approach, a number of problems where solved and, as an example, the scattering upon a thin dielectric structure is considered. In Fig.4 the filed distribution in the near zone is presented. The incident field is a plane wave propagating in the direction perpendicular to the big side of the parallelepiped. The use of the IAS in this case presenting main and auxiliary surfaces by rectangular patches allows to reduce significantly the total number of unknowns.

Fig. 4.
Scattering upon the dielectric parallelepiped. ($\lambda/2 \times \lambda/3 \times \lambda/25$)

Proceeding from this approach, a software package for development and optimization of an adaptive portable antenna was created [4]. The 2D model was investigated in the beginning. For simplicity, the point-like AS was used in this case. Further real 3D model of antenna structure was investigated.

REFERENCES

[1] R. Zaridze-Popovidi, Z. Tsverikmazashvili. "Numerical Solution of Diffraction Problem by Modified Method of Non-Orthogonal Series." Zurnal. Vichislit. Mat. i Mat. Fiz., Vol. 17, No 2, 1977, Moscow (Translation: Oxford – New-York - Paris, April, 1978).

[2] V.Schulz, G.Mrozynski. "Benchmark Catalog for Numerical Field Calculations in the Area of EMC German IEEE EMC-Chapter." Paderorn, Theoretische Elektrotechnik, 1999.

[3] R. Zaridze, D. Karkashadze, R. Djobava, D. Pommerenke, M. Aidam. "Numerical Calculations and Measurement of Transient Fields from Electrostatic Discharges." IEEE Transactions on Components, Packaging, and Manufacturing Technology, vol. 19, No 3, July 1996, pp. 178-183

[4] R. Zaridze, G. Bit-Babik, K. Tavzarashvili, A. Bijamov. "The MAS Applied to the Analysis of Adaptive Transverse Resonant Antennas." Proceedings of the IEEE AP International Symposium, July 11-16, 1999, Orlando, Florida, pp. 2524-2527.

SOLVING INTEGRAL EQUATIONS FOR ILL–POSED PROBLEMS OF ELETROMAGNETICS BASED ON THE ATOMIC FUNCTIONS

Victor F. Kravchenko* and Michael A. Basarab**

*Institute of Radio Engineering and Electronics of the Russian Academy of Sciences.
103907, Center, GSP - 3, ul. Mokhovaya, 11, Moscow, Russia.
Tel: (095) 9024737, 9214837; Fax: (095) 9259241; E-mail: kvf@mx.rphys.mipt.ru.

** A.N. Podgornyi Institute of Problems of Engineering Industry,
National Academy of Sciences of Ukraine
61046, ul. Dm. Pozharskogo, 2/10, Kharkov-46, Ukraine.
Tel: (0572) 959577, 942774; E-mail: rvachev@ipmach.kharkov.ua.

ABSTRACT

The problem of implicit regularization using approximation apparatus of atomic functions for numerical solution of Fredholm integral equations of the first kind is considered.

INTRODUCTION

To solve the problem of synthesis of linear antenna it is necessary to determine unknown current I distribution that generates the required directional diagram f. That is we should deal with solving Fredholm integral equation of the first kind

$$\int_{-a}^{a} I(t)e^{itx}dt = f(x), \tag{1}$$

where $x=k\sin\theta$; $k=2\pi/\lambda$ is wave number; $f(x)$ is directional diagram; θ is azimuth angle; $2a$ is a length of antenna. It is possible to distinguish two general approaches in solving Fredholm first kind integral equations. One of them is the most obvious and is concluded in application of numerical methods with preliminary regularization (by Tychonoff, Lavrentiev, statistical). However, recently particular attention is given to the methods of the so-called implicit regularization. Among them a method of partial diagrams should be noted. According to it the expression for unknown current distribution is presented by the set of the special system of functions (Kotelnikov set, Bessel functions, eigenfunctions of Fredholm operator. At the same time, the universal methods based on the approximation of both the unknown solution and the directional diagram by the systems of compactly supported functions are being developed. For example in [1] the method of "double spline-approximation" for solving Fredholm integral equation of the first kind is proposed. Recently the possibilities of the atomic functions apparatus in obtaining the solution of the problem of synthesis are being widely investigated [2]. These functions have certain advantages in comparison with other functions with compact support [3]. This work is devoted to the analysis of approximation properties of atomic functions $\text{fup}_n(x)$ in combination with collocation, Galerkin and least squares methods. The questions of implicit regularization in these cases are discussed.

NUMERICAL ALGORITHM

The Fredholm integral equation of the first kind should be solved in the form

$$\int_{a}^{b} K(x,t)y(t)dt = f(x), \quad c \leq x \leq d. \tag{2}$$

According to the partial diagrams method, let us represent both the unknown solution and the right part of the equation in the form of series with respect to the complete systems of functions $\{\varphi\}$ и $\{\psi\}$, respectively

$$\tilde{y}(x) = \sum_{k=0}^{N} \tilde{u}_k \varphi_k(x), \tag{3}$$

$$\tilde{f}(x) = \sum_{k=0}^{N} d_k \psi_k(x). \tag{4}$$

Here d_k are unknown coefficients, $\tilde{u}_k$ are those we should determine. Denote

$$h^{(k)}(x) = \int_a^b K(x,t)\varphi_k(t)dt \tag{5}$$

and expand the latter functions with respect to the $\{\psi\}$ system

$$\tilde{h}^{(k)}(x) = \sum_{j=0}^{N} b_j^{(k)} \psi_j(x) \tag{6}$$

Then algebraic system for determination of unknown coefficients $\tilde{u}_k$ will take the form

$$\sum_{k=0}^{N} \tilde{u}_k b_j^{(k)} = d_j, \quad (j = \overline{0,N})$$

or using matrix notation

$$B\tilde{U} = D. \tag{7}$$

Consider different methods of determination of matrix B and vector D components.

1.Collocation method. Determine elements of the column vectors of matrix B and vector D in the following way

$$\Psi B^{<k>} = H^{<k>}, \quad \Psi D = F,$$

$$\Psi_{i,j} = \psi_j(x_i), H_i^{<k>} = h^{(k)}(x_i), F_i = f(x_i), x_i = c + i\frac{d-c}{N}, (i, j = \overline{0,N}).$$

Obviously,

$$\Psi B = H,$$

and using (7) we obtain the following system with respect to unknown vector $\tilde{U}$

$$H\tilde{U} = F, \tag{8}$$

where

$$H_{i,j} = \int_a^b K(x_i,t)\varphi_j(t)dt, \quad F_i = f(x_i), \quad (i, j = \overline{0,N}) \tag{9}$$

2.Method of moments. Assuming

$$\Psi_{i,j} = (\psi_i, \psi_j), F_i = (f, \psi_i), H_i^{<k>} = (h^{(k)}, \psi_i), \quad (i, j = \overline{0,N}),$$

we obtain the system analogous to (8), in which

$$H_{i,j} = \int_c^d \psi_i(x)dx \int_a^b K(x,t)\varphi_j(t)dt, \quad F_i = \int_c^d f(x)\psi_i(x)dx, \quad (i, j = \overline{0,N}) \tag{10}$$

3.The least squares method. In such a case components of matrix H and vector F will be defined in the following way

$$H_{i,j} = \int_c^d \left[\int_a^b K(x,s)\psi_i(s)ds \int_a^b K(x,t)\varphi_j(t)dt \right] dx,$$

(11)

$$F_i = \int_c^d f(x)dx \int_a^b K(x,t)\psi_i(t)dt, \quad (i,j = \overline{0,N})$$

Further, we will consider sets of compactly supported functions $\{\varphi\}$, $\{\psi\}$ normalized in a natural way

$$\sum_{k=0}^N \varphi_k(x) \equiv 1, \quad \sum_{k=0}^N \psi_k(x) \equiv 1.$$

(12)

Let

$$\bar{y}(x) = \sum_{k=0}^N \bar{u}_k \varphi_k(x)$$

(13)

be the best approximation of the unknown solution $y(x)$. Then we have the true

Theorem. Solution of (8) system results in the following upper bounds for errors of approximate solution (3)

1) For the collocation method (9):

$$\left\| \tilde{y}(x) - y(x) \right\| \le \left\| \tilde{y}(x) - y(x) \right\| \left(1 + (b-a) \left\| H^{-1} \right\|_\infty \left\| K(x,t) \right\| \right);$$

(14)

2) For the method of moments (10):

$$\left\| \tilde{y}(x) - y(x) \right\| \le \left\| \tilde{y}(x) - y(x) \right\| \left(1 + (b-a)(c-d) \left\| H^{-1} \right\|_\infty \cdot \left\| K(x,t) \right\| \cdot \left\| \psi(x) \right\| \right);$$

(15)

3) For the least squares method (11):

$$\left\| \tilde{y}(x) - y(x) \right\| \le \left\| \tilde{y}(x) - y(x) \right\| \left(1 + (b-a)^2 (c-d) \left\| H^{-1} \right\|_\infty \cdot \left\| K(x,t) \right\|^2 \cdot \left\| \psi(x) \right\| \right).$$

(16)

From (14)–(16) we see that errors depend on the norm of the inverse matrix H^{-1}. The more N, the more $\left\| \tilde{y}(x) - y(x) \right\|$ tends to zero, while $\left\| H^{-1} \right\|_\infty$ approaches arbitrarily the infinity. The problem is to find the optimal value N that allows us to obtain a stable approximate solution with the least error.

As it was mentioned above, one of the most promising approaches in the approximation theory, including ill–posed problems, is using the apparatus of atomic functions [3]. Application of compactly supported atomic functions allows to simplify the procedure of evaluating integrals in (9)–(11).

CONCLUSION

The method proposed in this paper is similar to the method of partial diagrams, and represents the implicit regularization of the ill–posed synthesis problem. The method is more convenient in numerical realization in comparison with the Tychonoff regularization techniques. Numerical experiments demonstrate good accordance with theoretical estimations, and prove the effectiveness of the proposed algorithm.

REFERENCES

[1] Grebennikov A.I. The splines method and solving ill–posed problems of approximation theory. Moscow, MSU, 1983. (in Russian)
[2] Kravchenko V.F., Zamyatin A.A.// Proc. III Intern. Symp. MSMW'98, Kharkov, Sept. 15-17, 1998. P.413-415.
[3] Rvachev V.L., Rvachev V.A. Nonclassical methods of the approximation theory in boundary value problems. Kiev, Naukova Dumka, 1979. (in Russian)

THE METHOD OF SURFACE INTEGRAL IN THE THEORY OF WAVE SCATTERING

N.V. Bondarenko and N.F. Shul'ga [1]

Institute for Theoretical Physics

National Science Center «Kharkov Institute of Physics and Technology»,

Kharkov, 61108, Ukraine

E-mail: [1] shulga@kipt.kharkov.ua

ABSTRACT

The scattering of fast charged particles and electromagnetic waves on a scatterer, localized in a space domains is considered. It is shown that the scattering amplitude can be expressed in this case as an integral over an arbitrary closed surface enclosing the scatterer. This representation enables us to express the scattering amplitude as an integral over impact parameters in general case and to develop a simple method for calculation corrections to the eikonal amplitude.

INTRODUCTION

We review the recently proposed [1,2] method of surface integral in the theory of wave scattering. The method is applicable for scattering of electrons and electromagnetic waves on a scatterer, localized in a space domain. It consists in expressing the wave scattering amplitude as a certain integral over arbitrary surface, enclosing the scatterer. In particular, choice of the integration surface as a plane behind the scatterer, orthogonal to the incident wave vector, leads to the impact parameter representation for scattering amplitude. In that manner the impact parameter representation in our approach appears not as an amazing simplification of final formulas, but a feature established from the outset. The problem of integration plane coordinate elimination is discussed. As an example of the proposed representation virtue, we present a simple method of calculating corrections to the eikonal scattering amplitude.

THE THEORY OF THE ELECTRON SCATTERING

Let us consider at first the scattering of a fast electron in a stationary external field $U(\mathbf{r})$ localized in a spatial domain V. The amplitude for this process is given by [3]

$$a = -\frac{1}{4\pi}\int d^3r\,\overline{u}'e^{-i\mathbf{p}'\mathbf{r}}\gamma^0 U(\mathbf{r})\psi(\mathbf{r}),\qquad(1)$$

where $\psi(\mathbf{r})$ is the particle wave function in the filed $U(\mathbf{r})$, $\mathbf{p}'$ and $\overline{u}'$ are the momentum and bispinor of the final particle state. Using the Gauss theorem amplitude, (1) can be transformed to a surface integral over the surface S bounding the region V [1]

$$a = -\frac{i}{4\pi}\oint_S dS\,\overline{u}'e^{-i\mathbf{p}'\mathbf{r}}\gamma\psi(\mathbf{r})\qquad(2)$$

It is worth noting that the surface S in (2) is arbitrary. Specially, the surface S may be chosen near the domain of localization of the potential $U(\mathbf{r})$. Then, it suffices to know the wave function only within the domain of the potential $U(\mathbf{r})$. In the case of the diffraction scattering the surface is convenient to choose in the form of a cylinder whose plane side are orthogonal to the incident particle moment $\mathbf{p}$ and lateral surface is set far from the scattering center. Then, the scattering amplitude (2) reads for $\mathbf{p}'\neq\mathbf{p}$ as an integral over impact parameters ρ

$$a = -\frac{i}{4\pi}\int d^2\rho\,e^{-i\mathbf{p}'\mathbf{r}}\,\overline{u}'\,\gamma_z\,\psi(\rho,z)\Big|_{z=L},\qquad(3)$$

where L is the z-coordinate of the integration plane outside the domain of influence of the potential.

We would like to stress that the integral function in (3) depends on L. However, the amplitude (3) must not depend on L. That is very simple to show in eikonal approximation. We have in this case [1]

$$a = -\frac{i\overline{u}'\gamma_z u}{4\pi}\int d^2\rho\,e^{i(\mathbf{q}\rho+\chi_e(\rho))},\qquad(4)$$

where

$$\chi_e(\rho) = -\frac{1}{v}\int_{-\infty}^{L}dz\,U(\rho,z) = -\frac{1}{v}\int_{-\infty}^{\infty}dz\,U(\rho,z)\quad.\qquad(5)$$

A method was developed in [1,2] for calculation corrections to the eikonal scattering amplitude, which are proportional to the value p^{-1}. Eq. (3) with such accuracy given to us eq. (4) with changing $\chi_e \to \chi(\rho) = \chi_e(\rho) + \chi_1(\rho)$, where $\chi_1(\rho)$ is correction to the eikonal phase $\chi_e(\rho)$,

$$\chi_1(\rho) = \frac{1}{pv^2}\int_{-\infty}^{\infty}dz\,[z\frac{\partial}{\partial\rho}U(\rho,z)\frac{\partial}{\partial\rho}\int_{-\infty}^{z}dz'U(\rho,z') - \frac{1-v^2}{2}U(\rho,z)]\quad(6)$$

Here v is the particle velocity.

THE THEORY OF THE ELECTROMAGNETIC WAVE SCATTERING

The method of surface integral can be generalized for scattering waves of any types. Specially, let us consider the scattering of electromagnetic waves with frequency ω by a dielectric scatterer localized in a spatial domain V. The equation for electromagnetic field $\mathbf{E}(\omega, \mathbf{r})$ in this case is (see [4])

$$\left(\Delta + \frac{\omega^2}{c^2} \varepsilon(\omega, \mathbf{r}) - grad\ div \right) \mathbf{E}(\omega, \mathbf{r}) = 0, \tag{7}$$

where $\varepsilon(\omega, \mathbf{r})$ is the dielectric permittivity of the scatterer.

The amplitude of scattering for this process is given by

$$a = \frac{\omega^2}{4\pi c^2} \int d^3 r e^{-i\mathbf{kr}} (\varepsilon - 1) \mathbf{e}\, \mathbf{E}(\omega, \mathbf{r}), \tag{8}$$

where $\mathbf{k}$ is the wave vector of the scattered wave and $\mathbf{e}$ is the unit vector of his polarization. Using Eq. (7) we transform Eq. (8) to the form

$$a = -\frac{1}{4\pi} \int d^3 r e^{-i\mathbf{kr}} \mathbf{e} \left(\Delta + \frac{\omega^2}{c^2} - \nabla div \right) \mathbf{E}(\omega, \mathbf{r}). \tag{9}$$

Last term in this equation is proportional to $\mathbf{ek} = 0$. The second term in Eq. (9) is proportional to $-\Delta \exp(-i\mathbf{kr})$. Then, according to the Green's formula, the amplitude (9) can be represented in the form of an integral over surface S bounding the scatterer:

$$a = -\frac{1}{4\pi} \oint_S d\mathbf{S} \, [\nabla(\mathbf{e}\, \mathbf{E}(\omega, \mathbf{r})) + i\mathbf{k}\,(\mathbf{e}\, \mathbf{E}(\omega, \mathbf{r}))]e^{-i\mathbf{kr}}. \tag{10}$$

For impact parameter representation this equation has the form

$$a = -\frac{ik_z}{2\pi} \int d^2 \rho\, e^{-i\mathbf{kr}} \, \mathbf{e}\, \mathbf{E}(\omega, \rho, z)\Big|_{z=L>R}. \tag{11}$$

REFERENCES

[1] N.V. Bondarenko, N. F. Shul'ga // Phys. Lett. B427 (1998) 114.

[2] N.V. Bondarenko, N. F. Shul'ga // Theor. and Math. Phys.115 (1998) 588.

[3] A.I.Akhiezer, N. F. Shul'ga High-Energy Electrodynamics in Metter (Gordon and Breach Pub. Amsterdam, 1996).

[4] M.L.Ter-Mikaelian High-Energy Electromagnetic Processes in Condensed Media (Wiley-Interscience, New-York, 1972).

THE METHOD OF EIGENVALUE SPECTRUM DIACOPTIC PROCESS FOR THE REAL HESSENBERG MATRICES

V. I. Jordan

Altai State University, Dimitrov 66, Barnaul, 656099, Russia
Phone: (83852) 36-39-21 E-mail: Jordan@phys.dcn-asu.ru

INTRODUCTION

At present, the eigenvalue problem for the matrices of high order met in the boundary value problems of propagation and diffraction of electromagnetic waves has became actual, since memory, time and computational errors turn out to be considerable.

Traditionally, for a finite number of operations, for instance, in the Householder or Givens transformations, a real matrix is reduced to the compact form: for instance, non-symmetric matrices to the Hessenberg form, almost triangular, but symmetric matrices to the particular case of the latter, a tri-diagonal form. After that the compact-form matrix eigenvalues are normally found by iterative methods. In this paper, the method of eigenvalue spectrum diacoptic process for the real Hessenberg matrices is proposed [1, 2]. This method for the compact-form matrix is a result of iterative process reduced to block-triangular ("diacoptic") form of two incoherent Hessenberg matrix blocks on the diagonal. Then the incoherent Hessenberg matrix blocks are alternately decomposed into smaller-size incoherent Hessenberg matrix blocks by asymptotically tending to zero the "interaction" of the blocks.

PROBLEM FORMULATION AND BASIC EQUATIONS

As an NxN original matrix $A = A^{(0)}$, the upper Hessenberg form matrix (a right almost triangular form) is considered. The transformed matrix at the end of each k-"direct big iteration" (k-"direct" BI) is marked as $A^{(k)}$, which has also an upper Hessenberg form. In the structure (1.a), the upper block $A_{11}^{(k-1)}$ is an MxM matrix block, lower block $A_{22}^{(k-1)}$ is an $N-MxN-M$ matrix block, where $M = [N/2]$, $[N/2]$ is the integer part of $N/2$, and $k \geq 1$. The element of "interaction" of the matrix blocks $b^{(k-1)}$ is the element $a_{m+1,m}^{(k-1)}$ in the lower block $A_{21}^{(k-1)}$, in which all the block elements are zero except this one:

$$A^{(k-1)} = \begin{vmatrix} A_{11}^{(k-1)} & A_{12}^{(k-1)} \\ b^{(k-1)} & A_{22}^{(k-1)} \end{vmatrix}, \qquad A^{(k)} = \begin{vmatrix} A_{11}^{(k)} & A_{12}^{(k)} \\ b^{(k)} & A_{22}^{(k)} \end{vmatrix} \qquad (1)$$

$$(1.a) \qquad\qquad\qquad (1.b)$$

To ensure an asymptotic tending to the zero of the elements $b^{(k-1)}$ and $b^{(k)}$ under $k \to \infty$, one should use some method to calculate the eigenvalues τ_1 and τ_2, respectively, of the matrix block $A_{11}^{(k-1)}$ for k- "direct" BI and of the block $A_{22}^{(k)}$ for (k+1)-"inverse" BI, before k-"direct" BI and before (k+1)-"inverse" BI. For instance, by means of the algorithm "double QR-iterations with two Wilkinson tacit shifts", the eigenvalues τ_1 and τ_2 of the block $A_{11}^{(k-1)}$ can be determined normally after three to five iterations. As the tacit shifts, we choose two eigenvalues of lower 3x3 block:

$$\begin{vmatrix} a_{m-2,m-2}^{(k-1)} & a_{m-2,m-1}^{(k-1)} & a_{m-2,m}^{(k-1)} \\ a_{m-1,m-2}^{(k-1)} & a_{m-1,m-1}^{(k-1)} & a_{m-1,m}^{(k-1)} \\ 0 & a_{m,m-1}^{(k-1)} & a_{m,m}^{(k-1)} \end{vmatrix},$$

which are the closest to the eigenvalues of the lower 2x2 block. These two eigenvalues τ_1 and τ_2 enable us to start execution of the k-"direct" BI by means of transformation H_1, which starts from the first matrix column

$$\Phi = (A_{11}^{(k-1)} - \tau_2 \cdot E) \cdot (A_{11}^{(k-1)} - \tau_1 \cdot E) = (A_{11}^{(k-1)})^2 - (\tau_1 + \tau_2) \cdot A_{11}^{(k-1)} + \tau_1 \cdot \tau_2 \cdot E$$

and is defined as follows:

$$H_1 = E - U \cdot U^T / k^2 ; \quad U_i = \Phi_{i1} ; \quad i = 2,3,....,n ; \quad U_1 = \Phi_{11} \mp S$$

$$S = \sqrt{\Phi_{11}^2 + \Phi_{21}^2 + ... + \Phi_{n1}^2} , \quad k^2 = \mp U_1 \cdot S$$

Since the first column of the matrix Φ has only three nonzero elements:

$$\Phi_{11} = (a_{11}^{(k-1)})^2 + a_{12}^{(k-1)} \cdot a_{21}^{(k-1)} - (\tau_1 + \tau_2) \cdot a_{11}^{(k-1)} + \tau_1 \cdot \tau_2$$

$$\Phi_{21} = (a_{11}^{(k-1)} + a_{22}^{(k-1)} - \tau_1 - \tau_2) \cdot a_{21}^{(k-1)}$$

$$\Phi_{31} = a_{32}^{(k-1)} \cdot a_{21}^{(k-1)} ,$$

then at least nonzero elements (U_1, U_2, U_3) will form a vector U. Hence, the block $A_{11}^{(k-1)}$, after the transformation by means of H_1, will have nonzero elements located below the co-diagonal of this matrix block. These nonzero elements, by means of the Householder or Givens transformations, are removed from the lower part of transformed Hessenberg matrix. The sequence of matrix transformations H_i, where $i = 2,3,....,n-1$, together with matrix H_1 for the k-"direct" BI form the resulting matrix of transformations

$$Q = H_1 \cdot H_2 \cdots H_{n-1} . \qquad (2)$$

In other words, after the *(m-2)*-th step, the element $\tilde{a}_{m+1,m-2}^{(k-1)}$ equals to $a_{m+1,m}^{(k-1)} \cdot s_{m-1,m}^{(k,m-2)} \cdot s_{m-2,m-1}^{(k,m-2)}$ and after the *(m-10*-th step, by means of H_{m-1}, it is moved to the place of the element $a_{m-1,m-2}^{(k)}$:

$$a_{m-1,m-2}^{(k)} = \left| a_{m+1,m}^{(k-1)} \cdot s_{m-1,m}^{(k,m-2)} \cdot s_{m-2,m-1}^{(k,m-2)} \right| . \qquad (3)$$

The values $s_{m-1,m}^{(k,m-2)}$ and $s_{m-2,m-1}^{(k,m-2)}$ of rotations in the planes *(m-1, m)* and *(m-2, m-1)* at *the (m-2)*-step of the k-"direct" BI, form the matrix H_{m-2}. Transformation H_{m-1} consists only of rotation in the plane *(m-1, m+1)*, in which $c_{m-1,m+1}^{(k,m-1)} = 0$ and $\left| s_{m-1,m+1}^{(k,m-1)} \right| = 1$. The further removal of nonzero elements from the lower part of block $A_{22}^{(k-1)}$ by means of $\{H_i : i = m, m+1,...., n-1\}$ transformations terminate the k-"direct" BI and ensure conservation of the Hessenberg form for the matrix $A^{(k)}$.

Before *(k+1)*-"inverse" BI, similarly to the k-"directed" BI, the eigenvalues of the block $A_{22}^{(k)}$ are determined. As tacit shifts τ_1 and τ_2, we choose two eigenvalues of the 3x3 upper block:

$$\begin{bmatrix} a^{(k)}_{m-1,m-1} & a^{(k)}_{m-1,m} & a^{(k)}_{m-1,m+1} \\ a^{(k)}_{m,m-1} & a^{(k)}_{m,m} & a^{(k)}_{m,m+1} \\ 0 & a^{(k)}_{m+1,m} & a^{(k)}_{m+1,m+1} \end{bmatrix},$$

which are closer to the eigenvalues of 2x2 upper block. Then, as a *(k+1)-"inverse"* BI, a sequence of transformations $\{H_i : i = 1,2,....,n-1\}$ is realized, that converts "reduced upwards" matrix $A^{(k)}$ into the matrix $A^{(k+1)}$ by means of resulting matrix of transformations Q, similarly to equation (2). Besides, similarly to the "direct" BI, but only already with provision for a return in its former position, the element of interaction of blocks is

$$a^{(k+1)}_{m+1,m} = \left| a^{(k)}_{m-1,m-2} \cdot s^{(k+1,n-m)}_{m-1,m} \cdot s^{(k+1,n-m)}_{m,m+1} \right|. \tag{4}$$

The values $s^{(k+1,n-m)}_{m-1,m}$ and $s^{(k+1,n-m)}_{m,m+1}$ define rotations, respectively, in the planes *(m-1, m)* and *(m, m+1)* at the *(n-m)*-th step of the *(k+1)-"inverse"* BI.

PROOF OF CONVERGENCE OF ALGORITHM

In-turn usage of "direct" and "inverse" BI according to (3) and (4) ensures a progressive minimization to zero, by changing its position, of the element of "interaction" of blocks (analogously to the "fading fluctuations"). Zero limiting value of this element under $k \to \infty$ is absolutely guaranteed by the equations (3) and (4) if

$$\left| s^{(k,m-2)}_{m-2,m-1} \right| \le \sqrt{2}/2 \quad \text{и} \quad \left| s^{(k+1,n-m)}_{m-1,m} \right| \le \sqrt{2}/2. \tag{5}$$

Conditions (5) turn out to be realistic, since rotation in the planes *(m-2, m-1)* at the *(m-2)*-th step of the *k*-"direct" BI and *(m-1, m)* at the *(n-m)*-step of the *(k+1)-"inverse"* BI are the Jacobi rotations with a provision for sufficiently exact determination of shifts τ_1 and τ_2. Consequently, (3) and (4) determine a recurrence scheme of "compressing operator" that guarantees absolute convergence and computational stability of the eigenvalue spectrum diacoptic process for the real Hessenberg matrices. The number of operations [1] required for a full termination of the eigenvalue spectrum diacoptic process for the real Hessenberg matrices is determined by the value $k_1 \cdot n^2$ (for tri-diagonal symmetric matrices, by $k_2 \cdot n \cdot \log_2 n$). Other methods are characterized by computing expenses, respectively, of $k_3 \cdot n^3$ and $k_4 \cdot n^2$. The values of k_1, k_2, k_3, k_4 are some constants and n is the order of original matrices. The results of numerical experiments confirm these conclusions.

REFERENCES

[1]. Jordan V.I. The method of eigenvalue spectrum diacoptic process for matrices in the Hessenberg form, Barnaul, 1990. Manuscript presented by the Altai State University. Deposited at VINITI 20.06.90, № 3536-B90.
[2]. Jordan V.I. "Fading pendulum" algorithm of eigenvalue spectrum diacoptic process method for matrices in the Hessenberg form, *Proc. Int. Conf. "All-Siberia Readings on Mathematics and Mechanics"*, vol.1, Mathematics, Tomsk, Tomsk State University Press, 1997, p. 198.

NEW APPROACH TO DIFFRACTION PROBLEMS SOLUTION BY REDUCING IT TO VOLTERRA INTEGRAL EQUATION

Irena Vorgul

Kharkov National University

4 Svoboda Sq., Kharkov, 61077 Ukraine

e-mail: vorgul@info.kharkov.ua

Abstract: New approach to solving diffraction problems is proposed. It is based on combining integral equation for the electromagnetic field inside the diffracting object with integral expression, which determines the diffracted field in the external region after the field inside it. It allows to obtain Volterra integral equation with a free term containing the diffracted and incident fields, which can be solved by convergent iterations, giving as a result an expression for the field inside the object, determined after the external one. This expression enables one to obtain an equation connecting the external field and the object parameters, with lower dimension than the initial one. For the presented example as 1D problem, this equation is just an algebraic one, which allows solving the direct problem as well as the inverse one.

GENERAL IDEA

Electromagnetic field interaction with any object can be described by the Fredholm integral equation with the incident field as a free term. It has the following form for electric field amplitude in the case of time-harmonic incidence [1]:

$$\vec{E}_{in}(\vec{r}_{in}) = \vec{E}_0(\vec{r}_{in}) + \frac{1}{4\pi}\left(\text{graddiv} + k_1^2\right) \int_V \frac{\varepsilon_2(\vec{r}') - \varepsilon_1}{\varepsilon_1} \frac{e^{ik_1|\vec{r}_{in} - \vec{r}'|}}{|\vec{r}_{in} - \vec{r}'|} \vec{E}_{in}(\vec{r}') \, d\vec{r}', \quad (1)$$
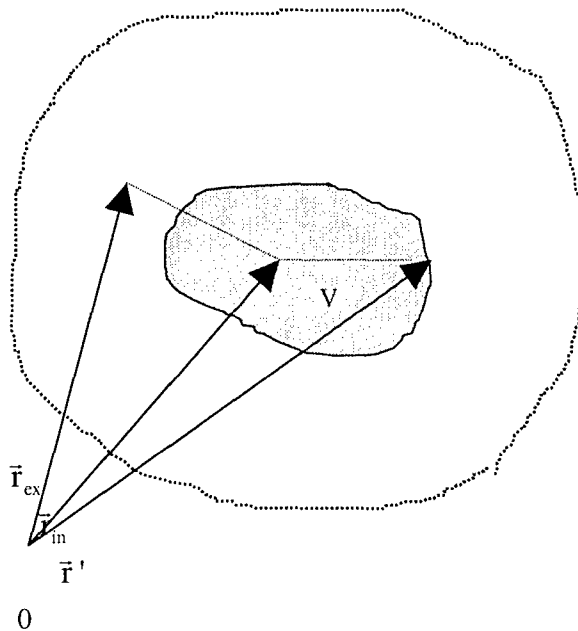

Fig.1

where ε_1 and k_1 are dielectric permittivity and wave vector in the external region, correspondingly, ε_2 is a permittivity inside the object, and V is the object volume. The permittivity of the object ε_2 in general case can be inhomogeneous and may contain imaginary part, but the external region is assumed homogeneous.

This is the integral equation for the field inside the object of diffraction, whereas the field in the external region is integrally expressed after the internal field.

$$\vec{E}_{ex}(\vec{r}_{ex}) = \vec{E}_0(\vec{r}_{ex}) + \frac{1}{4\pi}\left(\text{graddiv} + k_1^2\right) \int_V \frac{\varepsilon_2(\vec{r}') - \varepsilon_1}{\varepsilon_1} \frac{e^{ik_1|\vec{r}_{ex} - \vec{r}'|}}{|\vec{r}_{ex} - \vec{r}'|} \vec{E}_{in}(\vec{r}') \, d\vec{r}'. \quad (2)$$

Vectors $\bar{r}_{in}$ and $\bar{r}_{ex}$ determine the observation points inside and outside the object, correspondingly (Fig.1).

For a number of problems it is possible to combine these two integral formulas obtaining the Volterra integral equation with a free term as a combination of the incident and the reflected fields. It is possible due to that the integral at any point of the internal region (the more dark gray region in Fig.1) within a part of the object volume can be replaced with the integral at some point in the external region (The more light gray region in Fig.1), for which the length $\left|\bar{r}_{ex}-\bar{r}'\right|$ is equal to $\left|\bar{r}_{in}-\bar{r}'\right|$. Then, the another part of the integral will have variable limits of integration, depending on the observation point location $\bar{r}$. This part of the integral, left after the replacement, is the Volterra-type kernel [2].

The advantage of the Volterra equation is in that it can be solved by iterations with proved convergence [3]. This fact was used in [4], to find the solution of 1D stationary problem as a long-time approximation for the solution of the problem with the same geometry, but with time-varying parameters. It was possible as the fields in transient media are always described by Volterra equation, due to the processes casualty [5]. Even such a complication, with introduction of the additional dimension (time) gave there some advantages in comparison with conventional techniques. In the present work usage of the Volterra equation, in opposite, not leads to additional dimension, but make the problem with one dimension less.

For some objects this equation can be solved exactly by resolvent technique, otherwise the iteration procedure can be applied, giving as a result the expression for the internal diffracted field determined after the external one. The free term of the equation is taken as an initial guess, and each consequent iteration can be obtained by substitution of the previous one under the integral kernel. After substitution of this solution into the integral representation for the external field (2), one obtains the equation for the external field, which is more simple than the initial one, due to homogeneity of the external region. For some simple cases of incident field like plane or spherical waves, this equation is an algebraic one and can be easily solved.

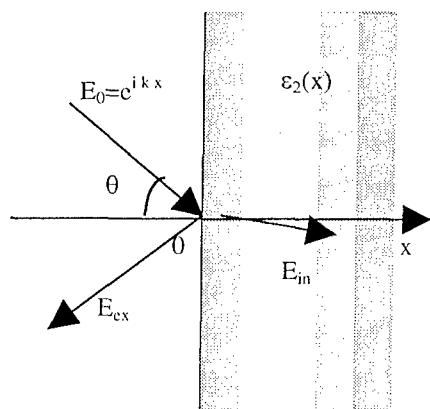## DEMONSTRATION OF THE METHOD APPLICATION IN 1D CASE

Fig.2

Consider 1D half-space with the permittivity profile $\varepsilon_2(x)$ (Fig.2). We assume it as a multilayer consisting of thin sub-layers of equal thickness Δa and different permittivities ε_i .

The Volterra integral equation here has the form

$$E_{in}(x)=e^{ikx}-\frac{\omega}{c\cos\theta}\int_0^\infty dx'\frac{\varepsilon(x')-\varepsilon_0}{\varepsilon_0}\sin k(x-x')\,E_{in}(x')\ .(3)$$

where $k\equiv\frac{\omega^2}{c^2}\cos^2\theta$. In operator representation it can be written as follows:

$$E=e^{ikx}+re^{-ikx}+\hat{K}E\ .\qquad(4)$$

Its solution can be obtained by iterations with proved convergence due to the collapsing Volterra operator. These iterations for the internal field have the following form in the operator representation:

$$E^k = e^{ikx} + re^{-ikx} + \hat{K}\left(e^{ikx} + re^{-ikx}\right) + \hat{K}\hat{K}\left(e^{ikx} + re^{-ikx}\right) + \dots$$
$$+ \hat{K}^k \left(e^{ikx} + re^{-ikx}\right)$$

(5)

In integral representation, after substitution into (2), it leads to the following equation connecting the reflection coefficient and the structure parameters:

$$r = \frac{1}{2i}\int_0^\infty dx' \, \tilde{\epsilon}(x')\left(e^{ikx'} + re^{-ikx'}\right)\left\{e^{ikx'} + \int_{x'}^\infty dx'' \, \tilde{\epsilon}(x'') \sin k(x''-x') \cdot \left\{e^{ikx''} + \int_{x''}^\infty dx''' \left\{\tilde{\epsilon}(x''') \sin k(x'''-x'')\dots\right\}\right\}\right\}$$

It can be proved that each consequent term in this sum is less than the previous one, and we can consider a few first terms of it. Then we can easily solve these integrals. If we consider only the first term of the sum (14) and assume that $\Delta\tilde{a}_j \equiv \tilde{a}_i - \tilde{a}_{i-1} << 1$ (where $\tilde{a}_j \equiv k_j a_j$ is the normalised width of the k-th sublayer), we obtain a very simple equation for the permittivity values:

$$-0.5 \cdot C_1 \cdot \sum_{k=1}^N \tilde{\epsilon}_k \, \Delta\tilde{a}_k + \sum_{k=1}^N \tilde{\epsilon}_k \, \Delta\tilde{a}_k \left[C_2 \cdot \left(\sum_{l=1}^{k-1}\Delta\tilde{a}_l + \frac{\Delta\tilde{a}_k}{2}\right) + \right.$$
$$\left. + C_3 \cdot \left(\Delta\tilde{a}_k \sum_{l=1}^{k-1}\Delta\tilde{a}_l + 2\sum_{l=1}^{k-1}\Delta\tilde{a}_l \sum_{j=1}^1 \Delta\tilde{a}_{jl}\right)\right] = 1$$

(6)

where $\tilde{\epsilon}_k = \dfrac{\epsilon_k - \epsilon_0}{\epsilon_0\sqrt{\epsilon_0}\cos\theta}$ is the normalised permittivity of kth sub-layer, $\Delta\tilde{a}_k = \dfrac{\Delta a_k \sqrt{\epsilon_0}}{c}\cos\theta$ is

its normalised thickness . The reflection coefficient and the incidence frequency is contained in the coefficients C, which are determined as follows:

$$C_1 = \omega\sin\varphi \quad, \quad C_2 = \omega^2\cos\varphi, \quad C_3 = \omega^3\sin\varphi \ .$$

The equation (6) written for different frequencies gives us a system of linear equations, which can be solved by standard techniques like the Gauss's method. It allows obtaining a set of linear equations for the permittivity values in different sub-layers, which can be solved directly, without involving the optimisation procedure or other techniques, usually used for solving inverse problems. Such an approximation, however, is valid mainly for the upper sub-layers, giving much less accuracy for the more embedded ones, so it can be probably useful for diagnostics of some thin layers – fabricated or natural ones.The advantage of this approach is in its simplicity and possibility to organise a very fast estimation of the profile.

For the problems which can be solved exactly, the presented approach leads to the known solutions. Advantages of the approach are in the proved convergence of the Volterra-type equations as well as in a possibility to obtain approximate analytical solutions appropriate for analysis of the fields diffracted by different parts of the object and for solving inverse problems.

1. N.A.Khizhnyak. Integral Equations of Macroscopic Electromagnetics. «Naukova Dumka» Publ., Kiev, 280 p. (in Russian)

2. V.Volterra.Theory of Functionals, Integral and Integro-Differential Equations. Moscow, Nauka Publ., (1982), 304 p (in Russian).

3. A.V.Samokhin, S.P.Kulikov. Iterative Method of Solving Integral Equations in Electrodynamics of Inhomogeneous Media. J. Theor. Physics, V.59, N 3 (1989), pp.47-53 (in Russian).

4. I.Y. Vorgul, M.Marciniak , «Reflection from 1D Quisi-periodical structures», Opt. Quantum Electron. no.6/8, vol. 32, pp. 1005-1012, 2000.

5. A.G.Nerukh and N.A.Khizhnyak, Modern Problems of Transient Macroscopic Electrodynamics, Test-Radio Publ., Kharkov, (1991) 324 p. (in Russian).

6. I.Yu.Vorgul and A.G.Nerukh, Inverse Problem for Medium with Transient Conductivity, Microwave and Optical Technology Letters, Vol. 19, N 3 (1998), 148-150.

WIENER-HOPF ANALYSIS OF THE VECTOR DIFFRACTION PROBLEM FOR A CYLINDRICAL WAVEGUIDE CAVITY

Dozyslav B. Kuryliak[1], Shoichi Koshikawa[2], Kazuya Kobayashi[3], and
Zinoviy T. Nazarchuk[1]

[1] Karpenko Physico-Mechanical Institute, National Academy of Sciences of Ukraine
5 Naukova St., 79601, Lviv, Ukraine
Tel: +380-322-637-038, Fax: +380-322-649-427, E-mail: doz@ipm.lviv.ua; nazarch@ipm.lviv.ua
[2] R&D Group, Laboratory, Antenna Giken Co., Ltd.
4-72 Miyagayato, Omiya 330-0011, Japan
Tel: +81-48-684-0712, Fax: +81-48-684-9960, E-mail: skoshi@mail.raidway.ne.jp
[3] Department of Electrical, Electronic, and Communication Engineering, Chuo University
1-13-27 Kasuga, Bunkyo-ku, Tokyo 112-8551, Japan
Tel: +81-3-3817-1869, Fax: +81-3-3817-1847, E-mail: kazuya@kazuya.elect.chuo-u.ac.jp

INTRODUCTION

The analysis of electromagnetic wave scattering by open-ended metallic waveguide cavities has received much attention recently in connection with the prediction and reduction of the radar cross section (RCS) of a target. This problem serves as a simple model of duct structures such as jet engine intakes of aircrafts and cracks occurring on surfaces of general complicated bodies. In our previous papers [1-2], we have considered a two-dimensional (2-D) cavity formed by a finite parallel-plate waveguide with a planar termination at the open end, and solved the plane wave diffraction problem rigorously using the Wiener-Hopf technique. In [3], the method developed in [1-2] has been further applied to analyze the diffraction by a three-dimensional (3-D) finite circular waveguide cavity for the axial symmetric case. In this paper, we shall consider the vector diffraction by a cavity formed by a semi-infinite circular waveguide with an interior planar termination as a generalization of our previous scalar problems, and analyze the non-symmetric electromagnetic wave diffraction by means of the Wiener-Hopf technique [4]. The time factor is assumed to be $e^{-i\omega t}$ and suppressed throughout this paper.

TRANSFORMED WAVE EQUATIONS

We consider a 3-D cavity formed by a semi-infinite circular waveguide with an interior planar termination, as shown in Fig. 1, where the cavity surface is perfectly conducting and of zero thickness, being defined in cylindrical coordinates (ρ, φ, z) as follows:

$$S = \left\{ (\rho, \varphi, z) | \rho = b, \ 0 \le \varphi \le 2\pi, \ z \in \left\{ \begin{array}{ll} (-\infty, L] & \text{for} \quad \rho = b+0 \\ [-L, L] & \text{for} \quad \rho = b-0 \end{array} \right\} \right\} \cup \left\{ (\rho, \varphi, z) | 0 \le \rho \le b, \ 0 \le \varphi \le 2\pi, \ z = -L \right\}.$$

The cavity is assumed to be excited by a hypothetical generator with voltage of unit amplitude across an infinitesimally small gap at $z = d \ (< | L |)$. Thus the applied electric field becomes a non-uniform ring source and is given by $e_z^i(z) = \delta(z-d)\sin(m\varphi + \varphi_0)$, for $m = 1,2,3,\ldots$ which is located at $(\rho, z) = (b-0, d)$. Let the total field be given by

$$u_l^t(\rho, z) = \left\{ \begin{array}{ll} u_l^i(\rho, z) + u_l(\rho, z) \text{ for } & 0 < \rho < b, \quad -L \le z < \infty, \\ u_l(\rho, z) \text{ for } & \rho > b, \quad -\infty < z < \infty, \end{array} \right. \tag{1}$$

where $u_l^i(\rho, z)$ for $l = 1$ and 2 are the TM and TE fields, respectively, which are excited in an infinitely long circular waveguide due to the ring source which take the form

$$u_1^i(\rho, z) = \frac{\omega \varepsilon}{2\pi i} \int_{-\infty}^{+\infty} \frac{I_m(\gamma_\beta \rho)}{\gamma_\beta^2 I_m(\gamma_\beta b)} e^{-i\beta(z-d)} d\beta, \quad u_2^i(\rho, z) = -\frac{m}{2\pi i b} \int_{-\infty}^{+\infty} \frac{\beta I_m(\gamma_\beta \rho)}{\gamma_\beta^3 I_m'(\gamma_\beta b)} e^{-i\beta(z-d)} d\beta,$$

where $\gamma_\beta = (\beta^2 - k^2)^{1/2}$ with $\text{Re}\,\gamma_\beta > 0$, and $k = k_1 + ik_2$, $0 < k_2 \ll k_1$; $I_m(\cdot)$ is the modified Bessel function of the first kind. Applying the method established in our previous papers [1-3], we
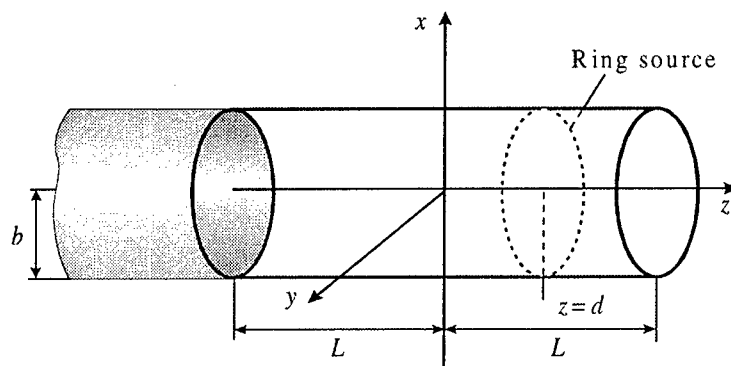
derive the transformed wave equations as in

$$\hat{T} U_l(\rho, \alpha) = 0 \quad \text{in} \quad \rho > b \quad \text{for} \quad |\tau| < k_2, \tag{2a}$$

$$\hat{T}\left[\Phi_l(\rho, \alpha) + e^{i\alpha L}\Psi_l^+(\rho, \alpha)\right] = e^{-i\alpha L}\left[\tilde{g}_l(\rho) - i\alpha \tilde{f}_l(\rho)\right] \quad \text{in} \quad 0 < \rho < b \quad \text{for} \quad \tau > -k_2 \tag{2b}$$

for $l = 1,2$ with $\hat{T} = \left[d^2 / d\rho^2 + \rho^{-1} d / d\rho - \left(\gamma^2 + m^2/\rho^2\right)\right]$, where $\gamma = (\alpha^2 - k^2)^{1/2}$ with

$\operatorname{Re}\gamma > 0$. In (2b), $\tilde{f}_l(\rho)$ and $\tilde{g}_l(\rho)$ are the unknown inhomogeneous terms defined by

$$\tilde{f}_l(\rho) = (2\pi)^{-1/2} u_l^i(\rho, -L), \quad \tilde{g}_l(\rho) = (2\pi)^{-1/2} \partial u_l^i(\rho, z)/\partial z \Big|_{z=-L}. \tag{3}$$

Fig. 1. Geometry of the problem.

The functions on the left-hand sides of (2a,b) are the Fourier transform of the functions appearing in (1), which are defined by

$$U_l(\rho, \alpha)\Big|_{\rho > b} = \frac{1}{\sqrt{2\pi}} \int_{-\infty}^{+\infty} u_l(\rho, z) e^{i\alpha z} \, dz, \quad U_l(\rho, \alpha)\Big|_{0 < \rho < b} = \frac{1}{\sqrt{2\pi}} \int_{-L}^{+\infty} u_l(\rho, z) e^{i\alpha z} \, dz \tag{4}$$

with $\alpha = \operatorname{Re}\alpha + i\operatorname{Im}\alpha \ (\equiv \sigma + i\tau)$ and

$$U_l(\rho, \alpha) = \Phi_l(\rho, \alpha) + e^{i\alpha L}\Psi_l^+(\rho, \alpha) - U_l^i(\rho, \alpha) \quad \text{for } 0 < \rho < b, \tag{5}$$

where

$$\Psi_l^+(\rho, \alpha) = U_l^+(\rho, \alpha) + Q_l^+(\rho, \alpha), \tag{6}$$

$$U_l^+(\rho, \alpha) = \frac{1}{\sqrt{2\pi}} \int_{+L}^{+\infty} u_l(\rho, z) e^{i\alpha(z-L)} dz, \quad \Phi_l(\rho, \alpha) = \frac{1}{\sqrt{2\pi}} \int_{-L}^{+L} u_l^i(\rho, z) e^{i\alpha z} dz. \tag{7}$$

Here $U_l^{(i)}(\rho, \alpha)$ and $Q_l^+(\rho, \alpha)$ are known functions. The functions $U_l^+(\rho, \alpha)$ and $Q_l^+(\rho, \alpha)$ are regular in the half-plane $\tau > -k_2$ and $\Phi_l(\rho, \alpha)$ with $l = 1,2$ are entire functions.

WIENER - HOPF SOLUTION OF THE PROBLEM

Since the scattered field for the region $\rho > b$ must vanish as $\rho \to \infty$ according to the radiation condition, we find that the solutions of (2a) are expressed as

$$U_1(\rho, \alpha) = V_1(\alpha) \frac{K_m(\gamma\rho)}{K_m(\gamma b)}, \qquad U_2(\rho, \alpha) = V_2(\alpha) \frac{K_m(\gamma\rho)}{\gamma K_m'(\gamma b)} \quad \text{for} \quad |\tau| < k_2, \tag{8}$$

where $V_l(\alpha)$ with $l = 1,2$ are the unknown functions. Taking into account the boundary conditions at the termination, we arrive at the solution of (2b) as in

$$\Phi_1(\rho,\alpha) + \Psi_1^+(\rho,\alpha)e^{i\alpha L} = \tilde{V}_1^+(\alpha)\frac{I_m(\gamma\rho)}{(\alpha - k)I_m(\gamma b)} + \frac{kZ^{-1}c_1 - \alpha a_1}{i\gamma^2}e^{-i\alpha L}\left(\frac{\rho}{b}\right)^m$$

$$+ i\alpha\sum_{n=1}^{\infty}\frac{e^{-i\alpha L}f_n}{\alpha^2 + \gamma_n^2}I_m(i\xi_n\rho/b), \quad \text{for} \quad \tau > -k_2,$$
(9a)

$$\Phi_2(\rho,\alpha) + \Psi_2^+(\rho,\alpha)e^{i\alpha L} = \tilde{V}_2^+(\alpha)\frac{I_m(\gamma\rho)}{\gamma(\alpha - k)I_m'(\gamma b)} + \frac{kZa_1 - \alpha c_1}{i\gamma^2}e^{-i\alpha L}\left(\frac{\rho}{b}\right)^m$$

$$- \sum_{n=1}^{\infty}\frac{e^{-i\alpha L}g_n}{\alpha^2 + \tilde{\gamma}_n^2}I_m(i\eta_n\rho/b), \quad \text{for} \quad \tau > -k_2$$
(9b)

with $\gamma_n = [(\xi_n/b)^2 - k^2]^{1/2}$, $\tilde{\gamma}_n = [(\eta_n/b)^2 - k^2]^{1/2}$, and $Z = \sqrt{\mu/\varepsilon}$, where $\tilde{V}_l^+(\alpha)$ for $l = 1,2$ are unknown functions, and ξ_n and η_n for $n = 1,2,3,...$ denote the zeros of $J_m(\cdot)$ and $J_m'(\cdot)$, respectively. Here $J_m(\cdot)$ is the Bessel function and the prime denotes differentiation with respect to the argument. The unknown coefficients f_n, g_n and a_1, c_1 are connected with values of the unknown functions $\tilde{V}_l^+(\alpha)$ at the discrete points k, $i\gamma_n$, $i\tilde{\gamma}_n$ by the relations which guarantee the regularity properties of (9a, b) in the half-plane $\tau > -k_2$. Taking into account the boundary conditions for the field components $e_z(\rho,z)$ and $e_\varphi(\rho,z)$ at the cylindrical surface $\rho = b$ and the continuity conditions for the field components $h_z(\rho,z)$ and $h_\varphi(\rho,z)$ at $\rho = b$ with $L < z < \infty$ in the Fourier transformed domain, we derive the Wiener - Hopf equation by using (9a, b). Then applying the decomposition procedure, we find that

$$\frac{i\omega\varepsilon E_1^+(b,\alpha)}{b(\alpha + k)M_2^+(\alpha)} + \frac{im^2 e^{ikL}F_1^+(\alpha)}{2b\chi}E_1^+(b,k)$$

$$+ \frac{\omega\varepsilon}{b}\sum_{n=1}^{\infty}\frac{(i\gamma_n + k)M_2^+(i\gamma_n)E_1^+(b,i\gamma_n)e^{-4\gamma_n L}}{\gamma_n(\alpha + i\gamma_n)} - \frac{im^2 ZP(b,k)F_1^+(\alpha)}{4b\chi} + R_1^+(\alpha) = 0.$$
(10)

Here $E_1^+(b,\alpha)$ is the Fourier transform of the unknown function $e_z(b,z)$; $F_1^+(\alpha)$, $R_1^+(\alpha)$, and $M_2^+(\alpha)$ are known functions regular in the half-plane $\tau > -k_2$; $P(b,k)$ and χ are known constants. Next we set $\alpha = k$, $i\gamma_n$ for $n = 1,2,3,...$ in (10). This leads to the infinite set of linear algebraic equations of the second kind which can be solved by the truncation method with pre-specified accuracy for a wide frequency range and geometrical parameters.

CONCLUSION

In this paper we have analyzed the vector diffraction problem for a circular waveguide cavity rigorously using the Wiener-Hopf technique. The method of solution is a generalization of the approach we have established previously for the analysis of the diffraction by a parallel-plate waveguide cavity [1-2] and the axial symmetric diffraction by a circular waveguide cavity [3]. The results rigorously involve the interaction between TM and TE types of waves. It is to be noted that (10) is the key result for investigation of the electromagnetic field scattered by the circular waveguide cavity in the vector case.

REFERENCES

[1] Kobayashi, K. and A. Sawai, "Plane wave diffraction by an open-ended parallel-plate waveguide cavity," *J. Electromagn. Waves Applics.*, vol. 6, no. 4, pp. 475-512, 1992.

[2] Koshikawa, S. and K. Kobayashi, "Wiener-Hopf analysis of the diffraction by a parallel-plate waveguide cavity with partial material loading," *IEICE Trans. Electron.*, vol. E77-C, no. 6, pp. 975-985, 1994.

[3] Kuryliak, D. B., T. Tsushima, K. Kobayashi, and Z. T. Nazarchuk, "Rigorous analysis of the axial symmetric diffraction problem for a circular waveguide cavity," *Rep. of the National Academy of Sciences of Ukraine*, no. 5, pp. 88-94, 1999.

[4] Kuryliak, D. B., S. Koshikawa, K. Kobayashi, and Z. T. Nazarchuk, "Wiener-Hopf analysis of the vector diffraction problem for a circular waveguide cavity" *Tech. Rep., The Institute of Electronics, Information and Communication Engineers(IEICE), Japan*, no. SANE 2000-20, 2000.

NON-CLASSICAL STRUCTURAL MATHEMATICAL MEANS AND OPTIC

V.K. Sorokin, and L.S. Lobanova
Ukrainian Engeneering-Pedagogical Academy,
16 Universitetskaja str., Kharkiv, Ukraine

ABSTRACT

In [1,2] it was shown that, for the body velocity comparable with the light velocity, the archimedean axiom and the archimedean arithmetic calculus rules (+,-,x,/) are not correct, if it is applied to the calculations in the mathematical methods in electromagnetic theory and optics. Nonarchimedean arithmetic rules and function are nonclassical structural mathematical means and must be used for calculations in the mathematical methods in electromagnetic theory. In this report, it is shown that the two-dimensional model can be constructed. This model admits to derive in numerous occasion the algebraic expressions of the nonarchimedean arithmetic rules, the nonarchimedean functions and algebraic expressions of the optical laws, for example, the optical laws for the light propagation and reflection on the two optical mediums boundary.

INTRODUCTION

Nonarchimedean arithmetic rules in algebraic field[1,2]

$$\Pi = (X \in R_{pr}(-\Gamma, \Gamma), \oplus, \oplus, \otimes, //) \tag{1}$$

where R_{pr} is a pseudorimanian set, $\Gamma = c$ is the maximal number of the noneuclidean sets. For example, nonarchimedean addition, subtraction rules have the form

$$v_1 \oplus v_2 = \frac{v_1 + v_2}{1 + \frac{v_1 v_2}{c^2}} . \tag{2}$$

$$v_1 \oplus v_2 = \frac{v_1 - v_2}{1 - \frac{v_1 v_2}{c^2}} . \tag{3}$$

the multiplication

$$v_1 \otimes v_2 = M[\exp(\eta \ln(N(v_1))\ln(N(v_2)))] = \frac{1}{\Phi}\left\{ \frac{\exp\left[\eta \ln\left|\frac{1+\Phi v_1}{1-\Phi v_1}\right|\ln\left|\frac{1+\Phi v_2}{1-\Phi v_2}\right|\right] - 1}{\exp\left[\eta \ln\left|\frac{1+\Phi v_1}{1-\Phi v_1}\right|\ln\left|\frac{1+\Phi v_2}{1-\Phi v_2}\right|\right] + 1} \right\}$$

the division

$$v_1 //v_2 = M[\exp(\frac{1}{\eta}\ln(N(v_1))(\ln(N(v_2)))^{-1}] = \frac{1}{\Phi}\left\{ \frac{\exp\left[\frac{1}{\eta}\ln\left|\frac{1+\Phi v_1}{1-\Phi v_1}\right|\ln^{-1}\left|\frac{1+\Phi v_2}{1-\Phi v_2}\right|\right] - 1}{\exp\left[\frac{1}{\eta}\ln\left|\frac{1+\Phi v_1}{1-\Phi v_1}\right|\ln^{-1}\left|\frac{1+\Phi v_2}{1-\Phi v_2}\right|\right] + 1} \right\} .$$

Where $\eta = (\ln(N(1))^{-1}$, $\Phi = 1/\Gamma$.

The auxiliary nonarchimedean productive direct and reciprocal function [1,2]:

$$M(s) = \Gamma\left(\frac{s-1}{s+1}\right), N(s) = \frac{1+s\Phi}{1-s\Phi}$$

MODEL DESCRIPTION

On the first step we use rough approximation to the real analytical model. It is the model in the form of the logarithmic spiral

$$\rho = Ce^{k\delta}, \tag{4}$$

where $k = arctg\,\alpha$ is the form parameter, ρ is the radius-vector, α is the rotation angle, C is const, δ is the angle between the tangent to a spiral point and the normal to the spiral at this point. We suppose that the deformed circle can be sufficiently precise represented in the form of the logarithmic spiral arcs. Let as definite the tangent line in a spiral curve point M:

$$K\,tg\,\varphi = K\frac{dy}{dx} = K\frac{x+y}{x-y}, \tag{5}$$

where $y = x\,tg\,\varphi + l$, $K = const.$ We will introduce the coordinates (5) coordinates, so that its analytical form can be equal to the analytical form of the productive nonarchimedean function and the propagation and reflection optical laws. For example, let us introduce the following coordinates $x = s, y = -1, K = \Gamma$:

$$K = \frac{dy}{dx} = K\frac{x+y}{x-y} = \Gamma\frac{s-1}{s+1} = M(s),$$

where M(s) is the auxiliary nonarchimedean productive direct function, s is archimedean variable. If $x = 1, y = \dfrac{S}{\Gamma}, K = 1$:

$$K\frac{dy}{dx} = K\frac{x+y}{x-y} = \frac{1+S\Phi}{1-S\Phi} = N(S),$$

where $\Phi = \dfrac{1}{\Gamma}$; $N(S)$ is the auxiliary nonarchimedean productive reciprocal function.

The nonarchimedean arithmetic rules can be obtained in the form of the Lorenz addition rule, if $x = N(S_1)N(S_2), y = -1, K = \Gamma$:

$$M[N(S_1)N(S_2)] = \Gamma\frac{N(S_1)N(S_2)-1}{N(S_1)N(S_2)+1} = \frac{S_1 + S_2}{1+\dfrac{S_1 S_2}{\Gamma^2}}. \tag{6}$$

The nonarchimedean arithmetic rule can be obtained in the form of the subtraction rule, if $x = N^{-1}(S_1)N(S_2), y = -1, K = \Gamma$:

$$M[N^{-1}(S_1)N(S_2)] = \Gamma\frac{N^{-1}(S_1)N(S_2)-1}{N^{-1}(S_1)N(S_2)+1} = \frac{S_2 - S_1}{1-\dfrac{S_1 S_2}{\Gamma^2}}. \tag{7}$$

There is the drop light intensity $I_e = E_s^2 + E_p^2$, the reflected - $I_r = R_s^2 + R_p^2$, the refracted - $I_d = D_s^2 + D_p^2$. If in (5) we put $x = n, y = -1, K = \dfrac{E_p}{\Gamma}$:

$$\frac{E_p}{\Gamma}\frac{dy}{dx} = \frac{E_p}{\Gamma}M(n) = E_p\frac{n-1}{n+1} = R_p. \tag{8}$$

If in (5) we put $x = M(n)$, $y = -1$, $K = \dfrac{1}{\Gamma}$:

$$\frac{1}{\Gamma}\frac{dy}{dx} = \frac{1}{\Gamma}M(n) = \frac{n-1}{n+1} = \rho, \tag{9}$$

where ρ^2 is the integral reflection coefficient. The reflection function R_s can be derived, if we put in (5) $x = N(n)$, $y = -1$, $K = \dfrac{-E_s}{\Gamma}$:

$$\frac{-E_s}{\Gamma}\frac{dy}{dx} = \frac{-E_s}{\Gamma}M(n) = -E_s\frac{n-1}{n+1} = R_s. \tag{10}$$

The reflection function r_e can be derived, if we put in (5)

$x = z_1$, $\quad y = -z_2$, $\quad K = 1$: $\qquad r_e = \dfrac{dy}{dx} = \dfrac{z_1 - z_2}{z_1 + z_2}$, , where $r_e = \dfrac{E_{yr}}{E_{yi}}$ is the reflection

coefficient, E_{yr} is the electrical vector component, which lie in the normal to x and z plane

, E_{yi} -drop light electrical component; $z_1 = \dfrac{E_{y1}}{H_{z1}}$, $z_2 = \dfrac{E_{y2}}{H_{z2}}$ is the medium wave

impedance; H_{zj} is the magnetic vector z-component; j=1, 2 the first and second media on their boundary, respectively.

CONCLUSION
Algebraic expressions of this optic laws are a direct consequence of the latent nonarchimedean functions, because if and only if then the mathematical model is adequate to the experimental data. There is an evidence of the significance of the new nonclassical structural mathematical means in the further development of mathematical methods in electromagnetic theory.

REFERENCES
[1] V.L. Rvachev. Non-Archimedean Arithmetic and other constructive mathematical means based on the concepts of special relativity theory // Reports of Academy of Sciences of USSR.-1991.-B.316, No 4.-P.884-889. (In Russian).
[2] V.L. Rvachev. From the special relativity theory to the mathematics without the Archimed axiom and back // Radiotekhnika.-1995.-No 2 (Electromagnetic waves.-No 1.-P.58-70). (In Russian).

MODIFIED ALGORITHM OF THE R-FUNCTIONS METHOD FOR SOLVING ELECTROMAGNETICS BOUNDARY VALUE PROBLEMS

Michael A. Basarab

A.N. Podgornyi Institute of Problems of Engineering Industry,
National Academy of Sciences of Ukraine.
61046, ul. Dm. Pozharskogo, 2/10, Kharkov, 61046, Ukraine
Tel: (0572) 959577, 942774; E-mail: rvachev@ipmach.kharkov.ua

ABSTRACT

Dirichlet problem for 2D second order partial differential equation in arbitrary domain is considered. To solve this problem, variational R-functions method (RFM) with the Kantorovich general structure of solution (GSS) is used. Instead of traditional RFM scheme, the complicated implicit function of boundary is substituted here with its approximation by a set of functions with compact supports. It is important that namely this set is also used in GSS. This approach allows to decrease significantly the quantity of numerically calculated integrals expressing the elements of matrices of systems of linear equations.

INTRODUCTION

Consider internal partial differential boundary value problem in 2D arbitrary domain S

$$LU(x, y) = -f(x, y), \tag{1}$$

(L is second order differential operator, f is known function) with Dirichlet conditions at boundary Γ

$$U(x, y)|_\Gamma = 0. \tag{2}$$

The main difficulty here is to satisfy boundary conditions (2). RFM [1] is an effective approach that allows to find unknown solution among the set of functions obeying (2) in advance. In this case we should use Kantorovich GSS [2] to represent unknown solution $U(x,y)$

$$U(x, y) = \omega(x, y) \sum_i c_i \varphi_i(x, y). \tag{3}$$

Here $\omega(x,y)$ is implicit real function of boundary S (this function is equal to zero on Γ, is positive inside S, and negative outside it), $\{\varphi_i\}$ are basic functions, $\{c_i\}$ is a set of undetermined coefficients. To find the latter, it is necessary to use any numerical method (Ritz, Galerkin, least squares, etc.). Application of GSS demands employing proper approximation apparatus, i.e. choosing convenient set of basic functions. Among them compactly supported functions such as Schoenberg splines or atomic functions are often used recently [3-5]. They have some advantages in comparison with the traditional polynomials. In the case of Galerkin method let us consider an approach allowing to simplify numerical realization of projection methods combined with RFM.

SETTING OF A PROBLEM

Consider the eigenvalue problem for the longitudinal electric field component E_z in cylindrical waveguide with a cross section S. In this case in (1) $L = \Delta + k^2$, where Δ is a Laplacian, and right part $f=0$. Using GSS (3) in combination with the Galerkin method leads to the following generalized eigenvalue problem with respect to the components of unknown vector C

$$AC = k^2 BC \qquad (4)$$

Elements of matrices A and B are defined in the following way

$$a_{i,j} = \int_S \left(\frac{\partial^2 (\omega \varphi_i)}{\partial x^2} + \frac{\partial^2 (\omega \varphi_i)}{\partial y^2} \right) \omega \varphi_j \, dx dy \qquad (5)$$

$$b_{i,j} = -\int_S \omega^2 \varphi_i \varphi_j \, dx dy \qquad (6)$$

Implicit function of boundary $\omega(x,y)$ constructed with the help of R-operations for domain S with complex shape will be complicated expression that makes difficult to calculate integrals (5), (6) repeatedly.

NUMERICAL ALGORITHM

Enclose domain S in a rectangle and approximate $\omega(x,y)$ with help of basic functions $\{\varphi_i\}$ arbitrary. We obtain an approximate implicit real function of boundary

$$w(x, y) = \sum_i d_i \varphi_i (x, y). \qquad (7)$$

Algebraic problem (4) – (6) in "perturbed" domain, characterized by $w(x,y)$ function will take the form

$$\tilde{A} \tilde{C} = k^2 \tilde{B} \tilde{C} \qquad (9)$$

$$\tilde{a}_{i,j} = \begin{cases} \int_S \Delta(\omega \varphi_i) \omega \varphi_j \, dx dy, & \mathrm{supp}(\varphi_i \cap \varphi_j) \not\subset S \\ \sum_k \sum_l d_k d_l \int_S \Delta(\varphi_k \varphi_i) \varphi_l \varphi_j \, dx dy, & \mathrm{supp}(\varphi_i \cap \varphi_j) \subset S \end{cases} \qquad (10)$$

$$\tilde{b}_{i,j} = \begin{cases} -\int_S \omega^2 \varphi_i \varphi_j \, dx dy, & \mathrm{supp}(\varphi_i \cap \varphi_j) \not\subset S \\ -\sum_k \sum_l d_k d_l \int_S \varphi_k \varphi_l \varphi_i \varphi_j \, dx dy, & \mathrm{supp}(\varphi_i \cap \varphi_j) \subset S \end{cases} \qquad (11)$$

In the cases when intersection of φ_i and φ_j supports is concluded in S, we can find corresponding components of the matrices A and B by using uniform integrals. The latter depend only on basic functions, not on the configuration of S. The quantity of elements computed in this way increases with increasing of the dimension of approximating space. Two-dimensional compactly supported functions φ_i are presented as tensor product of one-dimensional ones

$$\varphi_i(x, y) = \psi_i^{(1)}(x)\psi_i^{(2)}(y),$$

and second expressions in (10), (11) are presented in the form

$$\tilde{a}_{i,j} = \sum_k \sum_l d_k d_l \left(G_{i,j,k,l}^{(1)} J_{i,j,k,l}^{(2)} + G_{i,j,k,l}^{(2)} J_{i,j,k,l}^{(1)} \right) \tag{12}$$

$$\tilde{b}_{i,j} = -\sum_k \sum_l d_k d_l J_{i,j,k,l}^{(1)} J_{i,j,k,l}^{(2)}, \tag{13}$$

where

$$J_{i,j,k,l}^{(1)} = \int_{-\infty}^{\infty} \psi_i^{(1)}\psi_j^{(1)}\psi_k^{(1)}\psi_l^{(1)} dx, \quad J_{i,j,k,l}^{(2)} = \int_{-\infty}^{\infty} \psi_i^{(2)}\psi_j^{(2)}\psi_k^{(2)}\psi_l^{(2)} dx,$$

$$G_{i,j,k,l}^{(1)} = \int_{-\infty}^{\infty} \frac{d^2}{dx^2}(\psi_i^{(1)}\psi_k^{(1)})\psi_j^{(1)}\psi_l^{(1)} dx, \quad G_{i,j,k,l}^{(2)} = \int_{-\infty}^{\infty} \frac{d^2}{dy^2}(\psi_i^{(2)}\psi_k^{(2)})\psi_j^{(2)}\psi_l^{(2)} dy \tag{14}$$

Here the bounds of integrating are finite because of compactness of functions φ_i and φ_j. Integrals (14) do not depend on absolute values of indexes but on the pairwise differences between them. Using the integration by parts and symmetry reasons we can conclude that in fact it is not necessary to calculate integrals (14) for all possible combinations i, j, k, l, but only for some basic ones. So, in the case of cubic B-splines or atomic functions $fup_2(x)$ one has to find only 13 integrals $J_{i,j,k,l}^{(q)}$, $(q = 1,2)$ and 23 integrals $G_{i,j,k,l}^{(q)}$, $(q = 1,2)$. Analogous numbers for linear splines and functions $up(x)$ are 3 and 4, respectively. As it was mentioned above, expressions (14) do not contain any information about the domain S. The latter is contained in coefficients d_k in (12), (13). The problem of finding them is more simple than the initial boundary value problem.

CONCLUSION

The proposed algorithm of realization of RFM gives us a significant benefit in speed. To achieve an acceptable error, it is necessary to select proper dimension of approximating space. Numerical experiments with waveguides of complicated cross section shape prove the efficiency of the novel approach.

REFERENCES

[1] Rvachev V.L. Theory of R-functions and its applications. Kiev, Naukova Dumka, 1982. (In Russian)

[2] Kantorovich L.V., Krylov V.I. Approximate methods of superior calculus. Leningrad, Fizmatgiz, 1962. (In Russian)

[3] Rvachev V.L., Rvachev V.A. Nonclassical methods of approximation theory in boundary value problems. Kiev. Naukova Dumka, 1979. (In Russian)

[4] Kravchenko V.Ph., Rvachev V.A.// Zarubezhnaya radioelectronika. 1996. №8. PP.6-22.

[5] Kravchenko V.Ph., Zamyatin A.A.// Doklady RAN, 1999. 365. №4. PP.475-477.

INVESTIGATION OF THE INFLUENCE OF PERIODIC DISTURBANCES IN THE LAYERED MEDIUM BY THE METHOD OF AVERAGING OF KRYLOV-BOGOLYUBOV

K.Y. Kramarenko, and N.A. Khizhnyak

National Scientific Center "Kharkov Institute of Physics and Technology"

1 Akademicheskaya Ul., Kharkov, 61108, Ukraine

ABSTRACT

The influence of small periodic disturbance in periodic dielectric medium on propagation of TM-waves, investigated by the Krylov - Bogolyubov averaging method, results in the phenomenon of parametric resonance. As a result of periodic disturbance inside the allowed bands of undisturbed medium forbidden bands appear. The appearance of forbidden bands is conditioned by a parametric resonance between spatial harmonics of disturbance and plane waves, on which the solution of the wave equation in periodic medium is decomposed. The location, number and width of these bands are determined.

INTRODUCTION

Periodic structures with varying parameters may prove useful in many applications. In paper [1], the theory of wave propagation in periodic structures with smoothly varying parameters is developed with the help of the Wannier-function expansion. In particular, it is shown that the double periodic structure possesses a miniband structure. Such a spectrum has been observed in direct numerical simulations, described in paper [2]. The purpose of this paper is to describe the effects occurring when an electromagnetic wave propagates in a periodic medium with small periodic disturbances at an arbitrary period.

THE KRYLOV - BOGOLYUBOV AVERAGING METHOD

At first, we consider the propagation of a TM polarized wave in the periodic medium. The periodicity exists only in one direction, and propagation of the electromagnetic wave in that direction is governed by the equation:

$$\varepsilon \frac{d}{dz}\left(\frac{1}{\varepsilon}\frac{dD}{dz}\right) + L^2\left(k^2\varepsilon(z) - k_\perp^2\right)D = 0 \tag{1}$$

where $k = \frac{2\pi}{\lambda}$ is the wave number, $k_\perp$ is the transverse component of wave vector, L is the period of undisturbed medium, z is the undimensional variable and $\varepsilon(z+1) = \varepsilon(z)$. By replacing $U1 = D, U2 = \frac{1}{\varepsilon}\frac{dD}{dz}$ from the linear differential equation of the second order we arrive to a system of two equations of the first order:

$$\begin{cases} \dfrac{dU1}{dz} - \varepsilon(z)U2 = 0, \\ \dfrac{dU2}{dz} + \Omega(z)U1 = 0. \end{cases} \tag{2}$$

where $\Omega(z) = \dfrac{L^2}{\varepsilon(z)}\left(k^2\varepsilon(z) - k_\perp^2\right)$. The solution of the above system of linear homogeneous differential equations with periodic coefficients can be written in the Floquet form:

$$U1 = Cf_1 \exp(i\psi z) + C^* f_1^* \exp(-i\psi z)$$
$$U2 = Cf_2 \exp(i\psi z) + C^* f_2^* \exp(-i\psi z) \tag{3}$$

where f_1, f_2, ψ are determined by the fundamental solutions of (1). Functions f_1, f_2 are periodic ($f_1(z+1) = f_1(z)$, $f_2(z+1) = f_2(z)$), normalized by the following way: $f_1 f_2^* - f_2 f_1^* = -2i$.

In the case of periodic disturbance $\varepsilon(z) \to \varepsilon(z) + \Delta\varepsilon(z), \Delta\varepsilon(z+\Lambda) = \Delta\varepsilon(z)$, the set of equations (2) can be considered as inhomogeneous:

$$\begin{cases} \dfrac{dU1}{dz} - \varepsilon(z)U2 = \Delta\varepsilon(z)U2, \\[2mm] \dfrac{dU2}{dz} + \Omega(z)U1 = -\Delta\Omega U1 \end{cases} \tag{4}$$

where $\Delta\Omega = \dfrac{\Delta\varepsilon}{\varepsilon(\varepsilon + \Delta\varepsilon)} k_\perp^2$. The solution of inhomogeneous set of equations is as follows:

$$U1 = C(z)f_1 \exp(i\psi z) + C^*(z)f_1^* \exp(-i\psi z)$$

$$U2 = C(z)f_2 \exp(i\psi z) + C^*(z)f_2^* \exp(-i\psi z) \tag{5}$$

Where $C(z), C^*(z)$ are the solutions of the system of differential equations:

$$\frac{dC}{dz} = \frac{i}{2}\left[C\left(\Delta\varepsilon|f_2|^2 + \Delta\Omega|f_1|^2\right) + C^*\left(\Delta\varepsilon\left(f_2^*\right)^2 + \Delta\Omega\left(f_1^*\right)^2\right)\exp(-2i\psi z)\right]$$

$$\frac{dC^*}{dz} = -\frac{i}{2}\left[C^*\left(\Delta\varepsilon|f_2|^2 + \Delta\Omega|f_1|^2\right) + C\left(\Delta\varepsilon f_2^2 + \Delta\Omega f_1^2\right)\exp(2i\psi z)\right] \tag{6}$$

Application of the averaging method to equations (6) becomes possible if we assume that the following parameters $\Delta\varepsilon, \Delta\Omega$ are small. The application of the above method is based on the idea that if the derivatives are small, the values of functions can be naturally seen as the superposition of slowly varying part $\overline{C}$ and small rapidly oscillating terms. Assuming that these terms cause only small oscillations of real function about its mean part, it can be neglected in zero-order approximation: $C = \overline{C}$. The right-hand part of equations (6) is averaged on explicitly contained variable z:

$$\frac{dC}{dz} = i\left\langle\frac{1}{2}\left(\Delta\varepsilon|f_2|^2 + \Delta\Omega|f_1|^2\right)\right\rangle C + \left\langle\frac{i}{2}\left(\Delta\varepsilon\left(f_2^*\right)^2 + \Delta\Omega\left(f_1^*\right)^2\right)\exp(-2i\psi z)\right\rangle C^*$$

$$\frac{dC^*}{dz} = -i\left\langle\frac{1}{2}\left(\Delta\varepsilon|f_2|^2 + \Delta\Omega|f_1|^2\right)\right\rangle C^* + \left\langle\frac{i}{2}\left(\Delta\varepsilon f_2^2 + \Delta\Omega f_1^2\right)\exp(2i\psi z)\right\rangle C \tag{7}$$

Where $\langle...\rangle = \lim\limits_{T\to\infty}\dfrac{1}{T}\int\limits_0^T ....$ At first, consider the second items in the equations (7). The periodic functions can be decomposed in the Fourier series. After carrying out the averaging operation, only the items which satisfy the following condition remain:

$$\psi = \pi\left(\frac{l}{\Lambda} + n\right) + p = \psi_{n,l} + p \tag{8}$$

where $l = 0, \pm1, \pm2, ...$, $n = 0, \pm1, \pm2, ...$, $p \ll 1$. By introducing the following descriptions

$$\delta\psi = \left\langle\frac{1}{2}\left(\Delta\varepsilon|f_2|^2 + \Delta\Omega|f_1|^2\right)\right\rangle, \quad \Delta\psi = \left\langle\frac{i}{2}\left(\Delta\varepsilon\left(f_2^*\right)^2 + \Delta\Omega\left(f_1^*\right)^2\right)\exp(-2i\psi_{n,l}z)\right\rangle$$ one can

obtain the equations:

$$\frac{dC}{dz} = i\delta\psi C + \Delta\psi C^* \exp(-2ipz)$$

$$\frac{dC^*}{dz} = -i\delta\psi C^* + \Delta\psi^* C\exp(2ipz) \tag{9}$$

These equations (9) describe the phenomenon of a parametric resonance [3]. In the considered medium, the resonance is conditioned by the interaction of spatial harmonics of periodic disturbance and plane waves, on which the solution of wave equation in periodic medium is decomposed. The resonance bands correspond to forbidden bands of electromagnetic waves. As all previous presumptions were made only for objective ψ, the forbidden bands occur inside the allowed bands of undisturbed periodic medium. The position of the forbidden bands is given by the formula:

$$\psi = \pi\left(\frac{l}{\Lambda} + n\right) + \delta\psi = \psi_{n,l} + \delta\psi \tag{10}$$

where $l = 0,\pm1,\pm2,...$, $n = 0,\pm1,\pm2,...$. The width of the forbidden band is as follows:

$$2|\Delta\psi| = \left|\left\langle i\left(\Delta\varepsilon\left(f_2^*\right)^2 + \Delta\Omega\left(f_1^*\right)^2\right)\exp(-2i\psi_{n,l}z)\right\rangle\right| \tag{11}$$

The number of appearing bands depends on Λ. If Λ is integer ($\Lambda > 1$), in each allowed band of undisturbed medium $\Lambda - 1$ forbidden bands appear. If Λ is a rational number, $\Lambda = \frac{m}{j}$, $m - 1$ forbidden bands appear. Such forbidden band structure for layered medium with meander disturbance was observed in [4].

CONCLUSION

By using the averaging method, it is possible to evaluate the influence of the sum of disturbances on periodic medium dispersion properties. For example, for two disturbances with periods $\Lambda_1 = \frac{m_1}{j_1}, \Lambda_2 = \frac{m_2}{j_2}$ the number of forbidden bands is determined according to the formula: $(M - 1)$, where M is the least aliquot for m_1 and m_2.

REFERENCES

[1]. V.V. Konotop, "On wave propagation in periodic structures with smoothly varying parameters", *J. Opt. Soc. Am.*, B/Vol. 14, No. 2, 1997, pp. 364-369.

[2]. V.M. Agranovich, S.A. Kiselev, D.L. Mills, "Optical multistability in nonlinear superlattices with very thin layers", *Physical Review*, B/Vol. 44, No. 19, 1991, pp. 10917-10920.

[3]. A.A. Kolomensky, A.N. Lebedev, *"The theory of cyclic accelerators"*, Moscow, 1962 (in Russian).

[4]. N.A. Khizhnyak, E. Yu. Kramarenko, "Propagation of electromagnetic waves in space-periodic structures with dual periodicity", *Ukrainian Physical Journal*, Vol. 42, No. 10, 1997, pp. 1256-1259.

ANALYTICAL APPROACH TO THE THEORY OF RESONANCE DIFFRACTION BY PERIODICALLY MODULATED BOUNDARIES

A.V. Kats

Kharkiv Military University, P.O. Box 8847

Kharkiv, 61002, Ukraine, e-mail: avkats@akfirst.kharkiv.com

Light diffraction by gratings formed on high conducting surfaces can lead to great changes in the properties of diffracted waves if one of them is close to the surface electromagnetic wave (SEW) or, in other words, surface plasmon polariton (SPP), Ref. [1]. Resonance excitation of SEW can cause the total absorption of incident wave by the surface of high reflecting medium, Ref. [2], strong changes in polarization, including its full transformation, Ref. [3]. In spite of the fact that strong resonance effects caused by SEW were first discovered long ago by R. Wood, Ref. [4] (Wood anomalies), the effect still attracts attention of investigators. This is to be explained by unique properties of the resonance diffraction, allowing applications in many areas. As a result, many works have been devoted to theoretical investigation of resonance diffraction in the last years (see Ref. [5] and works cited therein), but complexity of the problem did not allow obtaining results in explicit analytical form that is of special interest.

From the other point of view, various possible applications in optics, optoelectronics [5], and radio-physics, make the problem of such research actual. Note that analytical approach allows both to make predictions of resonance properties of given grating (that is possible to do by numerical methods as well) and to formulate requirements for designing gratings with specified properties (this problem presents a very hard task for numerical methods).

This report presents new results in analytical approach to the problem. Possibility of obtaining results in explicit analytical form and investigating in details the peculiarities of the resonance diffraction is based upon some restrictions. Namely, we suppose the reflectivity of surface to be large. In other words, we suppose modulus of complex dielectric permeability ε to be large, or, equivalently, surface impedance ξ to be small, $|\xi| << 1$. This assumption allows simplification of the problem by using the Leontovich (impedance) boundary conditions. The assumption is not restrictive for metal surfaces and radiation wavelength from visible (or near infrared) range. One more assumption is that the gratings are "soft" enough, i.e. grooves depth is small in comparison with the period d and wavelength λ, or, for gratings formed by the modulation of dielectric properties of the surface, the modulation of the surface impedance $\tilde{\xi}(\vec{r})$ has to be much smaller than unity. Although the presented method allows to analyze both types of gratings (and combined gratings as well, see [6,7]), here for simplicity we present results for the case of impedance gratings.[1]

We start with the impedance boundary conditions

$$\vec{E}_t = \xi(\vec{r}) \cdot \vec{H}_t \times \vec{n}, \qquad z = 0 \qquad (1)$$

for the electric $\vec{E}(\vec{r})$ and magnetic $\vec{H}(\vec{r})$ monochromatic fields, index t denotes tangential components, $\vec{n}$ presents inner normal. For the plane boundary with periodically modulated impedance,

$$\xi(\vec{r}) = \xi_0 + \tilde{\xi}(\vec{r}), \qquad \tilde{\xi}(\vec{r}) = \sum \tilde{\xi}_n \exp(in\vec{g}\vec{r}), \qquad (2)$$

---

[1] The method used presents essential development of the one, described in Refs. [6-8], (see also Ref. [9]).

the total field is a sum of the incident wave $\vec{E}(\vec{r}) = \vec{E}\exp(ik_x x + ik_z z)$ and diffracted field $\vec{E}'(\vec{r})$. $\vec{E}'(\vec{r})$ can be presented as a sum of plane waves,

$$\vec{E}'(\vec{r}) = \sum \vec{E}_n \exp(i\vec{k}_{nt}\vec{r} + ik_{nz}z). \tag{3}$$

Here $\vec{k}_{nt}$ and k_{nz} are tangential and normal to the boundary components of wavevector, $\vec{k}_{nt} = \vec{k}_t + n\vec{g}$, $k_{nz} = -\sqrt{k^2 - k_{nt}^2}$, $n = 0, \pm 1, \pm 2, \ldots$, $\vec{k}_t = (k_x, 0, 0)$.

For the wave polarization amplitudes E_n^σ, $\vec{E}_n = \sum\limits_{\sigma=\pm} E_n^\sigma \vec{e}_n^\sigma$ (ort $\vec{e}_n^-$ lies in the n-th order propagation plane and $\vec{e}_n^+$ is perpendicular to it), one obtains the set of linear algebraic equations

$$\sum\limits_{\sigma'=\pm} D_{nm}^{\sigma\sigma'} E_m^{\sigma'} = V_n^\sigma. \tag{4}$$

All non-diagonal elements (both in number of diffracted order and polarization index) of the matrix $D_{nm}^{\sigma\sigma'}$ are of the order of $\tilde{\xi}_{n-m}$, and diagonal ones are of the order of unity: σ 1 , 2 , $D_{nn}^{--} = \beta_n + \xi_0$, where $\beta_n \equiv -k_{nz}/k$ are (dimentionless) propagating constants, $\mathrm{Re}(\beta_n) \geq 0$, $\mathrm{Im}(\beta_n) \geq 0$. Coefficients V_n^σ are linear in the incident wave and impedance amplitudes: $V_n^\sigma = \sum\limits_{\sigma'} V_n^{\sigma\sigma'} E_n^{\sigma'}$, $V_n^{\sigma\sigma'} \propto \tilde{\xi}_n$ for $n \neq 0$; for $n = 0$ $V_0^{\sigma\sigma'}$ is diagonal in polarization indices and does not depend on the impedance variation $\tilde{\xi}$. [2]

If all propagating constants are of the order of unity (nonresonanse case), one can solve the set of equations with the help of a perturbation theory in the small parameter $\tilde{\xi}$. In the case, the first term in the wave amplitudes expansion is of the order $\vec{E}_n \propto \tilde{\xi}_n (\beta_n + \xi_0)^{-1} \cdot \vec{E}$ for $n \neq 0$. Thus all amplitudes, excluding the specular reflected wave one, are small in comparison with the incident wave amplitude. But in the resonance case some of the propagation constants become small and the convenient perturbation theory fails: the denominators $\beta_r + \xi_0$, where index r corresponds to the resonance wave, i.e. $|\beta_r| \ll 1$, are small and the resonance wave amplitude can be greater than the incident one, $|E_r^-| \gg |\vec{E}|$.

The scattering matrix has a pole close to the real axis (due to small absorption); amplitude of resonance wave tends to infinity with $\mathrm{Re}(\xi_0) \to 0$ (if absorption vanishes, $\mathrm{Re}(\xi_0) = 0$, then the pole corresponds to real values of $\vec{k}_t$, $\vec{k}_{rt}^2 = k^2(1 + (\mathrm{Im}(\xi_0))^2)$). The last condition coincides with the dispersion law of SEW for ideal surface, see Ref. [1].

In the resonance case one can exclude the nonresonanse wave amplitudes E_N^σ and E_r^+ from the system (5) by perturbation method and obtain reduced system for the resonance wave amplitudes E_r^- only:

---

[2] For the relief grating, one can obtain a set of equations of the same form, but coefficients are infinite series in the Fourier amplitudes of the surface profile, [5]. These series converge for the grating relief without jumps. For the small grating depth, it is sufficient to take into account the first few terms of the expansion. Therefore, this case may be treated in analogy with the impedance grating case. The additional restriction here is assumption of Rayleigh's hypothesis validity that will take place for small enough grooves depth [1].

$$\sum_{r'} \tilde{D}_{rr'} E_{r'}^- = \tilde{V}_r \; . \tag{6}$$

If the coefficients of the reduced system (5) present convergent series in the grating Fourier amplitudes, then for analytical estimations one may use a few first terms of the expansion, that we call <u>main approximation.</u> The coefficients $\tilde{V}_r$ are linear functions of the incident wave amplitude; corresponding coefficients are power series in $\tilde{\xi}$, starting with proportional to $\tilde{\xi}_r$ term. Polarization amplitudes of all diffracted waves are linear functions of the incident wave amplitude,

$$E_n^\sigma = \sum_{\sigma'} R_n^{\sigma\sigma'} E^\sigma \; . \tag{7}$$

Transformation coefficients $R_r^{\sigma\sigma'}$ follow from (6), that can be solved explicitly. After this step, one can obtain $R_N^{\sigma\sigma'}$ and amplitudes of all non-resonance waves.

It is shown that theoretical results are in a good agreement with experimental ones, presented in the works [2], [3]; see also [5].

The explicit analytical results obtained, besides their theoretical interest, can be widely used in practice. For instance, they present interest in the problem of noncontact measurements, in constructing miniature optical and optoelectronics devices (rejecting filters, beam splitters, polarizers, etc.), in nonlinear optical effects. These effects increase due to the resonance growth of the local fields. Effects of resonance excitation of SEW are also principal in the nonlinear problem of surface structures formation under laser radiation action, see, for instance, Ref. [10].

REFERENCES

[1] "Electromagnetic theory of gratings", Ed. by R. Petit, Springer-Verlag, Berlin, 1980.

[2] M.C. Hutley, D. Maystre, Opt. Commun., 19, №3, pp. 431-436, 1976.

[3] G.P. Bryan-Brown, J.R. Sambles, J. Mod. Optics, 37, № 7, pp. 1227-232, 1990.

[4] R.W. Wood Philos. Mag., 4, p. 396, 1902.

[5] E.G. Loewen, E. Popov, "Diffraction gratings and applications", Marcel Dekker Inc., N-Y, 1997.

[6] A.V. Kats, P.D. Pavitskii, I.S. Spevak, Radiophysics and Quantum Electronics, 35, № 3-4, pp. 163-169, 1992.

[7] A.V. Kats, P.D. Pavitskii, I.S. Spevak, JETP, 78, № 1, pp. 42-48, 1994.

[8] A.V. Kats, V. V. Maslov, Sov. Phys. JETP, 35, № 2, pp. 264-267, 1972.

[9] A. Hessel, A.A. Oliner, Appl. Optics, 4, № 10, pp. 275-1297, 1965.

[10] I.S. Spevak, V.M. Kontorovich, A.V. Kats, V.K. Gavrikov, Sov. Phys. JETP, 66, № 1, pp. 58-65, 1987.

[11] A.V. Kats, I.S. Spevak, "Diffraction of electromagnetic waves", Kharkiv military university, Kharkiv, 1998, 178 pp. (In Ukrainian).

INTEGRAL EQUATIONS FOR DIELECTRIC-COATED THIN-WIRE ANTENNAS

Valerij I. Demidtchik

Belarusian State University, Department of Radiophysics, Minsk, Belarus

E-mail: valdem@rfe.bsu.unibel.by

ABSTRACT

The generalization of Pocklington's IE for thin-wire structures of arbitrary geometry with dielectric coating is offered in the paper. The deduction of IE is given. The deduction is based on the definition of the general electric field as the sum of field current on conductor surface, field of polarization current that is equivalent to dielectric coating, and primary field. Primary field can be the field of localized source (the problem of excitation) or the field of incident plane electromagnetic wave (the problem of scattering). Numerical results are found to be in a good agreement with experiments and with the data obtained by other authors.

INTRODUCTION

Thin-wire structures with dielectric coating are widely used in antenna techniques. The coating can be used for the improvement of antenna parameters, for solving problems connected with electric strength, for isolation, when no contacts between conductors and surrounding medium are permitted. The task of investigation of dielectric coating influence on electrodynamic properties is typical of grid reflectors.

The use of integral or integral-differential equations for current in conductors is one of the methods of analyzing such structures. For example, in [1] the solution of the problem of excitation of a thin-wire antenna with dielectric coating based on the Harrington-type integral equation is described, in [2] – based on Hallen's equation for rectilinear conductors.

INTEGRAL EQUATION DEDUCTION

Let us examine the solution of the given problem for thin conductors with gradually changing curvilinear geometry based on Pocklington's integral equation within the limits of quasi-static approximation. It is convenient to use curvilinear cylindrical coordinate system. The geometry is shown in Fig. 1.
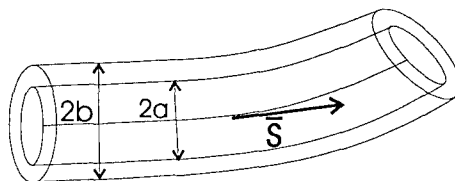
Fig. 1

The curvilinear conductor with a radius a, length L is covered with a layer of dielectric with a thickness b-a with absolute permittivity ε_a.

The electric field generated by the conductor can be found as $\overline{E} = \overline{E}_1 + \overline{E}_2$, where $\overline{E}_1$ is the field determined by surface currents and conductor charges, $\overline{E}_2$ is the field determined by the polarization currents and charges of dielectric coating.

If to introduce a simplifying suggestion that $a \ll \lambda$, where λ is the wavelength of electromagnetic field, it is possible to neglect the azimuth component of surface current and

to consider the current distributed along the conductor axis. This suggestion allows to obtain the known expression of tangent component of the field $\overline{E}_1$ on conductor surface [3]:

$$E_{1\tau} = \frac{1}{i\varpi\varepsilon} \int_L I(s') \left[k^2 \overline{s}\overline{s}' - \frac{\partial^2}{\partial s \partial s'} \right] G(s,s') ds', \tag{1}$$

$$G(s,s') = e^{-ikr} \Big/ 4\pi r, \quad r = \sqrt{(x-x')^2 + (y-y')^2 + (z-z')^2 + a^2},$$

where $\overline{s}, \overline{s}'$ are unit tangent vectors of source and observation points, x, y, z, x', y', z' are their coordinates, k is the free-space propagation coefficient.

The field $\overline{E}_2$ is found as:

$$\overline{E}_2 = -i\varpi\overline{A}_2 - \nabla\Phi_2, \tag{2}$$

where $\overline{A}_2$ and Φ_2 are the vector and scalar potentials determined by the polarization currents and charges.

Polarization current is connected with normal component of electric field on conductor surface, i.e. with the charge. In turn, longitudinal component of electric current is connected with the charge according to continuity equation.

Within the thin-wire approximation, as a result, the current of polarization can be found as:

$$\overline{J}_p = -\frac{\varepsilon_a - \varepsilon_0}{\varepsilon_a \, 2\pi a} \frac{\partial I(s')}{\partial s'}. \tag{3}$$

Consequently, $\overline{A}_2$ can be described as:

$$\overline{A}_2 = \frac{\mu_0}{\varepsilon_0} (\varepsilon_a - \varepsilon_0)(b-a) \int_L G(s,s') \frac{\partial I(s')}{\partial s'} \overline{n} \, ds', \tag{4}$$

where $\overline{n}$ is the unit vector of normal to the conductor surface.

Expression (4) was obtained on assumption that polarization current is not changed in the direction perpendicular to conductor surface.

The scalar potential Φ_2 is defined by surface density of polarization charges σ_{p1} and σ_{p2} on dielectric bounds $r=a$ и $r=b$. The values σ_{p1} and σ_{p2} are connected with normal component of polarization vector and, consequently, it is possible to say that:

$$\sigma_{p1} = \frac{\varepsilon_a - \varepsilon_0}{i\varpi\varepsilon_a \, 2\pi a} \frac{\partial I(s)}{\partial s}, \quad \sigma_{p2} = \frac{\varepsilon_a - \varepsilon_0}{i\varpi\varepsilon_a \, 2\pi b} \frac{\partial I(s)}{\partial s}. \tag{5}$$

Using (5) we can obtain an expression for Φ_2:

$$\Phi_2 = \frac{\varepsilon_a - \varepsilon_0}{i\varpi\varepsilon_a\varepsilon} \int_L (G(s,s') - \breve{G}(s,s')) \frac{\partial I(s')}{\partial s'} ds', \tag{6}$$

$$\breve{G}(s,s') = \frac{e^{-ik\breve{r}}}{4\pi\breve{r}}, \quad \breve{r} = \sqrt{(x-x')^2 + (y-y')^2 + (z-z')^2 + b^2}.$$

Tangent component of the field $\overline{E}_2$ on conductor surface is defined as:

$$E_{2\tau} = \overline{E}_2 \overline{s} = -i\varpi\overline{A}_2 \, \overline{s} - \frac{\partial\Phi_2}{\partial s} = \frac{k^2(\varepsilon_a - \varepsilon_0)}{i\varpi\varepsilon_0\varepsilon_a} (b-a) \int_L G(s,s') \frac{\partial I(s')}{\partial s'} \overline{n}\overline{s}' \, ds' +$$

$$+ \frac{\varepsilon_a - \varepsilon_0}{i\varpi\varepsilon_0\varepsilon_a} \int_L I(s') \frac{\partial^2 (G(s,s') - \breve{G}(s,s'))}{\partial s \, \partial s'} ds'. \tag{7}$$

The expression that describes the tangent component of the total field $\overline{E}$ is:

$$E_\tau = \frac{1}{i\varpi\varepsilon_0}\int_L I(s')\left[k^2\,\overline{ss}' - \frac{\partial^2}{\partial s\partial s'}\right]G(s,s')\,ds' + \frac{k^2(\varepsilon_a-\varepsilon_0)(b-a)}{i\varpi\varepsilon_0\varepsilon_a}\int_L G(s,s')\frac{\partial I(s')}{\partial s'}\overline{ns}'ds' +$$

$$+\frac{\varepsilon_a-\varepsilon_0}{i\varpi\varepsilon_0\varepsilon_a}\int_L I(s')\frac{\partial^2\big(G(s,s')-\breve{G}(s,s')\big)}{\partial s\,\partial s'}ds'. \tag{8}$$

The analysis shows, that the influence of the second item in (8) is not essential and can be neglected. Taking into consideration and using the boundary condition on the surface of an ideal conductor, we can obtain an integral equation of Pocklington's equation type:

$$E_\tau^i = -\frac{1}{i\varpi\varepsilon_0}\int_L\left[k^2 G(s,s')\overline{ss}' - \frac{\varepsilon_0}{\varepsilon_a}\frac{\partial^2 G(s,s')}{\partial s\partial s'} - \frac{\varepsilon_a-\varepsilon_0}{\varepsilon_a}\frac{\partial^2\breve{G}(s,s')}{\partial s\partial s'}\right]I(s')\,ds'. \tag{9}$$

where E_τ^i is the tangent component of the field of excitation source.

NUMERICAL RESULTS

The solution of the equation (9) was found using the methods described in [4], with choosing step-function as basis function and delta-function as weight function.

The field of incident plane wave can be used as the source of excitation or the field of the coaxial-line approximated by magnetic-current frill, or the field of a δ-function generator. The calculation of characteristics of radiation and scattering in far zone was carried out using the known current distribution.

In [1] the experimental and calculation data of current distribution are given for vertical monopole antenna with dielectric coating and for monopole-antenna with additional passive element. The comparison of these results with similar results, obtained according to integral equation (9), shows their good agreement.

Additionally, the calculation of electrodynamic characteristics of a helical antenna composed of dielectric-coated conductor was carried out. The influence of the dielectric on band properties of helical antenna is examined.

CONCLUSION

A method is presented for the analysis of thin-wire antennas of arbitrary geometry with dielectric coatings. The calculation results of characteristics of radiation and scattering are in a good agreement with experimental data for the structures with gradually changing geometry. Thereby the relative permittivity of the coating $\varepsilon_r < 10$ and its thickness is comparable with the conductor radius.

REFERENCES

[1] Popovic B.D., Djordjevic A.R., Kircanski N.M. The Radio and Electronic Engineer, v.51, № 3, p. 141.

[2] Motorin A.V. Electromagnetic Waves & Electronic Systems. 1997, v.2, № 2, p. 38. (in Russian).

[3] Mei K.K. IEEE Trans. , 1965, AP-13, №5, p. 374.

[4] Demidtchik V.I., Runov A.V., Kalashnikov N.V. Izvestija VUZov. Radioelektronika, Kyiv, 1983, vol. 26, №3, p. 82. (in Russian).

ELECTROMAGNETIC FIELDS, SCATTERED BY THE SYSTEM OF THE SUBSURFACE OBJECTS

O. I. Sukharevsky, G. S. Zalevsky
Kharkiv Military University
Ukraine, 61043, Kharkiv, maidan Svobody, 6

ABSTRACT

The numerical modeling problem of electromagnetic wave scattering by the system of the subsurface resonant objects is considered. The proposal technique based on using the integral equations, which were obtained by the authors in [1] for the case of local object. The mathematical modeling results for the system of perfectly conducting objects, located in the ground are discussed.

BASIC CALCULATION RELATIONS

Consider the system of the subsurface objects (SO), located in the dielectric lossy dispersive half-space V_2 (Fig.1). SO takes up the space with linear dimensions, which exceed some wavelength. For SO illumination the antenna of small electric dimensions – magnetic dipole, located in the free half-space V_1 at the distance of some wavelength from the boundary L of half-spaces V_1, V_2 is used. The problem consists in calculating of the electromagnetic responses, scattered from such the system of objects.
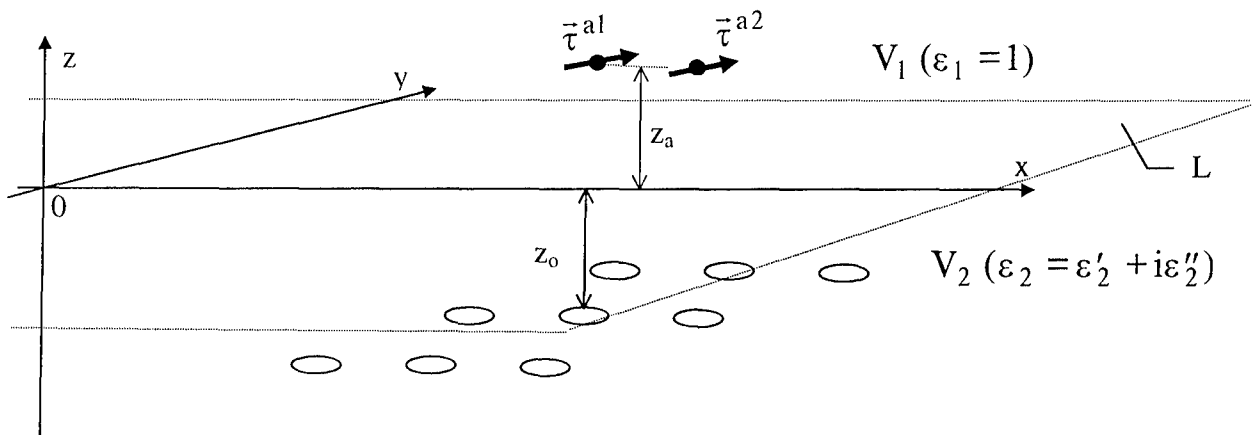
Fig. 1. System of the subsurface objects, located near the boundary of two dielectric half-spaces V_1, V_2.

In [1] the method for the calculating of the fields scattered by the local subsurface object are described. In the case of the perfectly conducting object there was obtained the Fredgolm surface integral equation of the second kind:

$$\left\|\begin{matrix} \vec{\tau}_2^0 \\ -\vec{\tau}_1^0 \end{matrix}\right\| \cdot (\vec{H}^\perp(Q_0) - 2\vec{H}^{m\perp}(Q_0)) = -\frac{2}{i\omega} \int_\Sigma \left\|\begin{matrix} \vec{E}_1^{mT}(Q|Q_0, \vec{\tau}_1^0) \\ \vec{E}_1^{mT}(Q|Q_0, \vec{\tau}_2^0) \end{matrix}\right\| \cdot \vec{H}^\perp(Q)ds \quad (Q_0 \in \Sigma), \quad (1)$$

where Q_0, Q are observation and integration points, respectively; $\vec{H}^\perp(Q_0)$ is the electric current density at the object surface Σ; $\vec{H}^{m\perp}(Q_0)$ is the electric current density, induced by the same source that the $\vec{H}^\perp(Q_0)$, but in the case of object absence; symbols $"\perp"$, $"T"$ denote vectors tangential to Σ: $\vec{a}^T = \vec{a} - \vec{n}(\vec{n}\cdot\vec{a})$, $\vec{b}^\perp = \vec{n}\times\vec{b}$ ($\vec{n}$ is normal unit vector to Σ). The kernel of integral equation is the field $\vec{E}_1^m(Q|Q_0, \vec{\tau}^0)$ of magnetic point source located at Q_0. Unit vectors $\vec{\tau}_1^0$, $\vec{\tau}_2^0$ indicate the orientation of magnetic vector-moment of considered point source. In the case of SO in equation (1) the integration surface is:

$$\Sigma = \bigcup_{n=1}^N \Sigma_n, \tag{2}$$

where Σ_n is the surface of local object in the system.

To solve the integral equation (1) when the number of objects is rather large is a difficult problem. It is attributed to large dimension of the system of linear equations to be solved and long time for the kernels calculating. So, we have done the mathematical modeling for the estimating of interaction between the objects in the system, located in the ground. The obtained results show that when the $\lambda=0.545$ m and the range between the two objects $\Delta=0.2$ m, 1 m and 2.2 m (in the H-plane) the changes of current densities on the object surface, caused by interaction with the other object make up 25%, 0.3% and 0.003% respectively; when the $\lambda=5$ m, $\Delta=6$ m the considered change amount to 10%. Using the obtained results the calculating algorithm can be simplified. To find the electromagnetic response of the system of N subsurface objects it is necessary to solve the integral equation for each object and then the H-component of the scattered field can be calculated by means of formula:

$$-i\omega\vec{\tau}^0(\vec{H}(Q_0) - \vec{H}^m(Q_0)) = \sum_{n=1}^N \int_{\Sigma_n} \vec{E}_1^{mT}(Q|Q_0, \vec{\tau}^0)\vec{H}^\perp(Q)ds. \tag{3}$$

Magnetic field strength of magnetic dipole, located in V_1 at the great distance from the boundary L can be calculated using relation:

$$\vec{H}^m(M) = \vec{H}^m(M|M_a, \vec{\tau}^a) \underset{z_a\to\infty}{\sim} \frac{e^{ik_1R_1}}{4\pi R_1}k_1\frac{\omega}{W_2}\left\{\vec{p}_2^n v_n + \vec{p}_2^\perp v_\perp\right\}e^{-ik_2(\vec{R}_2\vec{R}_2^0)}, \tag{4}$$

where M_a, M are location and observation points respectively; k_1, k_2 are the wave numbers in V_1, V_1 respectively; $W_2 = \sqrt{\dfrac{\mu_0\mu_2}{\varepsilon_0\varepsilon_2}}$; $R_1 = |\vec{R}_1|$, $\vec{R}_1^0 = \dfrac{\vec{R}_1}{|\vec{R}_1|}$, $\vec{R}_2^0 = \dfrac{\vec{R}_2}{|\vec{R}_2|}$;

$\vec{p}_1^n = \vec{n}_1(\vec{\tau}^{aT}\cdot\vec{n}_1)$, $\vec{p}_1^\perp = \vec{n}_1\times(\vec{\tau}^{aT}\times\vec{n}_1)$, $\vec{p}_2^n = \vec{n}_1\times(\vec{\tau}^{a\perp}\times\vec{n}_1)$, $\vec{p}_2^\perp = \vec{n}_1(\vec{\tau}^{a\perp}\cdot\vec{n}_1)$; $\vec{\tau}^{aT} = \vec{\tau}^a - \vec{R}_1^0(\vec{\tau}^a\cdot\vec{R}_1^0)$, $\vec{\tau}^{a\perp} = \vec{R}_1^0\times\vec{\tau}^a$; $\vec{n}_1$ is the normal to the plane of incidence of the illuminating wave; $v_n = \dfrac{2W_2\cos\alpha_1}{W_2\cos\alpha_2 + W_1\cos\alpha_1}$, $v_\perp = \dfrac{2W_2\cos\alpha_1}{W_2\cos\alpha_1 + W_1\cos\alpha_2}$.

The physical sense of vectors in (4) showed in fig. 2.

NUMERICAL MODELING RESULTS

In the paper the electromagnetic responses of the system of 15 perfectly conducting mine-like objects (fig 3a), buried in the ground are demonstrated and discussed. Objects were located at the depth of 6 cm. Transmitting and receiving antennas (magnetic dipoles) were located at the same height and separated in the plane, orthogonal to the direction of movement of radar system (fig 1). In fig. 4 were shown electromagnetic responses of considered SO in the case when the frequency of illumination made up 550 MHz for different direction of observation as shown in fig 3b.
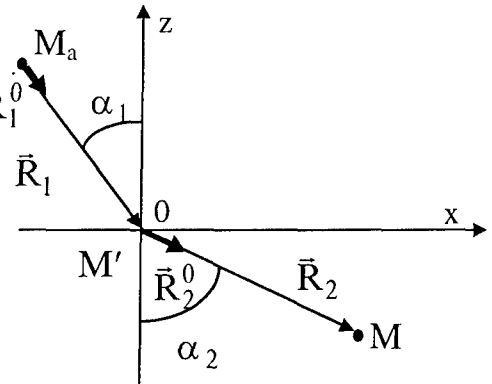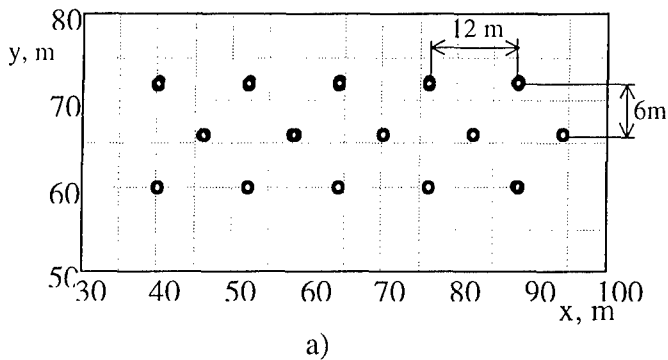
Fig. 2. Physical sense of vectors in relation (4).

a)

b)
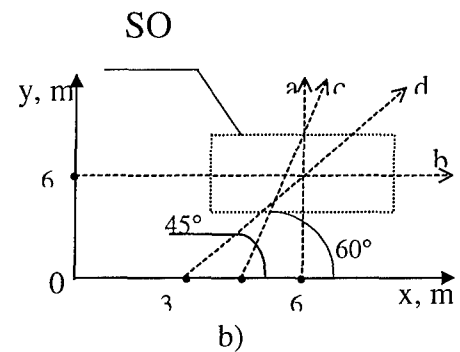
Fig. 3. a) System of subsurface objects; b) location of receiving points.
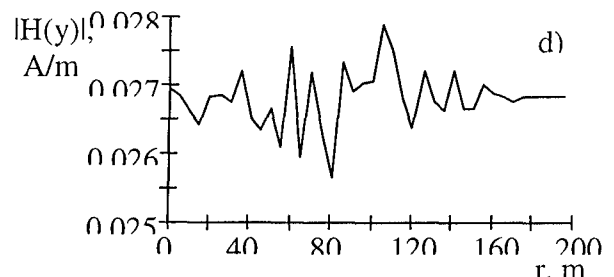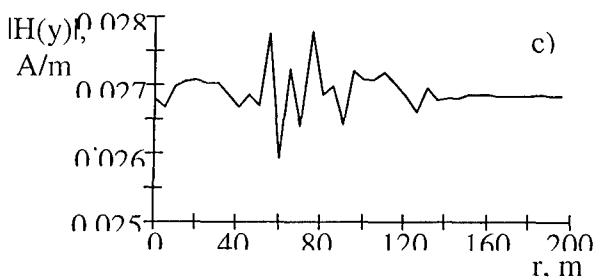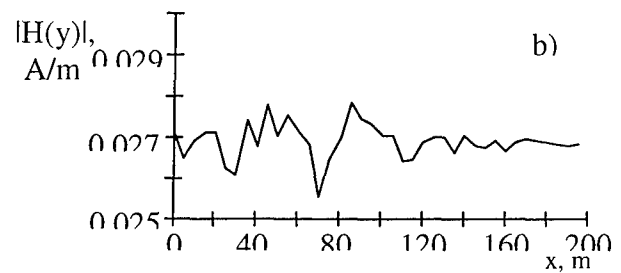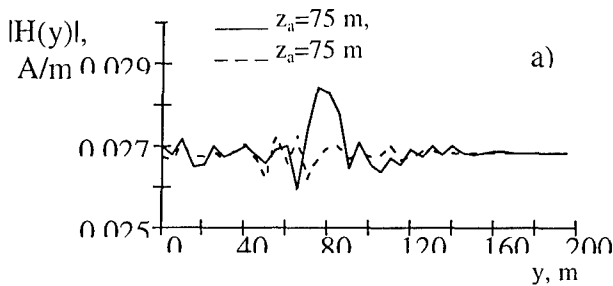
Fig. 4. Electromagnetic responses of the system of 15 subsurface objects in the cases showed in fig. 3b.

Reference

[1] O. I. Suharevsky, G. S. Zalevsky. Electromagnetic wave scattering by subsurface resonant object. // Radiophysic and radioastronomy. –1998. V.3, №1. –p. 37-42.

AUTHORS LIST

A

Afanasiev N.T.	334
Aksoy A.	61
Alexeev G.A.	586
Alpatova A.V.	459
Alpatova O.V.	193
Andrenko A.S.	295
Andriychuk M.I.	604
Antonova V.A.	355
Arai H.	163
Averkov Y.O.	323
Ayzatsky M.I.	506
Azarenkov N.A.	329

B

Bakunov M.I.	134
Balachonova N.A.	572
Baran R.	218, 224
Basarab M.A.	230, 682, 700
Batrakov D.O.	621
Bekker E.V.	27, 403
Beletskiy N.N.	343
Beletsky A.A.	283
Belov P.A.	259
Benson T.M.	27, 412, 541
Bijamov A.	286
Bit-Babik G.	286, 679
Blinova N.	485
Bliznyuk N.Y.	289
Bludov Y.V.	343
Bondarenko N.V.	685
Boriskin A.V.	397
Boriskina S.V.	397, 541
Borulko V.F.	550
Brovenko A.V.	196
Bryukhanova V.V.	253
Buharov S.V.	583
Bulgakov A.A.	346

C

Chen W.-T.	598
Chernish L.I.	676
Chernoblavskiy A.A.	406
Chernogor L.F.	233, 652
Chiu C.-C.	598
Chtchekaturov V.	137
Chumachenko V.P.	41, 512
Churmakov D.	332
Churyumov G.I.	355, 358

D

Daniel J.-P.	203
Daniele V.	432, 441, 673
Dautov R.	396
Demidtchik V.	709
Denisenko P.F.	630
Derevyanko S.A.	340
Di Fausto M.	68
Dikmen F.	202
Dobrovol'sky S.N.	114
Donchenko V.A.	661
Dotsenko O.	435
Drobakhin O.	215
Dumin A.N.	125
Dziech W.	218, 224
Dzyubanov D.A.	633

E

Engheta N.	34
Eren San S.	172
Ermakov G.V.	120, 143

F

Fedorenko A.I.	447
Fedotov F.	111
Filippov Y.F.	547
Fisch W.	137

R

S

T